Seabed Stability, Liquefaction and the Development of Fluid Mud During Dredging and Dumping at Miramichi Inner Bay

Seabed Stability, Liquefaction and the Development of Fluid Mud During Dredging and Dumping at Miramichi Inner Bay

Prepared For

Public Works and Government Services Canada
Architectural and Engineering Services
P.O. Box 7350
St. John, New Brunswick
E2L 4J4

SSC Contract # E0225-3-0020/01-OSC

Prepared By

C.L. Amos**, M. Brylinsky*, H.A. Christian** and G.R. Daborn*

*Acadia Centre for Estuarine Research, Acadia University
Wolfville, Nova Scotia B0P 1X0

** Atlantic Geoscience Centre, Bedford Institute of Oceanography
Dartmouth, Nova Scotia B2Y 4A2

February 1994

Acadia Centre for Estuarine Research Publication No. 32

EXECUTIVE SUMMARY

An evaluation of seabed stability, liquefaction and development of fluid muds during dredging and disposal was carried out in the Miramichi Inner Bay over a three week period during July 1993. The objective of the study was to determine if dredging and disposal activities cause instabilities that lead to enhanced sediment erodibility and resuspension. Measurements of sediment pore pressures, erosion thresholds, erosion rates, and settling rates were made at a number of sites representing the natural seabed, the navigation channel, and an experimental disposal site prior to and after disposal of spoils. The effect of ship passage on channel stability and sediment resuspension was also evaluated during passage of two commercial freighters.

Sediments in the Bay are characterized by high organic contents and minimal consolidation and are very close to liquefaction. Measurements of sediment settling rates, however, indicated that in most locations there is little potential for generation of fluid mud layers. Erosion thresholds were lowest at the Channel sites and were typical of fluidized gels. Erosion thresholds of dredge spoils were initially low, but quickly (within 60 hrs) increased to exceed those of the original dredge materials. This strengthening, however, was restricted to the surface 2 mm of sediment only. Immediately below this depth the strength of the disposed material remained extremely low, and was even in a fluidized state. Monitoring of *in situ* pore pressures at depths up to 50 cm before and after disposal of spoils indicated that spoils deposition has no effect on the long term stability of underlying sediments.

Continuous monitoring of suspended sediment concentrations indicated little evidence of either naturally occurring fluid mud layers or that dredging and disposal activities result in chronically high suspended sediment concentrations outside of the immediate area of the Channel where dredging is taking place. On two occasions high suspended sediment concentrations (>1000 mg^{-1}), lasting for periods of up to six hours, were detected near the Experimental disposal site. It was not clear if the source of these sediments was recently deposited spoils or river inputs resulting from high tides and strong precipitation events.

Ship passage produced elevated suspended sediment concentrations (>2000 mg^{-1}) at a site approximately 100 m north of the Channel, but these lasted for only a short period (<15 min). A more significant impact of ship passage was the generation of short term cyclic excess pore pressures by the wake which is a major factor leading to reduced stability of the Channel margin. Ship passage effects, however, may be relatively minor compared to the potential effects of sustained loading during extreme storm events.

TABLE of CONTENTS

LIST of TABLES

LIST of FIGURES

Page

Page

Page

Page

Page

Page

Seabed Stability, Liquefaction and the Development of Fluid Mud During Dredging and Dumping at Miramichi Inner Bay

1. INTRODUCTION

During 1981-1983 a capital dredging programme was undertaken in the Miramichi Bay and Estuary to deepen the navigable channel. Since that time, maintenance dredging has been required to ensure adequate depths for ship passage. Most of the material dredged from the Inner Bay during the capital project, and all of the spoils from maintenance dredging in the Inner Bay have been deposited at Disposal Site B. Examination of sediment cores from this site and nearby areas by Krank and Milligan (1989), together with other information, has given rise to the perception that the disposal site is unstable, and that much of the dredged material may have been remobilised, either as bedload or in suspension, to other parts of the estuary.

Dredging of the Miramichi Ship Channel has been a controversial project since its initiation. There is a widespread perception, particularly among the fishing community, that dredged spoils have caused an increase in turbidity of the water in the estuary, and that this has affected local fisheries, particularly for migratory species. Concern has also been expressed regarding contamination of the sediments, although existing data indicate that levels of contamination are not very high in the areas of the Inner Bay presently subject to maintenance dredging (MacKnight 1992).

In response to these concerns, and at the request of Public Works and Government Services Canada, the Acadia Centre for Estuarine Research of Acadia University and the Atlantic Geoscience Centre of the Bedford Institute of Oceanography carried out a preliminary field study during November 1991 to obtain measurements of sediment geotechnical properties and sediment strength and erodibility near Disposal Site B and the Ship Channel.

Results of this preliminary study (Brylinsky et al. 1992) indicated that erodibility of sediments on the spoils mound was less than at Control sites, and that the Channel sides exhibited the lowest stability. This study was conducted on spoils that had been deposited 1 or 2 years earlier, indicating there was little likelihood of well-weathered material becoming mobilized except under the most severe of conditions. It was not possible in that study to determine whether extensive loss of sediment was occurring within a short period of its deposition on the disposal site. In addition, direct measurements of pore pressure in control areas and adjacent to the channel indicated that the liquefaction potential of naturally deposited sediments appears to be high. This suggested that fluid muds might form under conditions of higher stress associated with storms, dredging and disposal of spoils, or, in the region of the Ship Channel, from the stresses exerted by passing ships. It was also evident that considerable variability exists between the sites examined as representative of the natural seabed, in terms of both sediment characteristics and critical erosion velocities. For these reasons, it was deemed advisable to re-examine the properties of naturally and anthropogenically deposited

sediments in the Bay, especially immediately after dredged spoils had been deposited on the disposal site. Accordingly, in July 1993 a field study was carried out in the Miramichi Inner Bay to address these concerns. The objectives of the study were to:

1. Obtain direct *in situ* measurements of the erodibility of sediments at up to 20 locations in Miramichi Inner Bay using a benthic flume. Sites were selected to represent natural seabed, seabed in the navigation channel and recently deposited dredge spoils on Disposal Site B.

2. Determine the characteristic patterns of erosion of deposited dredge spoils, with emphasis upon recently disposed material, and of the natural seabed.

3. Obtain long term measurements (i.e., over several tides) of suspended sediment concentrations in the vicinity of the Channel during dredging and at Disposal Site B following recent deposition of dredge spoils.

4. Obtain direct *in situ* measurements of suspended sediment concentrations in water near the Miramichi Ship Channel before, during and after passage of a commercial vessel using the Channel.

5. Obtain long term measurements (i.e., over several tides) of pore pressures and liquefaction potential of deposited sediments at sites in the Bay, with emphasis upon areas adjacent to the Miramichi Ship Channel.

6. Conduct an extensive survey to determine if fluid mud layers exist within the Bay, particularly in the region of recently disposed materials, and in association with dredging activities and/or ship passage.

7. Obtain Van Veen grab and gravity core samples from 10-20 locations representing natural seabed, recent spoil mounds, and areas adjacent to the Miramichi Ship Channel for determination of sediment geotechnical properties.

2. STUDY SITES and SAMPLING PROTOCOL

A total of 38 stations were occupied during the study. Table 2-1 lists the location and samples collected for each station. Appendix A is a cruise log providing details of times and activities for each station. The majority of activities were carried out in three general areas (Fig. 1)*: (1) a Control site located north of Reach 22; (2) a Channel site within Reach 22; and (3) an Experimental disposal site established within Disposal Site B. The Control site was located immediately north of the Channel and served also as the location for deployments carried out to monitor ship passage events. The Channel site was located in an area that was being dredged during the time of the field study. The Experimental disposal site was located in an area on the east margin of Disposal Site B that was unlikely to have had spoils deposited

*Located in map pocket at rear of document

Table 2-1. Summary of station locations and operations performed (SC - Sea Carousel; EXCAL - Excalibur; GC - Gravity Core; VV - Van Veen Grab; CTD - Salinity-Temperature Profile; CM - Current Meter; LAN - Lancelot; letters in parentheses next to station numbers indicate control (C), channel (Ch) and experimental disposal site (E)) .

DATE	STATION	POSITION		SC	EXCAL	GC	VV	CTD	CM	SOBS	LAN
14 July	1 (C)	47° 07.92'	65° 09.82'							X	
"	2 (C)	47° 07.89'	65° 09.66'						X		
"	3 (C)	47° 07.93'	65° 09.52'					X			
"	4 (C)	47° 07.99'	65° 09.97'								X
"	5 (E)	47° 06.64'	65° 09.74'						X		
15 July	6 (E)	47° 07.06'	65° 10.15'				X				
"	6 (E)	47° 07.06'	65° 10.15'			X					
"	6 (E)	47° 07.06'	65° 10.15'		X						
"	7 (E)	47° 06.98'	65° 10.30'			X					
"	7 (E)	47° 06.99'	65° 10.27'				X				
"	8 (E)	47° 06.85'	65° 10.33'				X				
"	8 (E)	47° 06.87'	65° 10.29'			X					
"	9 (E)	47° 06.92'	65° 10.30'			X					
"	9 (E)	47° 06.90'	65° 10.30'				X				
"	10 (E)	47° 07.03'	65° 10.24'				X				
"	10 (E)	47° 07.02'	65° 10.25'			X					
"	11 (E)	47° 07.01'	65° 10.26'		X						
16 July	6 (E)	47° 06.97'	65° 10.33'	X							
"	6 (E)	47° 06.96'	65° 10.33'					X			
"	7 (E)	47° 07.05'	65° 10.21'	X							
"	7 (E)	47° 07.05'	65° 10.21'					X			
"	7 (E)	47° 06.88'	65° 10.33'		X						
"	8 (E)	47° 06.88'	65° 10.33'	X							

DATE	STATION	POSITION		SC	EXCAL	GC	VV	CTD	CM	SOBS	LAN
18 July	8 (E)	47° 06.88'	65° 10.33'					X			
"	12 (Ch)	47° 07.70'	65° 09.20'				X				
"	12 (Ch)	47° 07.78'	65° 09.22'			X					
"	13 (Ch)	47° 07.80'	65° 09.40'			X					
"	13 (Ch)	47° 07.80'	65° 09.40'				X				
"	9 (E)	47° 06.87'	65° 10.29'	X							
"	9 (E)	47° 06.87'	65° 10.29'					X			
"	14 (Ch)	47° 06.78'	65° 14.69'								
"	14 (Ch)	47° 06.78'	65° 14.69'				X				
"	15 (Ch)	47° 06.80'	65° 14.57'				X				
"	15 (Ch)	47° 06.80'	65° 14.57'			X					
19 July	13 (Ch)	47° 07.83'	65° 09.41'		X						
"	13 (Ch)	47° 07.79'	65° 09.21'	X							
"	13 (Ch)	47° 07.83'	65° 09.41'					X			
"	12 (Ch)	47° 07.79'	65° 09.21'		X						
"	12 (Ch)	47° 07.79'	65° 09.21'	X							
"	12 (Ch)	47° 07.79'	65° 09.21'					X			
"	8 (E)	47° 06.96'	65° 10.29'		X						
"	8 (E)	47° 06.96'	65° 10.29'	X							
"	8 (E)	47° 06.96'	65° 10.29'					X			
"	16 (E)	47° 06.89'	65° 10.10'					X			
"	17 (C)	47° 08.05'	65° 09.77'		X						
20 July	38 (E)	47° 06.81'	65° 09.70'							X	
22 July	18 (C)	47° 08.13'	65° 09.39'								X
"	19 (E)	47° 06.82'	65° 10.09'					X			
"	20 (E)	47° 06.87'	65° 10.30'			X					
"	20 (E)	47° 06.87'	65° 10.30'				X				
"	20 (E)	47° 06.87'	65° 10.26'		X						
"	20 (E)	47 06.86'	65° 10.29'	X							
23 July	21 (E)	47° 06.89'	65° 10.26'			X					
"	21 (E)	47° 06.89'	65° 10.26'		X						

DATE	STATION	POSITION		SC	EXCAL	GC	VV	CTD	CM	SOBS	LAN
23 July	21 (E)	47° 06.86'	65° 10.26'	X							
"	21 (E)	47° 06.86'	65° 10.26'				X				
"	22 (E)	47° 06.90'	65° 10.29'				X				
"	22 (E)	47° 06.90'	65° 10.29'	X							
"	22 (E)	47° 06.90'	65° 10.29'			X					
"	23 (E)	47° 06.87'	65°10.23'			X					
"	23 (E)	47° 06 87'	65° 10 23'	X							
"	23 (E)	47° 06.87'	65° 10.23'		X						
"	24 (E)	47° 06.87'	65° 10.23'		X						
24 July	25 (C)	47° 08.01'	65° 09.46'	X							
"	25 (C)	47° 08.02'	65° 09.46'			X					
"	25 (C)	47° 08.03'	65° 09.46'				X				
"	25 (C)	47° 08.03'	65° 09.46'		X						
"	26 (C)	47° 08.02'	65° 09.49'	X							
"	26 (C)	47° 08.03'	65° 09.48'					X			
"	26 (C)	47° 08.04'	65° 09.48'				X				
"	26 (C)	47° 08.05'	65° 09.48'			X					
"	27 (C)	47° 08.01'	65° 09.46'	X							
"	27 (C)	47° 08.02'	65° 09.51'			X					
"	27 (C)	47° 08.02'	65° 09.48'				X				
"	28 (E)	47° 07.04'	65° 10.12'			X					
"	28 (E)	47° 07.03'	65° 10.13'				X				
"	28 (E)	47° 07.06'	65° 10.13'		X						
"	28 (E)	47° 07.02'	65° 10.12'	X							
25 July	29 (E)	47° 07.02'	65° 10.12'			X					
"	29 (E)	47° 07.02'	65° 10.12'		X						
"	29 (E)	47° 07.03'	65° 10.10'				X				
"	29 (E)	47° 07.03'	65° 10.12'	X							
"	30 (E)	47° 07.05'	65° 10.11'				X				
"	30 (E)	47°.07.02'	65° 10.10'			X					
"	30 (E)	47° 07.04'	65° 10.10'	X							

DATE	STATION	POSITION		SC	EXCAL	GC	VV	CTD	CM	SOBS	LAN
25 July	31 (E)	47° 06.05'	65° 10.11'		X						
26 July	32 (E)	47° 06.86'	65° 10.26'				X				
"	32 (E)	47° 06.86'	65° 10.25'			X					
"	32 (E)	47° 06.86'	65° 10.25'		X						
"	32 (E)	47° 06.85'	65° 10.31'	X							
"	33 (E)	47° 06.85'	65° 10.27'				X				
"	33 (E)	47° 06.86'	65° 10.25'		X						
"	33 (E)	47° 06.86'	65° 10.25'	X							
"	34 (E)	47° 06.86'	65° 10.31'				X				
"	34 (E)	47° 06.86'	65° 10.31'	X							
"	34 (E)	47° 06.88'	65° 10.31'			X					
"	35 (C)	47° 07.92'	65° 09.49'					X			
"	36 (C)	47° 07.88'	65° 09.49'		X						
"	37 (C)	47° 07.89'	65° 09.52'			X					

during previous dredging and disposal activities. Table 2-2 summarizes the amounts of spoil materials deposited at the Experimental disposal site, together with the times of deposition. A total of 4181 cubic meters scow measure (CMSM) of spoils were deposited, all of which was dredged from Area 22-28 of Reach 22. Figure 2-1 illustrates the distribution of spoils deposited at the Experimental disposal site based on sounding survey carried out on 13 August 1993 by the Miramichi Surveyor.

Dredging was carried out by the Beaver Bell, a 36 m long by 12 m wide, 405 ton dredge fitted with three spuds and equipped with a Model 1266 Koehring backhoe with a three cubic yard capacity. Dredged material was transported to the disposal site by the Beaver 9 and Beaver 10, both 34 m long and 10 m wide scows with a capacity of 400 cubic yards. The scows were towed by the Beaver Gamma (11.3 m long, 16.7 tons) and the Beaver Delta II (10.9 m long, 11 tons).

The sampling procedure at each station consisted of obtaining Van Veen grab samples for organic content and grain size analyses, gravity core samples for analysis of sediment index properties, CTD profiles for salinity and temperature measurements, Excalibur deployments for pore pressure analysis and liquefaction estimates, and Sea Carousel deployments for determination of erosion thresholds, friction angles and sediment settling rates. The general approach was to sample the Channel and Experimental sites prior to dredging/disposal and to then resample the same locations after dredging/disposal. Prior to deploying Sea Carousel on recently deposited dredge spoils at the Experimental disposal site, Van Veen grab samples were collected and visually examined to ensure that the specific area selected for deployment contained recently deposited dredge spoils.

Long term deployments of SOBS (Submersible Observatory for Benthic Stability) were made at the Control site (10 days) and in an area east of the Experimental disposal site (5 days). Two long term (six days each) deployments of Lancelot were made, one along the Channel margin and one at the Control site. In addition, two current meters were deployed over the entire field study (15 days), one at the Control site and one east of the Experimental disposal site.

The effect of ship passage on sediment stability was monitored on two occasions. During the first ship passage (15-16 July, M/V Mariner, 4950 gross tons, 112 m) Lancelot was deployed on the slope of the Channel margin and SOBS was deployed at the Control site. During the second ship passage (25-26 July, M/V Hubert Tanthier, 7964 gross tons, 133 m) Lancelot was deployed at the Control site.

Table 2-2. Summary of spoils deposited at the Experimental disposal site.

Date	Time (AST)*	Location Lat	Location Long	Volume (CMSM)	Source
July 20	12:30	47° 06.79'	65° 10.16'	280	22-28
July 20	15:25	47° 06.76'	65° 10.14'	293	22-28
July 20	17:50	47° 06.77'	65° 10.15'	305	22-28
July 20	21:00	47° 06.77'	65° 10.15'	280	22-28
July 20	23:30	47° 06.81'	65° 10.15'	280	22-28
July 21	02:30	47° 06.75'	65° 10.10'	280	22-28
July 21	06:00	47° 06.81'	65° 10.10'	280	22-28
July 21	07:55	47° 06.74'	65° 10.14'	280	22-28
July 21	11:00	47° 06.77'	65° 10.15'	280	22-28
July 21	15:10	47° 06.74'	65° 10.14'	280	22-28
July 21	19:50	47° 06.81'	65° 10.14'	280	22-28
July 21	22:55	47° 06.74'	65° 10.15'	280	22-28
July 22	02:15	47° 06.80'	65° 10.14'	280	22-28
July 22	04:00	47° 06.77'	65° 10.17'	305	22-28
July 22	21:30	47° 06.77'	65° 10.17'	305	22-28
July 23	00:30	47° 06.77'	65° 10.16'	293	22-28

*Atlantic Standard Time

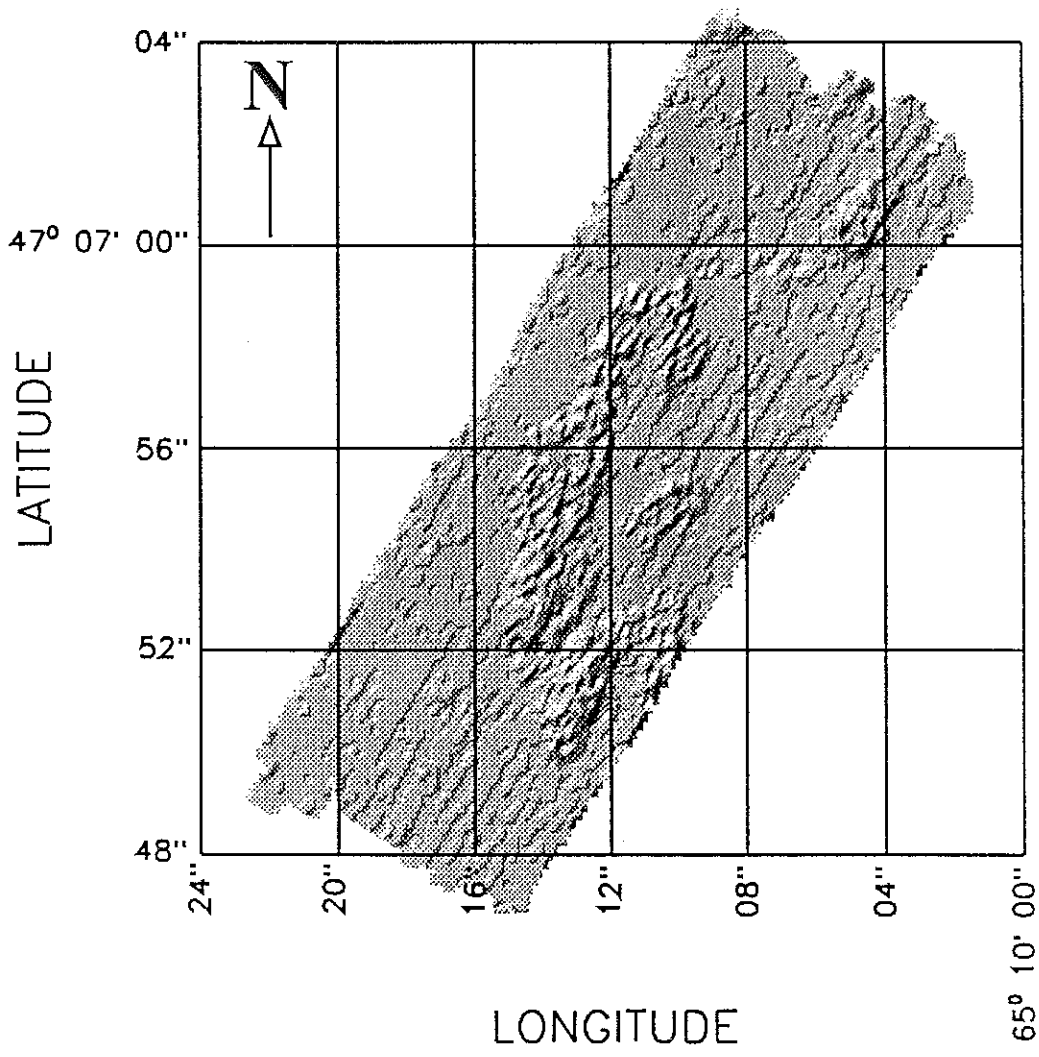

Figure 2-1. Distribution of spoils deposited on the Experimental disposal site.

3. METHODS

3.1 Seabed Sampling and Analyses

3.1.1 Sampling Procedure

Surficial (0-15 cm) sediment bulk samples were collected using a Van Veen grab sampler. Sediment core samples were collected using a 1 m long modified benthos gravity core sampler fitted with 45 kg of lead. Both samplers were deployed and recovered using a wheelhouse mounted line hauler. Twenty-two grab samples were collected. Immediately after collection, grab samples were placed in a tray for description and subsampled for organic content determination. Twenty-four core samples, ranging in length from 41 to 95 cm, were collected. Core samples were capped with plastic endcaps, wax sealed and stored upright in a refrigerated environment until laboratory analyses for water content, bulk density and grain size.

3.1.2 Multi-Sensor-Track Analysis

Multi-Sensor Track (MST) analysis was carried out on unsplit cores using the MST system housed at the Atlantic Geoscience Centre of the Bedford Institute of Oceanography, Dartmouth, Nova Scotia. This instrument logs sediment cores producing digital files of several geophysical and geotechnical parameters. The apparatus consists of a conveyor system on which the core is placed. The conveyor track is kevlar reinforced and forms a continuous loop that is coupled to a gearbox and a stepper motor, enabling both forward and reverse motion past the sensor head. The gearbox reduction ratio of 1:120 produces enough torque to carry the core at speeds of up to 2.5 m min^{-1}.

The measurement sensors on the system consist of a magnetic susceptibility sensor, a pair of compressional wave transducers, a gamma ray source (for measurement of bulk density), and a pair of displacement transducers. Magnetic susceptibility is useful in identifying gaps within the core as well as tracing sediment provenance. Core diameter is measured by a pair of displacement transducers that are mounted on the faces of the compressional wave transducers. The track and sensor array is coupled to a personal computer via an RS232 interface.

Magnetic susceptibility is sensed through the whole core using a Bartington loop. The fixed loop diameter favors large diameter cores, so the small diameter of the Miramichi Bay cores made it necessary to run the instrument at longer time intervals to gain the required magnetic detail.

3.1.3 Core Splitting and Analyses of Physical Properties

Core samples were split longitudinally, photographed and described. Subsamples were then taken for determination of water content, bulk density, organic content, undrained shear

strength and grain size analyses. The presence of disposed material was noted on the description log along with colour, lithology and sedimentary structures.

Water content was determined according to the following formula:

$$W_n = M_w / (M_d - (M_t - r)) \ 100\% ,$$

where M_w is wet mass minus dry mass, M_d is dry mass, M_t is wet mass and r is salinity. Dry weight was determined from samples that had been oven dried at 110 °C for 24 hrs. Salinity was measured using an optical refractometer.

A constant volume sampler (9.723 cm^3) was used to obtain samples of known volume for determination of bulk density which was determined according to the following equation:

$$\rho_S = M_t / V_t ,$$

where V_t is wet volume.

Undrained shear strength S_u (peak strength) was recorded using a miniature shear vane interfaced to a personal computer. Grain size samples were taken and analyzed for the full grain size distribution. After subsampling, the working half of each core was wrapped with cellophane, placed in a plastic storage case, along with the archived section, and returned to cold storage.

3.1.4 Grain Size Analyses

Grain size analyses were performed on 21 Van Veen subsamples and 22 core subsamples, taken at different depth increments within three specific cores. Detailed analyses of grain size, organic content and bulk density variation with depth were carried out on three core samples, chosen on the basis of location and because they were the longest cores recovered at each particular site. These included cores taken at Station 13 (Channel; 7 subsamples), Station 25 (Control; 8 subsamples) and Station 28 (Post-disposal Experimental site; 7 subsamples).

Complete grain size analyses involved a number of laboratory pre-treatment procedures for sieve, settling tube and sedigraph analyses. Samples rich in organics were pre-treated to remove the organic matter in order to allow the trapped fine sediment to be processed. Raw samples of *circa* 100 g wet weight were pre-weighed and oven dried at 50-60 °C for approximately six hrs and then reweighed for determination of dry weight. Samples were then placed in 1 liter glass beakers to which 2-3 drops of 25 percent hydrogen peroxide were added. Heat and fumes were controlled, when excessive, with spray bottles containing distilled water. Gradually, additional hydrogen peroxide was added while the sample was stirred. Once the reaction began to subside, greater quantities of the peroxide (up to 500 ml for a 100 g sample) were added to ensure that organic removal was complete. The samples were placed in a warm water bath for 3-4 hrs to complete the reaction. Finally, the water bath was set to boil for a further 3-4 hrs. The samples were then placed in an ultrasonic bath for

approximately 5 min and stirred to assist in desegregating the mud from the coarser fraction. The samples were then poured through a 0.053 mm wet sieve and separated into mud and coarser fractions. Excess water in the basin was decanted and the mud residue added to the initial separated mud fractions. The coarse fractions contained in the sieve were transferred to pre-weighed filters and washed to remove any hydrogen-peroxide residue. The filters were then placed on pre-weighed dishes, oven dried at 50-60 °C for approximately 48 hrs, reweighed, separated from the filter and further split into sand and gravel fractions using a 1.00 mm dry sieve. The gravel portion was weighed and any subsamples exceeding 8 percent of total sample weight were subjected to further sieving. The sand fractions were microsplit into 1 g subsamples to give representative samples for the settling tube.

The mud fractions from the wash were transferred to 750 ml centrifuge bottles and spun at 3000 rpm for 90 min. The bottles were then decanted and the remaining mud transferred to 250 ml centrifuge bottles which were spun at 3000 rpm for an additional 60 min. The consecutive centrifuge runs helped to clean the mud of hydrogen peroxide residue. These bottles were also decanted and the mud transferred to pre-weighed beakers and dried at 50-60 °C for 3-5 days. The dry mud samples were then re-weighed, placed in distilled water and riffle-split to between 3.5 g and 5.5 g. The final mud splits were spun at 3000 rpm for 60 min, decanted to remove the distilled water which was then replaced with an electrolyte solution. The mud splits were then placed on a mechanical shaker for 2-3 hrs prior to the sedigraph analyses.

A Micromeritics Instrument Corporation Model 5000D sedigraph was used for grain size analysis of the mud fraction. This instrument uses an x-ray measurement technique. The mud sample is pumped through a sample cell and the transmitted radiation is detected by a scintillation counter, amplified, passed through a noise discriminator and clipped to a constant voltage. A dedicated computer logs the signal from the instrument.

The settling column analysis, used for grain size analysis of the coarser particle fraction, is based on the principle that a sample's grain size distribution can be obtained from measurement of the mass-velocity distribution of sand grains, settling through an otherwise turbid free liquid. It is assumed that the grains settle out individually and are not hindered by other settling particles, involved in convective plumes of high concentration, or retarded by upward flow of displaced fluid. The settling column is comprised of a pyrex pipe approximately 2 m high and 15 cm in diameter. A balance (interfaced with a computer) at the top of the column is connected through a thin cable to a collecting plate at the bottom of the pipe. An introduction system below the balance is connected to a computer via a microswitch. Once the sample is spread over the introduction system and released, the sediment particles begin to fall through the water column, eventually arriving at the collection pan below. The accumulating weight of the particles on the pan is registered by the balance and recorded by the computer.

Merging software accumulated the data from the settling tube computer and sedigraph computer to produce the proper convergence of grain size from the mud to sand spectrum.

Grain size percentages for total sample weight had previously been computed through the various fraction weights added throughout the lab procedures.

3.2 Sea Carousel

Sea Carousel, named after the carousels of Postma (1967) and Hydraulic Research Limited (Burt 1984), is a benthic annular flume designed for field use in intertidal and subtidal settings. The carousel is 1.0 m in radius with an annulus 0.15 m wide and 0.30 m high (Fig. 3.2-1). It weighs approximately 150 kg in air and 40 kg in water and is made entirely of aluminum. Flow in the annulus is induced by rotating a movable lid that is driven by a 0.35 hp DC motor powered from the surface. Eight small paddles, spaced equidistantly beneath the lid, induce a flow of water in the annulus. The width of the annulus (D) was made 0.15 m to give a relative roughness (e/D) $\pm$ 0.004 (where the wall roughness, e = $\pm$ 0.0006 m; after Shames (1962)). The water depth in the annulus was minimized to 0.25 m to ensure conditions for Nikuradse's "rough-pipe zone of flow" wherein changes in wall friction factor with changes in Reynolds number are at a minimum (Shames 1962).

A schematic diagram of the Sea Carousel configuration is shown in Figure 3.2-2. It is equipped with three optical backscatter sensors (OBS's; Downing 1983). Two of these are located non-intrusively on the inner wall of the annulus at heights of 0.03 and 0.18 m above the skirt (the skirt is a horizontal flange situated around the outer wall of the annulus 0.04 m above the base; it was designed to standardize penetration of the flume into the seabed; see Figure 3.2-2). The third OBS detects ambient particle concentration outside the annulus, or it may be used to detect internal sediment concentration at a height between the other two. The OBS sensors give linear responses to particle concentration (of a constant size) for both mud and sand over a concentration range of 0.1 to 50 g l^{-1} (Downing and Beach 1989). They are unaffected by flows below 1.5 m sec^{-1} and are stable through time. A sampling port is situated in the outer wall of the annulus at a height of 0.2 m above the skirt through which water samples can be drawn to calibrate the three sensors under well mixed conditions.

Flow within the carousel was determined from a relationship between azimuthal speed and lid rotation presented in Amos et al. (1992). Mean tangential lid rotational speed (U_r) is detected through a shaft end-coder resting on the lid. Controller boards for each sensor and the necessary power (12 VDC) are derived from an underwater pod located above the annulus. Output voltages from all sensors are digitized and transformed to scientific units on a Campbell Scientific CR10 data logger and stored on a Campbell Scientific SM192 storage module (storage capacity of 96,000 data values), also located in the underwater pod. The data logger is interrogated and programmed from the surface using a microcomputer linked to the data logger through an RS232 interface. Maximum sampling rate of all channels is approximately 2 Hz, whereas U_y and U_w may be logged at rates up to 10.66 Hz. All channels may be monitored and displayed on the surface computer allowing the operator to control the experiment interactively. Bed shear stress is varied in time by varying the power supplied to the underwater motor up to 350 watts via a surface power supply. The data stored from each deployment may be downloaded remotely through the RS232 cable at the end of each experiment and the storage module reinitialized.

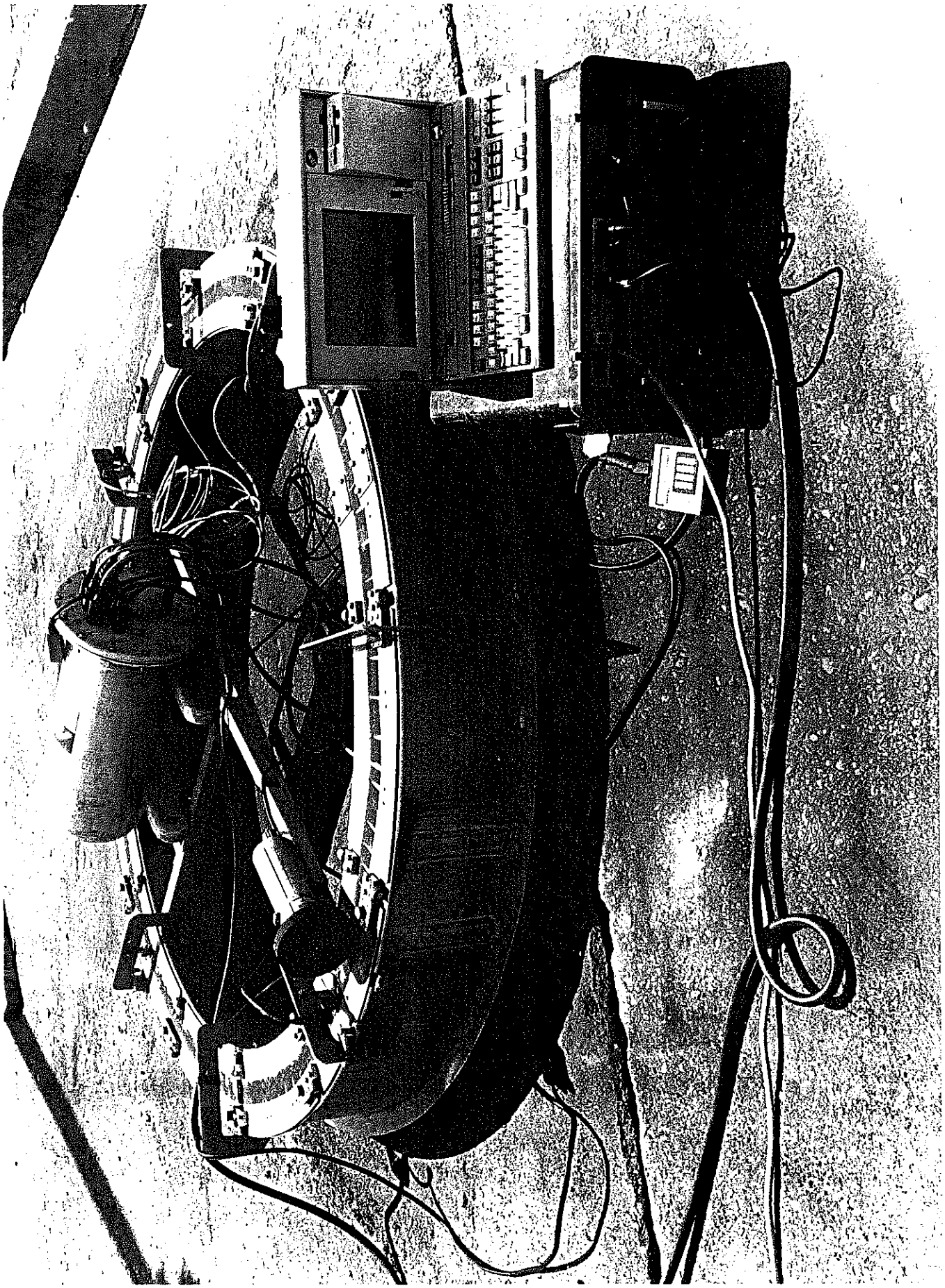

Figure 3.2-1. The Sea Carousel system.

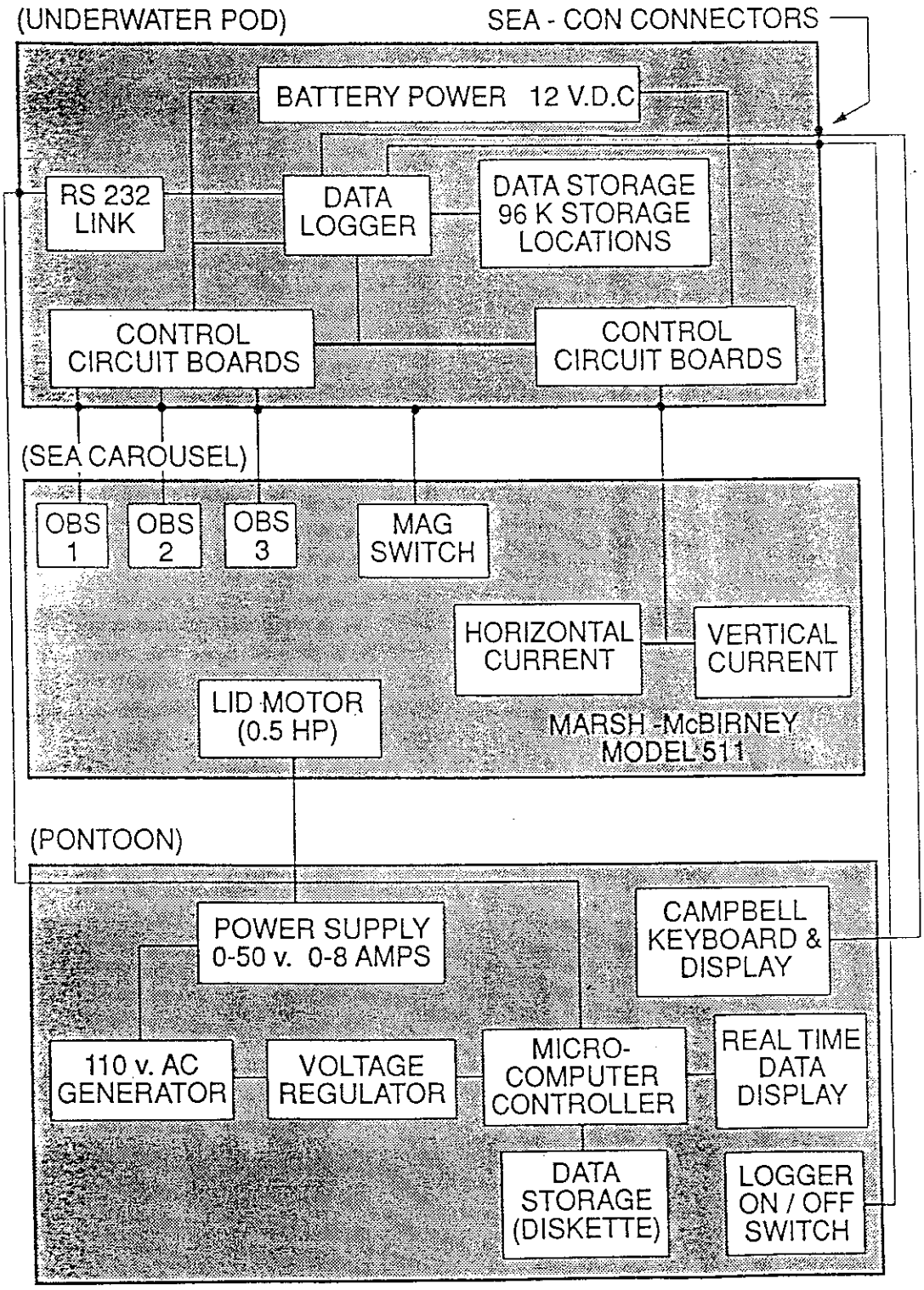

Figure 3.2-2. Schematic diagram of the configuration of the Sea Carousel.

A window is located in the inner flume wall for purposes of observing and recording the mechanics of bed failure. A perspex wedge at the base of the window sections the sediment upon deployment. Thus the upper 20 mm of sediment and the lower 10 cm of the water column can be viewed in section. Visual observations are made using a Sony Handycam 8 mm video recorder model CCD-V11 held in an Amphibico Amphibian V11 underwater housing. Light is provided by two 100 watt underwater lights powered from the surface. The housing has a lens that corrects for underwater geometric distortions and so is suitable for accurate image scaling. The camera lens is located approximately 0.2 m from the window. Horizontal and vertical scale lines are present on the window and situated within the field of view. The camera images 100 frames sec^{-1}. A co-axial cable connects the camera to a surface monitor for real-time detection. Video records are stored on a standard VHS video cassette recorder, also at the surface. Sequential video images are digitized for particle trajectories at varying heights above the bed. From these, velocity profiles are constructed. From such profiles, thicknesses of the logarithmic part of the benthic boundary layer are determined and friction velocities computed. These latter values were then compared with laboratory measures.

Dispersion of suspended sediment out of the rotating annulus was observed on the video to take place during submerged deployments of Sea Carousel. Dispersion results from exchanges of water mass between the annulus (at concentration S_1) and the open marine environment (at concentration S_o) where $S_1 = S_o$. The rate of diffusion of mass (M) may be defined per unit cross-section area as:

$$\partial M/\partial t = - \delta \, \partial S/\partial x \qquad (1)$$

where δ is the coefficient of diffusivity (L^2T^{-1}) and x is a typical horizontal length scale, which in our case is unknown. Similarly, the change in mass in Sea Carousel may be defined as:

$$\partial M/\partial t = - \delta \, \partial S/\partial x \, A\in/V \qquad (2)$$

where A is the area over which diffusion takes place (0.012 m^2), V is the volume of Sea Carousel (0.218 m^3), and $\in$ is an efficiency term dependent on the azimuthal velocity ($\in \propto U_y$). Measurements of $\partial M/\partial t$ at different constant azimuthal velocities yield a concentration half-life ($S_{1/2}$) of 2400 sec, setting $\in = U_y$ and $\partial S/\partial x$ to ($S_1 - S_o$), the quotient ($- \delta A/\partial x$) is derived:

$$\partial M = - 3.3 \times 10^{-3}(S_1 - S_o)U_y \, \partial t \qquad (3)$$

The loss of mass through dispersion, calculated using equation 3, is added to measured annulus mass (SV) to derive a measure of the total mass, where V is the annulus volume (0.218 m^3).

3.3 Submersible Observatory of Benthic Stability (SOBS)

The Submersible Observatory of Benthic Stability (SOBS) is a benthic tripod that is equipped with six Optical Backscatter Sensors (OBS); Downing and Beach (1989), a pressure transducer and a down-looking Hi8 SONY video camera (Fig. 3.3-1). The lower OBS sensor is oriented in a down-looking mode at a height of 0.13 m above the base. The remaining five sensors are located from 0.16 to 1.80 m above the base in a logarithmic progression.

The SONY Hi8 video camera was housed in an Amphibico underwater housing. It was installed 0.43 m above the tripod base and was oriented approximately 45^{o} from the horizontal to give a field of view of *circa* 1 m^{2}. The seabed was illuminated by two Amphibico 75 watt lights mounted normal to the field of view of the camera.

Two AccuStar clinometers, installed in the pressure case, give information on the attitude of the tripod from horizontal along two orthogonal axes. These sensors are sensitive to changes of 0.001^{o}. A Data Instruments pressure sensor records hydrostatic pressure to 200 psi (132 m). It is sensitive to 1 psi (0.7 m) changes.

The system is powered by two 12-volt Sonnichsen batteries capable of delivering 126 amp-hours of power. System control and data logging are controlled by a TattleTale 6 (Onset Data Corporation) data logger attached to a 20 Mbyte hard-drive. Data from each of the OBS sensors and the pressure sensor are logged at a rate of 1 Hz and stored on the hard-drive. The video camera was operated to record for 5 sec every 2 min.

The following information is logged on the header of the data file: start time, end time, disposal time, version, scans per min, battery voltage, burst rate, burst length, camera interval, camera duration, X inclinometer, and Y inclinometer.

The calibration of the OBS sensors was undertaken using reduced, blackened sediments collected in the navigation channel. This was done as we were largely concerned with this material in a dredged and disposed form. The calibration curve for each sensor is shown in Figure 3.3-2. At low suspended sediment concentrations (< 1000 mg^{-1}) the sensors showed a linear response. The equations defining these linear responses are given in Table 3.3-1. Above 1000 mg^{-1}, the sensors showed virtually no response to changing concentrations suggesting that the sensors were saturated. This response is presumed to be due to the colour of the bottom sediment which is black due to the highly-reduced, organic-rich nature of the material. As the sensors rely on the reflection of deep-red light (660 nannometres wavelength) to detect material is suspension, we presume that the light is fully absorbed by the sediment rather than reflected.

3.4 Shear Strength Analysis

Seabed instability is governed by soil mechanics principles. The stability of a sediment mass can best be described in engineering terms by means of the concept of "effective stress", whereby shear strength is decomposed into two independent components, the effective stress

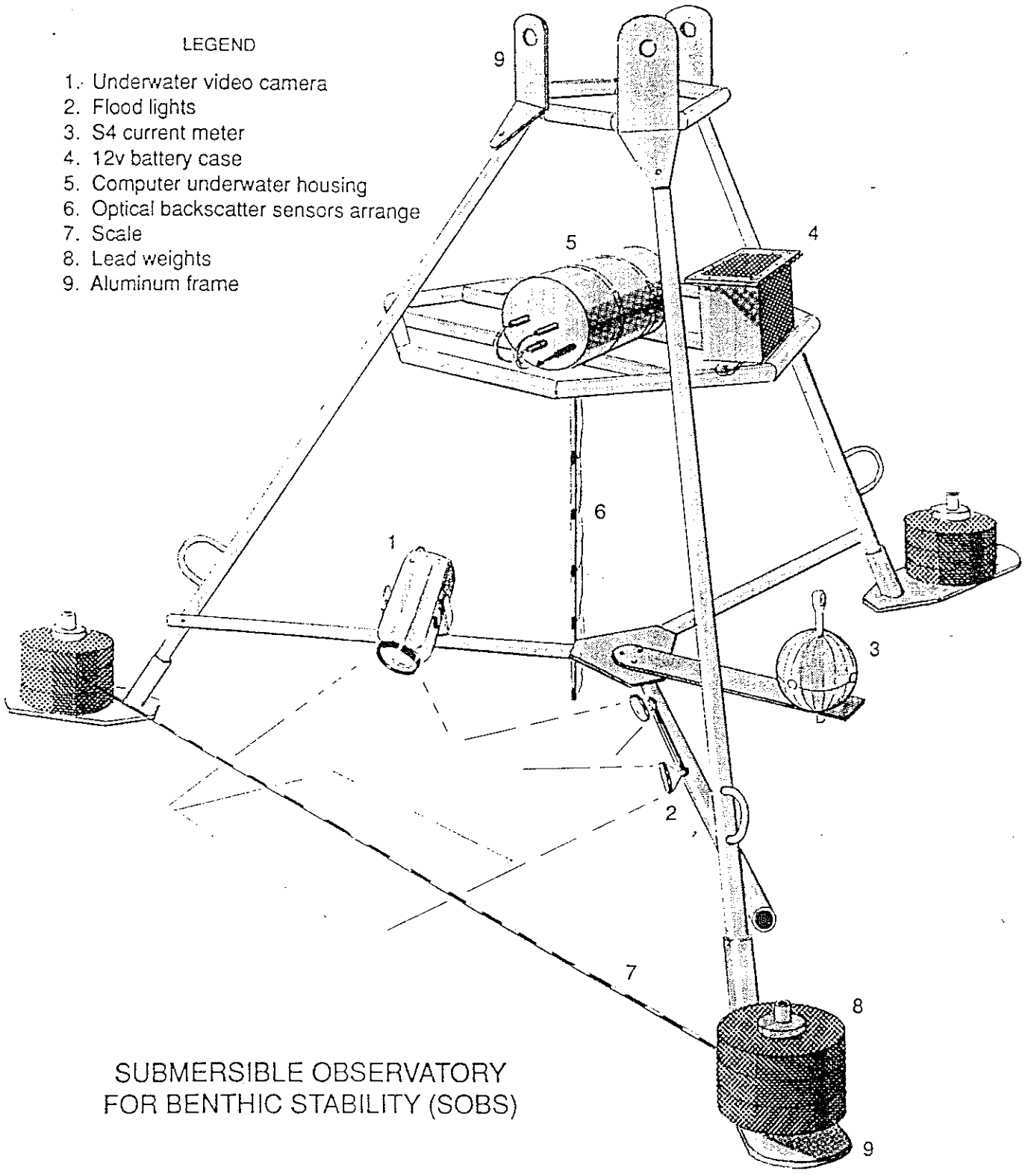

Figure 3.3-1. The SOBS system (note that the current meter was not installed during this study).

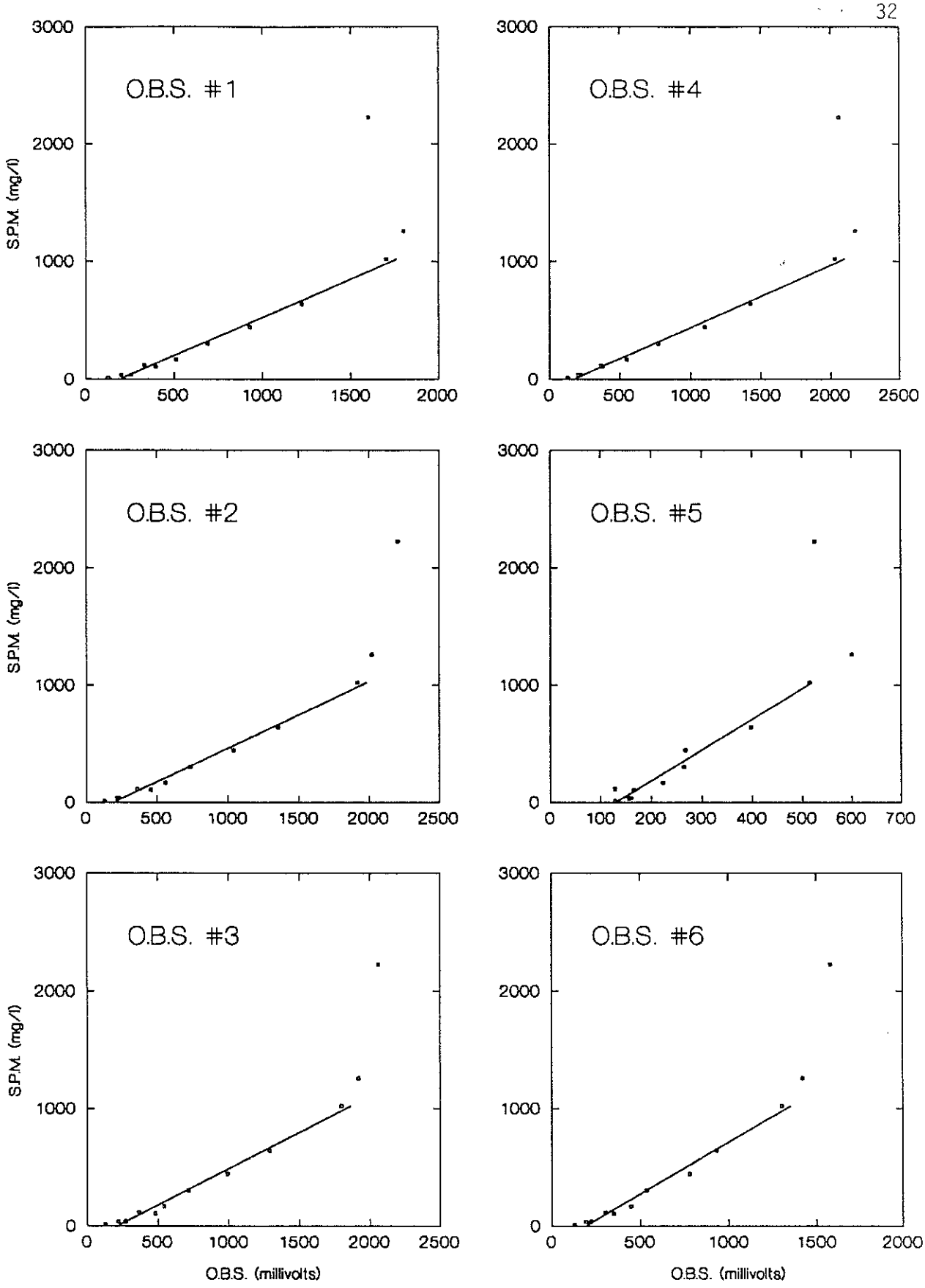

Figure 3.3-2. Calibration curves for SOBS Optical Backscatter Sensors.

Table 3.3-1. Calibration equations for Optical Backscatter Sensors on SOBS.

OBS SENSOR	HEIGHT (m)	CALIBRATION
1	0.13	-119 + 0.642 (OBS1)
2	0.16	-105 + 0.564 (OBS2)
3	0.27	-125 + 0.609 (OBS3)
4	0.41	-85 + 0.523 (OBS4)
5	0.95	-325 + 0.250 (OBS5)
6	1.80	-158 + 0.863 (OBS6)

shear strength parameters. The shear strength and consolidation of marine sediments responds to changes in effective stress, while the movement of porewater is controlled by hydraulic gradients within the bed, as well as sediment permeability.

Before one can develop an understanding of the triggering mechanisms involved in liquefaction failure of the seabed, it is necessary to determine the manner in which shear strength is mobilized within the bed, the nature of resulting deformations and the role of excess porewater pressure. To provide a basis for developing an understanding of the reasons why a loose sediment deposit can lose strength during shear, compared to a dense deposit which stiffens and sustains additional load without appreciable deformations, some basic soil mechanics theory is given below.

The strength of a sediment mass τ is expressed in terms of effective stress σ_{vo}', which is given simply as the sum of gravitational forces minus buoyant forces according to the Mohr-Coulomb failure criterion (Terzaghi and Peck 1967) wherein,

$$\tau = c' + \sigma_{vo}' \tan \phi' \ ,$$

where $\tan \phi'$ is the slope of the failure envelope (Fig. 3.4-1).

The failure envelope represents a bounding condition within which all effective stress states must exist. Any stress state approaching the failure envelope is indicative of internal shearing of the sediment, which occurs associated with changes in excess pore water pressure (positive during contraction and negative during dilation). The shear strength at zero effective stress is referred to as the effective cohesion intercept c', which is roughly equivalent to the critical shear stress for erosion. Cohesion can only exist in fine-grained sediments (arising through attractive forces between clay particles), or in organically-bonded sediments and is non-existent in clean sands. Referring to Figure 3.4-1, point *a* represents the *in situ* stress state of an element at a distance z below the seabed. Effective vertical stress is governed by the thickness of overlying sediment, as well as the bulk density ρ_S of the sediment. However, by the principle of effective stress, any excess porewater pressure dU reduces the effective vertical stress according to,

$$\sigma_{vo}' = (\rho_S - \rho_{SW})\, g\, z - dU$$

where ρ_{SW} is the density of seawater and g is the constant of gravitational acceleration.

The difficulty of measuring excess pore pressures has led in many instances to a general assumption of fully drained, hydrostatic conditions. Subsequent analysis of the state of consolidation has suggested that excess pore pressures have been overlooked (Silva and Jordan 1984; Richards 1984). This problem was overcome with the development of new techniques for *in situ* hydrogeologic measurement (Christian et al. 1993) and is especially important in any study that seeks to identify the causal trigger for liquefaction events.

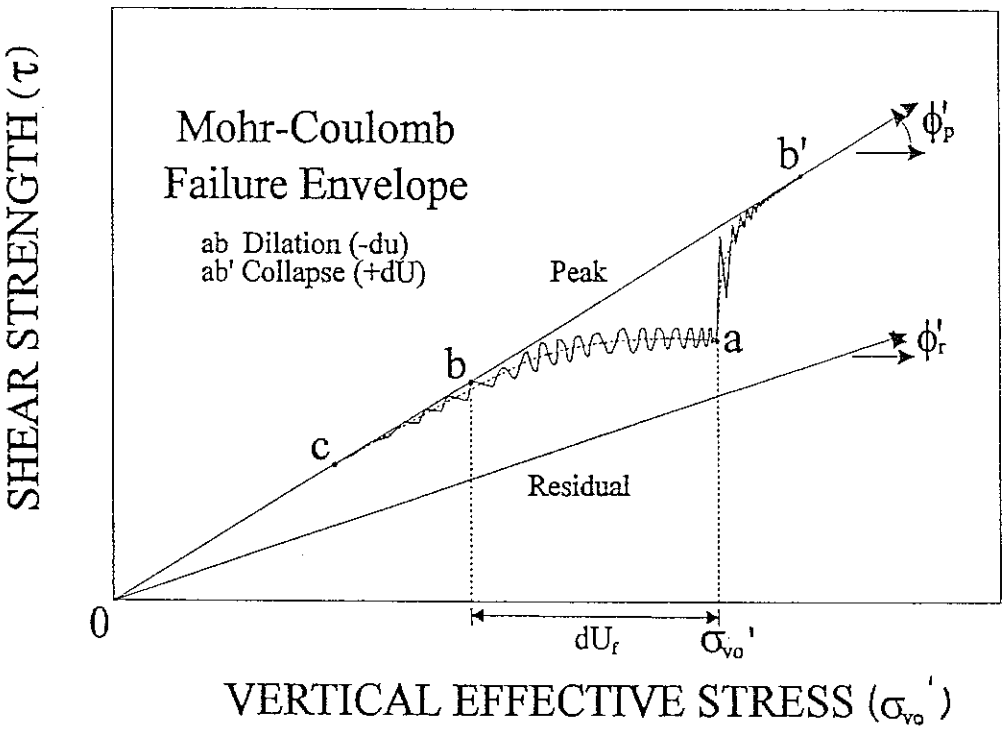

Figure 3.4-1. Relationship between shear strength and vertical effective stress.

The effective stress at any depth can be estimated only by measuring the sediment bulk density from high-quality core samples. The effect of residual hydraulic gradients can be included in the calculation of effective stress by measuring the porewater pressure *in situ*.

As the sediment experiences shear, it begins to deform, and its stiffness changes. If the initial state was loose, then shearing with no drainage leads to structural collapse, resulting in the development of excess pore pressure. Progressive failure is rapid and a point on the failure envelope is reached (point ***b***), after which unlimited deformations can occur under sustained shear stress. If the initial state of the sediment is dense, then the sediment structure attempts to expand (dilation). Again, if drainage is prevented, then no volume change occurs and the pore pressure becomes negative, increasing the effective stress. The sediment becomes stronger, as indicated by the stress path that rises up the failure envelope, ending at point ***b'***. After large deformations, both stress paths end up at point ***c*** on the failure envelope. If the shear strength at ***c*** is less than it was initially at ***a***, then the failed mass will continue to move in response to the driving stress, until it diminishes to the same level. Shown along with the dashed idealized stress paths ***ab*** and ***ab'*** are idealized stress paths followed during cyclic shear loading, such as might occur during storm events.

Referring again to the Mohr-Coulomb failure criterion, the peak shear strength is maximized in dense angular cohesionless materials, but is substantially less following collapse if conditions are loose before shear. Due to the high pore pressures generated during shear-induced collapse, sediments existing on a slope may subsequently undergo catastrophic flow-type downslope movements. Such mobile sediments may exist as a viscous fluid following failure and continue to deform under external forces.

Excess porewater pressure causes the effective stress state within the seabed to shift to the left toward the failure envelope. Any process which initiates and sustains excess porewater pressure can lead to failure. As sediment is sheared in this manner, it begins to yield, is progressively weakened by the rupture of interparticle bonds and begins to deform. If the sediment is initially loose, then a collapse of the structural arrangement of particles occurs, giving rise to further increase in pore pressure. At the point of failure, the effective stress is essentially zero, and the sediment suffers a complete loss of shearing resistance (Clukey et al. 1985). The subsequent type of deformation ranges from rapid flowslide (for very loose cohesionless materials), to limited spreading-type movements (in marginally collapsible sediments), to no significant movement (in dense or dilatant sediments). For a period of time after initial failure, the weakened sediment mass is more susceptible to erosion by currents and waves.

This is illustrated in schematic form in Figure 3.4-2, showing how waves can lead to internal shearing, which destabilizes the sediment structure, resulting in a large buildup in excess pore pressure. Once the effective stress state reaches zero, liquefaction is said to have occurred. Wave energy attenuates exponentially with water depth and the stability of a sediment deposit is governed by the amount of energy imparted by the wave, the looseness and potential for collapse of the seabed, as well as its permeability, or ability to allow the movement of porewater. Thus, the wave period becomes important, as silty sediments are able to dissipate

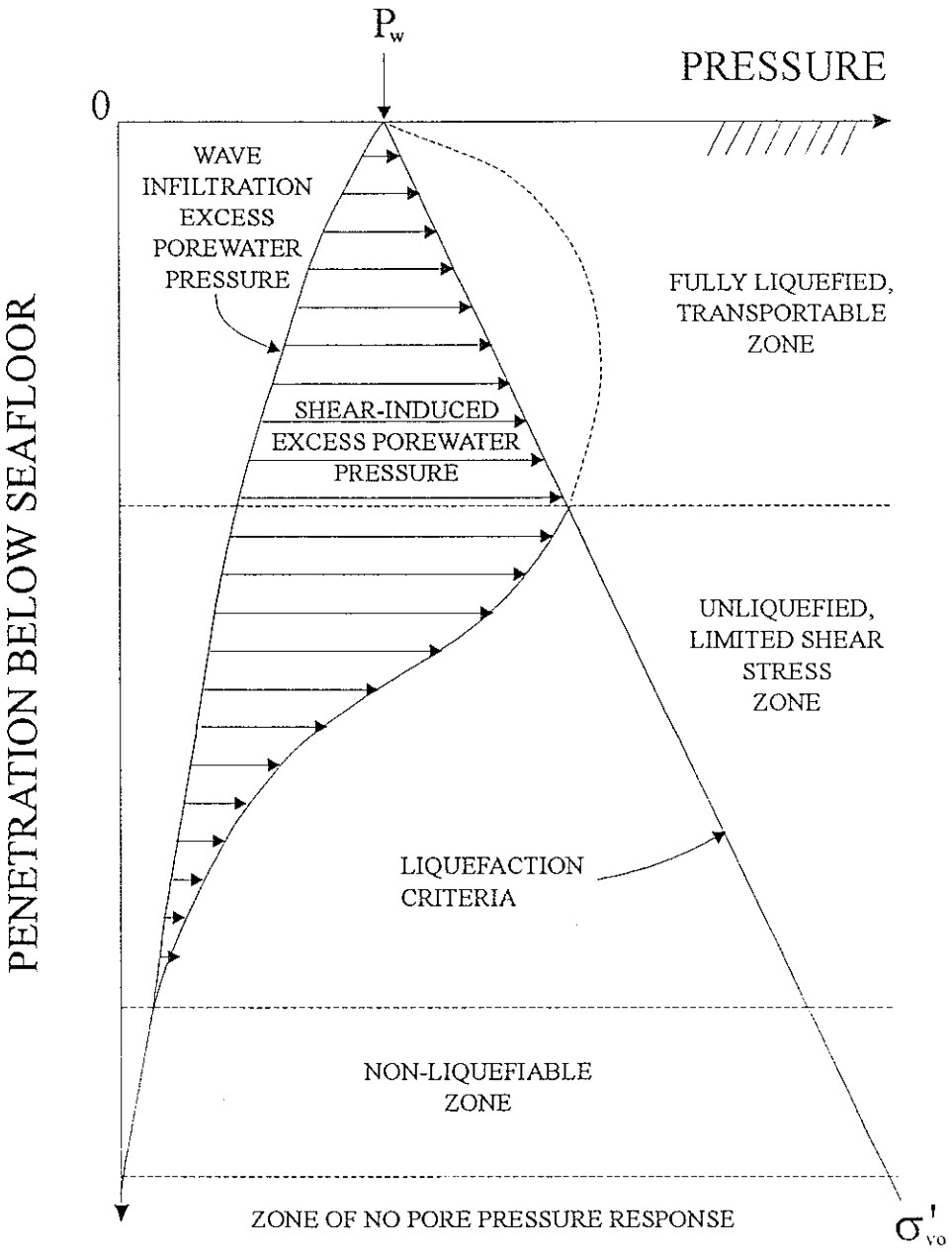

Figure 3.4-2. Diagram illustrating how waves can cause internal shearing and lead to the destabilization of sediment structure.

large amplitude standing waves (i.e., tides), given sufficient time, without a reduction in stability. Small-amplitude, high frequency waves, however, can lead to excess pore pressure buildup and, ultimately, liquefaction failure.

Pore pressure measurements were carried using Lancelot (long term) and Excalibur (short term). Appendix F contains the operation log for both instruments.

3.4.1 Lancelot

Lancelot is an instrument used to measure the *in situ* porewater pressure regime beneath the seabed, providing data required in engineering stability calculations. Excess porewater pressures may develop in certain loading situations and are of concern, as they directly reduce sediment shear strength (Christian et al. 1993). Previous investigations in Miramichi Inner Bay detailing use of the Lancelot system are reported in Brylinsky et al. (1992) and Christian and Heffler (1993).

Lancelot is configured to push a slender probe with a pressure port to a predetermined distance beneath the seabed, and to make measurements over an extended time frame, at various data sampling rates. The instrument (Fig. 3.4.1-1) consists of a wide baseplate, a rigidly-mounted pressure case and a slender probe (outside dia of 1.6 cm). The probe contains an oil-filled tube that connects a porous filter stone mounted behind the tip to a differential pressure transducer (Validyne Model DP9) inside the electronics housing. This transducer records pore differential fluid pressure changes within the seabed to an accuracy of ± 1.4 mm of head. The back side of the transducer is ported to the water column, giving a continuous pressure reference. There is also an absolute pressure transducer (Data Instruments Model AB), located at the top of the instrument pressure case, which gives a continuous record of water depth to an accuracy of ± 100 mm. Sensors for recording pitch and roll (vertical tilts) are located inside the pressure case, along with a vertical accelerometer, which records orientation and dynamic motion of the instrument during the deployment period. Data are stored within a TattleTale 6 (Onset Corporation) datalogger, which was programmed to sample all sensors at rates ranging from 55 to 100 scans per min. The instrument is capable of autonomous operation for periods lasting up to 20 days at a rate of 55 scans per min. All data are written to an internal 20 Mbyte hard drive, and is downloaded after recovery for playback and analysis. The data are stored in sequential files that are time-referenced to an onboard clock. A lithium battery prevents data loss in the event of a power failure.

A diagram of Lancelot in the deployed configuration is given in Figure 3.4.1-2, wherein the probe tip has been driven into the seabed by the weight of the instrument, and is in the process of collecting data. An idealized penetration record is shown in Figure 3.4.1-3, illustrating the dilatant and contractant pore pressure response that might be encountered. There are five pieces of information that can be obtained from the data record. The initial response in the water column is shown at **1**, where wire motion and ship heave result in a coupled sensor response. During each deployment and recovery, 5 to 10 min are allowed for this stage, providing a temperature-corrected baseline calibration for the differential pressure transducer.

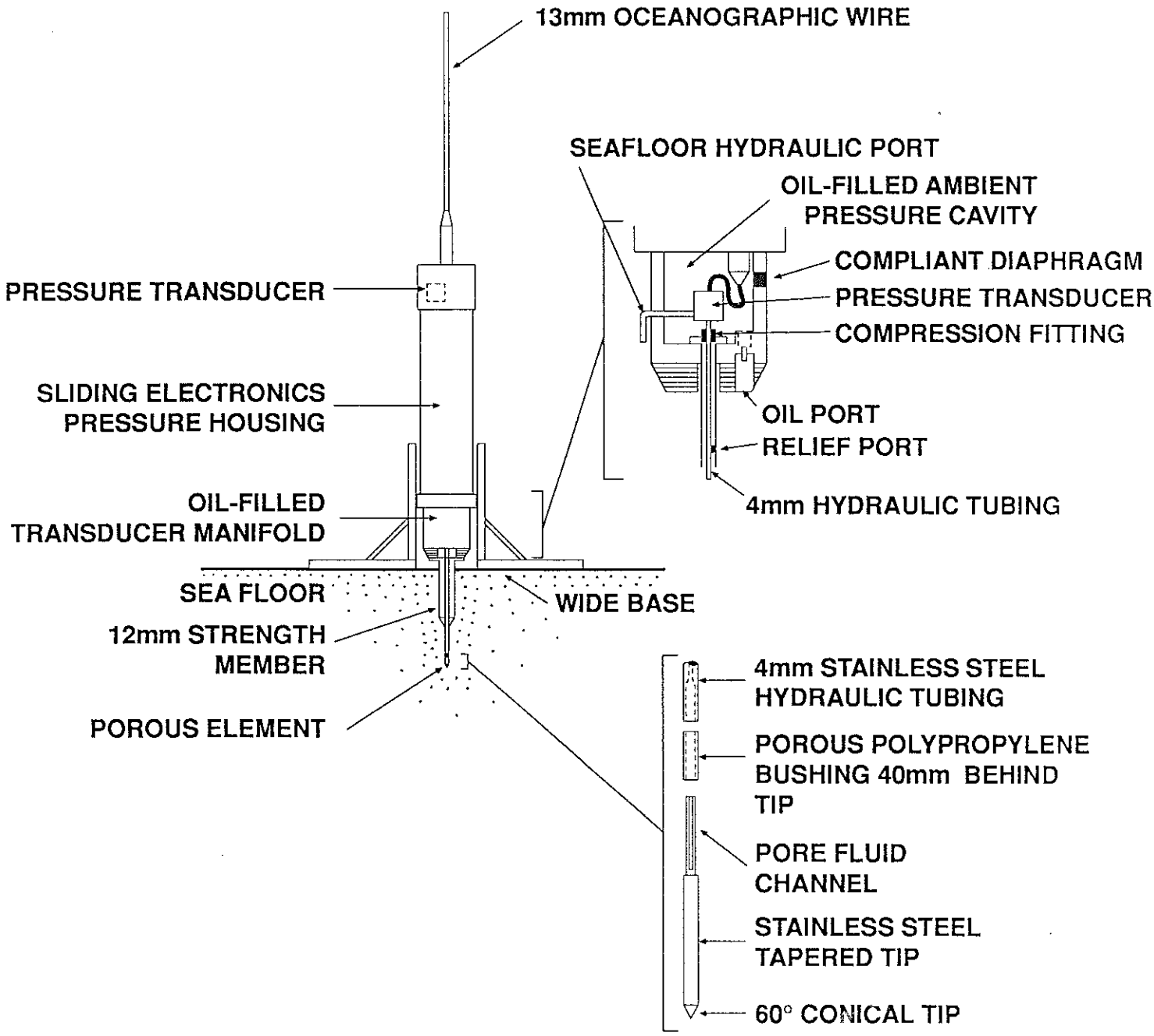

Figure 3.4.1-1. Schematic diagram of Lancelot.

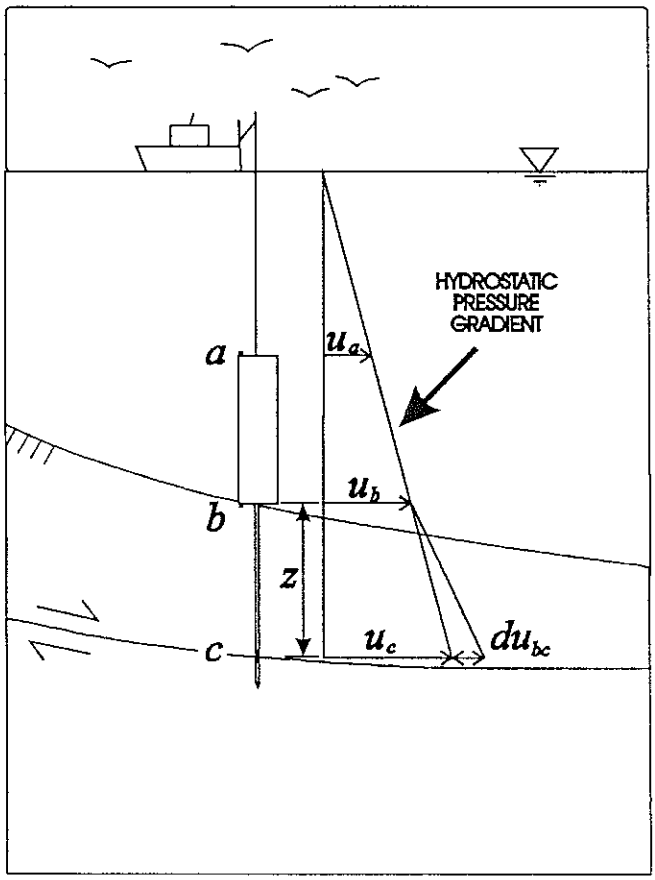

Figure 3.4.1-2. Diagram of Lancelot in the deployed configuration.

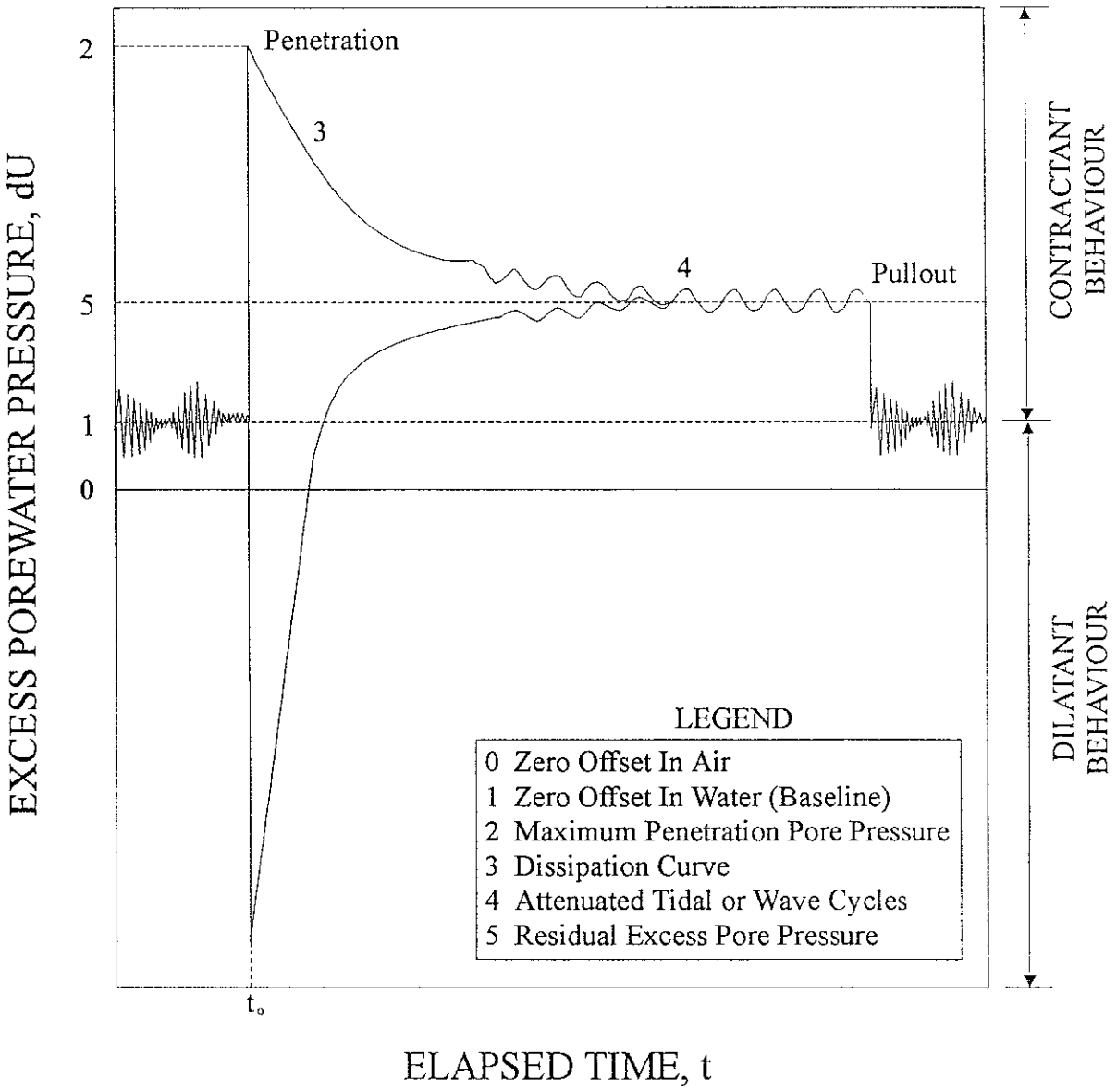

Figure 3.4.1-3. An idealized penetration record produced by Lancelot.

The maximum penetration pore pressure denoted by **2** can provide an accurate estimate of undrained shear strength in clayey sediments. The consolidation or dissipation response is shown at **3**, again for the case of soft fine-grained sediment. Wave or tidal cycling can induce a cyclic excess porewater pressure response, as indicated at **4**, which, if large, can lead to liquefaction failure. The equilibrium or residual excess porewater pressure, given by **5** provides data for an evaluation of effective stress, when combined with a high-quality bulk density sample from the test site, which is used in an evaluation of liquefaction. Only stages **1**, **4** and **5** can be obtained in Miramichi sediments, due to their high silt content, which can lead to partially drained conditions around the probe during penetration.

3.4.2 Excalibur

Excalibur is a newer version of the Lancelot system developed to have the additional capability of obtaining pressurized porewater/gas samples after completion of the pore pressure measurement test stage (Christian 1993). The salinity of the porewater sample is measured using a handheld refractometer. The volume of free gas existing within the sample is computed by subtracting the volume of porewater recovered from the total volume of the sample cylinder.

The physical configuration of Excalibur is very similar to that of Lancelot. The length of the probe is 55 cm. The tube inside the probe is filled with distilled water before each deployment, in a similar manner as with Lancelot. The volume of water initially within the hydraulic circuit is about 0.5 cc, which represents a 1.1 percent dilution of the porewater sample. The quantity of *in situ* porefluid recovered is obtained by measuring the salinity of the recovered sample and that of the water column.

The differential transducer is a Validyne Model DP300, and has a similar accuracy to that in Lancelot. Identical transducers as in Lancelot are used to record pressures and instrument orientation. No accelerometer exists in Excalibur, however. The absolute gauge was located inline with the control valve and the porous filter stone on the tip instead of on the top of the pressure case, in order to record pressure changes within the 40 cc sample cylinder. The valve position is controlled through pre-programming by computer to open and close the line to the sample cylinder at preset times. For deployments where the instrument was left on site longer than the available memory would allow, a facility for storing the most recent data was enabled.

3.5 Current Meters

Aanderaa RCM-7 current meters were deployed continuously at two locations (Stations 2 and 5) at a depth of *circa* 1 m above the seabed. Station 2 was located in the control area and Station 5 was located *circa* 500 m east of the Experimental disposal site. Current velocity (m sec^{-1}), current direction (degrees true), pressure (dbars), temperature (°C), conductivity (μ mhos cm^{-1})and salinity (ppt) were recorded at 15 min intervals.

3.6 CTD

CTD deployments were carried out using an Applied Microsystems EMP-2000 CTD fitted with salinity, temperature and OBS turbidity sensors.

3.8 Positioning

Geographic positioning was carried out using a ship mounted Koden Model KGP-97 GPS navigator. All station locations were recorded in latitude and longitude. The corresponding UTM coordinates (converted by Public Works and Government Services Canada personnel using GSRUG developed by Energy, Mines and Resources) are presented in Appendix B.

4. RESULTS

4.1 Sediment Properties

The results of analyses for sediment properties of Van Veen grab and gravity core samples are presented in Appendix C. Colour photographs of gravity core samples are contained in Appendix D.

Sediments from all sites were similar and were characterized by high organic content (8-20 percent), high water content (generally >100 percent) and low bulk densities. Detailed analysis of representative cores from each study site revealed a decrease in organic content with depth (Fig. 4.1-1) and a strong correlation between organic content and water content (Fig. 4.1-2). Grain size analyses on these same cores indicated clay, silt and sand contents of *circa* 50, 40 and 10 percent, respectively, with little variation with depth (Fig. 4.1-3).

4.2 Sea Carousel Results

4.2.1 Summary

Good results were obtained from all 20 stations undertaken in this survey. A list of these stations is shown in Table 4.2.1-1 and results are summarized in Table 4.2.1-2. Results were obtained from water depths of 4.9 m to 8.5 m. Video results (VHS) were obtained at 17 stations, while high resolution Sony Hi8 records were obtained from 19 stations. Four stations were occupied within the Experimental disposal site prior to disposal (MIR1, MIR2, MIR3, and MIR4); two stations were taken in the Channel within Reach 22 (MIR4 and MIR5); three stations were occupied north of the Channel at a natural Control site (MIR12, MIR13, and MIR14); and eleven stations were occupied on newly disposed material within the Experimental disposal site (MIR7, MIR8, MIR9, MIR10, MIR11, MIR15, MIR16, MIR17, MIR18, MIR19, and MIR20).

Water depths at the Control site ranged from 5.8 to 6.2 m. The water temperature was between 15.0 and 15.1 °C and the salinity was *circa* 22 ppt. Water depth at the two Channel

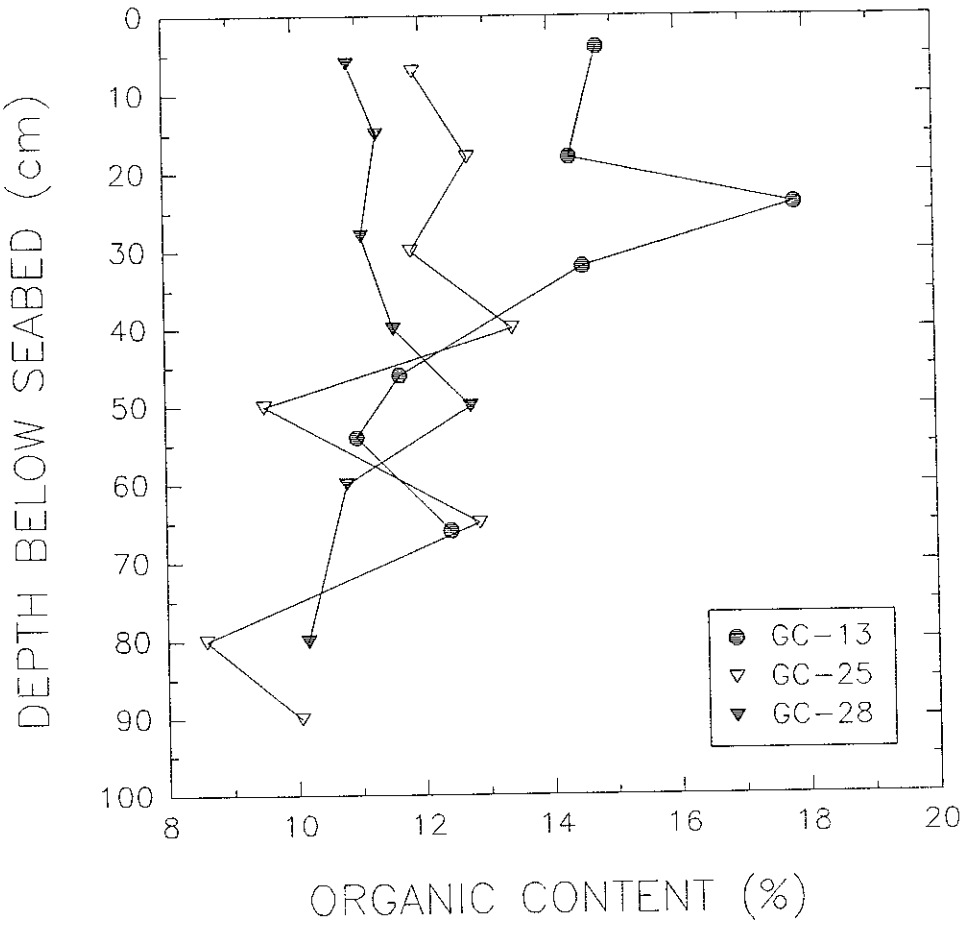

Figure 4.1-1. Variation in sediment organic content with depth for core samples taken in the Channel (GC-13), Control site (GC-25) and the post-disposal Experimental site (GC-28).

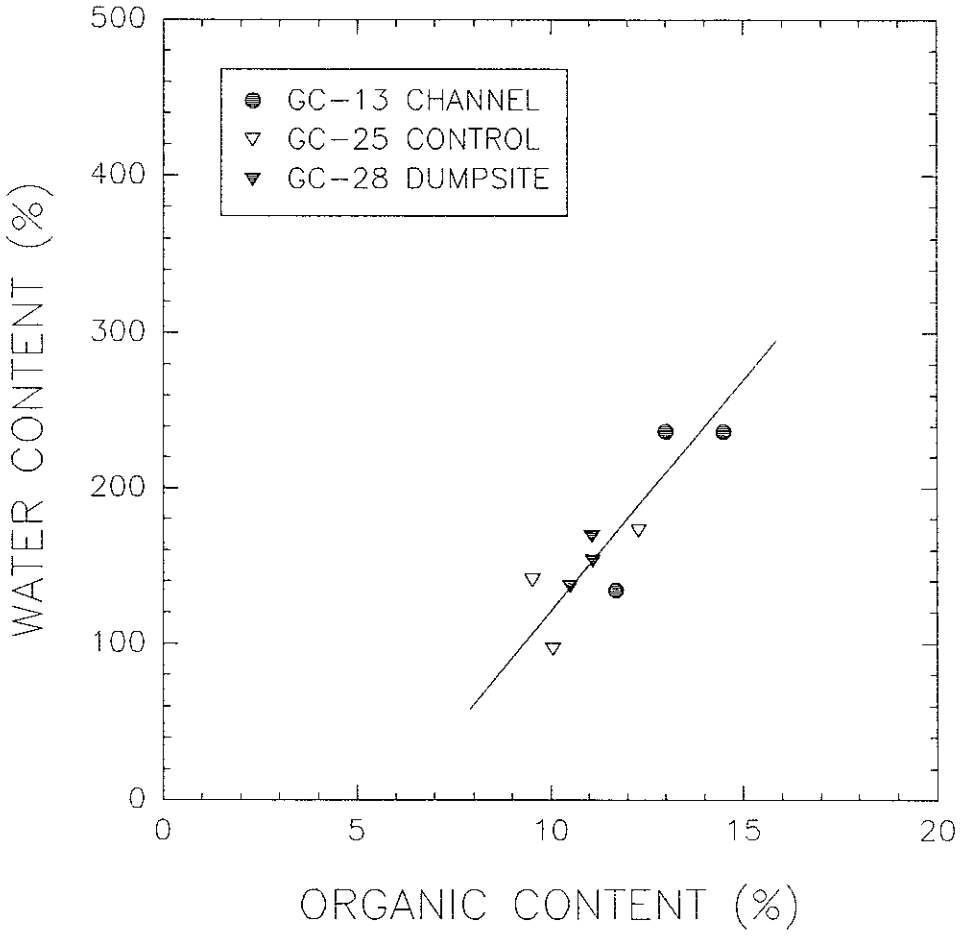

Figure 4.1-2. Relationship between sediment water content and organic content.

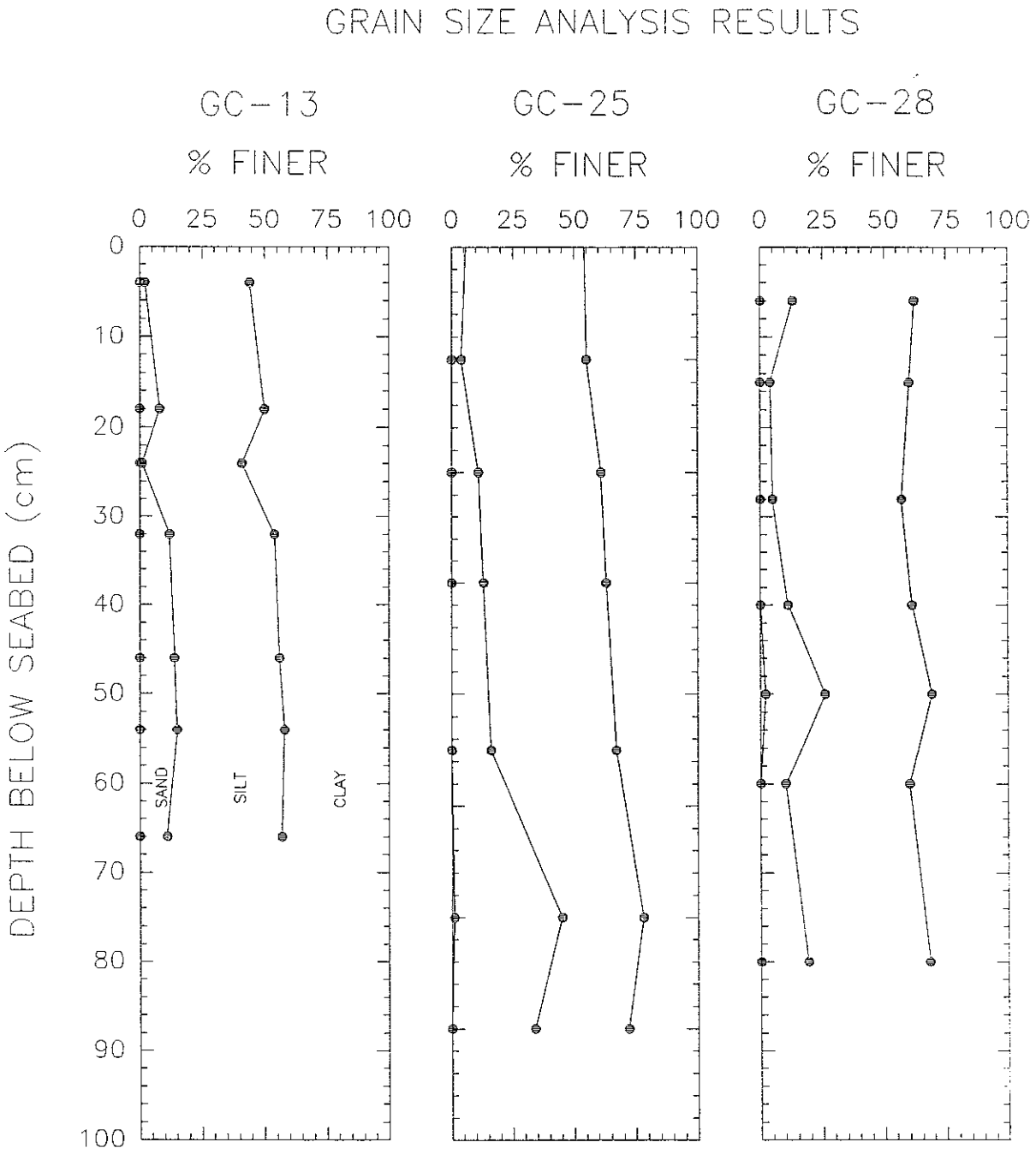

Figure 4.1-3. Variation in sediment grain size with depth for core samples taken in the Channel (GC-13), Control site (GC-25) and the post-disposal Experimental site (GC-28).

Table 4.2.1-1. Summary of Sea Carousel deployments (station numbers in parentheses; Video, 1 - Sony Hi8, 2 - VHS (low resolution)).

STATION*	LATITUDE	LONGITUDE	DEPTH (m)	TIME (min)	SUB-SAMPLE	VIDEO
MIR1(6)-PD	47° 06.97'	65° 10.33'	5.2	83	12	1
MIR2(7)-PD	47° 07.05'	65° 10.21'	5.5	75	12	1
MIR3(8)-PD	47° 06.88'	65° 10.33'	5.8	84	12	1,2
MIR4(9)-PD	47° 06.87'	65° 10.39'	5.2	91	11	1,2
MIR5(13)-CH	47° 07.79'	65° 09.21'	8.5	102	11	1,2
MIR6(12)-CH	47° 07.79'	65° 09.21'	8.5	106	11	1,2
MIR7(8)-D	47° 06.96'	65° 09.90'	5.2	86	11	1,2
MIR8(20)-D	47° 06.86'	65° 10.29'	5.2	59	7	2
MIR9(21)-D	47° 06.86'	65° 10.26'	4.9	80	11	1,2
MIR10(22)-D	47° 06.90'	65° 10.29'	5.0	83	13	1,2
MIR11(23)-D	47° 06.87'	65° 10.23'	5.0	67	12	1,2
MIR12(25)-CO	47° 08.01'	65° 09.46'	6.4	88	12	1,2
MIR13(26)-CO	47° 08.02'	65° 09.49'	6.1	74	13	1,2
MIR14(27)-CO	47° 08.01'	65° 09.46'	5.8	78	12	1,2
MIR15(28)-D	47° 07.02'	65° 10.12'	5.2	76	13	1,2
MIR16(29)-D	47° 07.03'	65° 10.12'	5.5	82	12	1,2
MIR17(30)-D	47° 07.04'	65° 10.10'	5.2	80	12	1,2
MIR18(32)-D	47° 06.85'	65° 10.31'	5.5	D	10	1,2
MIR19(33)-D	47° 06.86'	65° 10.25'	5.5	71	12	1,2
MIR20(34)-D	47° 06.86'	65° 10.31'	5.2	80	13	1,2

*PD - pre-disposal Experimental site; CH - Channel site; D -post-disposal Experimental site; CO - Control site.

Table 4.2.1-2. Summary of the results of Sea Carousel measurements from the twenty stations occupied during the study. (Stations fall into four settings: pre-disposal experimental site (PD), the navigation channel (CH), control site (CO), and the post-disposal material in the experimental disposal site (D). The stations fall into five broad groups based on the shear stress profiles and friction angles. These are: (1) stable beds (positive friction angles where $\phi > 10°$); (2) unstable beds (negative friction angles where $\phi < -10°$); (3) neutral beds (where $10° > \phi > -10°$, and where $\tau > 0$); (4) fluidized beds (where $10° > \phi > -10°$, and where $\tau \Rightarrow 0$); and (5) a surface phenomenon of bed strengthening interpreted as sediment biostabilizing due to microorganisms.)

STATION	COHESION (Pa)	FRICTION ANGLE	EROSION TYPE	BED STATE
MIRI (6)	1.5	-29	IA	BIOSTABILIZED
PD		- 19	IB	UNSTABLE
		-5	IB	UNSTABLE
MIR2(7)	1.5	-75	IB	BIOSTABILIZED
PD		2	IB	STABLE
MIR3(8)	1.4	-16	IB	BIOSTABILIZED
PD		6	IB	STABLE
MIR4(9)	0.7	-5	IB	UNSTABLE
PD		16	IB	STABLE
MIR5(13)	1.0	-45	IA	UNSTABLE
CH		- 10	II	UNSTABLE
MIR6(12)	0.8	-13	IB	BIOSTABILIZED
CH		0	IB	UNSTABLE
		4	IB	STABLE
MIR7(8)	0.7	-8	IB	UNSTABLE
D		10	IB	STABLE
MIR8(20)	0.3	-34	II	BIOSTABILIZED
D		- 10	II	UNSTABLE
		0	II	FLUIDIZED BED
MIR9(21)	0.6	70	IA	BIOSTABILIZED
D		- 13	IB	UNSTABLE
		11	IB	STABLE
MIR 10(22)	0.5	78	IB	STABLE
D		29	IB	STABLE
		4	IB	NEUTRAL

Table 4.2.1-2. (Continued)

STATION	COHESION (Pa)	FRICTION ANGLE	EROSION TYPE	BED STATE
MIR11(23)	1.0	29	IB	BIOSTABILIZED
D		-4	IB/II	UNSTABLE
		1	II	FLUIDIZED BED
MIR12(25)	1.3	-21	IB	UNSTABLE
CO		-3	IB	NEUTRAL
		16	IB	STABLE
MIR 13 (26)	1.4	- 18	IB	UNSTABLE
CO		0	IB	NEUTRAL
		18	IB	STABLE
MIR 14(27)	1.4	-22	IB	UNSTABLE
CO		-6	IB	NEUTRAL
		12	IB	STABLE
MIR15(28)	0.8	-8	IB	UNSTABLE
D		17	IB/II	STABLE
		-63	II	UNSTABLE
MIR 16(29)	0.0	70	IA	STABLE
D		37	IB	STABLE
		57	IB	STABLE
MIR17(30)	0.5	18	IB	STABLE
D		-4	IB	NEUTRAL
		21	IB	STABLE
		- 10	IB	UNSTABLE
		13	IB	STABLE
MIR18(32)	1.2	-27	IA	BIOSTABILIZED
D		-4	IB	NEUTRAL
		-1	II	FLUIDIZED BED
MIR19(33)	0.9	-34	IA	BIOSTABILIZED
D		-5	IB	NEUTRAL
		-1	II	FLUIDIZED BED
MIR20(34)	1.1	-34	IA	BIOSTABILIZED
D		- 15	IB	UNSTABLE
		-2	II	NEUTRAL/FLUIDIZED

sites was 8.5 m, while the water temperature was 16.5 °C and the salinity was *circa* 23 ppt. Water depths at the pre-disposal Experimental stations ranged from 5.2 to 5.8 m; the water temperature was constant at 17.9 °C and the salinity was *circa* 22 ppt. Water depths at the post-disposal Experimental stations ranged from 4.9 to 5.5 m; the water temperature varied between 15.0 and 15.6 °C and the salinity varied between 19.1 and 20.1 ppt. The 2 °C range in water temperature is considered to have had only a small effect on the viscosity (2 percent) and density (0.1 percent) of the eroding fluids and, therefore, has not been considered further. Salinity also varied with depth, being greatest at the deeper (Channel) stations, but again a 2 ppt change in salinity results in only a 0.1 percent change in viscosity and so has also been ignored as a variable.

4.2.2 Sensor Calibration

The calibration of the two internal OBS sensors (OBS1 and OBS3) was undertaken by sampling the sediment/water slurry by pumping from a sample port in the side of Sea Carousel. This was carried out at each station. Samples were collected at each speed increment yielding 12-13 samples of systematically increasing suspended sediment concentration (SSC). Sediment concentration was determined by vacuum filtering a known volume of water through 0.45-micron pore diameter Nuclepore filters. The filtered samples yielded a strong correlation with the OBS voltage detected at the time of pump sampling. The calibration equations and correlations for the two internal sensors are presented in Table 4.2.2-1. The relationships between OBS voltage and suspended sediment concentration for each station are shown in Appendix E.

The lid rotational speed derived from the shaft end-coder was verified by monitoring it in the VHS video tapes of stations MIR4 and MIR20. The correlation between these two measures was almost perfect (Fig. 4.2.2-1). The Sea Carousel pressure sensor was calibrated against physical measures of depth. The pressure output (in millivolts) showed a linear calibration with depth (Fig. 4.2.2-2) of the following form:

$$\text{DEPTH (m)} = 1.54 + 7.03\ (\text{PRESSURE})$$

The current speed in the flume was verified by the digitization of particle trajectories in the high-resolution Sony tapes. The height of these particle trajectories *(circa* 6 cm) differed from that of the E.M. flow meter. The transform to the height of the current meter follows "Law of the Wall" to compute first the friction velocity U*:

$$U(Z) = (U*/k).\ \ln(Z/Z_O)$$

where U* is the friction velocity (τ/ρ), k is the von Karman's constant (0.40), Z is the height of the velocity measurement (U), and Z_O is the roughness length (herein equated with 2.5 times the grain diameter, d_{50} = 40 microns, Z_O = 0.10 mm). Thereafter, the Law of the Wall is used to recompute the current velocity at a height (Z) of 0.20 m, the height of the flow meter. The results are shown in Figure 4.2.2-3. The transform is a clear water one, and does not consider turbulent dampening by suspended solids through an increase in density and the

Table 4.2.2-1. Calibration equations of the lower (OBS1) and upper (OBS3) optical sensors used to determine suspended sediment mass (mg^{-1}) from output voltage (CC is the correlation coefficient).

STATION	OBS 1	OBS3	CC	N
MIR1(6)	446 + 2.70 (0BS1)	-861 + 3.20 (0BS3)		12
MIR2(7)	547 + 2.28 (0BS1)	-793 + 2.96 (0BS3)	0.92	12
MIR3(8)	431 + 2.10 (0BS1)	-681 + 2.72 (0BS3)	0.94	12
MIR4(9)	495 + 2.00 (0BS1)	-649 + 2.50 (0BS3)	0.98	11
MIR5(13)	-304 + 3.33 (0BS1)	-786 + 3.33 (0BS3)	0.90	11
MIR6(12)	BURIED	-834 + 3.05 (0BS3)		11
MIR7(8)	602 + 2.13 (0BS1)	-677 + 2.63 (0BS3)	0.98	11
MIR8(20)	BURIED	-4160 + 14.3 (0BS3)		7
MIR9(21)	436 + 3.38 (0BS1)	1211 - 8.90 (0BS3)	0.96	11
MIR10(22)	BURIED	-1025 + 4.14 (0BS3)	0.96	13
MIR11(23)	BURIED	3132 + 10.29 (0BS3)	0.83	12
MIR12(25)	-468 + 2.24 (0BS1)	-815 + 2.97 (0BS3)	0.99	12
MIR13(26)	520 + 2.20 (0BS1)	-683 + 2.8 1 (OBS3)	0.98	13
MIR14(27)	441 + 2.35 (0BS1)	-848 + 3.04 (0BS3)	0.99	12
MIR15(28)	873 + 3.89 (0BS1)	-1228 + 4.98 (0BS3)	0.98	13
MIR16(29)	BURIED	-805 + 3.52 (0BS3)	0.81	12
MIR17(30)	1044 + 4.12 (0BS1)	-1356 + 5.43 (0BS3)	0.92	13
MIR18(32)	677 + 6.00 (0BS1)	-1973 + 7.28 (0BS3)	0.85	10
MIR19(33)	758 + 6.03 (0BS1)	-2300 + 7.41 (0BS3)	0.90	12
MIR20(34)	986 + 8.39 (0BS1)	-2745 + 9.75 (0BS3)	0.85	13

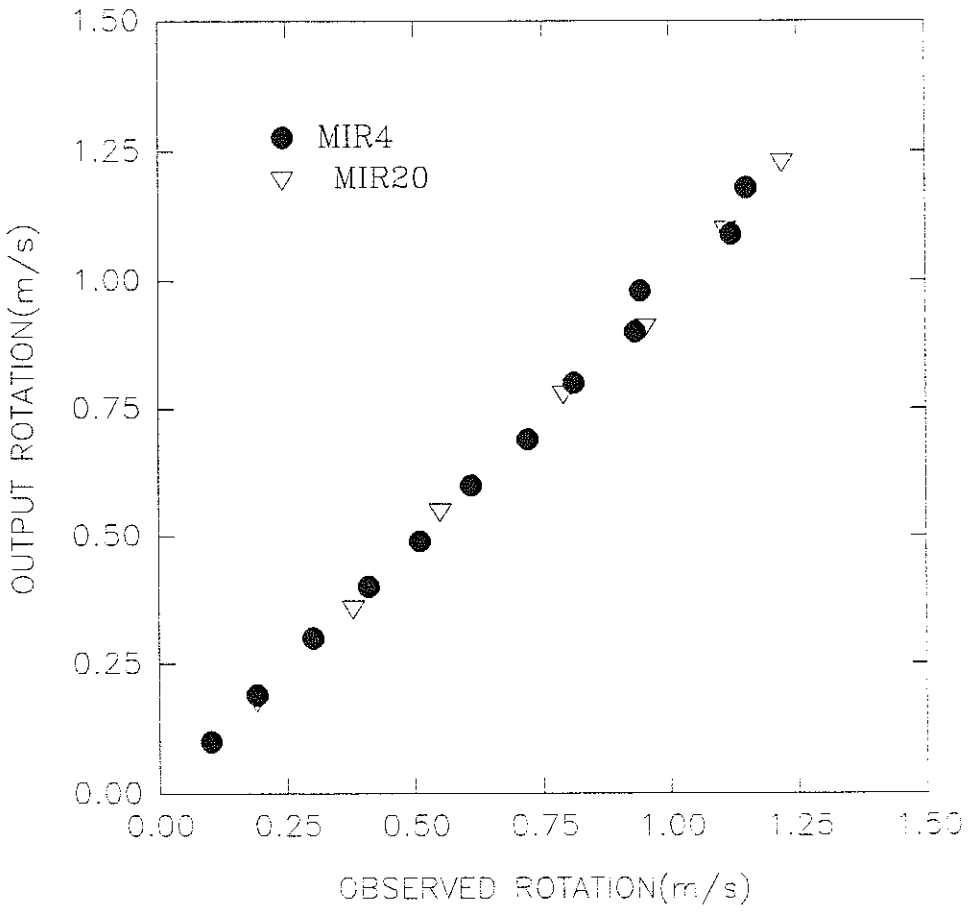

Figure 4.2.2-1. Relationship between shaft end-coder speed measurement (output) and lid rotation speed (observed).

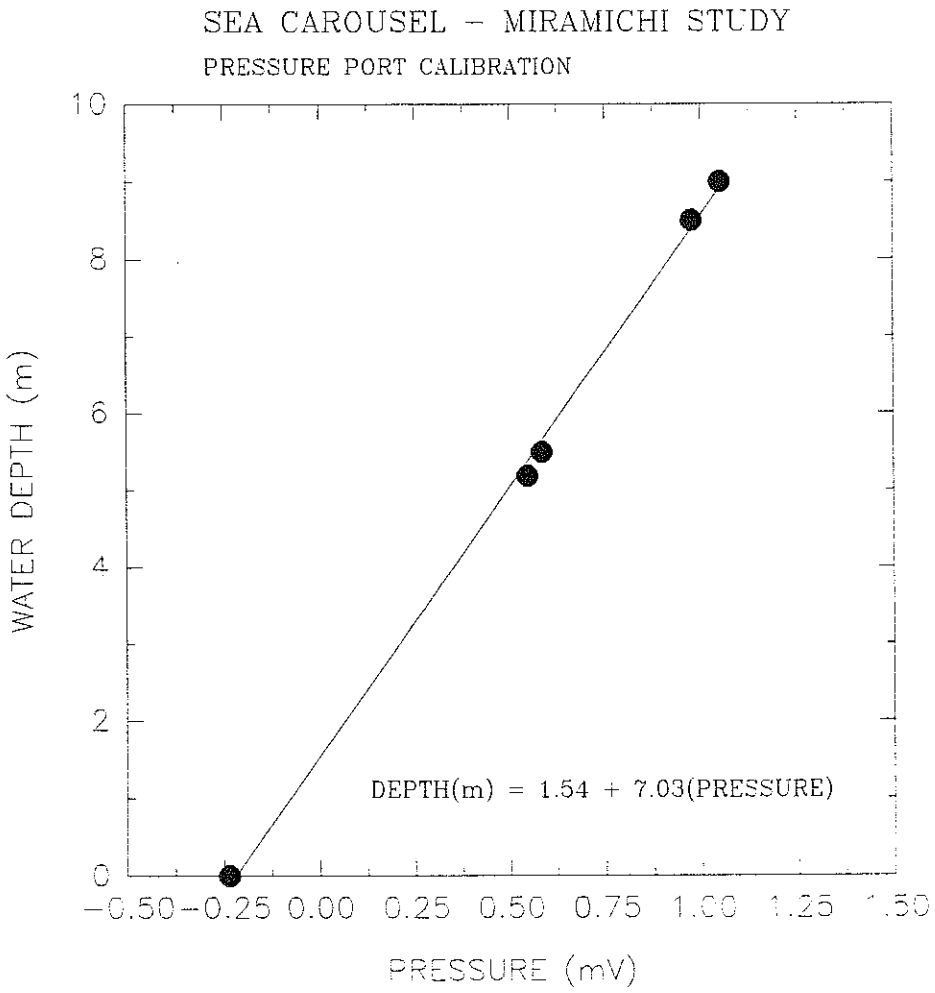

Figure 4.2.2-2. Relationship between pressure sensor measurement and water depth.

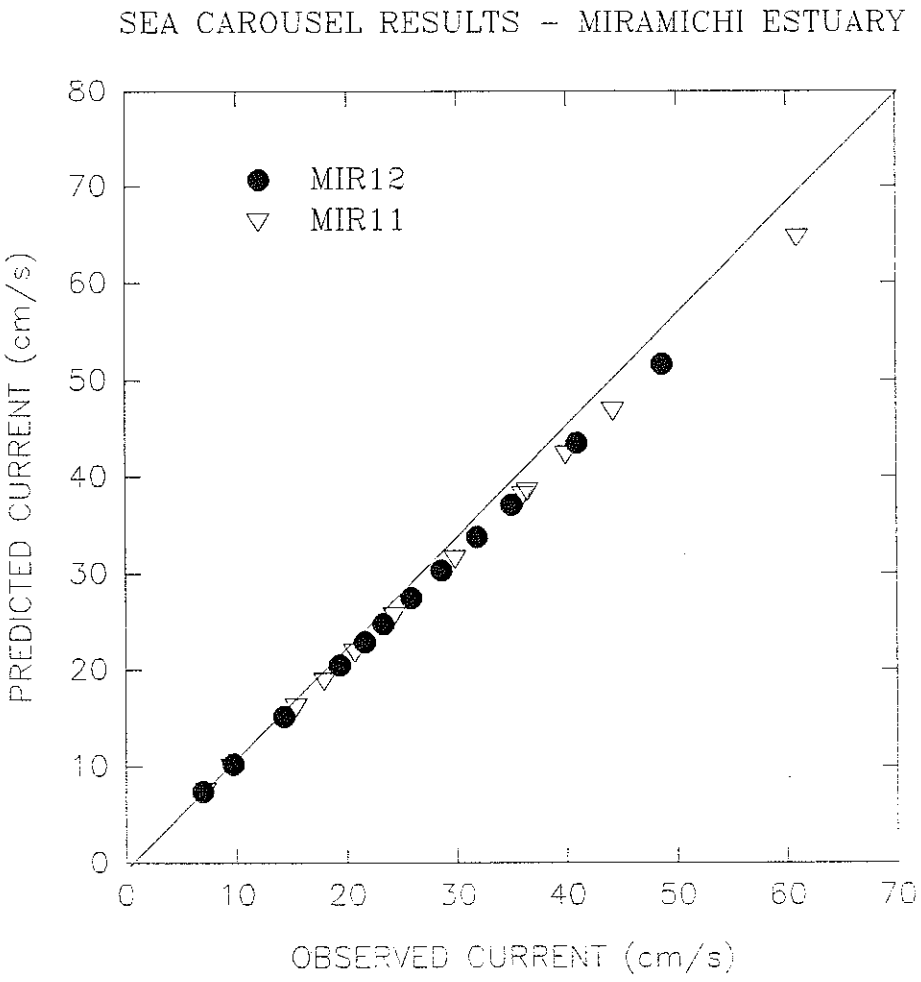

Figure 4.2.2-3. Relationship between observed and predicted current velocity.

consequent enhancement of the viscous sub-layer. Nevertheless, a good relationship between the two methods for determining current speed was found. The plot suggests that our sensed values of current speed may be underestimated by a maximum of 5 percent at the highest speeds. This equates to an under-prediction of bed shear stress of *circa* 25 percent.

4.2.3 Control Site

Time series of the results from the Sea Carousel at the Control sites (MIR12, MIR13, and MIR14) are shown in Figures 4.2.3-1 to 4.2.3-3, respectively. The seabed was tested under 12 increments of speed ranging up to a maximum lid rotational speed of *circa* 1.2 m sec^{-1}. The increments of lid rotation were all of equal magnitude.

The video records showed the seabed at the Control site to be smooth, but bioturbated, probably largely by shrimp. We saw no evidence for a fluid mud layer as the visibility of the seabed was good in all cases.

4.2.3.1 Threshold Stresses for Bed Erosion

The threshold for seabed erosion varies with depth in the sediment as a function of the friction angle. It is equated with the applied bed shear stress at sediment failure during the erosion process. For present purposes, we use this to define the sediment strength at the mudline. It is used as our index of sediment strength. Within the context of bed erosion, it is "the threshold stress for bed erosion". It is also known as "cohesion" because the effective stress (sediment weight-induced) is zero. The thresholds are summarized in Table 4.2.1-2 (as cohesion) for all stations. Also listed is the friction angle (in degrees), the erosion type (Amos et al. 1992), and the bed states (stable, unstable, neutral, fluidized, and biostabilized).

The results from the Control site showed remarkably consistent trends (Figs. 4.2.3.1-1 to 4.2.3.1-3). The thresholds varied by only 0.1 Pa (1.3-1.4 Pa), and were amongst the highest detected in the survey. The sediment state was in all cases unstable (negative friction angle) at the surface, neutral immediately beneath, and stable at the lowest eroded sections (positive friction angle). The erosion type was IB; that is, there is a peak in the erosion rate at the onset of the applied bed shear stress that diminishes asymptotically with time (over 5 min). Sediments were of low consolidation, as friction angles were less than *circa* 20°.

4.2.3.2 Erosion Rates

The erosion rates for the Control sites are plotted in panels C of Figures 4.2.3-1 to 4.2.3-3. The patterns of erosion largely follow type I (asymptotically decaying with time). Initially, we see a relatively high erosion rate at very low flows (< 0.1 m sec^{-1}), that corresponds to the suspension of loose organic "fluff". This erosion is short lived and accounts for a small proportion of the bed. Peak erosion rates are on the order of 5×10^{-4} kg m^{-2} sec^{-1}. At intermediate flows (0.1 to 0.3 m sec^{-1}), type IB erosion prevails and the peak erosion (EP) shows a systematic increase with current speed, from 2×10^{-4} to 10^{-2} kg m^{-2} sec^{-1}. The base erosion rate (EB) is the minimum erosion rate detected at the end of each speed

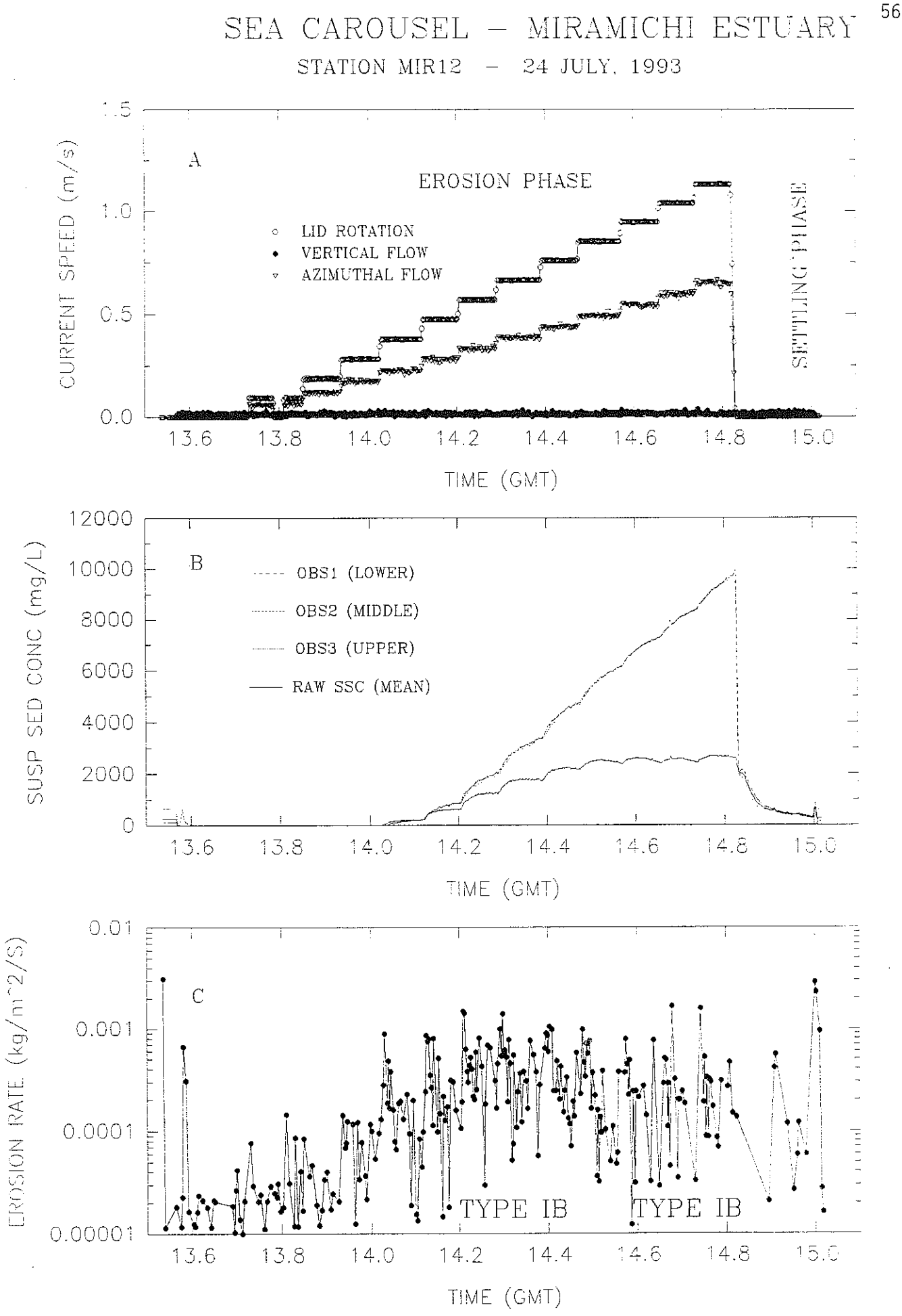

Figure 4.2.3-1. Time series of Sea Carousel results at Control site MIR12 (Station 25).

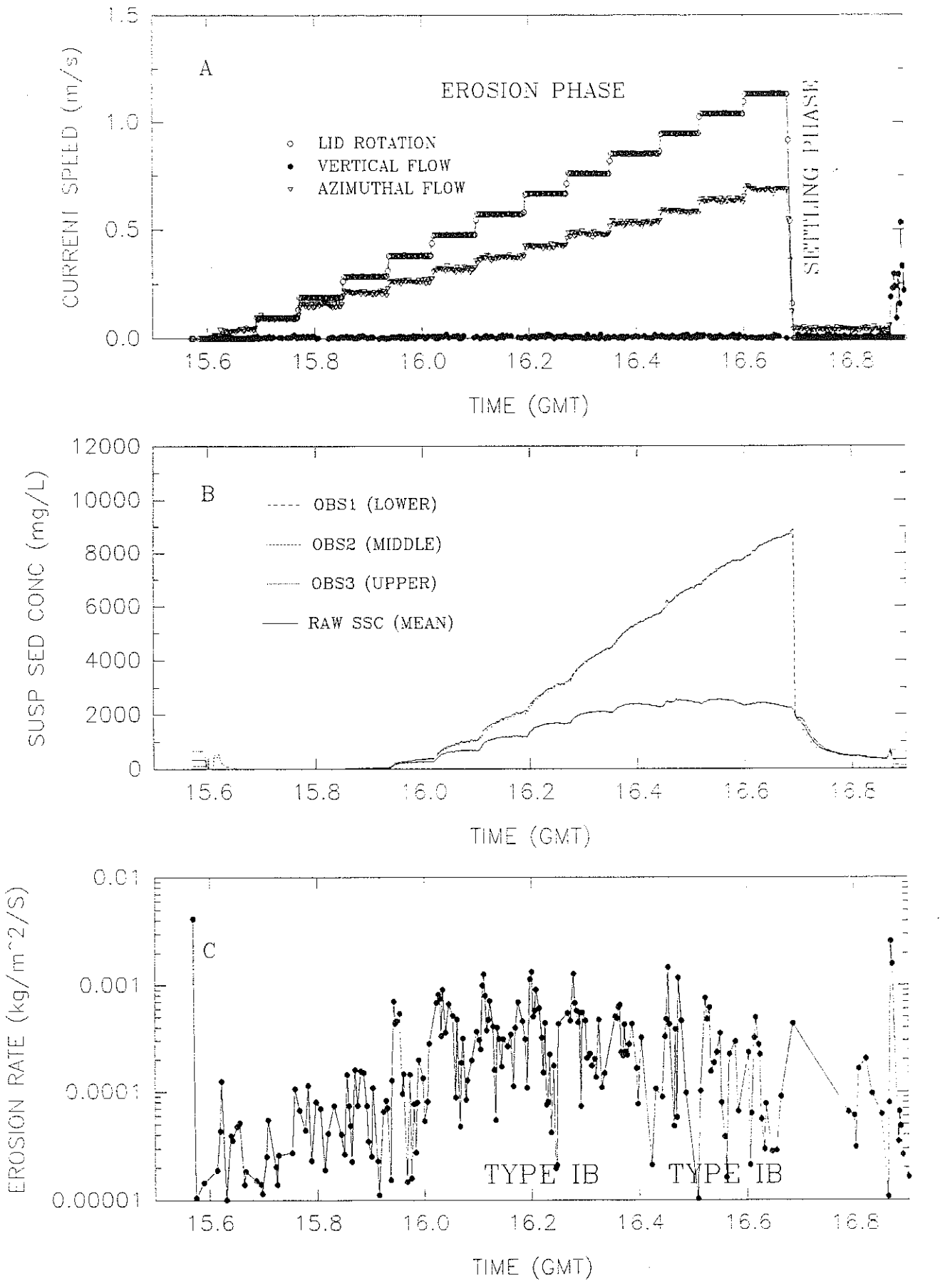

Figure 4.2.3-2. Time series of Sea Carousel results at Control site MIR13 (Station 26).

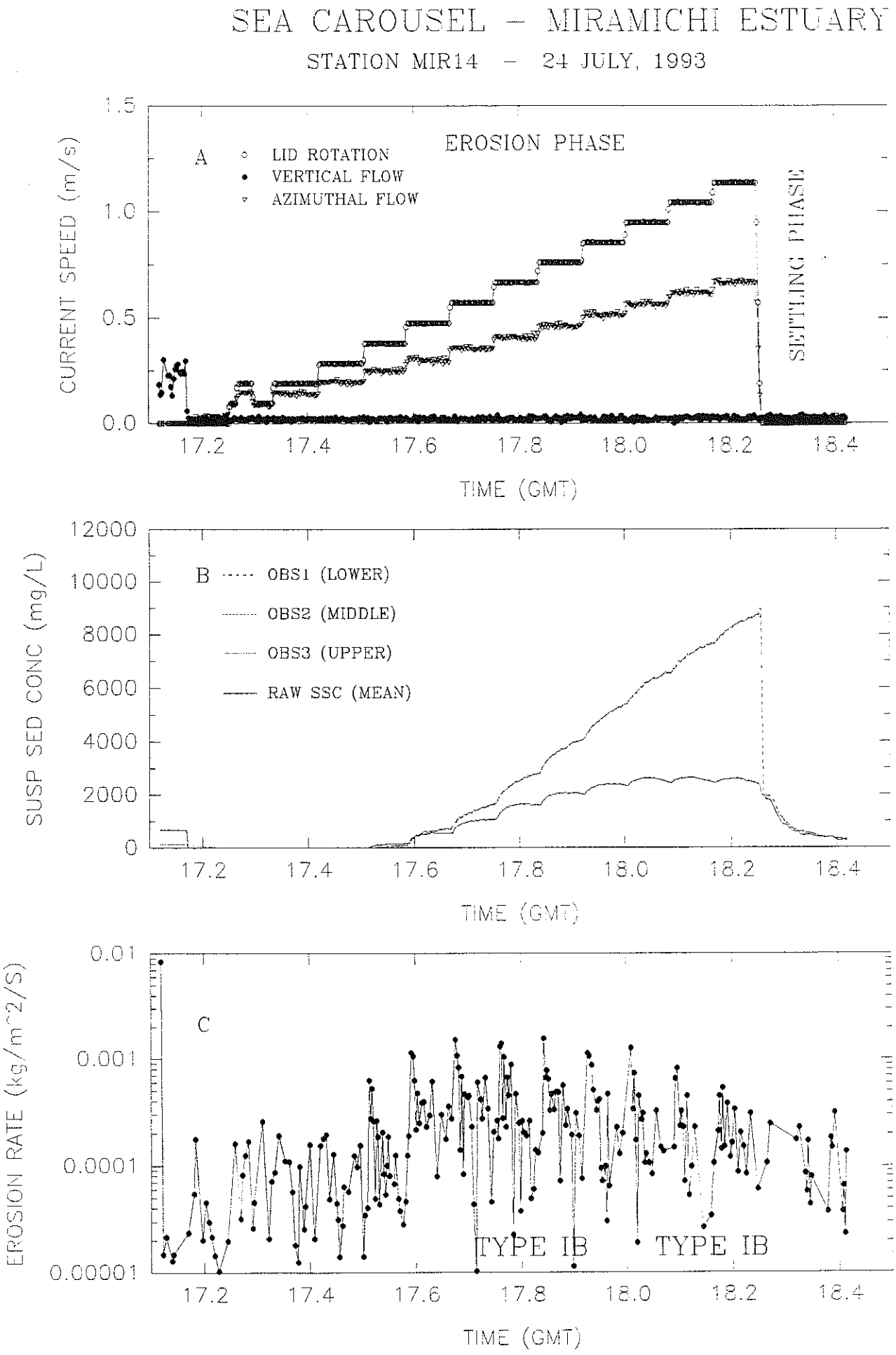

Figure 4.2.3-3. Time series of Sea Carousel results at Control site MIR14 (Station 27).

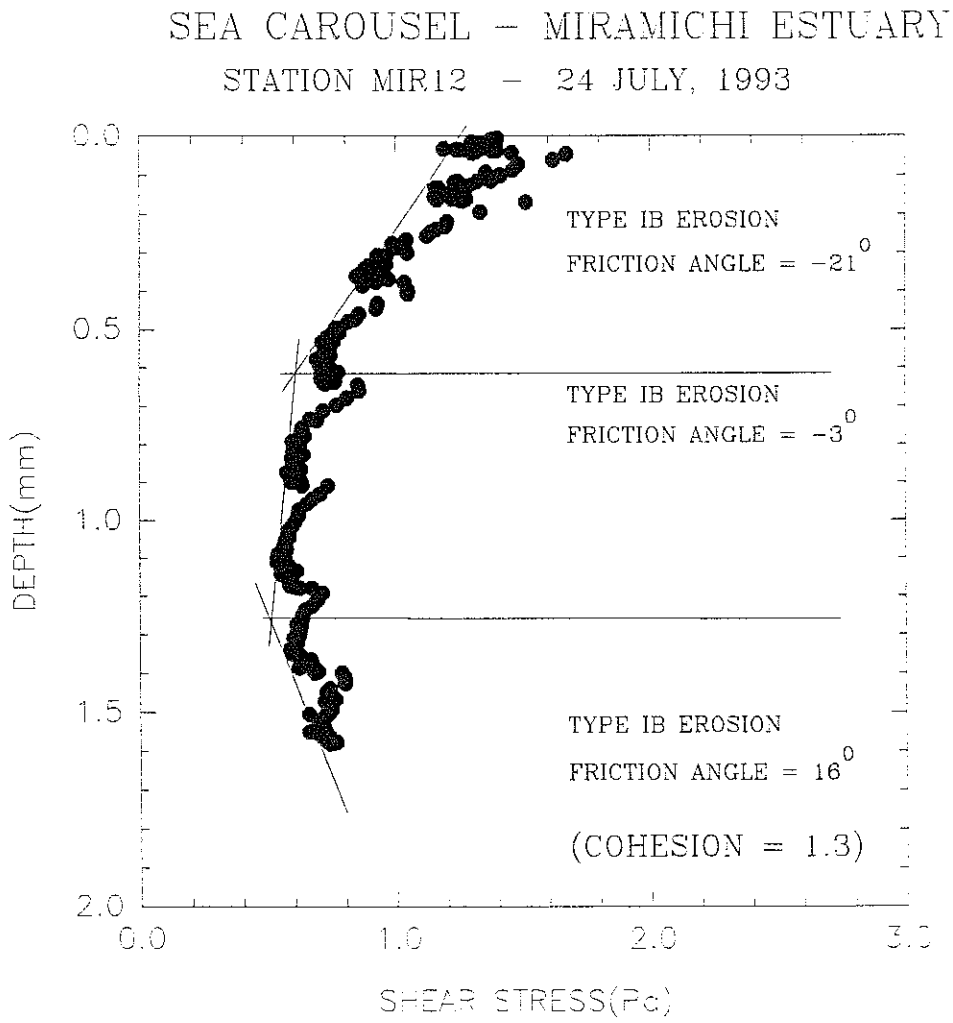

Figure 4.2.3.1-1. Relationship of shear stress and depth at Control site MIR12 (Station 25).

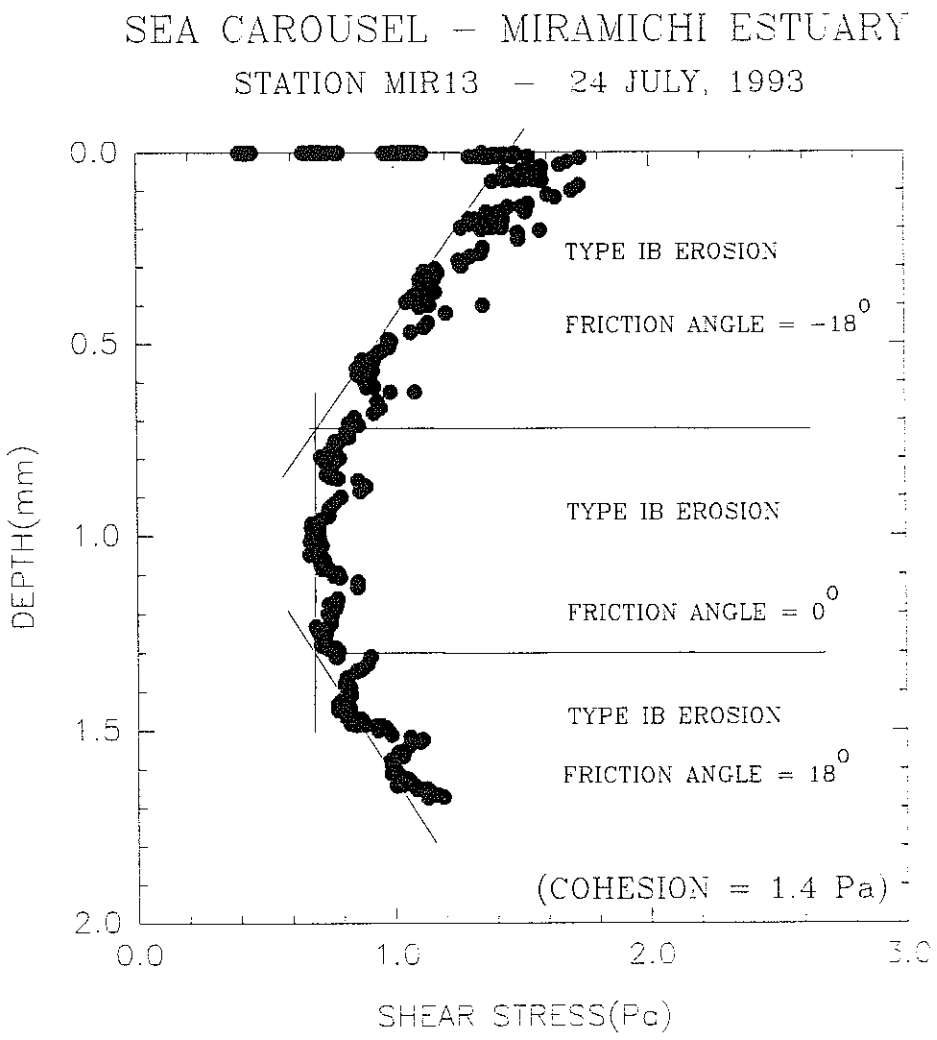

Figure 4.2.3.1-2. Relationship of shear stress and depth at Control site MIR13 (Station 26).

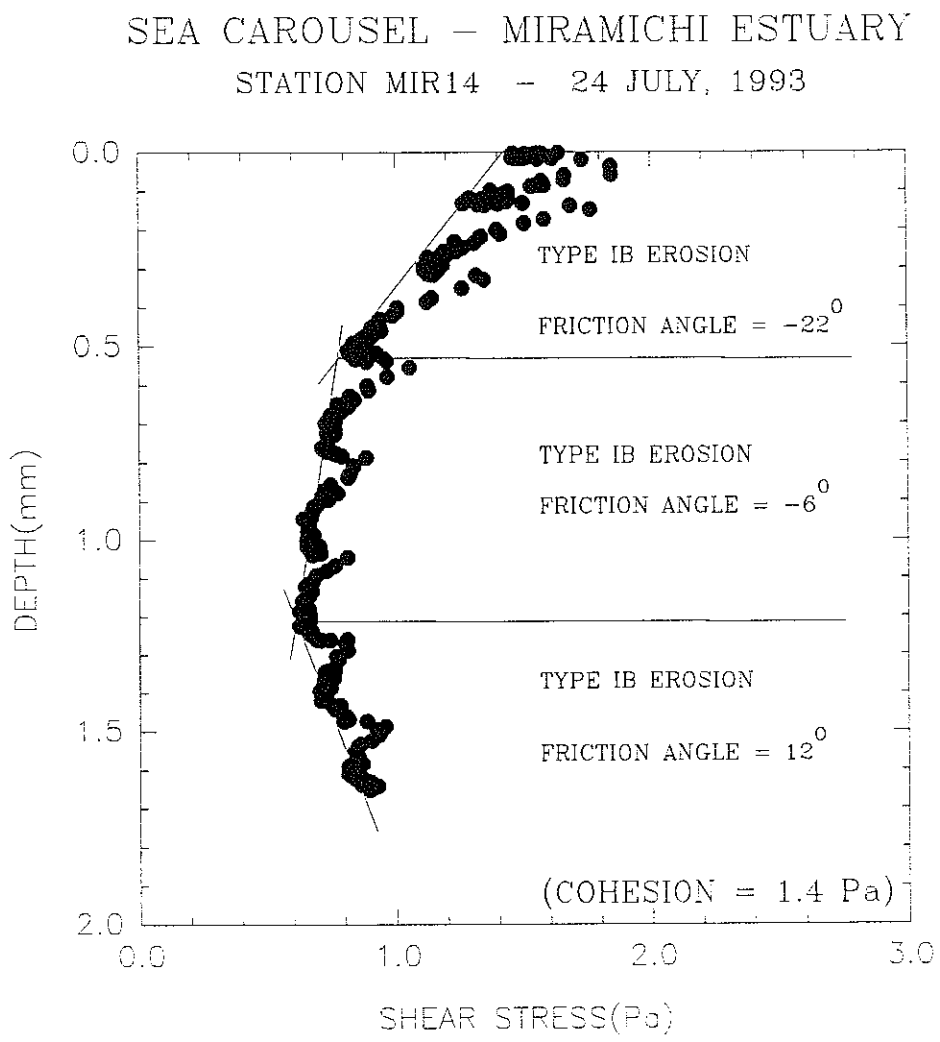

Figure 4.2.3.1-3. Relationship of shear stress and depth at Control site MIR14 (Station 27).

increment. It too shows a systematic increase with current speed from 3×10^{-5} to 7×10^{-4} kg m^{-2} sec^{-1}. At current speeds in excess of 0.4 m sec^{-1}, both EP and EB remain relatively constant at values of 10^{-3} and 2×10^{-4} kg m^{-2} sec^{-1}, respectively. Neither EP nor EB show any overall relationship to either current speed or bed shear stress, as the highest erosion rates takes place at intermediate current speeds.

4.2.3.3 Deposition Rates

The deposition rates of suspended sediment were determined at the end of each experiment under still water conditions. The purpose of this procedure was to evaluate the potential for fluid mud generation under ambient, natural conditions. These tests supplement results of laboratory settling experiments on Miramichi sediment samples previously performed by the Acadia Centre for Estuarine Research (Amos et al. 1992). Still water settling of suspended matter results in an exponential decrease in sediment concentration with time. This may be expressed as:

$$SSC(t) = SSC_0 \exp[-kt]$$

where SSC_0 is the initial concentration, t is elapsed time, and k is the decay constant (in units of reciprocal seconds). The decay constant is an index of mass settling rate and is always negative during settling. Also, the greater the value, the greater is the settling rate. The potential for fluid mud generation increases as k approaches 0. Estimates of k are summarized in Table 4.2.3.3-1.

The suspended sediment concentration at two heights within the Sea Carousel for the Control stations are shown in Figures 4.2.3.3-1 to 4.2.3.3-3. The concentration half-lives of suspended material show differences between the near-surface and near-bed in the Carousel. These differences are not, however, systematic, and so no general conclusions can be made regarding the settling rates as a function of height above the bed. For the Control sites, the half-lives vary between 133 and 198 sec, and the equivalent decay constants vary between -0.0025 and -0.0052 (a factor of two). These values fall within the range presented by Amos et al. (1992), but are generally higher for equivalent starting sediment concentrations. We conclude that the potential for the generation of fluid muds is low, as settling takes place quickly.

4.2.4 Channel Site

Two stations were occupied within the navigation channel of Miramichi Bay, MIR5 (Station 13) and MIR6 (Station 12). The stations were situated in 8.5 m within Reach 22. The water temperature at the stations was 16.5 °C and the salinity was 23 ppt. Good data were obtained from both stations, although the lower OBS sensor was buried during deployment MIR6. The time-series of the two stations are shown in Figures 4.2.4-1 and 4.2.4-2. The seabed was tested under twelve increments of velocity ranging up to a maximum lid rotational speed of *circa* 1.2 m sec^{-1}. The speed increments were all of equal magnitude. The video observations showed the bed to be in a gel-like state and heavily bioturbated. We saw no

Table 4.2.3.3-1. Summary of the concentration half-lives ($t_{0.5}$) and the decay constants (k) for the settling of suspended material within the Sea Carousel (k is valid for units of sediment concentration in mg l^{-1}; they should be multiplied by 1000 to be comparable to those reported by Amos et al. 1992).

Station	Near Surface		Near Bed	
	$t_{0.5}$ (sec)	k (sec^{-1})	$t_{0.5}$ (sec)	k (sec^{-1})
MIR1(6)	298	-0.00232	122	-0.00566
MIR2(7)	106	-0.00664	129	-0.00535
MIR3(8)	122	-0.00566	122	-0.00566
MIR4(9)	57	-0.01200	111	-0.00621
MIR5(13)	183	0.00378	14	-0.04810
MIR6(12)	90	-0.00770	buried	buried
MIR7(8)	190	0.00363	237	-0.00292
MIR8(20)	187	-0.00370	buried	buried
MIR9(21)	82	0.00837	90	-0.00770
MIR10(22)	180	0.00385	183	0.00378
MIR 12(25)	133	0.00520	154	0.00448
MIR13(26)	198	-0.00250	190	0.00363
MIR14(27)	176	0.00393	194	0.00357
MIR15(28)	151	0.00458	187	-0.00370
MIR 16(29)	82	0.00837	buried	buried
MIR 17(30)	82	-0.00838	111	-0.00621
MIR18(32)	176	-0.00363	133	-0.00520
MIR19(33)	165	0.00419	129	0.00535
MIR20(34)	320	0 00216	90	-0.00770

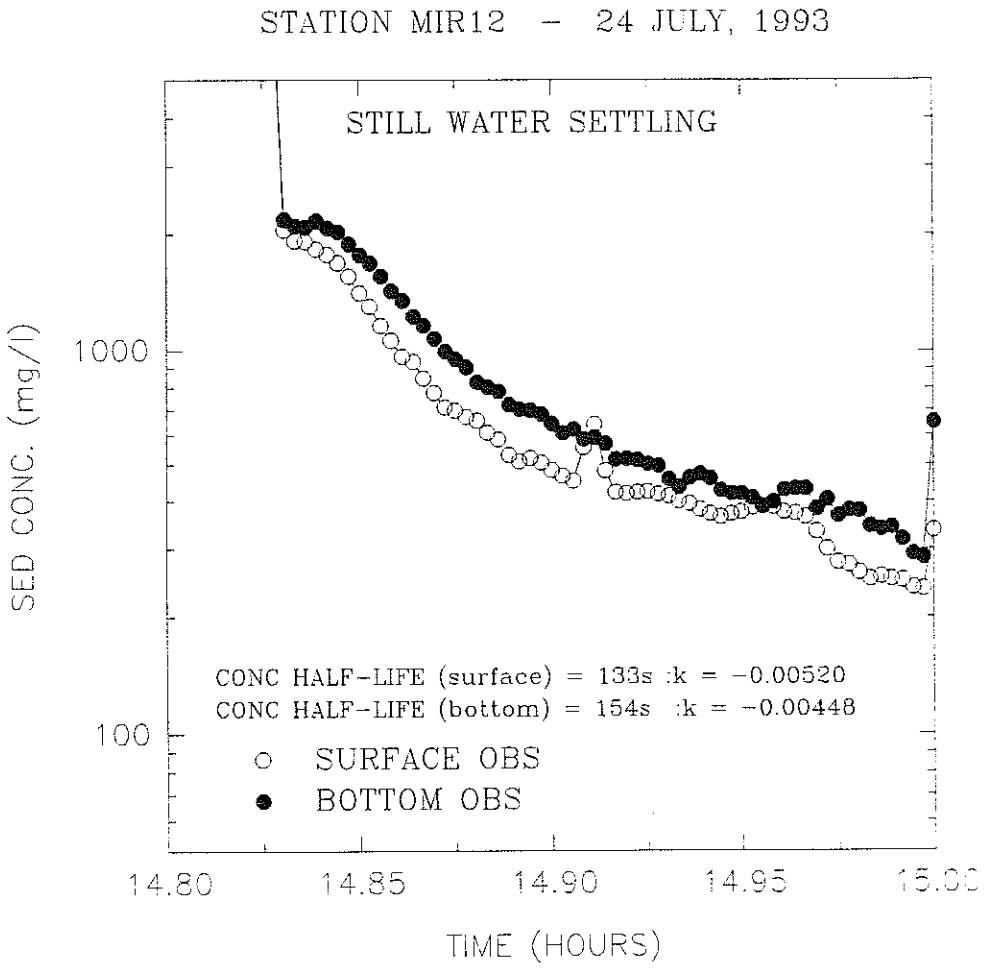

Figure 4.2.3.3-1. Relationship between sediment concentration and time during Sea Carousel settling rate measurements at Control site MIR12 (Station 25).

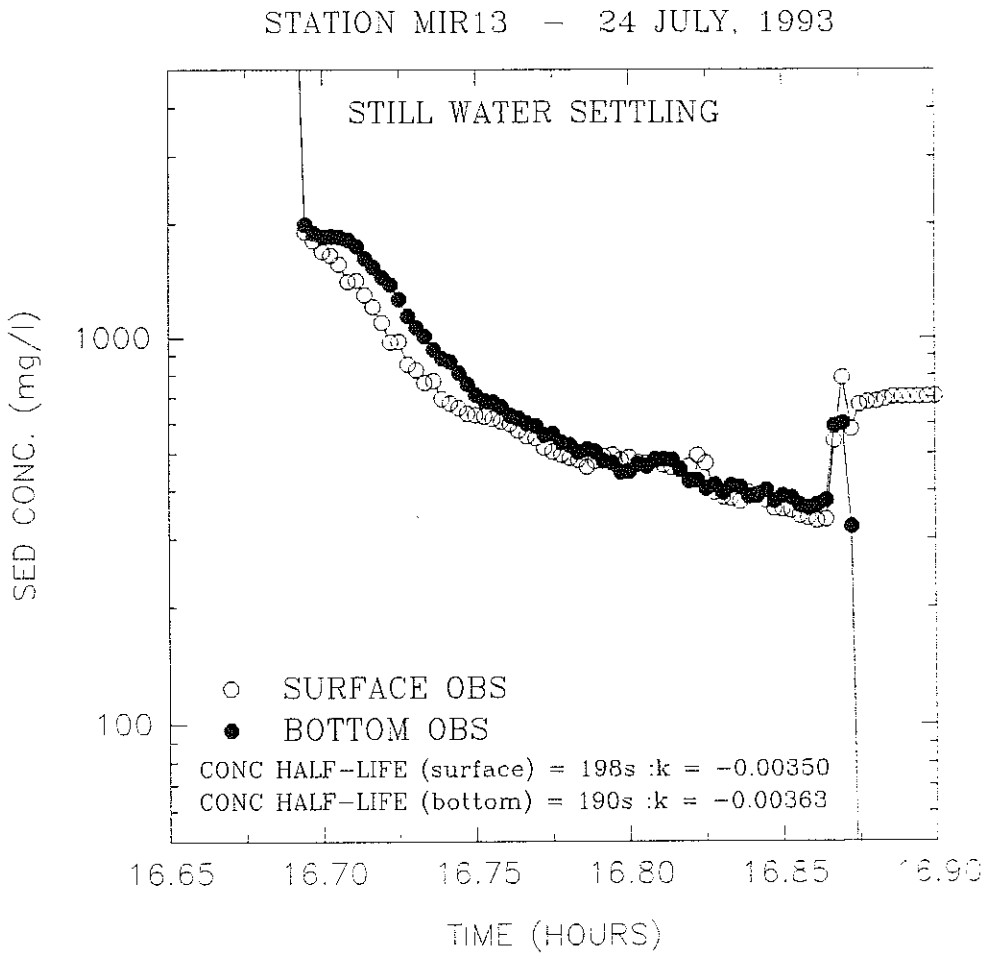

Figure 4.2.3.3-2. Relationship between sediment concentration and time during Sea Carousel settling rate measurements at Control site MIR13 (Station 26).

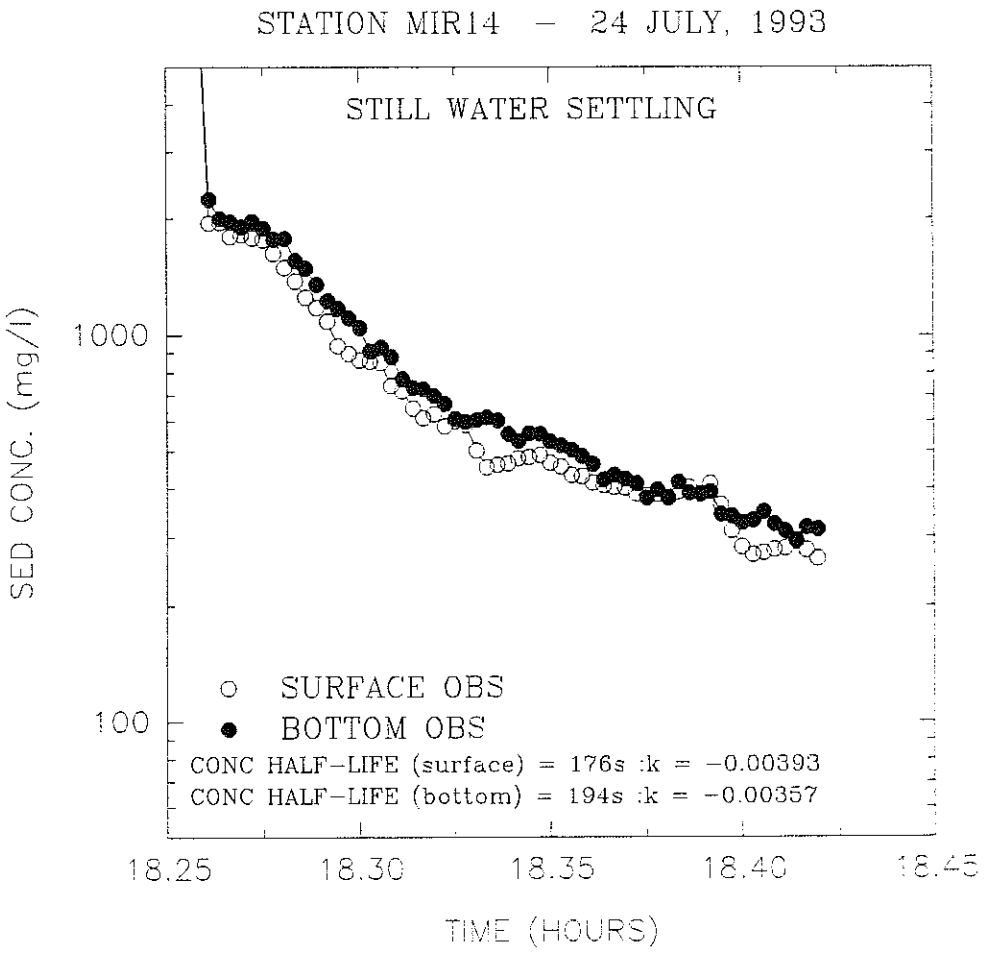

Figure 4.2.3.3-3. Relationship between sediment concentration and time during Sea Carousel settling rate measurements at Control site MIR14 (Station 27).

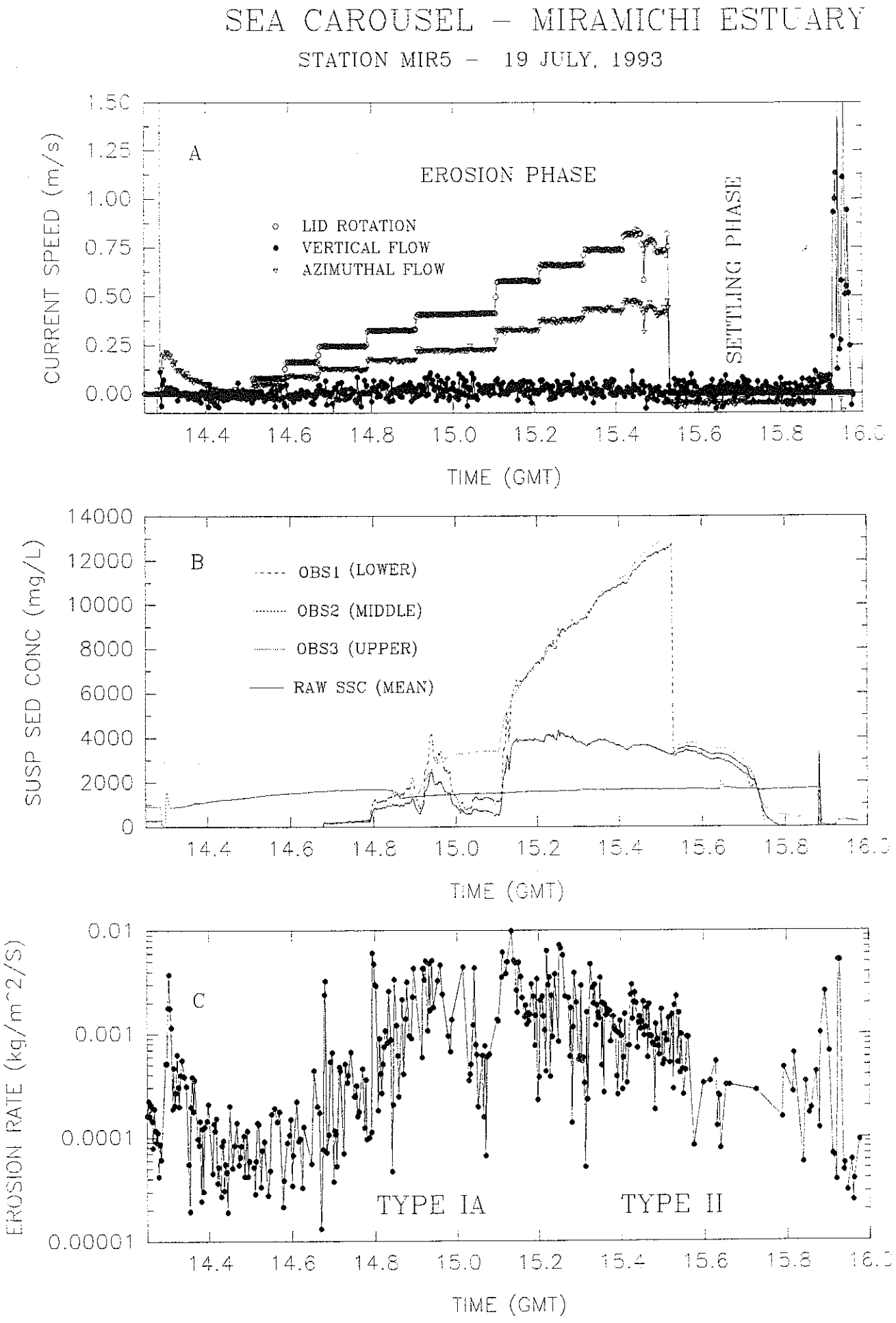

Figure 4.2.4-1. Time series of Sea Carousel results at Channel site MIR5 (Station 13).

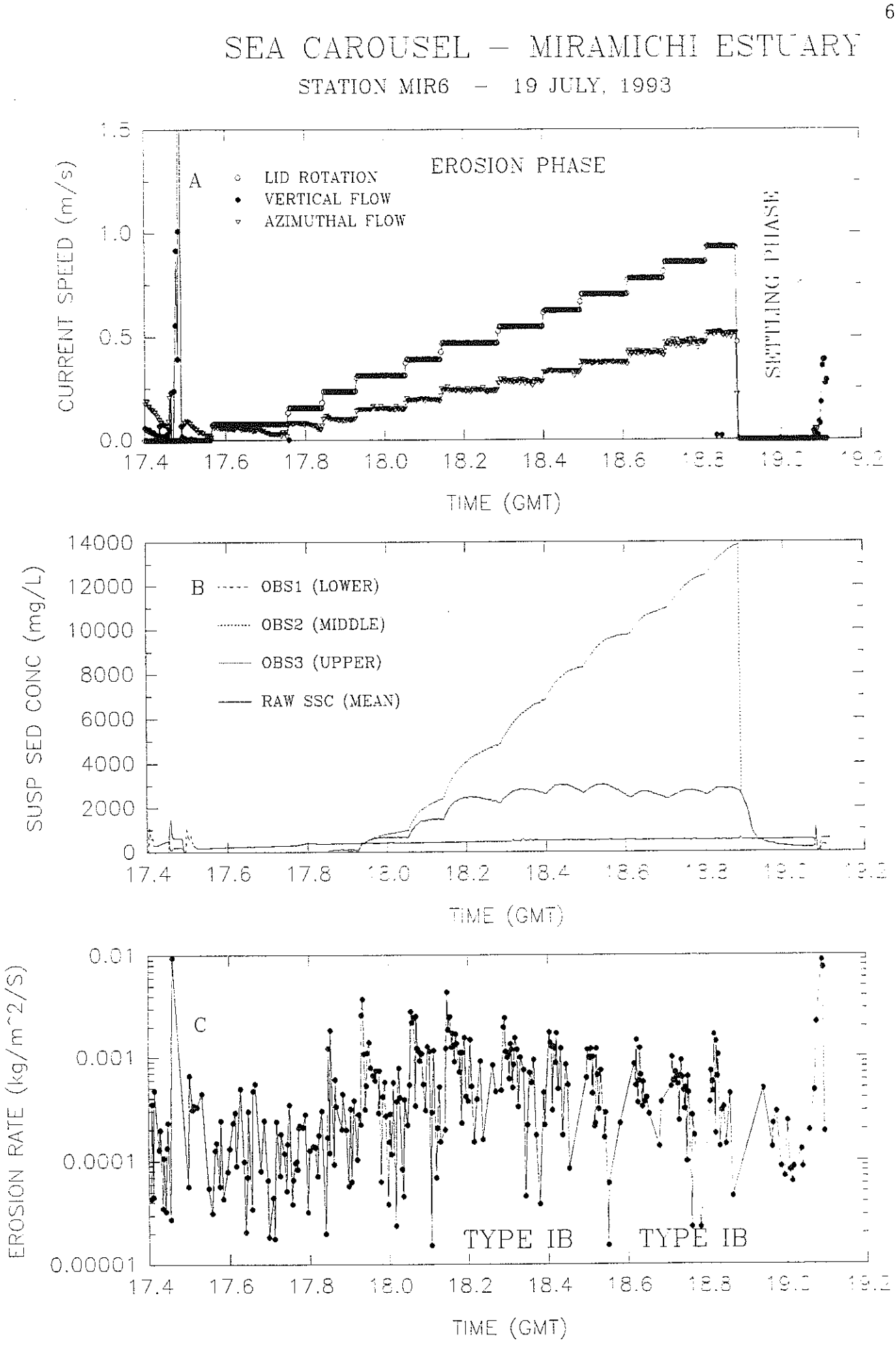

Figure 4.2.4-2. Time series of Sea Carousel results at Channel site MIR6 (Station 12).

evidence of a fluid mud layer as the visibility of the bed was good, and the penetration of the Carousel was limited, though greater than at the Control site.

4.2.4.1 Threshold Stresses for Bed Erosion

The thresholds for bed erosion were determined from Figures 4.2.4.1-1 and 4.2.4.1-2. The threshold stresses for bed erosion were 1.0 and 0.8 Pa. Both stations demonstrate a decrease in strength with depth from the surface over the top 2 mm. The sediment strength at 1 mm in station MIR5 virtually went to zero, suggestive of a fluidized bed. At station MIR6, the strength increased below 2 mm diagnostic of consolidation, although the low friction angles attest to their potential mobility. The surface strength values are consistently below the values for the Control site. If we ascribe the surface strength, experienced at this or other locations, to either biological or physico-chemical stabilization process acting at the surface, a reduced strength would be expected below the surface where bioturbation and decay process may be dominant.

4.2.4.2 Erosion Rates

The erosion rates for the Channel sites are plotted in panels C of Figures 4.2.4-1 and 4.2.4-2. The patterns of erosion largely follow type I (asymptotically decaying with time). Initially, we see a relatively high erosion rate at very low flows (< 0.1 m sec^{-1}), that corresponds to the suspension of a loose organic "fluff". This layer may be indicative of disturbance by benthic microinvertebrates. This erosion is short-lived and accounts for a small proportion of the bed. Peak erosion rates are in the order of 5×10^{-4} kg m^{-2} sec^{-1}. At intermediate flows (0.1 to 0.3 m sec^{-1}), type IB erosion prevails and the peak erosion (EP) shows a systematic increase with current speed, from 2×10^{-4} to 10^{-2} kg m^{-2} sec^{-1}. The base erosion rate (EB) is the minimum erosion rate detected at the end of each velocity increment. It too shows a systematic increase with current speed from 3×10^{-5} to 7×10^{-4} kg m^{-2} sec^{-1}. At current speeds in excess of 0.4 m sec^{-1}, both EP and EB remain relatively constant at values of 10^{-3} and 2×10^{-4} kg m^{-2} sec^{-1}, respectively. Neither EP nor EB show any overall relationship to either current speed or bed shear stress, as the highest erosion rates take place at intermediate current speeds. Thus we observe two domains to bed erosion. The first, at flow speeds below 0.3 m sec^{-1}, is where erosion rate increases with current speed. The second, at flow speeds in excess of 0.3 m sec^{-1}, is where erosion rate remains more or less constant and independent of current speed.

4.2.4.3 Deposition Rates

The deposition rates were determined from the time-series plotted in Figures 4.2.4.3-1 and 4.2.4.3-2. The settling rates varied considerably between the two stations, and so a trend is not evident. Results for MIR5 suggest a brief period (12 min) when negligible settling took place despite the absence of flow. This phenomenon is called "hindered settling", and is a major factor in the development of fluid muds. The hindered settling takes place at a starting concentration of *circa* 4000 mg/l. We interpret this to be the result of very high organic

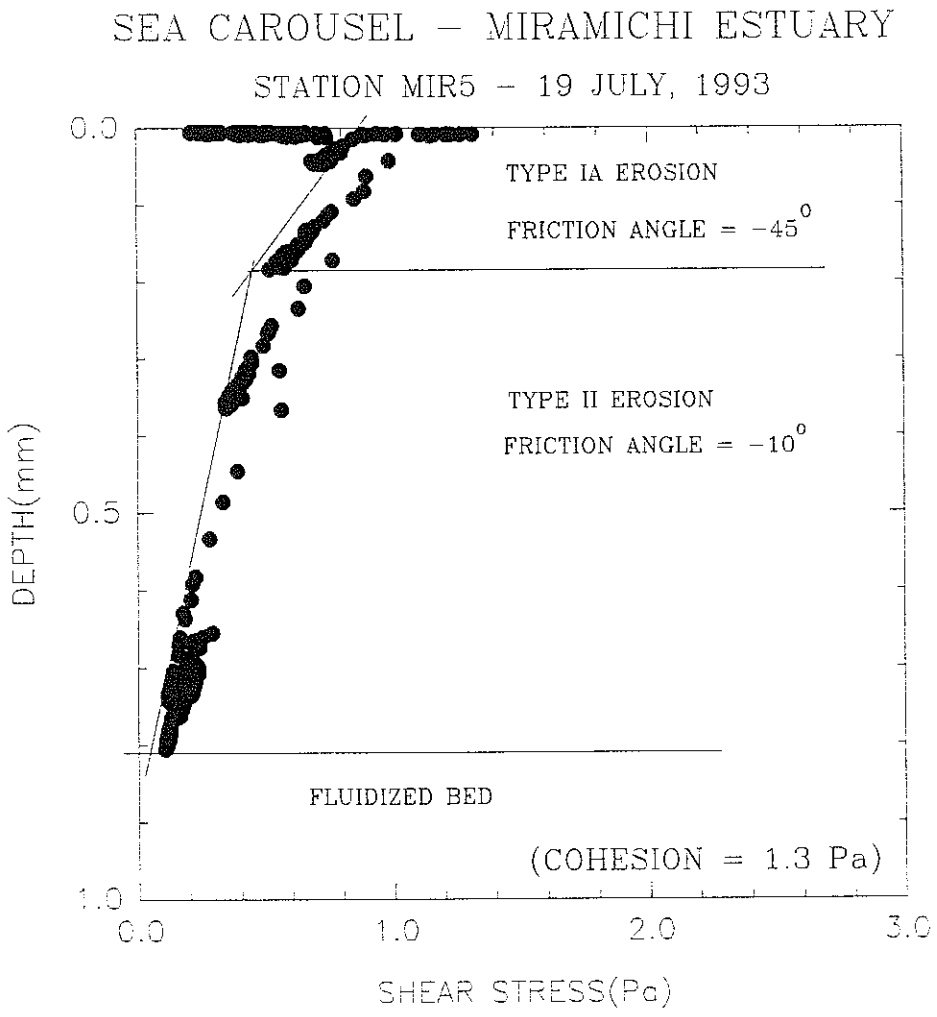

Figure 4.2.4.1-1. Relationship of shear stress and depth at Channel site MIR5 (Station 13).

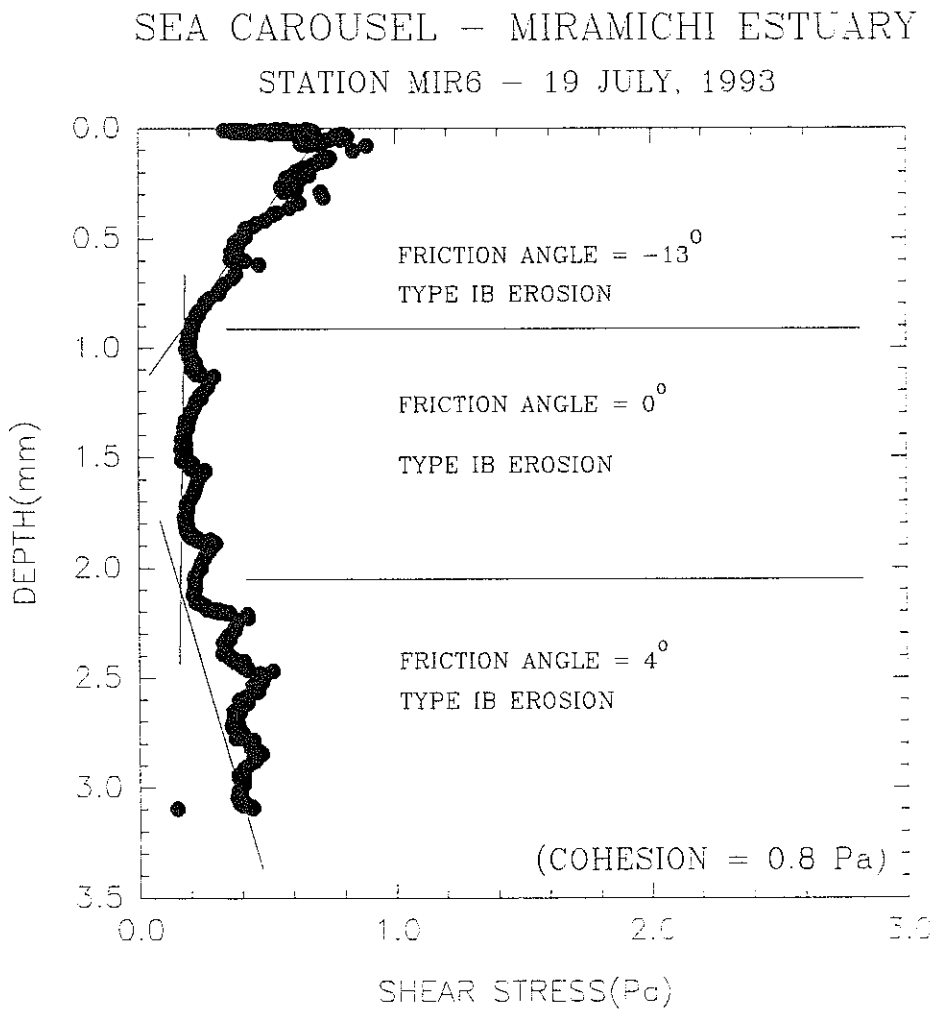

Figure 4.2.4.1-2. Relationship of shear stress and depth at Channel site MIR6 (Station 12).

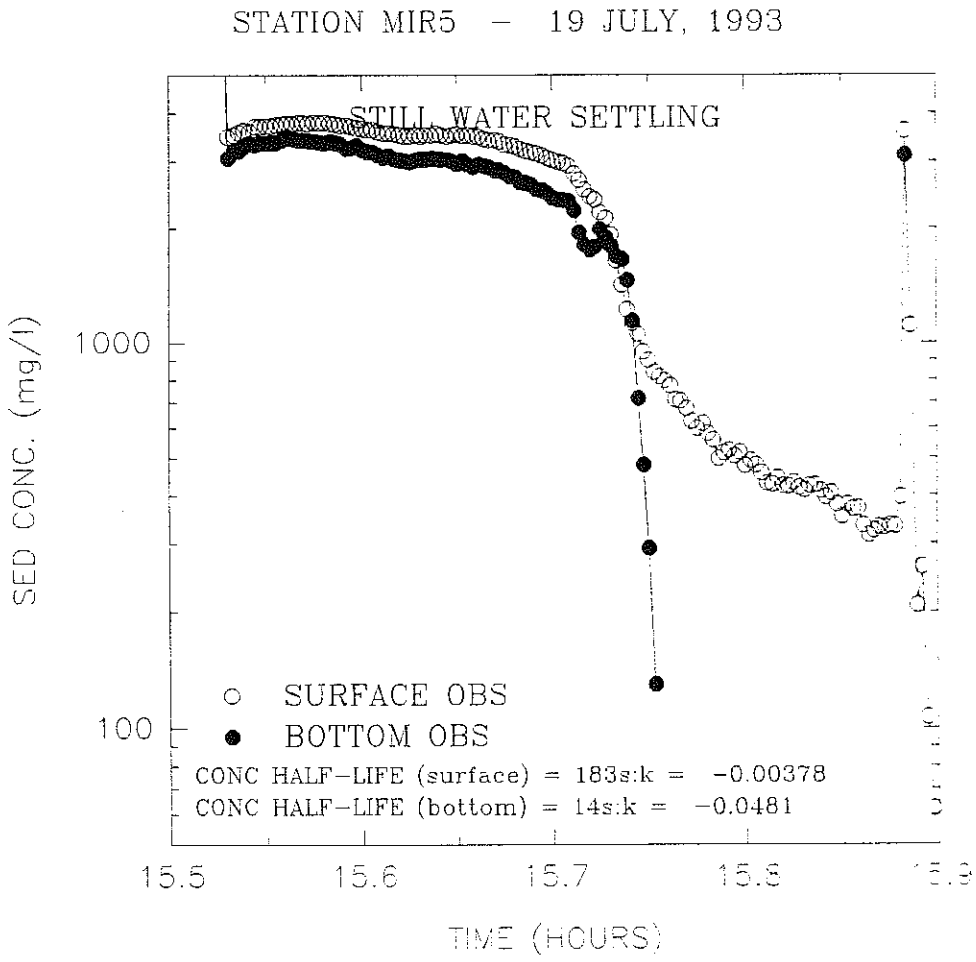

Figure 4.2.4.3-1. Relationship between sediment concentration and time during Sea Carousel settling rate measurements at Channel site MIR5 (Station 13).

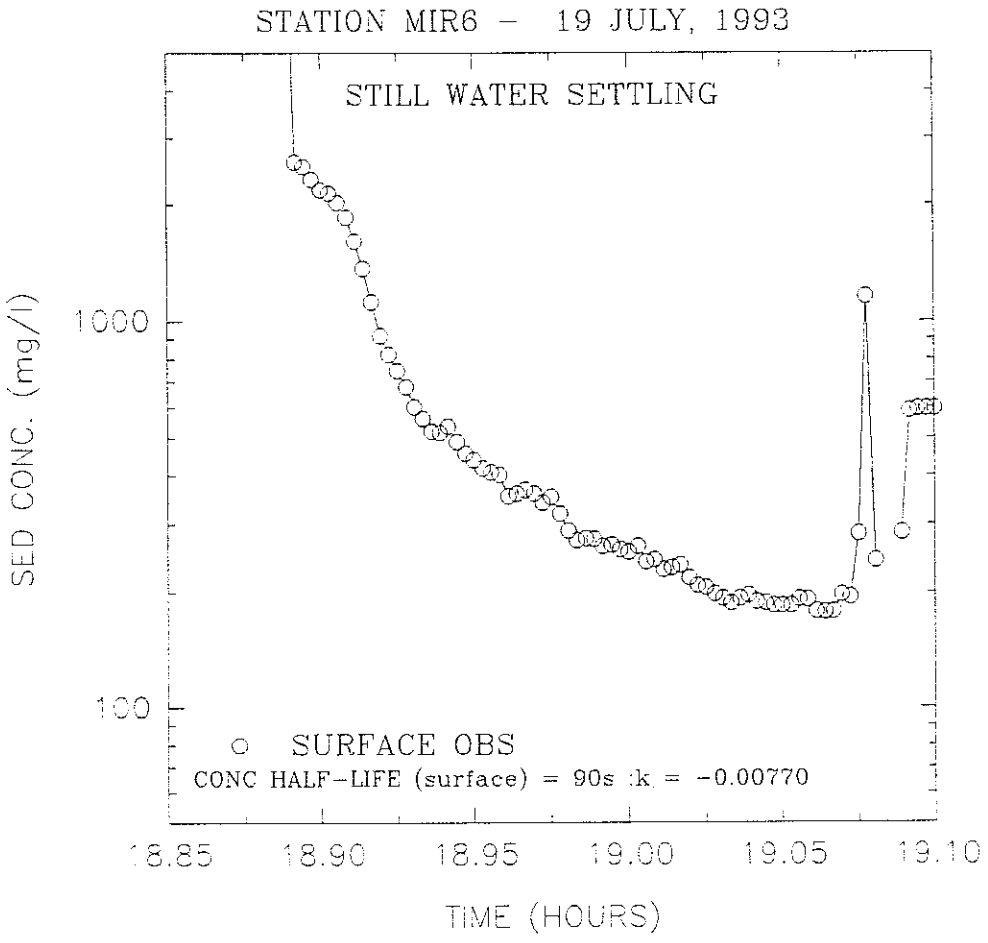

Figure 4.2.4.3-2. Relationship between sediment concentration and time during Sea Carousel settling rate measurements at Channel site MIR6 (Station 12).

contents within the Channel sediment. We also note that hindered settling was not detected in the Amos et al. (1992) laboratory study, nor was it evident at station MIR6.

4.2.5 Pre-disposal Experimental Site

Four stations were occupied at the Experimental site prior to deposition of spoils: MIR1 (Station 6); MIR2 (Station 7); MIR3 (Station 8); and MIR4 (Station 9). The water depths at these locations varied between 5.2 and 5.8 m. The water temperature was consistently 17.9 °C, and the seawater salinity was *circa* 22 ppt. Good results were obtained at all stations, although the low-light VHS system failed at the first two sites. The seabed was tested under eleven increments of velocity up to a lid rotational speed of *circa* 1.2 m sec^{-1}. Temporary failure of the power supply to the Sea Carousel motor led to a small gap in the results during station MIR1. Nevertheless, the stations show reasonably consistent trends in strength and stability. The time-series of the four stations are shown in Figures 4.2.5-1 to 4.2.5-4. The highest bed strengths of the survey were detected at this site. Also, all appear to have a stabilized surface and to be stable at depths below 2 mm.

4.2.5.1 Threshold Stresses for Bed Erosion

The plots used to derive the threshold stresses (surface) for stations MIR1 to MIR4 are shown in Figures 4.2.5.1-1 to 4.2.5.1-4, respectively. The values are generally the highest detected in the survey, varying up to 1.5 Pa. Stations MIR1 to MIR3 are remarkably similar suggesting a relatively homogenous seabed. The friction angles are all negative at the surface suggestive of biostabilization: i.e., adhesion produced by the mucilage of microorganisms (e.g., benthic diatoms, bacteria and fungi) has a stronger effect than does the cohesive strength of the sediment. This layer is between 1 and 2 mm thick. Beneath this surface layer, the bed strength increases with depth, presumably due to the dominating influences of consolidation by the overlying sediment column.

4.2.5.2 Erosion Rates

The erosion rates for the pre-disposal Experimental stations are plotted in panels C of Figures 4.2.5-1 to 4.2.5-4. The patterns of erosion largely follow type I (asymptotically decaying with time). The peaks in erosion rate at the onset of each speed increment are clearly seen in Figure 4.2.5-2, and the subsequent asymptotic decay is exemplified in Figures 4.2.5-3 and 4.2.5-4. We see no evidence for type IA erosion, as was evident in the Channel. We attribute this to lower levels of organic matter at this site, together with lower benthic invertebrate activity (seen in the video tapes). Type IB erosion prevails throughout. With reference to MIR1, the peak erosion (EP) shows a systematic increase with current speed, from 2×10^{-4} to 4×10^{-3} kg m^{-2} sec^{-1}. The base erosion rate (EB) is the minimum erosion rate detected at the end of each velocity increment. It too shows a systematic increase with current speed from 4×10^{-5} to 4×10^{-4} kg m^{-2} sec^{-1}. At current speeds in excess of 0.3 m sec^{-1}, both EP and EB remain relatively constant at values of 4×10^{-3} and 3×10^{-4} kg m^{-2} sec^{-1}, respectively. Neither EP nor EB show any overall relationship to either current speed or bed shear stress, as the highest erosion rates take place at intermediate current speeds. As at the

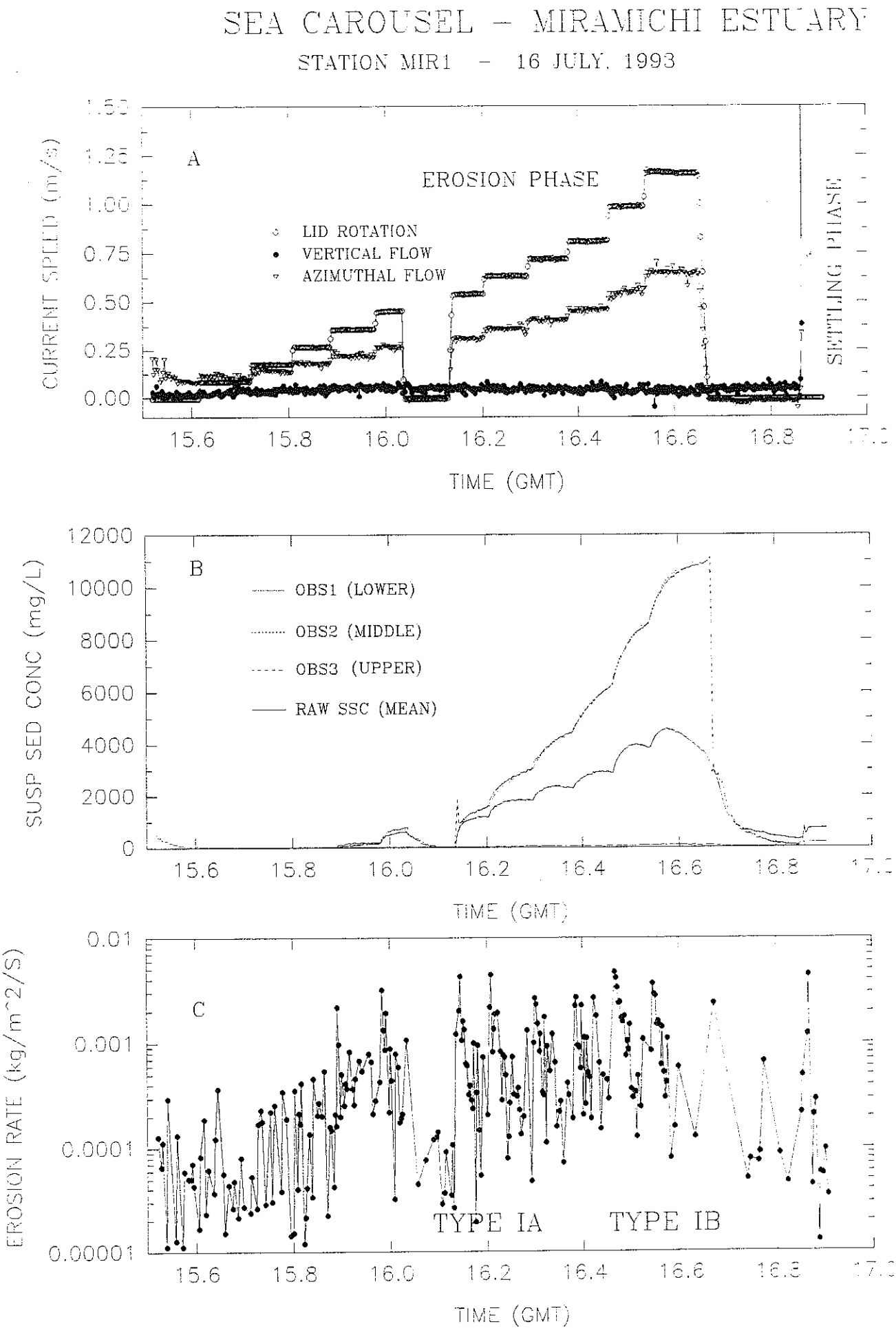

Figure 4.2.5-1. Time series of Sea Carousel results at pre-disposal Experimental site MIR1 (Station 6).

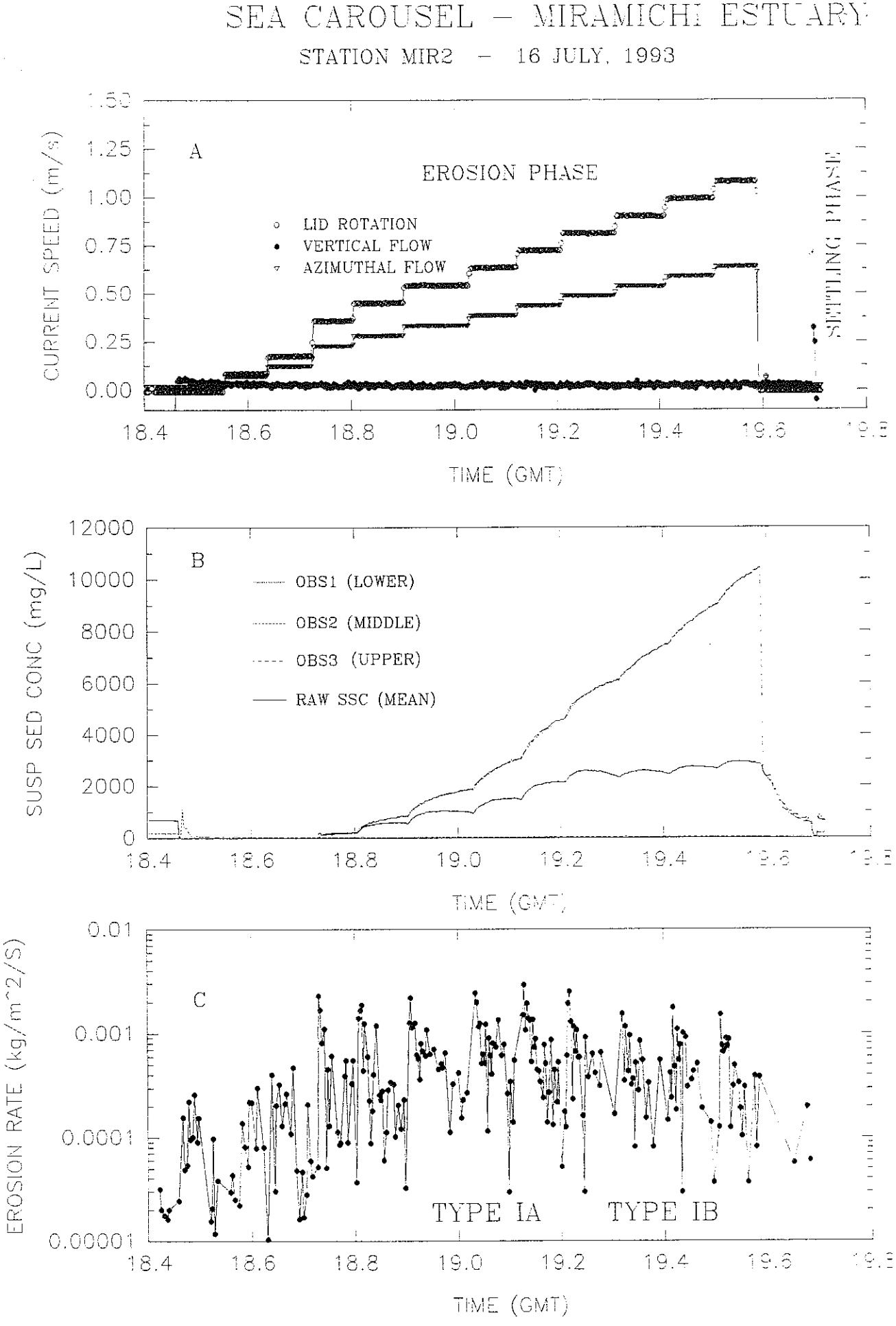

Figure 4.2.5-2. Time series of Sea Carousel results at pre-disposal Experimental site MIR2 (Station 7).

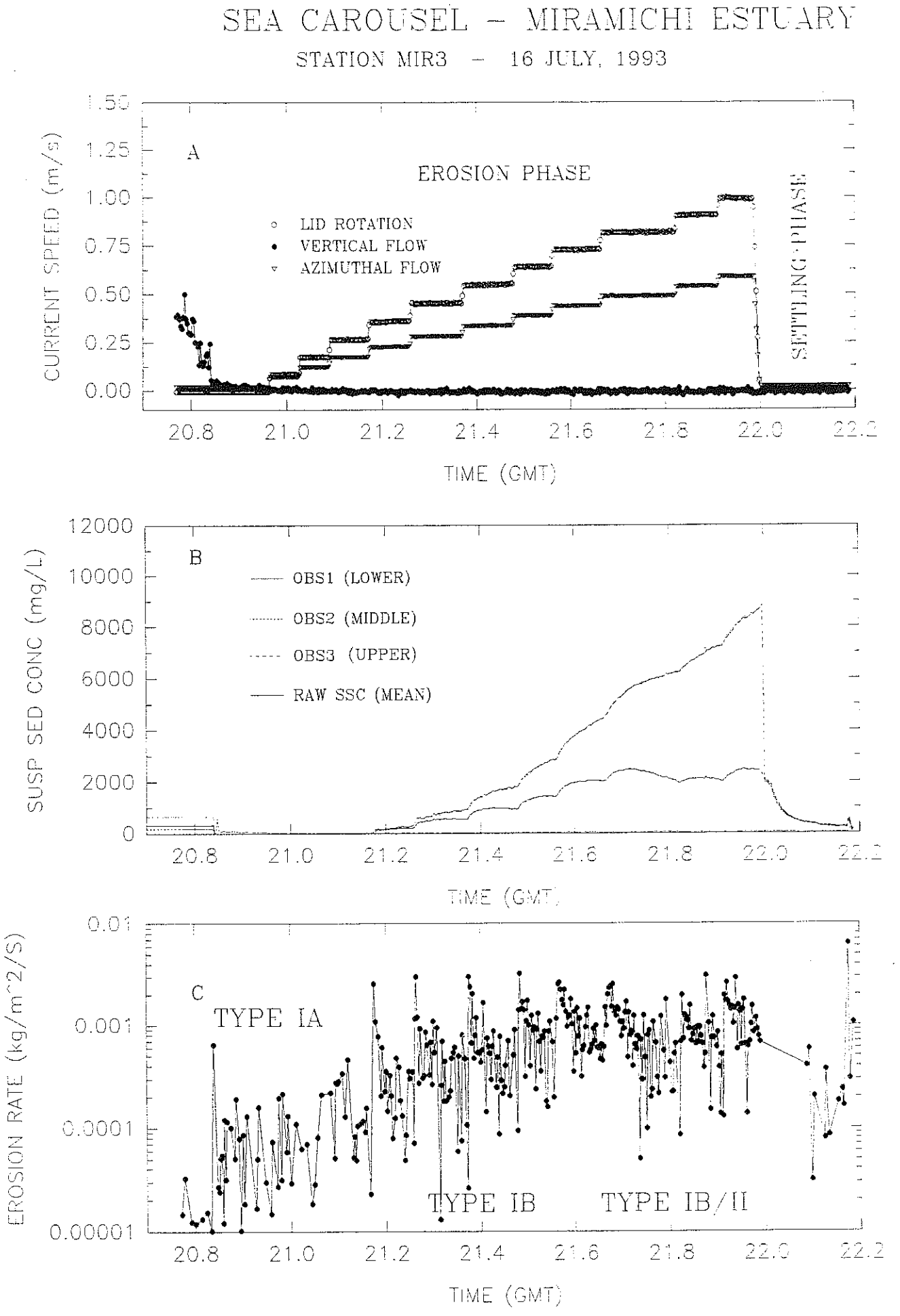

Figure 4.2.5-3. Time series of Sea Carousel results at pre-disposal Experimental site MIR3 (Station 8).

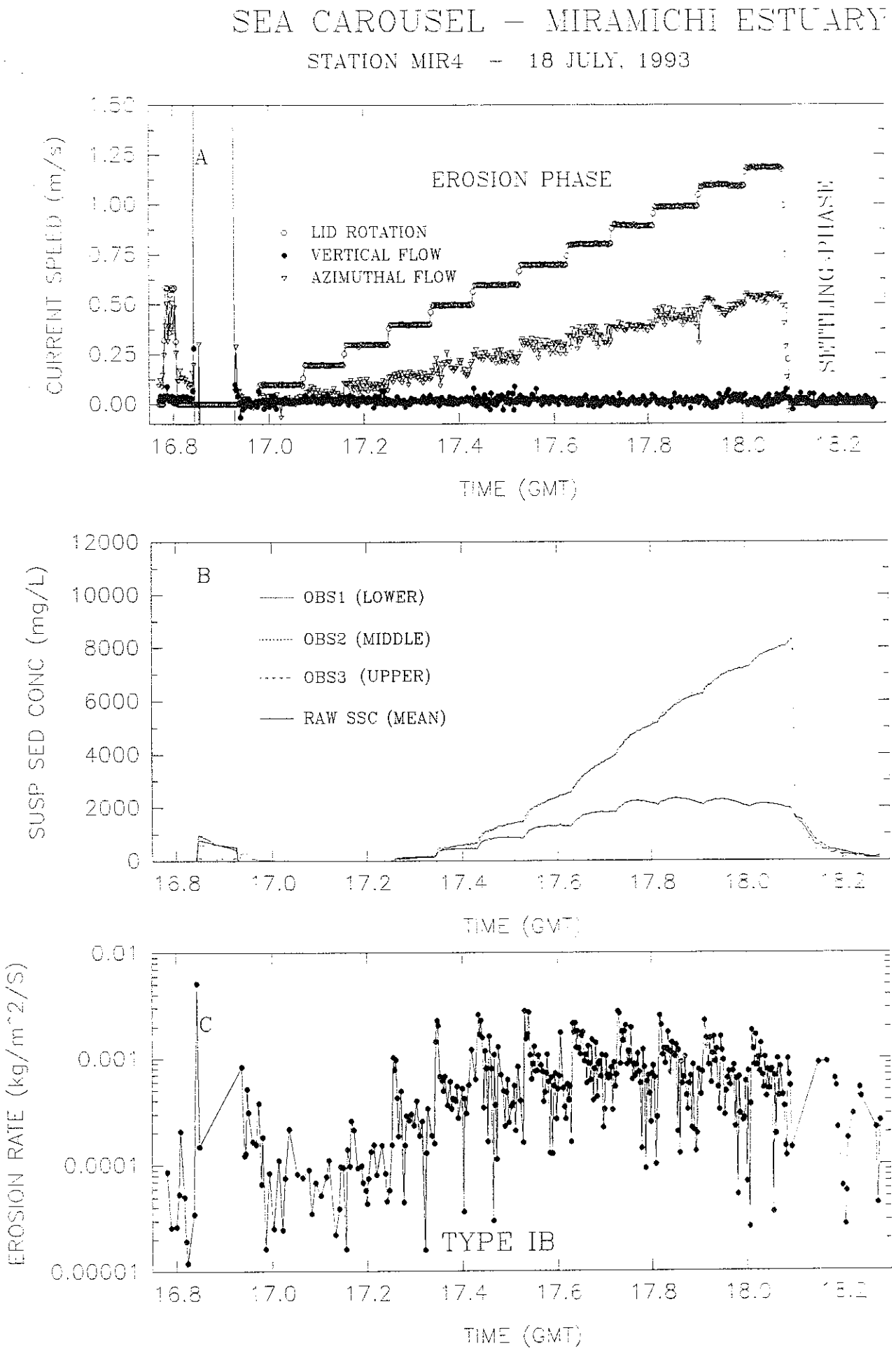

Figure 4.2.5-4. Time series of Sea Carousel results at pre-disposal Experimental site MIR3 (Station 9).

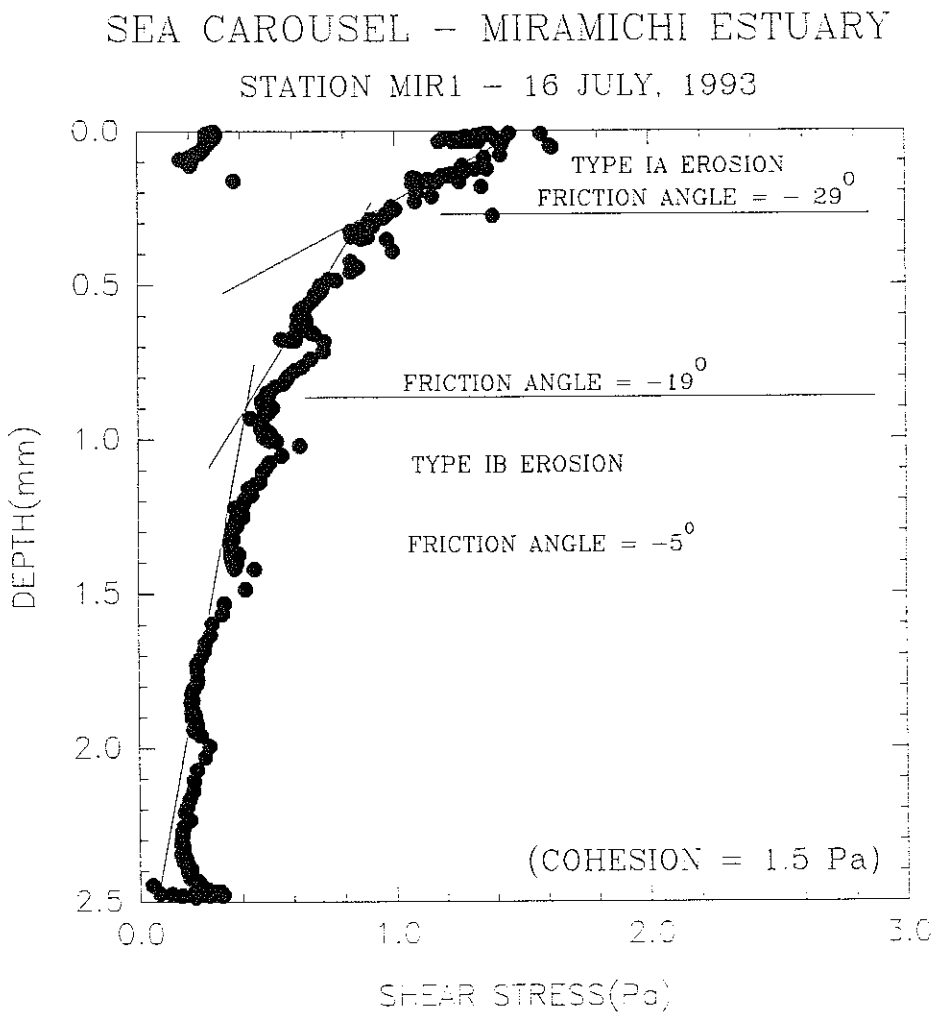

Figure 4.2.5.1-1. Relationship of shear stress and depth at pre-disposal Experimental site MIR1 (Station 6).

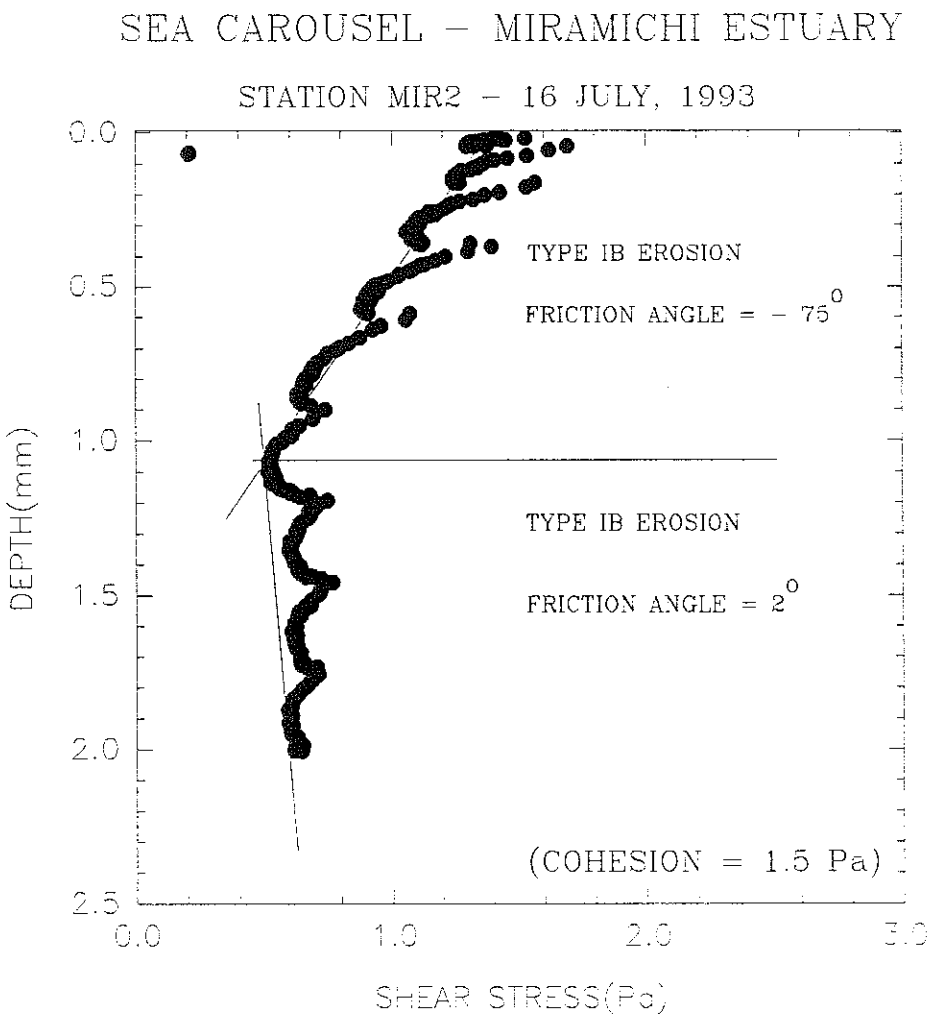

Figure 4.2.5.1-2. Relationship of shear stress and depth at pre-disposal Experimental site MIR2 (Station 7).

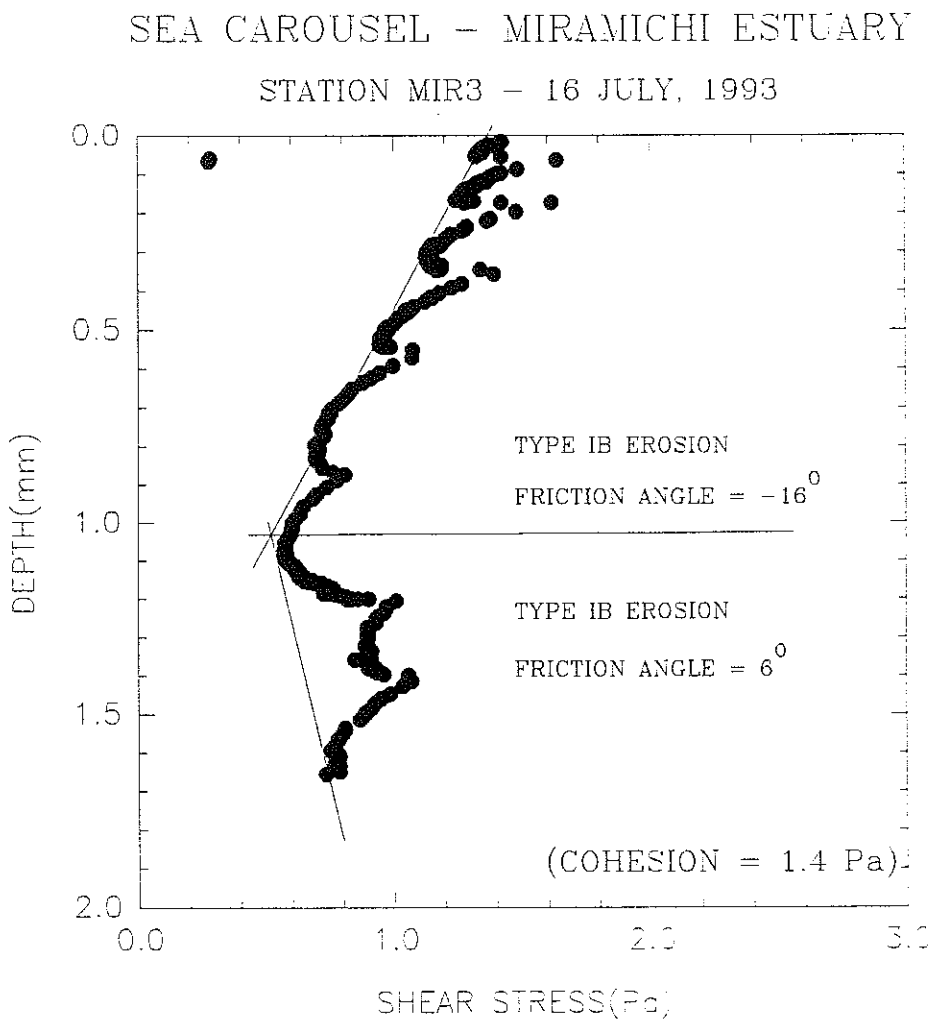

Figure 4.2.5.1-3. Relationship of shear stress and depth at pre-disposal Experimental site MIR3 (Station 8).

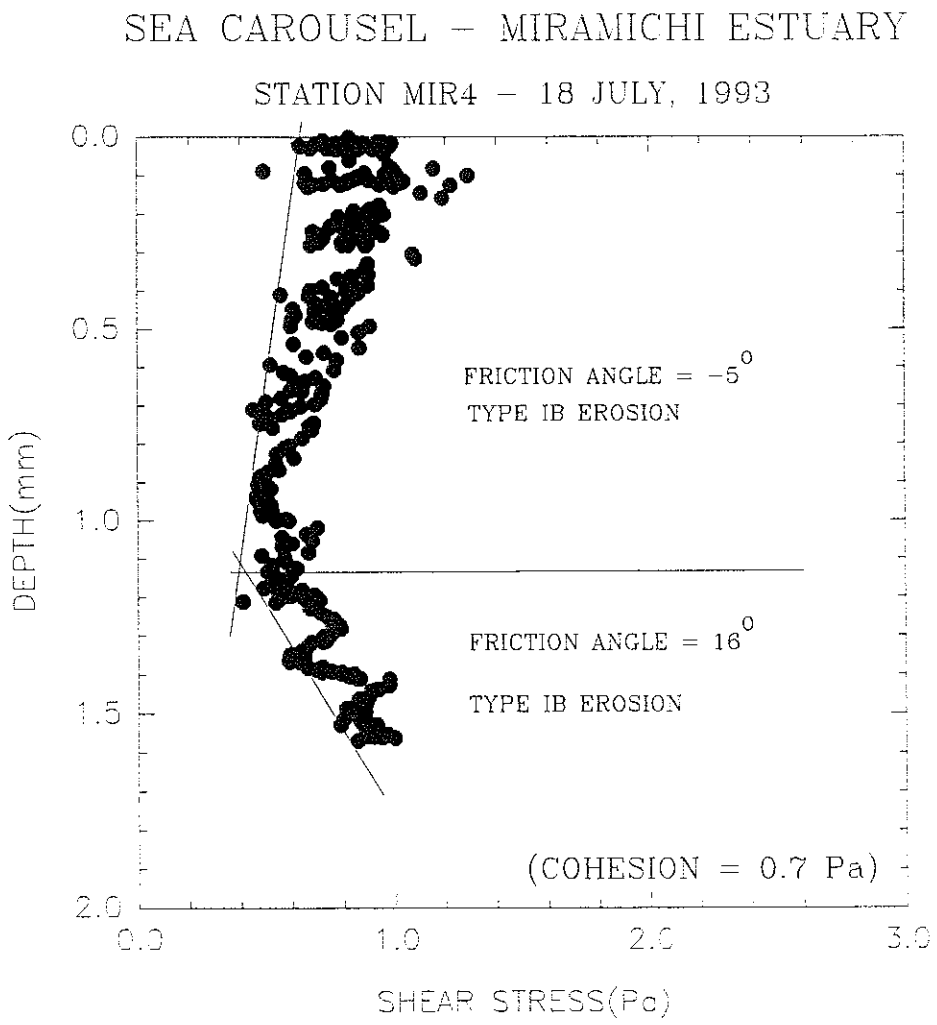

Figure 4.2.5.1-4. Relationship of shear stress and depth at pre-disposal Experimental site MIR4 (Station 9).

Channel sites, we observe two domains to bed erosion. The first, at flow speeds below 0.3 m sec^{-1}, is where erosion rate increases with current speed. The second, at flow speeds in excess of 0.3 m sec^{-1}, is where erosion rate remains more or less constant and independent of current speed.

4.2.5.3 Deposition Rates

The time-series for settling for stations MIR1 to MIR4 are shown in Figures 4.2.5.3-1 to 4.2.5.3-4, respectively. The deposition rates show a significant variation in trends between the near-surface and near-bed measures. The near-surface half-lives vary from 57 to 298 sec (a factor of 6). By contrast, the near-bed measures are stable and constant, varying only between 111 and 129 sec. That is, the SSC will be approximately halved each 2 min. Even the highest SSC's generated in Sea Carousel (6000 mg l^{-1}) settled to near-ambient conditions within 10 min. This indicates that the potential for long term fluid mud generation at these sites is very low.

4.2.6 Post-disposal Experimental Site

Eleven stations were occupied on material excavated from the navigation channel and newly disposed within the Experimental disposal site. These stations are MIR7 (Station 8), MIR8 (Station 20), MIR9 (Station 21), MIR10 (Station 22), MIR11 (Station 23), MIR15 (Station 28), MIR16 (Station 29), MIR17 (Station 30), MIR18 (Station 32), MIR19 (Station 33) and MIR20 (Station 34). The time-series of the eleven stations are shown in Figures 4.2.6-1 to 4.2.6-11. Most stations were subjected to twelve increments of increasing lid rotation of equal magnitude. Stations MIR5, MIR8 and MIR18 were subjected to less increments of longer intervals due to logistical constraints. The change in procedure produced no obvious effect on the results. These stations exhibited the greatest variability in both the threshold for erosion and in terms of sediment stability (friction angle). The mean threshold stress (*circa* 0.7 Pa) is approximately half that of the underlying pre-disposal seabed. It is also significantly less than the original Channel material before dredging, indicating a loss of strength during the dredging and disposal process. Nevertheless, there is a general trend towards increasing strength with time. Within three days, it had recovered much of its former strength. This recovery may be related to biostabilization process by microorganisms, particularly bacteria and fungi.

4.2.6.1 Threshold Stresses for Bed Erosion

The thresholds for erosion were derived from Figures 4.2.6.1-1 to 4.2.6.1-11. These thresholds varied considerably from site to site and with time. The mean threshold was 0.7 Pa. The friction angles were also highly variable, being both negative and positive. The scatter in results is probably due to the blocky nature of the dredged material. Upon disposal, these blocks will present, at the mudline, sediment from a range of depths that is controlled by the dredging depth. As well, a range of orientations and attitudes would be expected in the blocky disposed material. Despite the scatter, there appears to be a trend in results that suggests an increase in the erosion threshold with time. The approximate age of the disposed

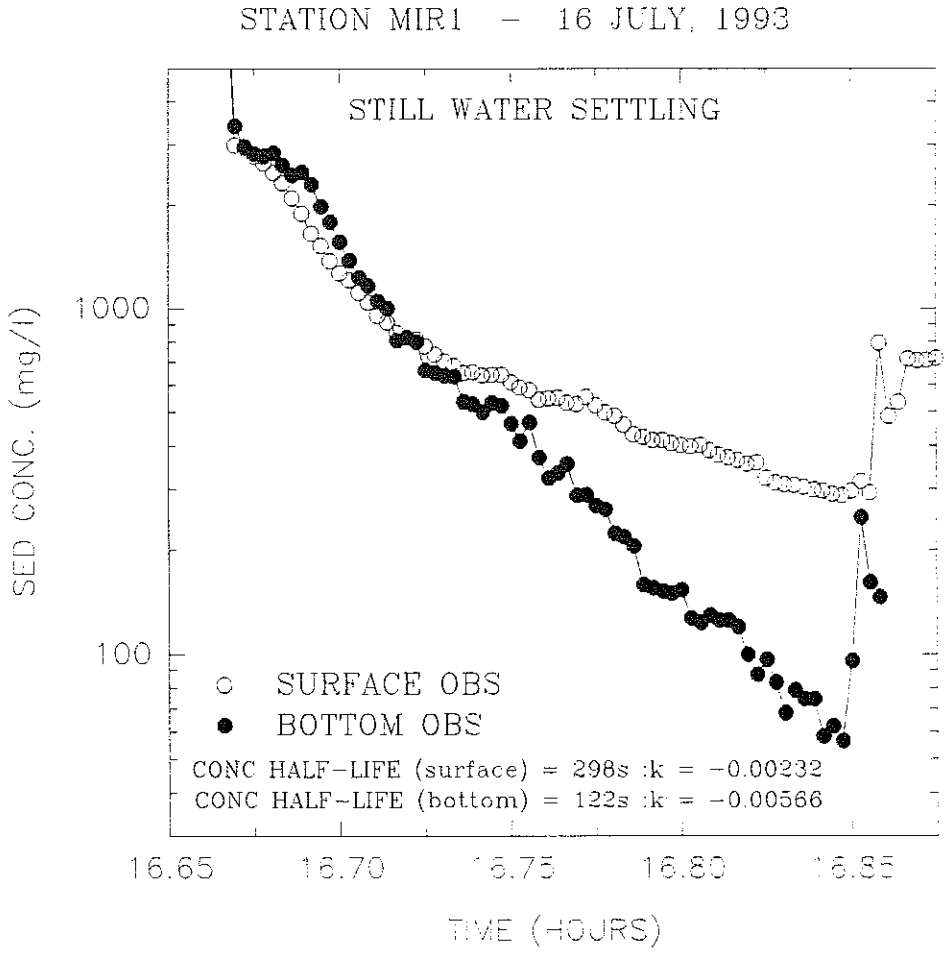

Figure 4.2.5.3-1. Relationship between sediment concentration and time during Sea Carousel settling rate measurements at pre-disposal Experimental site MIR1 (Station 6).

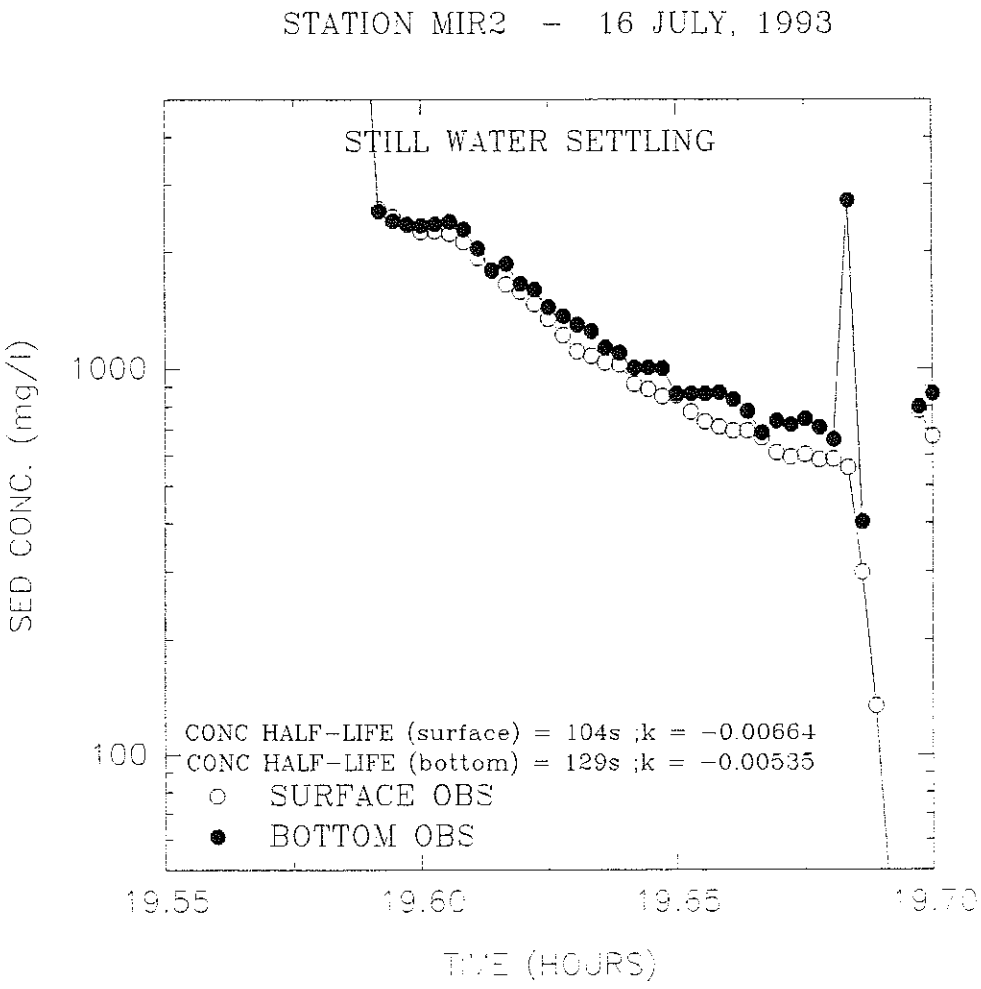

Figure 4.2.5.3-2. Relationship between sediment concentration and time during Sea Carousel settling rate measurements at pre-disposal Experimental site MIR2 (Station 7).

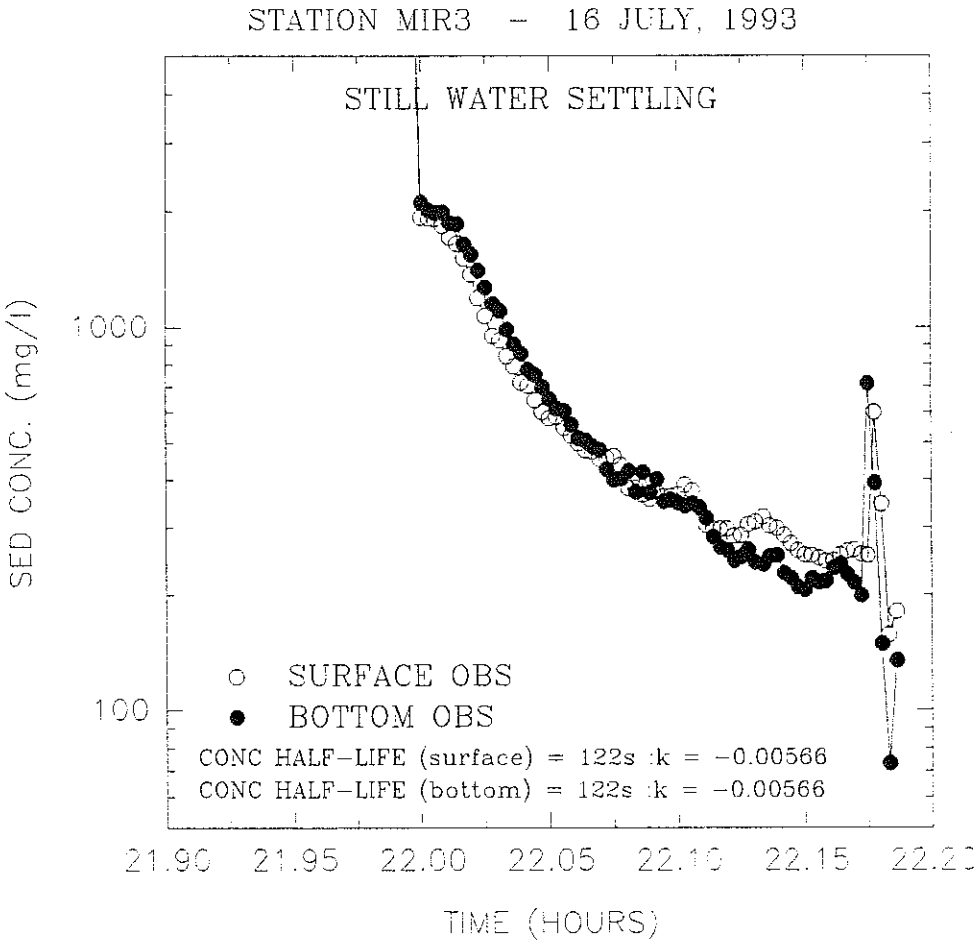

Figure 4.2.5.3-3. Relationship between sediment concentration and time during Sea Carousel settling rate measurements at pre-disposal Experimental site MIR3 (Station 8).

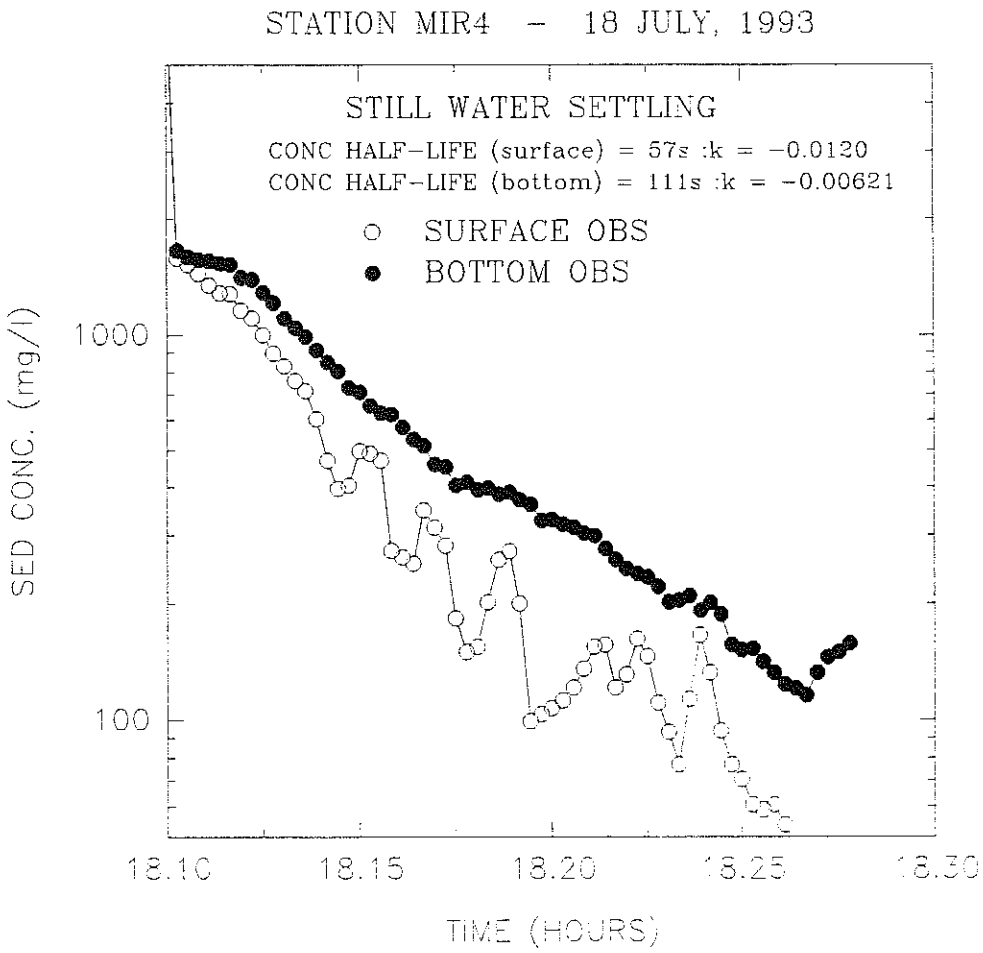

Figure 4.2.5.3-4. Relationship between sediment concentration and time during Sea Carousel settling rate measurements at pre-disposal Experimental site MIR4 (Station 9).

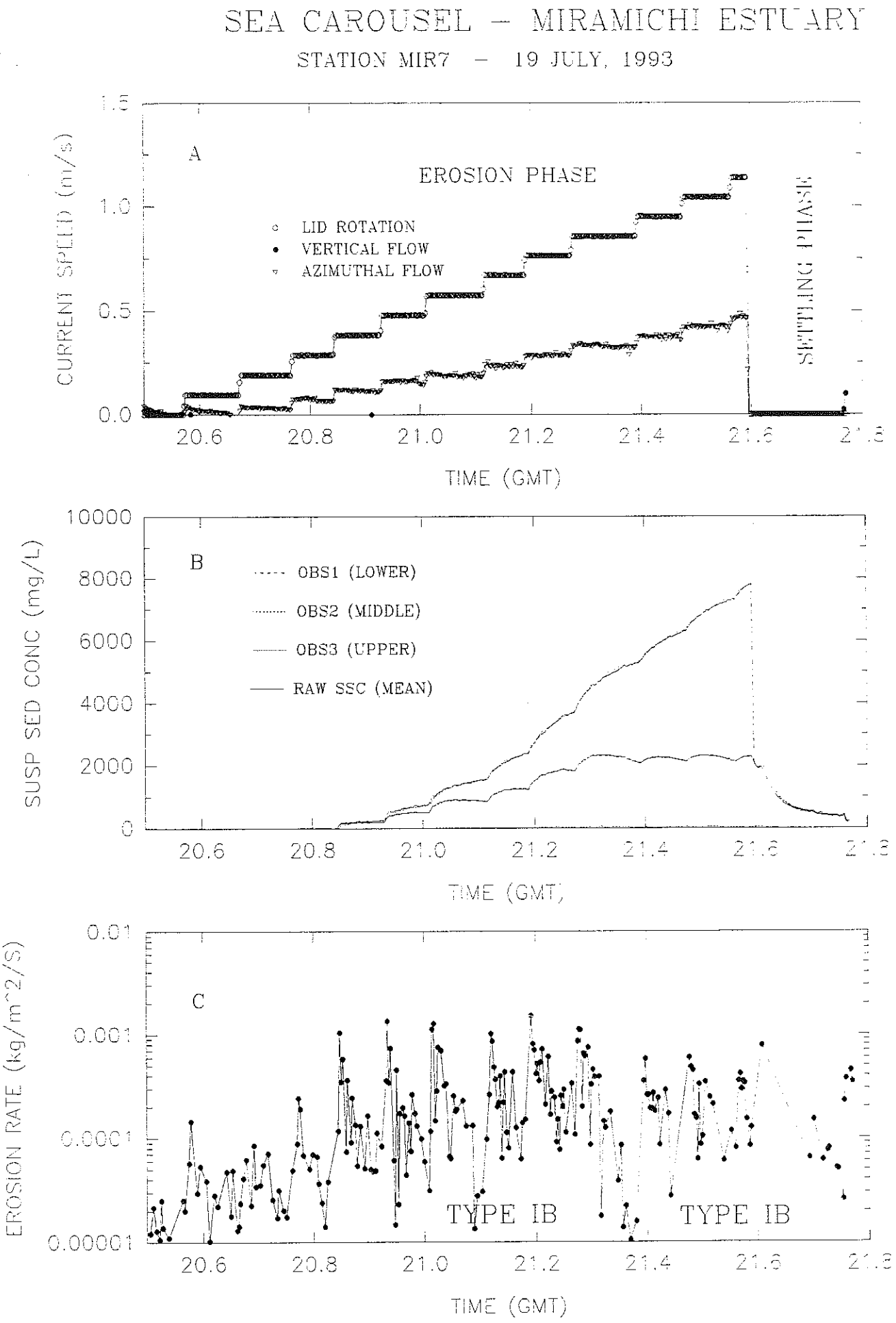

Figure 4.2.6-1. Time series of Sea Carousel results at post-disposal Experimental site MIR7 (Station 8).

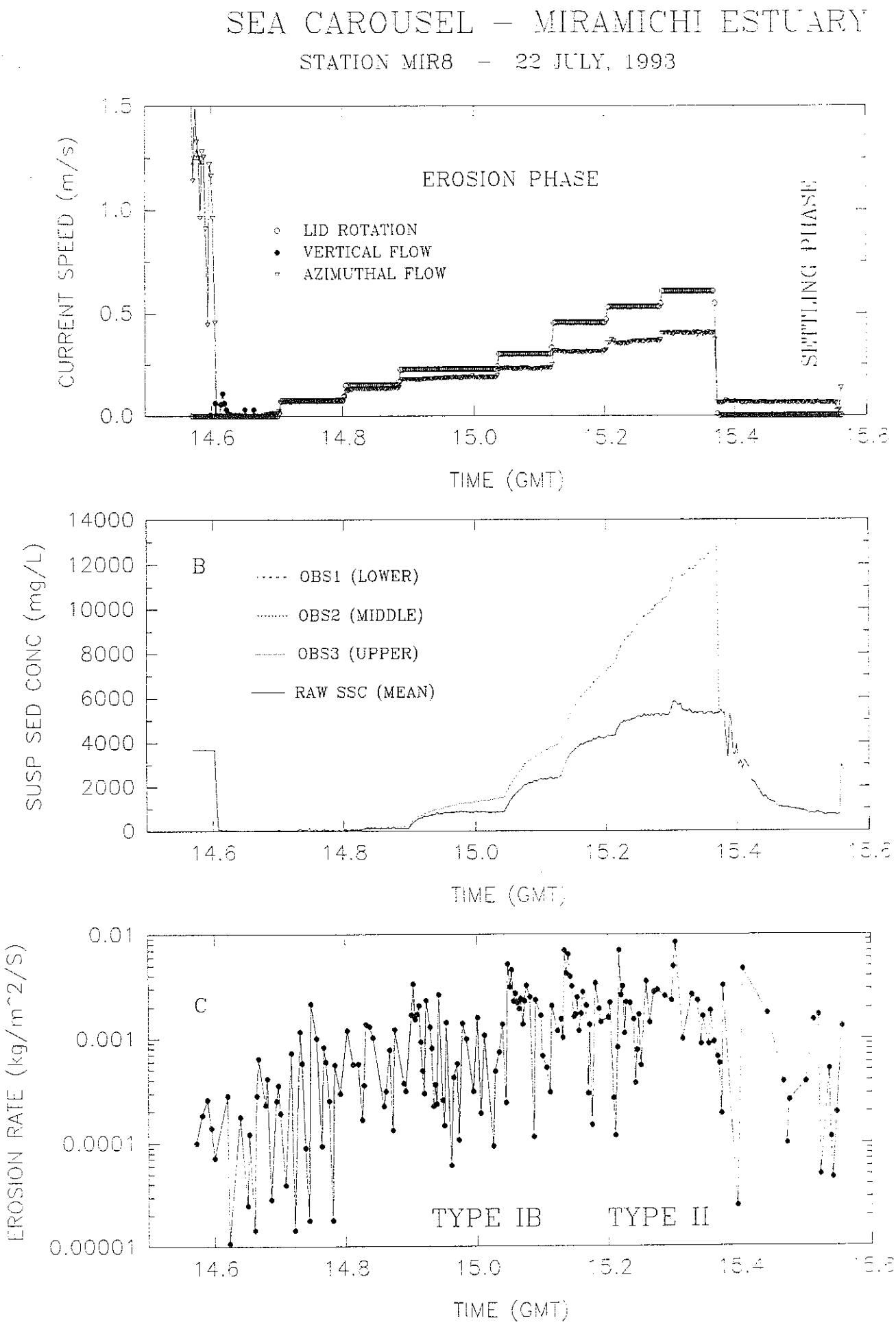

Figure 4.2.6-2. Time series of Sea Carousel results at post-disposal Experimental site MIR8 (Station 20).

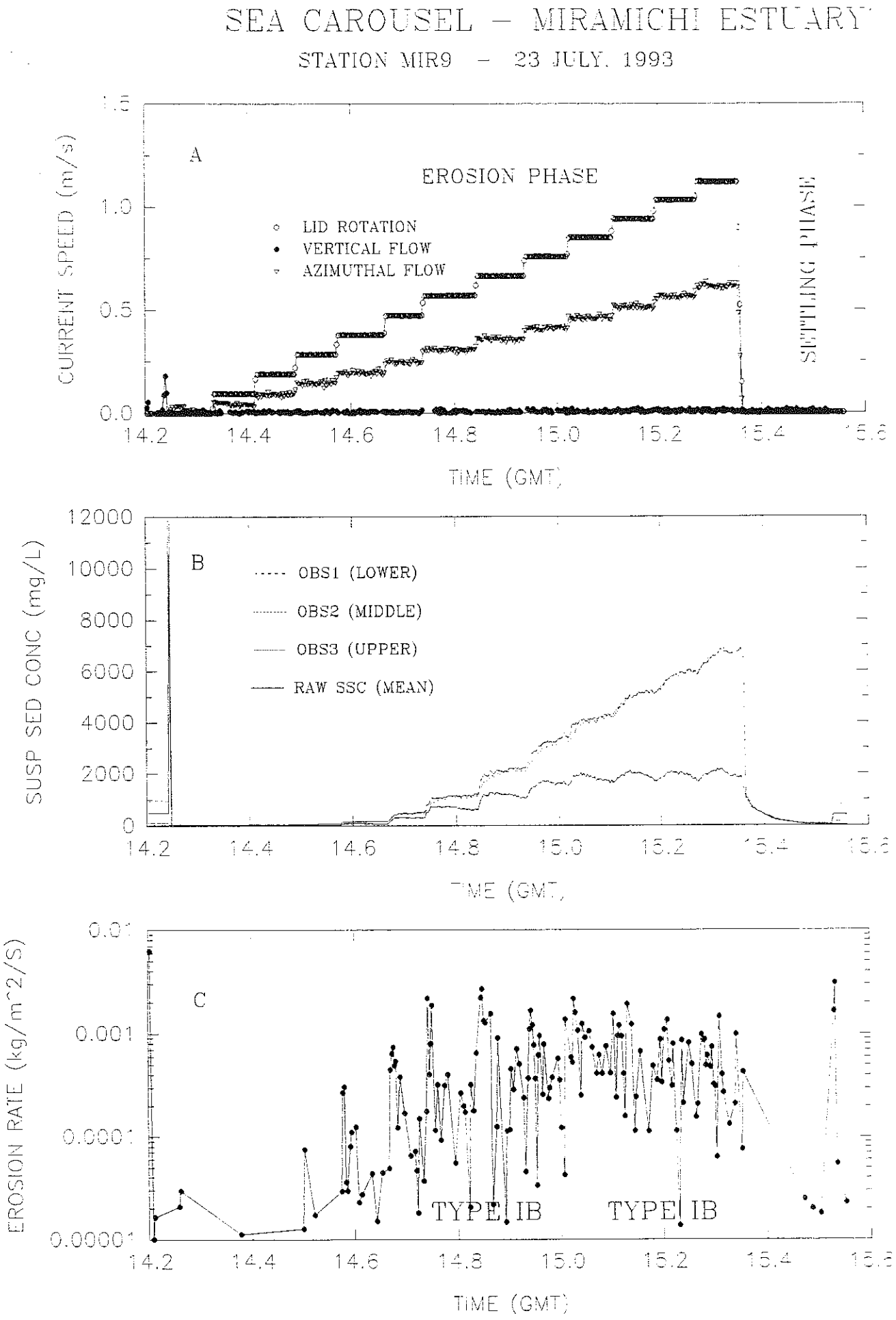

Figure 4.2.6-3. Time series of Sea Carousel results at post-disposal Experimental site MIR9 (Station 21).

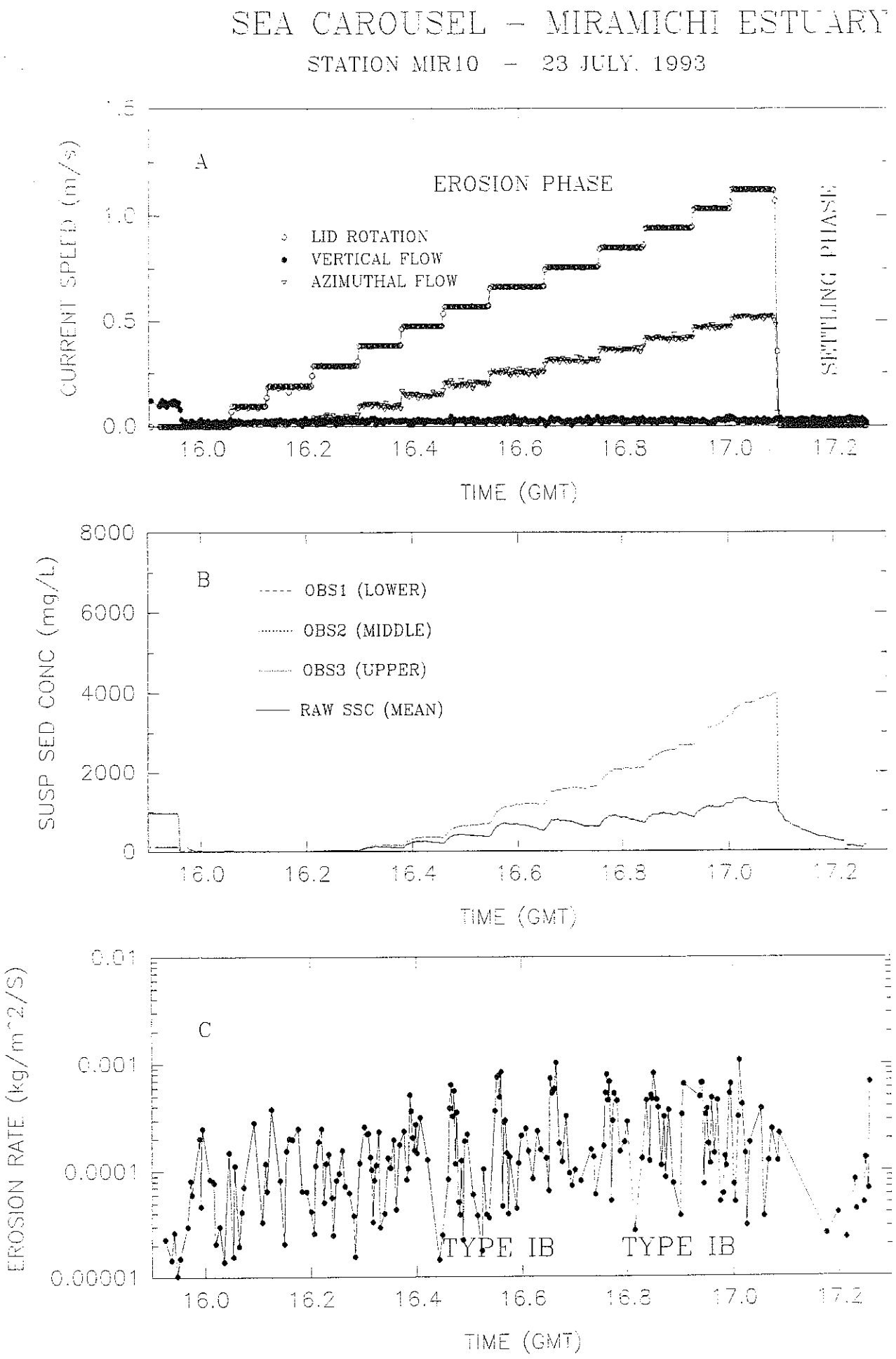

Figure 4.2.6-4. Time series of Sea Carousel results at post-disposal Experimental site MIR10 (Station 22).

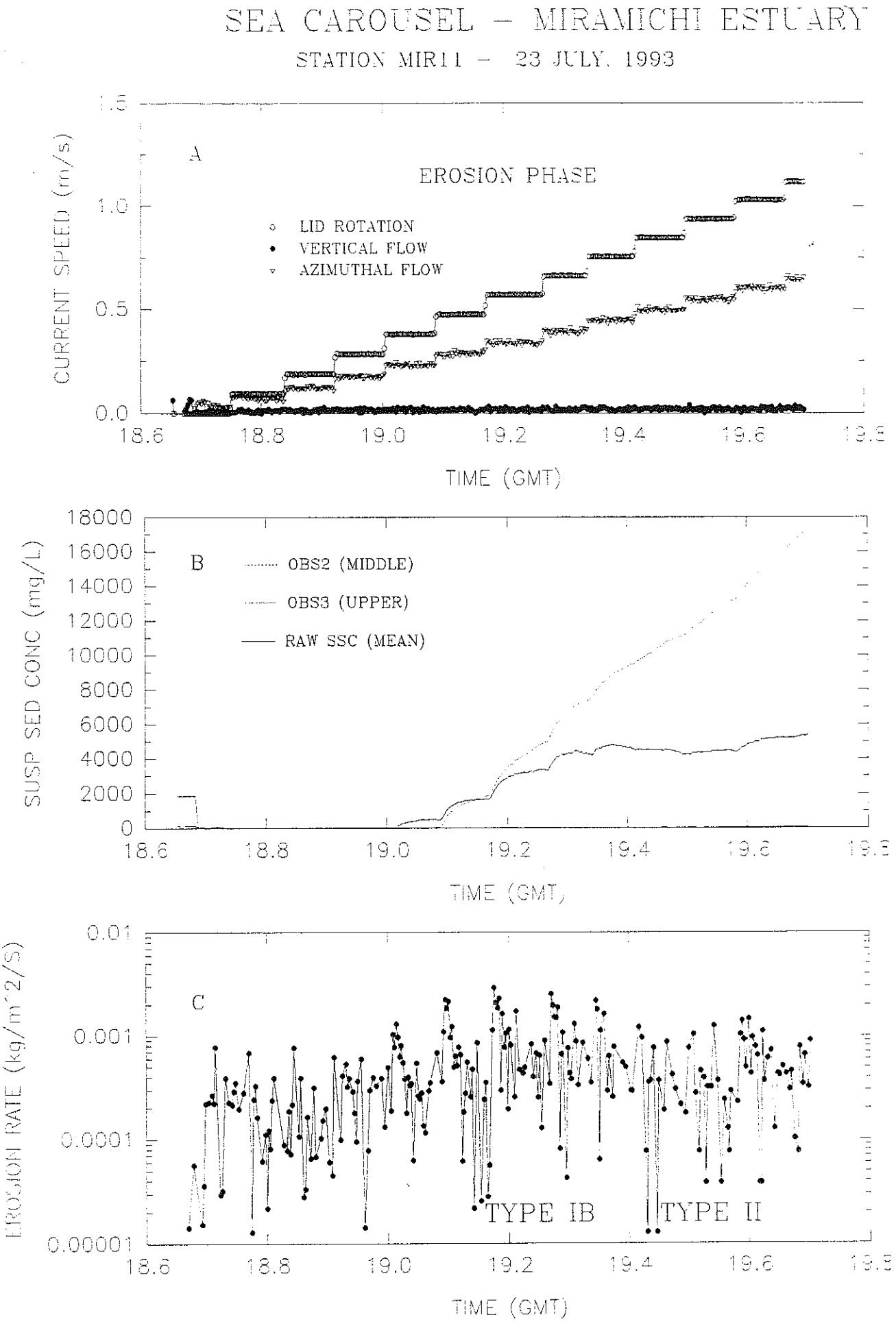

Figure 4.2.6-5. Time series of Sea Carousel results at post-disposal Experimental site MIR11 (Station 23).

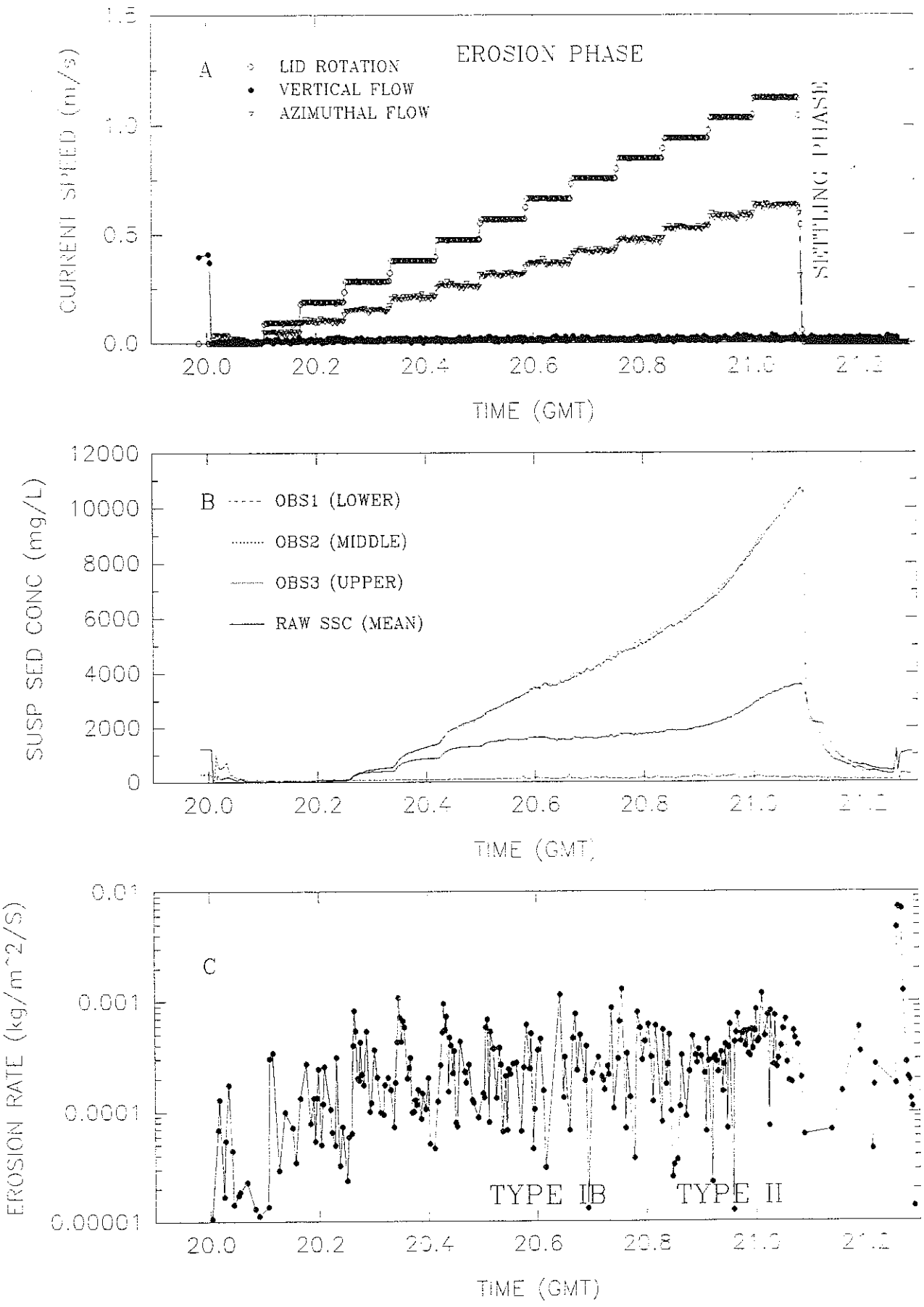

Figure 4.2.6-6. Time series of Sea Carousel results at post-disposal Experimental site MIR15 (Station 28).

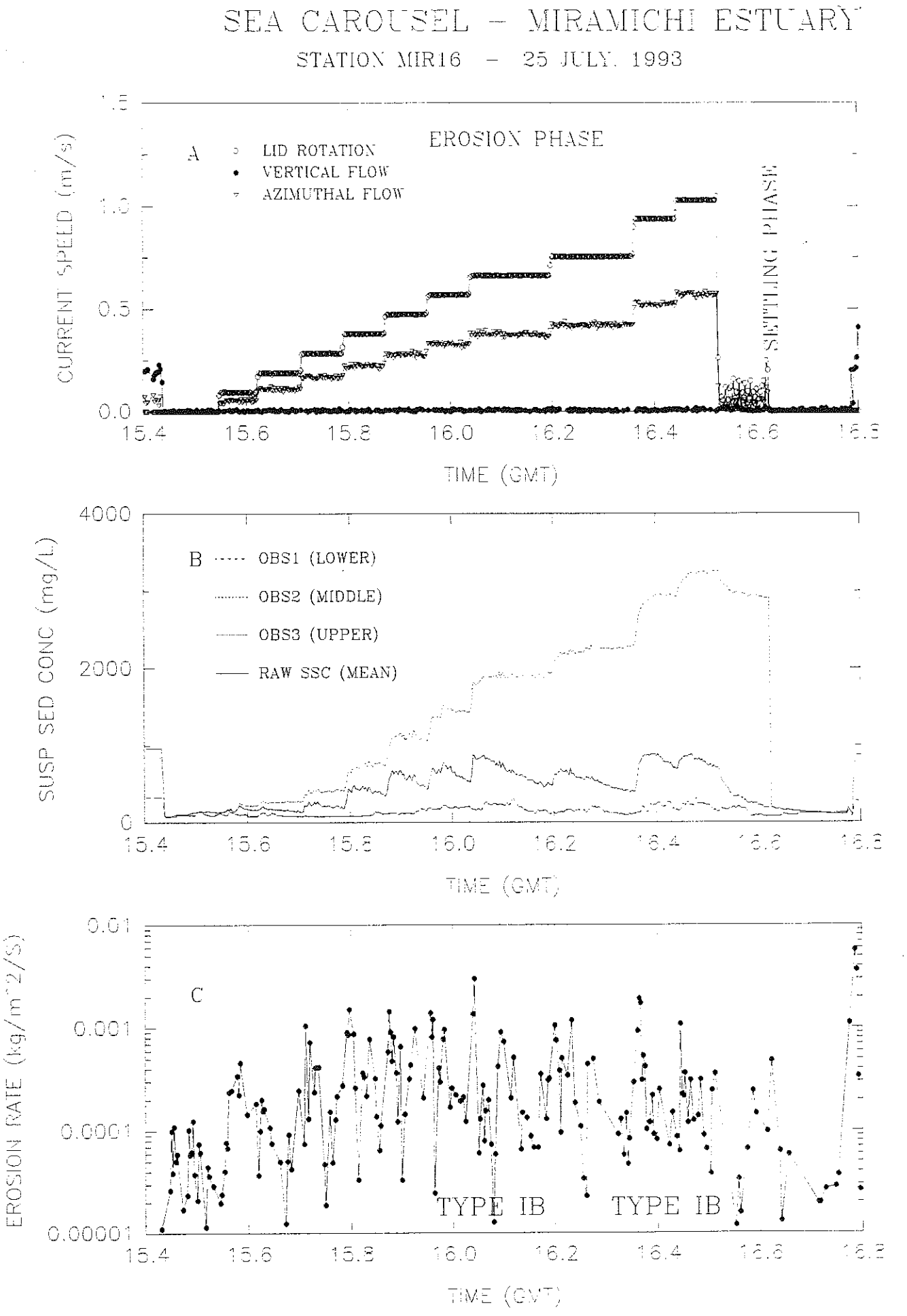

Figure 4.2.6-7. Time series of Sea Carousel results at post-disposal Experimental site MIR16 (Station 29).

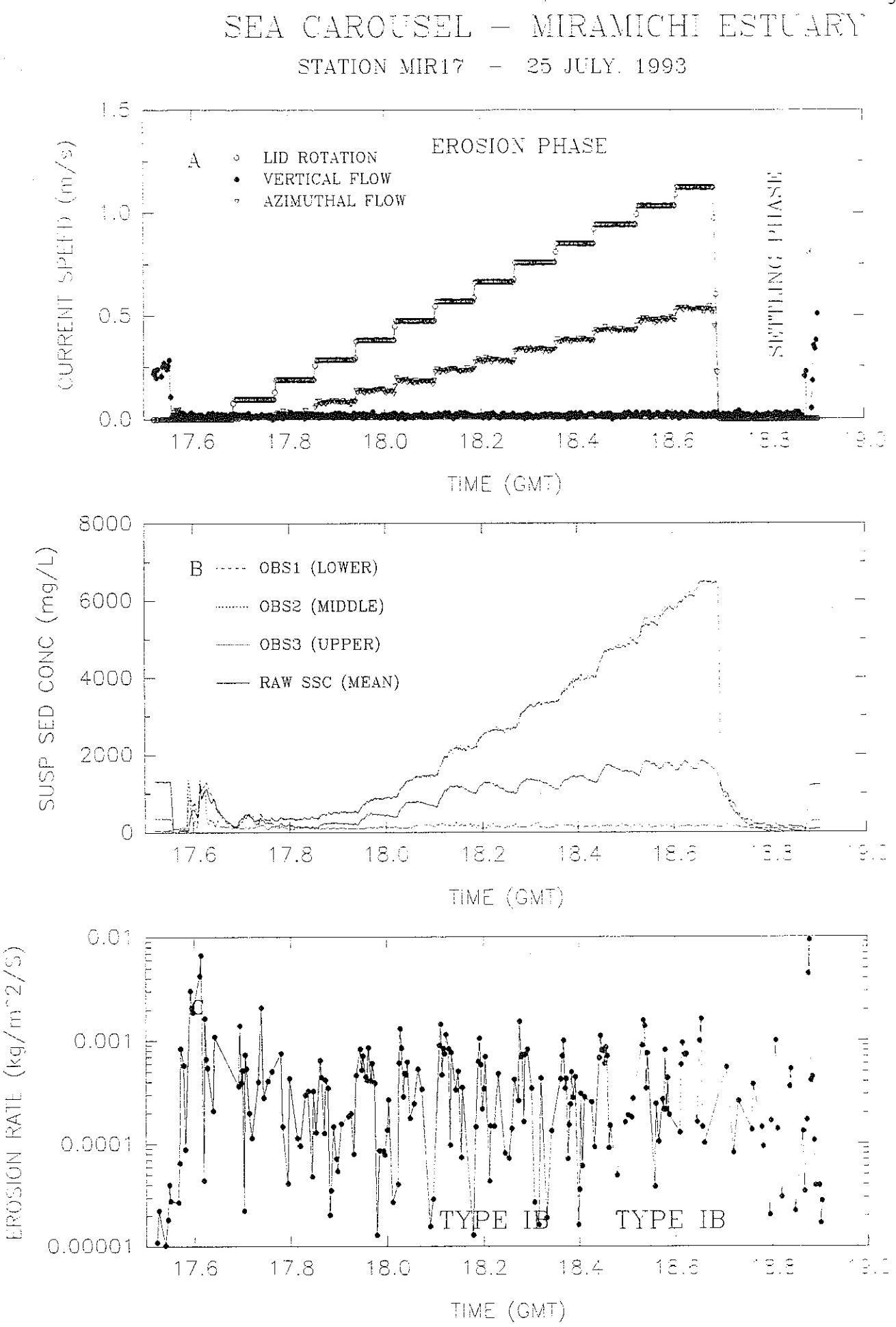

Figure 4.2.6-8. Time series of Sea Carousel results at post-disposal Experimental site MIR17 (Station 30).

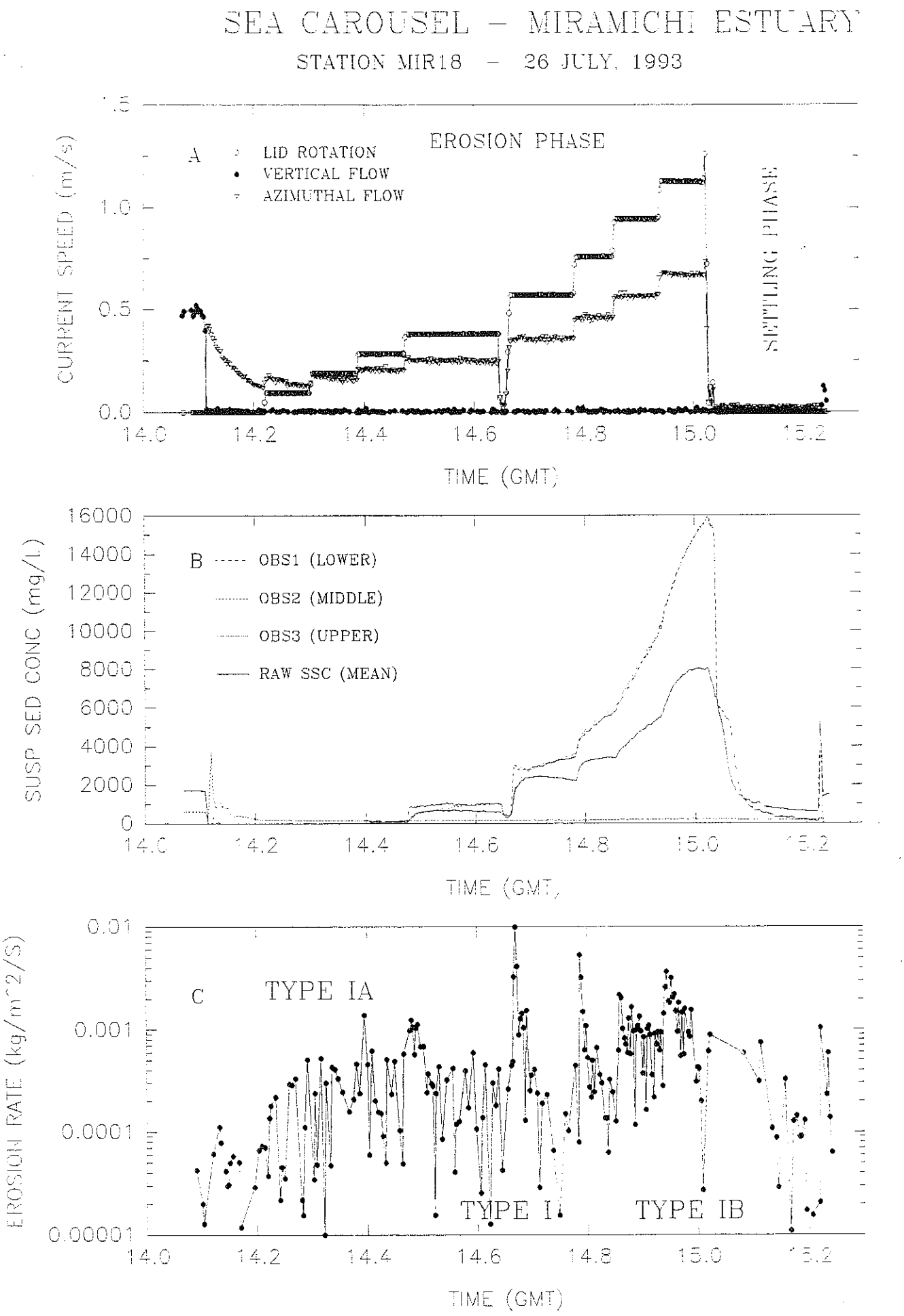

Figure 4.2.6-9. Time series of Sea Carousel results at post-disposal Experimental site MIR18 (Station 32).

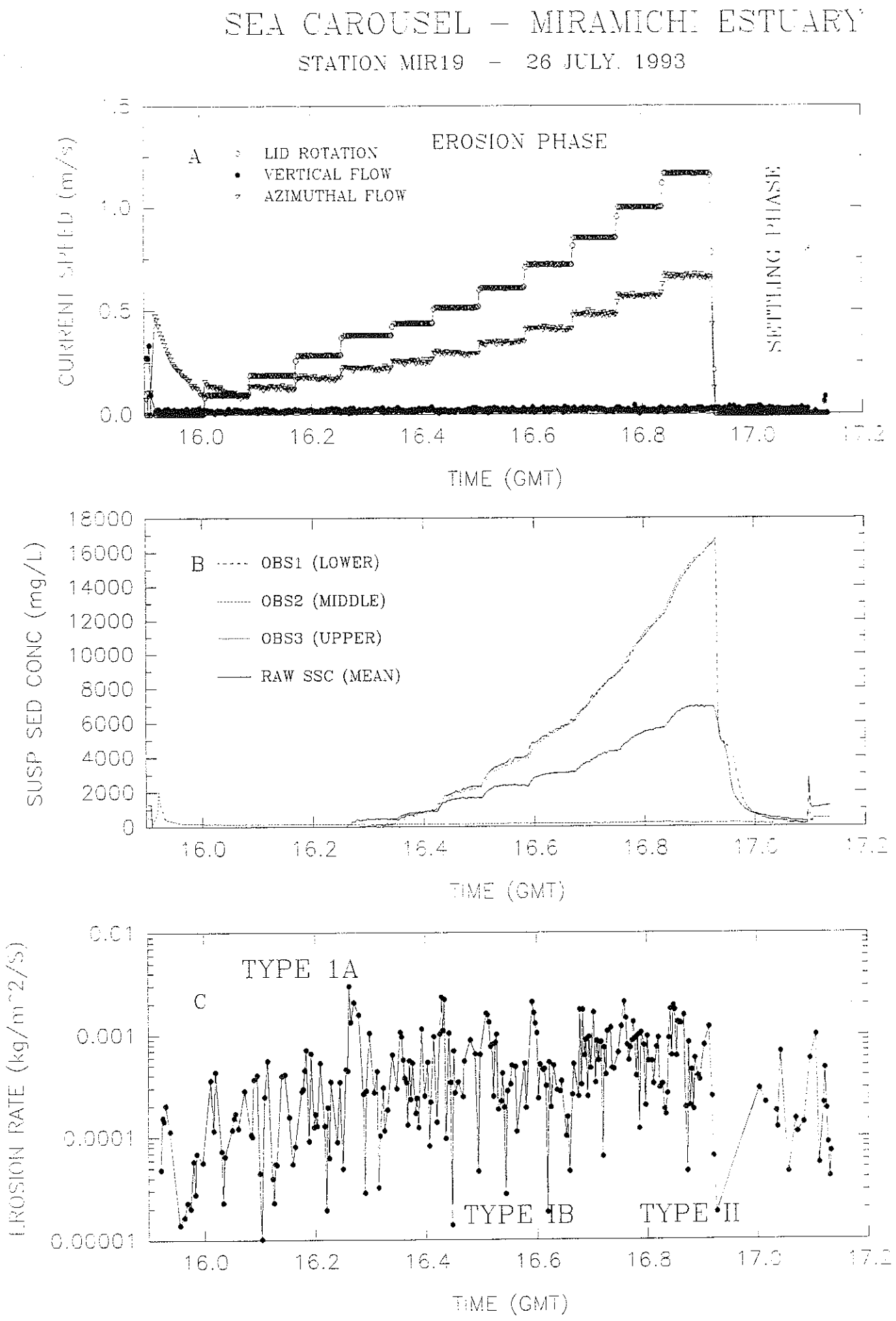

Figure 4.2.6-10. Time series of Sea Carousel results at post-disposal Experimental site MIR19 (Station 33).

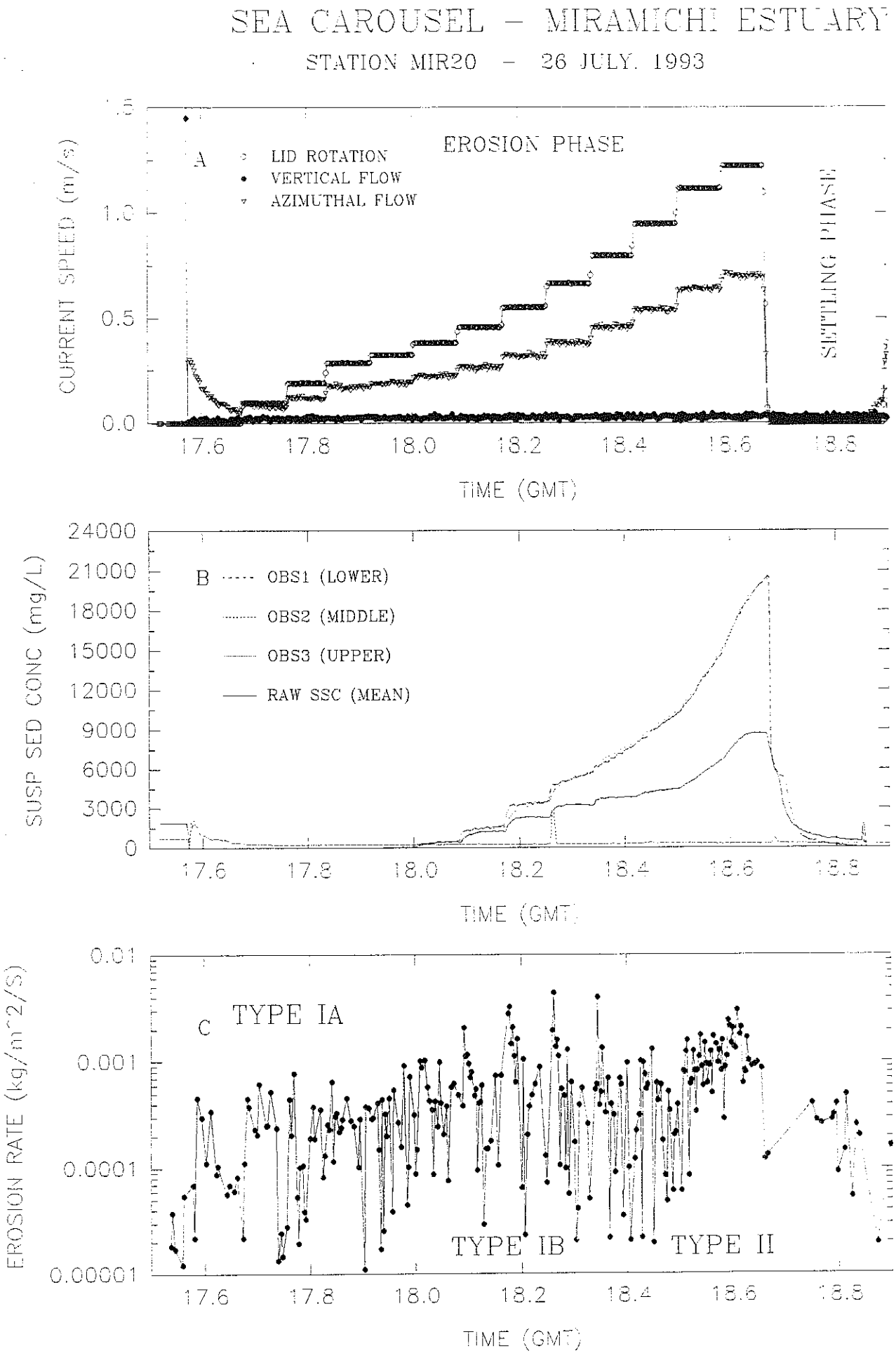

Figure 4.2.6-11. Time series of Sea Carousel results at post-disposal Experimental site MIR20 (Station 34).

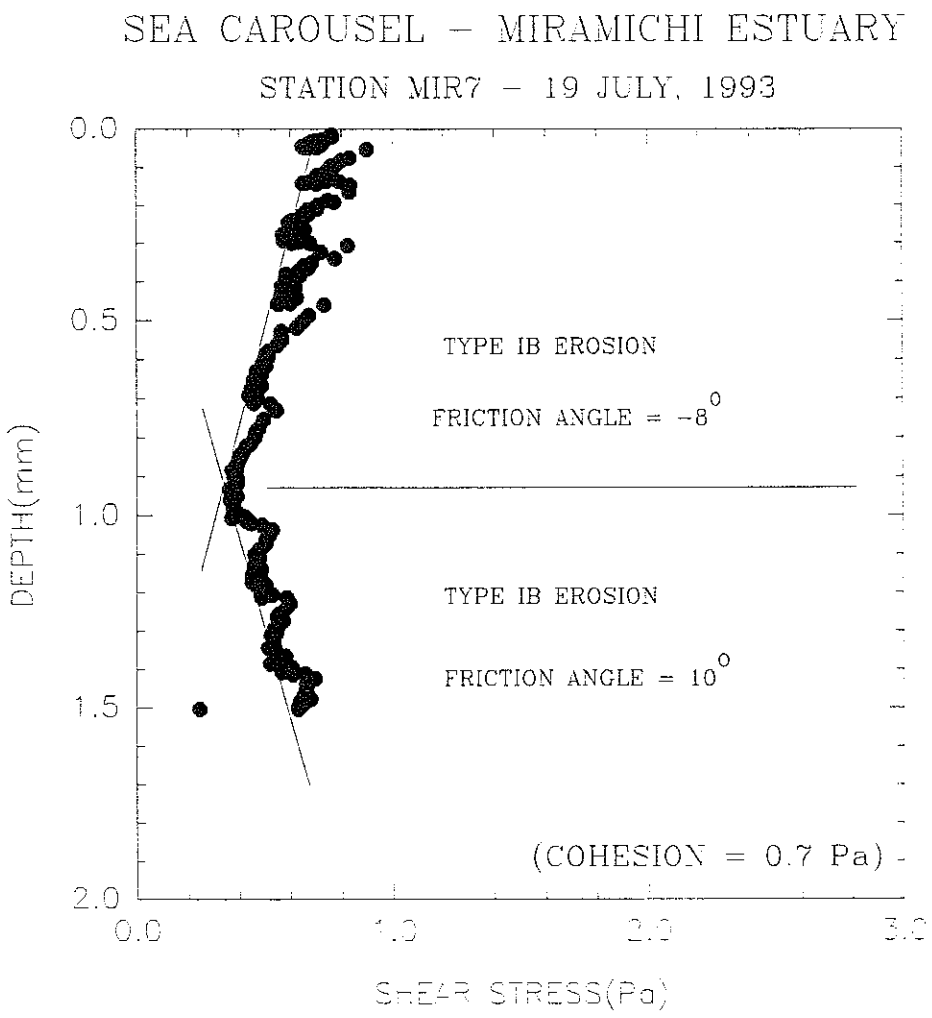

Figure 4.2.6.1-1. Relationship of shear stress and depth at post-disposal Experimental site MIR7 (Station 8).

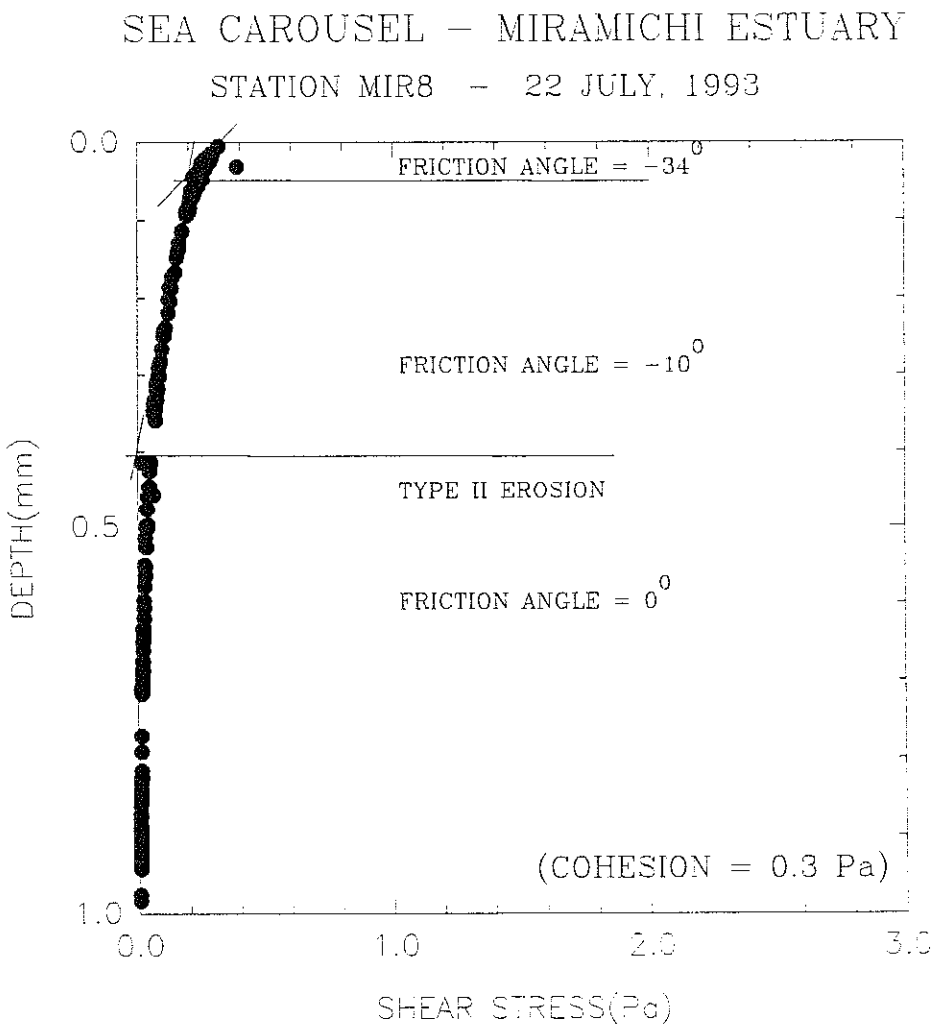

Figure 4.2.6.1-2. Relationship of shear stress and depth at post-disposal Experimental site MIR8 (Station 20).

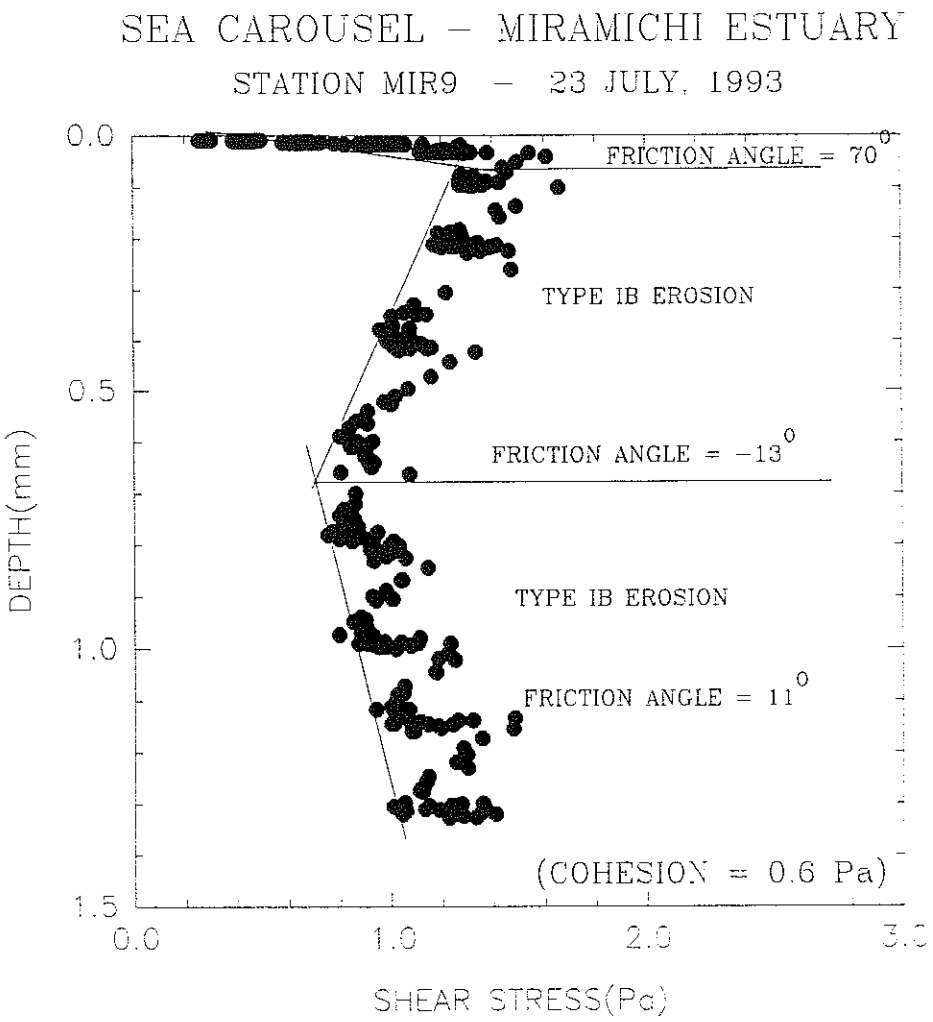

Figure 4.2.6.1-3. Relationship of shear stress and depth at post-disposal Experimental site MIR9 (Station 21).

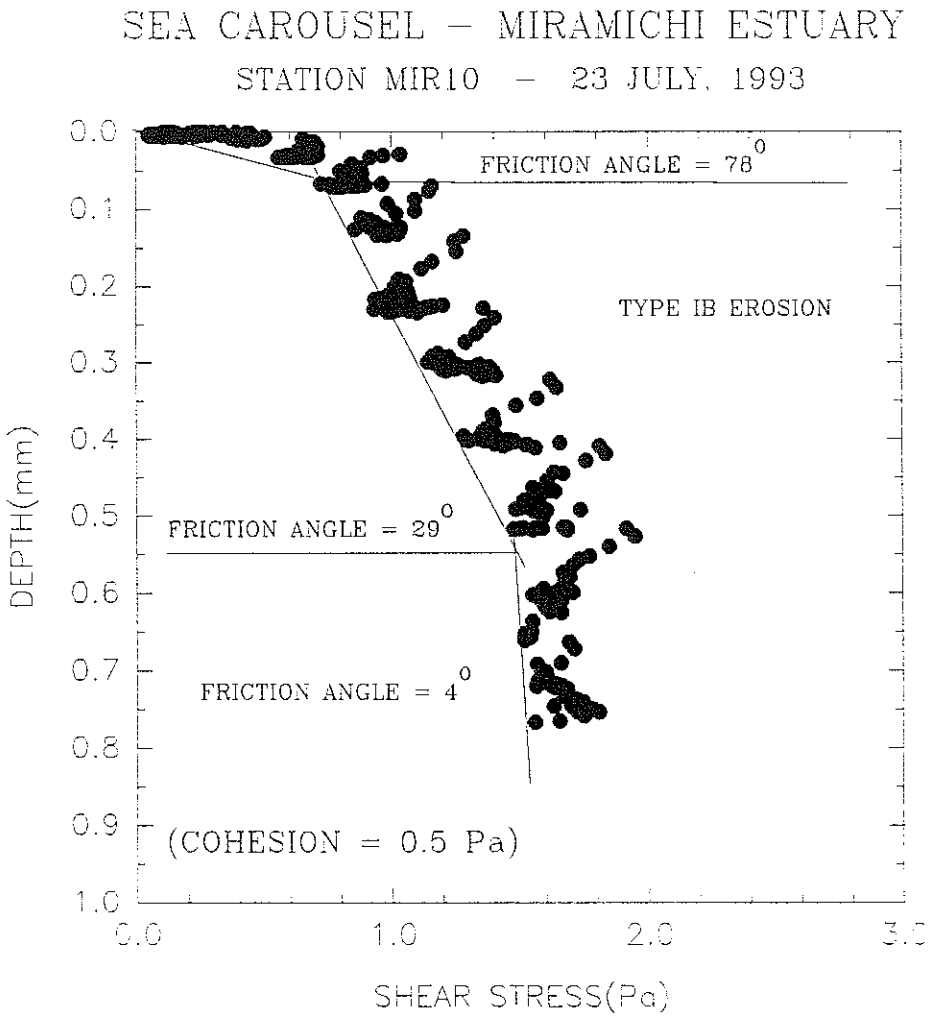

Figure 4.2.6.1-4. Relationship of shear stress and depth at post-disposal Experimental site MIR10 (Station 22).

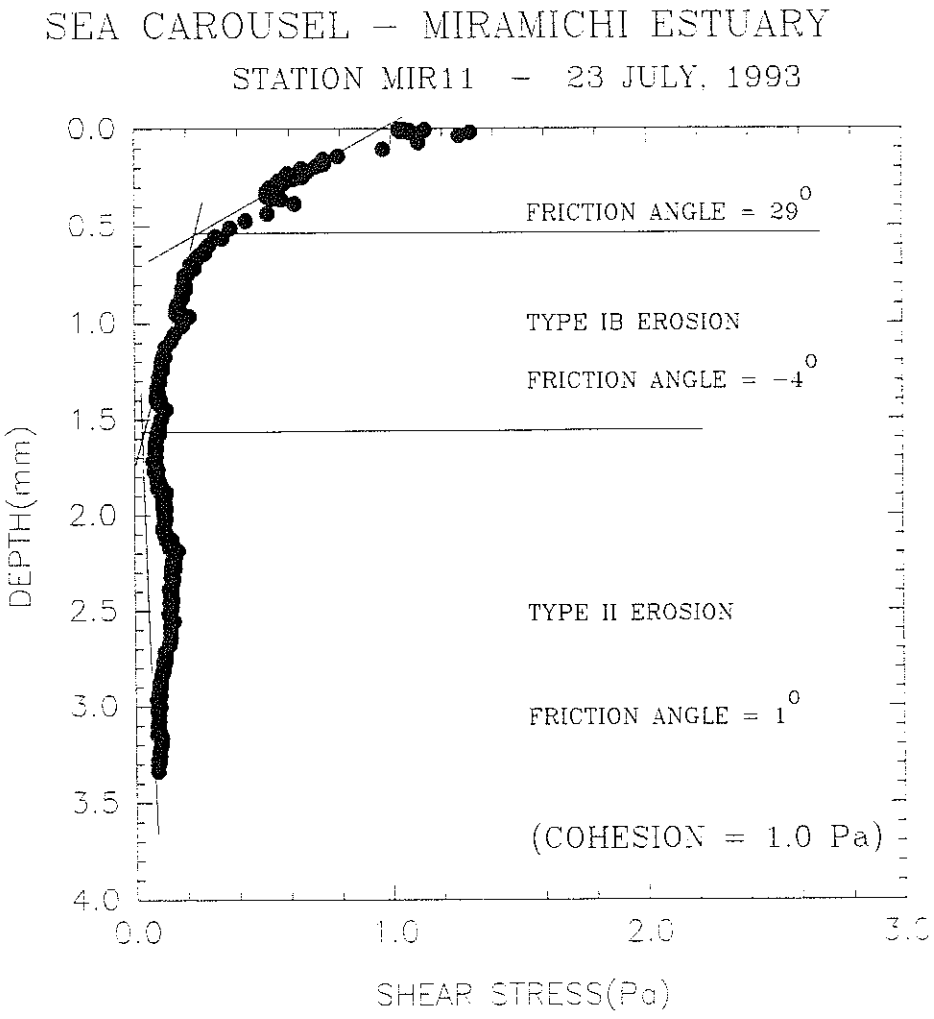

Figure 4.2.6.1-5. Relationship of shear stress and depth at post-disposal Experimental site MIR11 (Station 23).

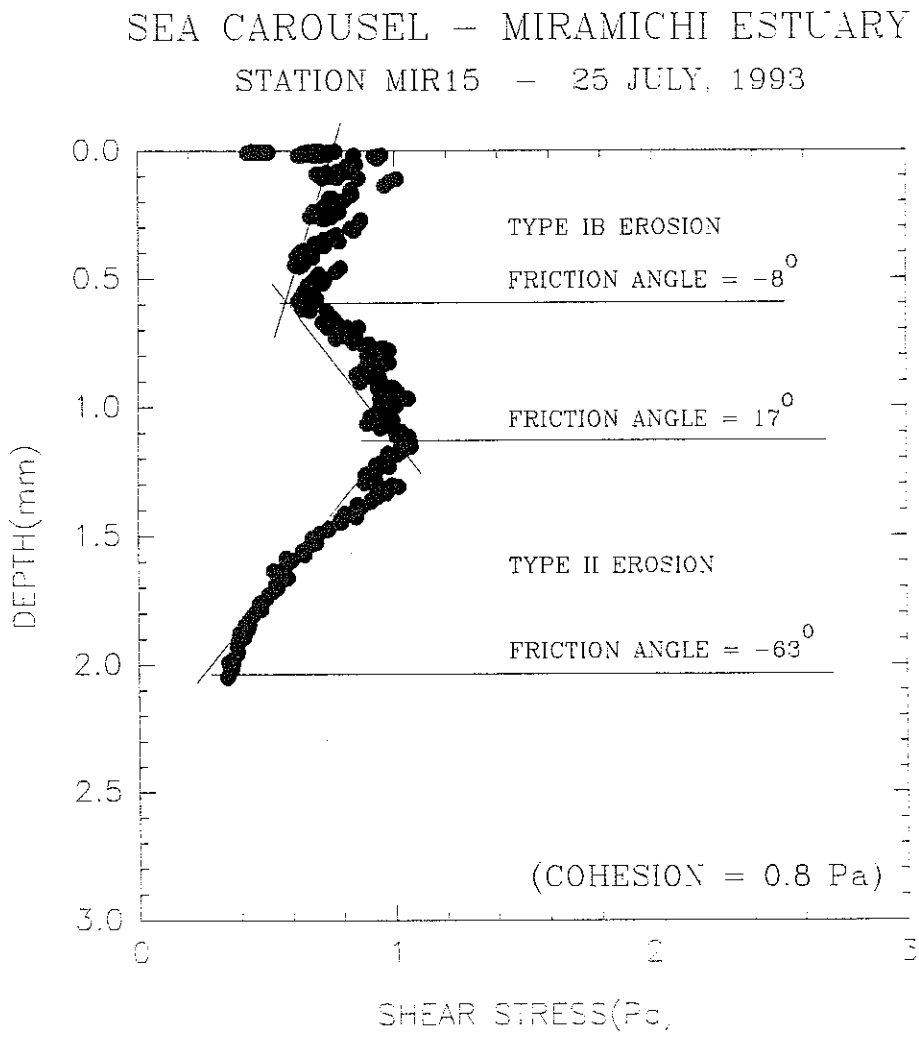

Figure 4.2.6.1-6. Relationship of shear stress and depth at post-disposal Experimental site MIR15 (Station 28).

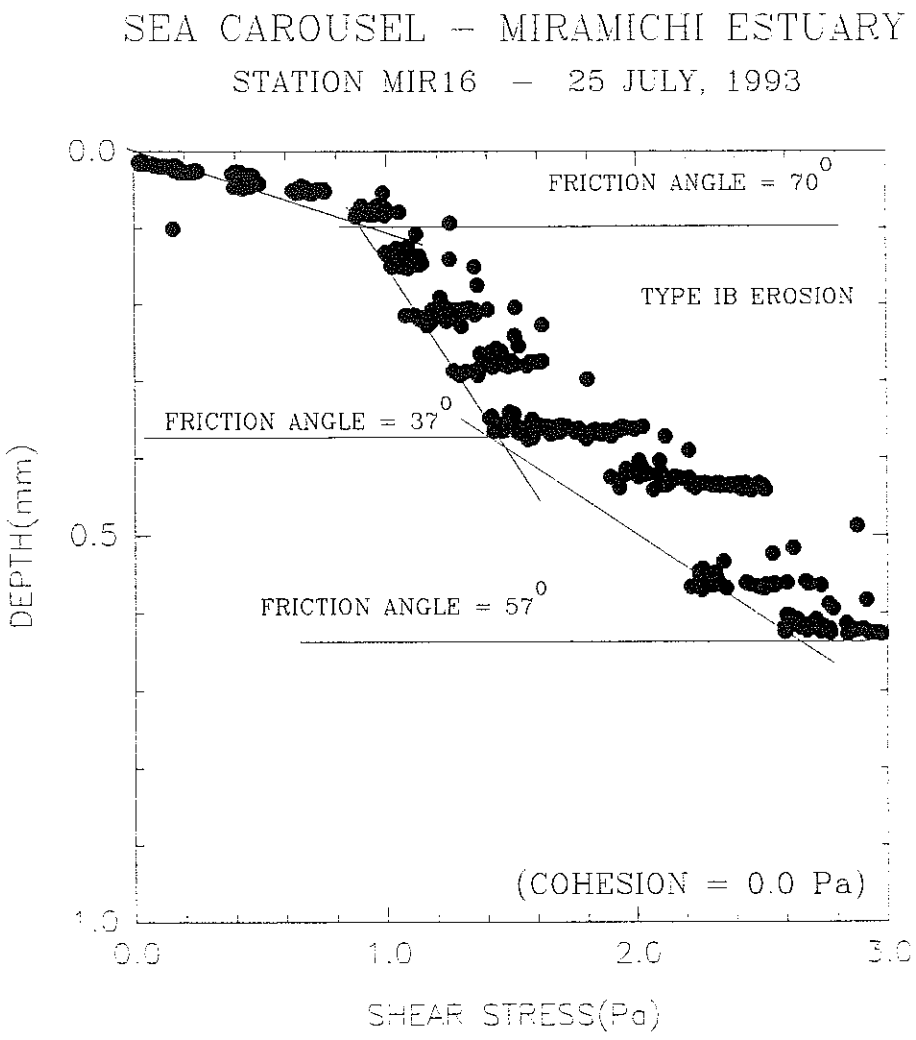

Figure 4.2.6.1-7. Relationship of shear stress and depth at post-disposal Experimental site MIR16 (Station 29).

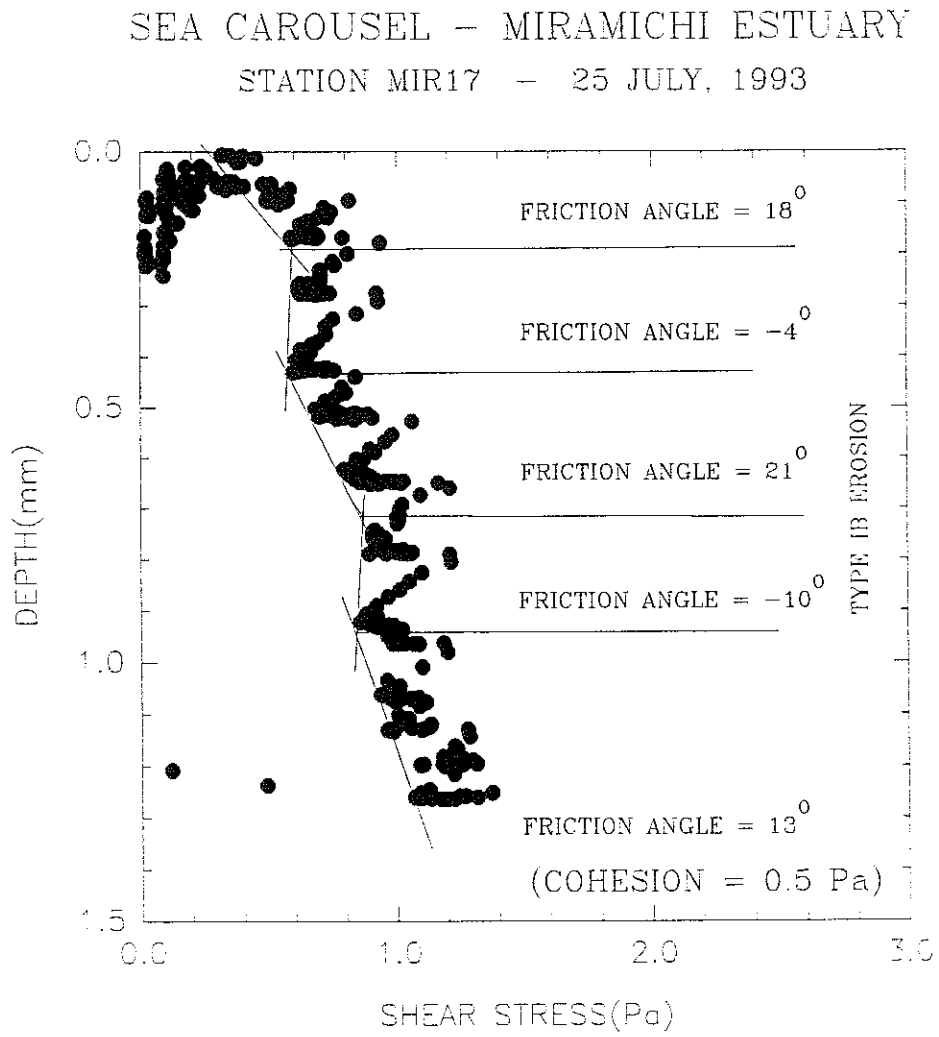

Figure 4.2.6.1-8. Relationship of shear stress and depth at post-disposal Experimental site MIR17 (Station 30).

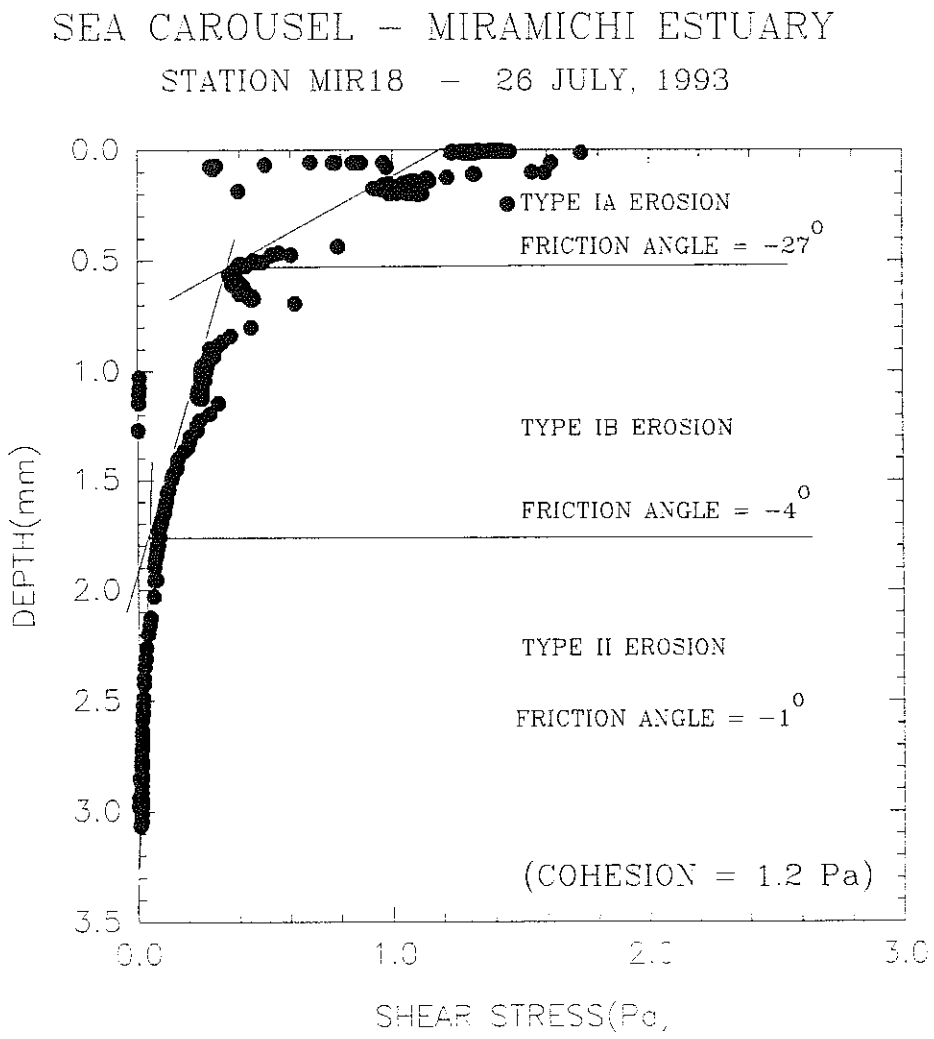

Figure 4.2.6.1-9. Relationship of shear stress and depth at post-disposal Experimental site MIR18 (Station 32).

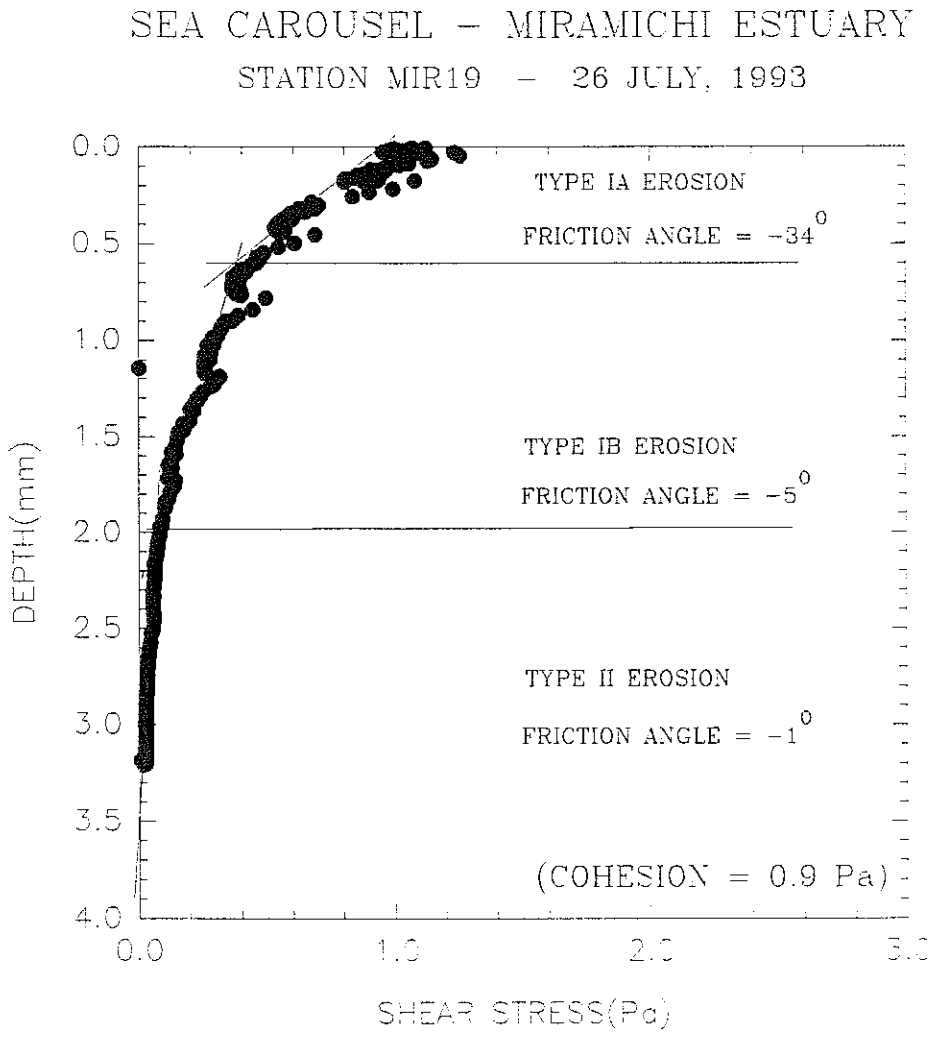

Figure 4.2.6.1-10. Relationship of shear stress and depth at post-disposal Experimental site MIR19 (Station 33).

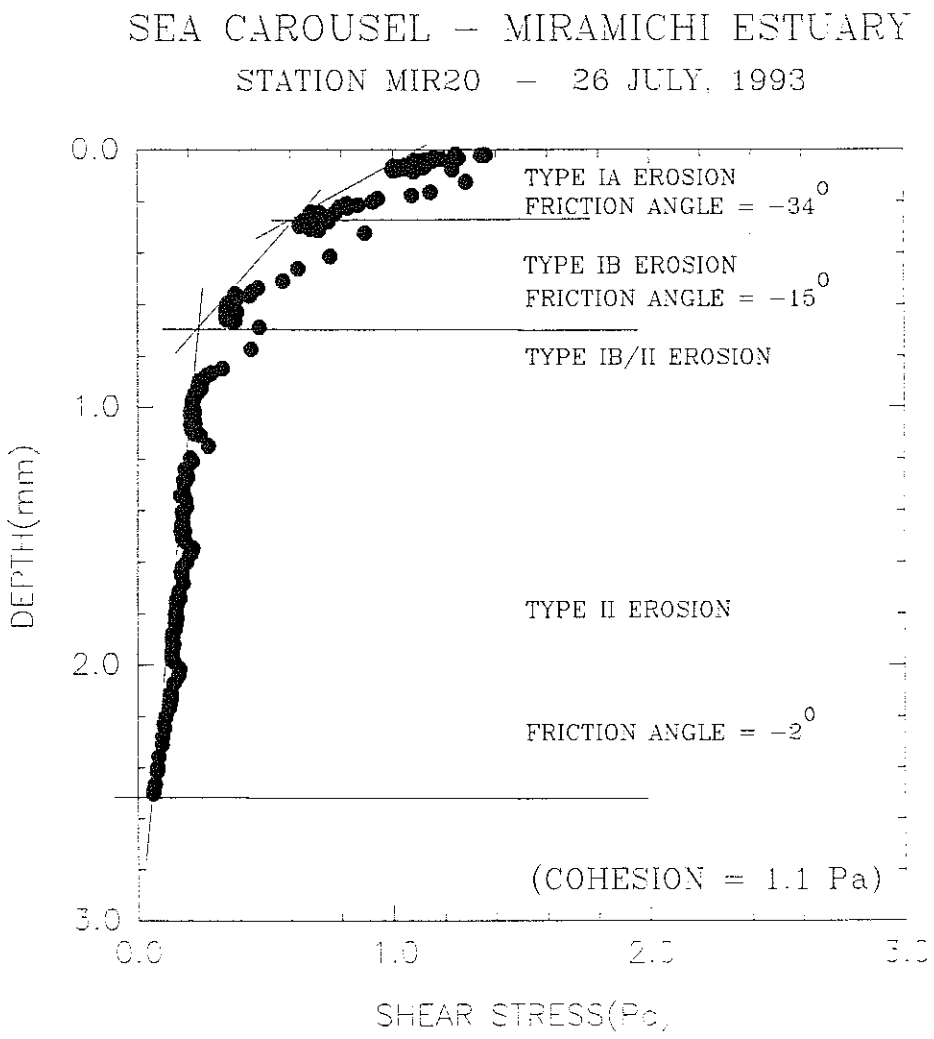

Figure 4.2.6.1-11. Relationship of shear stress and depth at post-disposal Experimental site MIR20 (Station 34).

material, the sediment strengths, and the (near-surface) friction angles are shown in Table 4.2.6.1-1. Notice that we analyzed disposed material from within 2 hrs after emplacement to approximately 62 hrs after emplacement. The time-series of the erosion threshold (ET) of the disposed material over this period of time is shown in Figure 4.2.6.1-12. The increase in bed strength is clear. This strength increase is a linear function of time, of the form:

$$ET = 0.30 + 0.0106\ (t)$$

where the erosion threshold (ET) is defined in pascals and time (t) is defined in hours. Notice that the strength of the disposed material exceeds that of the original Channel sediment (0.8 - 1.0 Pa) within approximately 48 hrs, and that by the end of the survey it was slightly stronger than the original Channel material (1.0 - 1.2 Pa).

The time-series of the near-surface friction angle is shown in Figure 4.2.6.1-13. In this figure we see a stabilization of the sediment over the first 28 hrs, reflected by a rapid increase in friction angle. This we attribute to normal consolidation processes. Thereafter, we see a decrease in friction angle to values typically associated with biostabilized seabeds. This period of time (28-62 hrs after disposal) we interpret as a period of re-colonization by benthic communities, and the development of an adhesive strength at the surface of the deposited material.

4.2.6.2 Erosion Rates

The erosion rates for the post-disposal Experimental sites are plotted in panels C of Figures 4.2.6-1 to 4.2.6-11. The patterns of erosion largely follow type IB (asymptotically decaying with time). The peaks in erosion rate at the onset of each speed increment are clearly seen in Figure 4.2.6-3. The subsequent asymptotic decay is also exemplified in this figure. This type of erosion prevails at current speeds less than 0.5 m sec^{-1}. We see no evidence for type IA erosion, which is evident in the Channel. We attribute this to lower levels of organic matter at this site, together with lower benthic biological activity (seen in the video tapes). Type II erosion prevails in the latter stages of stations MIR8, MIR11, MIR15, MIR19, and MIR20. Type II erosion occurs at current speeds in excess of 0.5 m sec^{-1}. The peak erosion (EP) in general shows a systematic increase with current speed up to *circa* 0.2 m sec^{-1}, from 2 x 10^{-4} to 4 x 10^{-3} kg m^{-2} sec^{-1}. Thereafter, EP remains roughly constant with speed and has values that vary between 7 x 10^{-4} to 10^{-2} kg m^{-2} sec^{-1}. The base erosion rate (EB) is the minimum erosion rate detected at the end of each velocity increment. It generally shows a systematic increase over the range of current speeds, from 4 x 10^{-5} to 10^{-3} kg m^{-2} sec^{-1}.

4.2.6.3 Deposition Rates

The time-series for the suspended sediment settling monitoring for the post-disposal stations are shown in Figures 4.2.6.3-1 to 4.2.6.3-10. The nearsurface settling rates show significant variations in concentration half-lives between 82 and 320 sec (mean $t_{0.5}$ = 146 sec). Nevertheless, the concentration decay generally follows an exponential decay pattern. The decay constant (k) has a mean value of -0.0051 sec^{-1}. The decay constants (and half-lives) are

Table 4.2.6.1-1. Erosion thresholds (cohesion) and friction angles of disposed material, listed in terms of age (time) after disposal.

STATION	AGE (hrs)	COHESION (Pa)	FRICTION ANGLE
MIR8(20)	2	0.3	-34
MIR15(28)	3	0.8	-8
MIR9(21)	12	0.6	70
MIR16(29)	21	0.0	70
MIR17(30)	23	0.5	18
MIR10(22)	24	0.5	78
MIR11(23)	26	1.0	29
MIR18(32)	55	1.2	-27
MIR19(33)	60	0.9	-34
MIR20(34)	62	1.1	-34

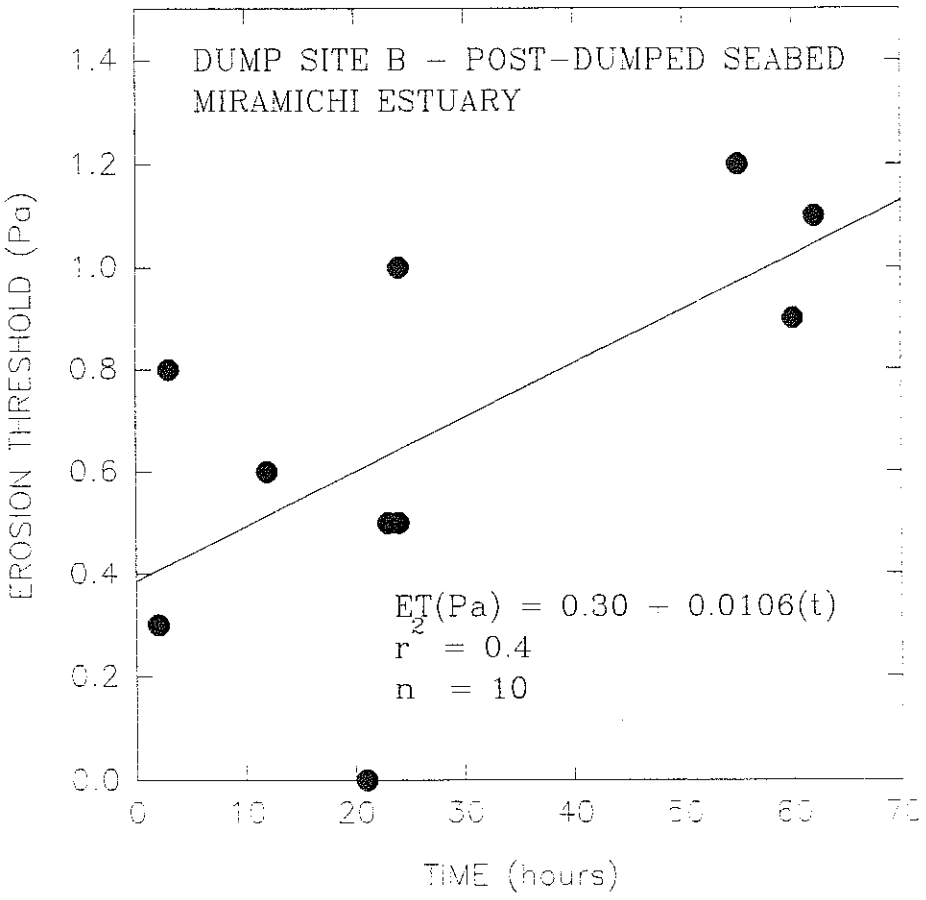

Figure 4.2.6.1-12. Time series of the erosion threshold of spoils deposited at the Experimental disposal-site.

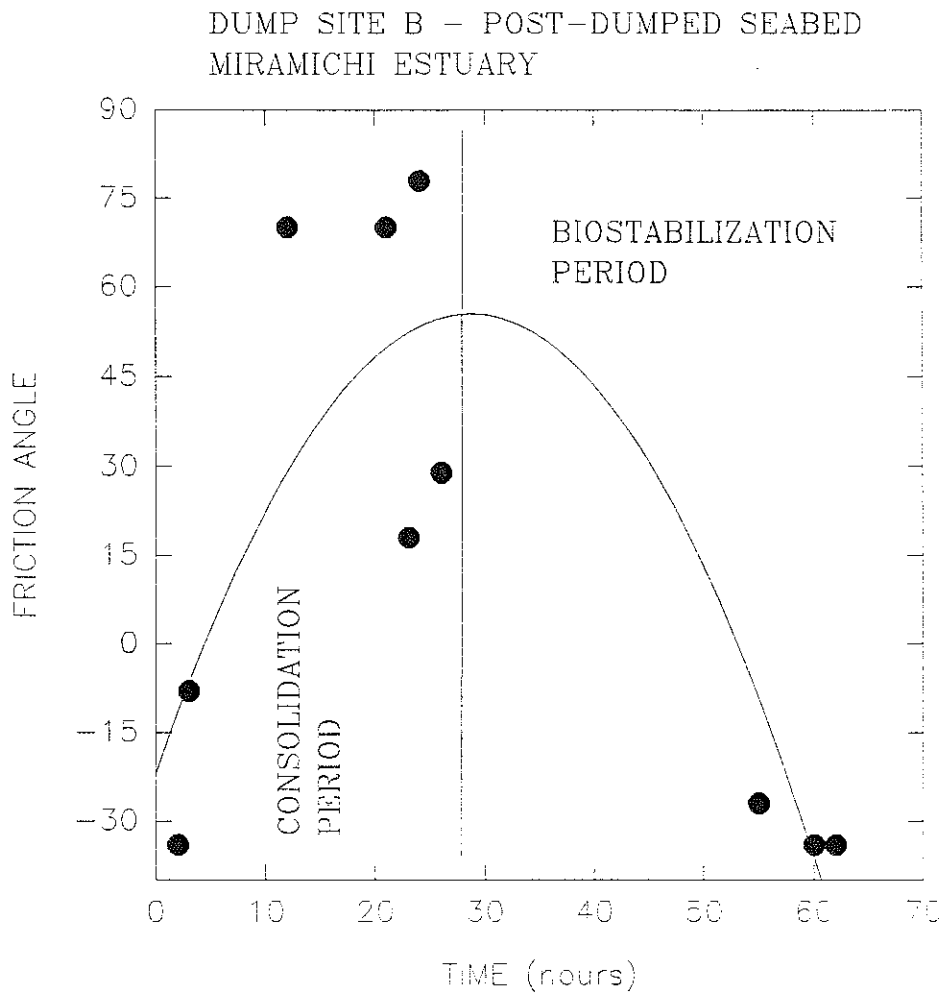

Figure 4.2.6.1-13. Time series of the near-surface friction angle at the post-disposal Experimental site.

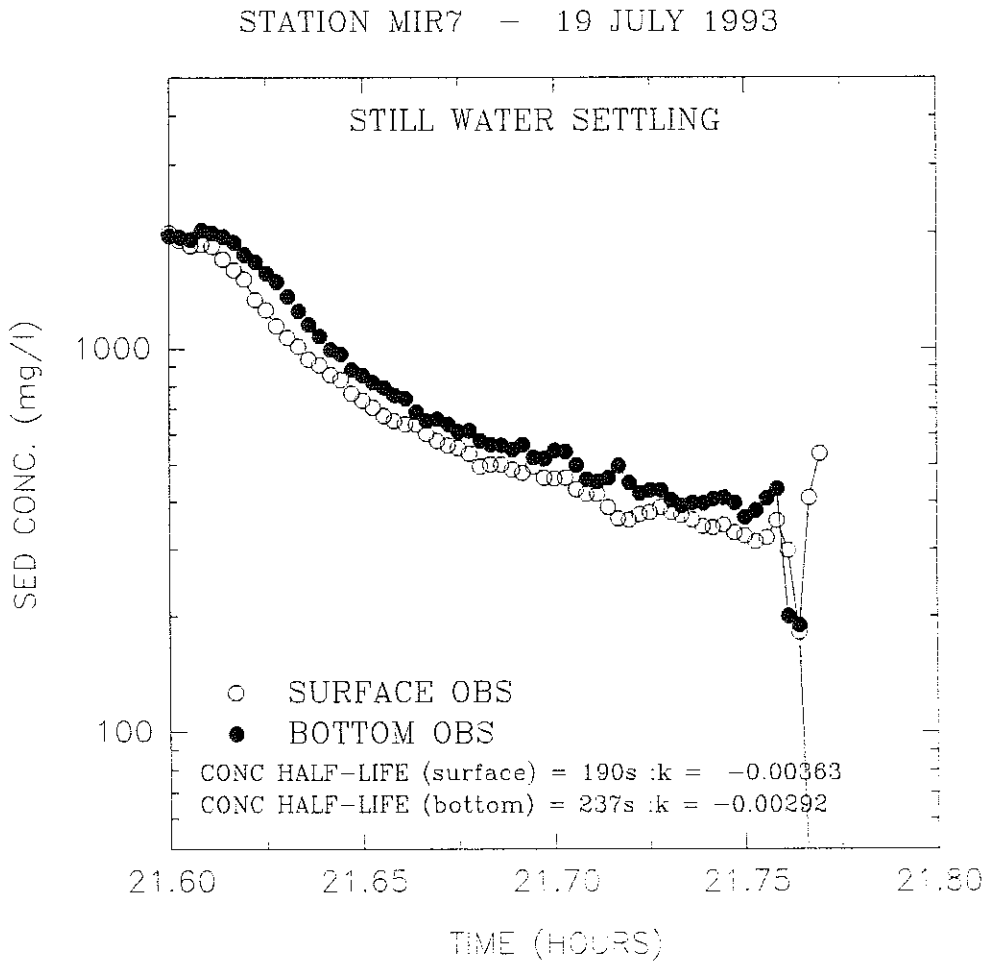

Figure 4.2.6.3-1. Relationship between sediment concentration and time during Sea Carousel settling rate measurements at post-disposal Experimental site MIR7 (Station 8).

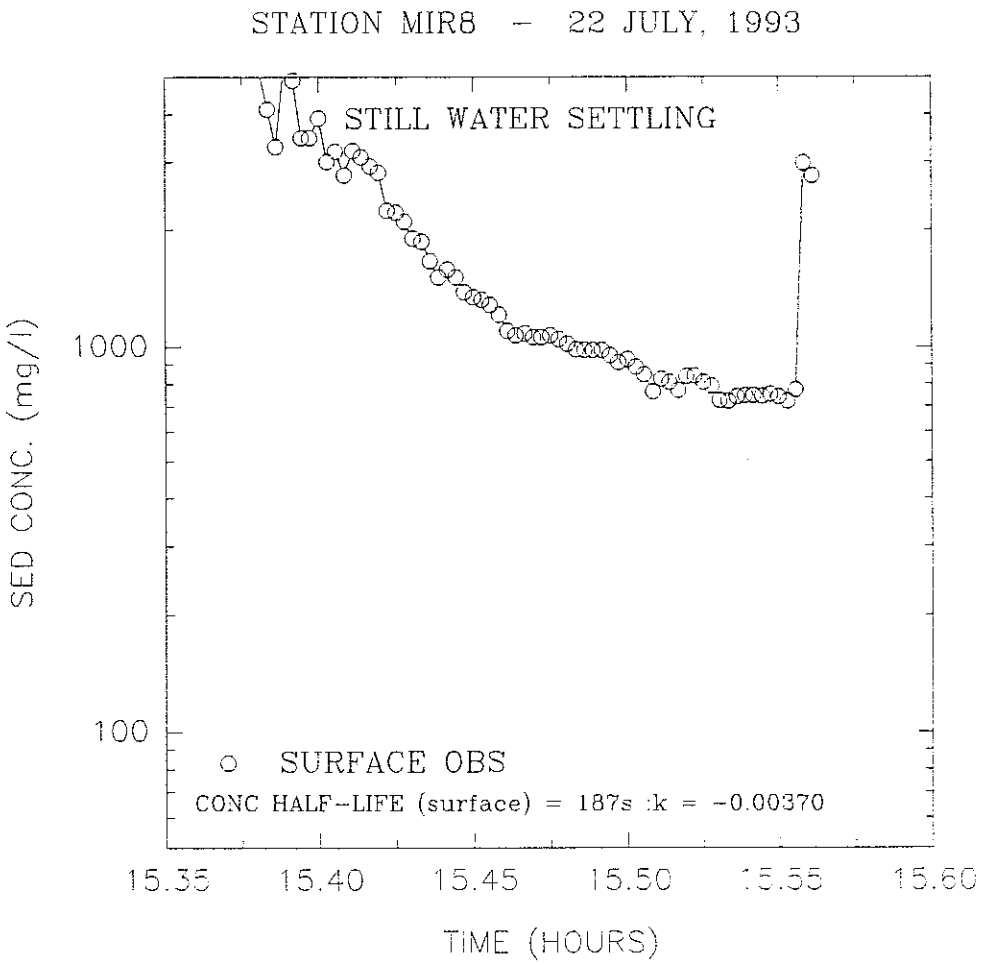

Figure 4.2.6.3-2. Relationship between sediment concentration and time during Sea Carousel settling rate measurements at post-disposal Experimental site MIR8 (Station 20).

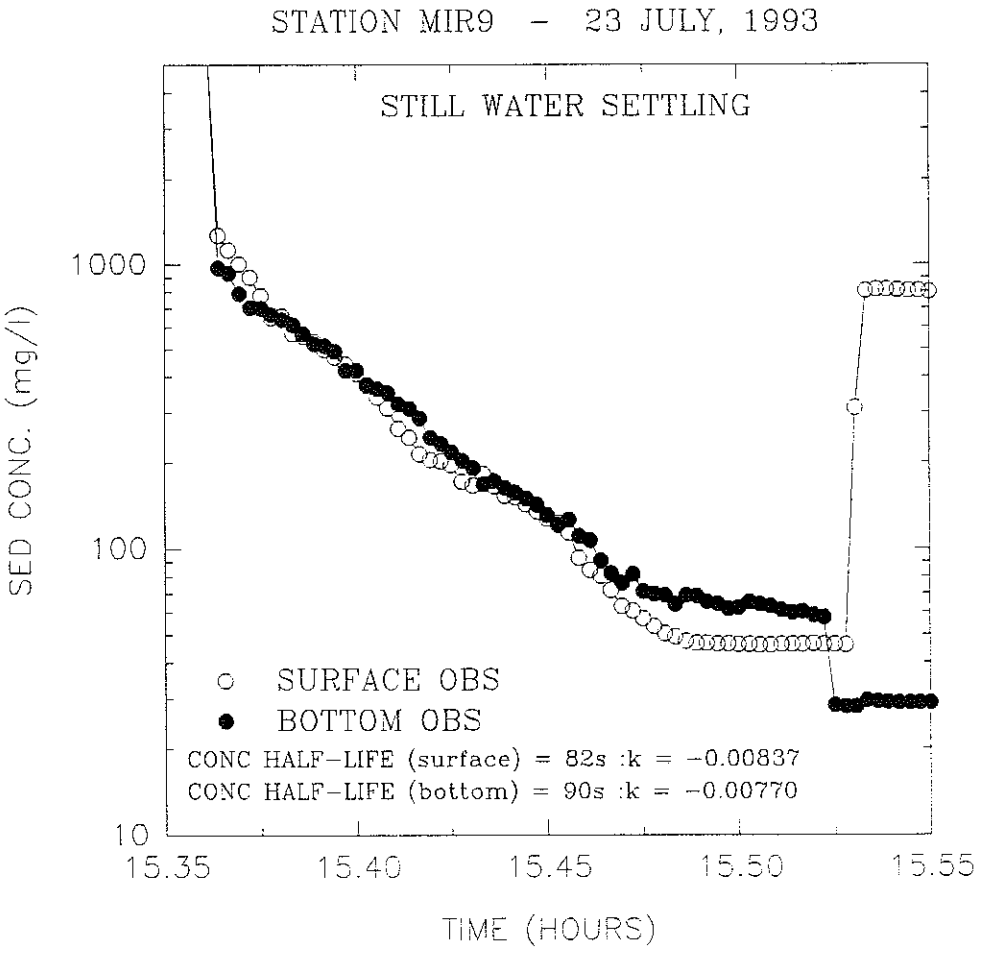

Figure 4.2.6.3-3. Relationship between sediment concentration and time during Sea Carousel settling rate measurements at post-disposal Experimental site MIR9 (Station 21).

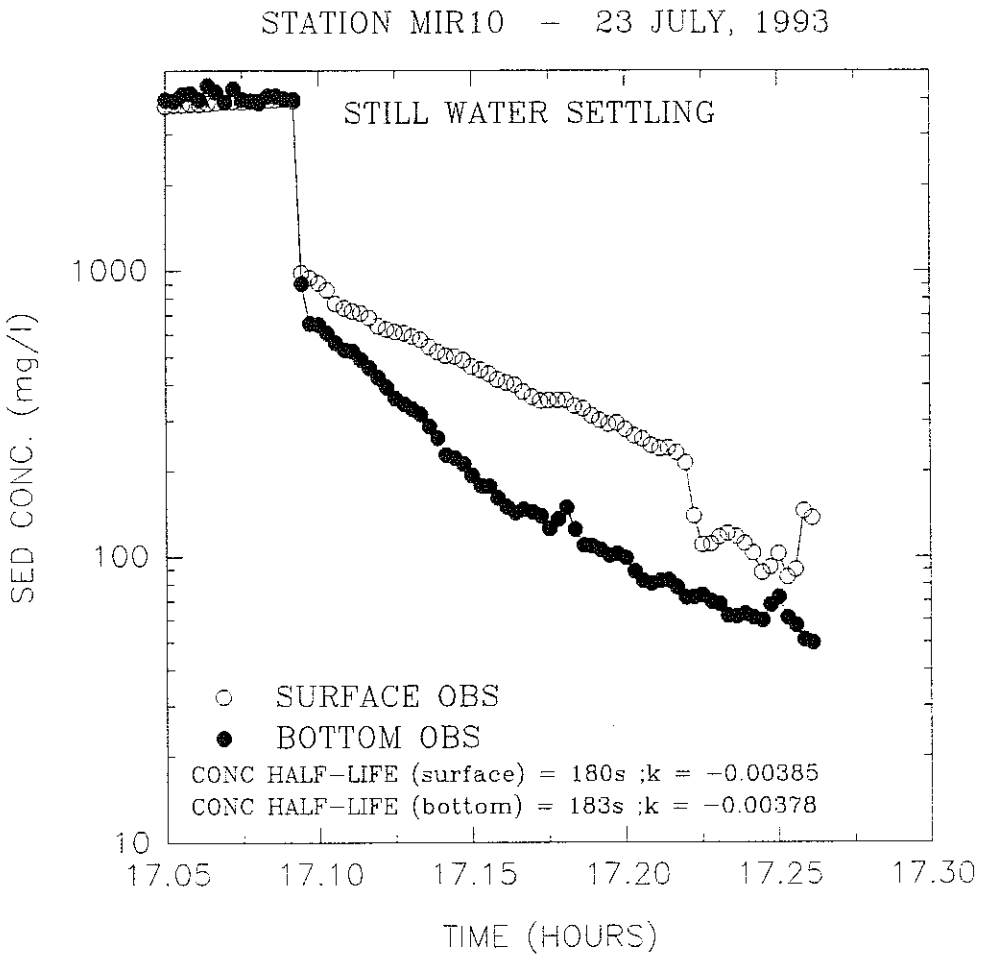

Figure 4.2.6.3-4. Relationship between sediment concentration and time during Sea Carousel settling rate measurements at post-disposal Experimental site MIR10 (Station 22).

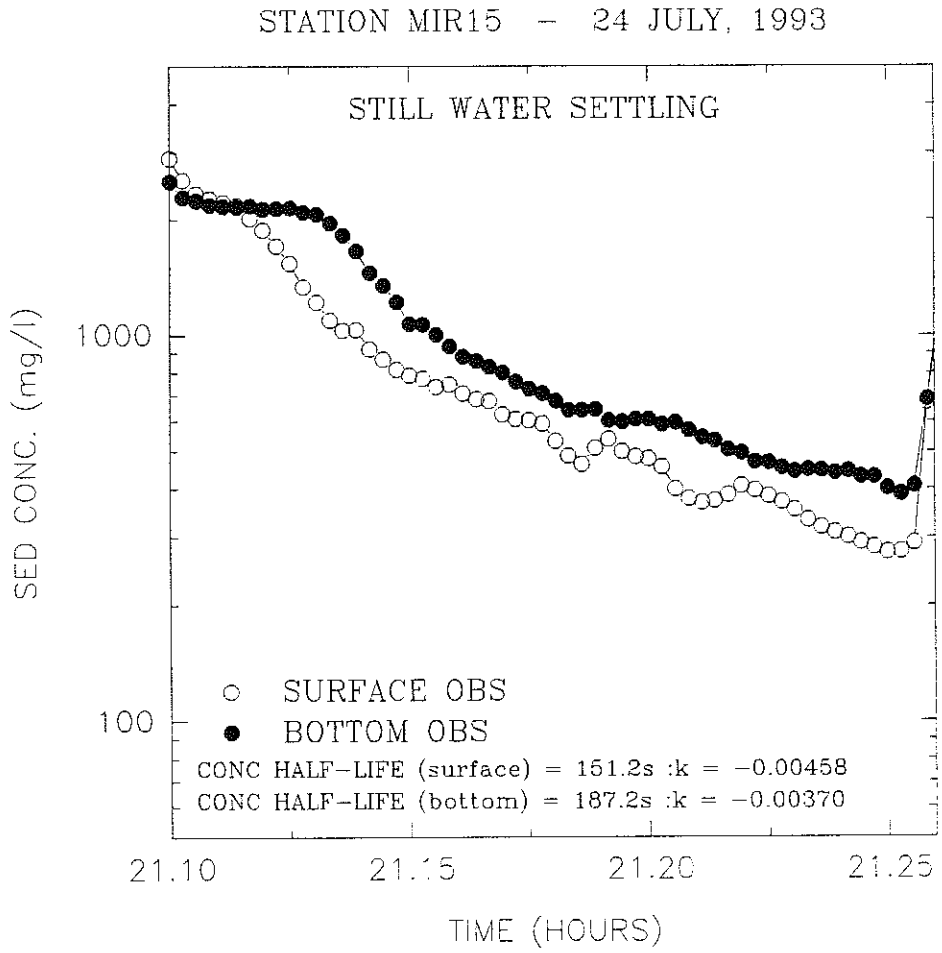

Figure 4.2.6.3-5. Relationship between sediment concentration and time during Sea Carousel settling rate measurements at post-disposal Experimental site MIR15 (Station 28).

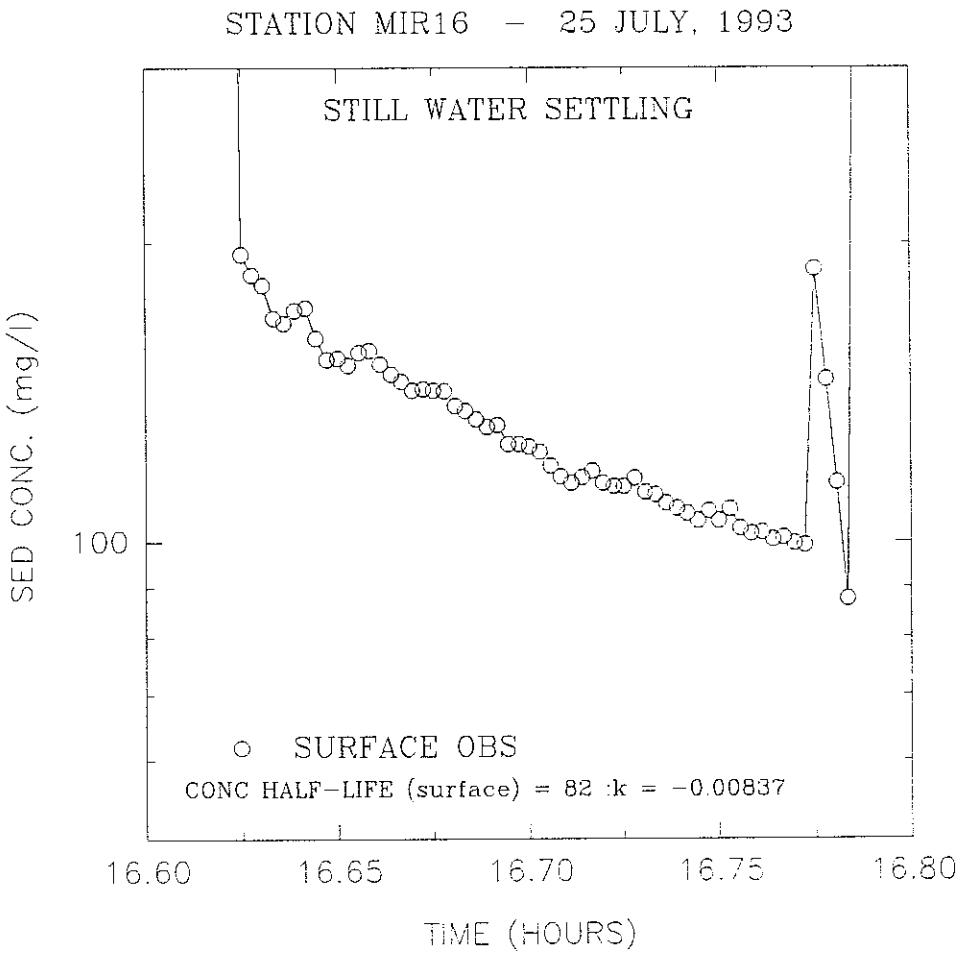

Figure 4.2.6.3-6. Relationship between sediment concentration and time during Sea Carousel settling rate measurements at post-disposal Experimental site MIR16 (Station 29).

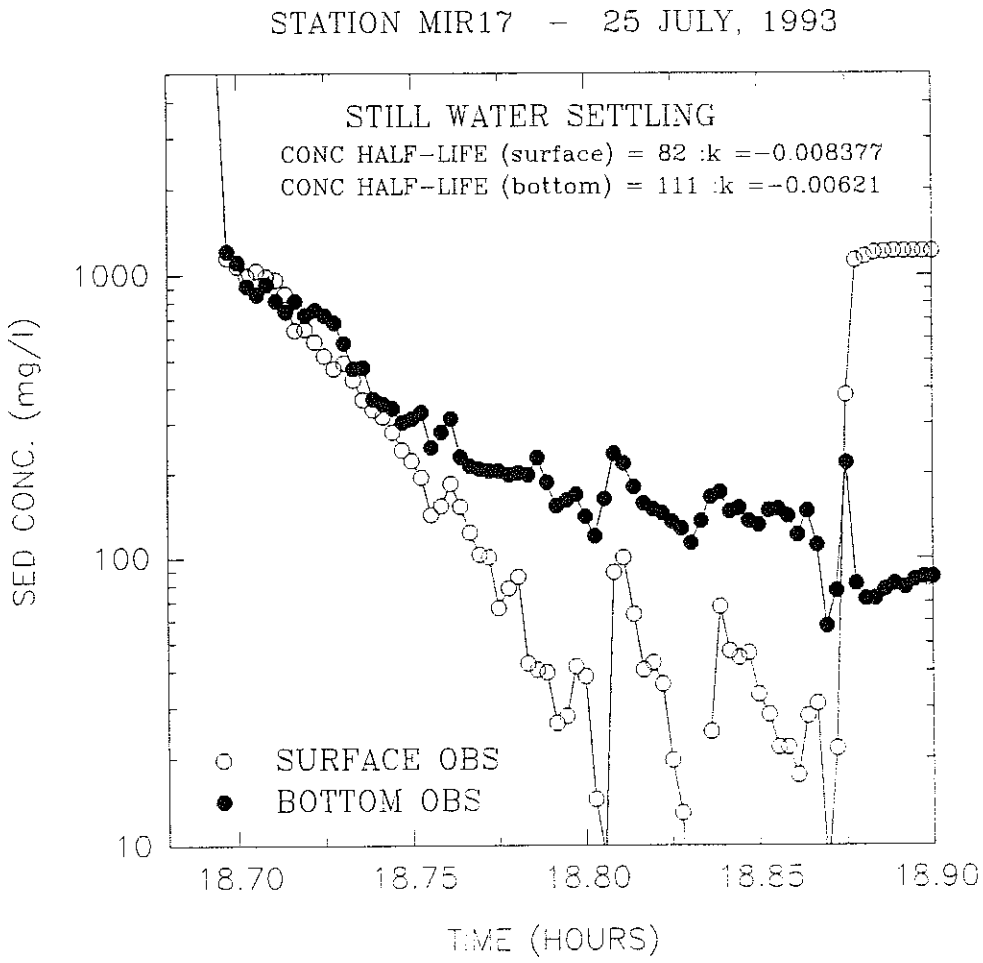

Figure 4.2.6.3-7. Relationship between sediment concentration and time during Sea Carousel settling rate measurements at post-disposal Experimental site MIR17 (Station 30).

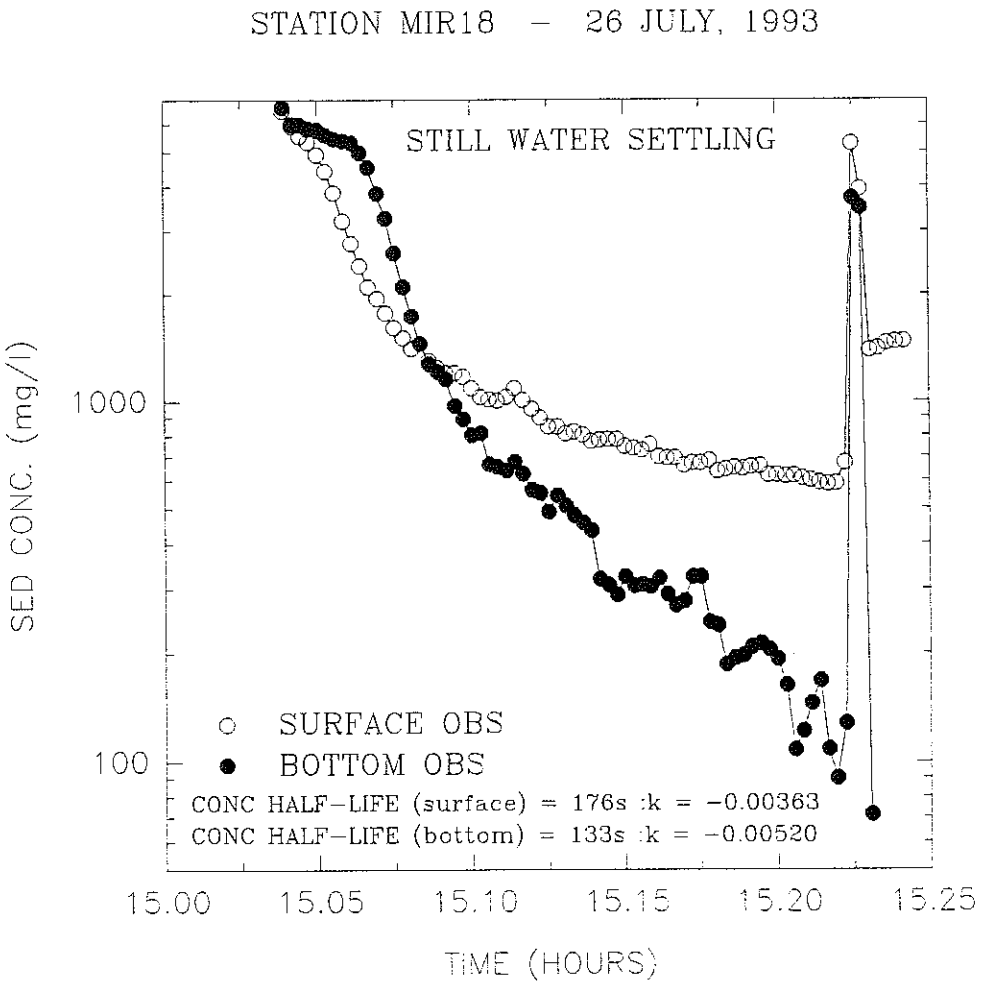

Figure 4.2.6.3-8. Relationship between sediment concentration and time during Sea Carousel settling rate measurements at post-disposal Experimental site MIR18 (Station 32).

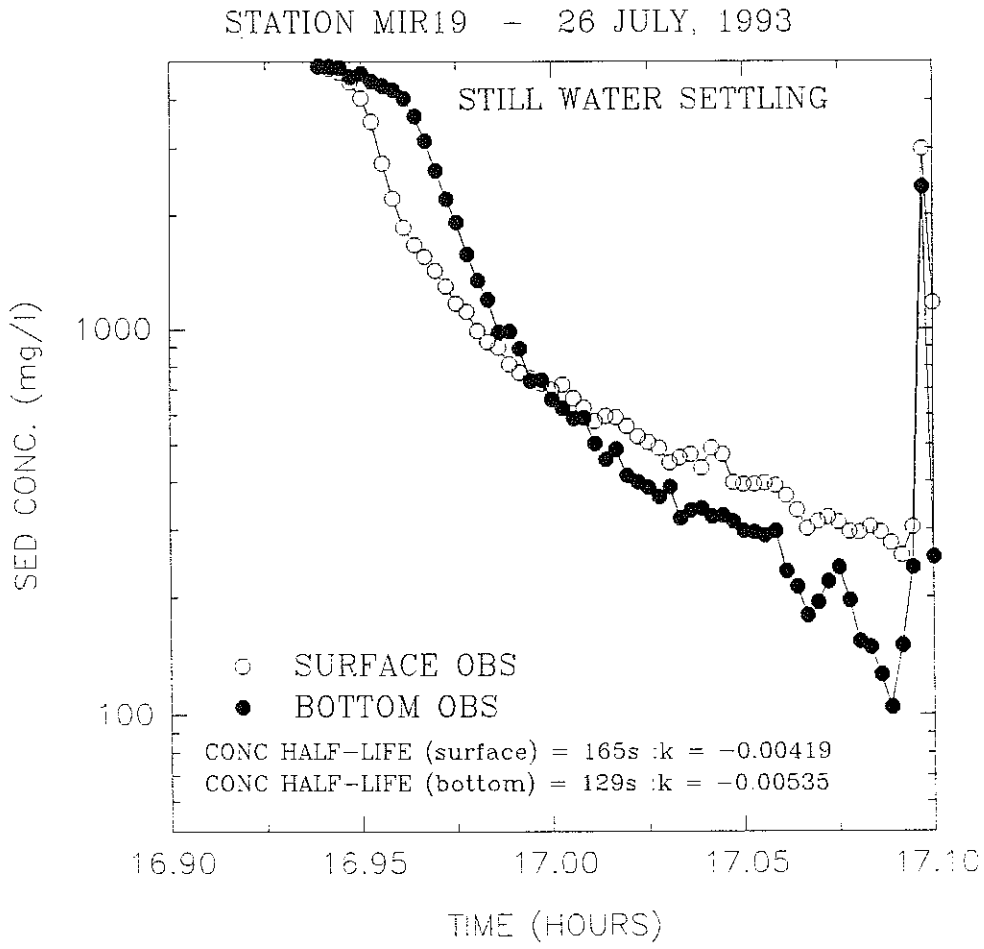

Figure 4.2.6.3-9. Relationship between sediment concentration and time during Sea Carousel settling rate measurements at post-disposal Experimental site MIR19 (Station 33).

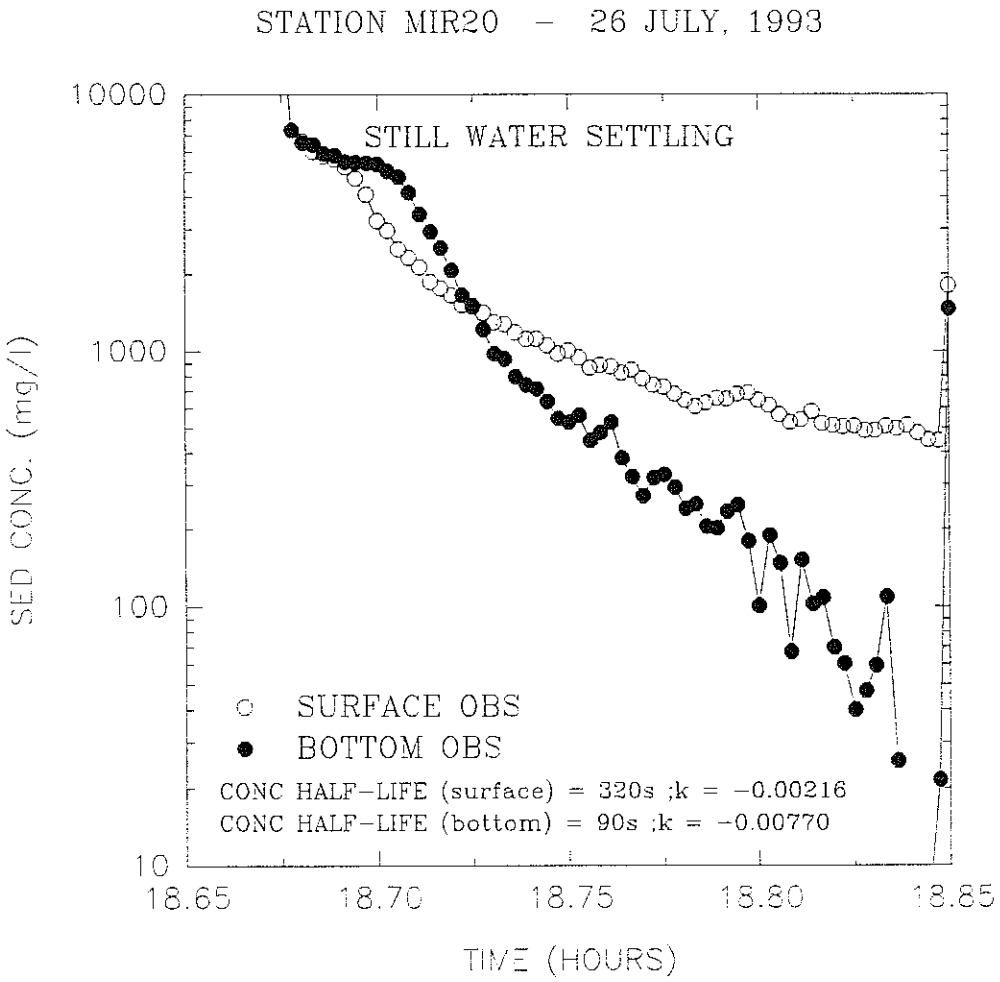

Figure 4.2.6.3-10. Relationship between sediment concentration and time during Sea Carousel settling rate measurements at post-disposal Experimental site MIR20 (Station 34).

listed in Table 4.2.3.3-1. The nearbed concentration half-lives are much more consistent that the near surface ones, and show a mean concentration half-life of 164 sec. The associated mean decay constant (k) is -0.0050 sec^{-1}. These settling rates are consistent with results presented by Amos et al. (1993) and suggest a low potential for fluid mud generation.

4.3 SOBS Results

4.3.1 Control Site

The SOBS deployment at the Control site (SOBS1) was located at Lat: 47° 07.92' W, Lon: 65° 09.82' N (Station 1). The site was situated in 5.8 m of water approximately 75 m north of Reach 22 of the Miramichi Channel. It was deployed at 14:36 Atlantic Daylight Time (ADT), on 14 July 1993 (Julian Day 195) and was recovered at 12:35 ADT, on 20 July 1993 (Julian Day 201); a duration of 142 hrs. SOBS worked continuously throughout the deployment. It detected coherent resuspension events associated with the flooding tidal currents and with periods of strong wave activity. The OBS sensors also detected coherent resuspension events associated with the arrival of the M/V Mariner at 0745 ADT, 15 July 1993 and again with this ship's departure at 0700 ADT, 16 July 1993. Numerous other non-coherent events were detected. None could be firmly ascribed to dredging activities.

The time-series of results from SOBS1 are shown on Figures 4.3.1-1 to 4.3.1-16. The figures illustrate the suspended sediment concentration (to a maximum of *circa* 3000 mg^{-1}) from the six OBS sensors, as well as the depth recorded by the pressure sensor. Each figure shows approximately 9 hrs of data. Full saturation of OBS1 suggests that it was close to the seabed or buried within it. All remaining OBS sensors showed backgrounds of between 100 and 200 mg^{-1}. OBS2 (the lowermost horizontal sensor) showed the greatest activity, while OBS's 5 and 6 showed the least. This suggests that small scale local resuspension events take place, but are restricted to the lowermost part of the water column. Many of these events may be ascribed to resuspension of organic "fluff" by tidal flow. Figure 4.3.1-2 (hrs 6 and 8) show events in OBS's 2, 3, and 4 that may be linked to the strongly flooding tide (see depth plot). Similar phenomena are evident in Figure 4.3.1-7 (hrs 2-5) for the subsequent flood tide and also in Figure 4.3.1-10 (hrs 2-4). The ebbing tide shows less evidence of resuspension, although events in Figure 4.3.1-8 (hrs 2-5) may be the result of an ebb tide current.

The 17th July 1993 (Julian Day 198) was extremely rough (see depth plot Fig. 4.3.1-9 and wind velocity data Fig. 4.6-3). We see evidence for resuspension of bottom material within the lower 0.5 m throughout this rough period. Peaks in SSC are *circa* 300 - 400 mg^{-1}, and are relatively short-lived. The 18th July 1993 (Julian Day 199) was also rough. During this period, we see evidence of large plumes of turbid water within the lower 0.5 m of the water column (see Fig. 4.3.1-12; hrs 0-2). Again, we believe that these plumes are due to wave resuspension of natural bed material, and are not related to dredging or disposal activities in the region.

The most significant resuspension events took place during the arrival of the M/V Mariner at 0745 ADT, 15 July 1993 (Fig. 4.3.1-3) and again with this ship's departure at 0700 ADT, 16

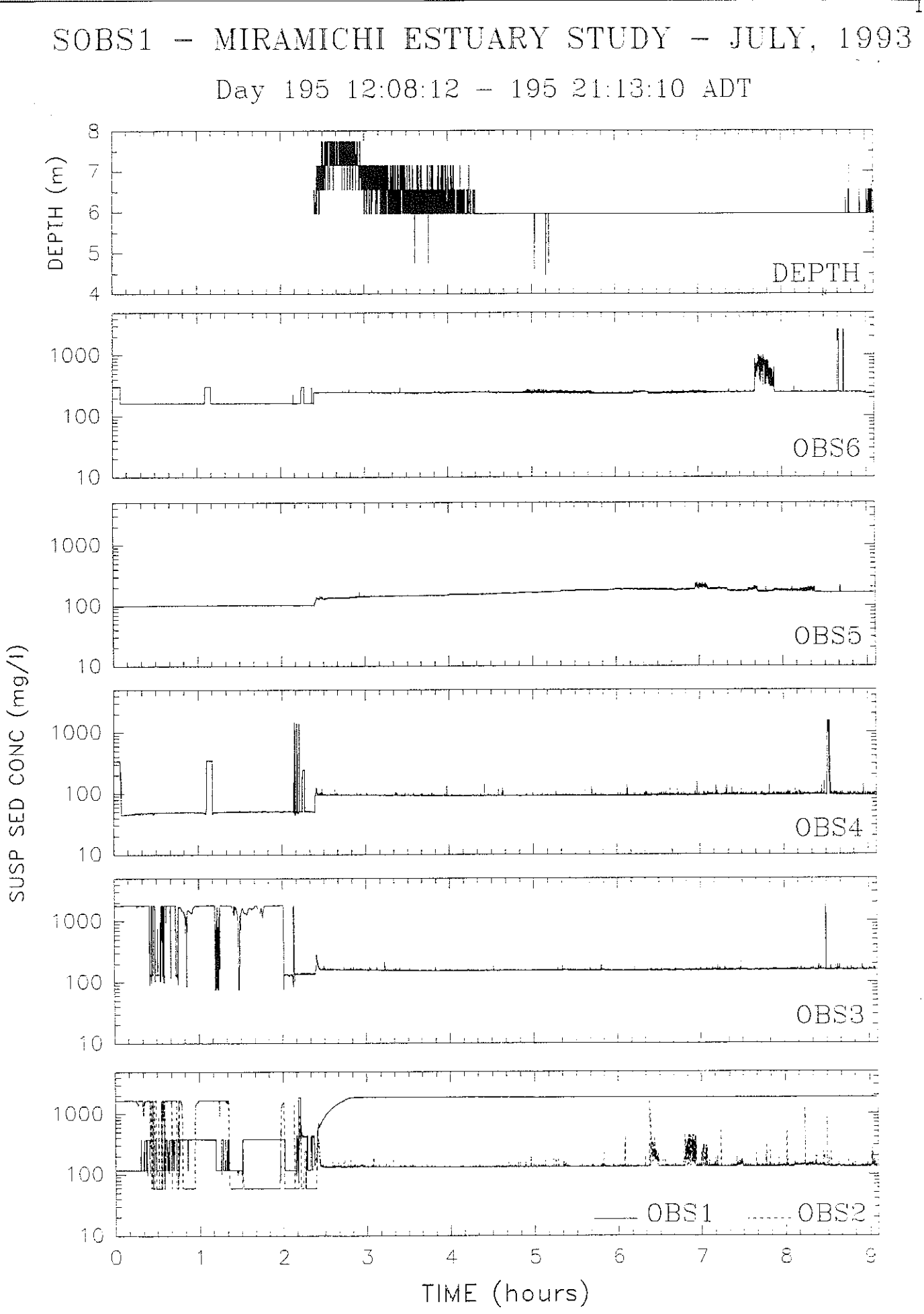

Figure 4.3.1-1. Time series of results from SOBS1 deployment at the Control site.

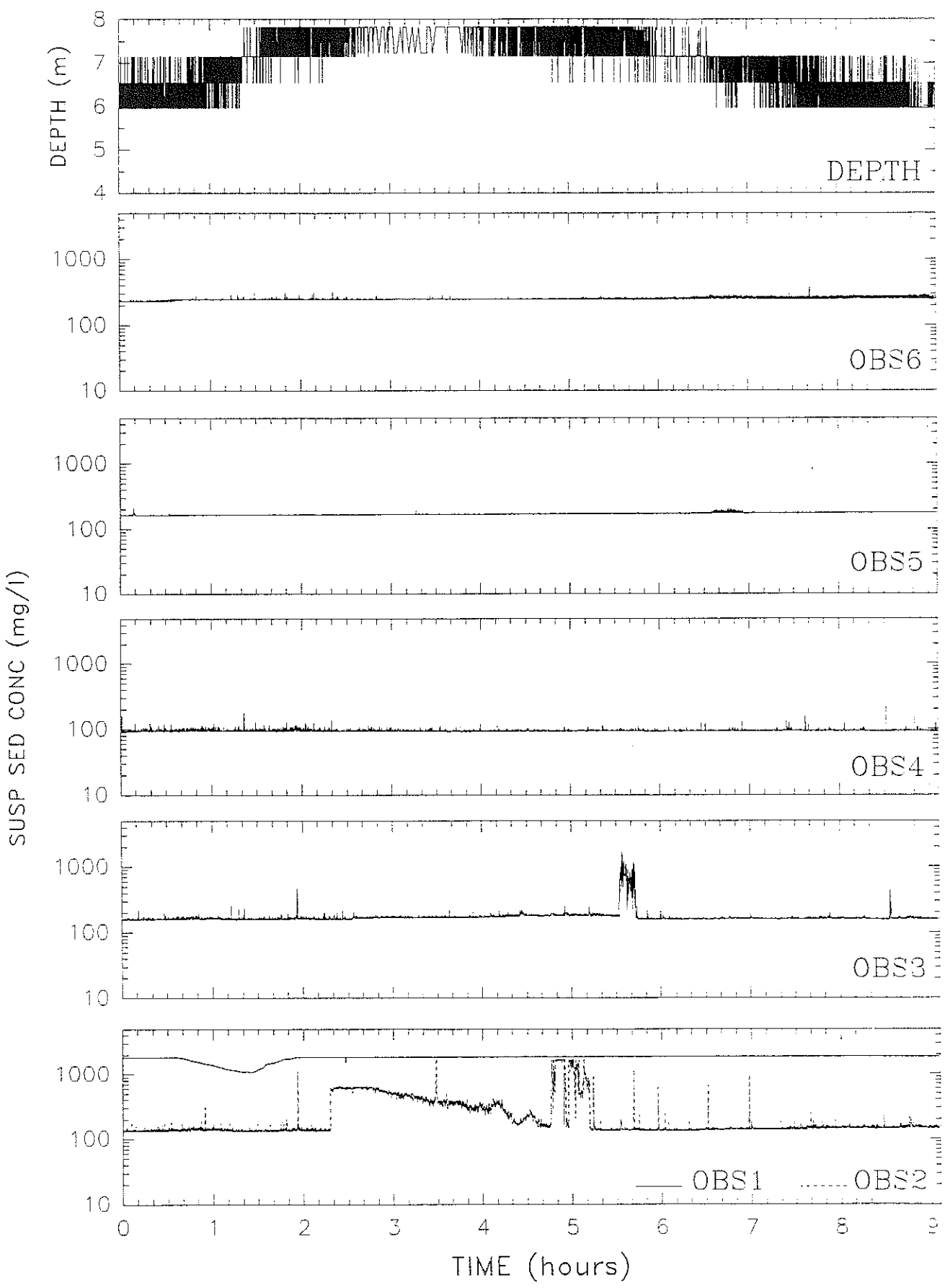

Figure 4.3.1-2. Time series of results from SOBS1 deployment at the Control site.

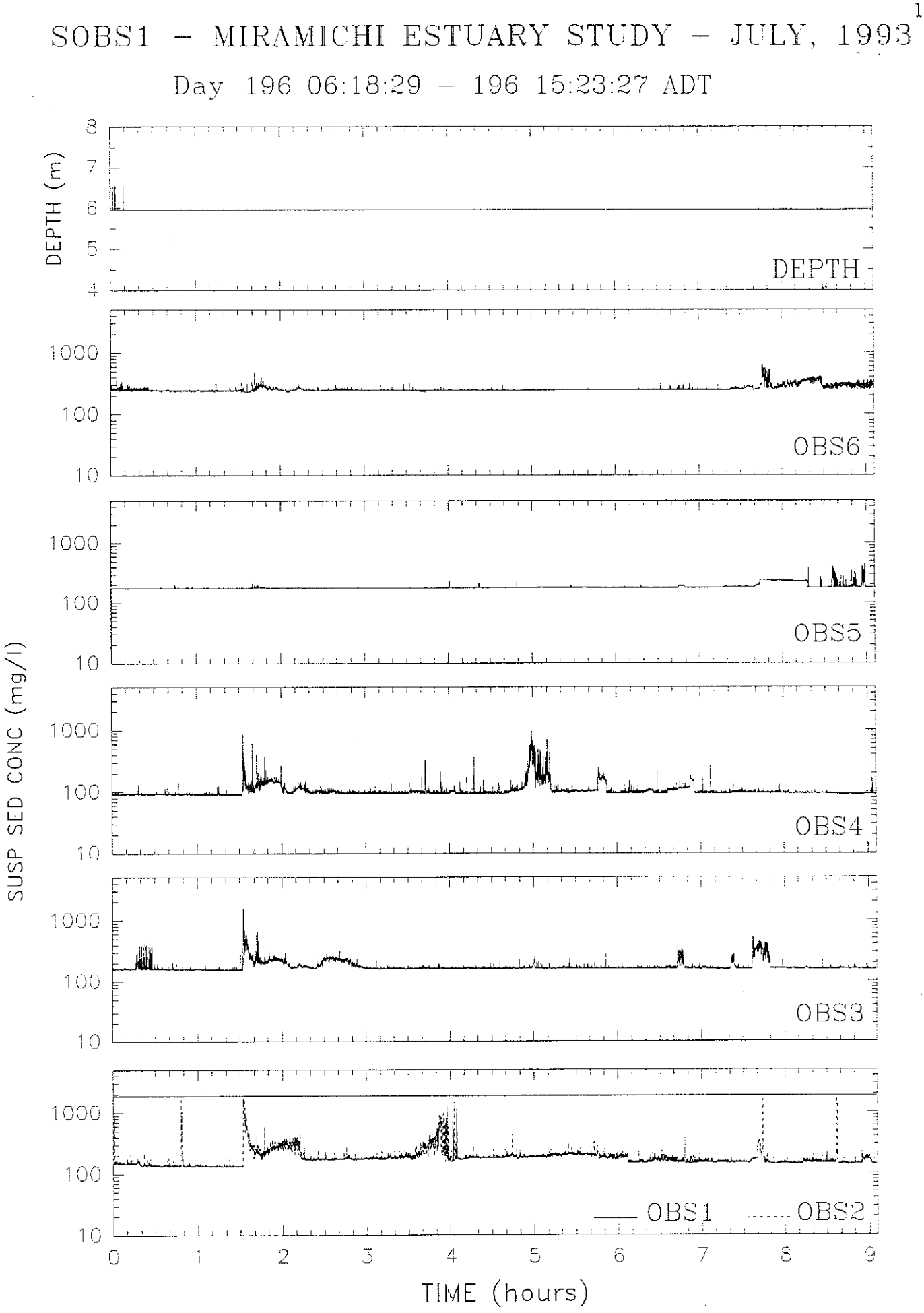

Figure 4.3.1-3. Time series of results from SOBS1 deployment at the Control site.

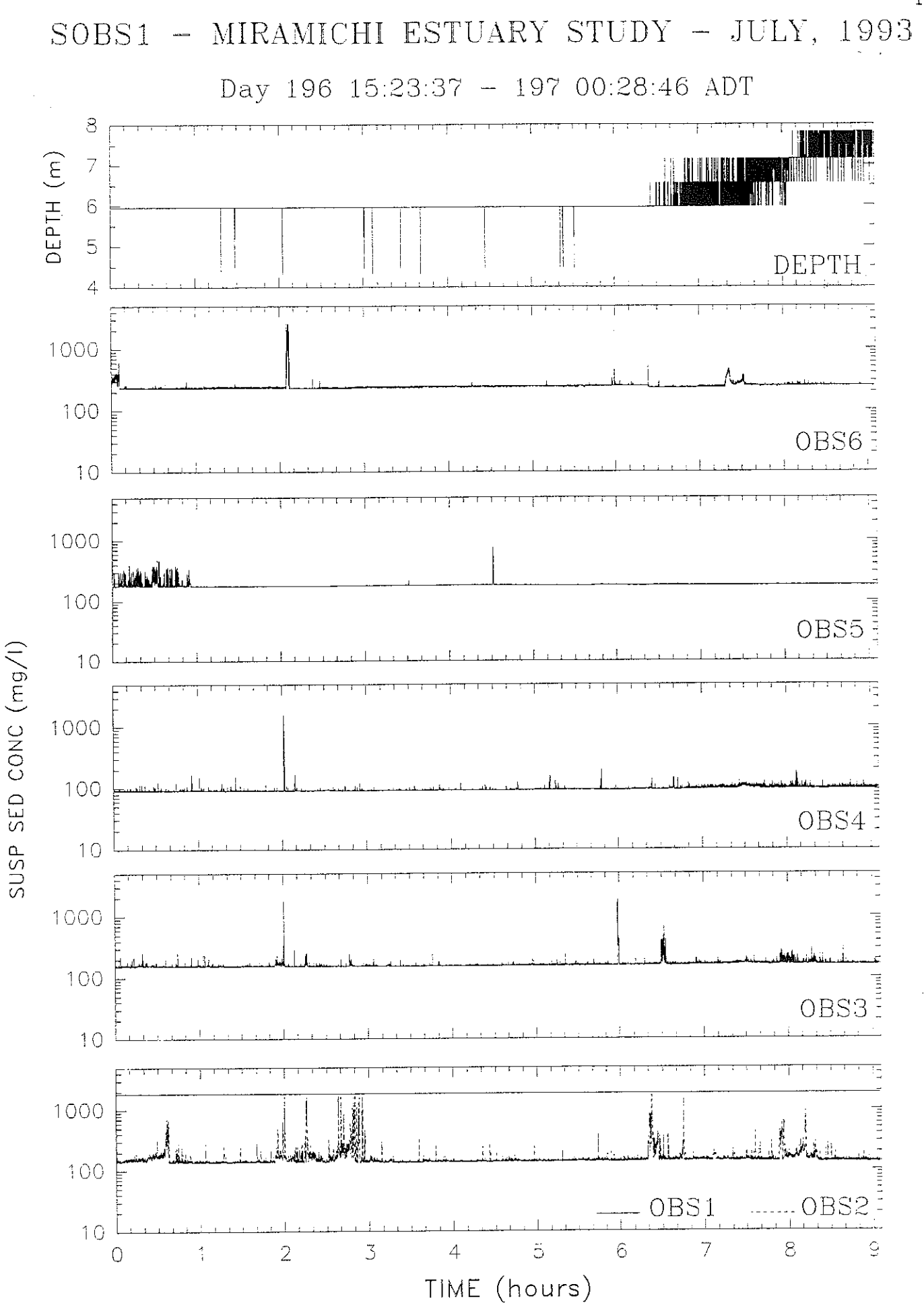

Figure 4.3.1-4. Time series of results from SOBS1 deployment at the Control site.

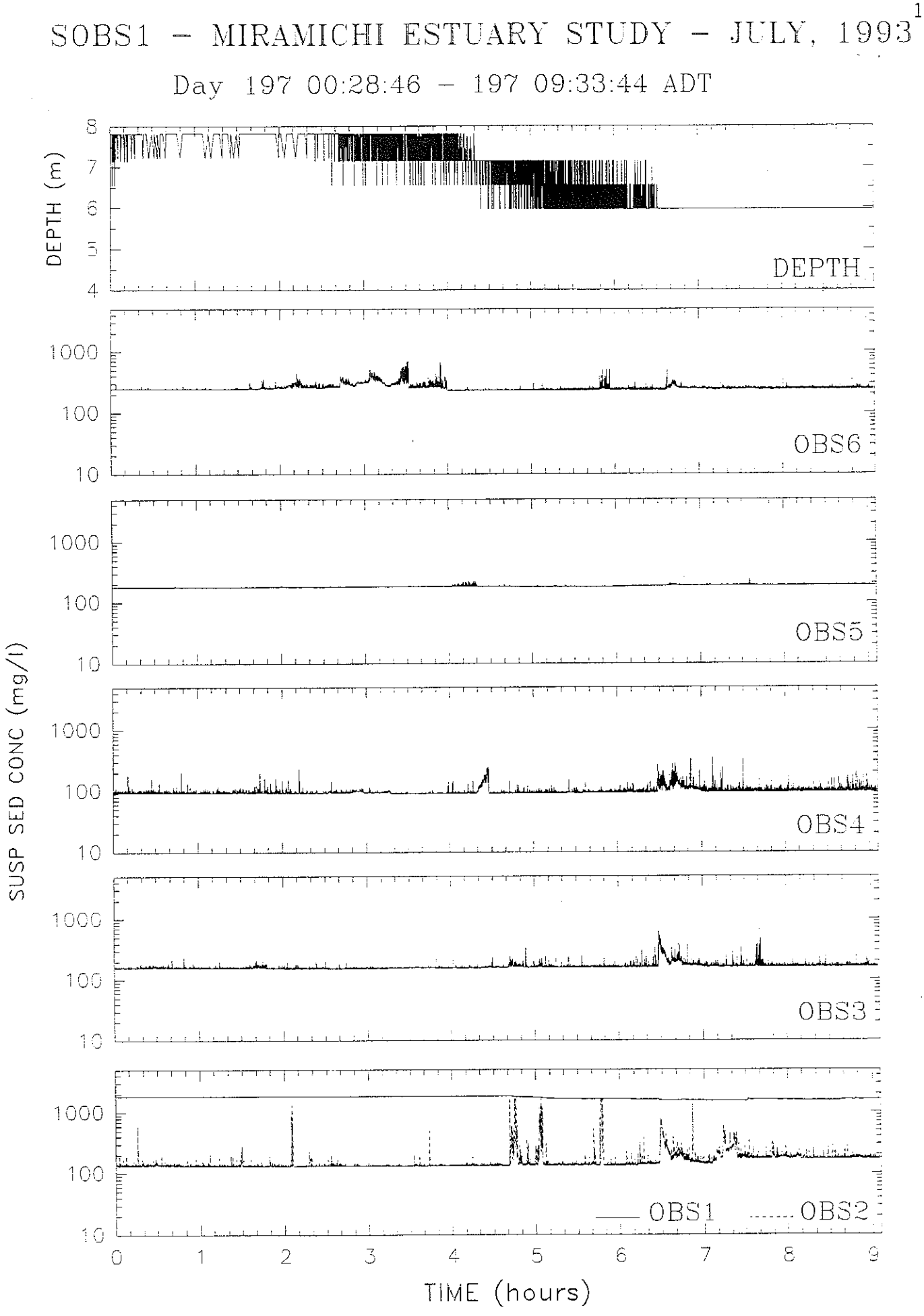

Figure 4.3.1-5. Time series of results from SOBS1 deployment at the Control site.

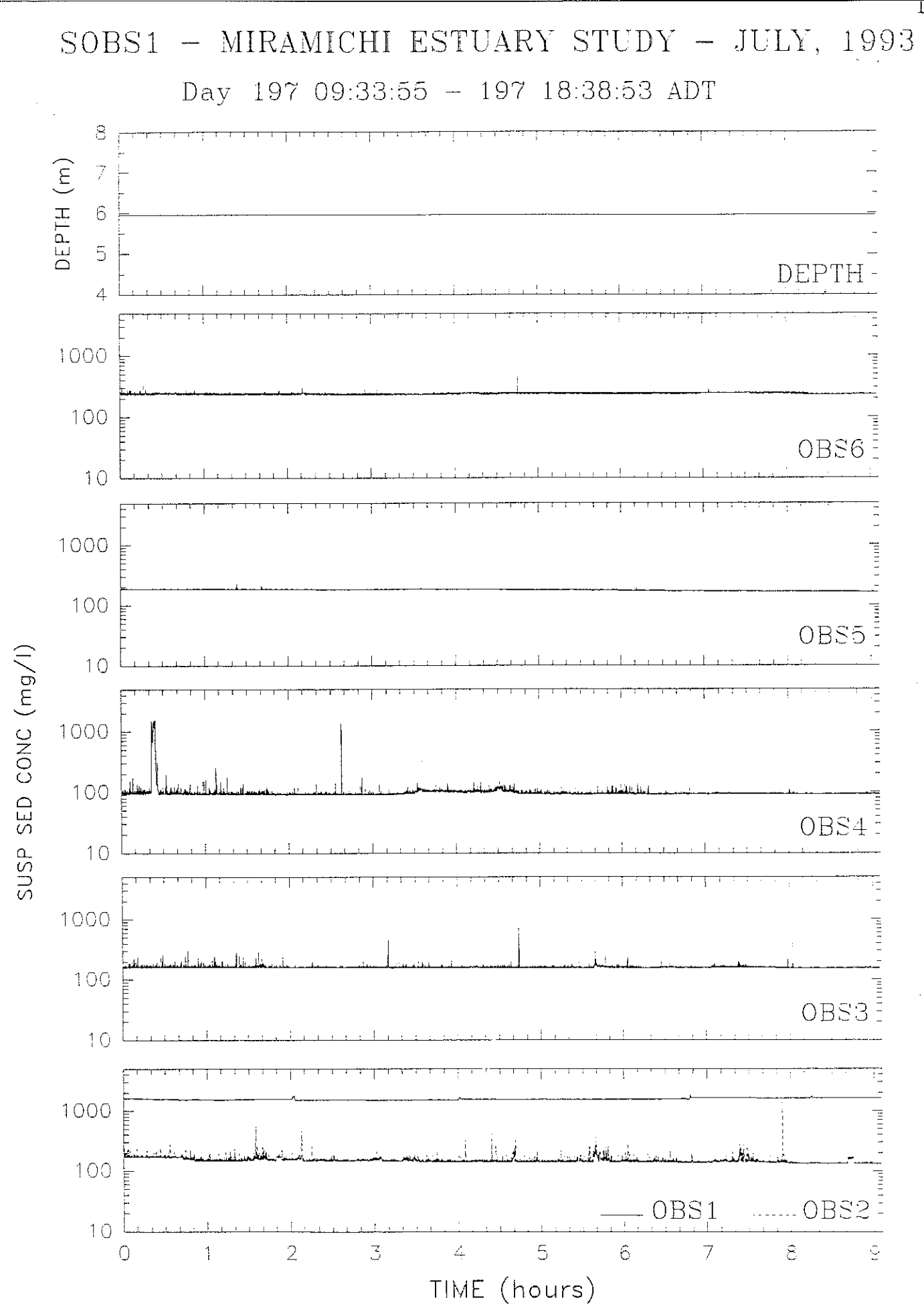

Figure 4.3.1-6. Time series of results from SOBS1 deployment at the Control site.

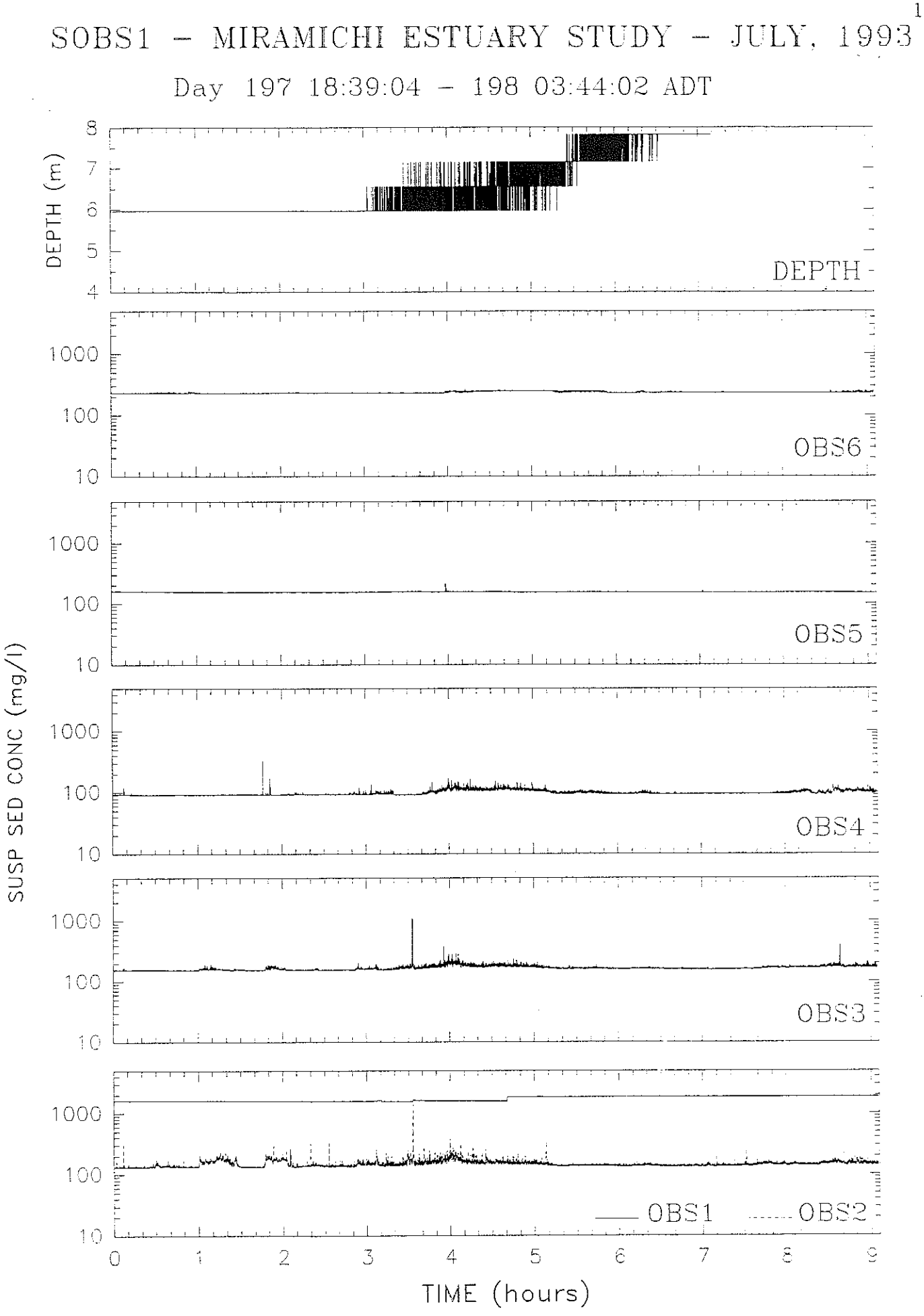

Figure 4.3.1-7. Time series of results from SOBS1 deployment at the Control site.

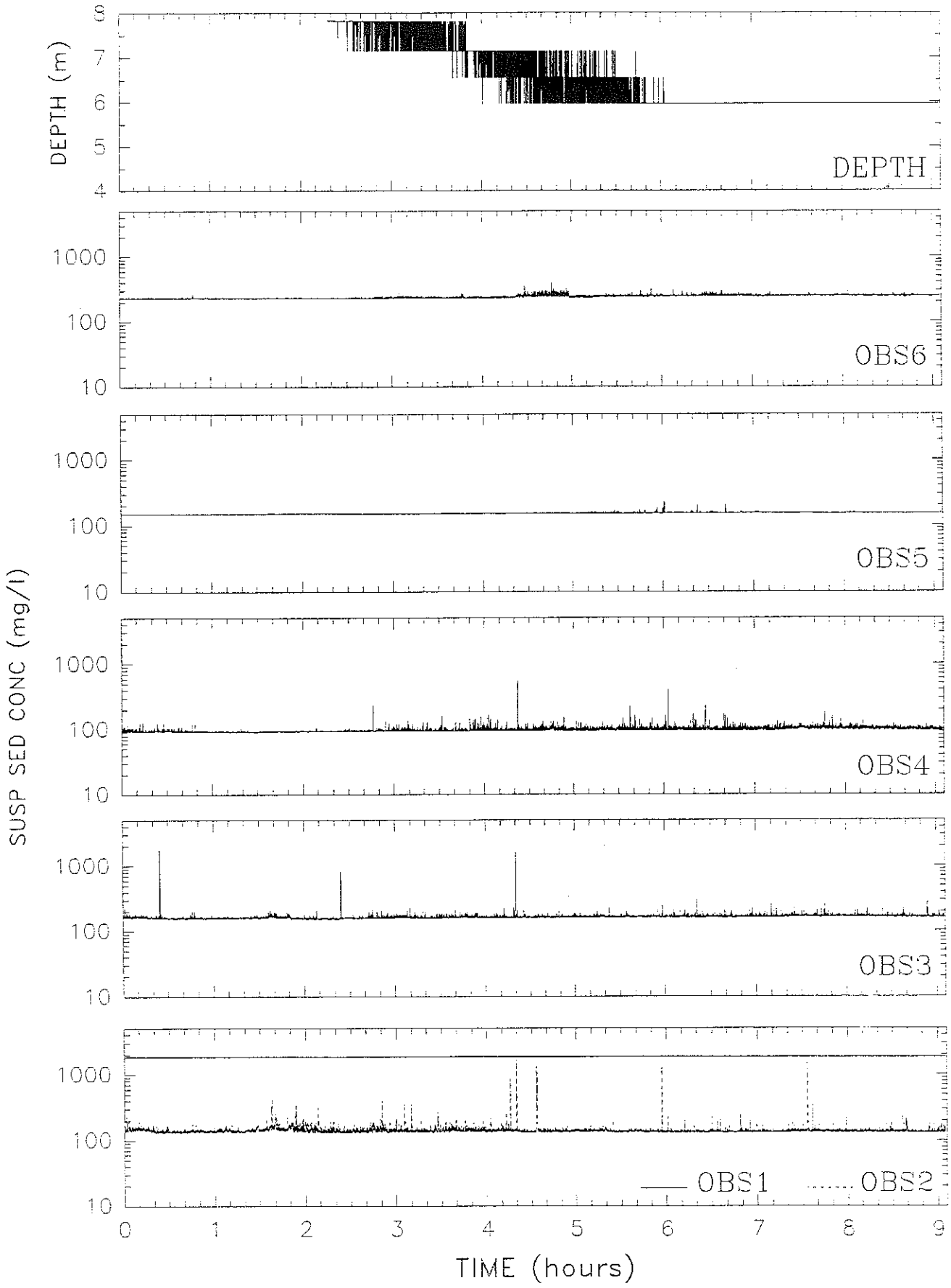

Figure 4.3.1-8. Time series of results from SOBS1 deployment at the Control site.

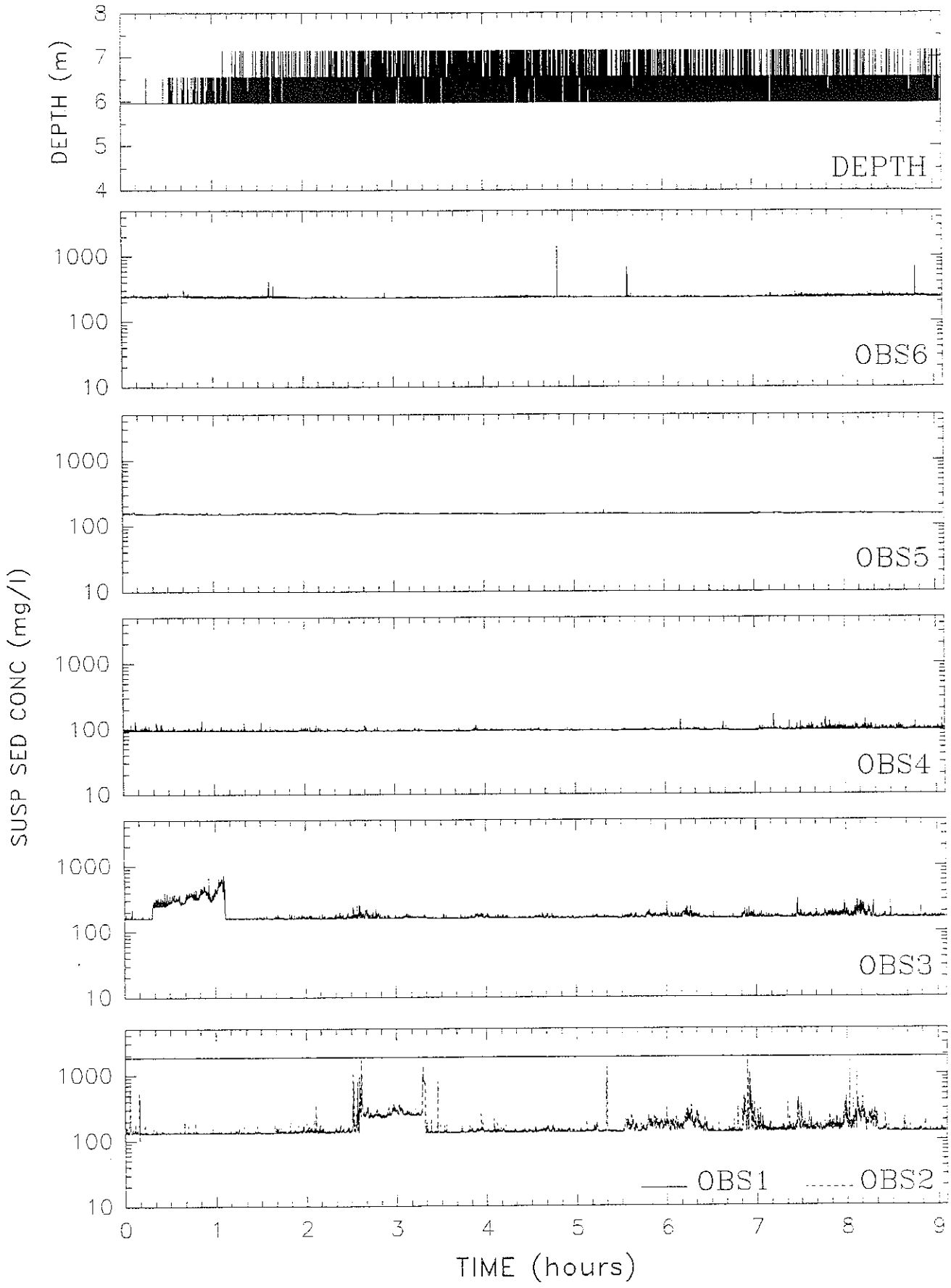

Figure 4.3.1-9. Time series of results from SOBS1 deployment at the Control site.

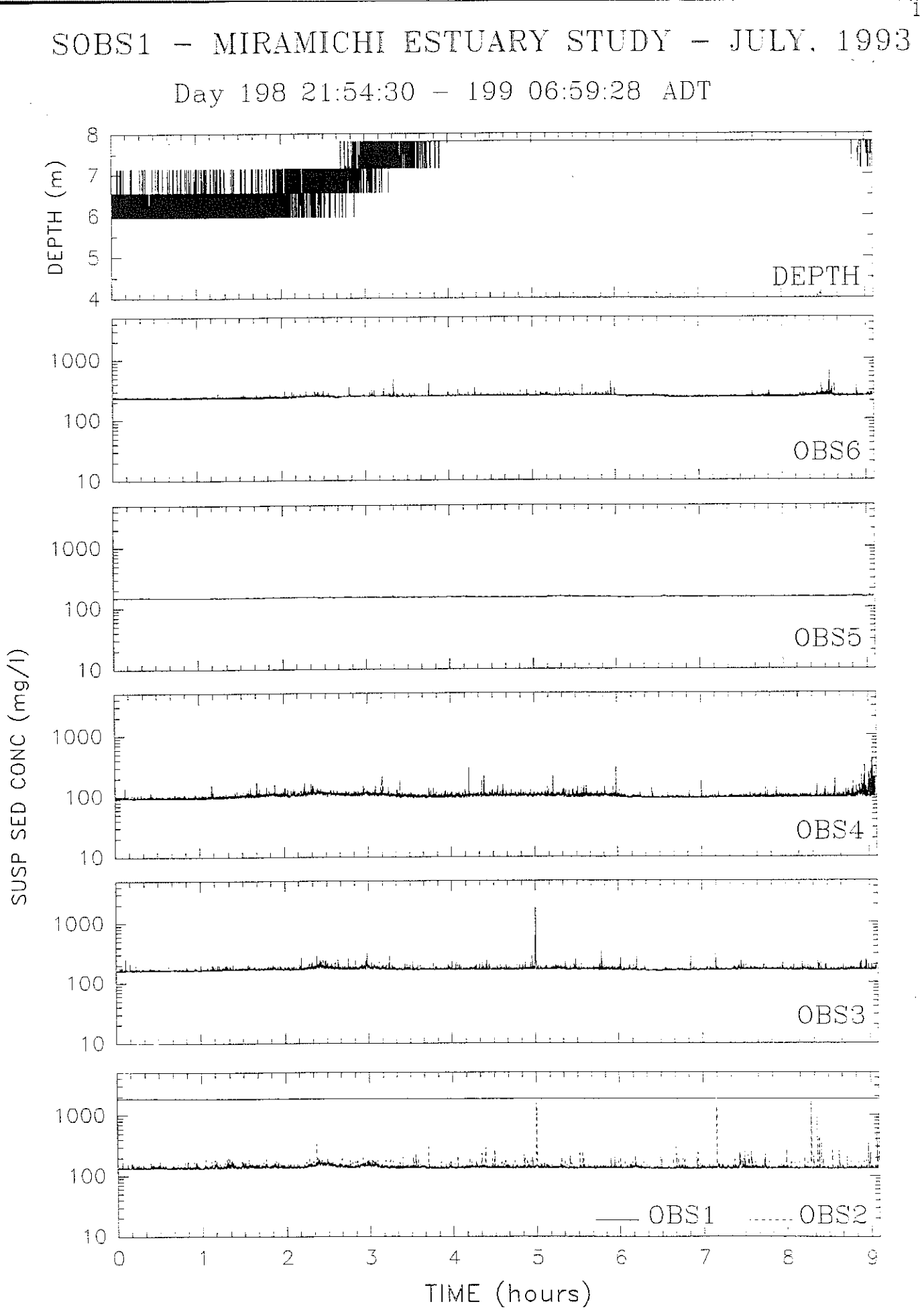

Figure 4.3.1-10. Time series of results from SOBS1 deployment at the Control site.

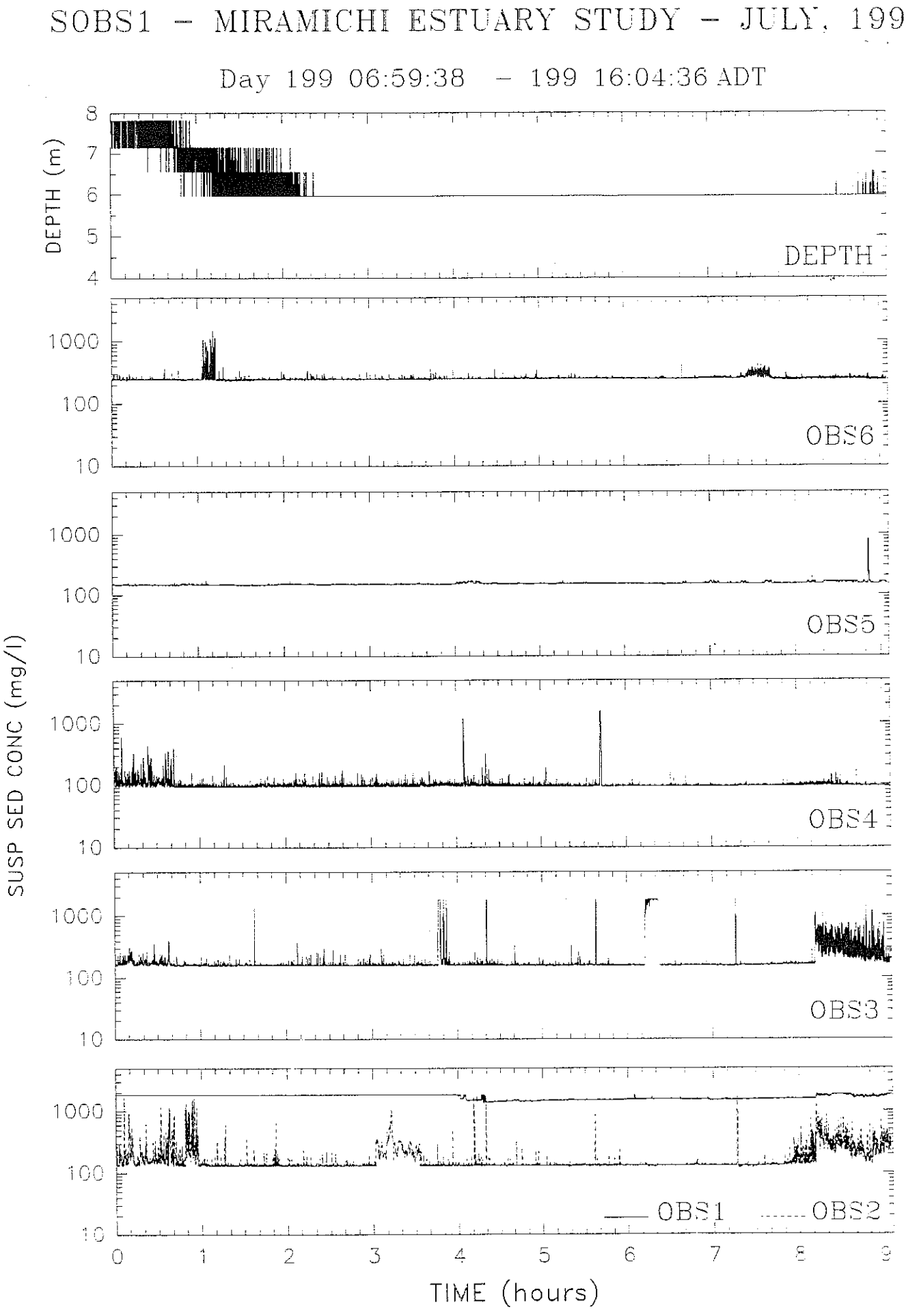

Figure 4.3.1-11. Time series of results from SOBS1 deployment at the Control site.

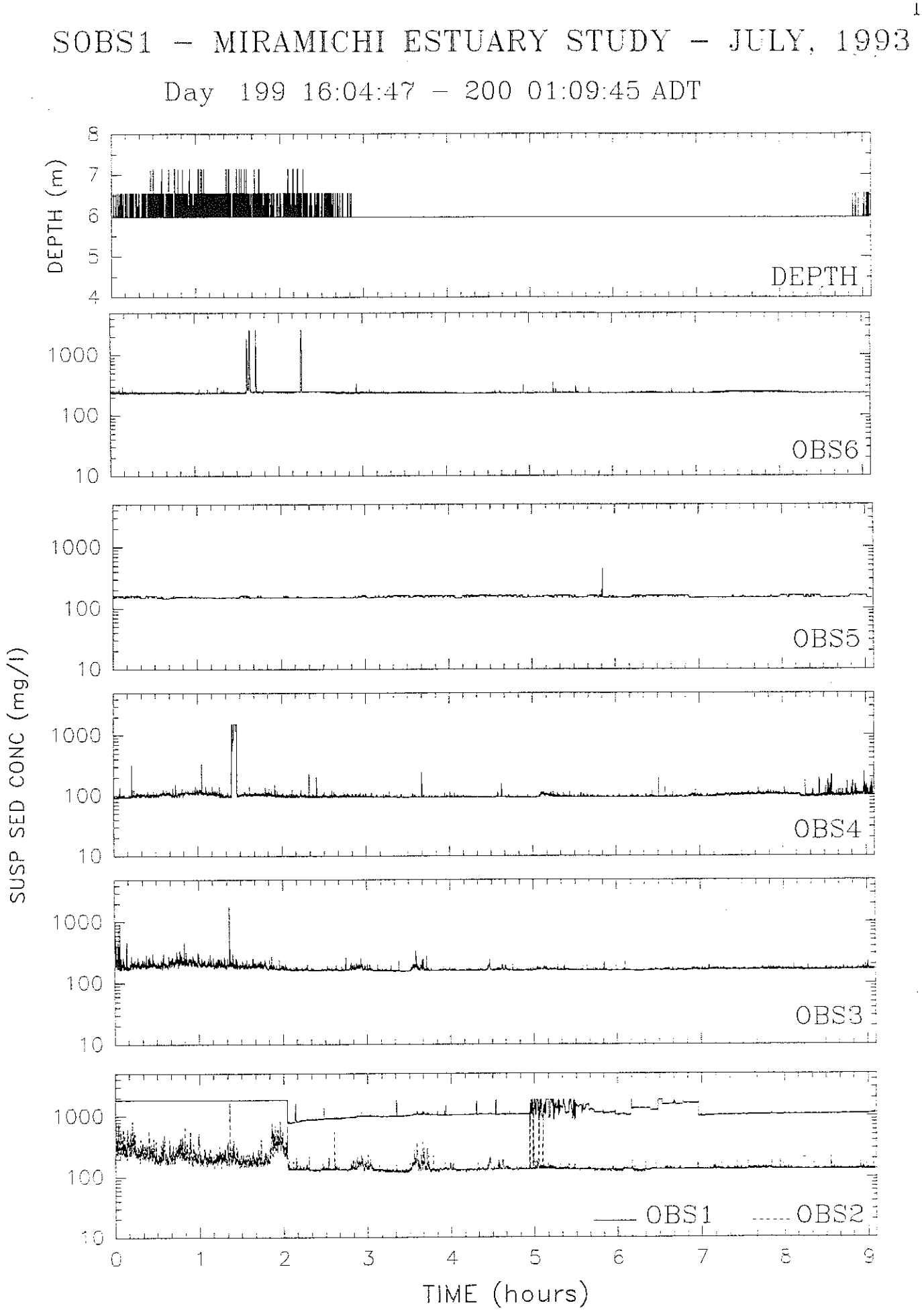

Figure 4.3.1-12. Time series of results from SOBS1 deployment at the Control site.

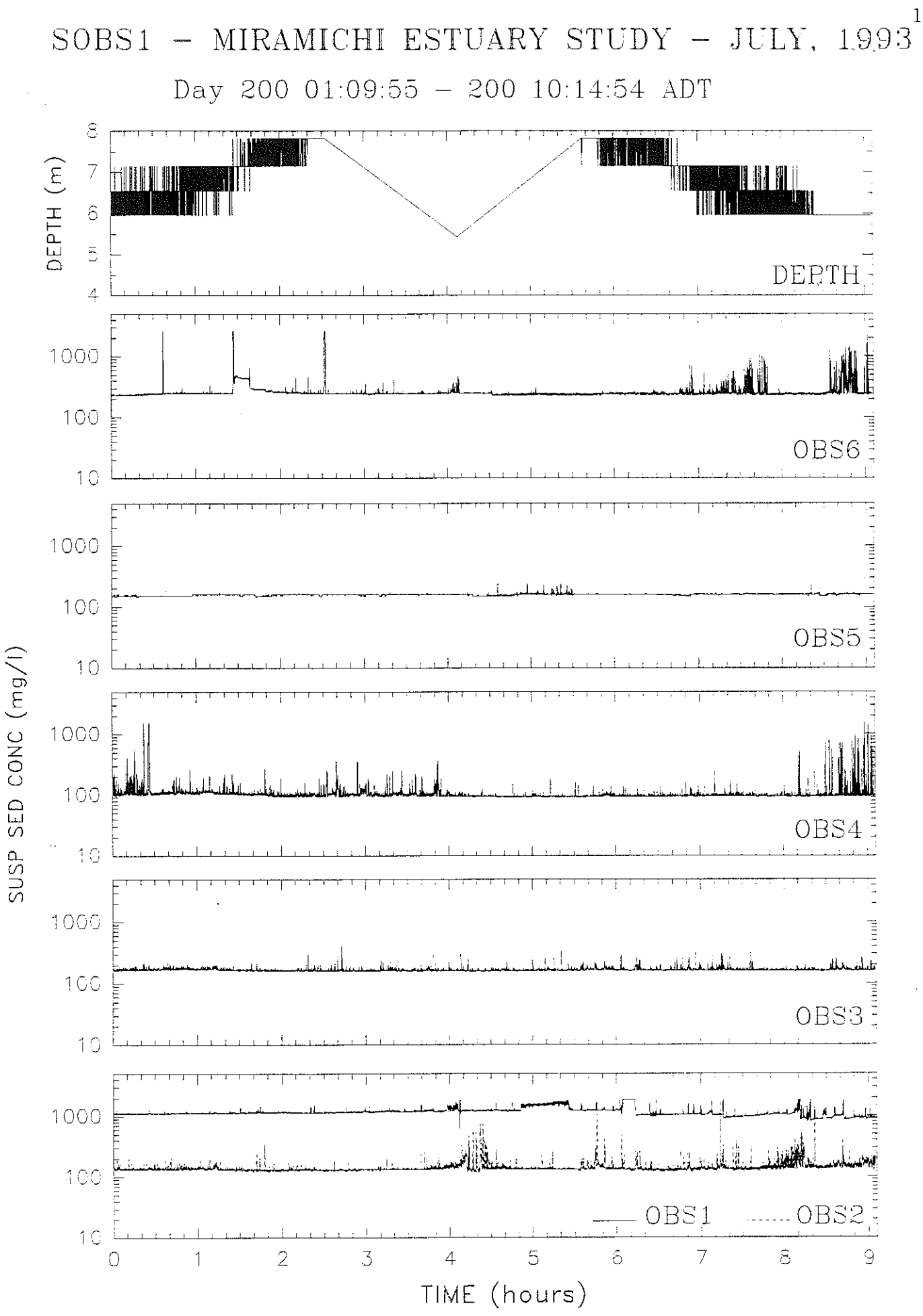

Figure 4.3.1-13. Time series of results from SOBS1 deployment at the Control site.

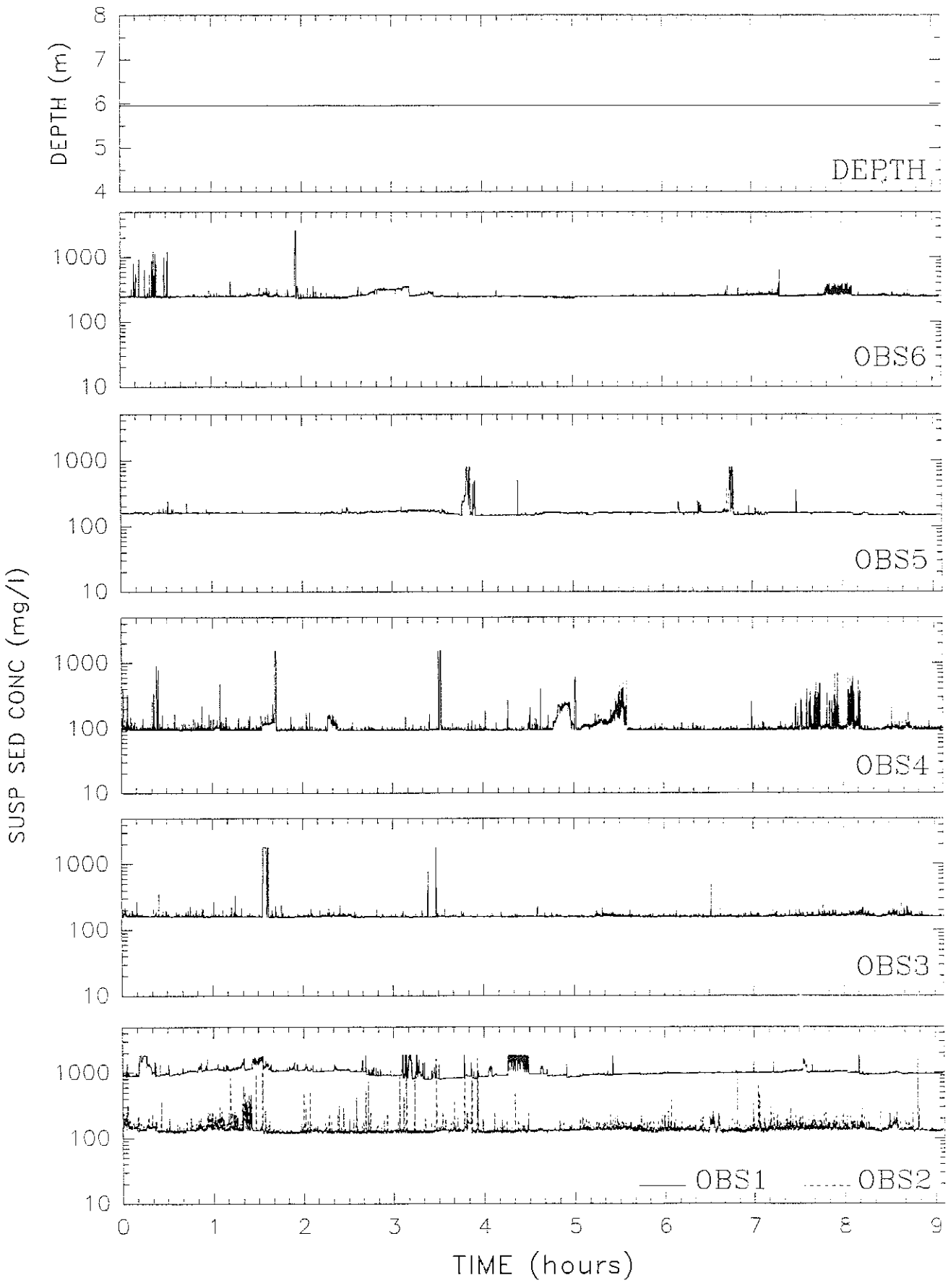

Figure 4.3.1-14. Time series of results from SOBS1 deployment at the Control site.

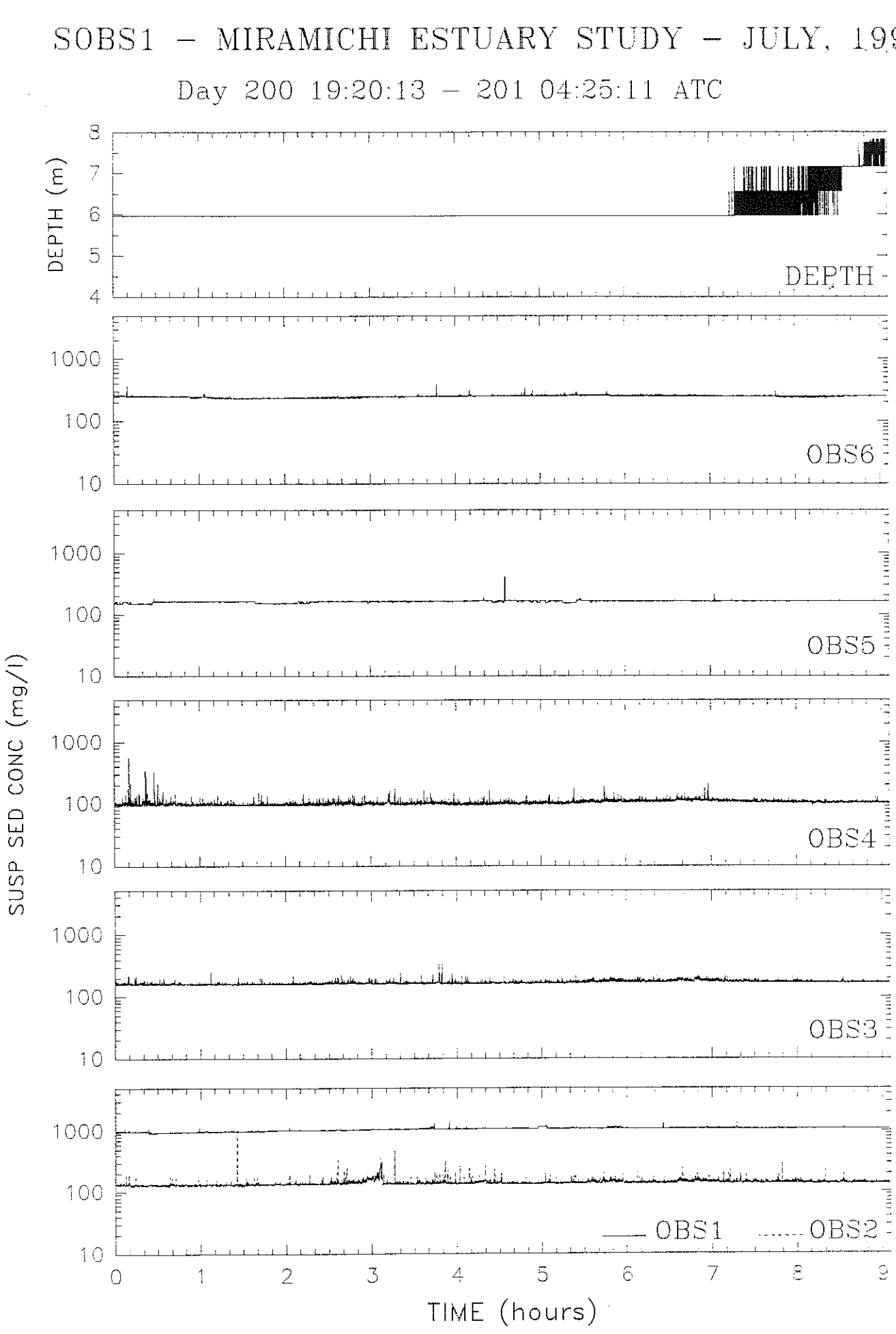

Figure 4.3.1-15. Time series of results from SOBS1 deployment at the Control site.

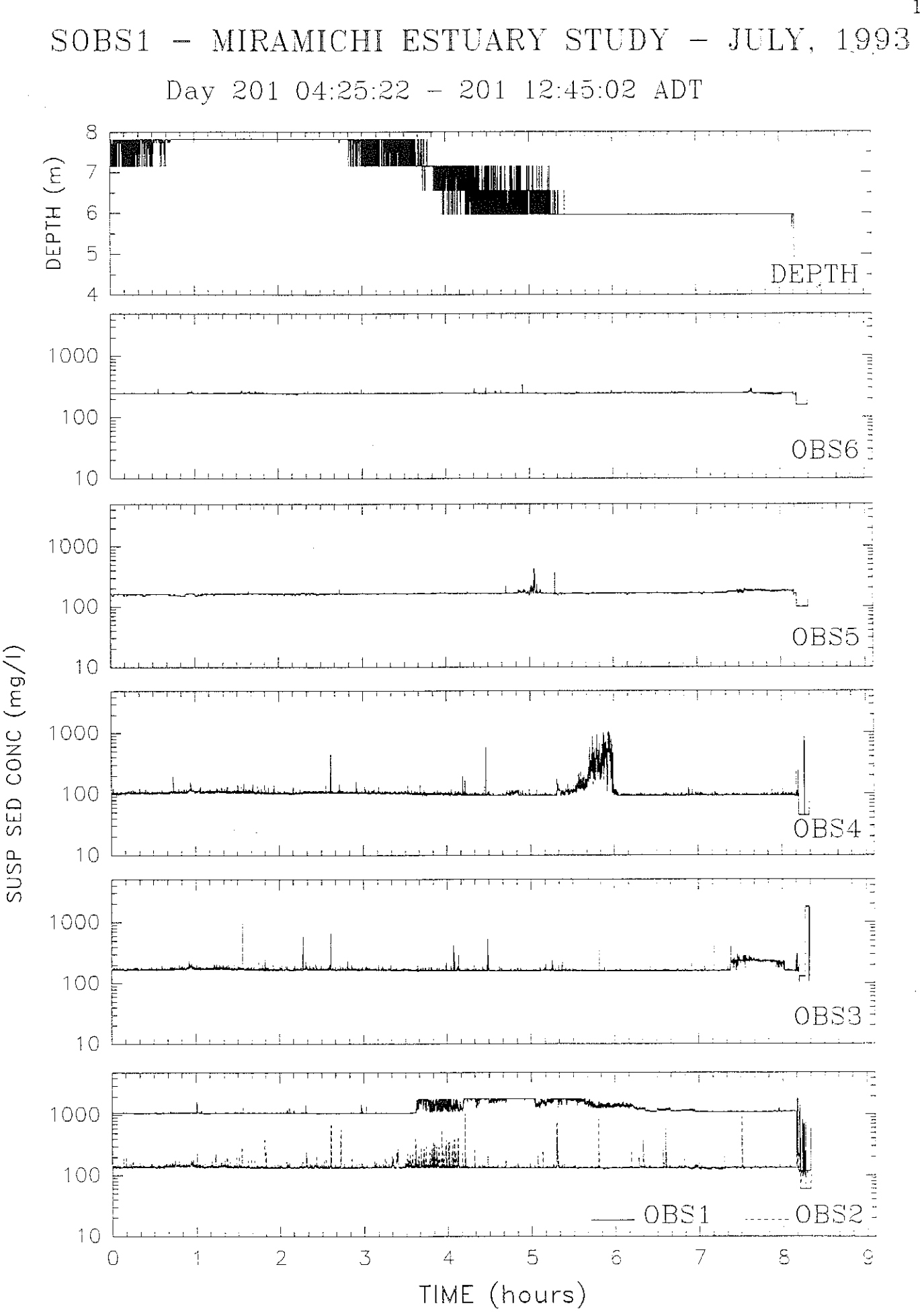

Figure 4.3.1-16. Time series of results from SOBS1 deployment at the Control site.

July 1993 (Fig. 4.3.1-5). These events produced a coherent response in all six OBS sensors. The bow wave of the ship caused seabed material to be resuspended to at least 1.8 m above the bed, and resulted in SSC's in excess of 2000 mg^{-1}. The bow wave resuspension event lasted only about 12 min. It peaked very sharply and thereafter decayed exponentially to background. A second broader resuspension event trailed the bow wave event; the wake resuspension cloud. This cloud persisted for up to 1 hr, was of lower concentration (300-400 mg^{-1}), and appeared to show undulations which we associate with cloud advection by the tide.

No coherent resuspension events could be firmly related to dredging of the Channel. Although resuspension during dredging was detected in the Channel (as reflections on the boat depth sounder), no sediments appeared to spill out of the Channel.

4.3.2 Experimental Dump Site

The SOBS deployment at the disposal site (SOBS2) was located at Lat: 47° 06.81' W, Lon: 09.70' N (Station 38). The site was situated in 5.5 m of water approximately 600 m east of the Experimental disposal site. It was deployed at 14:00 ADT, on 20 July 1993 (Julian Day 201) and was recovered at 11:05 ADT, on 27 July 1993 (Julian Day 208); a duration of 165 hrs. SOBS worked continuously throughout the deployment. The OBS sensors detected many resuspension events, but none that could be firmly linked to disposal activities.

The time-series of results from SOBS2 are shown on Figures 4.3.2-1 to 4.3.2-19. The figures illustrate the suspended sediment concentration (to a maximum of *circa* 3000 mg^{-1}) from the six OBS sensors, as well as the depth recorded by the pressure sensor. Each figure shows approximately 9 hrs of data. Full saturation of OBS1 suggests that it was close to the seabed or buried within it. All remaining OBS sensors showed backgrounds of between 100 and 200 mg^{-1}. OBS2 (the lowermost horizontal sensor) showed the greatest activity, while OBS's 5 and 6 showed the least. This suggests that small scale local resuspension events take place, but are restricted to the lowermost part of the water column. Many of these events may be ascribed to resuspension of organic "fluff" by tidal flow. Such tidal resuspension events are evident in Figures 4.3.2-2 (hrs 5-7). Evidence for wave resuspension is apparent in Figures 4.3.2-5 and 4.3.2-6 (22 July 1993) and in Figure 4.3.2-8 (the afternoon of 23 July, 1993). Most of the disposal of dredged material at the Experimental disposal site took place between days 201-204 (20-23 July 1993). Coherent events within the water column were detected by OBS's 4, 5 and 6 on days 202 and 203 (Figs. 4.3.2-3 and 4.3.2-5). However, these events were of low concentration (200-300 mg^{-1}). Furthermore, a similar event is evident in Figure 4.3.2-16 (Julian Day 207) when no disposal was taking place. Consequently, these events cannot be directly linked with disposal activities.

The sea state on 25 July 1993 (Julian Day 206) was rough. This period of rough weather corresponds to the highest and longest-lasting turbid events. Though largely restricted to OBS sensors 2 and 3, concentrations exceeded 2000 mg^{-1} and the sensors were saturated for up to 6 hrs over a 24 hr period (Figs. 4.3.2-13 to 4.3.2-16). This turbid layer was restricted to the lowermost 0.27-0.41 m of the water column. The dramatic difference in responses

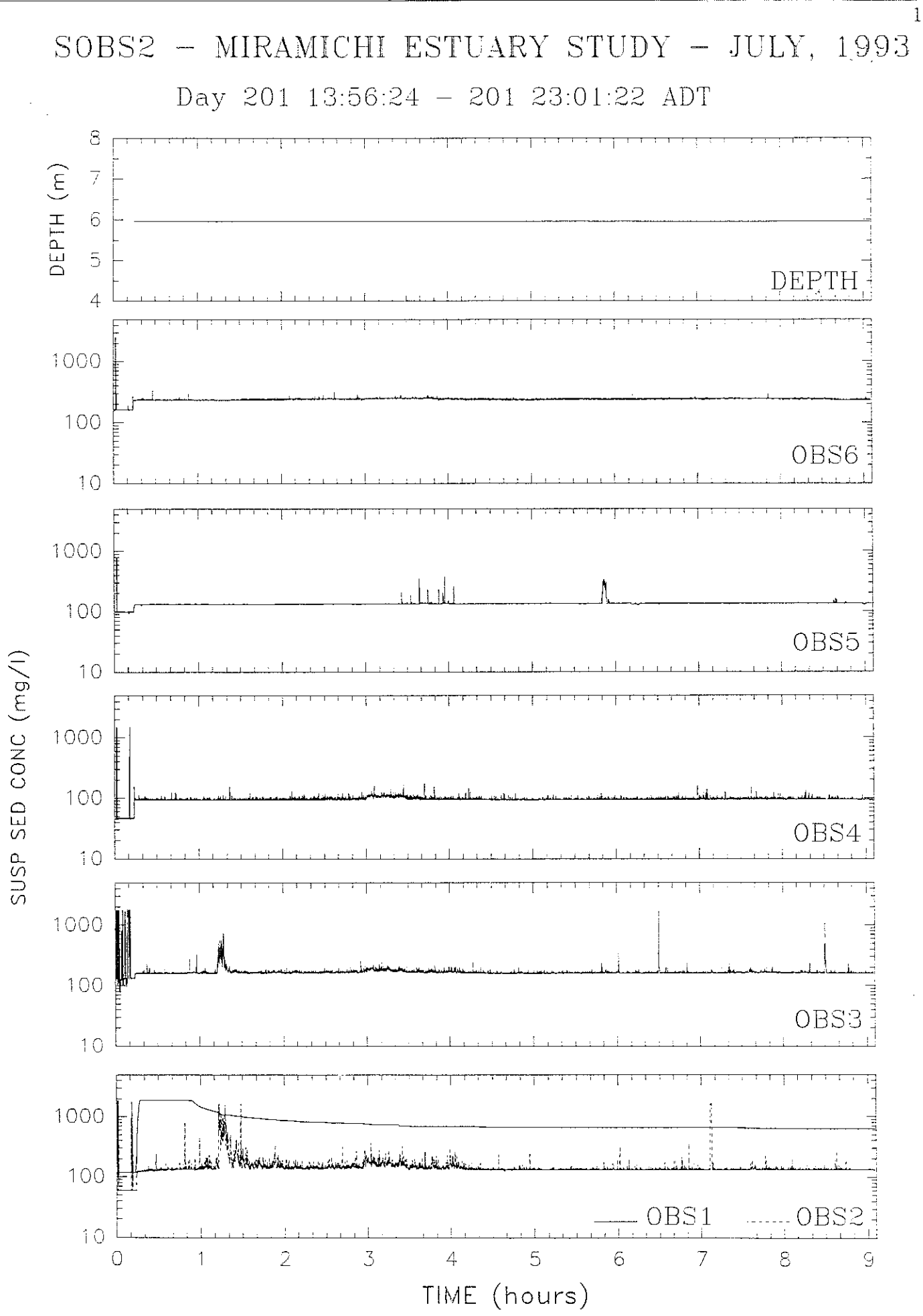

Figure 4.3.2-1. Time series of results from SOBS2 deployment at the Experimental site.

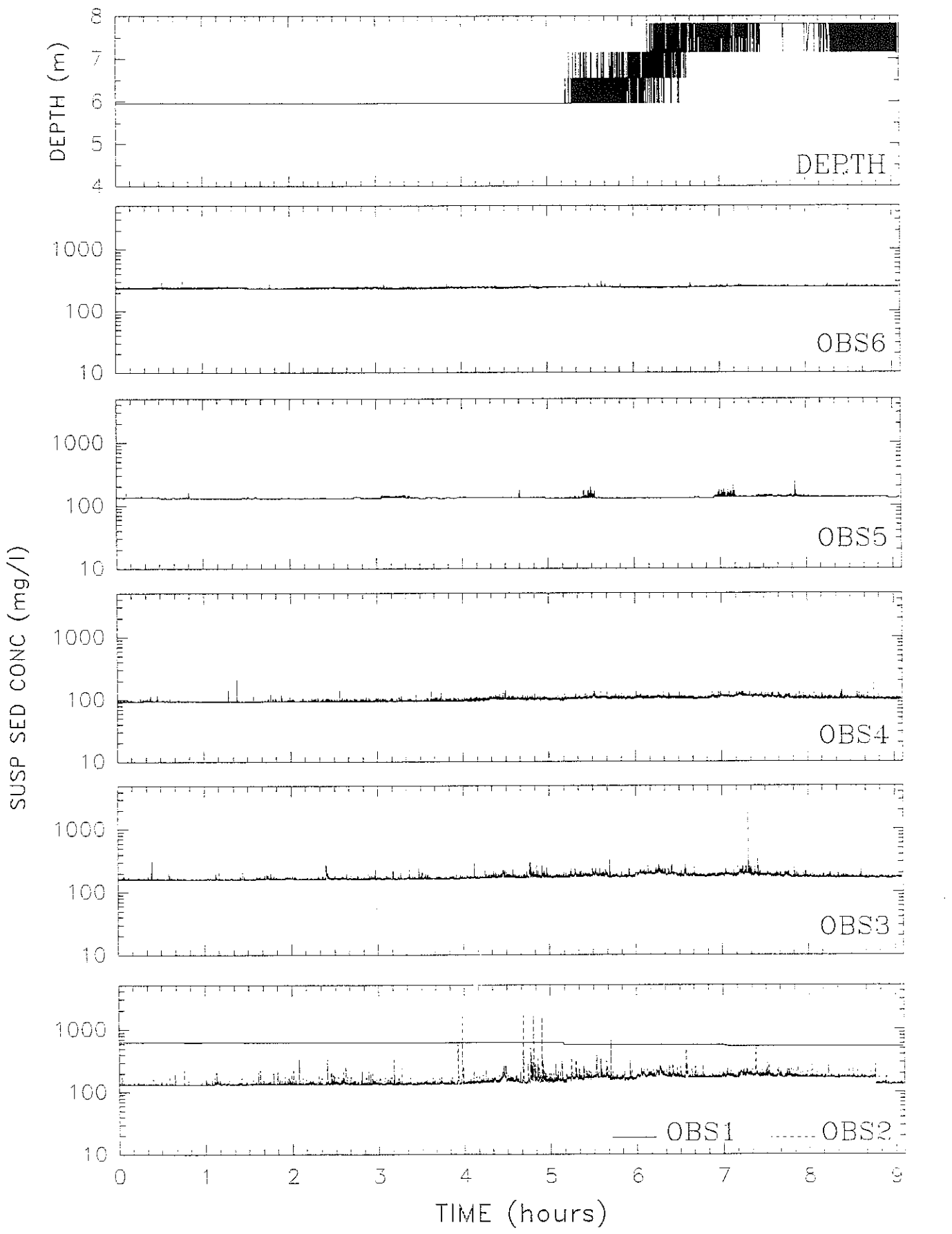

Figure 4.3.2-2. Time series of results from SOBS2 deployment at the Experimental site.

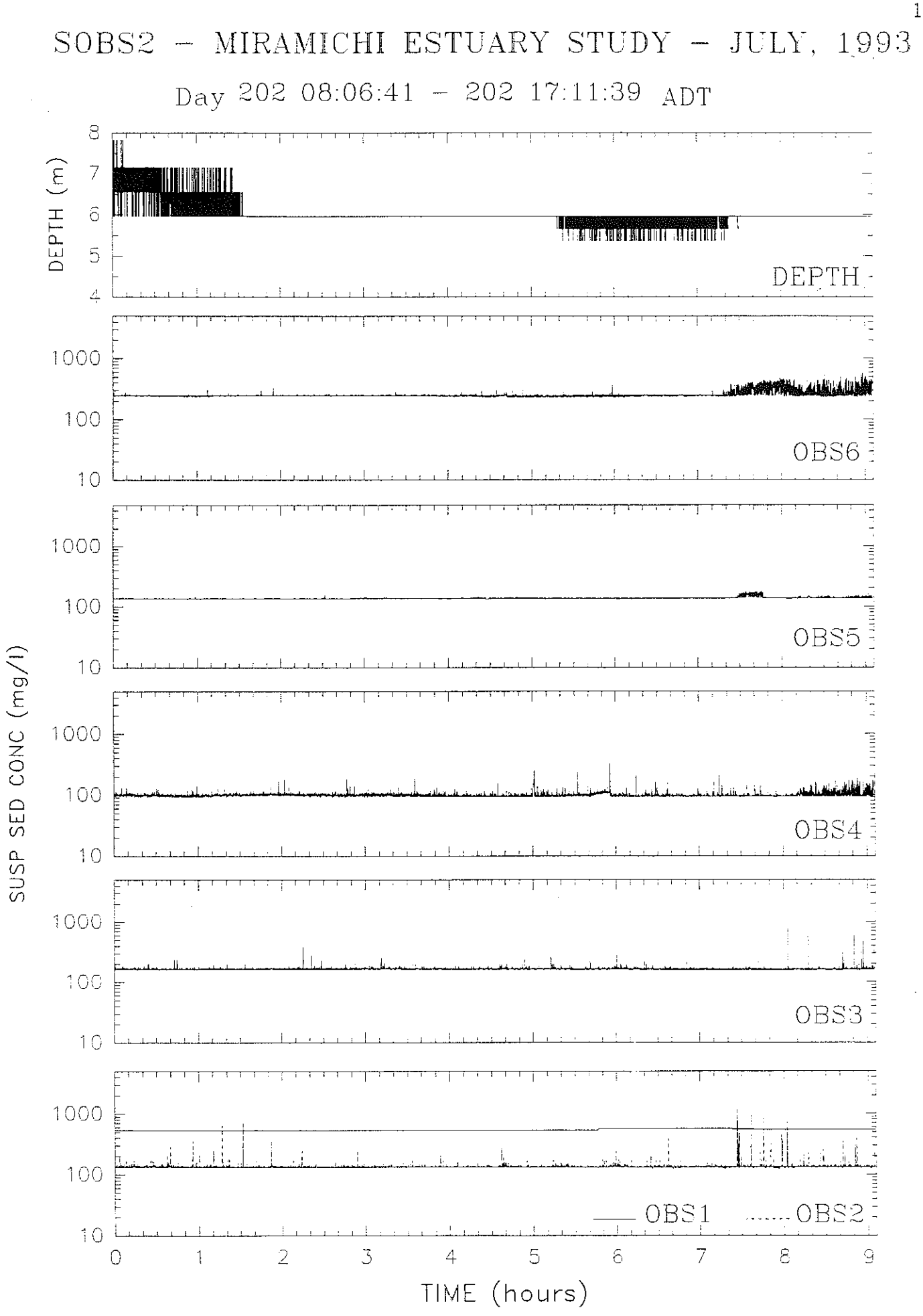

Figure 4.3.2-3. Time series of results from SOBS2 deployment at the Experimental site.

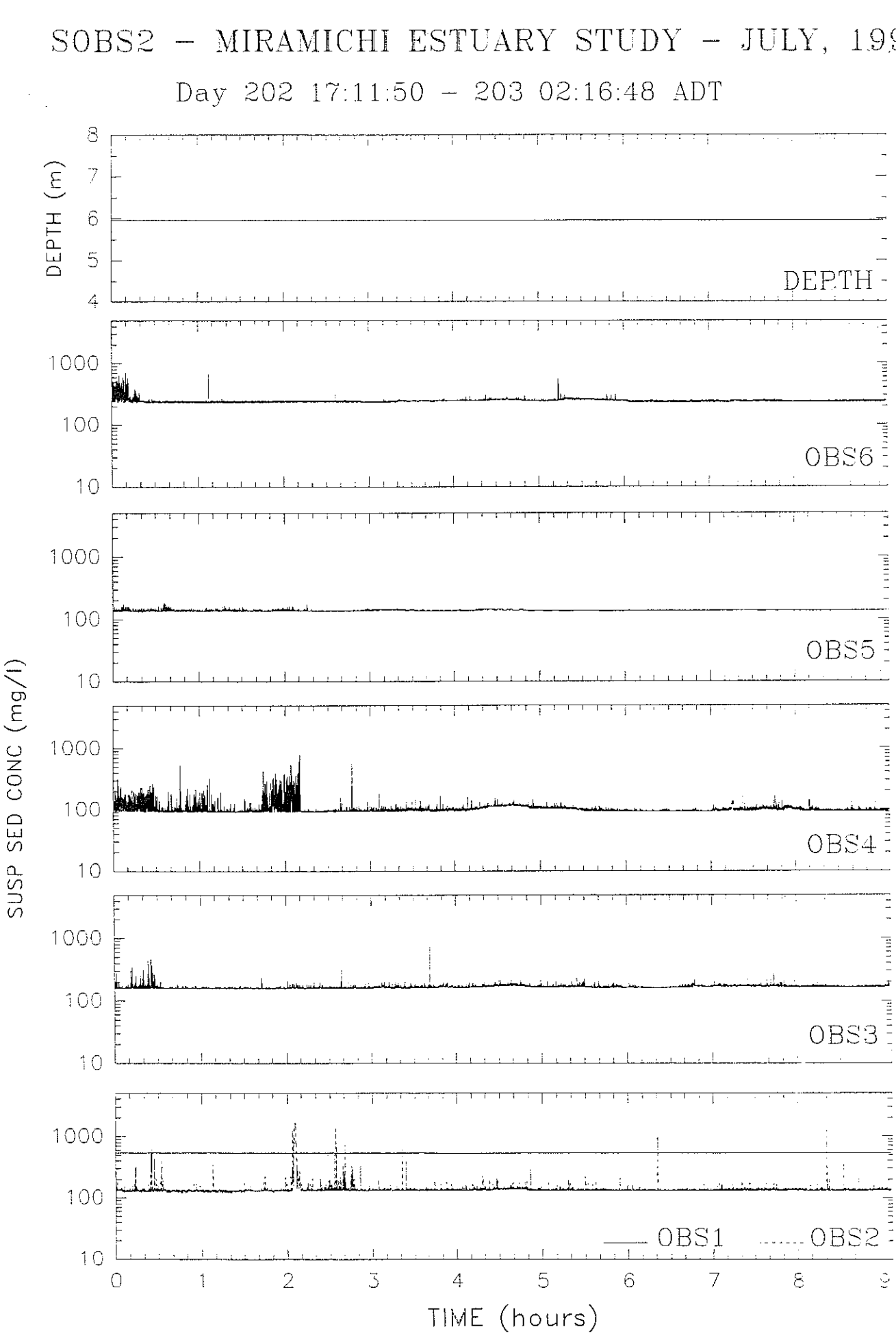

Figure 4.3.2-4. Time series of results from SOBS2 deployment at the Experimental site.

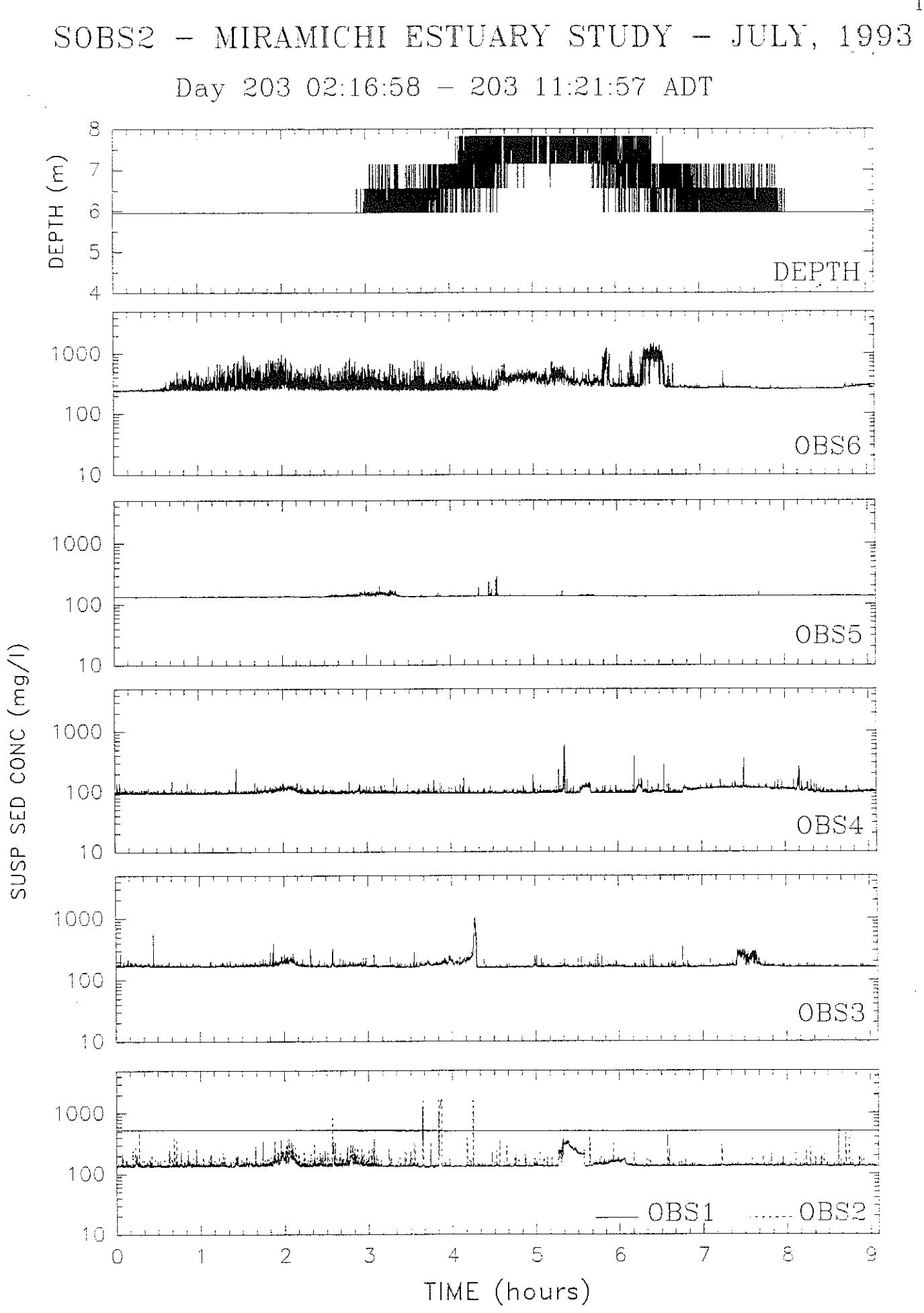

Figure 4.3.2-5. Time series of results from SOBS2 deployment at the Experimental site.

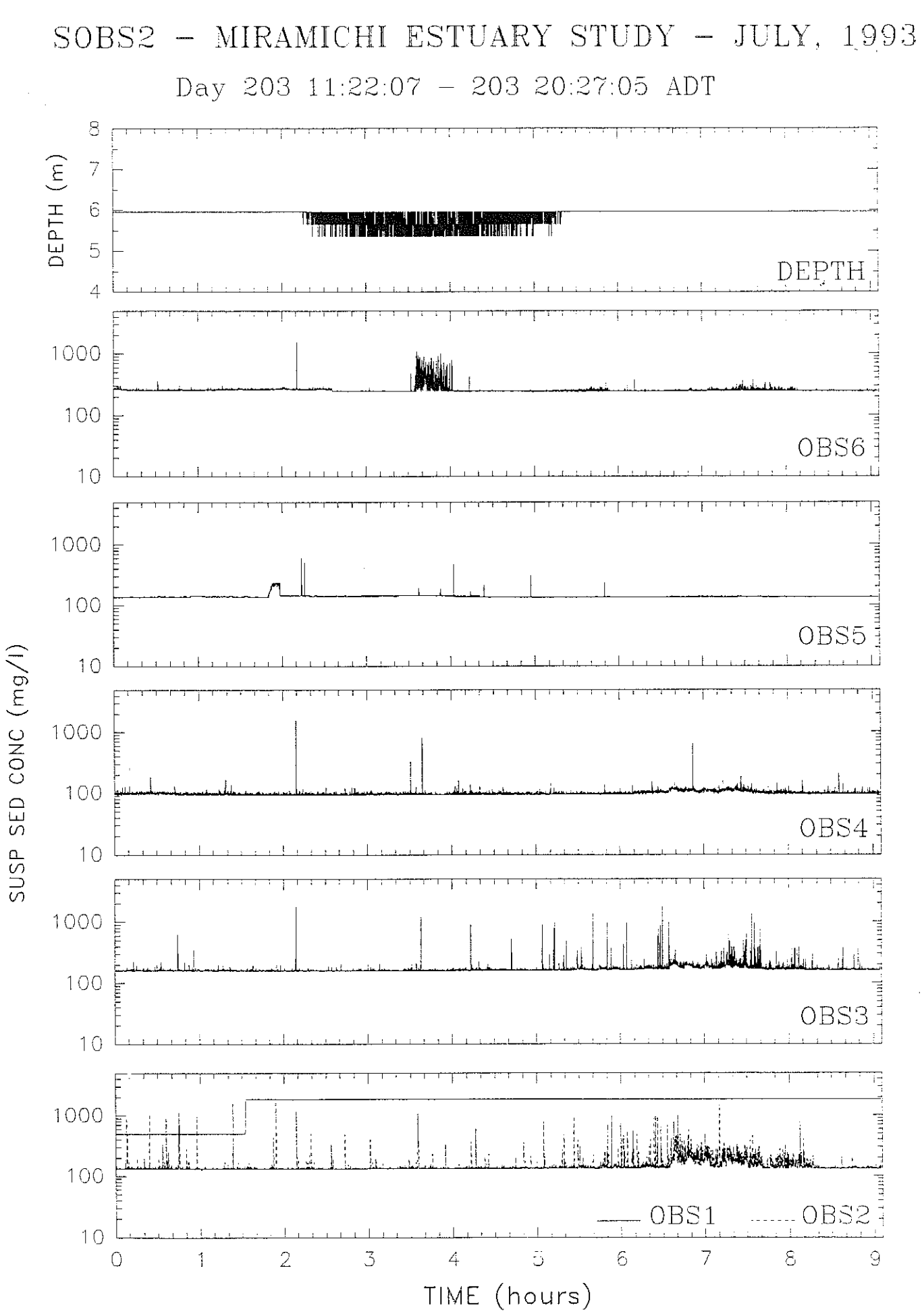

Figure 4.3.2-6. Time series of results from SOBS2 deployment at the Experimental site.

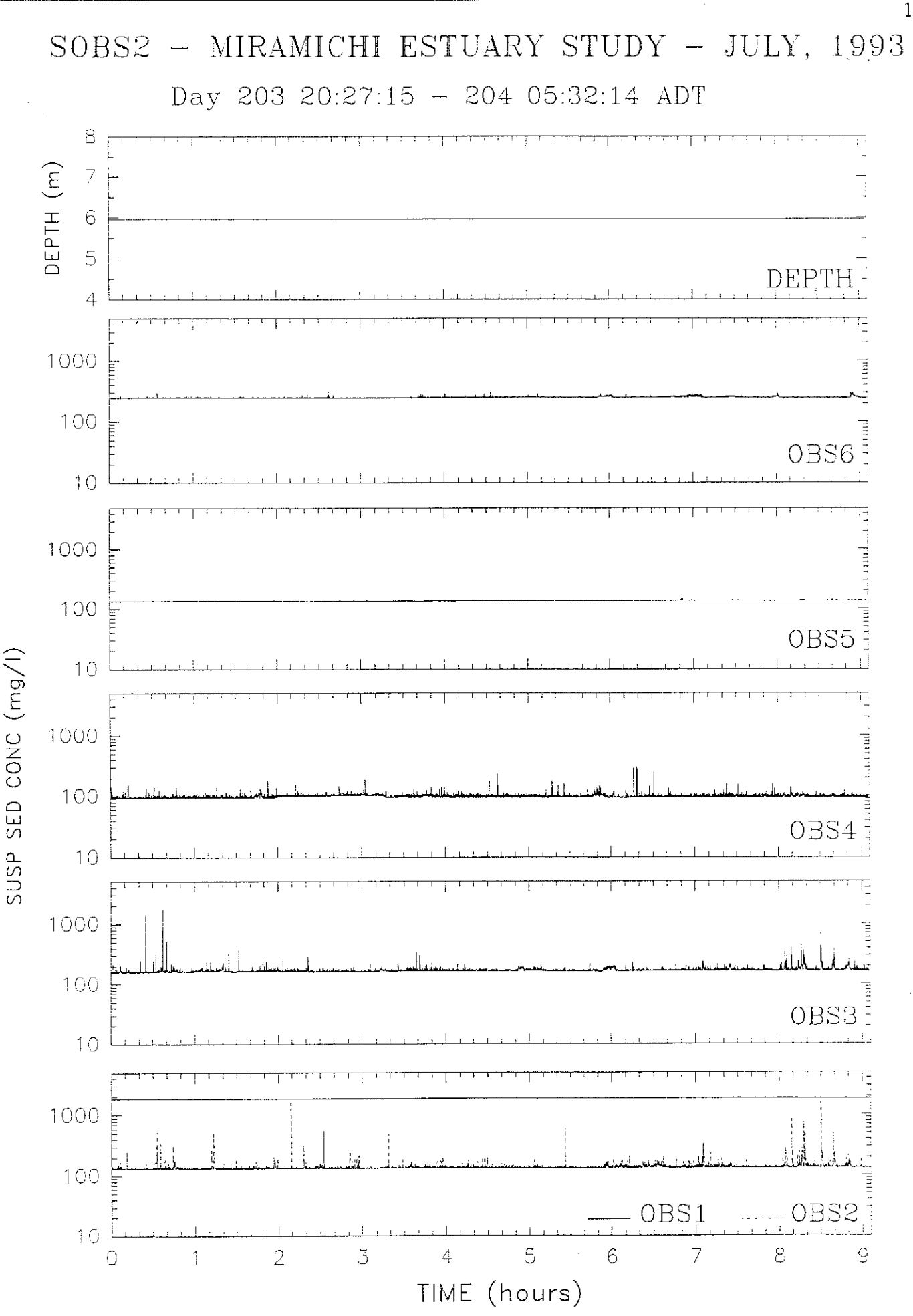

Figure 4.3.2-7. Time series of results from SOBS2 deployment at the Experimental site.

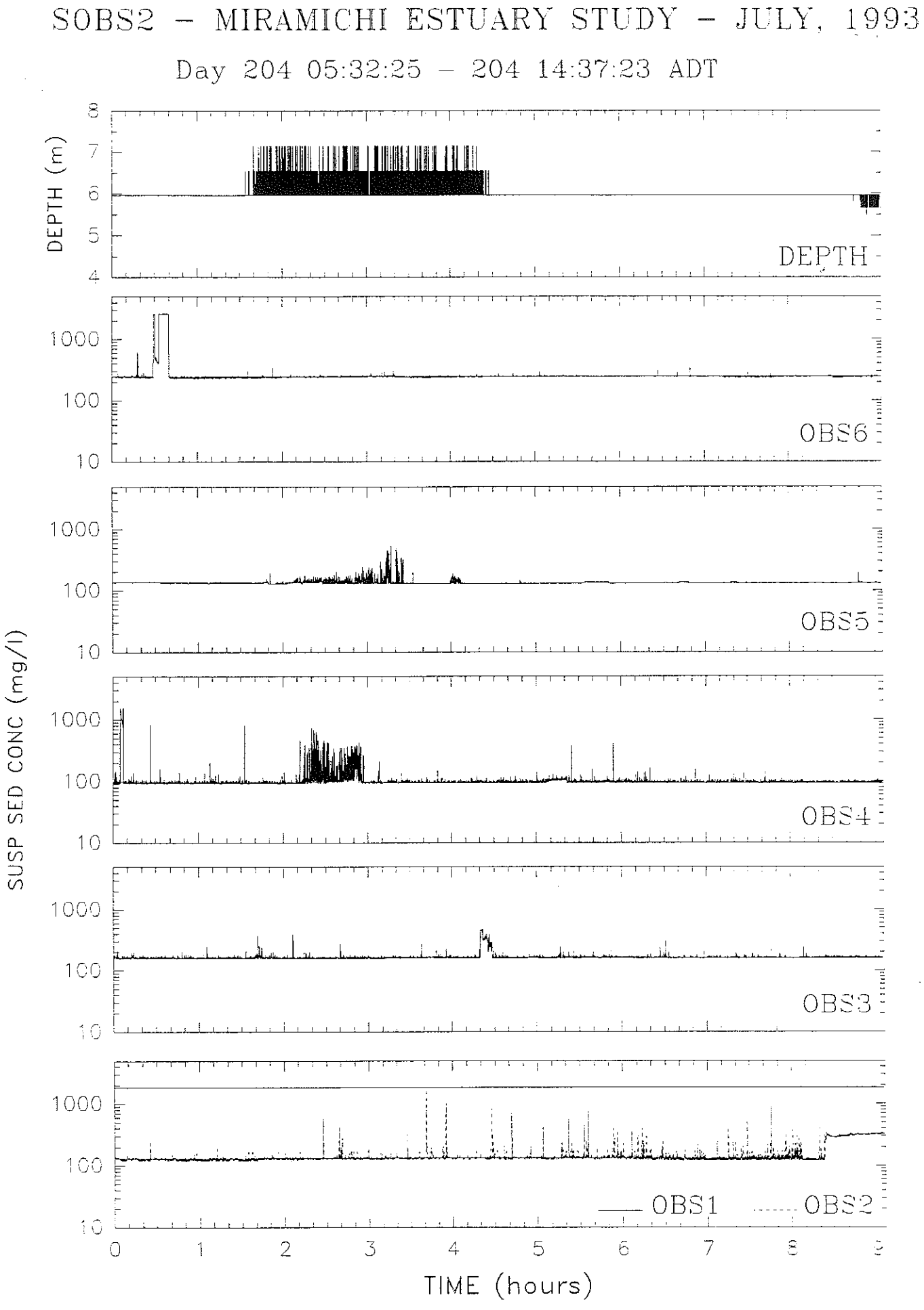

Figure 4.3.2-8. Time series of results from SOBS2 deployment at the Experimental site.

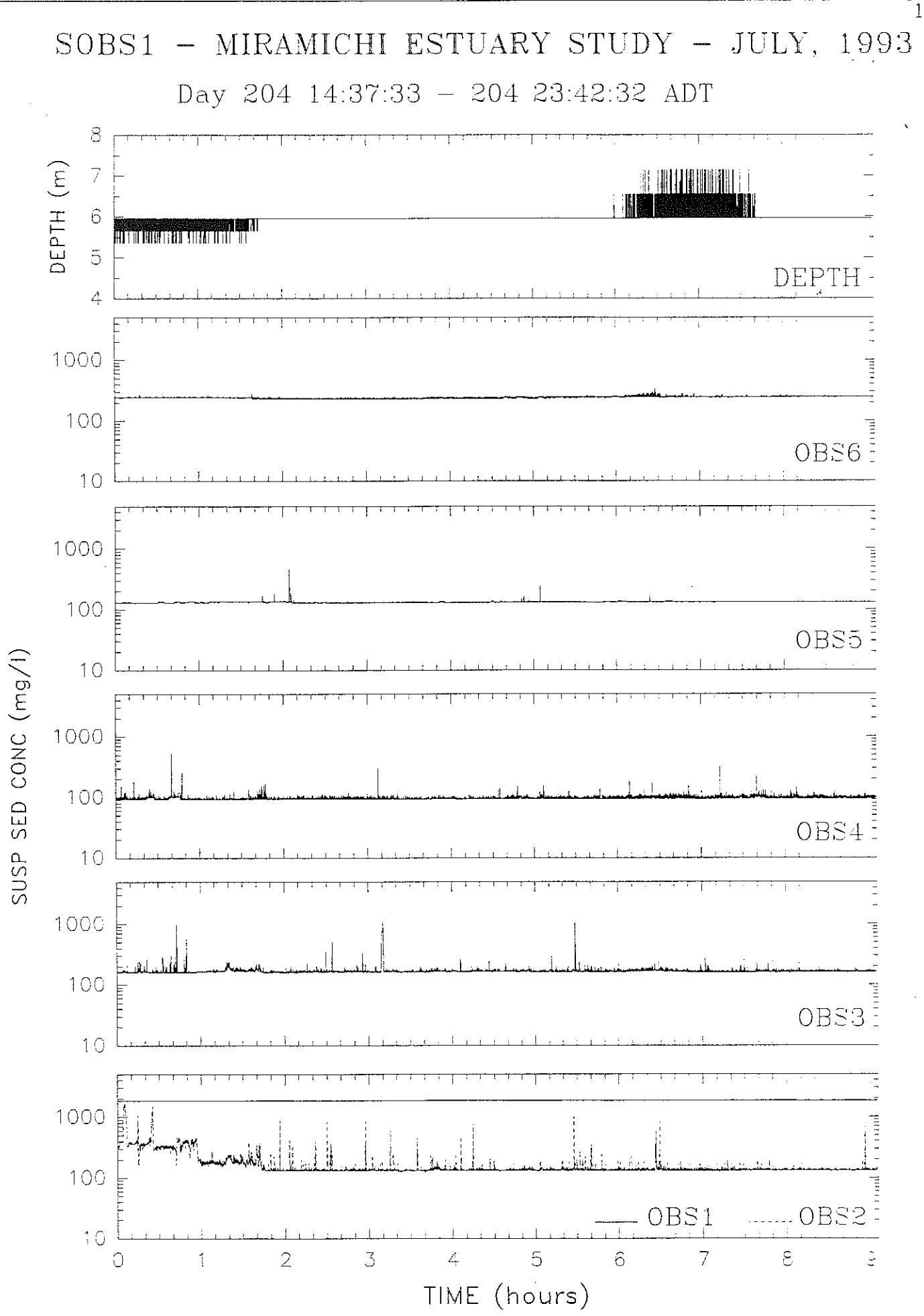

Figure 4.3.2-9. Time series of results from SOBS2 deployment at the Experimental site.

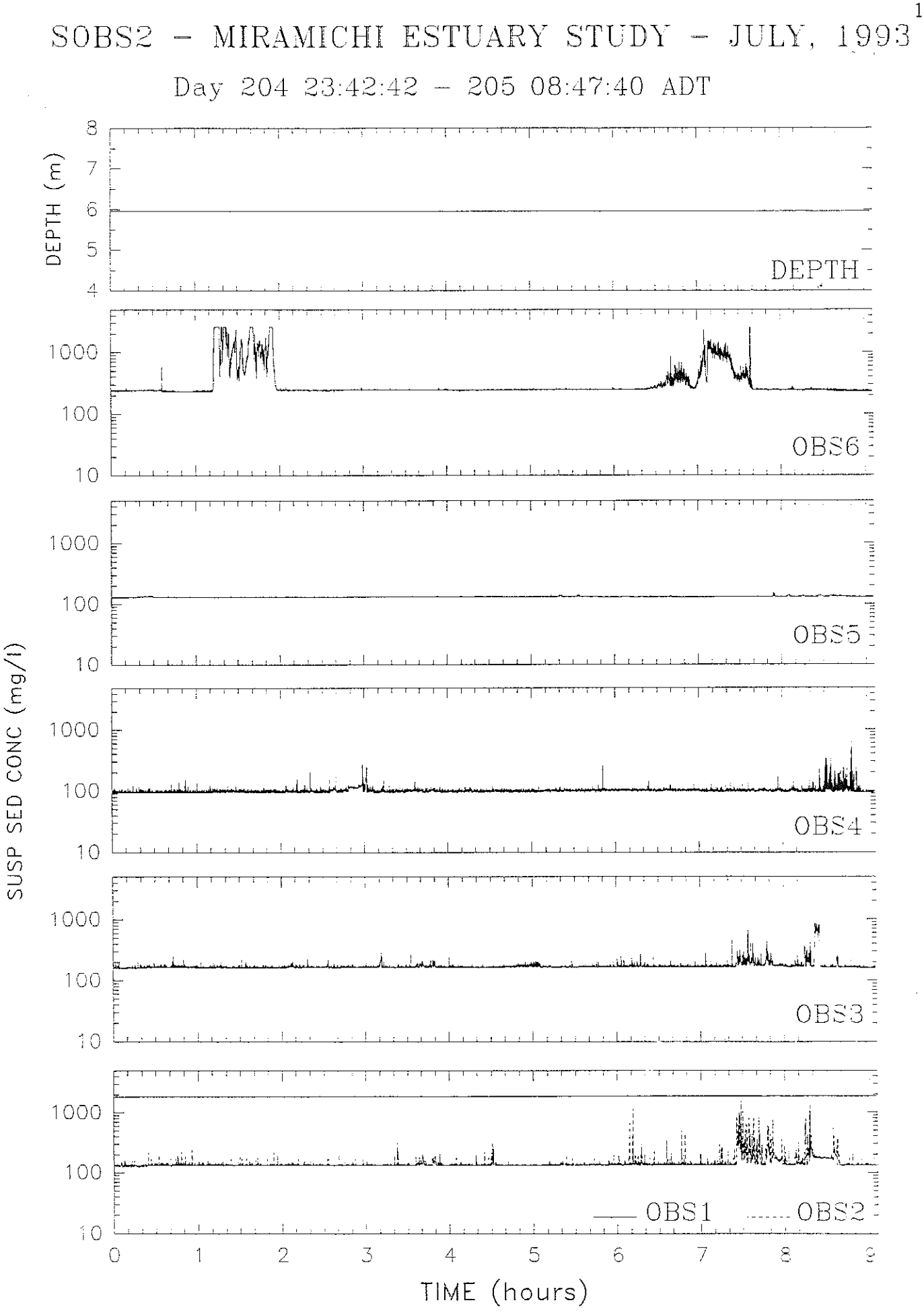

Figure 4.3.2-10. Time series of results from SOBS2 deployment at the Experimental site.

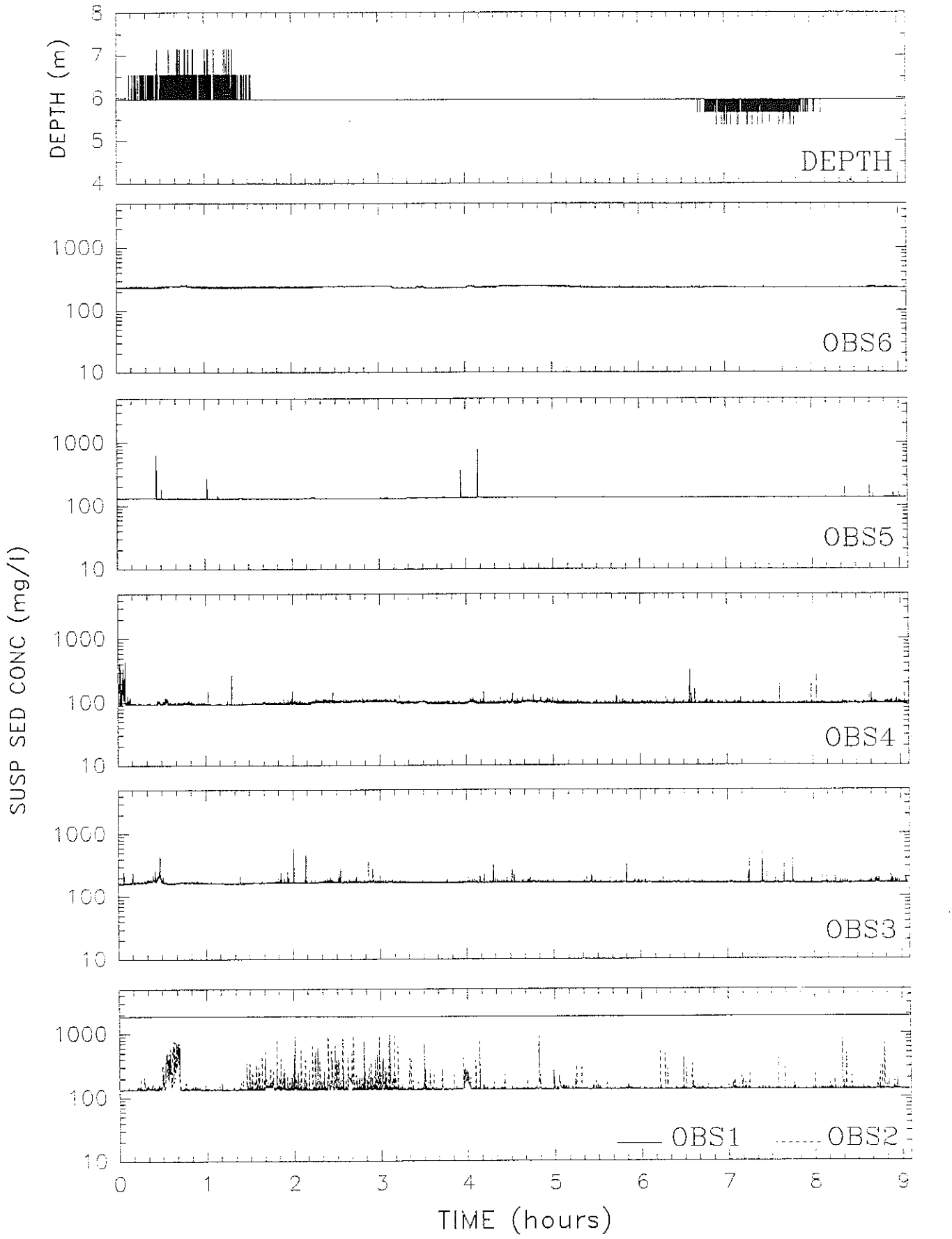

Figure 4.3.2-11. Time series of results from SOBS2 deployment at the Experimental site.

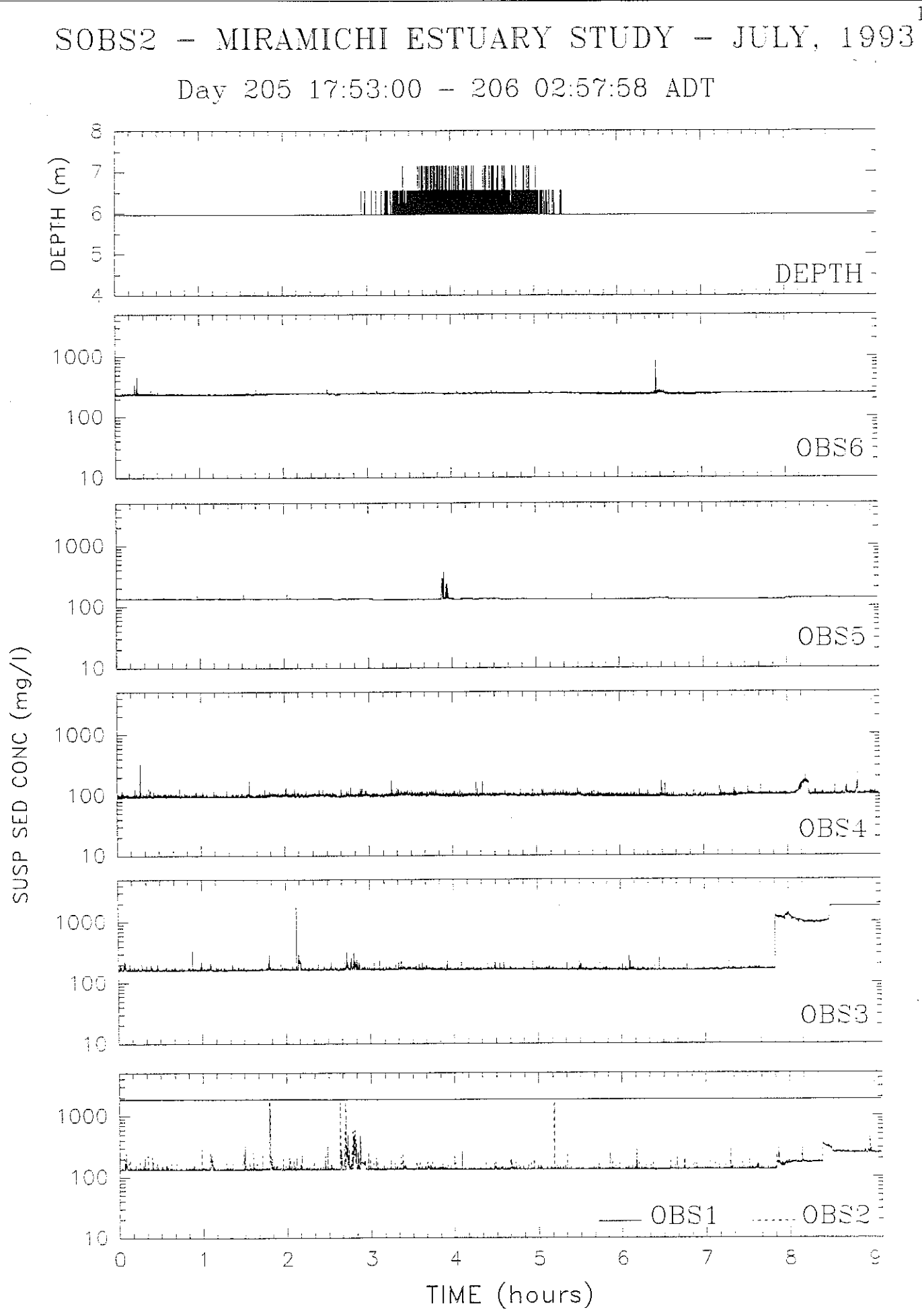

Figure 4.3.2-12. Time series of results from SOBS2 deployment at the Experimental site.

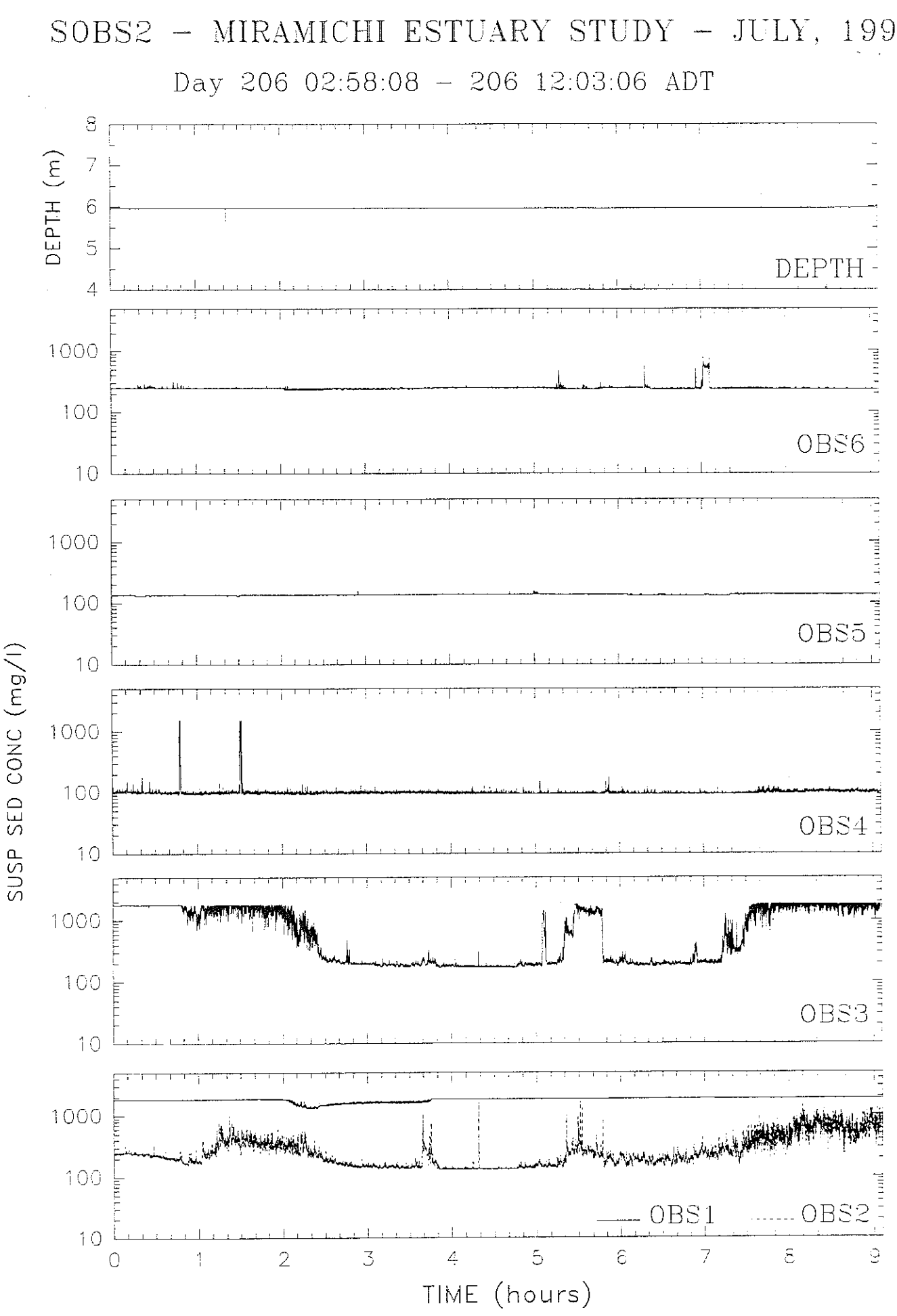

Figure 4.3.2-13. Time series of results from SOBS2 deployment at the Experimental site.

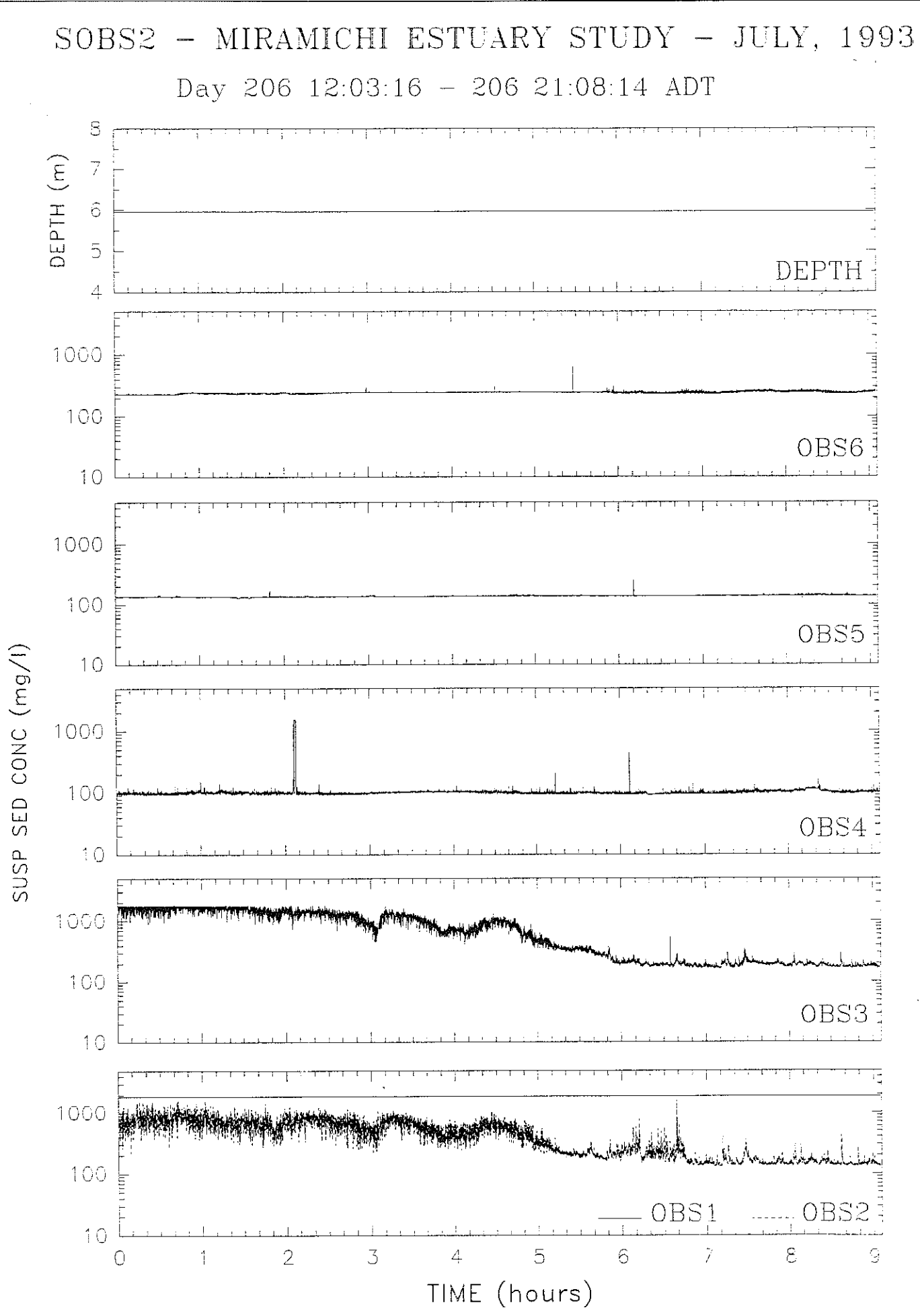

Figure 4.3.2-14. Time series of results from SOBS2 deployment at the Experimental site.

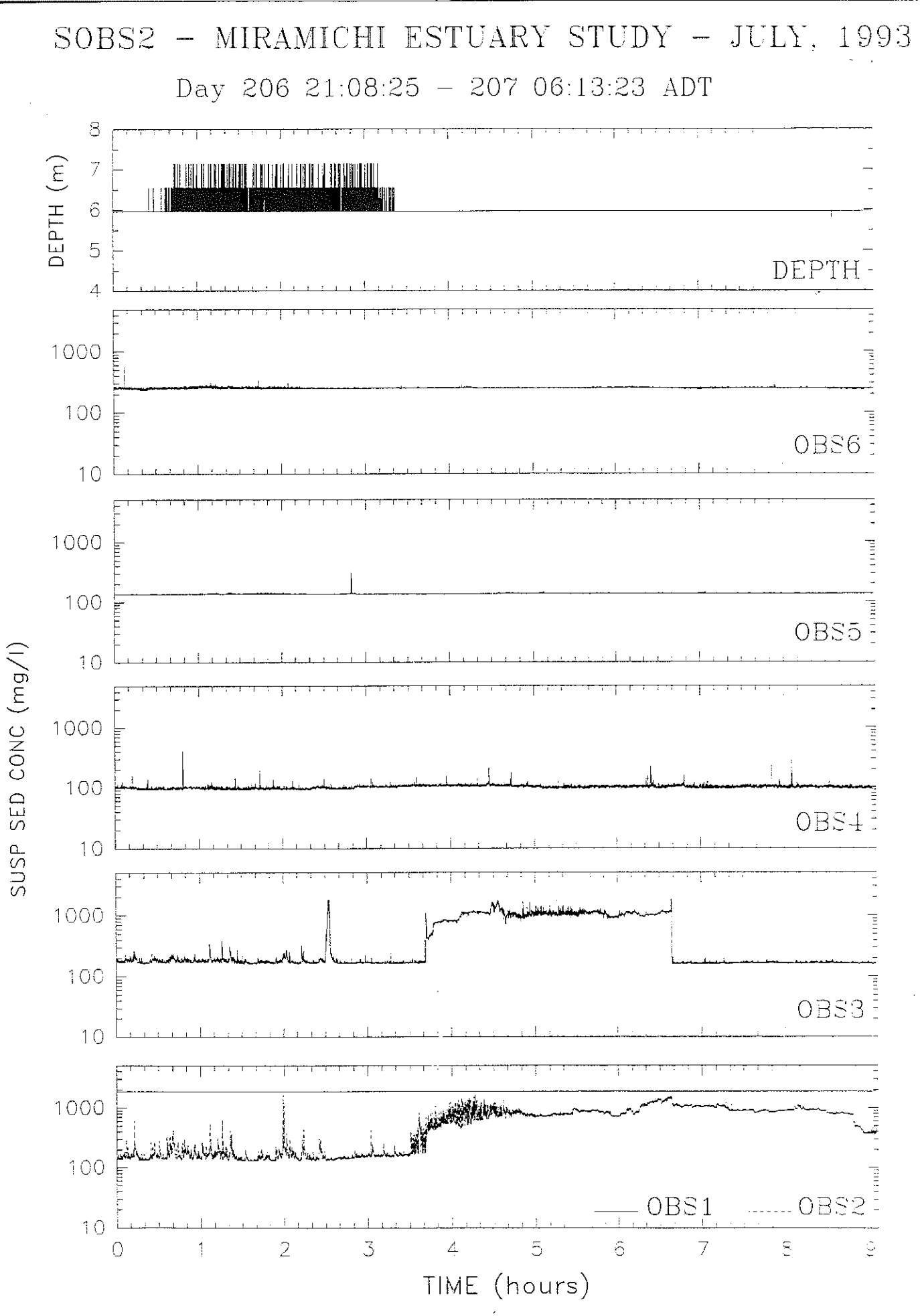

Figure 4.3.2-15. Time series of results from SOBS2 deployment at the Experimental site.

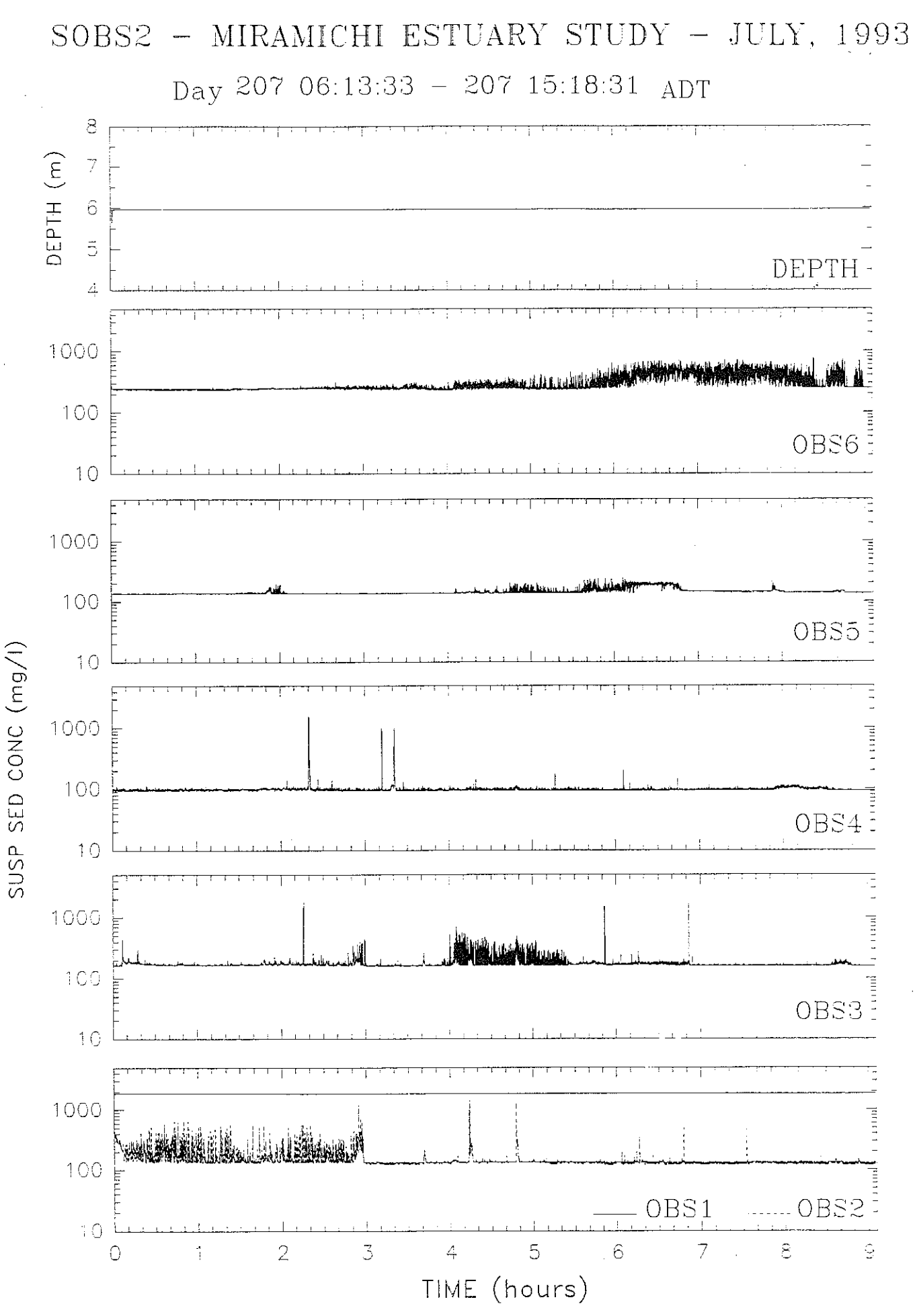

Figure 4.3.2-16. Time series of results from SOBS2 deployment at the Experimental site.

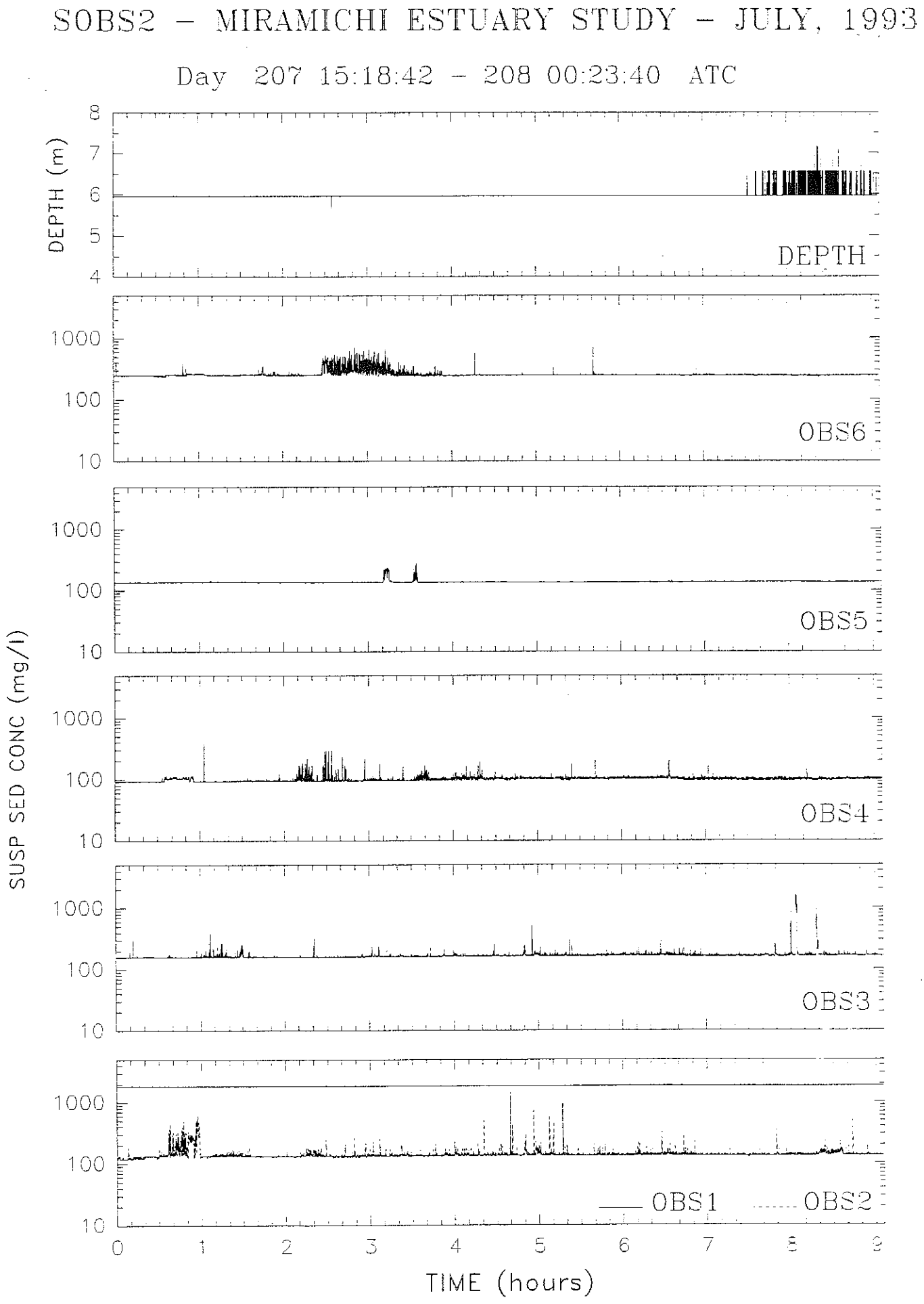

Figure 4.3.2-17. Time series of results from SOBS2 deployment at the Experimental site.

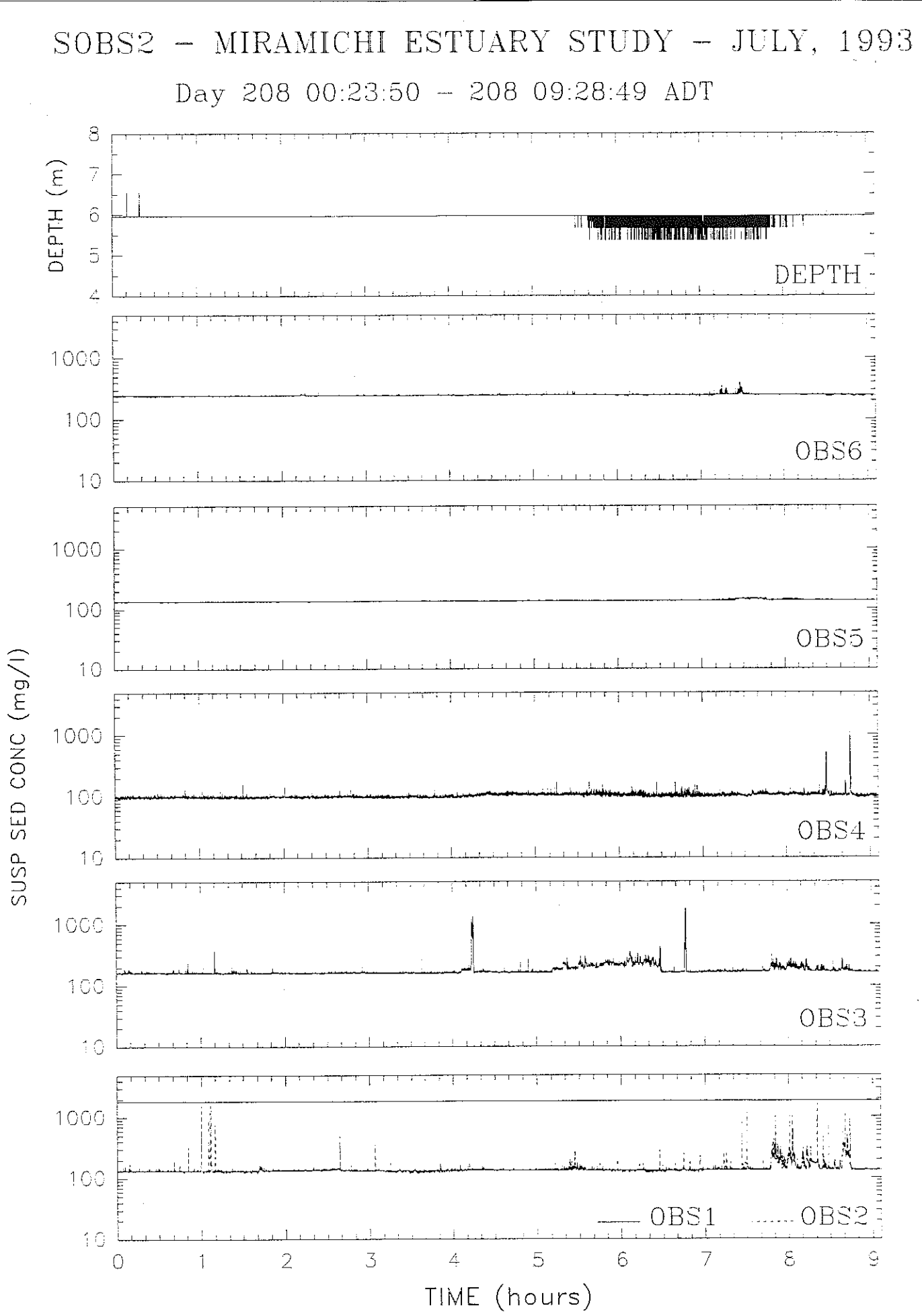

Figure 4.3.2-18. Time series of results from SOBS2 deployment at the Experimental site.

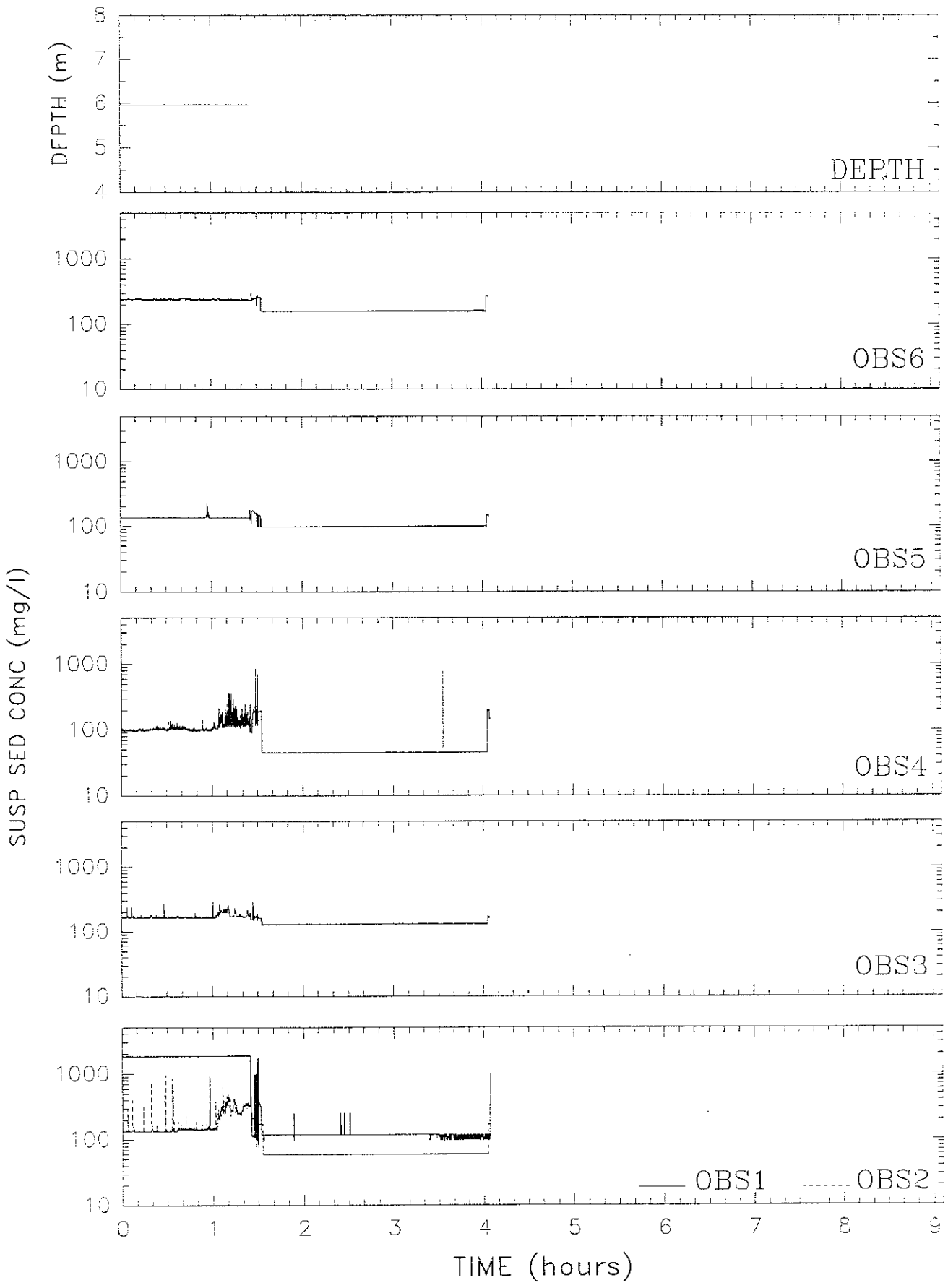

Figure 4.3.2-19. Time series of results from SOBS2 deployment at the Experimental site.

between OBS sensor 3 (saturated) and OBS sensor 4 (low response) suggests that this turbid layer mud has a well defined surface situated between the heights of these sensors. The rapid rise in sensor response suggests that the sediments were advected to the SOBS site, rather than resuspended from the vicinity.

4.4 Lancelot Results

Lancelot was deployed at two sites, Station 4 (Channel margin) and Station 18 (Control), to assess long term residual excess pore pressures and to determine the natural degree of consolidation. Time series for Lancelot deployments are presented in Figures 4.4-1 to 4.4-13. The first deployment encountered sediments on the Channel margin that were much softer than expected, as the vertical load imposed by the instrument itself resulted in a masking of the residual pore pressure levels. This was corrected before the second deployment at the Control Site by replacing the steel baseplate with a more buoyant plywood base. The imposed weight of the instrument was determined to be equivalent to a head of water about 110 and 54 mm for Lancelot deployments 1 and 2, respectively. These levels correspond to the end of primary consolidation, as indicated in the long term excess pore pressure decay curves (Figs. 4.4-1 and 4.4-2). The decay curve for the Lancelot 1 deployment indicates substantial capacity for secondary consolidation (creep settlement), which is typical of sediments containing high organic contents (Mesri and Castro 1987).

The records for both Lancelot deployments suggest a minor degree of excess pore pressure resident within the seabed at both the Channel margin and Control site, but the actual level near the Channel margin is difficult to quantify due to the high compressibility of the organics. The record for Lancelot 2 indicates a small degree of cyclic movement of pore fluids, probably as a result of tidal forcing. This has been observed in other studies as well (Schultheiss 1990). Although these effects are detectable, they appear to be relatively insignificant and indicate that sediment permeabilities are high enough to dissipate small excess pore pressures over a period of several hours. This was confirmed during ship passage events (see below).

The estimated effective stresses (assuming hydrostatic pore pressure) were calculated to be 4.61 kPa and 5.54 kPa at the depth of the probe tip for the Channel and Control sites, respectively. The pore pressure parameter r_u is given by Morgenstern and Sangrey (1978) as:

$$r_u = dU / \gamma' z$$

This parameter is used in stability analyses to characterize the influence of pore pressure during shear. Values of the pore pressure parameter range from 0 for no excess pore pressure (fully grain-supported) to 1 (fully pore fluid-supported). Estimates of r_u were made for sites that had dissipated penetration pore pressures (Table 4.4-1). These values indicate that the Channel margin is close to failure under natural conditions, whereas the Control site is essentially fully stabilized.

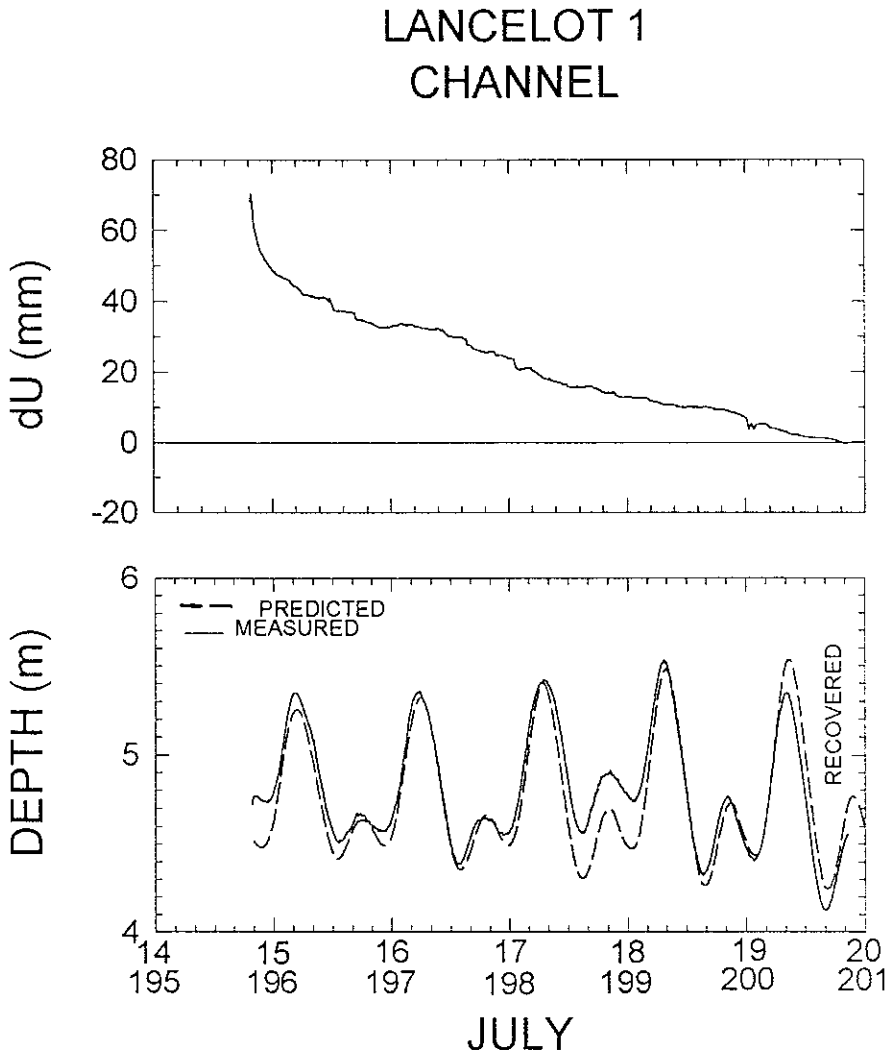

Figure 4.4-1. Pore pressure decay curve for Lancelot 1 deployment at the Channel site (Station 4).

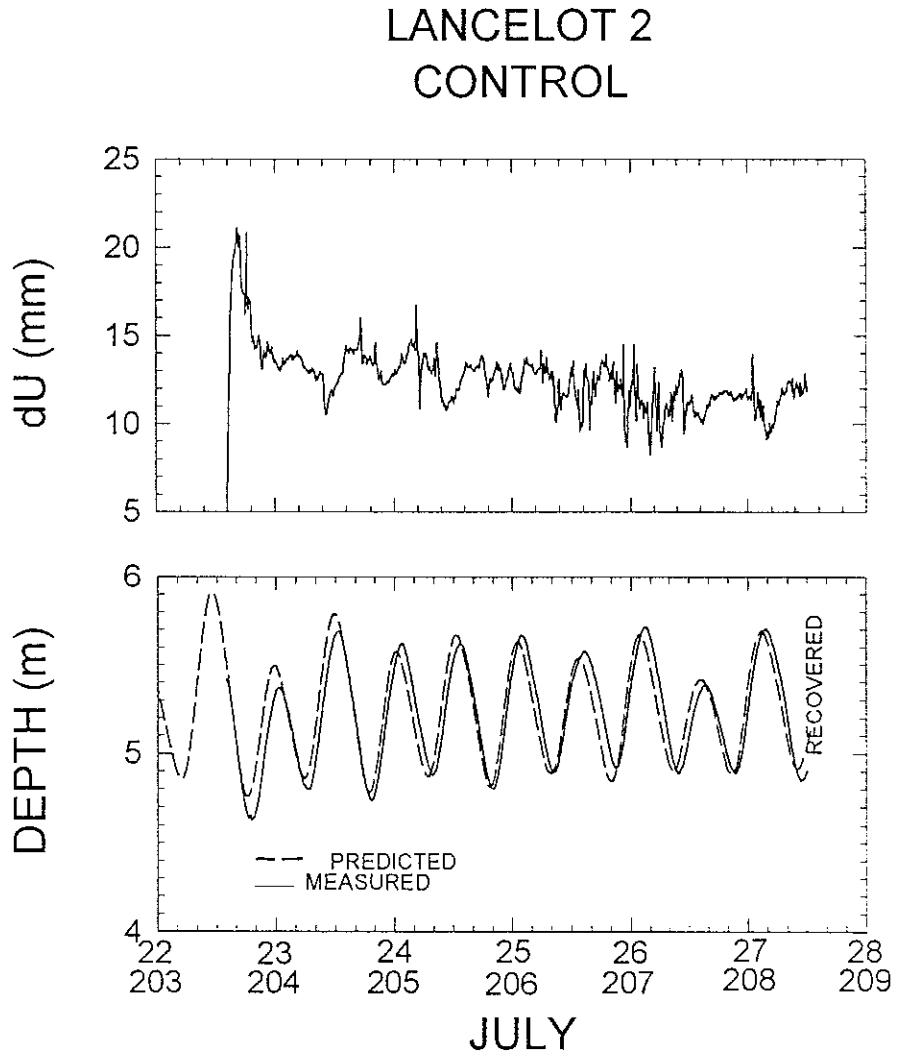

Figure 4.4-2. Pore pressure decay curve for Lancelot 2 deployment at the Control site (Station 18).

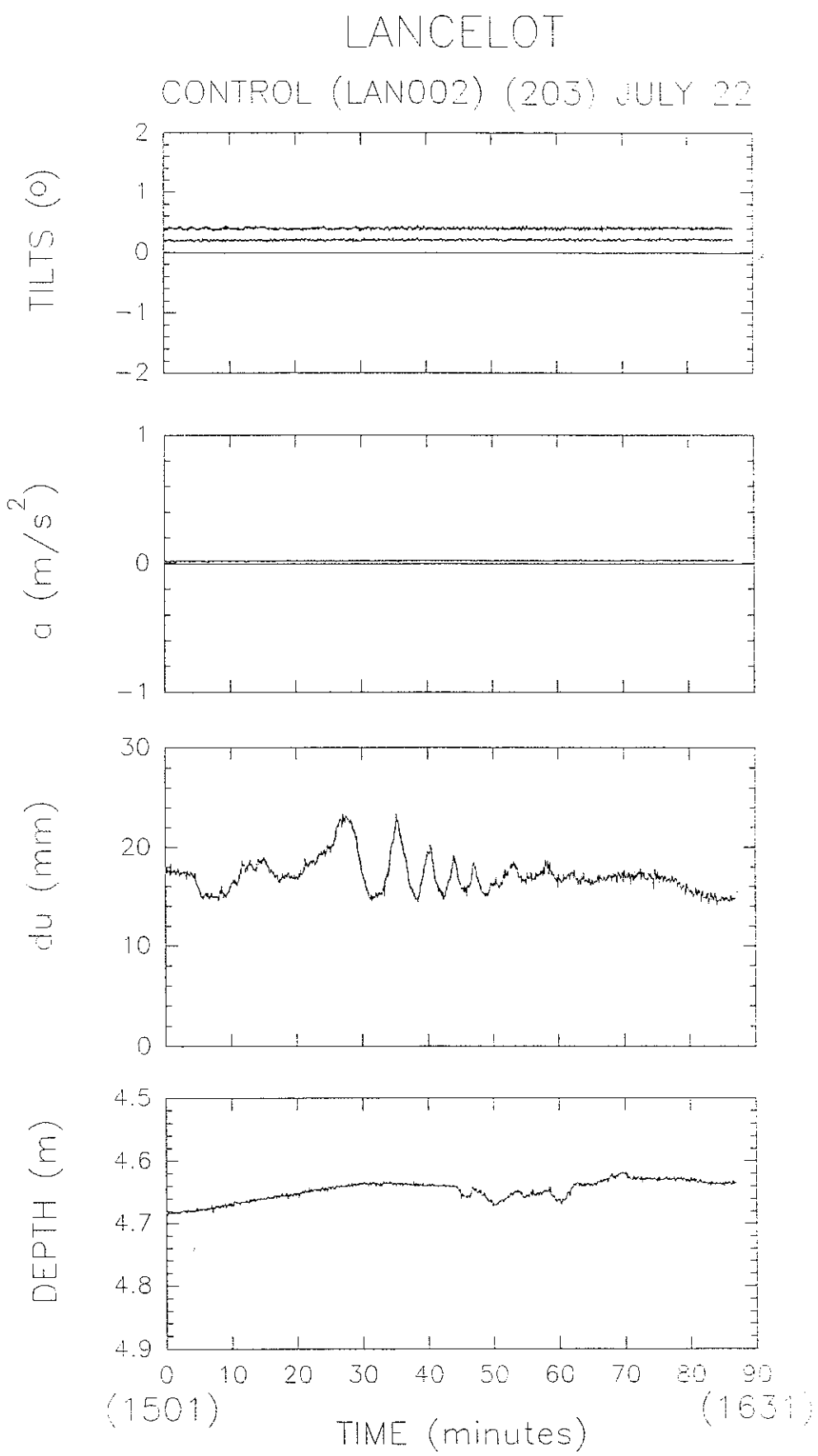

Figure 4.4-3. Lancelot results during event of unknown origin (22 July 1993) at the Channel site.

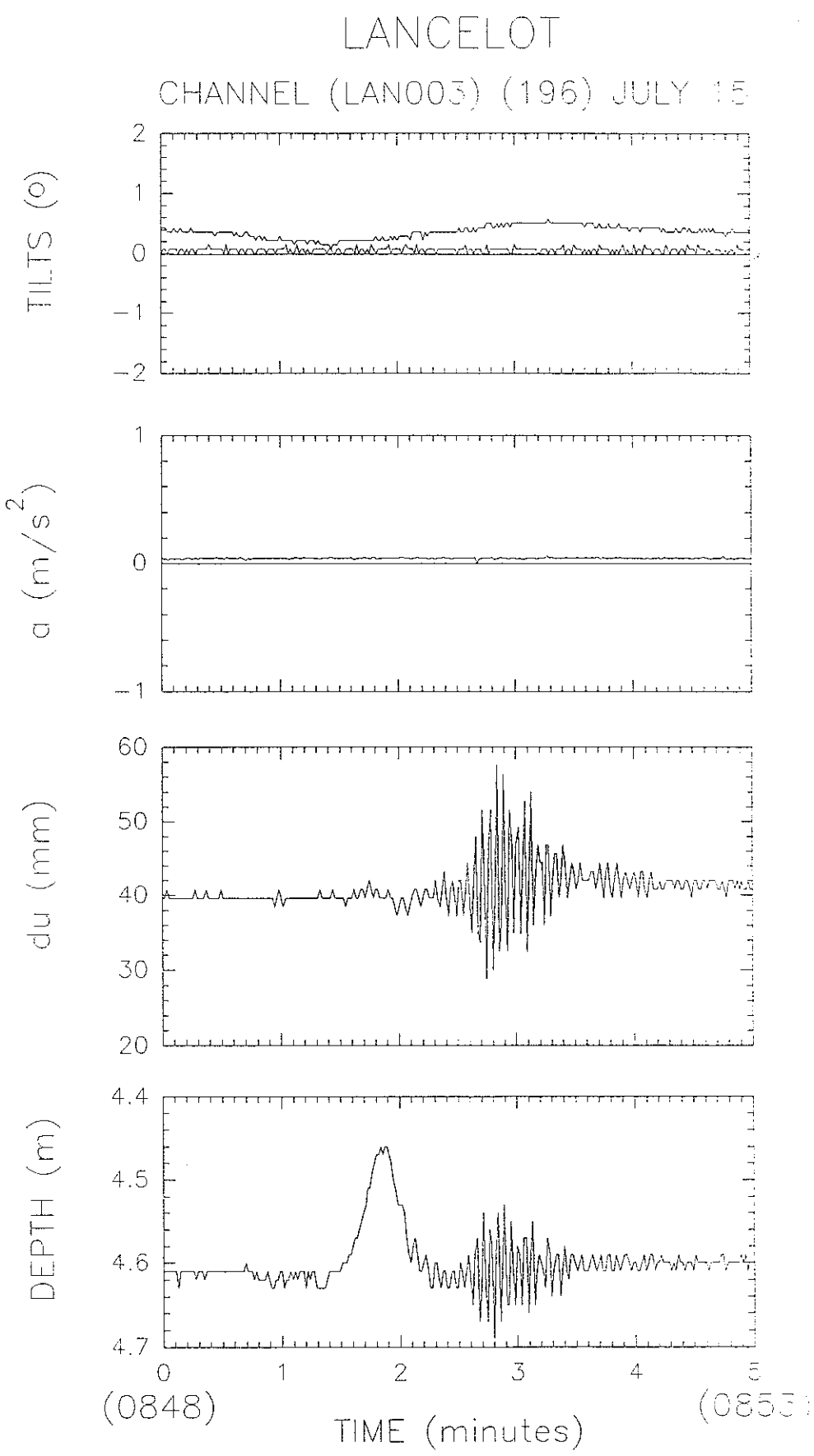

Figure 4.4-4. Lancelot results during passage (incoming) of the M/V Mariner (15 July 1993) at the Channel site.

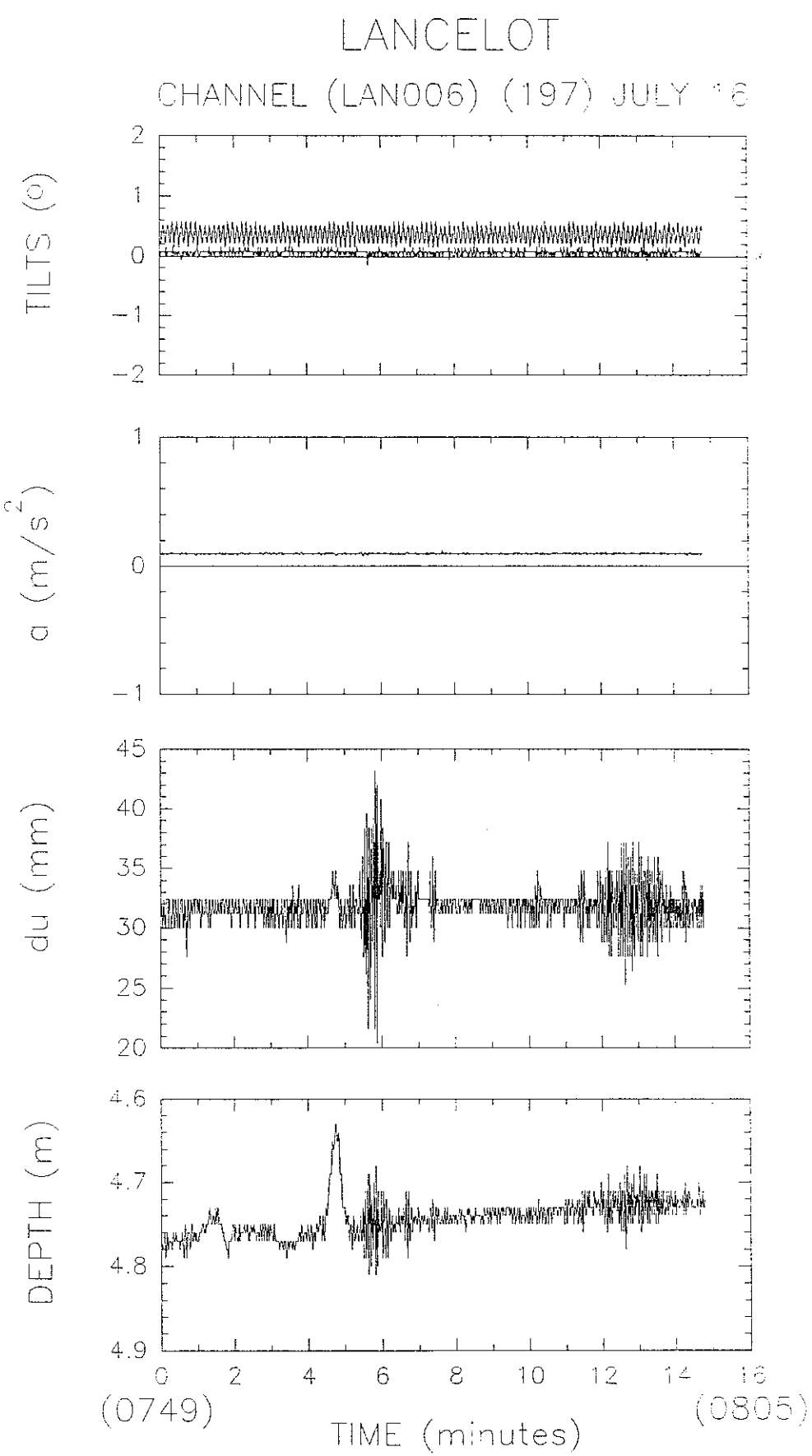

Figure 4.4-5. Lancelot results during passage (outgoing) of the M/V Mariner (16 July 1993) at the Channel site.

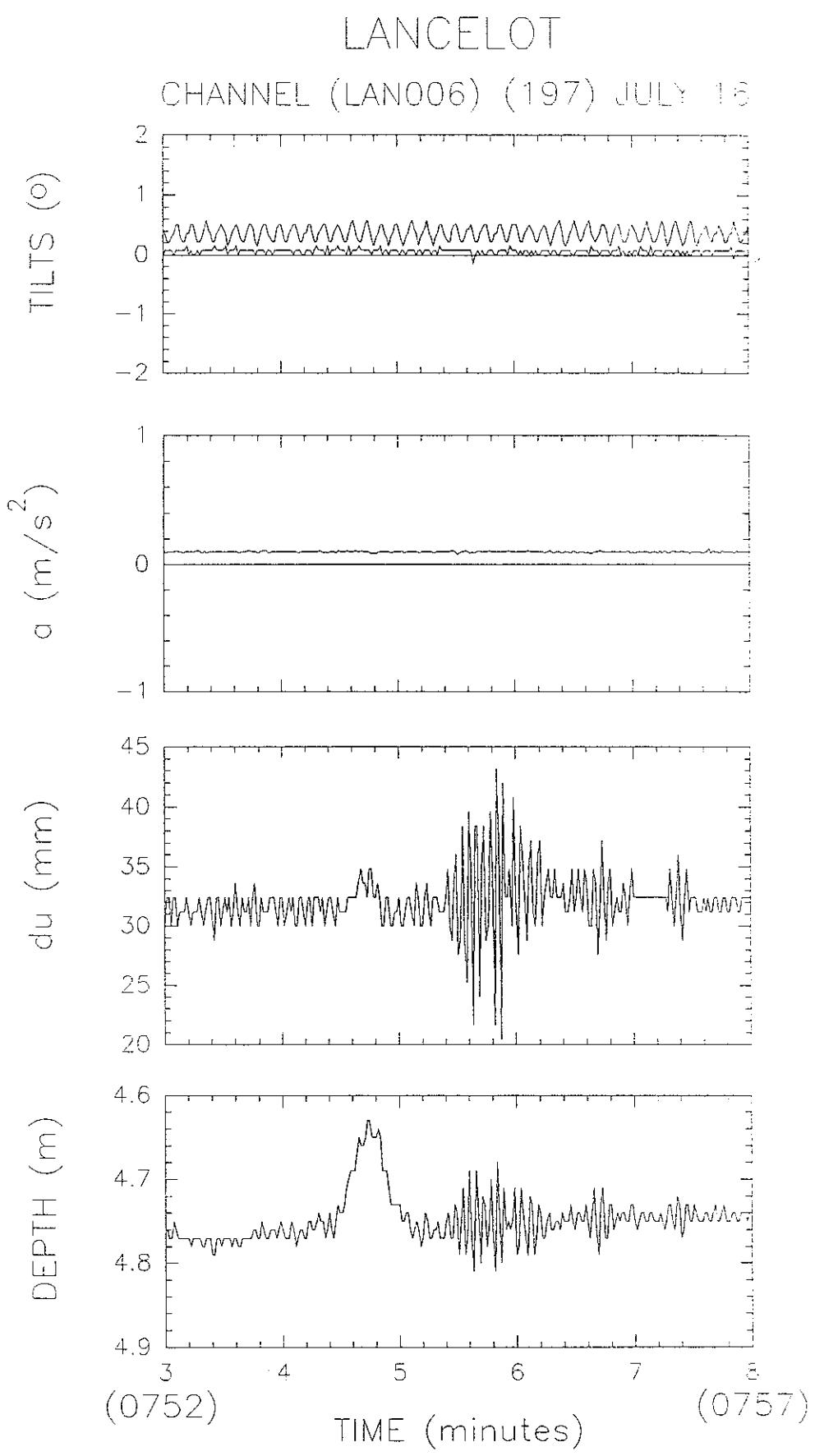

Figure 4.4-6. Expanded view of Lancelot results during passage (outgoing) of the M/V Mariner (16 July 1993) at the Channel site.

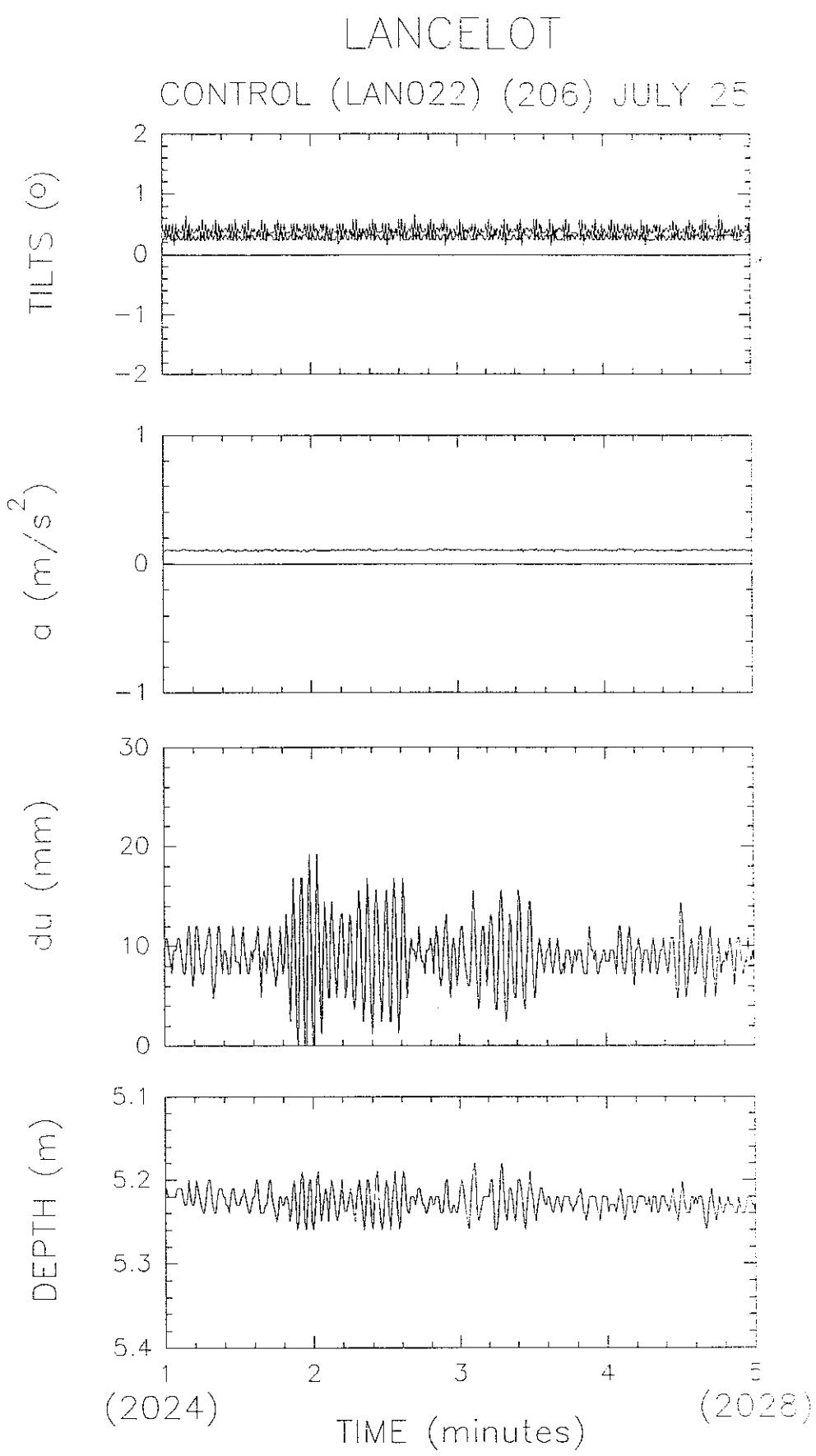

Figure 4.4-7. Lancelot results during passage (incoming) of the Hubert Tanthier (25 July 1993) at the Control site.

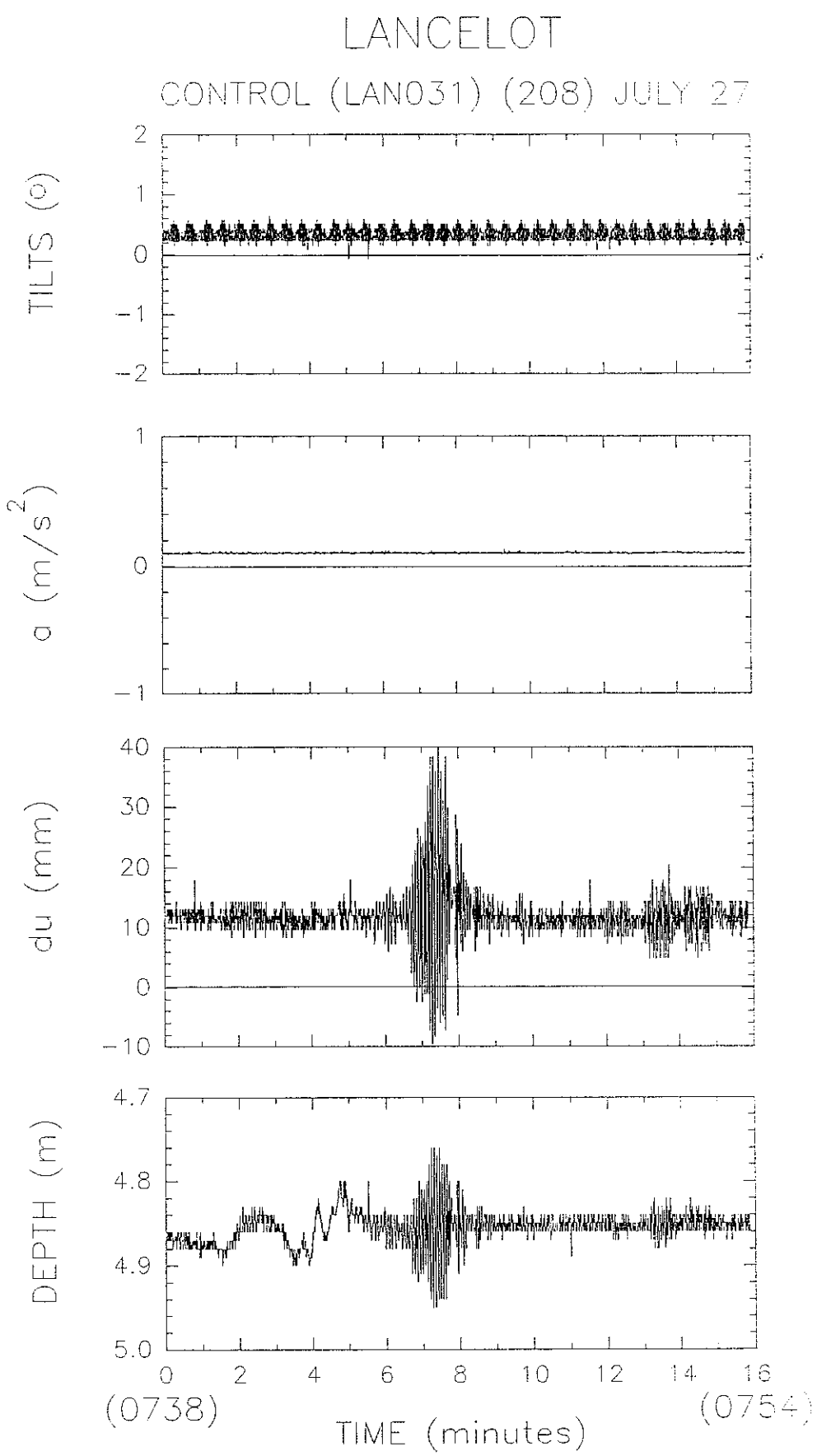

Figure 4.4-8. Lancelot results during passage (outgoing) of the Hubert Tanthier (27 July 1993) at the Control site.

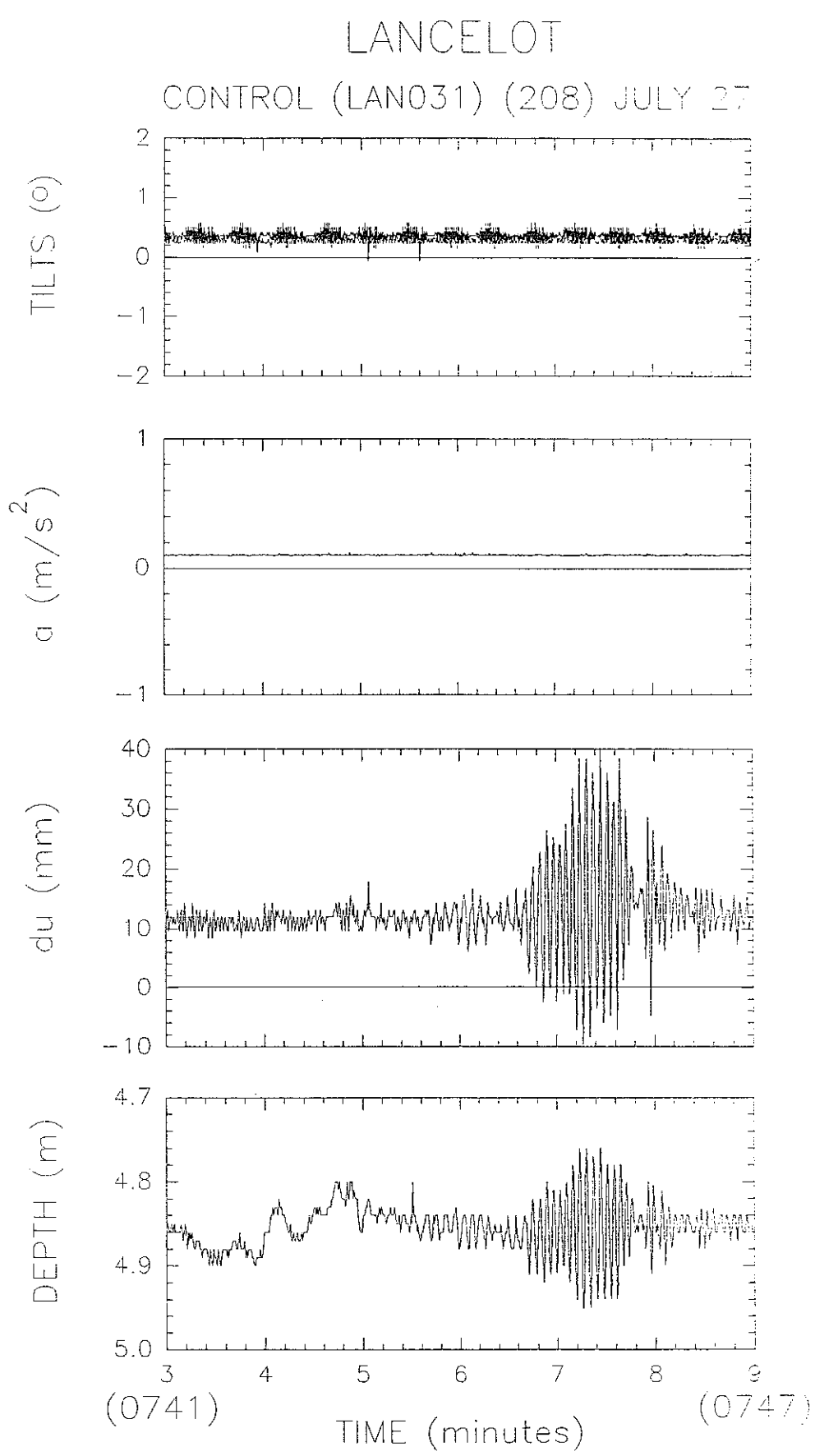

Figure 4.4-9. Expanded view of Lancelot results during passage (outgoing) of the Hubert Tanthier (27 July 1993) at the Control site.

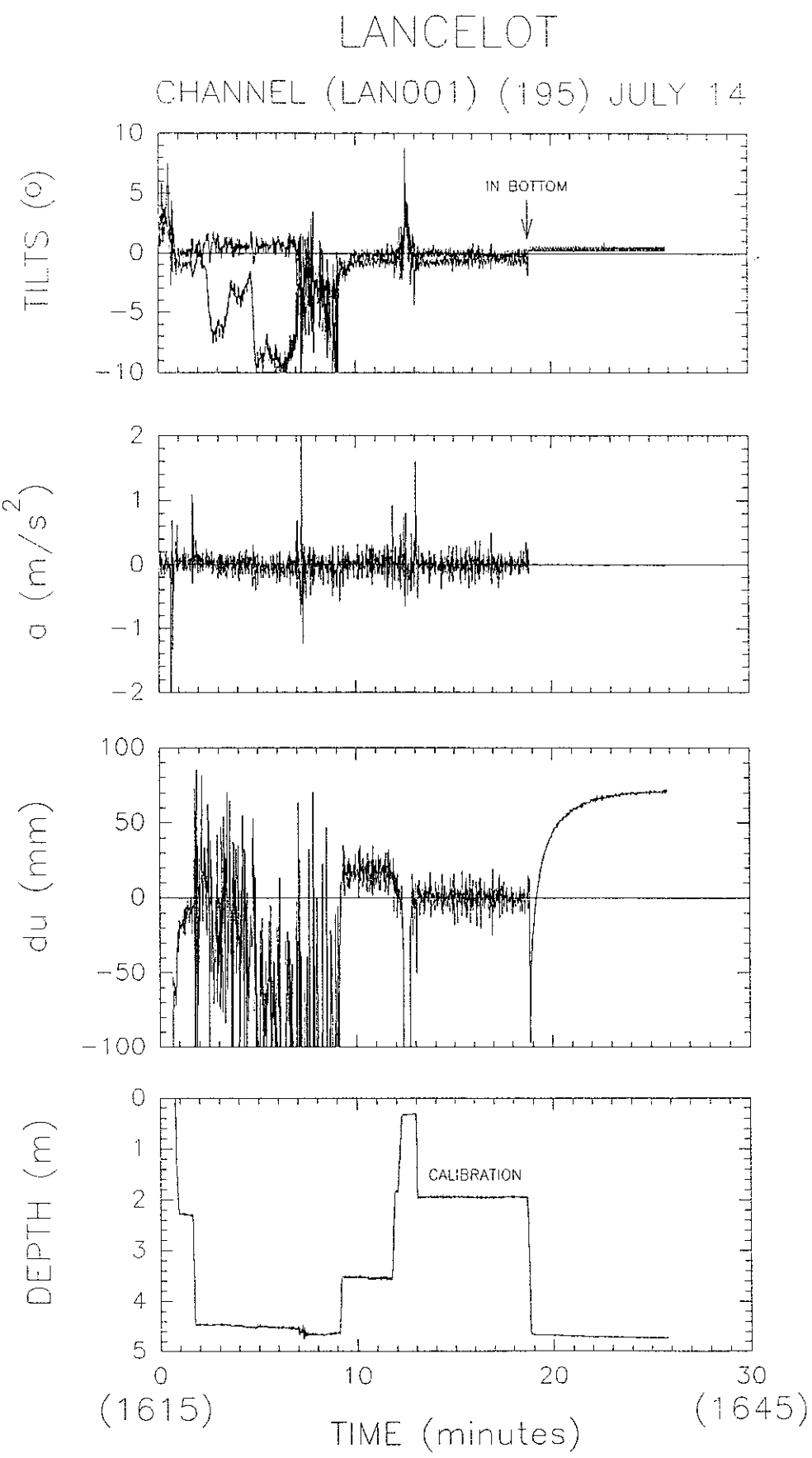

Figure 4.4-10. Calibration records for Lancelot from deployment recovery and data files (July 14 1993).

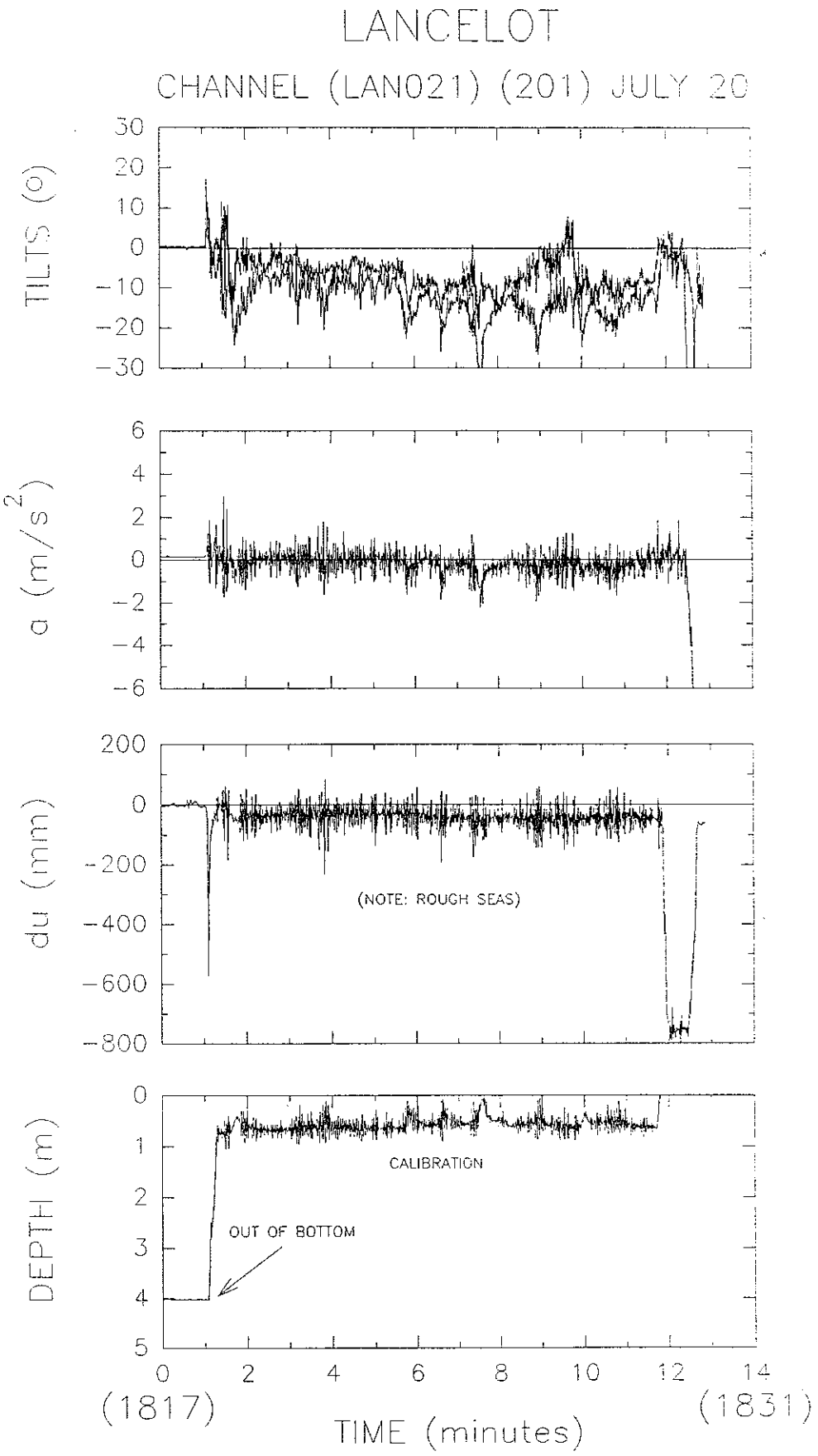

Figure 4.4-11. Calibration records for Lancelot from deployment recovery and data files (20 July 1993).

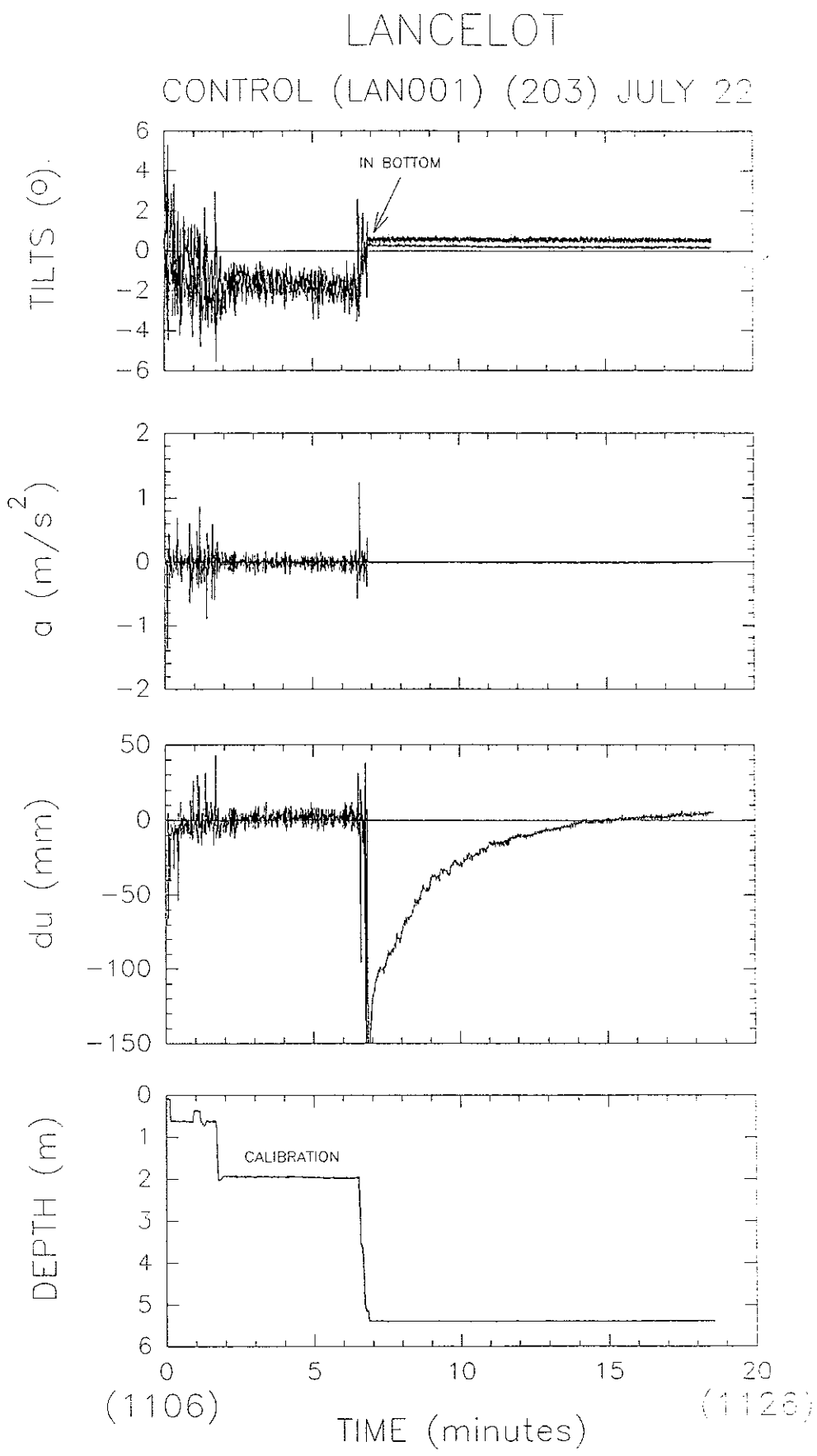

Figure 4.4-12. Calibration records for Lancelot from deployment recovery and data files (22 July 1993).

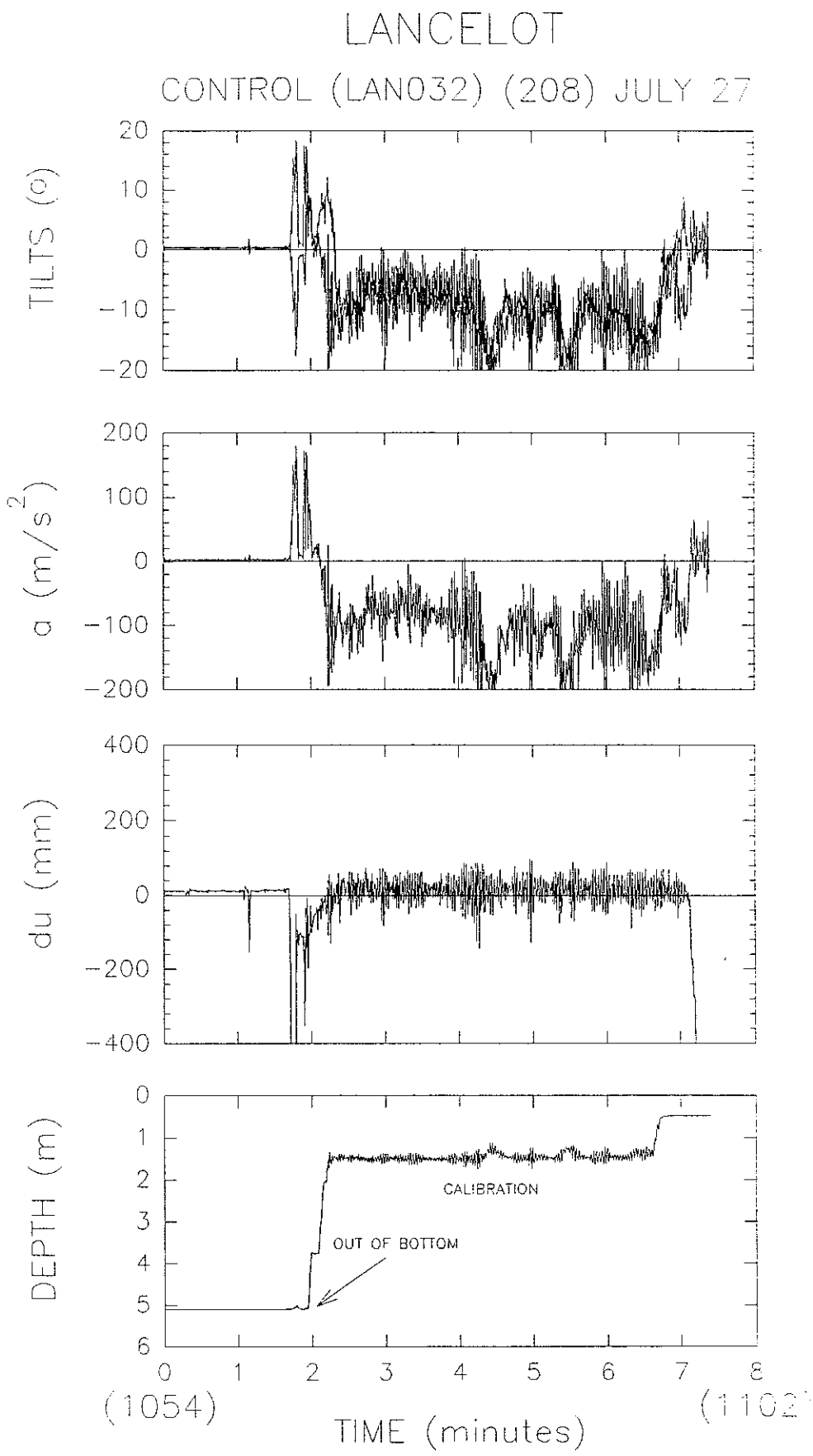

Figure 4.4-13. Calibration records for Lancelot from deployment recovery and data files (27 July 1993).

Table 4.4-1. Summary of residual excess pore pressures and r_u values obtained for Lancelot deployments. (0 indicates no instability; 1 indicates seabed is liquefied).

Deployment	Site	Core	ρ_s (g cm^{-3})	dU (mm)	r_u
Lancelot 1	Channel	GC-13	1.15	40*	0.75*
Lancelot 2	Control	GC-25	1.36	12	0.08

*These values may not represent real long-term values (see discussion in Section 4.4)

Lancelot was deployed during two ship passage events (a third event, which also appeared to be a ship passage, was recorded (Fig. 4.4-3), but its exact cause is unknown). The times of these events are summarized in Table 4.4-2.

The pressure disturbance from vessel passage was detected initially as a reduction in water level (trough ahead of the bow wave), followed thereafter by a quiet interval of about 1 min and a well-defined sequence of high-frequency waves (Figs. 4.4-4 to 4.4-6). This high-frequency component was concluded to be the ship wake. Its effect was quite dramatic, as indicated by the higher excess pore pressures generated as compared to the bow wave. This indicates that the amplitude of waves in the ship wake is the major destabilizing factor along the Channel margin.

Note that for event four (Fig. 4.4-7), there was very low amplitude or no bow wave. As this deployment of Lancelot was at the Control site, it can be concluded that the effects of shipping are negligible away from the Ship Channel. Presumably, these waves break on the Channel banks and dissipate the majority of their energy there. During event six Excalibur was deployed in the Channel margin and registered a bow wave that immediately preceded the wake (Figs. 4.4-14 and 4.4-15), compared to Lancelot 1 which was slightly farther away and showed a time gap between the bow wave and the wake (Figs. 4.4-3 and 4.4-5). The degree of stress transfer to the fluid phase was also considerably higher. Apparently, the confines of the Channel preclude time for seabed restabilization between the long-period bow wave and the high frequency wake.

4.5 Excalibur Results

A total of 18 Excalibur deployments were made. The results are summarized in Table 4.5-1 and Figures 4.5-1 to 4.5-18. The problem of the long time required for dissipation of penetration pore pressures became evident in some of the Excalibur deployments. Some deployments had not achieved full dissipation of pore pressures developed during penetration of the probe, making a calculation of long term pore pressures and stability impossible. Deployments at Stations 6 and 11 were influenced by the weight of the instrument, as with Lancelot, so a lighter plywood base was installed for subsequent deployments. This resulted in an imposed vertical stress on the seabed equivalent to 12 mm of head which was less than all but one of the measurements of residual excess pore pressure. Station 36 actually showed a long term excess pore pressure that was slightly negative, which probably resulted from shearing during the previous ship passage. This indicates that the instrument effects were negligible.

Figure 4.5-19 shows residual excess pore pressures for all sites, in comparison with the level at which liquefaction would have existed, based on estimates of effective vertical stress. Penetration pore pressures are a local effect, and ambient conditions can be recognized only after the penetration pressure has dissipated. Therefore, the data on excess pore pressure were not used to calculate values of r_u for these sites. Instead, the undrained strength determined from gravity cores was used to empirically estimate maximum excess pore pressures that could be generated during penetration. Bennett et al. (1985) concluded that

Table 4.4-2. Known ship movements adjacent to Lancelot and Excalibur.

Event No.	Vessel	Date	Time (AST)	Instrument Deployed	Test Site
1	M/V Mariner (incoming)	July 15	08:49	Lancelot 1	Channel
2	M/V Mariner (outgoing)	July 16	07:50	Lancelot 1	Channel
3	Unknown Vessel (n/a)	July 22	15:05	Lancelot 2	Control
4	Hubert Tanthier (incoming)	July 25	20:26	Lancelot 2	Control
5	Hubert Tanthier (outgoing)	July 27	07:40	Lancelot 2	Control
6	Hubert Tanthier (outgoing)	July 27	06:40	Excalibur 36	Channel

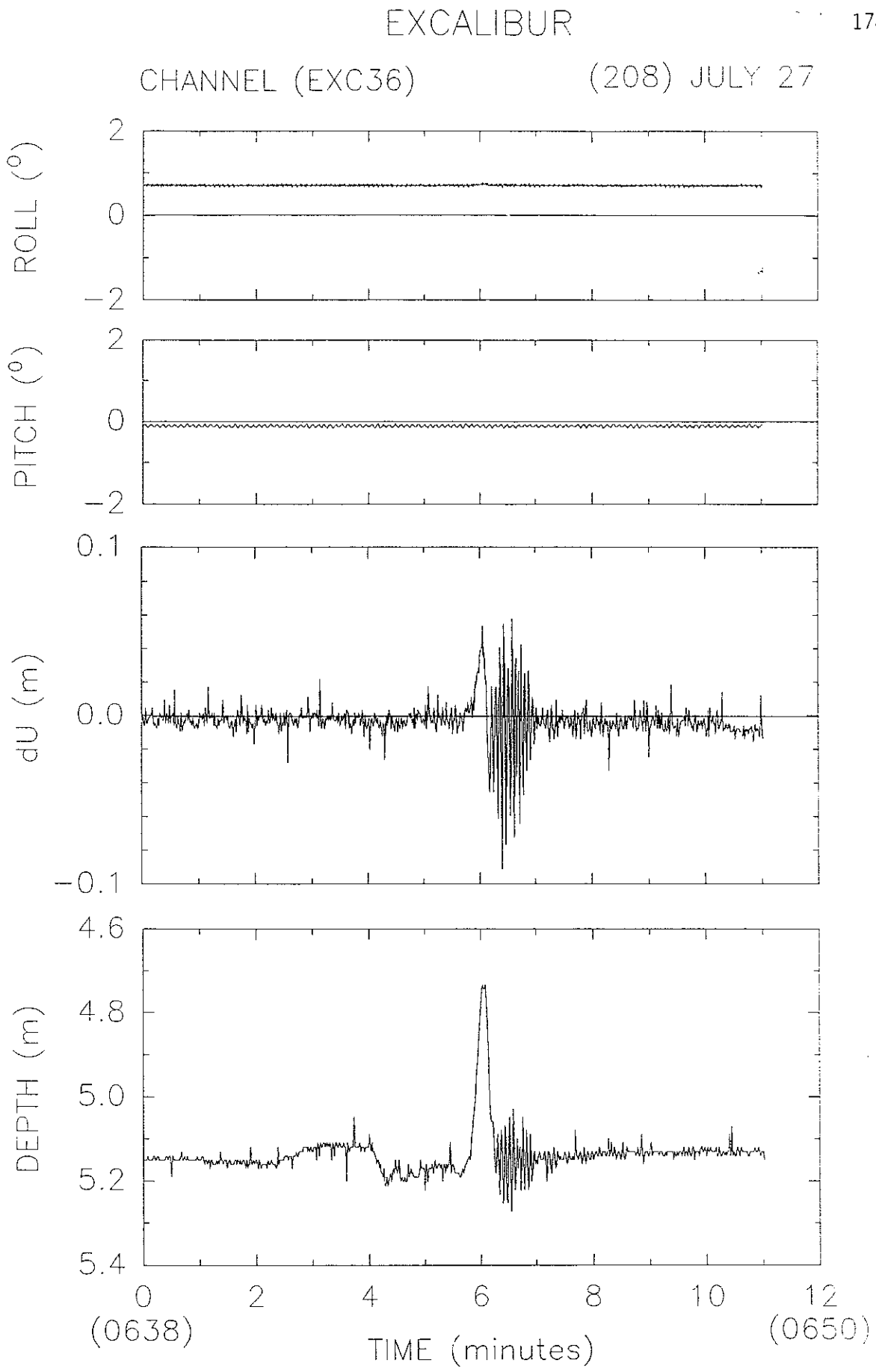

Figure 4.4-14. Excalibur results during passage (outgoing) of the Hubert Tanthier (27 July 1993) at the Channel site.

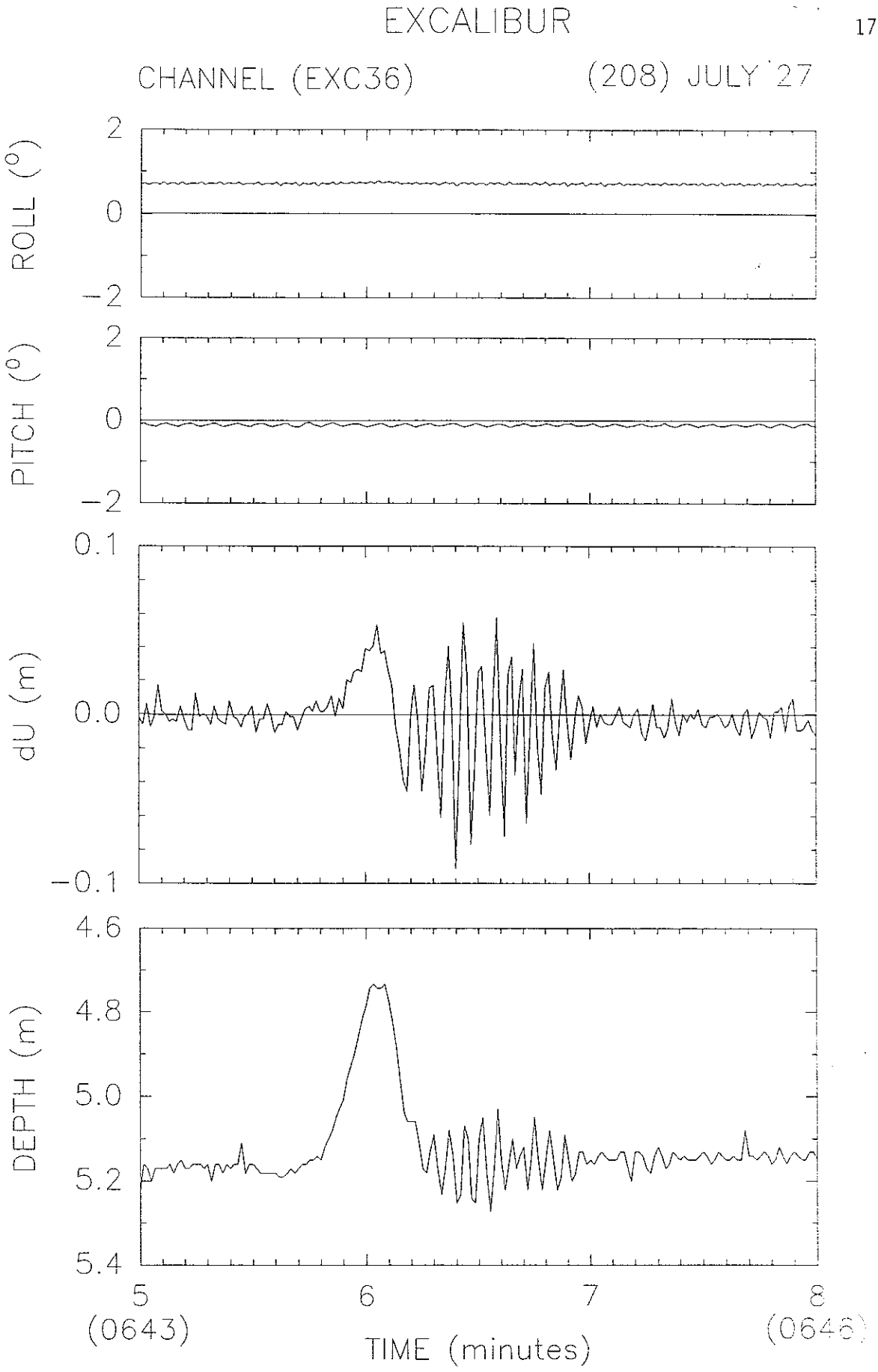

Figure 4.4-15. Expanded view of Excalibur results during passage (outgoing) of the Hubert Tanthier (27 July 1993) at the Channel site.

Table 4.5-1. Summary of Excalibur excess pore pressure data and calculated values of effective vertical stress and pore pressure parameter.

Site	Station No.	Date	Time	Depth (m)	ρ_s (g cm^{-3})	γ' (kN m^{-3})	dU (m)	r_u
Control	25	July 24	1500	5.59	1.37	3.35	0.042	0.22
Channel	13	July 19	1300	6.72	1.38	3.45	0.773	-
Channel	12	July 19	1700	7.82	1.21	1.78	0.361	-
Channel	17	July 20	1200	5.68	1.38	3.45	0.595	-
Channel	36	July 27	0900	5.33	1.30	2.66	-	0.02
Pre-Dump	6	July 15	1700	NA	1.38	3.45	0.339	-
Pre-Dump	11	July 15	1900	NA	1.38	3.45	0.453	-
Pre-Dump	07	July 16	1830	5.75	1.38	3.45	0.033	0.17
Post-Dump	08	July 19	2000	5.84	1.38	3.45	1.305	-
Post-Dump	20	July 22	1600	4.82	1.38	3.45	1.572	-
Post-Dump	21	July 23	1300	5.55	1.32	2.86	0.082	0.51
Post-Dump	23	July 23	1700	5.18	1.34	3.05	0.034	0.02
Post-Dump	24	July 23	1900	5.28	1.38	3.45	0.110	0.57
Post-Dump	28	July 25	0900	5.59	1.36	3.25	0.016	0.09
Post-Dump	29	July 25	1400	5.93	1.30	2.66	0.648	-
Post-Dump	31	July 26	1100	5.40	1.38	3.45	0.012	0.06
Post-Dump	32	July 26	1300	5.62	1.34	3.05	0.039	0.23
Post-Dump	33	July 27	1700	4.73	1.53	4.92	0.122	0.44

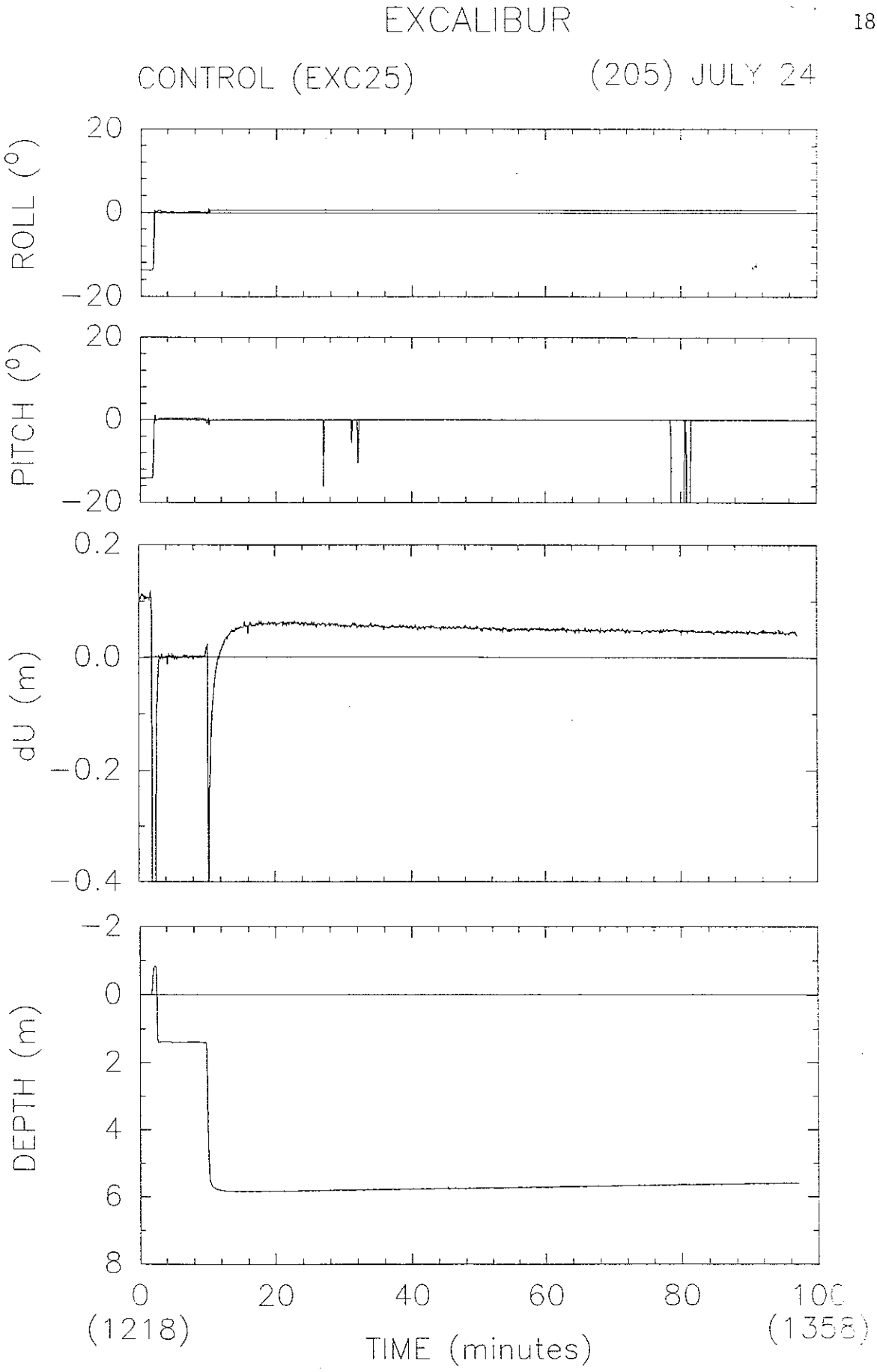

Figure 4.5-1. Time series results for Excalibur deployment at Control site (Station 25).

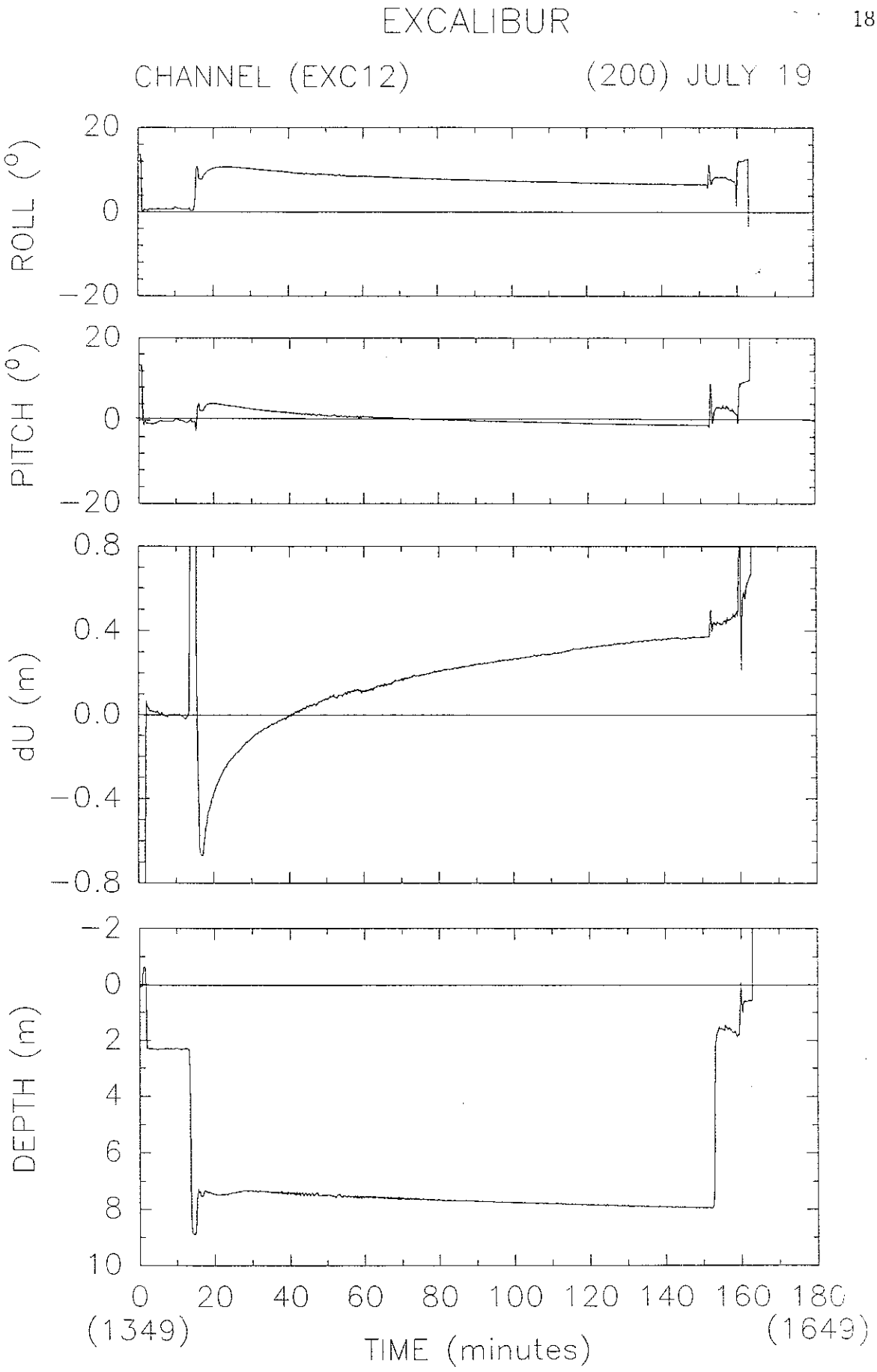

Figure 4.5-2. Time series results for Excalibur deployment at Channel site (Station 12).

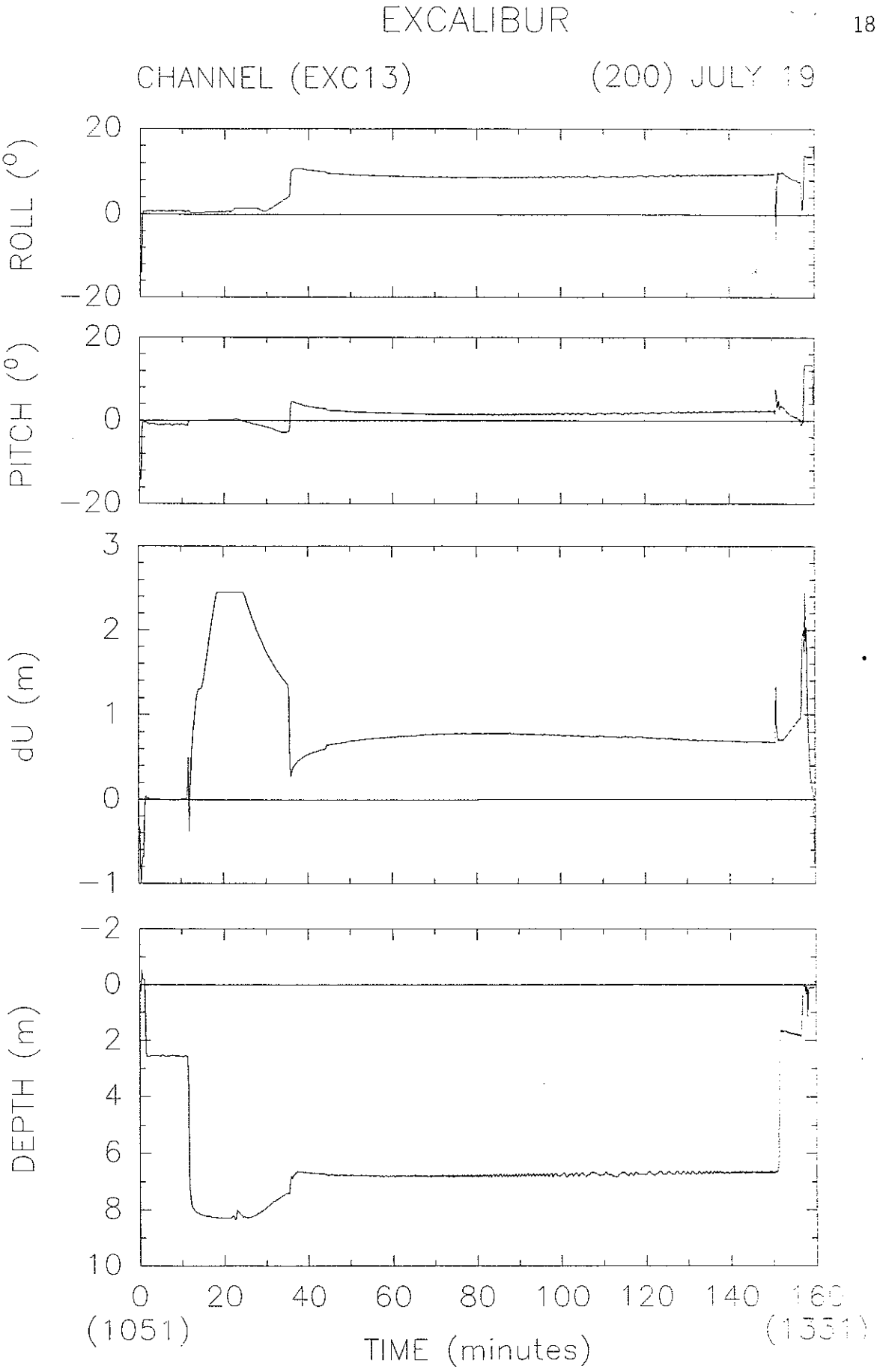

Figure 4.5-3. Time series results for Excalibur deployment at Channel site (Station 13).

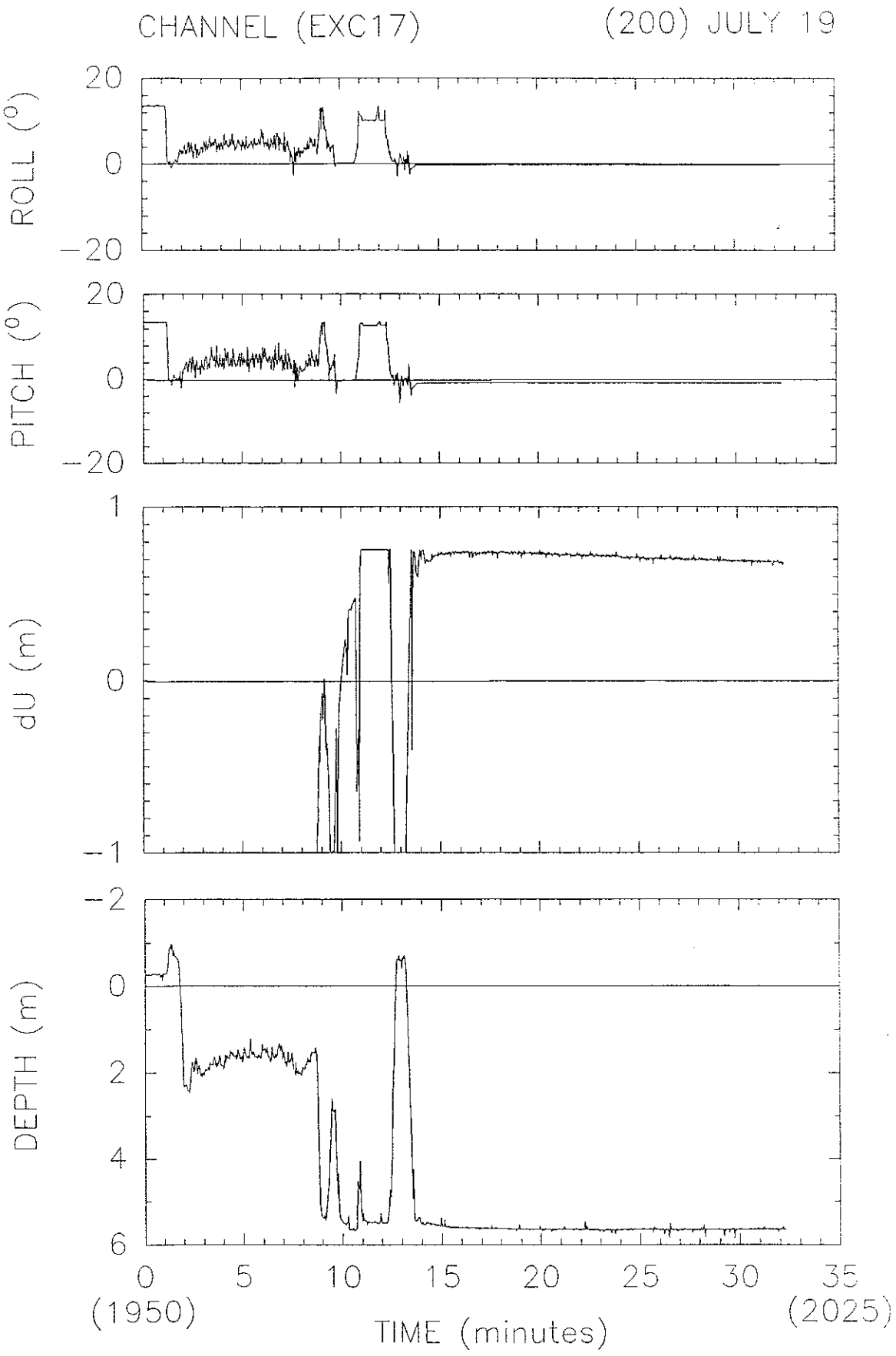

Figure 4.5-4. Time series results for Excalibur deployment at Channel site (Station 17).

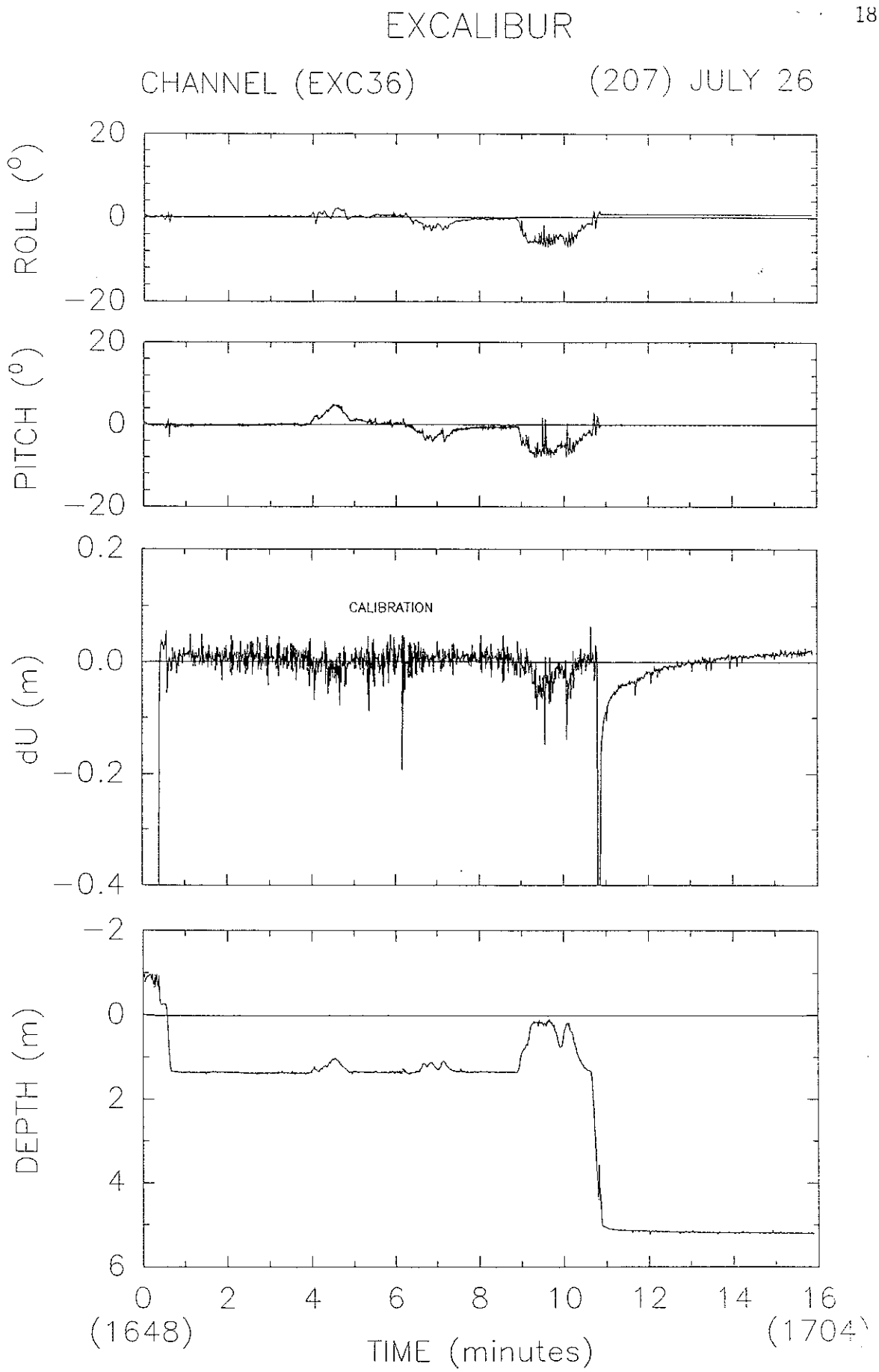

Figure 4.5-5. Time series results for Excalibur deployment at Channel site (Station 36).

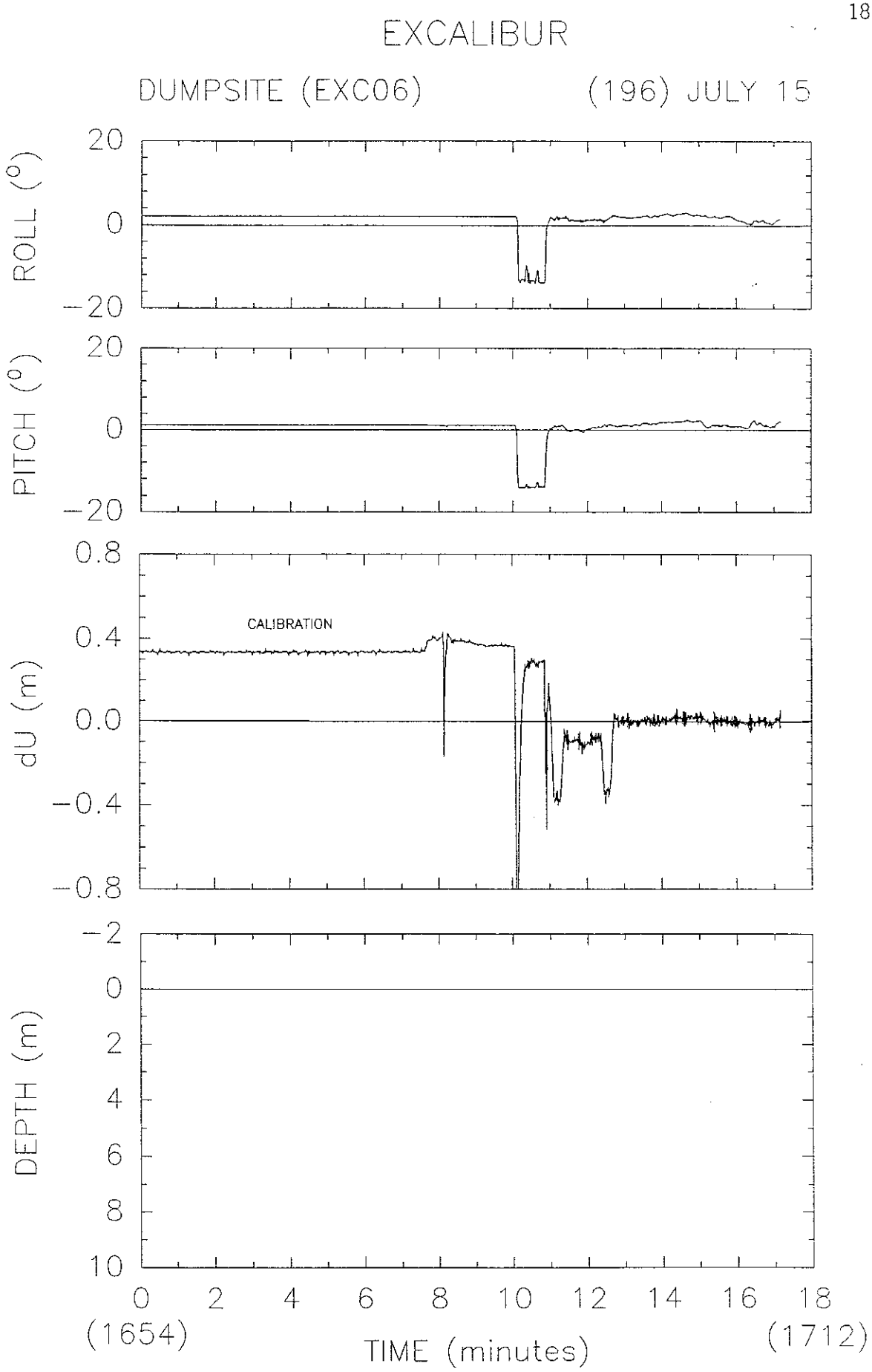

Figure 4.5-6. Time series results for Excalibur deployment at Experimental site (Station 6).

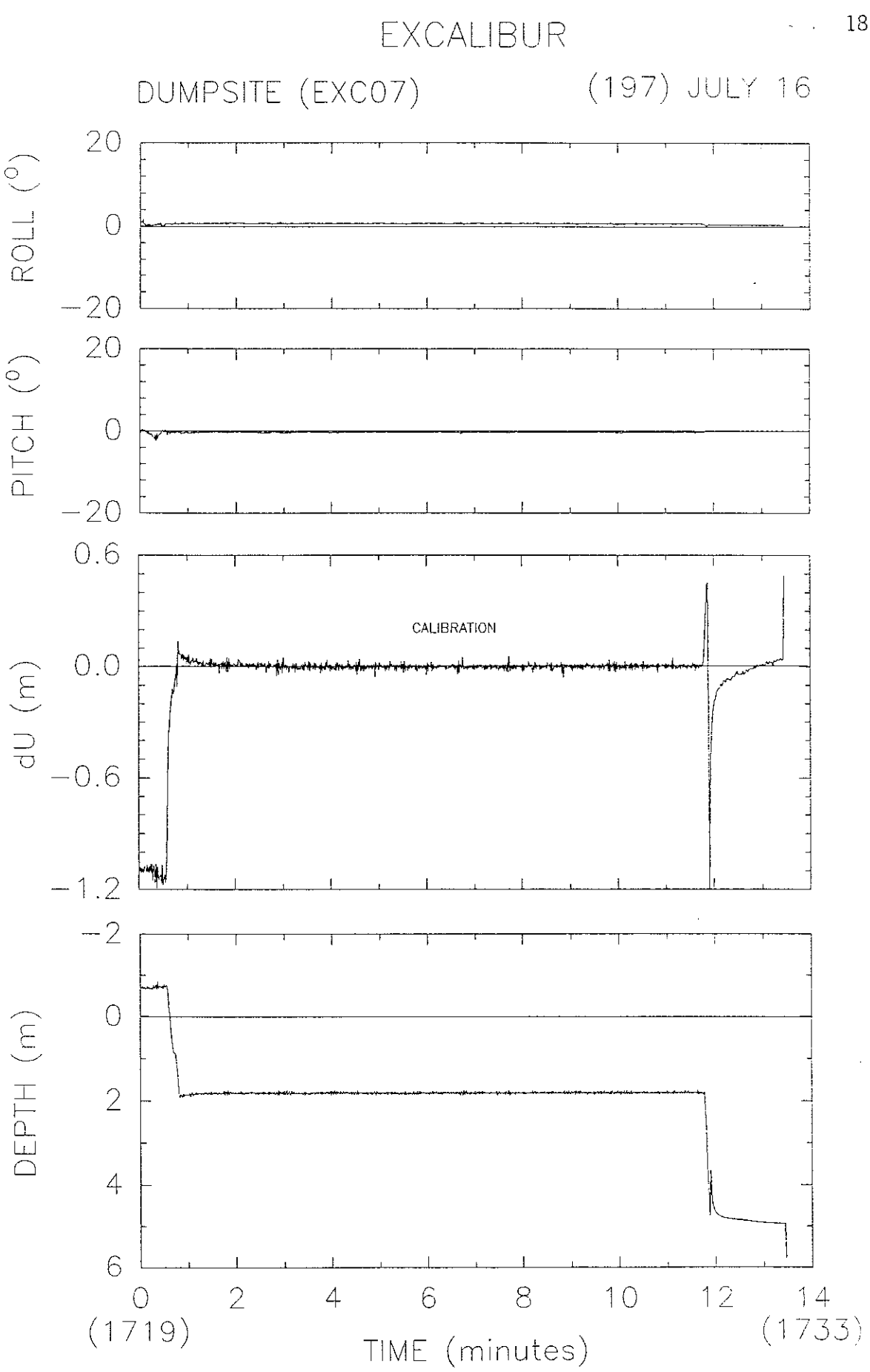

Figure 4.5-7. Time series results for Excalibur deployment at Experimental site (Station 7).

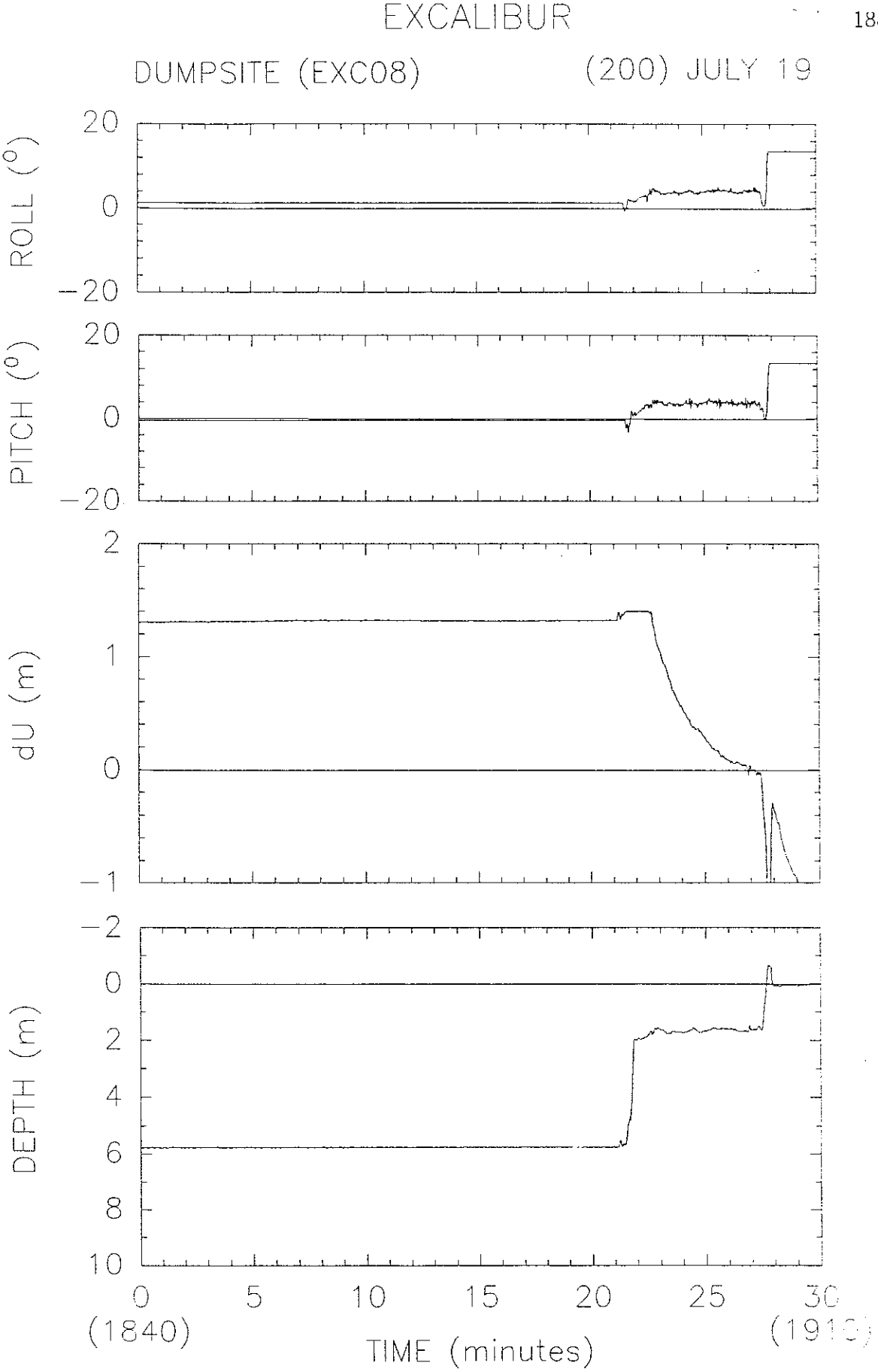

Figure 4.5-8. Time series results for Excalibur deployment at Experimental site (Station 8).

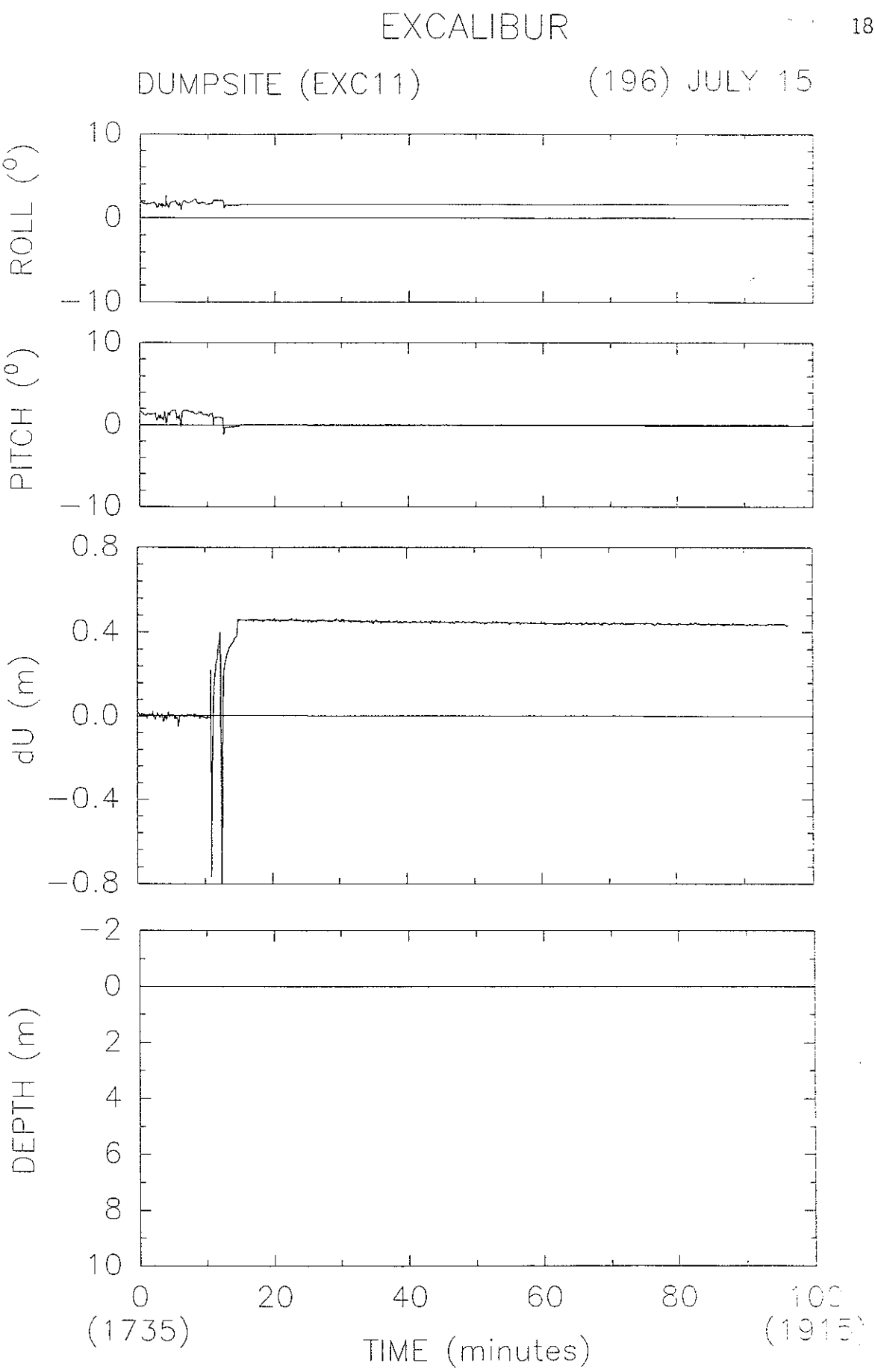

Figure 4.5-9. Time series results for Excalibur deployment at Experimental site (Station 11).

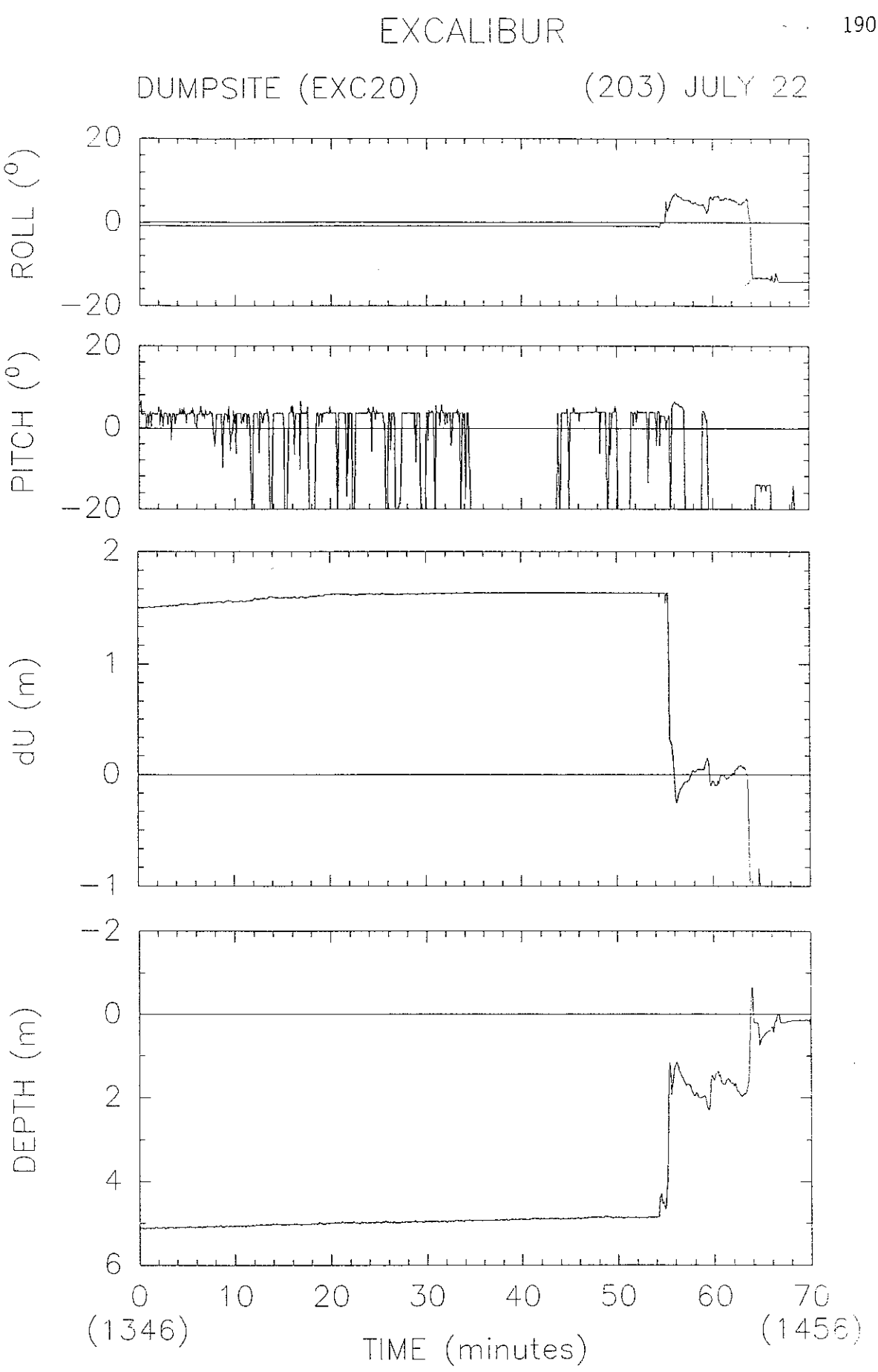

Figure 4.5-10. Time series results for Excalibur deployment at Experimental site (Station 20).

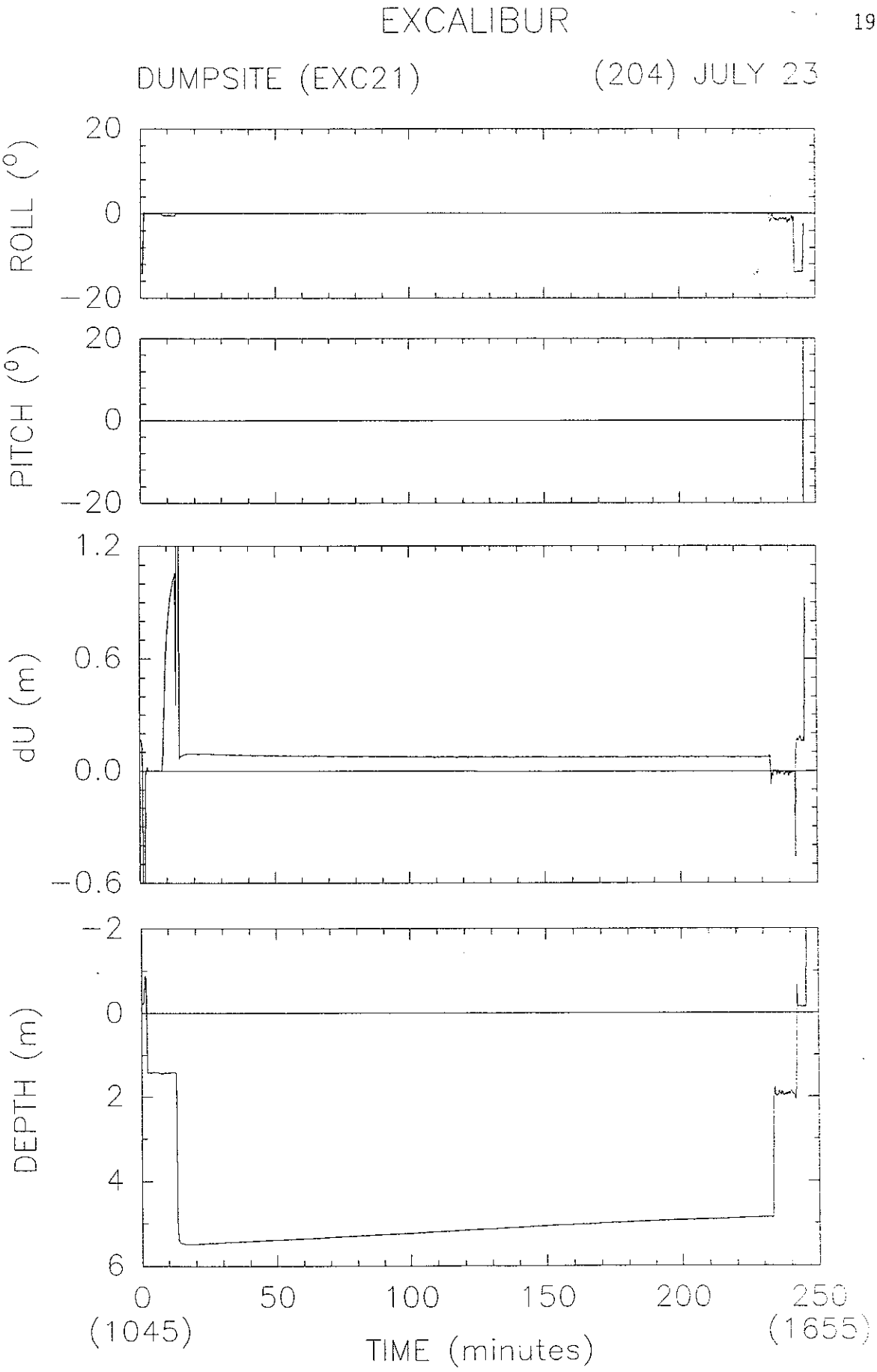

Figure 4.5-11. Time series results for Excalibur deployment at Experimental site (Station 21).

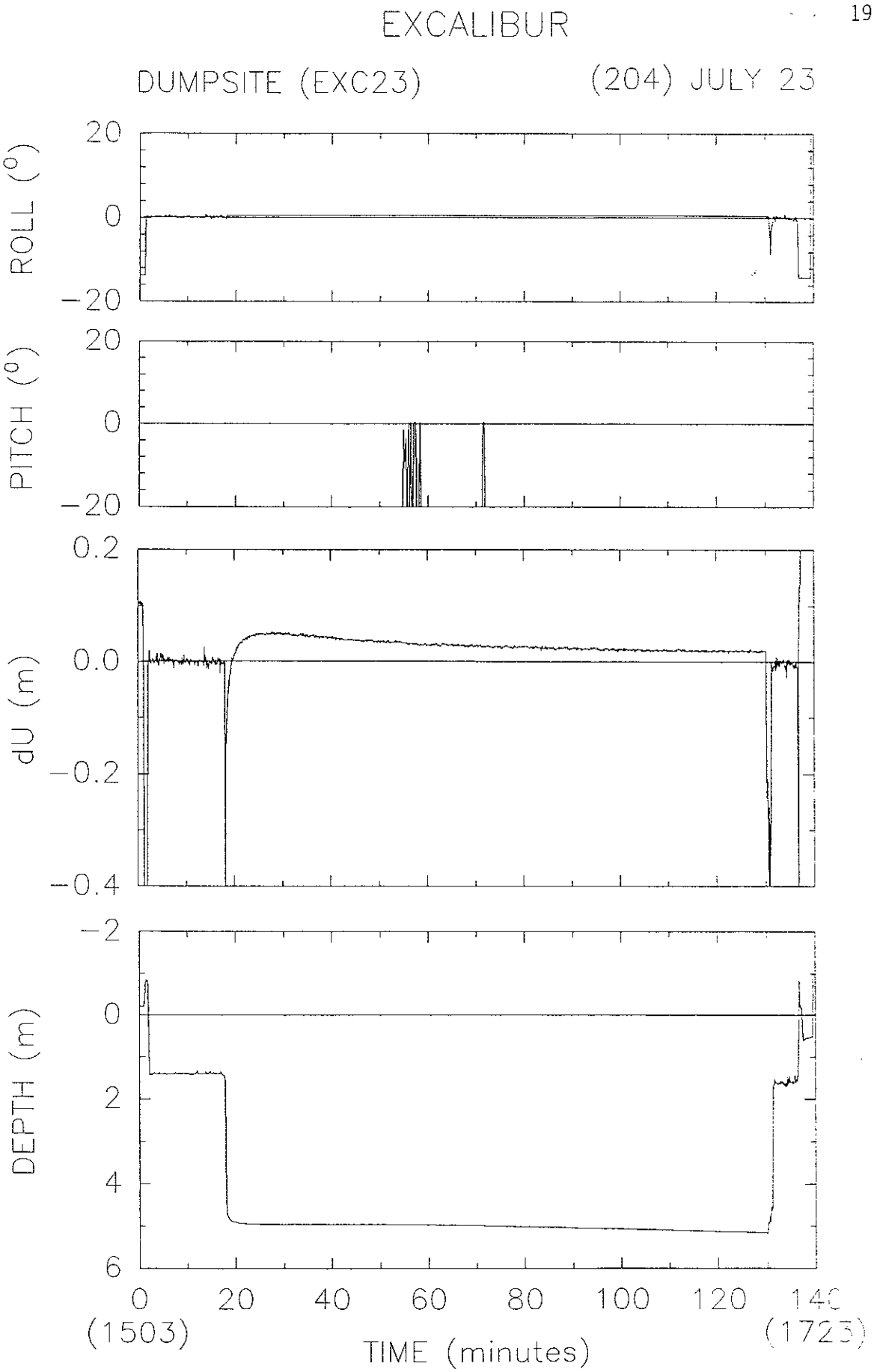

Figure 4.5-12. Time series results for Excalibur deployment at Experimental site (Station 23).

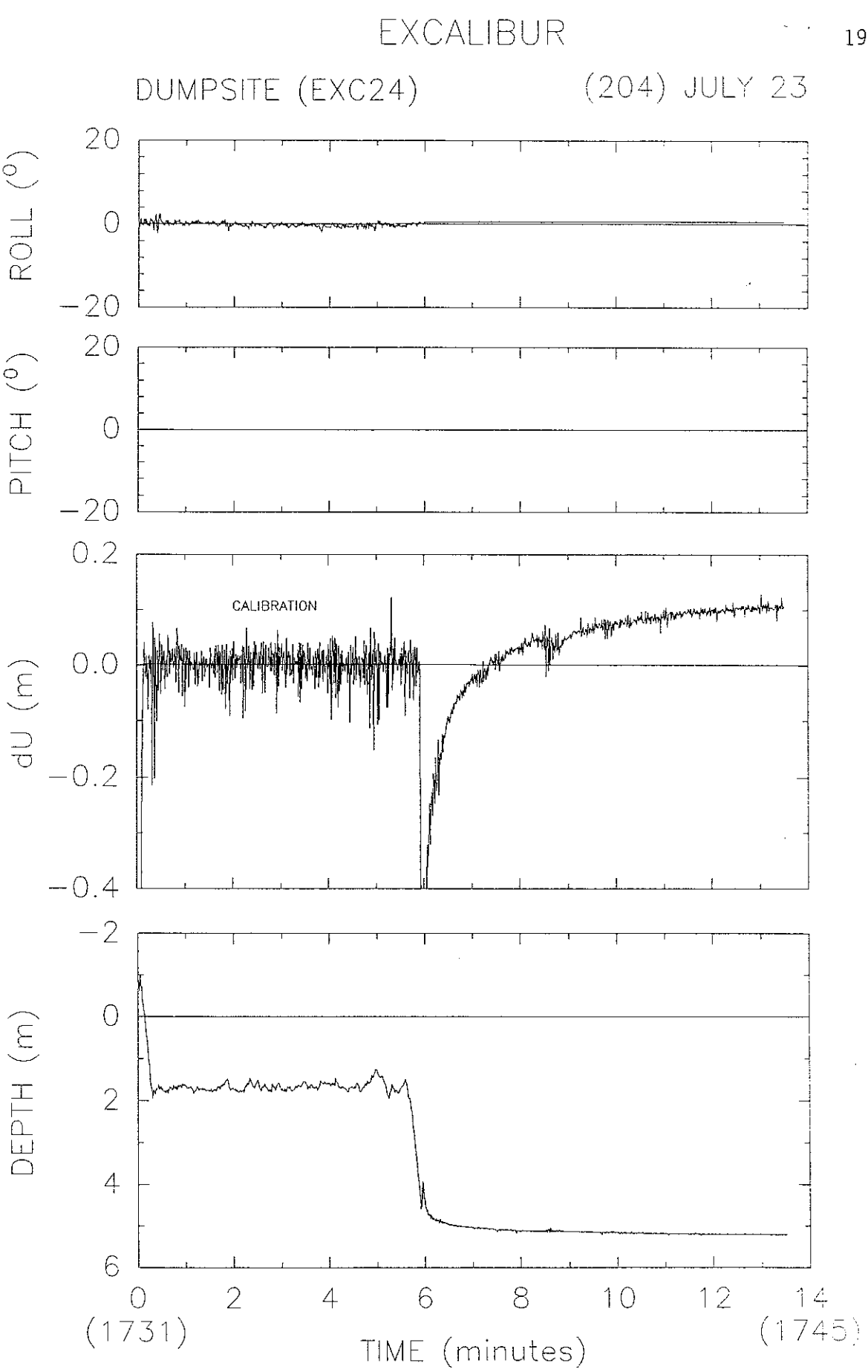

Figure 4.5-13. Time series results for Excalibur deployment at Experimental site (Station 24).

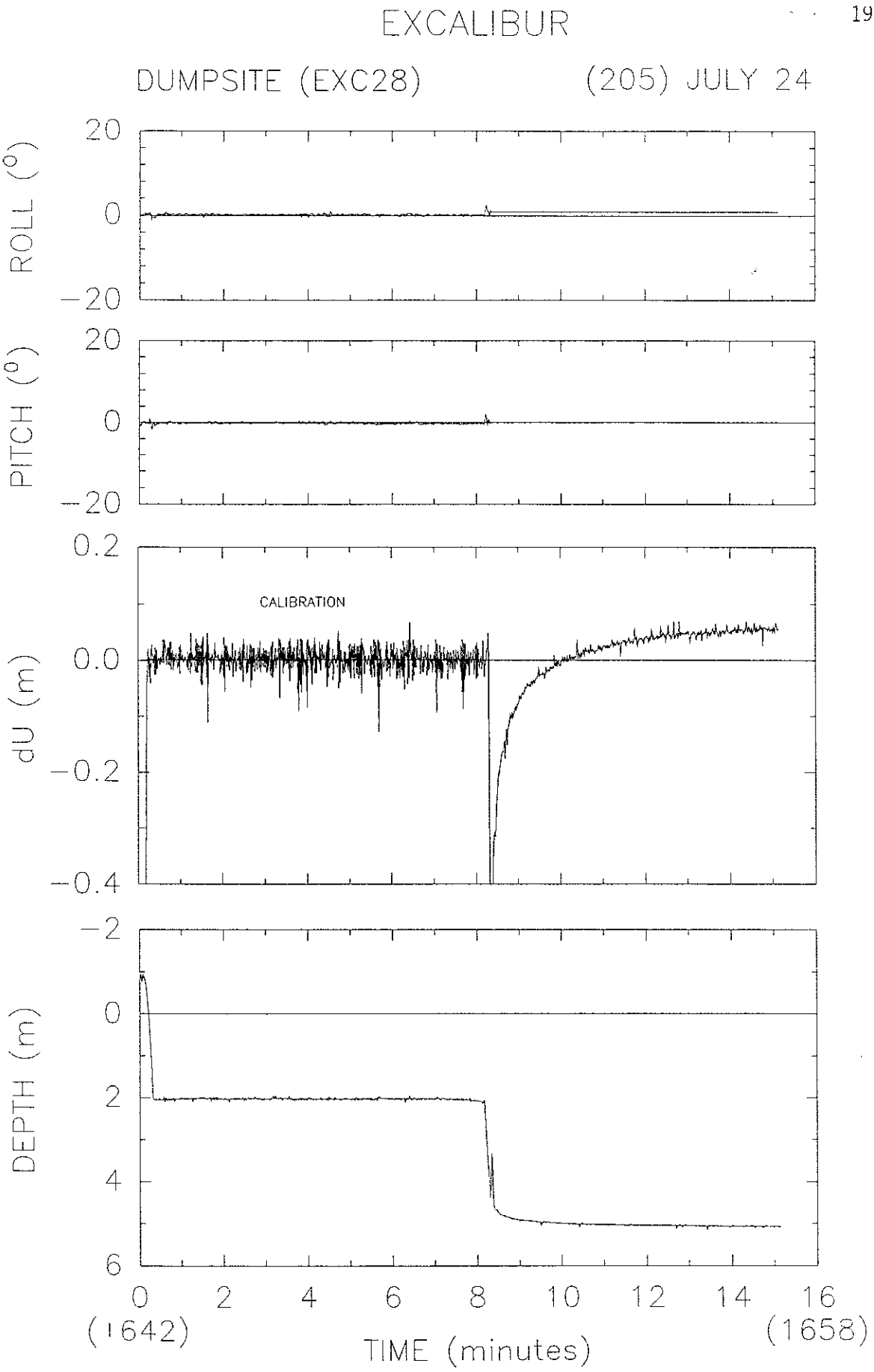

Figure 4.5-14. Time series results for Excalibur deployment at Experimental site (Station 28).

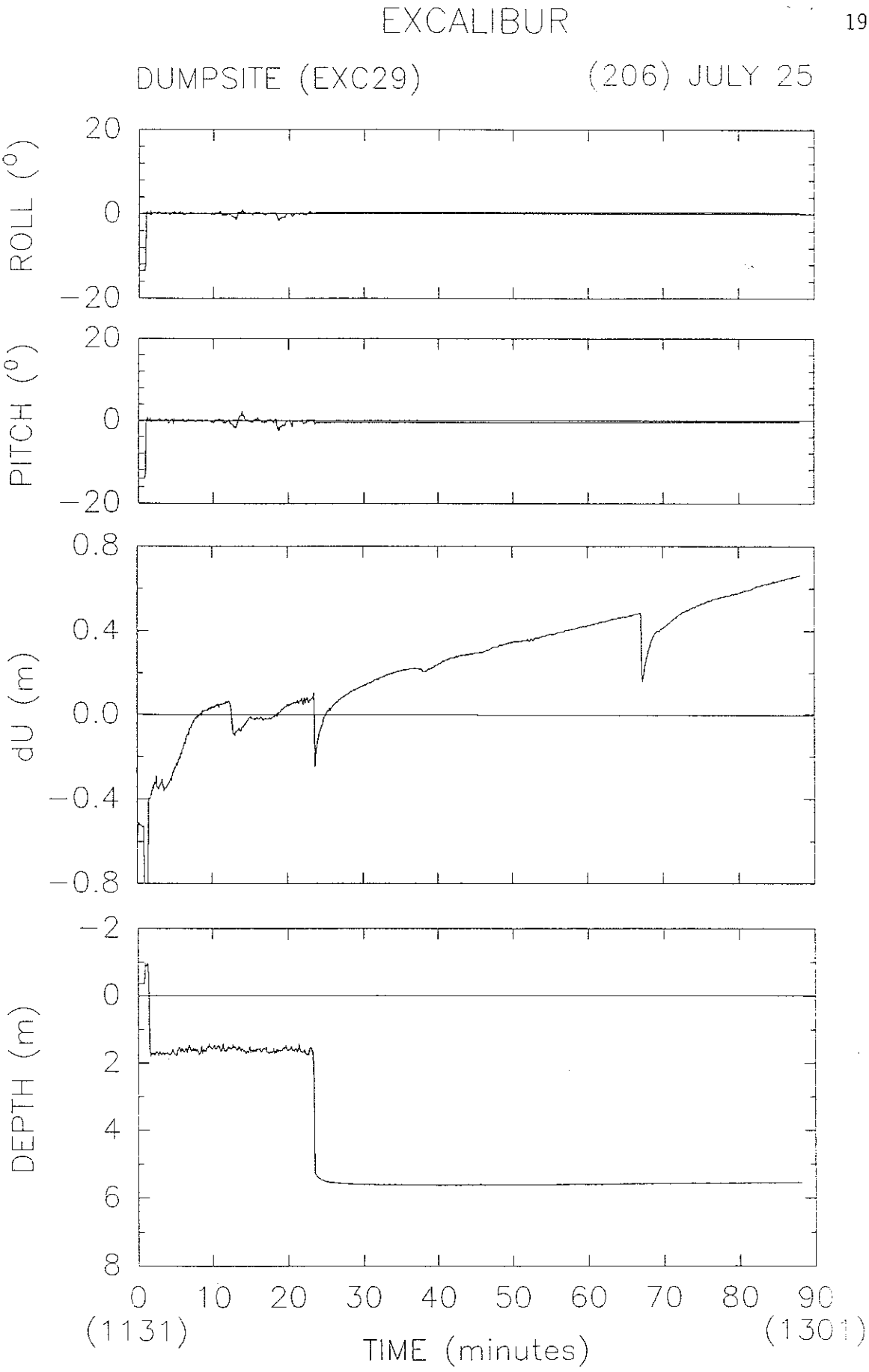

Figure 4.5-15. Time series results for Excalibur deployment at Experimental site (Station 29).

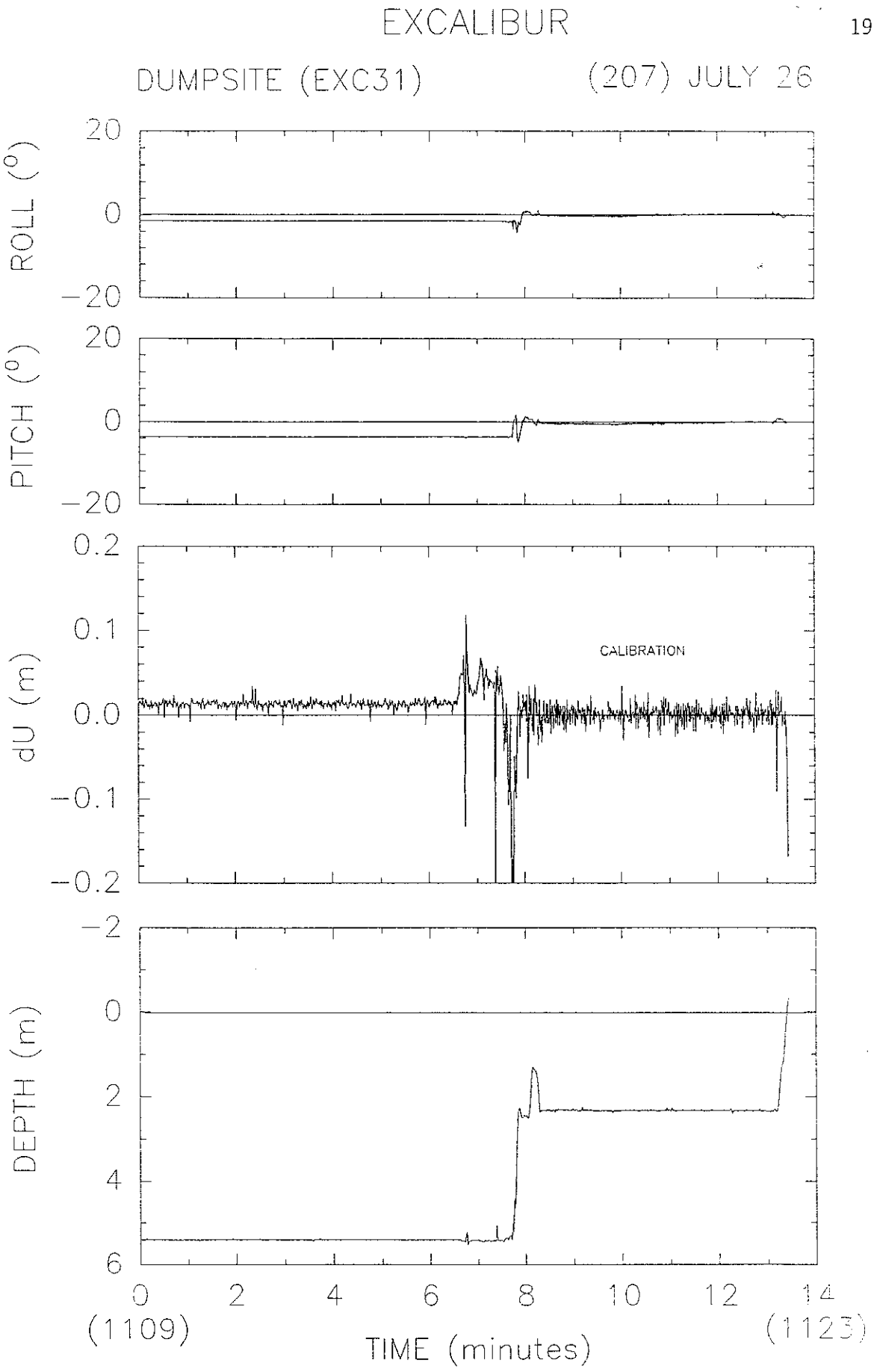

Figure 4.5-16. Time series results for Excalibur deployment at Experimental site (Station 31).

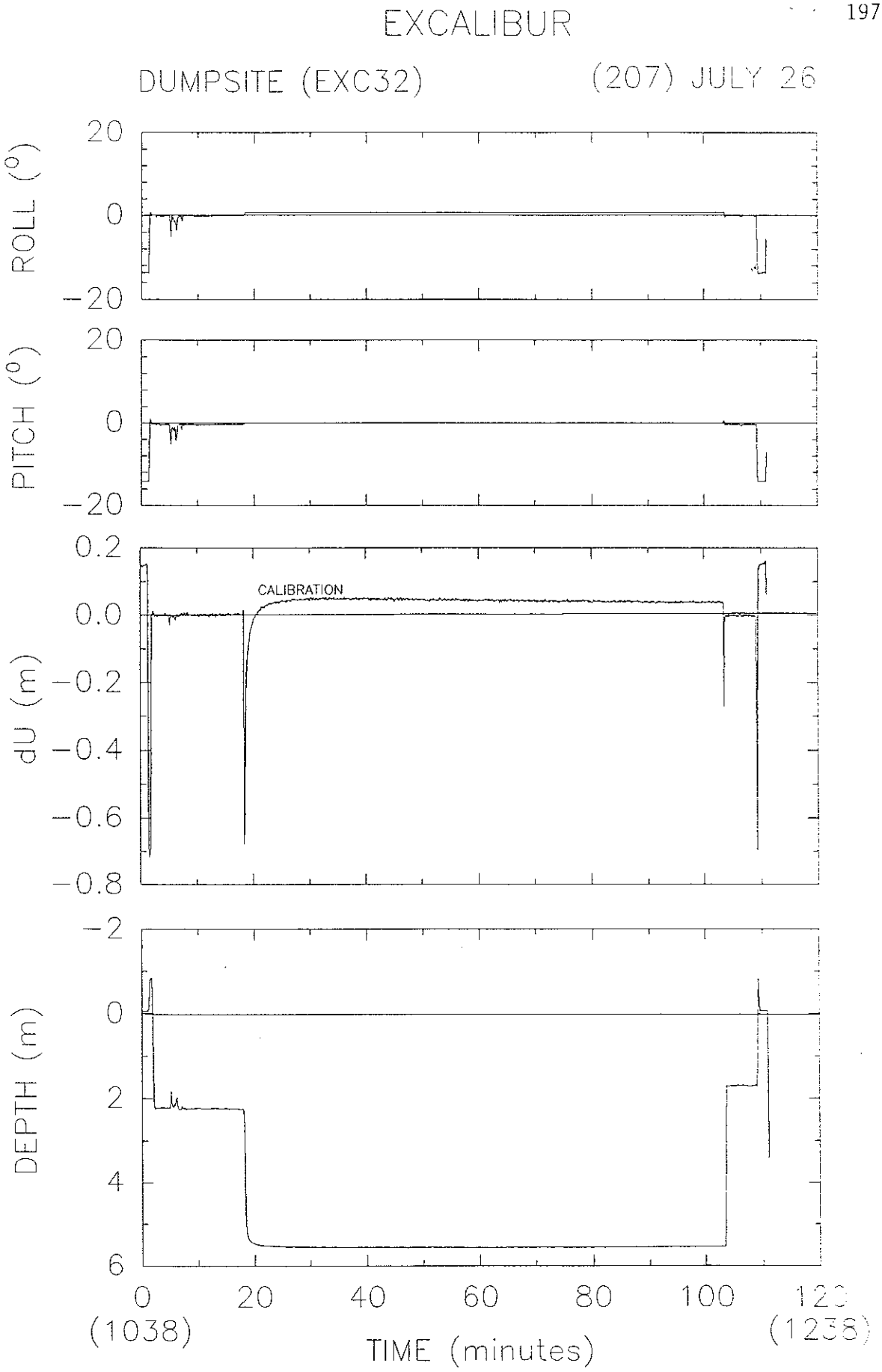

Figure 4.5-17. Time series results for Excalibur deployment at Experimental site (Station 32).

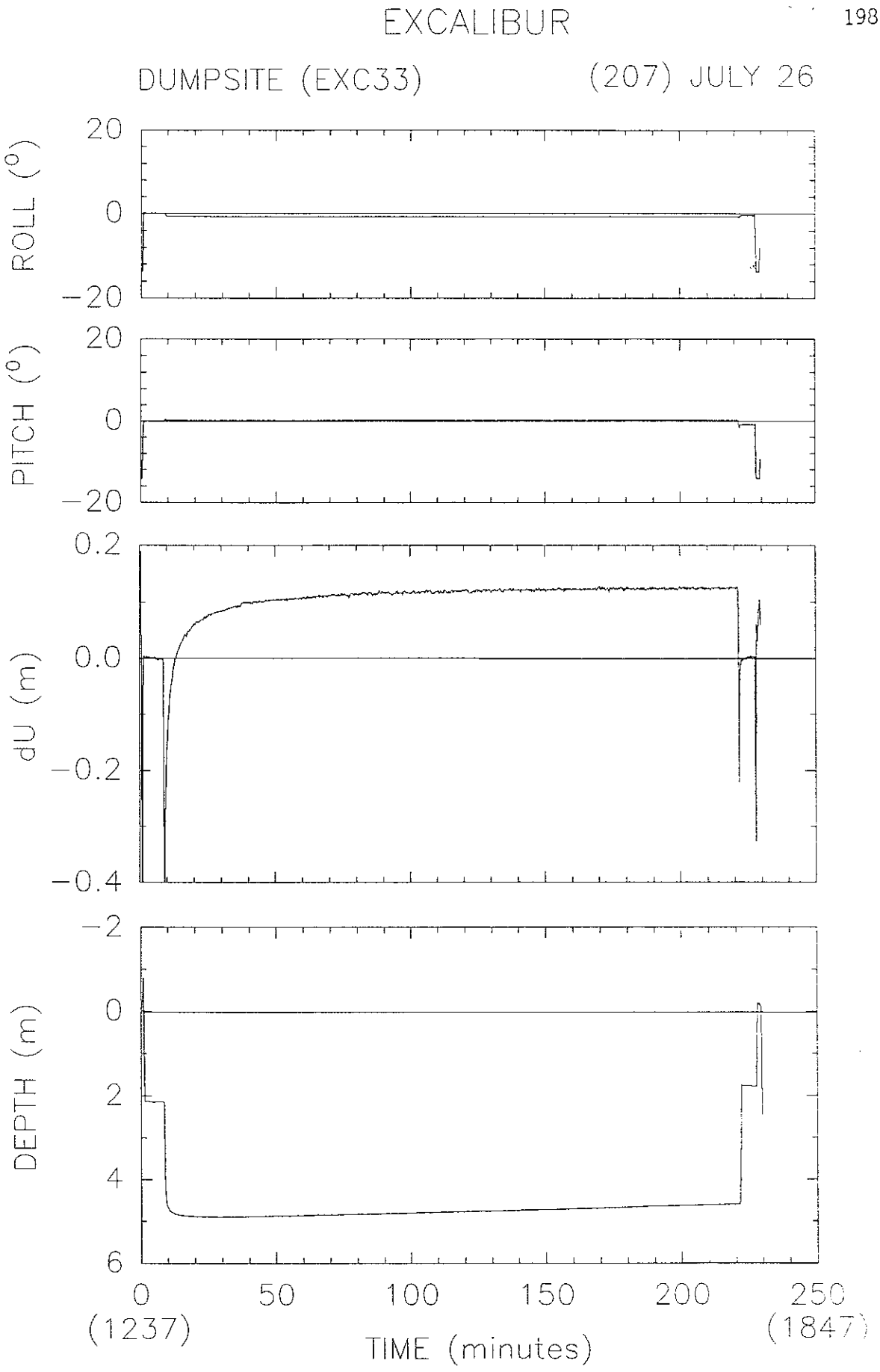

Figure 4.5-18. Time series results for Excalibur deployment at Experimental site (Station 33).

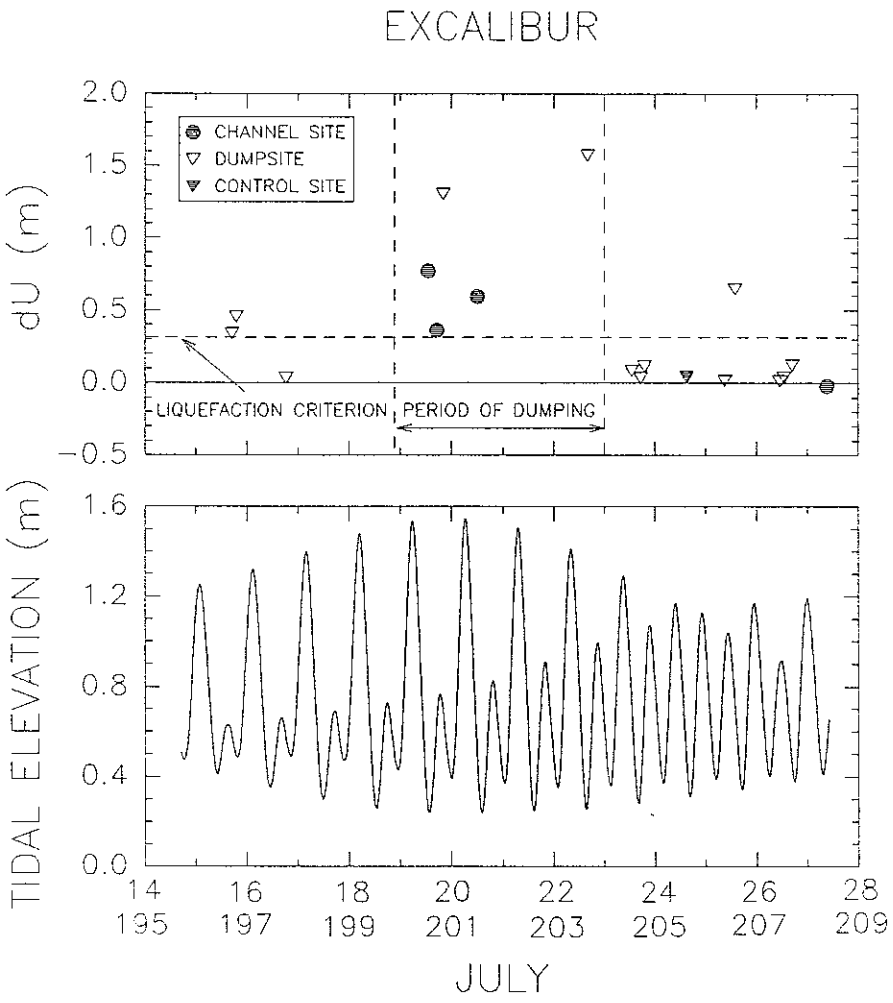

Figure 4.5-19. Time series of Excalibur residual excess pore pressures for all sites in relationship to time frame for disposal activities.

penetration pore pressures could be as high as six times the undrained shear strength in fine-grained sediments. Christian (1993) confirmed this finding; however, a lower factor is more appropriate for less plastic sediments. A multiplication factor of 4 adequately predicted pore pressures in this study. (The maximum penetration pore pressure may have been higher but not recorded due to the slight dilation behavior within the surficial denser crust.)

Undrained strengths ranged from 2 to 4 kPa (equivalent to 0.2-0.4 m of head), which is extremely low. Therefore, using a conversion factor of 4, the maximum excess pore pressures range from 0.8-1.6 m of head. The maximum excess pore pressure was measured at Station 20 to be at a level of 1.57 m of head, which is in agreement with the prediction. As previously noted, it is not possible for a sediment deposit to be stable if its excess pore pressure exceeds the vertical effective stress. Thus deployments at Stations 6, 11, 13, 12, 8, 17, 20 and 29 can be considered to have been of insufficient duration to determine the long term stability. All other stations gave a fully dissipated response within the duration of measurement.

Dumping of dredgings appears to have had no long term impact on seabed stability at a depth of 0.5 m (the depth of the probe) for stations 21, 23, 24, 28, 31, 32, and 33. Excess pore pressures are shown in excess of the maximum permissible for stability for some stations, but cannot be concluded to represent actual long term values. It is curious that the higher values were recorded immediately after disposal, and that after disposal had ceased, conditions appeared to become stable, as they were before disposal at Station 7.

4.6 Current Velocity and Direction

Current velocities at Station 2 (Fig. 4.6-1), located within the Control site, had a mean velocity of 0.13 m sec^{-1}. The currents were generally rotary, with a weakly defined ebb and somewhat better defined flood. The westerly flood is more strongly defined than the ebb, and has a maximum rate of almost 0.5 m sec^{-1}. Current velocities at Station 5, located just east of the Experimental disposal site (Fig. 4.6-2), had a mean value of 0.11 m sec^{-1}, slightly less than at the Control site. There was little difference between ebb and flood tide current velocities.

Wind velocity during the study period (obtained from Environment Canada for the Point Escuminac weather station) ranged from 0 to 56 km hr^{-1} (Fig. 4.6-3).

5. DISCUSSION

5.1 Sediment Properties

The sediments at all sites examined ranged from very loose to extremely loose organic silty clays and clayey silts with exceptionally high organic contents, high water content and low bulk density. These characteristics suggest that they are very susceptible to collapse during shear. In addition, the high organic contents and lack of consolidation enhance the potential for remobilization of dredged and deposited sediments through cyclic pore pressure generation and liquefaction failure during major storms or other loading events.

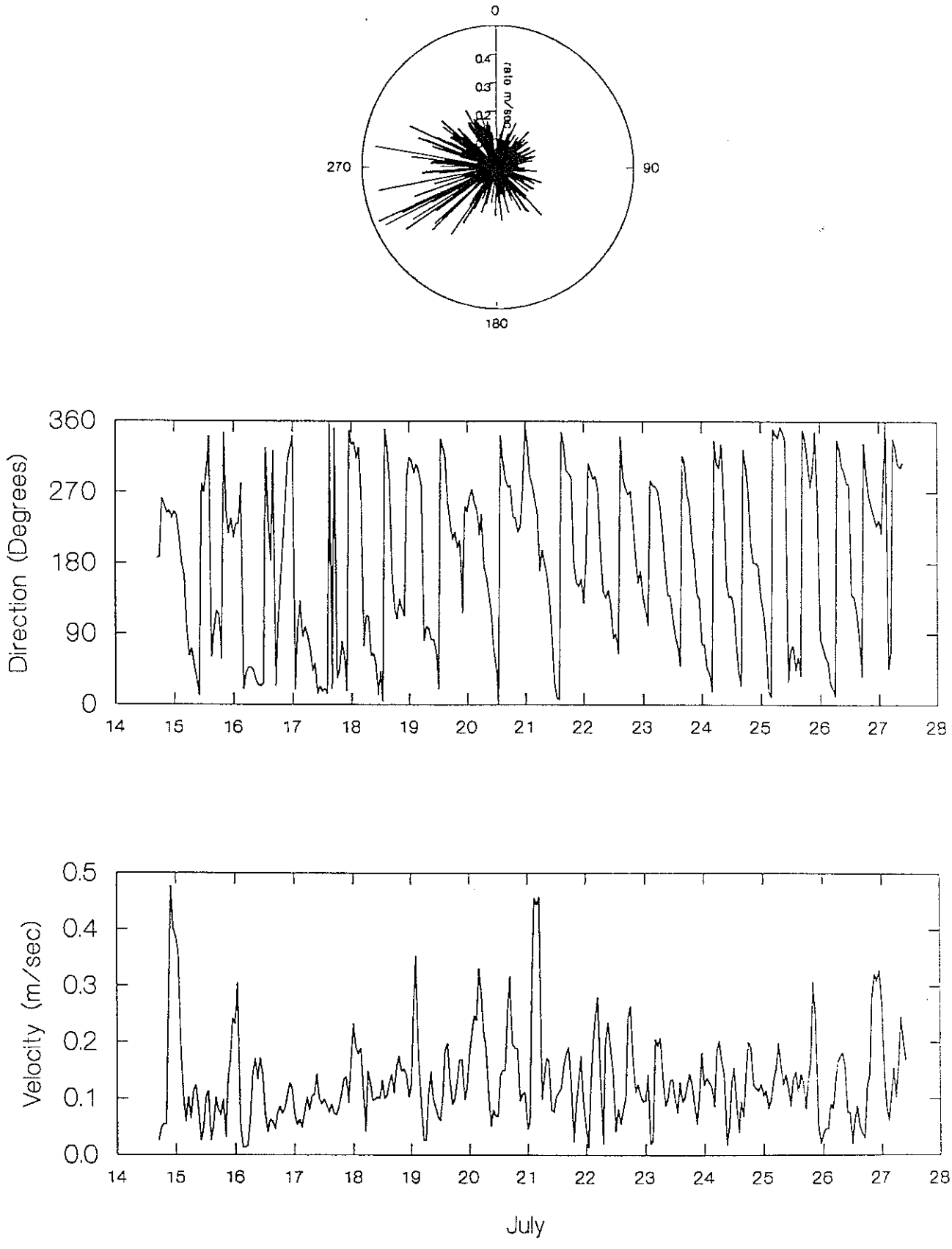

Figure 4.6-1. Current velocity and direction at the Control site (Station 2).

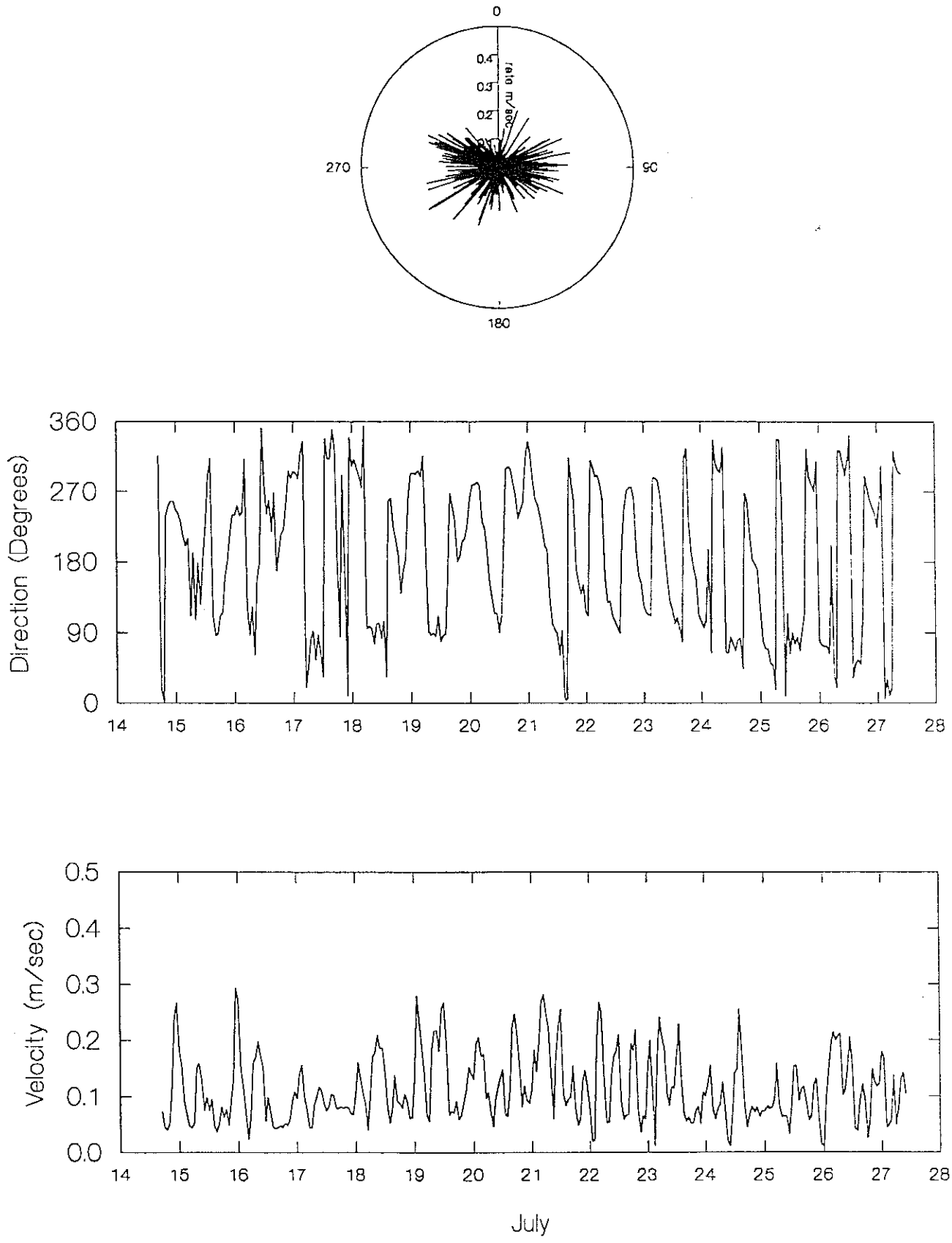

Figure 4.6-2. Current velocity and direction at the Experimental site (Station 5).

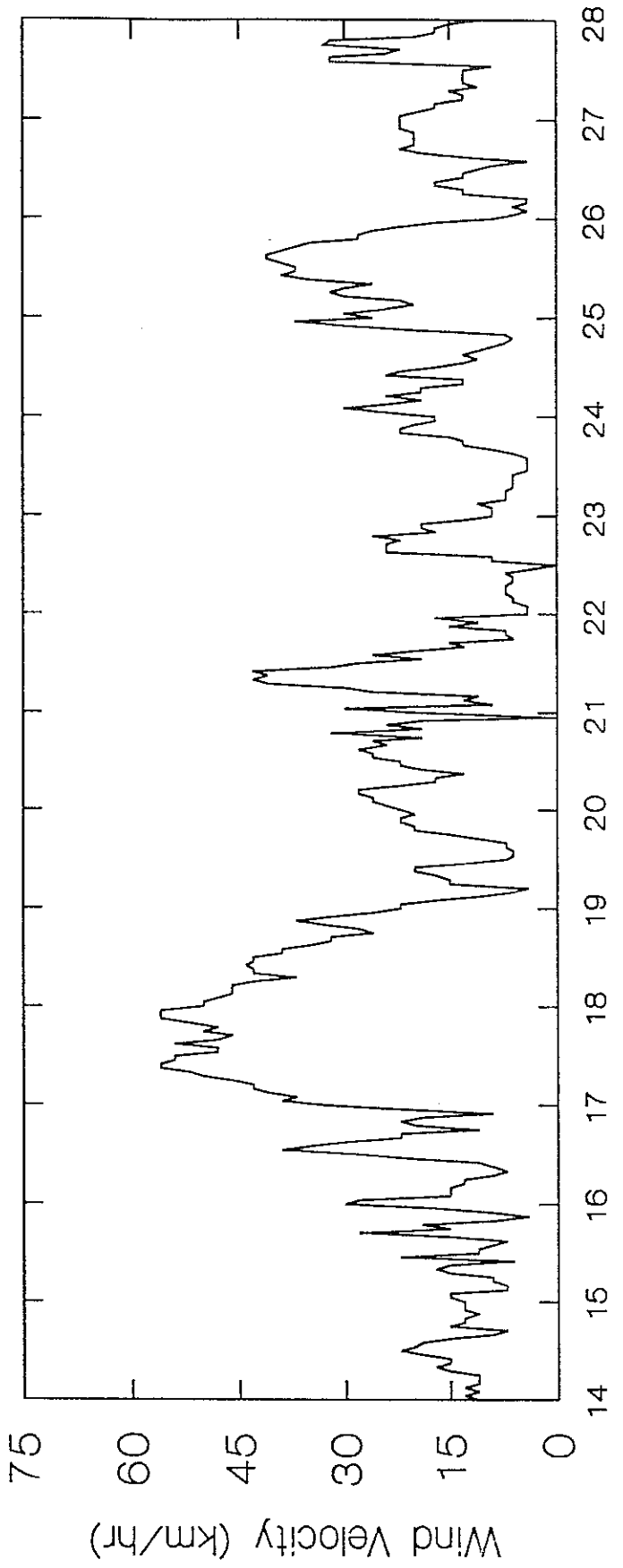

Figure 4.6-3. Wind velocity during the study period (for the Point Escuminac weather station).

The negative initial penetration pore pressure response from Lancelot and Excalibur measurements suggested the presence of a thin surficial crust. This was verified in subsequent analysis of gravity cores, which showed decreasing bulk density with depth over the top 10-15 cm (Section 4.1). Although high organic contents are often indicative of a highly compressible sediment structure, they may in some cases prevent drainage from within the consolidating mass, sustaining it in a weak condition indefinitely. The presence of an impermeable organic cap on the sediment column has been reported (Siva and Jordan 1984) as a possible explanation for a lack of consolidation at depth in other marine sediments.

5.2 Patterns of Erosion

The patterns of erosion determined in this study show a series of trends that help understand the stability of disposed sediment. These trends are illustrated in Figure 5.2-1 in the form of the erosion threshold (cohesion) and friction angle. The results are clustered into Control sites, the navigation channel, the pre-disposal sites and the post-disposal sites. The triplicate Control experiments (MIR12, MIR13, and MIR14) clearly demonstrate the reproducibility of results from the Sea Carousel, and the relatively homogeneous seabed, at least on spatial scales of tens of meters. The seabed sediments exhibit a threshold stress which is within the range of fine-grained marine sediments. The negative friction angle is suggestive of biostabilization of the sediment surface, leading us to believe that the sediment strength is derived from adhesion produced by benthic organisms.

The Channel sites show a significant reduction in erosion threshold compared to the Control sites. The extremely low thresholds encountered during the erosion process is diagnostic of fluidized gels. The high organic contents of these sediments (the highest of all sites in this survey) are believed to contribute to the development of the gel state.

The pre-disposal stations at the Experimental disposal site show a range in erosion thresholds typical of a heterogeneous seabed and may be a result of the region being previously used for disposal of dredge material. The highest erosion thresholds of the survey were detected within the Experimental disposal site. This finding confirms results from a similar survey in the region reported in Brylinsky et al. (1992), wherein disposed material quickly developed a strength that exceeded the surrounding natural material.

The majority of our study was devoted to monitoring the stability of disposed material within the Experimental disposal site. An examination of Figure 5.2-1 clearly shows that the disposed material shows a much greater degree of variability in results than was evident at the other three locations. This is reflected in both the threshold for erosion as well as in the friction angles. This result is to be expected given the nature of the material disposed, which is blocky in form and which retains much of its original character (Fredette et al. 1992). Despite this heterogeneity of the disposed material, we feel that several interesting trends are evident in our results. The most important is the rapid development of strength of the surface of the disposed material. Within the first 12 hrs after disposal, the material possesses a strength which is about 50 percent that of the original dredged material. However, the

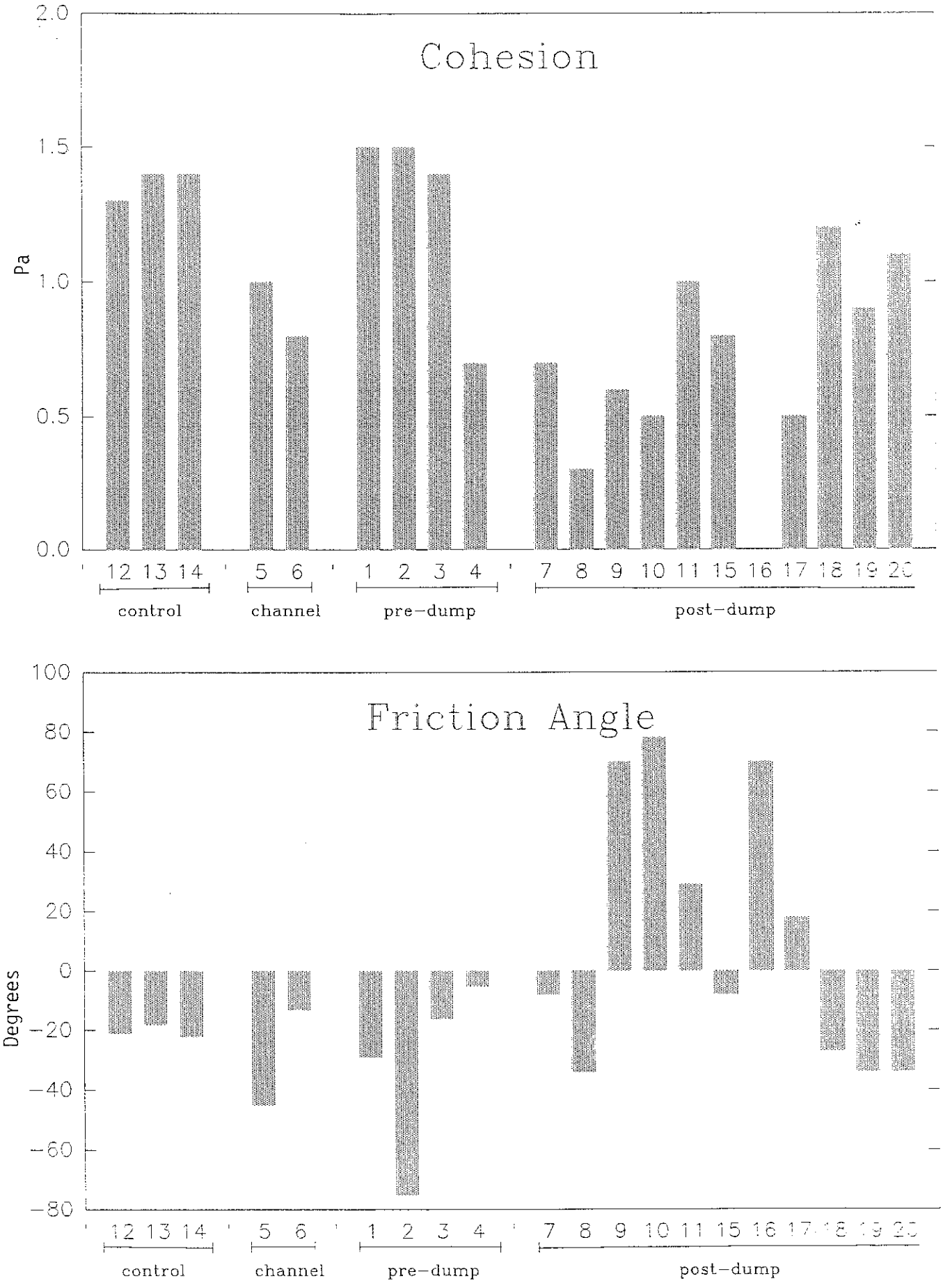

Figure 5.2-1. Trends in erosion threshold (cohesion) and friction angle.

strength increases rapidly over a period of 60 hrs, at which time it possesses a strength which exceeds that of the original dredged Channel material. At the same time there is a systematic decrease in the friction angle. The reason for these apparently-contradictory trends may be explained by reference to Figures 4.2.6.1-9 to 4.2.6.1-11 (MIR18, MIR19, and MIR20). These figures illustrate Sea Carousel results of the spoils approximately 60 hrs after disposal. Notice the rapid decrease in the erosion threshold with depth in the sediment. This is typical of the effects of colonization by benthic microflora as described by Paterson (1989). Also, work undertaken by T. Sutherland (Dalhousie University) has shown that this trend of surface strengthening may be a result of microphytobenthos production. The sediment strength is, however, restricted to the surface 2 mm of sediment only. Immediately below this "skin" the strength of the disposed material remained extremely low, and was even in a fluidized state (Fig. 4.2.6.1-9). We conclude, therefore, that disposed material is quick to develop a surface strength due to biological colonization of its surface. However, if this surface layer is damaged or broken, the underlying material would be easily mobilized.

5.3 SSC Concentrations and Development of Fluid Muds

5.3.1 Natural

The concentration of suspended material was observed at two sites: at the edge of the navigation channel; and at the edge of the Experimental disposal site. At the first site, there is clear evidence for tidal resuspension of bottom sediment during the flooding tide. This accounts for a small increase in SSC only, and is largely restricted to the lower 0.5 m of the water column. The ebbing tide was less effective in the resuspension of bed material. The most significant resuspension events were associated with periods of rough seas. Wave resuspension was particularly evident at Station 38 near the Experimental disposal site. On 25 July 1993 (Figs. 4.3.2-13 to 4.3.2-16), we see the most significant turbid events to be detected in the survey. These persist for periods of up to 6 hrs and occur at intervals over a 24 hr period of rough weather. The rapid onset of the turbid events suggests that the material was not resuspended *in situ*, but was advected in from a nearby source. Examination of current velocities and directions (Fig. 4.6-2) at the time of these events suggests that this source may be the freshly deposited material at Disposal Site B. However, these events also coincided with a period of high tides, strong precipitation and low salinity suggesting they may have resulted from sediments carried into the Bay by the river.

The synthesis of the settling experiments from each of the Sea Carousel deployments is shown in Figure 5.3.1-1. The irregular results of the near-surface OBS in the Carousel indicate that surface effects contribute to the signal and that it cannot be used with confidence to indicate fluid mud potential. The near-bed OBS, by contrast, produces consistent results in the Control examples (MIR12, MIR13, and MIR14). Omissions in this plot are due to burial of the sensor. Nevertheless, we see that the pre-disposal sites produce a rapid settling rate ($k < -0.0004$), which is diagnostic of a low fluid mud potential. The post-disposal Stations show a trend of increasing settling rate with time. The low initial settling rates we associate with disaggregated, remoulded material. The rapidly settling material that characterizes MIR18, MIR19, and MIR20 are the highest detected in the survey, and are diagnostic of an extremely

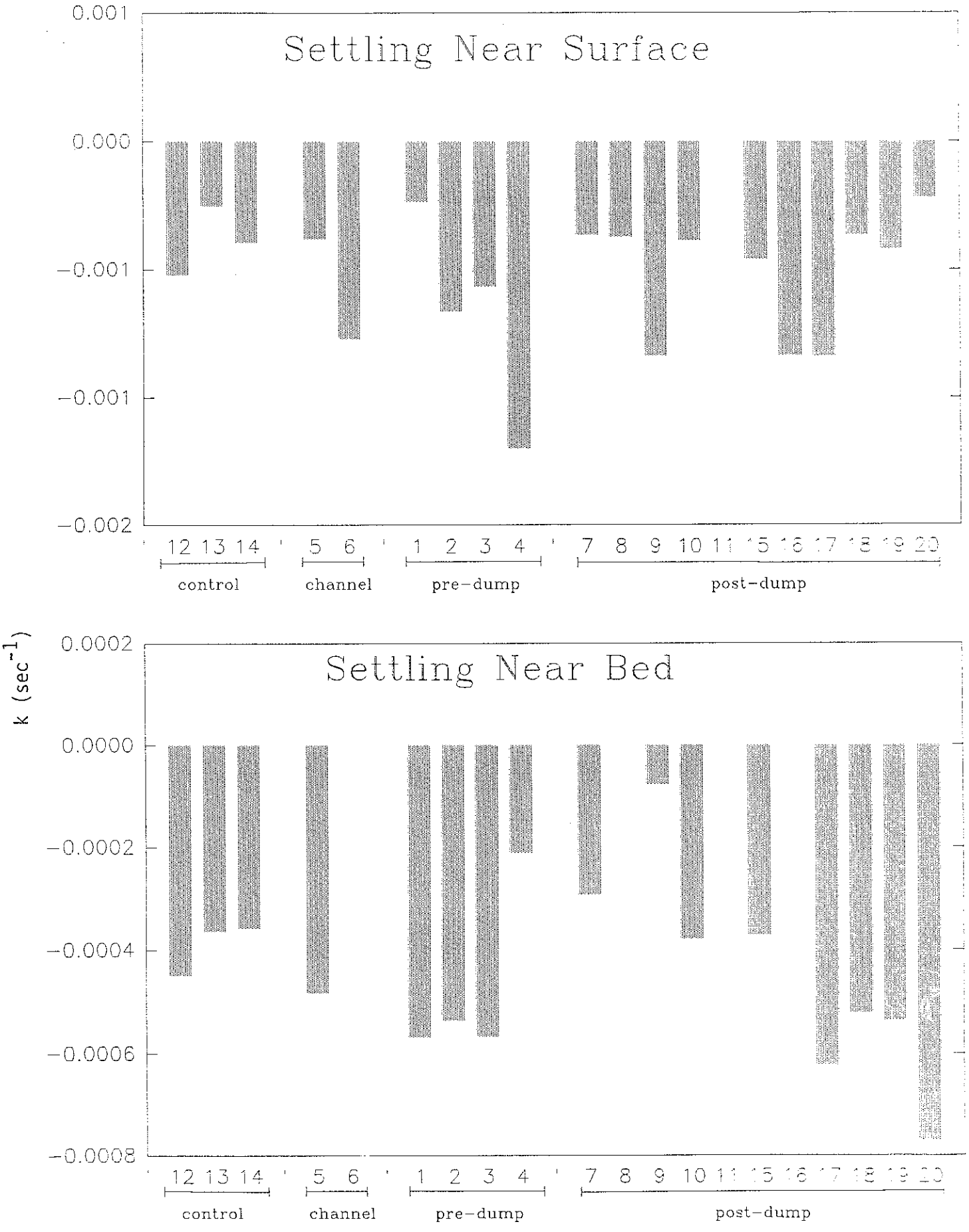

Figure 5.3.1-1. Summary of results of settling experiments.

low potential for fluid mud generation. This, we presume, is due to the pelletization, and aggregation of material brought about by biological activity; the same process contributes to sediment biostabilization.

Previous studies have demonstrated the loose state of Miramichi sediments (Brylinsky et al. 1992) which, together with the results of the present study, suggests that there is a potential for widespread instability during major natural loading events, such as autumn storms. Short-term loading events may also lead to destabilization of the seabed to some depth. Wave loading is commonly thought to result in excess pore pressure development through cyclic shear reversal within the seabed, progressively weakening the seabed. In actual fact, only certain wave amplitudes and frequencies will lead to shearing and excess pore pressure buildup within the seabed, as wave energy attenuates exponentially with increasing water depth and is absorbed by intergranular friction within the bed. Also, water depths limit the period of the longest storm waves that can develop, so an evaluation of the effects of wave loading requires a more complete consideration of the wave climate along with the local geometric setting, as well as the sediment shear response.

The results of Lancelot measurements indicate that the Channel margin may be close to failure under natural conditions, whereas the Control site is essentially fully stabilized. It is probable that the high sediment organic contents inhibit the expulsion of pore water along the Channel margin, resulting in a long term high susceptibility to liquefaction. The effect of repeated ship passage (discussed below) may partially account for the lack of stability along the Channel margins.

5.3.2 Ship Passage Effects

At the time of the passage of the M/V Mariner SOBS was at location at Station 1, near the Channel margin. The effect of the ship entering the Channel can be clearly seen in Figure 5.3.2-1. All OBS's show a rapid increase in SSC which is interpreted to be local resuspension from the bow wave of the ship. The turbid layer so generated has a peak concentration of *circa* 2000 mg^{-1}, and is largely evident to a height of approximately 1 m above the bed. The highest SSC is coincident with the bow wave, and drops rapidly with time in an exponentially decaying fashion, similar to the Sea Carousel settling experiments. During the concentration decay period a second pulse occurs evident as a secondary increase in SSC. This pulse occurs within 2 min of the bow wave, and is explained as local resuspension from the turbulent wake region caused by the ship's propellers. The turbidity associated with this turbulent wake region is sustained for 1 to 2 hrs. It appears oscillatory in OBS3 of Figure 5.3.2-1. This we presume is due to tidal advection of the turbid plume left behind after the ship's passage.

The effects of the outgoing ship's passage on day 197 is clearly seen in Figure 5.3.2-2. The signature of turbidity detected by the OBS sensors is similar to that seen in Figure 5.3.2-1, although the magnitude of the event was lower. We see a rapid onset of a highly turbid event that is associated with the passage of the ship's bow wave. The SSC shows a decrease with height above the bed from a maximum of 1000 mg^{-1}. It is evident even in the highest sensor (1.8 m above the seabed). This peak is followed by a lesser, but nevertheless distinct,

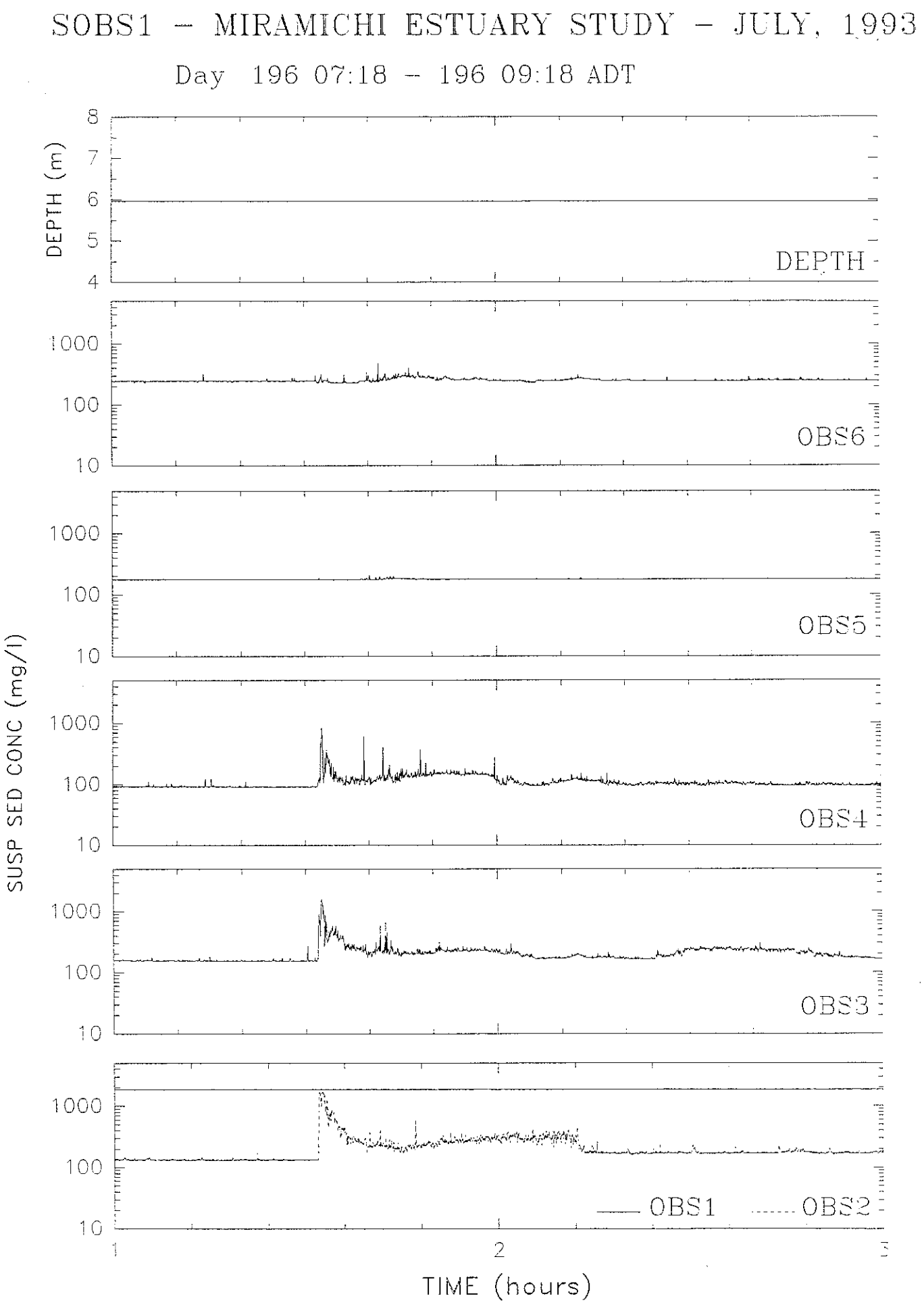

Figure 5.3.2-1. SOBS1 record during passage (incoming) of the M/V Mariner.

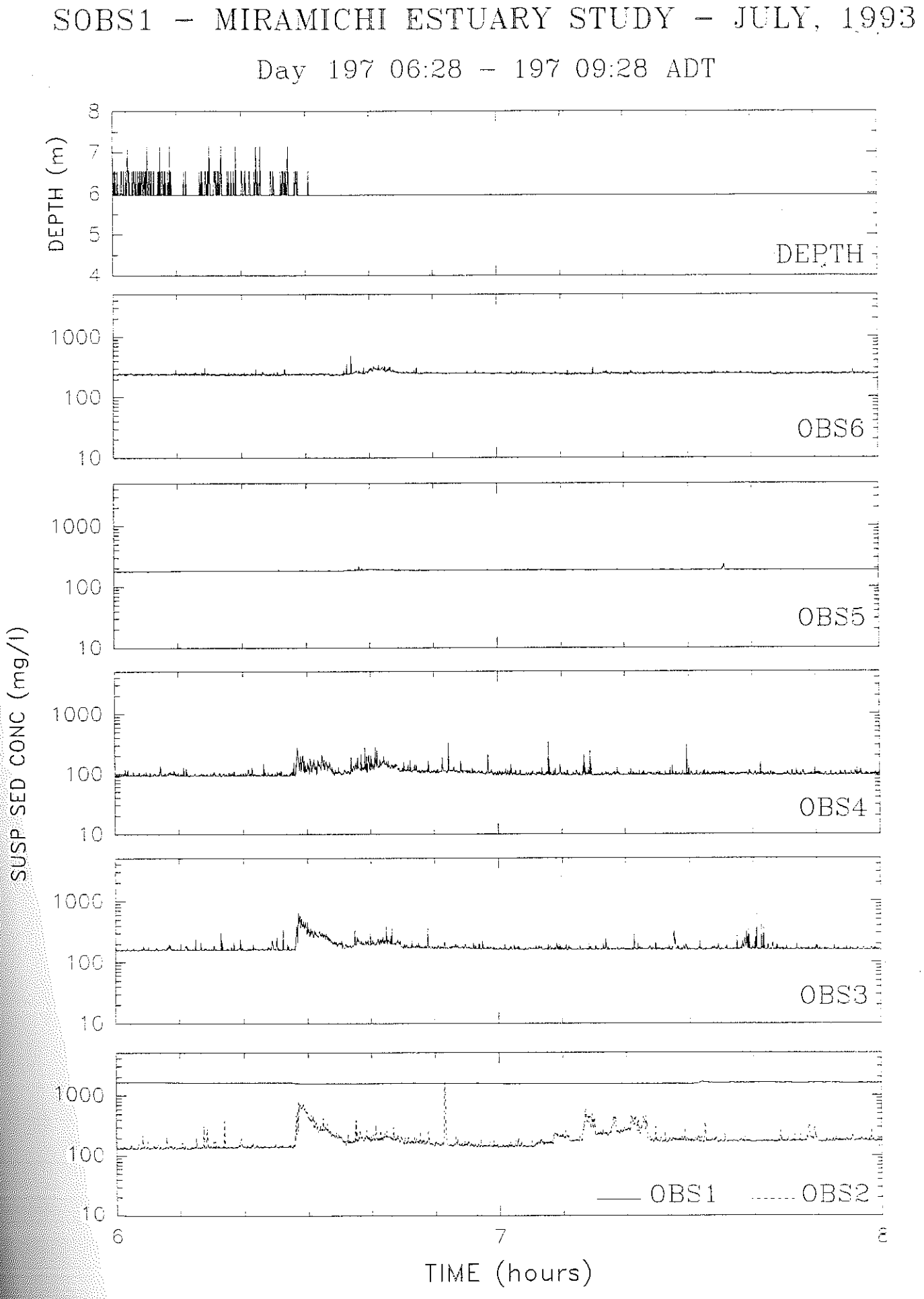

Figure 5.3.2-2. SOBS1 record during passage (outgoing) of the M/V Mariner.

secondary turbid event some 4 min later. The secondary plume we associate again with the turbulent wake region generated by the ship's propellers. The turbid wake region again takes approximately 1 hr to dissipate. The lower magnitude of the second event we attribute to the lower displacement of the outgoing vessel, which had unloaded its cargo. These two turbid events dominate the entire record of SOBS1. It is greater than tidal resuspension or wave resuspension.

Lancelot and Excalibur results indicated that ship passage caused a rapid cyclic loading that was closely coupled to excess porewater pressure cycling, indicating that shear stress reversal was occurring and that the seabed was being sheared, at least to the depth of the probe (0.55m). This process closely simulates what would happen during a major storm. It is not possible at this time to state whether or not ship passage effects are more destabilizing than storm waves since wave spectra measurements were not made during this study.

Several instances of the onset of cyclic liquefaction failure were observed adjacent to the Ship Channel (Figs. 4.4-4, 4.4-6, 4.4-9, 4.4-14 and 4.4-15). Sediments there and over the entire study area in general, are very close to the liquefaction threshold (or failure envelope), due to a lack of consolidation. This loose condition is probably a result of the high organic content of the sediments, which may play a role in preventing egress of porewater during wave loading, and to a lesser degree, during tidal loading, as indicated by the sinusoidal excess porewater pressure records recorded for the ship passages. A reduction in water depth (during passage of a wave trough or during an ebbing tide) is manifested by a coincident increase in excess pore pressure beneath the seabed, indicating that there is a time lag for equalization. This indicates that the stress state within the seabed is cycling in response to loading, and on one occasion, nearly resulted in liquefaction failure beneath the instrument.

The major excess pore pressure events recorded by Lancelot and Excalibur occurred in each case at exactly the time that a large vessel passed the deployment site. Shearing of the seabed during the incoming passage had evidently weakened the sediment (Fig. 4.4-4), as indicated by the onset of excess pore pressure generation during the outgoing passage the following day (Fig. 4.4-6). The bow wave on the incoming passage did not result in an excess pore pressure response; energy was fully absorbed by internal shearing and/or compression in the pore gas phase. The degree of shear stress transferred to the pore water in percent is given in Table 5.3.2-1, indicating that there may have been some free gas within the sediment. Event six resulted in the greatest degree of liquefaction under the action of the wake, as indicated by the 60 percent excess pore pressure response.

It is noteworthy that flowslide mobility is controlled by the geometry of the seabed, by the potential for excess porewater pressure generation during collapse, and by the viscous drag resistance offered by the overlying water column. They have been observed on very flat slopes, below 1 degree, in loose sandy sediment. Furthermore, there is minimal data on flowslides in material as rich in organics as in the Miramichi Bay which are much weaker than sediment deposits that have failed in reported case histories. Unfortunately, it is unlikely that flattening the side slopes on the Ship Channel would have any significant mitigating effect on channel bank slumping and infilling. Channel margin stability could be enhanced, however, if

Table 5.3.2-1. Excess pore pressures arising from cyclic wave loading during ship passage events.

Event No.	Max Ht. Bow Wave (mm)	Peak Ampl. *dU* (mm)	Max Ht. Wake Wave (mm)	Peak Ampl. *dU* (mm)	*dU*/Ht Bow	*dU*/Ht Wake
1	170	2	160	28	1.2%	18%
2	140	4	130	23	2.9%	18%
3	-	-	-	-	-	-
4	0	0	80	20	-	25%
5	50	5	190	40	10%	21%
6	430	55	250	150	13%	60%

ship passages were conducted at slower speeds, particularly in sections known to be prone to failure.

5.3.3 Dredging Effects

Dredging of the navigation channel took place within Reach 22 during deployment of SOBS1. The dredging operation was at times close (within 100 m) to the location of SOBS1. We observed reflectors on the ship's echo sounder while undertaking Sea Carousel deployments in the Channel that were obviously associated with the dredging operation. Even so, no evidence of the dredging operation was observed at SOBS1. We conclude from this that, although increases in turbidity are evident in the Channel, none of this turbid water spills over the Channel margins. Consequently, all effects of dredging the Channel appear to be contained within the Channel.

One immediate impact of dredging is undoubtedly the oversteepening of ship channel banks, which would fail back to a flatter slope, over a short period of time. These slumps would be of local extent, but would gradually infill the Channel, making periodic dredging a necessity. The preceding section discussed the problem presented in terms of the ambient levels of excess pore pressure and the loose nature of the sediments. It is evident that it will not be possible to avoid continuing to dredge to maintain adequate draft for vessel traffic. Furthermore, any attempt to flatten the side slopes would have minimal impact, as the degree of flattening required is excessively expensive.

The sediment exposed at the base of the cut is likely somewhat more stable than the overlying material, due to the effects of self-weight consolidation. However, the actual activity of dredging itself creates localized pockets of resuspended material, which returns to a stable condition very slowly, after it settles out of the water column. As no measurements were made in freshly-dredged locations, no conclusions can be made regarding the characteristics of redeposited material at the dredge site, or of the stiffer substrate that becomes exposed after dredging.

5.3.4 Dumping Effects

The majority of disposal at the Experimental disposal site took place between 20-23 July 1993 (Julian Days 201-204). SOBS during this period of time was located adjacent to the Experimental disposal site (Station 38). SOBS output for this period of time is presented in Figures 4.3.2-1 to 4.3.2-19. No clear evidence for increased turbidity caused by disposal can be seen. Several turbid events were detected, but similar events were also seen during periods when no disposal was taking place.

Excalibur measurements suggest that disposal has no effect on the long term stability of the seabed (Fig. 4.5-1). Pore pressures within recently deposited spoils, as well as within the underlying seabed, quickly (within days) returned to ambient levels. The weight of sediment added to the deposit is initially taken up as a rise in the porewater pressure above hydrostatic levels at depth, which then dissipate with time to the seabed. In the case of disposal of

dredged spoils, the imposition of stress and development of excess porewater pressure is sudden, which may be manifested through a deep-seated failure and the creation of fluid-expulsion features on the seabed (pockmarks or craters). With time, this condition disappears and the seabed returns to equilibrium conditions. During this period of stabilization, the disposed spoils, and perhaps the underlying seabed, exists in a weakened state and, consequently, there is a higher potential for resuspension under surface wave events.

6. CONCLUSIONS

(1) The sediments at all sites examined ranged from very loose to extremely loose organic silty clays and clayey silts with exceptionally high organic contents, high water content and low bulk density. These characteristics suggest that they are very susceptible to collapse when subjected to shear forces.

(2) The seabed at all sites, and particularly the Channel, is poorly consolidated and very close to liquefaction. The poor consolidation is a result of the high organic contents of the sediments.

(3) Erosion thresholds at the Channel sites were considerably lower than the Control site and were diagnostic of fluidized gels. The high organic contents of the Channel sediments (the highest of all sites in this survey) are believed to contribute to the development of the gel state.

(4) The strength of spoils deposited at the Experimental disposal-site increased rapidly. After 60 hrs sediment strength exceeded that of the original dredged Channel material. This however, was restricted to the surface 2 mm of sediment. Immediately below this depth the strength of the disposed material remained extremely low, and was even in a fluidized state.

(5) Excalibur measurements suggest that disposal has minimal impact on the long term stability of the original seabed. Although *in situ* pore pressures initially increased in sediments below spoil deposits, they quickly (within days) returned to ambient levels.

(6) Sediment settling rate measurements showed that the sediments encountered are generally not of a nature that would lead to hindered settling and the development of fluid mud layers. Continuous measurement of SSC concentrations and video observations by both Sea Carousel and SOBS did not detect the presence of fluid mud layers during the study period. High SSC (>2000 mg^{-1}), lasting for periods of hours were, however, observed on two occasions during the SOBS deployment near the Experimental disposal site. The origin of the sediments causing these events is unclear.

(7) Ship passage produced elevated SSC concentrations (> 2000 mg^{-1}) at sites located outside of the Channel, but this lasted for only a short period (<15 min).

(8) Ship passage caused a rapid cyclic loading that was closely coupled to excess porewater pressure cycling, indicating that the seabed was being sheared. The ship wake (as opposed to the bow wave) is a major destabilizing force along the Channel margin. The effects of ship speed and frequency of ship passage may be a major factor accounting for reduced stability along portions of the Channel margins.

(9) The source of sediment that results in infilling of the navigation channel within the Bay is unclear. If infilling is largely a result of slumping along Channel margins, as opposed to deposition of sediment carried into the Bay by the river, Channel margin stability could be enhanced if ship passages were conducted at lower speeds, particularly in sections known to be prone to failure.

7. RECOMMENDATIONS FOR FUTURE STUDIES

Previous studies (Brylinsky et al. 1992) of sediment stability at Disposal Site B indicated little difference between sediments at a spoils mound one year after deposition and the sediments at a natural undisturbed Control site in the Miramichi Inner Bay. The present study has shown that recently deposited spoils are initially unstable, but the surface strength quickly increases to exceed that of the original dredge materials. This stability, however, was still less than at the Control site, and was limited to the surface 2 mm of sediment.

In order to obtain a more comprehensive data set on the effects of wind and tidal forcing on resuspension process at Disposal Site B, it is recommended that SOBS and Lancelot, together with a current meter and wave rider, be deployed during any further dredging progamme, and for a period of three to four months thereafter (e.g., until ice-up). This would provide a long term data set that could be analyzed to determine the frequency and strength of forcing factors associated with natural and dredging related resuspension events. This information should also provide appropriate data for development of resuspension algorithms and validation data for numerical models.

Present information suggests that dredged spoils from the Channel area of the Miramichi Inner Bay do not consolidate readily, possibly because of the low gravitational stress levels resulting from the high organic content, and that this inhibits development of long-term sediment stability. Frequent (bimonthly or semi-annual) high quality bathymetric surveys of spoils at Disposal Site B, together with information on changes in bulk density obtained from core sample measurements, should provide data on the rate and degree of consolidation of spoils and could be used to determine if spoils remain where they are originally deposited.

Studies should be carried out to determine the relative contributions of channel margin slumping and river-borne sediments toward infilling of the navigation channel within the Bay.

If channel slumping is found to be a major factor, policy regarding the velocity and frequency of ship passage should be reviewed with the aim of developing guidelines that may reduce the amount and frequency of dredging activities.

8. REFERENCES

Amos, C.L., Daborn, G.R., Christian, H.A., Atkinson, A., and Robertson, A. 1992. *In situ* erosion measurements on fine-grained sediments from the Bay of Fundy. Marine Geology, 108, pp. 175-196.

Amos, C.L., Gibson, A.J., and Brylinsky, M. 1992. Sediment settling rate analyses for a sediment stability study of the Inner Miramichi Bay (Public Works and Government Services Contract No. 2105182). Acadia Centre for Estuarine Research Publication No. 23. Acadia University, Wolfville, Nova Scotia. 16 p.

Bennett, R.H., Li, H., Valent, P.J., Lipkin, J., and Esrig, M.I. 1985. *In-situ* undrained shear strengths and permeabilities derived from piezometer measurements. *In:* Strength Testing of Marine Sediments: Laboratory and *In-Situ* measurements, ASTM STP 883, R.C. Chaney and K.R. Demars, Eds., American Society for Testing and Materials, Philadelphia, pp. 83-100.

Brylinsky, M., Gibson, J., Daborn, G.R., Amos, C.L., and Christian, H. 1992. Miramichi Inner Bay Sediment Stability Study. Report to Public Works Canada. Acadia Centre for Estuarine Research Publication No. 22. Acadia University, Wolfville, Nova Scotia.

Burt, T.N. 1984. The Carousel: commissioning of a circular flume for sediment transport research. Hydraulic Research Limited Report SR 33.

Christian, H.A. 1993. *In situ* measurement of consolidation and permeability of soft marine sediments. Proceedings of the 4th Canadian Conference on Marine Geotechnical Engineering, St. John's, Newfoundland, 28-30 June, 2, pp. 662-679.

Christian, H.A. and Heffler, D.E. 1993. Lancelot - A seabed piezometer for geotechnical studies. Geo-Marine Letters, 13, pp. 189-195.

Christian, H.A., Heffler, D.H., and Davis, E.E. 1993. Lancelot - an *in-situ* piezometer for soft marine sediments. Deep-Sea Research, 40(7), pp. 1509-1520.

Clukey, E.C., Kulhawy, F.H., Liu, P.L.F., and Tate, G.B. 1985. The impact of wave loads and pore-water pressure generation on initiation of sediment transport. Geo-Marine Letters, 5, pp. 177-183.

Downing, J.P. and Beach, R.A. 1989. Laboratory apparatus for calibrating optical suspended solids sensors. Marine Geology, 86, pp. 243-249.

Fredette, T.J., Germano, J.D., Carey, D.A., Murray, P.M., and Kullberg, P.G. 1992. Chemical stability of capped dredged material disposal mounds in Long Island Sound, USA. Chemistry and Ecology, 7, pp. 173-194.

Hydraulics Research Limited. 1987. Deposition of cohesive sediments in an annular flume. Unpublished Internal Report: 5 p.

Krank, K. and T.G. Milligan. 1989. Effects of a major dredging program on the sedimentary environment of Miramichi Bay, New Brunswick. Can. Tech. Rep. Hydrogr. Ocean Sci., No. 112, iv + 61 p.

MacKnight, S. 1990. Contaminants in the Miramichi Estuary system. Report to the Acadia Centre for Estuarine Research, Acadia University, Wolfville, Nova Scotia. 24 p.

Mesri, G. and Castro, A. 1987. C'/Cc concept and Ko during secondary compression. Journal of Geotechnical Engineering, American Society of Civil Engineers, 113(GT3), pp. 230-247.

Morgenstern, N.R. and Sangrey, D.A. 1978. Methods of stability analysis. *In*: Landslides - Analysis and Control, R.L. Schuster and R.J. Krizek, Eds., Special Report 176, Transportation Research Board, National Academy of Sciences, Washington, D.C., pp. 15-171.

Paterson, D.M. 1989. Short-term changes in the erodibility of intertidal cohesive sediments related to the migratory behavior of epipelic diatoms. Limnology and Oceanography, 34(1), pp. 223-234.

Postma, H. 1967. Sediment transport and sedimentation in the estuarine environment. *In:* Estuaries, G.M. Lauff, Ed., Publ. American Association for the Advancement of Science, No. 83, pp. 158-179.

Richards, A.F. 1984. Modelling and the consolidation of marine soils. *In:* Seabed Mechanics, B. Denness, Ed., Graham and Trotham, London, pp. 3-8.

Schultheiss, P.J. 1990. *In-situ* pore-pressure measurements for a detailed geotechnical assessment of marine sediments: state of the art. *In:* Geotechnical Engineering of Ocean Waste Disposal, ASTM STP 1087, K.R. Demars and R.C. Chaney, Eds., American Society of Testing and Materials, Philadelphia, pp. 190-205.

Shames, I. 1962. Mechanics of Fluids. Publ. McGraw-Hill Book Company, New York: 555 p.

Silva, A.J. and Jordan, S.A. 1984. Consolidation properties and stress history of some deep sea sediments. *In:* Seabed Mechanics, B. Denness, Ed., Graham and Trotham, London, pp. 25-39.

Terzaghi, K. and Peck, R.B. 1967. Soil Mechanics in Engineering Practice. Wiley, New York, 729 p.

9. APPENDICES

APPENDIX A

Cruise Log

CRUISE LOG

MIRAMICHI BAY SEDIMENT STABILITY STUDY
Acadia Center for Estuarine Research
Atlantic Geoscience Centre

14-27 July 1993

DATE	TIME	OPERATION	STATION	DEPTH	POSITION	
14 July	12:27	Depart Chatham Wharf				
"	14:36	SOBS Deployed	1	19'	47° 07.92'	65° 09.82'
"	14:46	Current Meter 8707 Deployed	2	20'	47° 07.89'	65° 09.66'
"	14:56	CTD Deployed	3	19'	47° 07.93'	65° 09.52'
"	15:37	Lancelot Deployed	4	17'	47° 07.99'	65° 09.97'
"	16:30	Current Meter 8207 Deployed	5	18'	47° 06.64'	65° 09.74'
"	16:40	Depart for Chatham Wharf				
"	18:42	Arrive Chatham Wharf				
15 July	11:24	Depart Chatham Wharf				
"	13:20	Arrive Disposal Site				
"	13:58	Buoys Deployed by Miramichi Surveyor				
"	14:11	Van Veen Grab Deployed	6	18'	47° 07.06'	65° 10.15'
"	14:21	Gravity Core Deployed	6	18'	47° 07.06'	65° 10.15'
"	14:49	Excalibur Deployed	6	18'	47° 07.06'	65° 10.15'
"	15:26	Gravity Core Deployed	7	18'	47° 06.98'	65° 10.30'
"	15:37	Van Veen Grab Deployed	7	18'	47° 06.99'	65° 10.27'
"	15:48	Van Veen Grab Deployed	8	18'	47° 06.85'	65° 10.33'
"	15:54	Gravity Core Deployed	8	18'	47° 06.87'	65° 10.29'
"	16:10	Gravity Core Deployed	9	18'	47° 06.92'	65° 10.30'

15 July	16:22	Van Veen Grab Deployed	9	18'	47° 06.90'	65° 10.30'
"	16:36	Van Veen Grab Deployed	10	18'	47° 07.03'	65° 10.24'
"	16:43	Gravity Core Deployed	10	18'	47° 07.02'	65° 10.25'
"	17:10	Excalibur Retrieved				
"	17:46	Excalibur Deployed	11	17'	47° 07.01'	65° 10.26'
"	17:55	Depart for Chatham Wharf				
"	19:50	Arrive Chatham Wharf				
16 July	09:10	Depart Chatham Wharf				
"	10:50	Arrive Disposal Site (Station 6)				
"	12:32	Sea Carousel Deployed	6	17'	47° 06.97'	65° 10.33'
"	12:35	CTD Profile	6	17'	47° 06.97'	65° 10.33'
"	12:40	Eckman Grab Deployed	6	17'	47° 06.97'	65° 10.33'
"	13:50	Sea Carousel Terminated				
"	14:31	Excalibur Retrieved				
"	14:35	Depart for Station 7				
"	14:51	Arrive Station 7				
"	15:30	Sea Carousel Deployed	7	18'	47° 07.05'	65° 10.21'
"	15:35	CTD Profile	7	18'	47° 07.05'	65° 10.21'
"	15:45	Eckman Grab Deployed	7	18'	47° 07.05'	65° 10.21'
"	16:45	Sea Carousel Terminated				
"	17:25	Excalibur Deployed	7	18'	47° 06.88'	65° 10.33'
"	17:30	Depart for Station 8				
"	17:40	Arrive Station 8				
"	17:50	Sea Carousel Deployed	8	18'	47° 06.88'	65° 10.33'
"	17:55	CTD Profile	8	18'	47° 06.88'	65° 10.33'
"	18:00	Eckman Grab Deployed	8	18'	47° 06.88'	65° 10.33'
"	19:14	Sea Carousel Terminated				
"	19:20	Depart for Station 3				
"	19:30	Retrieved CTD from Station 3				
"	19:34	Depart for Chatham Wharf				

16 July	20:30	Return Chatham Wharf				
18 July	08:35	Depart Chatham Wharf				
"	10:05	Arrive Disposal Site				
"	10:24	Excalibur Retrieved from Station 7				
"	12:00	Aborted attempt @ Sea Carousel Deployment (too stormy)				
"	12:05	Depart for Station 12				
"	12:12	Arrive Station 12				
"	12:14	Van Veen Grab Deployed	12	23'	47° 07.70'	65° 09.20'
"	12:29	Gravity Core Deployed	12	24'	47° 07.78'	65° 09.22'
"	12:30	Depart for Station 13				
"	12:32	Arrive Station 13				
"	12:36	Gravity Core Deployed	13	31'	47° 07.80'	65° 09.40'
"	12:43	Van Veen Grab Deployed	13	31'	47° 07.80'	65° 09.40'
"	12:45	Depart for Station 9				
"	13:30	Arrive Station 9				
"	13:55	Sea Carousel Deployed	9	18'	47° 06.87'	65° 10.29'
"	14:06	CTD Deployed (Depth Profile)	9	18'	47° 06.87'	65° 10.29'
"	15:27	Sea Carousel Terminated				
"	15:35	Depart for Station 14				
"	16:00	Arrive Station 14				
"	16:02	Gravity Core Deployed	14	31'	47° 06.78'	65° 14.69'
"	16:12	Van Veen Grab Deployed	14	31'	47° 06.78'	65° 14.69'
"	16:15	Depart for Station 15				
"	16:20	Arrive Station 15				
"	16:22	Van Veen Grab Deployed	15	31'	47° 06.80'	65° 14.57'
"	16:29	Gravity Core Deployed	15	31'	47° 06.80'	65° 14.57'
"	16:40	Depart for Chatham Wharf				
"	18:30	Arrive Chatham Wharf				
19 July	09:00	Depart Chatham Wharf				

19 July	10:42	Arrive Station 13				
"	11:02	Excalibur Deployed	13	27'	47° 07.83'	65° 09.41'
"	11.17	Sea Carousel Deployed	13	28'	47° 07.79'	65° 09.21'
"	11:40	CTD deployed (Depth Profile)	13	27'	47° 07.83'	65° 09.41'
"	12:59	Sea Carousel Retrieved				
"	13:24	Excalibur Retrieved				
"	13:30	Depart for Station 12				
"	13:40	Anchored At Station 12				
"	14:02	Excalibur Deployed	12	28'	47° 07.79'	65° 09.21'
"	14:30	Sea Carousel Deployed	12	28'	47° 07.79'	65° 09.21'
"	14:40	CTD Deployed (Depth Profile)	12	28'	47° 07.79'	65° 09.21'
"	16:05	Sea Carousel Retrieved				
"	16:31	Depart for Station 8				
"	17:00	Anchored at Station 8				
"	17:05	Excalibur Deployed	8	18'	47° 06.96'	65° 10.29'
"	17:10	CTD Deployed (Depth Profile)	8	18'	47° 06.96'	65° 10.29'
"	17:30	Sea Carousel Deployed	8	18'	47° 06.96'	65° 10.29'
"	18:40	Sea Carousel Retrieved				
"	19:00	Excalibur Retrieved				
"	19:05	Depart for Station 16				
"	19:29	Anchored at Station 16				
"	19:30	CTD Deployed	16	18'	47° 06.89'	65° 10.10'
"	19:32	Depart for Station 17				
"	19:50	Anchored at Station 17				
"	20:05	Excalibur Deployed	17	18'	47° 08.05'	65° 09.77'
"	20:07	Depart for Chatham Wharf				
"	22:00	Arrive Chatham Wharf				
21 July	08:45	Depart Chatham Wharf				
"	10:30	Arrive Experimental Site				
"	11:27	ROV Deployed (Experimental Site)		18'	47° 06.88'	65° 10.26'

21 July	11:57	ROV Retrieved				
"	12:05	ROV Deployed (Experimental Site)				
"	12:40	ROV Retrieved				
"	12:48	ROV Deployed (Disposal Site B)		17'	47° 06.73'	65° 10.46'
"	13:00	ROV Retrieved				
"	13:15	ROV Deployed (Disposal Site B)		16'	47° 07.21'	65° 10.74'
"	13:30	ROV Retrieved				
"	13:40	ROV Deployed (Channel - Reach 22)		26'	47° 06.76'	65° 14.70'
"	14:30	Depart for Chatham Wharf				
"	16:20	Arrive Chatham Wharf				
22 July	08:01	Depart Chatham Wharf				
"	10:00	Arrive Station 18				
"	10:16	Lancelot Deployed	18	23'	47° 08.13'	65° 09.39'
"	10:20	Depart for Station 19				
"	10:25	Arrive Station 19				
"	10:37	CTD Deployed	19	19'	47° 06.82'	65° 10.09'
"	10:39	Depart for Station 20				
"	10:40	Arrive Station 20				
"	10:43	Gravity Core Deployed	20	17'	47° 06.87'	65° 10.30'
"	10:54	Van Veen Grab Deployed	20	17'		
"	11:16	Excalibur Deployed	20	18'	47° 06.87'	65° 10.26'
"	11:40	Sea Carousel Deployed	20	17'	47° 06.86'	65° 10.29'
"	12:34	Sea Carousel Retrieved				
"	13:41	Excalibur Retrieved				
"	14:45	Depart for Chatham Wharf				
"	16:40	Arrive Chatham Wharf				
23 July	08:30	Depart Chatham Wharf				
"	10:30	Arrive Experimental Site				
"	10:31	Gravity Core Deployed	21	15'	47° 06.87'	65° 10.23'

23 July	10:45	Excalibur Deployed	21	15'	47° 06.87'	65° 10.23'
"	11:15	Sea Carousel Deployed	21	15'	47° 06.86'	65° 10.26'
"	12:31	Sea Carousel Retrieved				
"	12:33	Van Veen Grab Deployed	21	15'	47° 06.86'	65° 10.26'
"	12:35	Depart for Station 22				
"	12:40	Arrive Station 22				
"	12:41	Van Veen Grab Deployed	22	15'	47° 06.90'	65° 10.29'
"	12:57	Sea Carousel Deployed	22	15'	47° 06.90'	65° 10.29'
"	14:17	Sea Carousel Retrieved				
"	14:18	Gravity Core Deployed	22	15'	47° 06.90'	65° 10.29'
"	14:37	Excalibur Retrieved				
"	15:00	Depart for Station 23				
"	15:04	Arrive Station 23				
"	15:05	Gravity Core Deployed	23	14'	47° 06 87'	65° 10.23'
"	15:41	Sea carousel Deployed	23	14'	47° 06 87'	65° 10.23'
"	15:58	Sea Carousel Retrieved				
...."	16:00	Depart for Chatham Wharf				
24 July	08:04	Depart Chatham Wharf				
"	10:00	Arrive Experimental Site				
"	10:04	Excalibur Retrieved				
"	10:10	Depart for Control Site				
"	10:30	Arrive Control Site (Station 25)				
"	10:40	Sea Carousel Deployed	25	19'	47° 08.01'	65° 09.46'
"	12:05	Sea Carousel Retrieved				
"	12:06	Gravity Core Deployed	25	19'	47° 08.02'	65° 09.46'
"	12:22	Van Veen Grab Deployed	25	19'	47° 08.03'	65° 09.46'
"	12:29	Excalibur Deployed	25	19'	47° 08.03'	65° 09.46'
"	12:30	Depart for Station 26				
"	12:33	Arrive Station 26				
"	12:38	Sea Carousel Deployed	26	19'	47° 08.02'	65° 09.49'

24 July	12:53	CTD Deployed (Depth Profile)	26	19'	47° 08.03'	65° 09.48'
"	13:52	Sea Carousel Retrieved				
"	13:55	Van Veen Grab Deployed	26	19'	47° 08.04'	65° 09.48'
"	14:02	Gravity Core Deployed	26	19'	47° 08.05'	65° 09.48'
"	14:08	Depart for Station 27				
"	14:10	Arrive station 27				
"	14:11	Sea Carousel Deployed	27	19'	47° 08.01'	65° 09.46'
"	15:26	Sea Carousel Retrieved				
"	15:28	Gravity Core Deployed	27	19'	47° 08.02'	65° 09.51'
"	15:37	Van Veen Grab Deployed	27	19'	47° 08.02'	65° 09.48'
"	15:52	Excalibur Retrieved				
"	16:10	Depart for Station 28				
"	16:17	Arrive Station 28				
"	16:30	Gravity Core Deployed	28	17'	47° 07.04'	65° 10.12'
"	16:43	Van Veen Grab Deployed	28	17'	47° 07.03'	65° 10.13'
"	16:51	Excalibur Deployed	28	17'	47° 07.06'	65° 10.13'
"	17:00	Sea Carousel Deployed	28	17'	47° 07.02'	65° 10.12'
"	18:16	Sea Carousel Retrieved				
"	18:20	Depart for Chatham Wharf				
"	20:15	Arrive Chatham Wharf				
25 July	08:45	Depart Chatham Wharf				
"	10:42	Arrive Experimental Site				
"	10:50	Excalibur Retrieved				
"	10:55	Depart for Station 29				
"	11:30	Arrive Station 29				
"	11:34	Gravity Core Deployed	29	18'	47° 07.02'	65° 10.12'
"	11:52	Excalibur Deployed	29	18'	47° 07.02'	65° 10.12'
"	12:17	Van Veen Grab Deployed	29	18'	47° 07.03'	65° 10.10'
"	12:29	Sea Carousel Deployed	29	18'	47° 07.03'	65° 10.12'
"	13:48	Sea carousel Retrieved				

25 July	14:20	Van Veen Grab Deployed	30	18'	47° 07.05'	65° 10.11'
"	14:25	Gravity Core Deployed	30	18'	47° 07.02'	65° 10.10'
"	14:37	Sea Carousel Deployed	30	18'	47° 07.02'	65° 10.10'
"	15:54	Sea carousel Retrieved				
"	16:15	Excalibur Retrieved				
"	16:45	Excalibur Deployed	31	18'	47° 07.05'	65° 10.11'
"	16:50	Depart for Chatham Wharf				
"	18:45	Arrive Chatham Wharf				
26 July	08:25	Depart Chatham Wharf				
"	10:12	Arrive Experimental Dump Site				
"	10:17	Excalibur Retrieved				
"	10:20	Depart for Station 32				
"	10:30	Arrive Station 32				
"	10:50	Van Veen Grab Deployed	32	17'	47° 06.86'	65° 10.26'
"	10:55	Gravity Core Deployed	32	17'	47° 06.86'	65° 10.25'
"	10:58	Excalibur Deployed	32	17'	47° 06.86'	65° 10.25'
"	11:06	Sea Carousel Deployed	32	17'	47° 06.85'	65° 10.31'
"	12:15	Sea Carousel Retrieved				
"	12:20	Excalibur Retrieved				
"	12:22	Depart for Station 33				
"	12:30	Arrive Station 33				
"	12:36	Van Veen Grab Deployed	33	18'	47° 06.85'	65° 10.27'
"	12:40	Gravity Core Deployed	33	18'	47° 06.86'	65° 10.25'
"	12:47	Excalibur Deployed	33	18'	47° 06.86'	65° 10.25'
"	12:55	Sea Carousel Deployed	33	18'	47° 06.86'	65° 10.25'
"	14:07	Sea Carousel Retrieved				
"	14:10	Depart for Station 34				
"	14:20	Arrive Station 34				
"	14:25	Van Veen Grab Deployed	34	17'	47° 06.86'	65° 10.31'
"	14:35	Sea Carousel Deployed	34	17'	47° 06.86'	65° 10.31'

26 July	15:52	Sea Carousel Retrieved				
"	16:00	Gravity Core Deployed	34	17'	47° 06.88'	65° 10.31'
"	16:30	CTD Retrieved				
"	16:58	CTD Deployed	35	17'	47° 07.92'	65° 09.49'
"	17:00	Excalibur Deployed	36	18'	47° 07.88'	65° 09.49'
"	17:05	Gravity Core Deployed	37	17'	47° 07.89'	65° 09.52'
"	17:06	Depart for Chatham Wharf				
27 July	08:00	Depart Chatham Wharf				
"	09:40	Excalibur Retrieved				
"	10:05	CTD Retrieved				
"	10:15	Lancelot Retrieved				
"	10:37	Current Meter 8208 Retrieved				
"	10:50	Current Meter 8207 Retrieved				
"	11:05	SOBS Retrieved				
"	11:10	Depart for Chatham Wharf				
"	13:05	Arrive Chatham Wharf				

APPENDIX B

UTM Coordinates For Station Locations

Department of ENERGY MINES AND RESOURCES
GEODETIC SURVEY OF CANADA - Program GSRUG

Geographic to UTM

ACADIA SEDIMENT STABILITY STUDY

01:12:199
Semi-Major Axis = 6378137.0000
Minor Axis = 6356752.3142

False Easting = 500000.0000
Northing = .0000
Scale Factor = .99960000

Station Name	Latitude	Longitude	Northing	Easting	Zone	CM	Scale Factor
1	N47 7 55.200001	W65 9 49.200001	5222104.219	335914.410	63	0 W	.99993091
2	N47 7 53.400000	W65 9 39.600001	5222043.061	336115.098	63	0 W	.99993010
4	N47 7 59.400000	W65 9 58.200001	5222239.115	335728.418	63	0 W	.99993166
5	N47 6 38.400000	W65 9 44.400000	5219730.797	335949.930	63	0 W	.99993077
6	N47 7 3.600001	W65 10 9.000001	5220523.020	335453.110	63	0 W	.99993277
11	N47 7 .600001	W65 10 15.600001	5220434.279	335311.471	63	0 W	.99993335
6	N47 6 58.200001	W65 10 19.800000	5220362.656	335220.914	63	0 W	.99993371
7	N47 7 3.000001	W65 10 12.600000	5220506.606	335376.741	63	0 W	.99993308
7	N47 6 52.800000	W65 10 19.800000	5220195.972	335216.281	63	0 W	.99993373
8	N47 6 52.800000	W65 10 19.800000	5220195.972	335216.281	63	0 W	.99993373
9	N47 6 52.200001	W65 10 17.400000	5220176.046	335266.339	63	0 W	.99993353
13	N47 7 49.800000	W65 9 24.600001	5221923.208	336428.009	63	0 W	.99992884
13	N47 7 47.400000	W65 9 12.600001	5221842.153	336678.755	63	0 W	.99992783
12	N47 7 47.400000	W65 9 12.600001	5221842.153	336678.755	63	0 W	.99992783
12	N47 7 47.400000	W65 9 12.600001	5221842.153	336678.755	63	0 W	.99992783
8	N47 6 57.600001	W65 9 17.400000	5220307.739	336535.253	63	0 W	.99992841
8	N47 6 57.600001	W65 9 17.400000	5220307.739	336535.253	63	0 W	.99992841
17	N47 8 3.000001	W65 9 46.200001	5222343.236	335984.269	63	0 W	.99993063
38	N47 6 48.600001	W65 9 42.000001	5220044.246	336009.213	63	0 W	.99993053

18	N47 8 7.800000	W65 9 23.400000	5222478.126	336468.622	63	0 W	.99992868
20	N47 6 52.200001	W65 10 15.600001	5220174.993	335304.269	63	0 W	.99993337
20	N47 6 51.600001	W65 10 17.400000	5220157.526	335265.825	63	0 W	.99993353
21	N47 6 53.400000	W65 10 15.600001	5220212.034	335305.298	63	0 W	.99993337
21	N47 6 53.400000	W65 10 15.600001	5220212.034	335305.298	63	0 W	.99993337
22	N47 6 54.000001	W65 10 17.400000	5220231.608	335267.883	63	0 W	.99993352
23	N47 6 52.200001	W65 10 13.800000	5220173.939	335342.198	63	0 W	.99993322
24	N47 6 52.200001	W65 10 13.800000	5220173.939	335342.198	63	0 W	.99993322
25	N47 8 .600001	W65 9 27.600001	5222258.322	336374.018	63	0 W	.99992906
25	N47 8 1.800000	W65 9 27.600001	5222295.363	336375.041	63	0 W	.99992905
26	N47 8 1.200001	W65 9 29.400001	5222277.890	336336.613	63	0 W	.99992921
27	N47 8 .600001	W65 9 27.600001	5222258.322	336374.018	63	0 W	.99992906
28	N47 7 3.600001	W65 10 7.800000	5220522.319	335478.395	63	0 W	.99993267
28	N47 7 1.200001	W65 10 7.200001	5220447.886	335488.982	63	0 W	.99993263
29	N47 7 1.200001	W65 10 7.200001	5220447.886	335488.982	63	0 W	.99993263
29	N47 7 1.800000	W65 10 7.200001	5220466.406	335489.496	63	0 W	.99993263
30	N47 7 2.400000	W65 10 6.000000	5220484.225	335515.295	63	0 W	.99993252
31	N47 7 3.000001	W65 10 6.600001	5220503.096	335503.166	63	0 W	.99993257
32	N47 6 51.600001	W65 10 15.000000	5220156.121	335316.398	63	0 W	.99993333
32	N47 6 51.000001	W65 10 18.600001	5220139.708	335240.024	63	0 W	.99993364
33	N47 6 51.600001	W65 10 15.000000	5220156.121	335316.398	63	0 W	.99993333
33	N47 6 51.600001	W65 10 15.000000	5220156.121	335316.398	63	0 W	.99993333
34	N47 6 51.600001	W65 10 18.600001	5220158.228	335240.538	63	0 W	.99993363
35	N47 7 55.200001	W65 9 29.400001	5222092.684	336331.498	63	0 W	.99992923
36	N47 7 52.800000	W65 9 29.400001	5222018.602	336329.452	63	0 W	.99992924

APPENDIX C

Results of Analyses of Sediment Properties

MIRAMICHI ESTUARY STUDY 1993

CORE BULK DENSITY & WATER CONTENT

CONTROL SITE

CORE #	DEPTH cm	Vt cm3	Mt g	Md g	Mw g	r ppt	Bd g/cm3	w %
6	12	9.723	13.79	6.61	7.18	25.0	1.42	108.62
	34	9.723	12.49	4.58	7.91	25.0	1.28	172.71
	56	9.723	13.42	6.06	7.36	25.0	1.38	121.45
7	10	9.723	14.14	6.93	7.21	25.0	1.45	104.04
	34	9.723	13.38	5.6	7.78	25.0	1.38	138.93
	72	9.723	13.42	5.68	7.74	25.0	1.38	136.27
25	12	9.723	12.46	4.57	7.89	25.0	1.28	172.65
	50	9.723	13.27	5.52	7.75	25.5	1.36	140.40
	90	9.723	14.24	7.25	6.99	25.5	1.46	96.41
26	8	9.723	13.6	6.19	7.41	25.0	1.40	119.71
	40	9.723	13.22	5.65	7.57	25.0	1.36	133.98
	70	9.723	14.07	7.03	7.04	25.0	1.45	100.14
27	8	9.723	12.58	4.96	7.62	25.0	1.29	153.63
	40	9.723	12.99	5.36	7.63	25.0	1.34	142.35
	70	9.723	14.15	6.86	7.29	25.0	1.46	106.27

MIRAMICHI ESTUARY STUDY 1993

CORE BULK DENSITY & WATER CONTENT

CHANNEL SITE

CORE #	DEPTH cm	Vt cm3	Mt g	Md g	Mw g	r ppt	Bd g/cm3	w %
12	20	9.723	11.63	3.12	8.51	25.0	1.20	272.76
	58	9.723	11.75	3.74	8.01	25.0	1.21	214.17
	82	9.723	14.28	7.63	6.65	25.0	1.47	87.16
13	10	9.723	11.88	3.53	8.35	25.0	1.22	236.54
	40	9.723	11.15	3.31	7.84	25.5	1.15	236.86
	60	9.723	13.2	5.64	7.56	26.5	1.36	134.04
14	10	9.723	12.42	3.96	8.46	25.0	1.28	213.64
	30	9.723	11.72	5.48	6.24	25.0	1.21	113.87
	60	9.723	14.05	6.98	7.07	25.0	1.45	101.29
15	4	9.723	11.86	3.5	8.36	25.0	1.22	238.86
	20	9.723	12.61	4.51	8.1	25.0	1.30	179.60
	40	9.723	16.13	7.46	8.67	25.0	1.66	116.22
36	8	9.723	12.75	5.03	7.72	25.0	1.31	153.48
	20	9.723	13.08	5.68	7.4	25.0	1.35	130.28
	50	9.723	12.66	4.47	8.19	25.0	1.30	183.22

MIRAMICHI ESTUARY STUDY 1993

CORE BULK DENSITY & WATER CONTENT

EXPERIMENTAL PRE-DUMP SITE

CORE #	DEPTH cm	Vt cm3	Mt g	Md g	Mw g	r ppt	Bd g/cm3	w %
9	4	9.723	16.46	12	4.46	25.0	1.69	37.17
	24	9.723	13.14	5.53	7.61	25.0	1.35	137.61
	60	9.723	13.13	5.43	7.7	25.0	1.35	141.80
10	8	9.723	13.99	7.15	6.84	25.0	1.44	95.66
	22	9.723	12.58	5	7.58	25.0	1.29	151.60
	40	9.723	12.67	4.9	7.77	25.0	1.30	158.57

MIRAMICHI ESTUARY STUDY 1993

CORE BULK DENSITY & WATER CONTENT

EXPERIMENTAL POST-DUMP SITE

CORE #	DEPTH cm	Vt cm3	Mt g	Md g	Mw g	r ppt	Bd g/cm3	w %
8	8	9.723	15.71	9.61	6.1	25.0	1.62	63.48
	32	9.723	12.66	4.86	7.8	25.0	1.30	160.49
	62	9.723	13.37	6.12	7.25	25.0	1.38	118.46
20	8	9.723	12.63	5.06	7.57	25.0	1.30	149.60
	30	9.723	15.49	9	6.49	25.0	1.59	72.11
	70	9.723	13.18	5.85	7.33	25.0	1.36	125.30
21A	8	9.723	15.25	8.44	6.81	25.0	1.57	80.69
	50	9.723	12.86	5.21	7.65	25.0	1.32	146.83
	70	9.723	13.93	6.78	7.15	25.0	1.43	105.46
21B	10	9.723	14.43	7.58	6.85	25.0	1.48	90.37
	40	9.723	14.14	7.29	6.85	25.0	1.45	93.96
	60	9.723	12.77	4.98	7.79	25.0	1.31	156.43
22	14	9.723	13.15	5.68	7.47	25.0	1.35	131.51
	44	9.723	13.4	6.08	7.32	25.0	1.38	120.39
	56	9.723	12.52	4.6	7.92	25.0	1.29	172.17
23	6	9.723	14.73	7.96	6.77	25.0	1.51	85.05
	40	9.723	12.44	4.14	8.3	25.0	1.28	200.48
	60	9.723	13.09	5.43	7.66	25.0	1.35	141.07

MIRAMICHI ESTUARY STUDY 1993

CORE BULK DENSITY & WATER CONTENT

EXPERIMENTAL POST-DUMP SITE

CORE #	DEPTH cm	Vt cm3	Mt g	Md g	Mw g	r ppt	Bd g/cm3	w %
29	10	9.723	13.18	5.76	7.42	25.0	1.36	128.82
	40	9.723	12.56	4.81	7.75	25.0	1.29	161.12
	70	9.723	12.75	5.05	7.7	25.0	1.31	152.48
30	12	9.723	13.17	5.72	7.45	25.0	1.35	130.24
	30	9.723	12.5	4.54	7.96	25.0	1.29	175.33
	70	9.723	13.25	5.63	7.62	25.0	1.36	135.35
32	10	9.723	12.78	5.17	7.61	25.0	1.31	147.20
	50	9.723	13	5.36	7.64	25.0	1.34	142.54
	70	9.723	14.16	6.83	7.33	25.0	1.46	107.32
33	10	9.723	14.65	8.44	6.21	25.0	1.51	73.58
	20	9.723	16.98	11.88	5.1	25.0	1.75	42.93
	30	9.723	14.86	8.35	6.51	25.0	1.53	77.96
34	10	9.723	13.63	6.38	7.25	25.0	1.40	113.64
	40	9.723	13.27	5.67	7.6	25.0	1.36	134.04
	60	9.723	12.34	4.53	7.81	25.0	1.27	172.41

MIRAMICHI ESTUARY STUDY 1993

CORE GRAIN SIZE & ORGANICS

CHANNEL SITE

CORE # & DEPTH cm	TOTAL SAMPLE WT g	GRAVEL WT g	SAND WT g	MUD WT g	GRAIN SIZE MEAN mm	ORGANIC WT g	ORGANIC %
13-04	16.98	0.00	0.31	14.16	0.00256	2.51	14.78
13-18	18.42	0.00	1.44	14.34	0.00357	2.64	14.33
13-24	12.89	0.04	0.08	10.47	0.00224	2.30	17.84
13-32	18.31	0.01	2.06	13.58	0.00424	2.66	14.53
13-46	22.85	0.01	3.08	17.10	0.00498	2.66	11.64
13-54	21.44	0.00	3.15	15.94	0.00515	2.35	10.96
13-66	19.91	0.00	2.08	15.36	0.00458	2.47	12.41

MIRAMICHI ESTUARY STUDY 1993

CORE GRAIN SIZE & ORGANICS

CONTROL SITE

CORE # & DEPTH cm	TOTAL SAMPLE WT g	GRAVEL WT g	SAND WT g	MUD WT g	GRAIN SIZE MEAN mm	ORGANIC WT g	
25-07	20.51	0.01	1.49	16.57	0.00443	2.44	11.90
25-18	19.71	0.01	1.21	15.98	0.00410	2.51	12.73
25-30	17.23	0.00	0.70	14.49	0.00377	2.04	11.84
25-40	22.29	0.00	2.40	16.90	0.00588	2.99	13.41
25-50	30.33	0.00	3.91	23.53	0.00576	2.89	9.53
25-65	21.39	0.00	3.41	15.23	0.00749	2.75	12.86
25-80	33.13	0.23	13.85	16.20	0.0240	2.85	8.60
25-90	28.42	0.01	9.24	16.31	0.0121	2.86	10.06

MIRAMICHI ESTUARY STUDY 1993

CORE GRAIN SIZE & ORGANICS

EXPERIMENTAL POST-DUMP SITE

CORE # & DEPTH cm	TOTAL SAMPLE WT g	GRAVEL WT g	SAND WT g	MUD WT g	GRAIN SIZE MEAN mm	ORGANIC WT g	
28-06	18.95	0.03	2.42	14.44	0.00609	2.06	10.87
28-15	23.60	0.00	1.07	19.86	0.00481	2.67	11.31
28-28	20.33	0.00	1.08	17.00	0.00410	2.25	11.07
28-40	20.70	0.00	2.14	16.17	0.00523	2.39	11.55
28-50	25.59	0.46	5.57	16.30	0.0125	3.26	12.74
28-60	19.45	0.00	1.99	15.36	0.00515	2.10	10.80
28-80	25.17	0.00	4.75	17.86	0.00820	2.56	10.17

MIRAMICHI ESTUARY STUDY 1993

CORE GRAVEL-SAND-SILT-MUD RATIOS

CHANNEL SITE

CORE # & DEPTH cm	GRAVEL %	SAND %	SILT %	CLAY %	MUD %	MEAN GRAIN SIZE mm
13-04	0.00	2.15	42.00	55.86	97.85	0.00256
13-18	0.00	8.48	42.34	49.17	91.52	0.00357
13-24	0.38	0.76	39.86	59.01	98.87	0.00224
13-32	0.04	12.25	41.76	45.95	87.71	0.00424
13-46	0.06	14.43	42.21	43.30	85.50	0.00498
13-54	0.00	15.24	42.95	41.82	84.76	0.00515
13-66	0.00	11.21	45.80	42.99	88.79	0.00458

MIRAMICHI ESTUARY STUDY 1993

CORE GRAVEL-SAND-SILT-MUD RATIOS

CONTROL SITE

CORE # & DEPTH cm	GRAVEL %	SAND %	SILT %	CLAY %	MUD %	MEAN GRAIN SIZE mm
25-07	0.07	7.50	49.26	43.17	92.43	0.00443
25-18	0.06	6.33	48.19	45.42	93.61	0.00410
25-30	0.00	4.11	51.05	44.84	95.89	0.00377
25-40	0.00	11.30	50.41	38.29	88.70	0.00588
25-50	0.00	12.55	49.78	37.66	87.45	0.00576
25-65	0.00	16.19	50.64	33.17	83.81	0.00749
25-80	0.75	44.04	32.70	22.51	55.21	0.0240
25-90	0.04	33.78	37.91	28.27	66.18	0.0121

MIRAMICHI ESTUARY STUDY 1993

CORE GRAVEL-SAND-SILT-MUD RATIOS

EXPERIMENTAL POST-DUMP SITE

CORE # & DEPTH cm	GRAVEL %	SAND %	SILT %	CLAY %	MUD %	MEAN GRAIN SIZE mm
28-06	0.21	13.38	49.08	37.34	86.41	0.00609
28-15	0.00	4.25	56.06	39.69	95.75	0.00481
28-28	0.00	5.34	52.24	42.42	94.66	0.00410
28-40	0.00	10.67	50.28	39.05	89.33	0.00523
28-50	2.04	23.72	43.39	30.85	74.23	0.0125
28-60	0.00	10.11	50.35	39.54	89.89	0.00515
28-80	0.02	18.89	48.89	32.20	81.09	0.00820

MIRAMICHI ESTUARY STUDY 1993

VAN VEEN GRAIN SIZE & ORGANICS

CONTROL SITE

STATION #	TOTAL SAMPLE WT g	GRAVEL WT g	SAND WT g	MUD WT g	GRAIN SIZE MEAN mm	ORGANIC WT g	ORGANIC %
6	59.10	0.09	7.57	48.32	0.00588	3.12	5.28
25	57.90	0.02	4.64	49.87	0.00396	3.37	5.82
26	53.50	0.02	3.52	47.04	0.00424	2.92	5.46
27	52.10	0.02	5.34	44.27	0.00443	2.47	4.74

MIRAMICHI ESTUARY STUDY 1993

VAN VEEN GRAIN SIZE & ORGANICS

CHANNEL SITE

STATION #	TOTAL SAMPLE WT g	GRAVEL WT g	SAND WT g	MUD WT g	GRAIN SIZE MEAN mm	ORGANIC WT g	ORGANIC %
12	37.41	0.00	2.35	32.37	0.00340	2.69	7.19
13	21.81	0.00	0.70	17.19	0.00319	3.92	17.97
14	25.09	0.26	3.34	17.68	0.00685	3.81	15.19
15	49.34	1.32	16.47	27.04	0.0166	4.51	9.14

MIRAMICHI ESTUARY STUDY 1993

VAN VEEN GRAIN SIZE & ORGANICS

EXPERIMENTAL PRE-DUMP SITE

STATION #	TOTAL SAMPLE WT g	GRAVEL WT g	SAND WT g	MUD WT g	GRAIN SIZE MEAN mm	ORGANIC WT g	ORGANIC %
9	80.52	0.95	37.01	38.58	0.0242	3.98	4.94
10	46.74	0.00	3.68	39.12	0.00446	3.94	8.43

MIRAMICHI ESTUARY STUDY 1993

VAN VEEN GRAIN SIZE & ORGANICS

EXPERIMENTAL POST-DUMP SITE

STATION #	TOTAL SAMPLE WT g	GRAVEL WT g	SAND WT g	MUD WT g	GRAIN SIZE MEAN mm	ORGANIC WT g	ORGANIC %
8	68.30	0.10	8.72	56.56	0.00537	2.92	4.28
20	83.50	0.11	22.84	58.36	0.00897	2.19	2.62
21	74.60	0.04	16.91	53.29	0.00770	4.36	5.84
22	86.10	0.36	26.12	54.85	0.0118	4.77	5.54
23	86.30	0.09	21.86	60.21	0.00975	4.14	4.80
28	67.80	0.06	16.55	47.75	0.00942	3.44	5.07
29	73.40	0.05	19.33	49.37	0.00955	4.65	6.34
30	59.10	0.15	12.45	43.36	0.00803	3.14	5.31
32	60.50	0.80	13.54	41.81	0.00975	4.35	7.19
33	83.60	0.06	19.17	59.65	0.00873	4.72	5.65
34	104.70	21.92	33.13	47.15	0.0544	2.50	2.39

MIRAMICHI ESTUARY STUDY 1993

VAN VEEN GRAIN SIZE & ORGANICS

STATION #	TOTAL SAMPLE WT g	GRAVEL WT g	SAND WT g	MUD WT g	GRAIN SIZE MEAN mm	ORGANIC WT g	ORGANIC %
	CONTROL SITE						
6	59.10	0.09	7.57	48.32	0.00588	3.12	5.28
25	57.90	0.02	4.64	49.87	0.00396	3.37	5.82
26	53.50	0.02	3.52	47.04	0.00424	2.92	5.46
27	52.10	0.02	5.34	44.27	0.00443	2.47	4.74
	CHANNEL SITE						
12	37.41	0.00	2.35	32.37	0.00340	2.69	7.19
13	21.81	0.00	0.70	17.19	0.00319	3.92	17.97
14	25.09	0.26	3.34	17.68	0.00685	3.81	15.19
15	49.34	1.32	16.47	27.04	0.0166	4.51	9.14
	EXPERIMENTAL PRE-DUMP SITE						
9	80.52	0.95	37.01	38.58	0.0242	3.98	4.94
10	46.74	0.00	3.68	39.12	0.00446	3.94	8.43
	EXPERIMENTAL POST-DUMP SITE						
8	68.30	0.10	8.72	56.56	0.00537	2.92	4.28
20	83.50	0.11	22.84	58.36	0.00897	2.19	2.62
21	74.60	0.04	16.91	53.29	0.00770	4.36	5.84
22	86.10	0.36	26.12	54.85	0.0118	4.77	5.54
23	86.30	0.09	21.86	60.21	0.00975	4.14	4.80
28	67.80	0.06	16.55	47.75	0.00942	3.44	5.07
29	73.40	0.05	19.33	49.37	0.00955	4.65	6.34
30	59.10	0.15	12.45	43.36	0.00803	3.14	5.31
32	60.50	0.80	13.54	41.81	0.00975	4.35	7.19
33	83.60	0.06	19.17	59.65	0.00873	4.72	5.65
34	104.70	21.92	33.13	47.15	0.0544	2.50	2.39

MIRAMICHI ESTUARY STUDY 1993

VAN VEEN GRAVEL-SAND-SILT-CLAY RATIOS

CONTROL SITE

STATION #	GRAVEL %	SAND %	SILT %	CLAY %	MUD %	GRAIN SIZE MEAN mm
6	0.16	12.82	48.10	38.92	87.02	0.00588
25	0.04	7.85	47.12	45.00	92.12	0.00396
26	0.04	6.30	49.46	44.21	93.66	0.00424
27	0.04	10.00	46.76	43.19	89.96	0.00443

MIRAMICHI ESTUARY STUDY 1993

VAN VEEN GRAVEL-SAND-SILT-CLAY RATIOS

CHANNEL SITE

STATION #	GRAVEL %	SAND %	SILT %	CLAY %	MUD %	GRAIN SIZE MEAN mm
12	0.00	6.33	44.22	49.44	93.67	0.00340
13	0.00	3.37	47.47	49.16	96.63	0.00319
14	1.22	15.14	45.04	38.60	83.64	0.00685
15	2.95	35.77	31.70	29.59	61.28	0.0166

MIRAMICHI ESTUARY STUDY 1993

VAN VEEN GRAVEL-SAND-SILT-CLAY RATIOS

EXPERIMENTAL PRE-DUMP SITE

STATION #	GRAVEL %	SAND %	SILT %	CLAY %	MUD %	GRAIN SIZE MEAN mm
9	1.24	47.57	28.97	22.22	57.19	0.0242
10	0.00	7.94	48.82	43.24	92.06	0.00446

MIRAMICHI ESTUARY STUDY 1993

VAN VEEN GRAVEL-SAND-SILT-CLAY RATIOS

EXPERIMENTAL POST-DUMP SITE

STATION #	GRAVEL %	SAND %	SILT %	CLAY %	MUD %	GRAIN SIZE MEAN mm
8	0.15	12.54	44.79	42.52	87.31	0.00537
20	0.14	26.28	39.06	34.53	73.59	0.00897
21	0.06	22.36	41.35	36.23	77.58	0.00770
22	0.44	30.30	39.38	29.87	69.26	0.0118
23	0.11	25.02	42.01	32.85	74.87	0.00975
28	0.09	24.47	43.88	31.55	75.43	0.00942
29	0.07	26.77	41.12	32.03	73.16	0.00955
30	0.27	21.24	43.59	34.90	78.49	0.00803
32	1.42	22.50	43.74	32.33	76.07	0.00975
33	0.08	22.69	44.45	32.79	77.24	0.00873
34	21.45	31.97	23.04	23.53	46.58	0.0544

MIRAMICHI ESTUARY STUDY 1993

VAN VEEN GRAVEL-SAND-SILT-CLAY RATIOS

STATION #	GRAVEL %	SAND %	SILT %	CLAY %	MUD %	GRAIN SIZE MEAN mm
	CONTROL SITE					
6	0.16	12.82	48.10	38.92	87.02	0.00588
25	0.04	7.85	47.12	45.00	92.12	0.00396
26	0.04	6.30	49.46	44.21	93.66	0.00424
27	0.04	10.00	46.76	43.19	89.96	0.00443
	CHANNEL SITE					
12	0.00	6.33	44.22	49.44	93.67	0.00340
13	0.00	3.37	47.47	49.16	96.63	0.00319
14	1.22	15.14	45.04	38.60	83.64	0.00685
15	2.95	35.77	31.70	29.59	61.28	0.0166
	EXPERIMENTAL PRE-DUMP SITE					
9	1.24	47.57	28.97	22.22	57.19	0.0242
10	0.00	7.94	48.82	43.24	92.06	0.00446
	EXPERIMENTAL POST-DUMP SITE					
8	0.15	12.54	44.79	42.52	87.31	0.00537
20	0.14	26.28	39.06	34.53	73.59	0.00897
21	0.06	22.36	41.35	36.23	77.58	0.00770
22	0.44	30.30	39.38	29.87	69.26	0.0118
23	0.11	25.02	42.01	32.85	74.87	0.00975
28	0.09	24.47	43.88	31.55	75.43	0.00942
29	0.07	26.77	41.12	32.03	73.16	0.00955
30	0.27	21.24	43.59	34.90	78.49	0.00803
32	1.42	22.50	43.74	32.33	76.07	0.00975
33	0.08	22.69	44.45	32.79	77.24	0.00873
34	21.45	31.97	23.04	23.53	46.58	0.0544

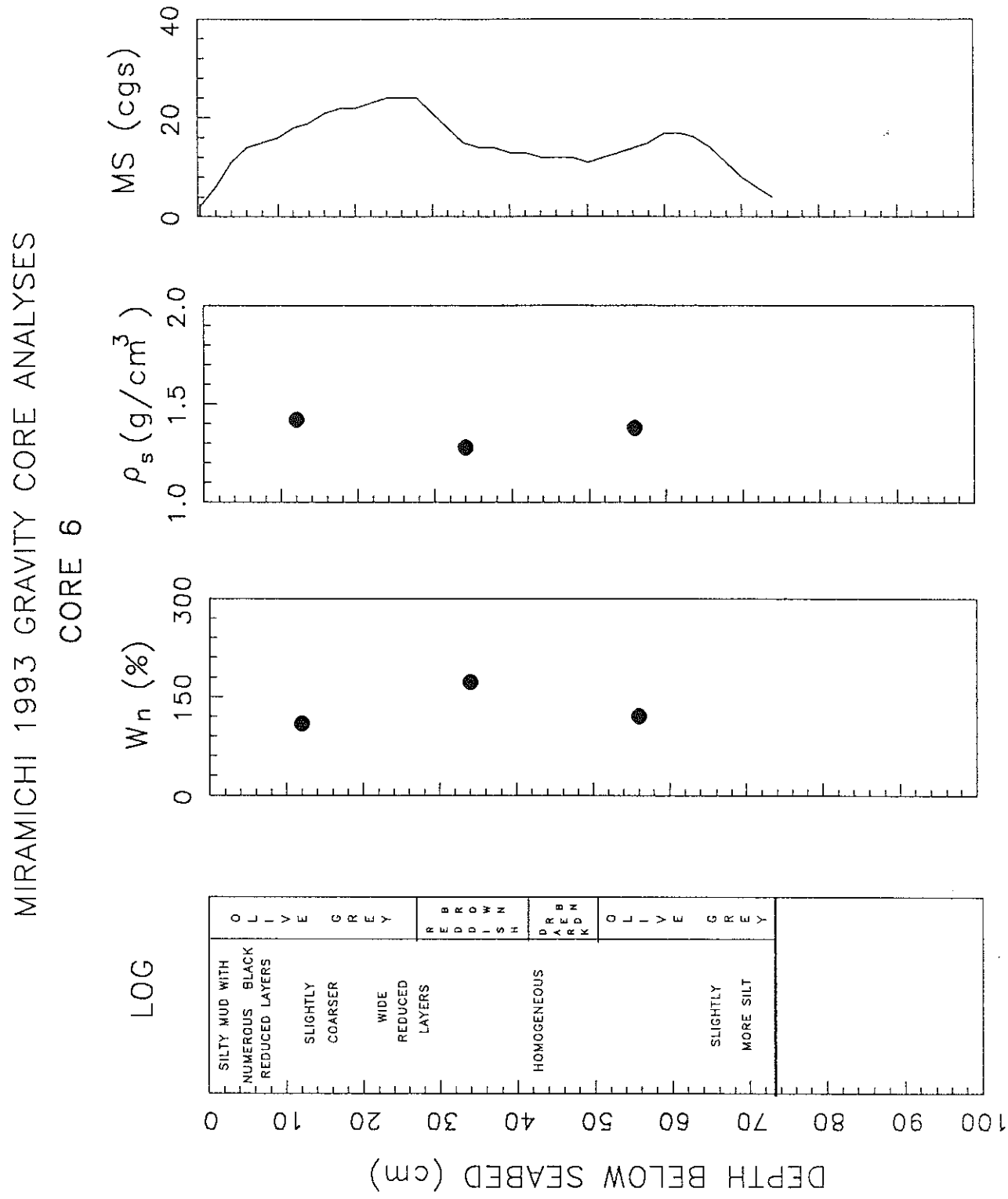
MIRAMICHI 1993 GRAVITY CORE ANALYSES
CORE 6
LOG
SILTY MUD WITH NUMEROUS BLACK REDUCED LAYERS
SLIGHTLY COARSER
WIDE REDUCED LAYERS
HOMOGENEOUS
SLIGHTLY MORE SILT
OLIVE GREY
REDDISH BROWN
DARK BROWN
OLIVE GREY
W_n (%)
0
150
300
ρ_s (g/cm^3)
1.0
1.5
2.0
MS (cgs)
0
20
40
DEPTH BELOW SEABED (cm)
0
10
20
30
40
50
60
70
80
90
100

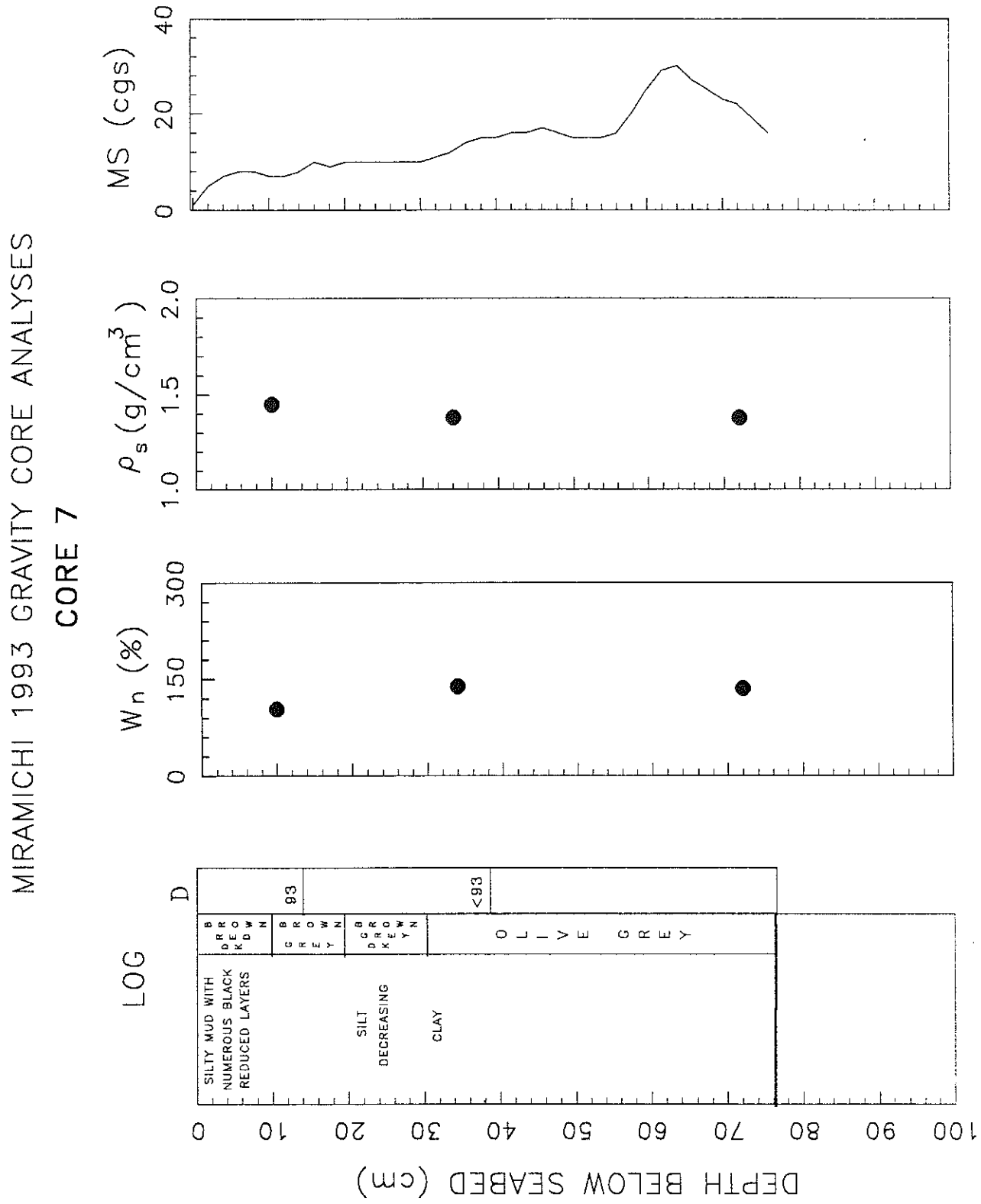
MIRAMICHI 1993 GRAVITY CORE ANALYSES
CORE 7
LOG
D
MS (cgs)
0
20
40
ρ_s (g/cm^3)
1.0
1.5
2.0
W_n (%)
0
150
300
93
<93
SILTY MUD WITH NUMEROUS BLACK REDUCED LAYERS
BROWN
GREY BROWN
SILT DECREASING CLAY
OLIVE GREY
DEPTH BELOW SEABED (cm)
0
10
20
30
40
50
60
70
80
90
100

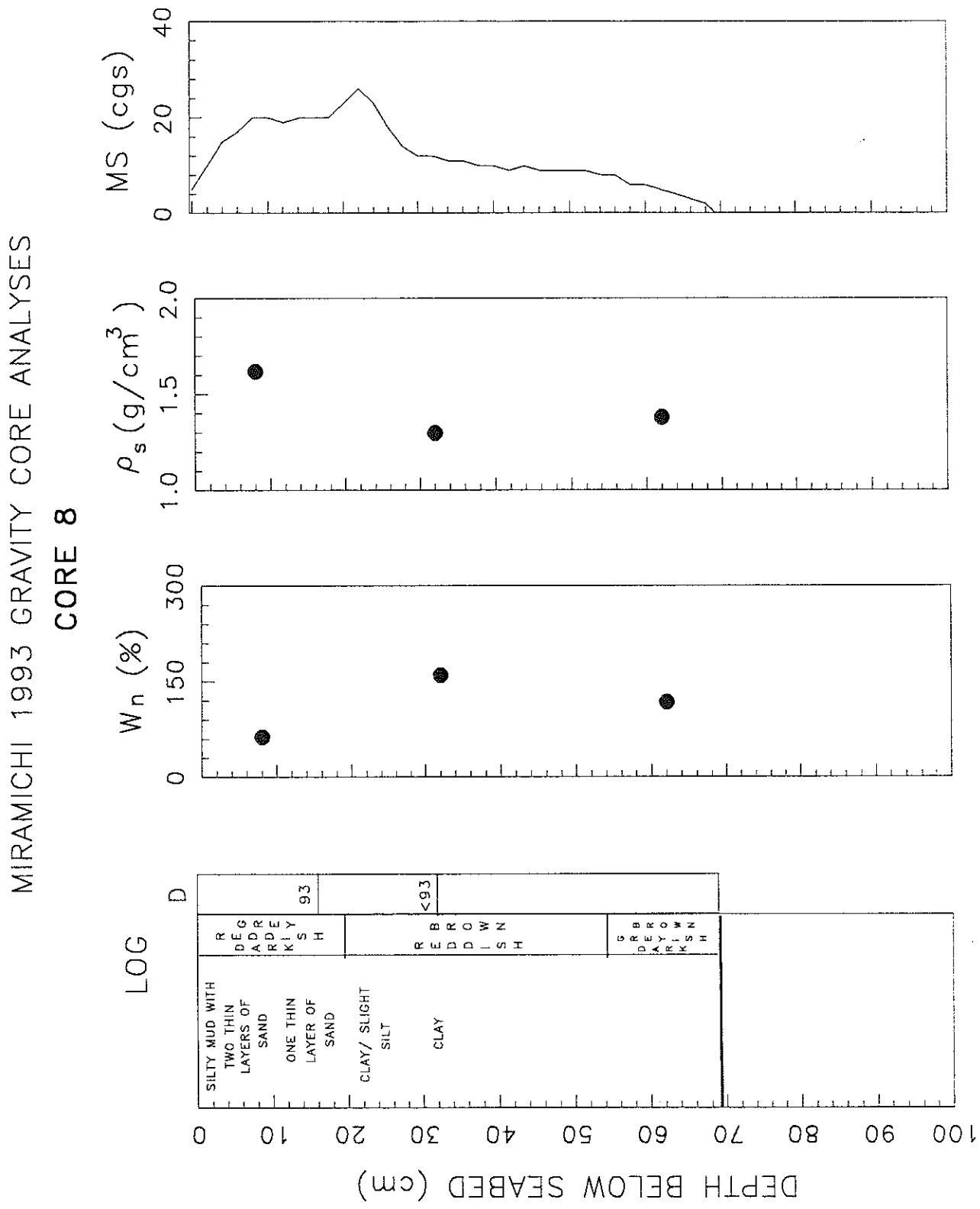
MIRAMICHI 1993 GRAVITY CORE ANALYSES
CORE 8
MS (cgs)
0
20
40
ρ_s (g/cm^3)
1.0
1.5
2.0
W_n (%)
0
150
300
LOG
D
93
<93
REDRADE KISH
REDRDOWSNH
GRDERAYOKSNH
SILTY MUD WITH TWO THIN LAYERS OF SAND
ONE THIN LAYER OF SAND
CLAY/ SLIGHT SILT
CLAY
DEPTH BELOW SEABED (cm)
0
10
20
30
40
50
60
70
80
90
100

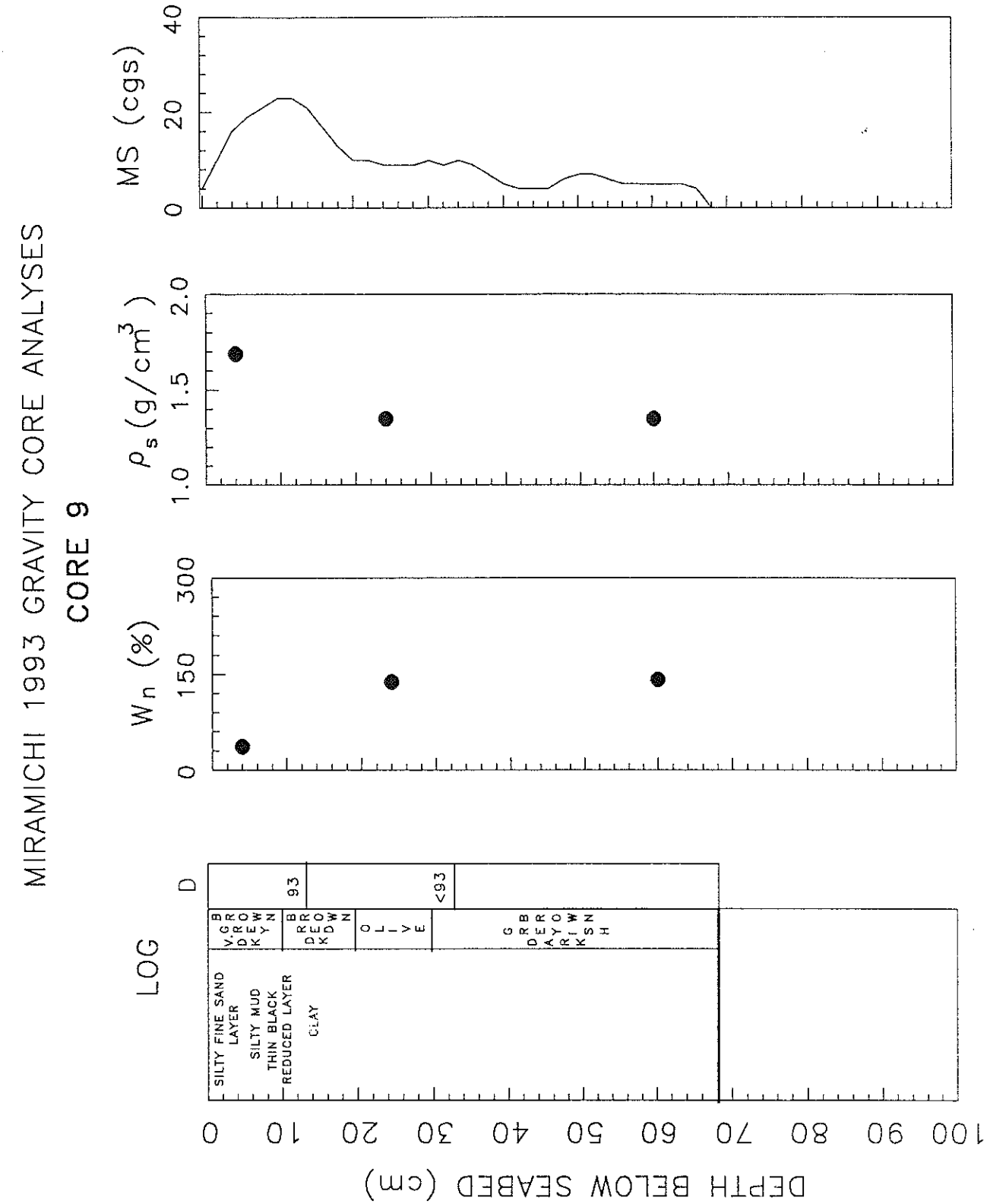
MIRAMICHI 1993 GRAVITY CORE ANALYSES
CORE 9
MS (cgs)
0
20
40
ρ_s (g/cm^3)
1.0
1.5
2.0
W_n (%)
0
150
300
LOG
D
93
<93
SILTY FINE SAND LAYER
SILTY MUD
THIN BLACK REDUCED LAYER
CLAY
DEPTH BELOW SEABED (cm)
0
10
20
30
40
50
60
70
80
90
100

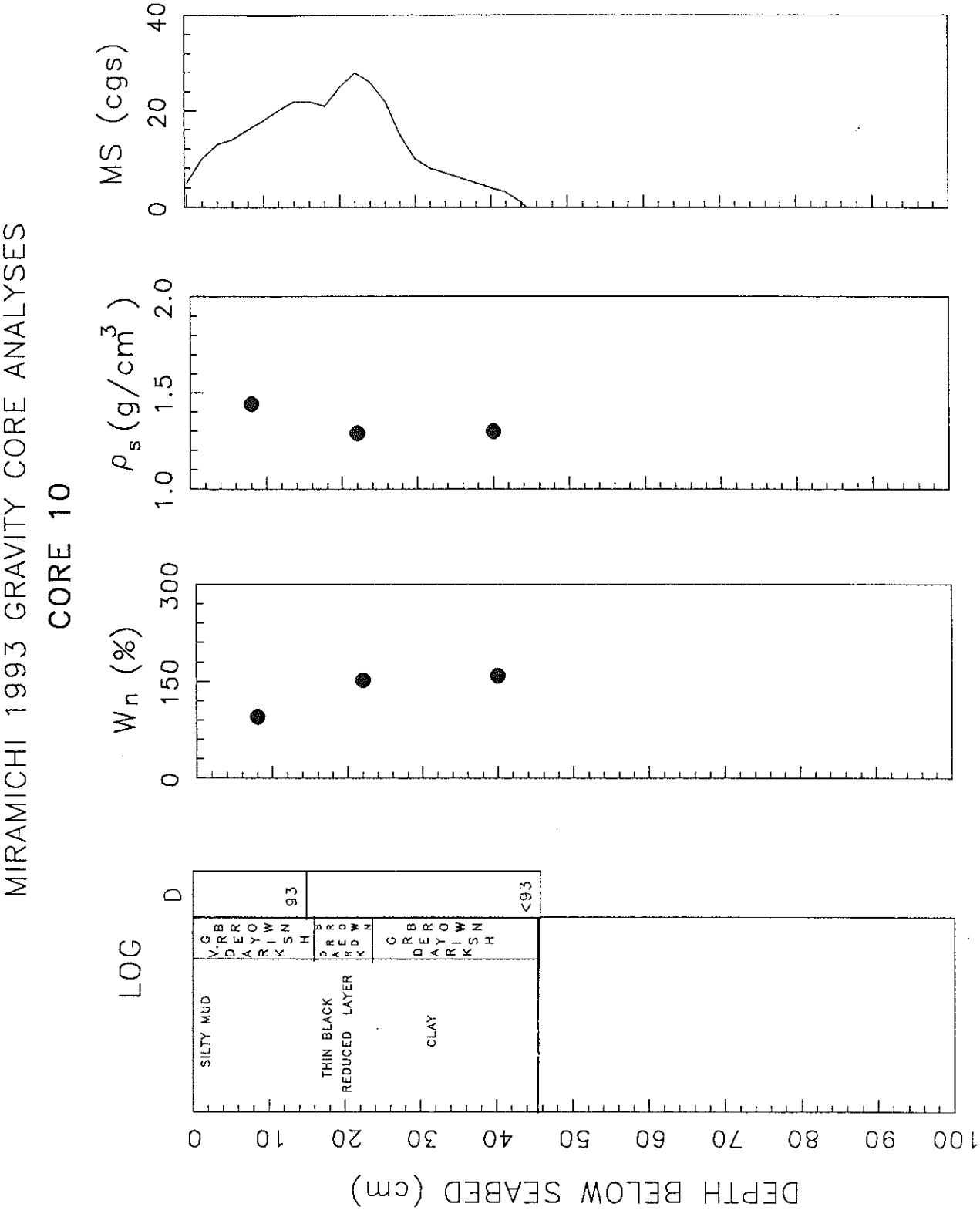
MIRAMICHI 1993 GRAVITY CORE ANALYSES
CORE 10
LOG
D
93
<93
SILTY MUD
THIN BLACK REDUCED LAYER
CLAY
W_n (%)
0
150
300
ρ_s (g/cm^3)
1.0
1.5
2.0
MS (cgs)
0
20
40
DEPTH BELOW SEABED (cm)
0
10
20
30
40
50
60
70
80
90
100

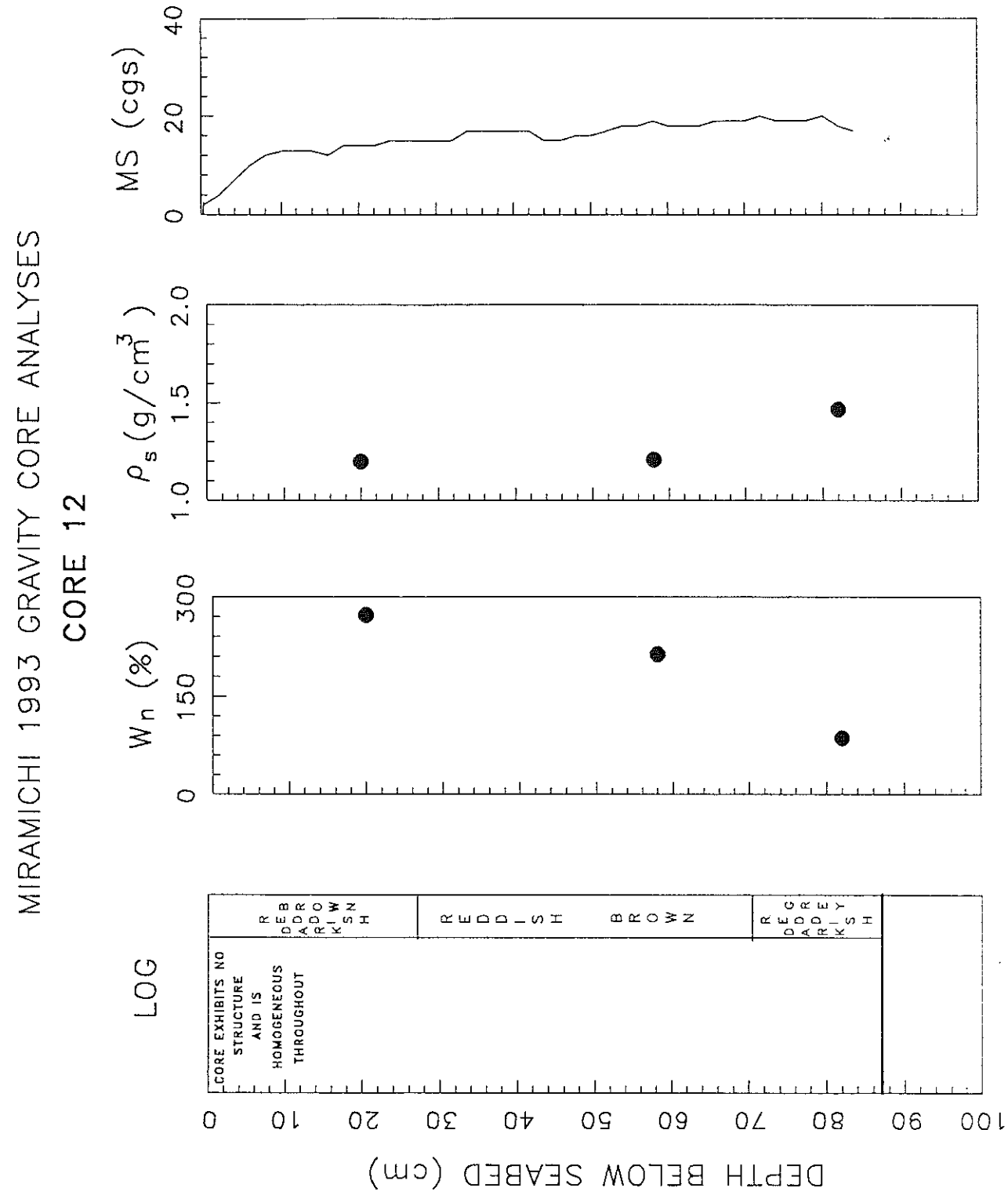
MIRAMICHI 1993 GRAVITY CORE ANALYSES
CORE 12
MS (cgs)
0
20
40
ρ_s (g/cm^3)
1.0
1.5
2.0
W_n (%)
0
150
300
LOG
CORE EXHIBITS NO STRUCTURE AND IS HOMOGENEOUS THROUGHOUT
REDDISH BROWN
DEPTH BELOW SEABED (cm)
0
10
20
30
40
50
60
70
80
90
100

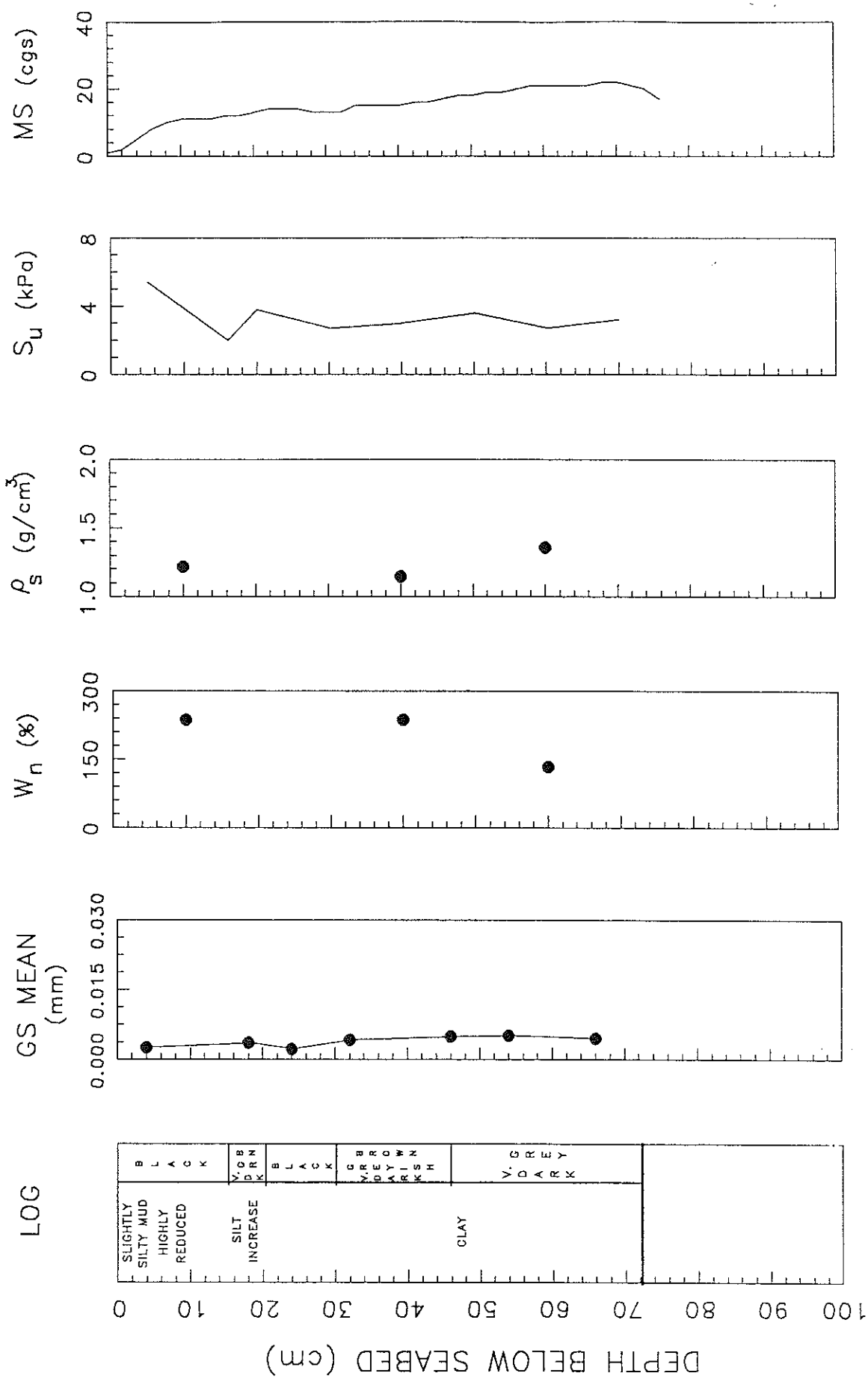
MIRAMICHI 1993 GRAVITY CORE ANALYSES
CORE 13
LOG
GS MEAN (mm)
0.000 0.015 0.030
W_n (%)
0 150 300
ρ_s (g/cm^3)
1.0 1.5 2.0
S_u (kPa)
0 4 8
MS (cgs)
0 20 40
SLIGHTLY SILTY MUD
HIGHLY REDUCED
BLACK
V.DARK BROWN
SILT INCREASE
BLACK
GRADED BROWN/OLIVE GREEN
V.DARK GREY
CLAY
DEPTH BELOW SEABED (cm)
0 10 20 30 40 50 60 70 80 90 100

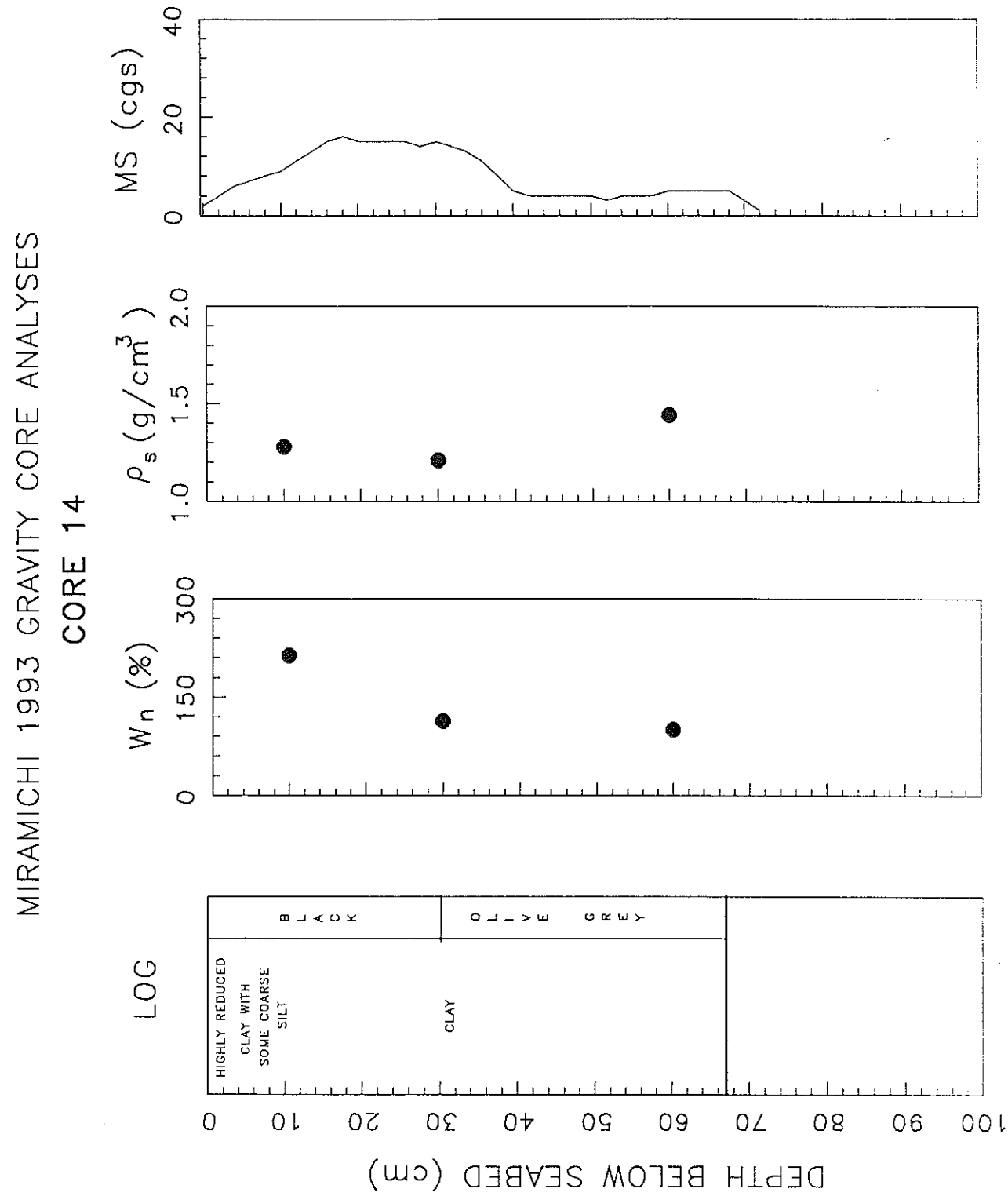
MIRAMICHI 1993 GRAVITY CORE ANALYSES
CORE 14
MS (cgs)
0
20
40
ρ_s (g/cm^3)
1.0
1.5
2.0
W_n (%)
0
150
300
LOG
BLACK
OLIVE GREY
HIGHLY REDUCED CLAY WITH SOME COARSE SILT
CLAY
DEPTH BELOW SEABED (cm)
0
10
20
30
40
50
60
70
80
90
100

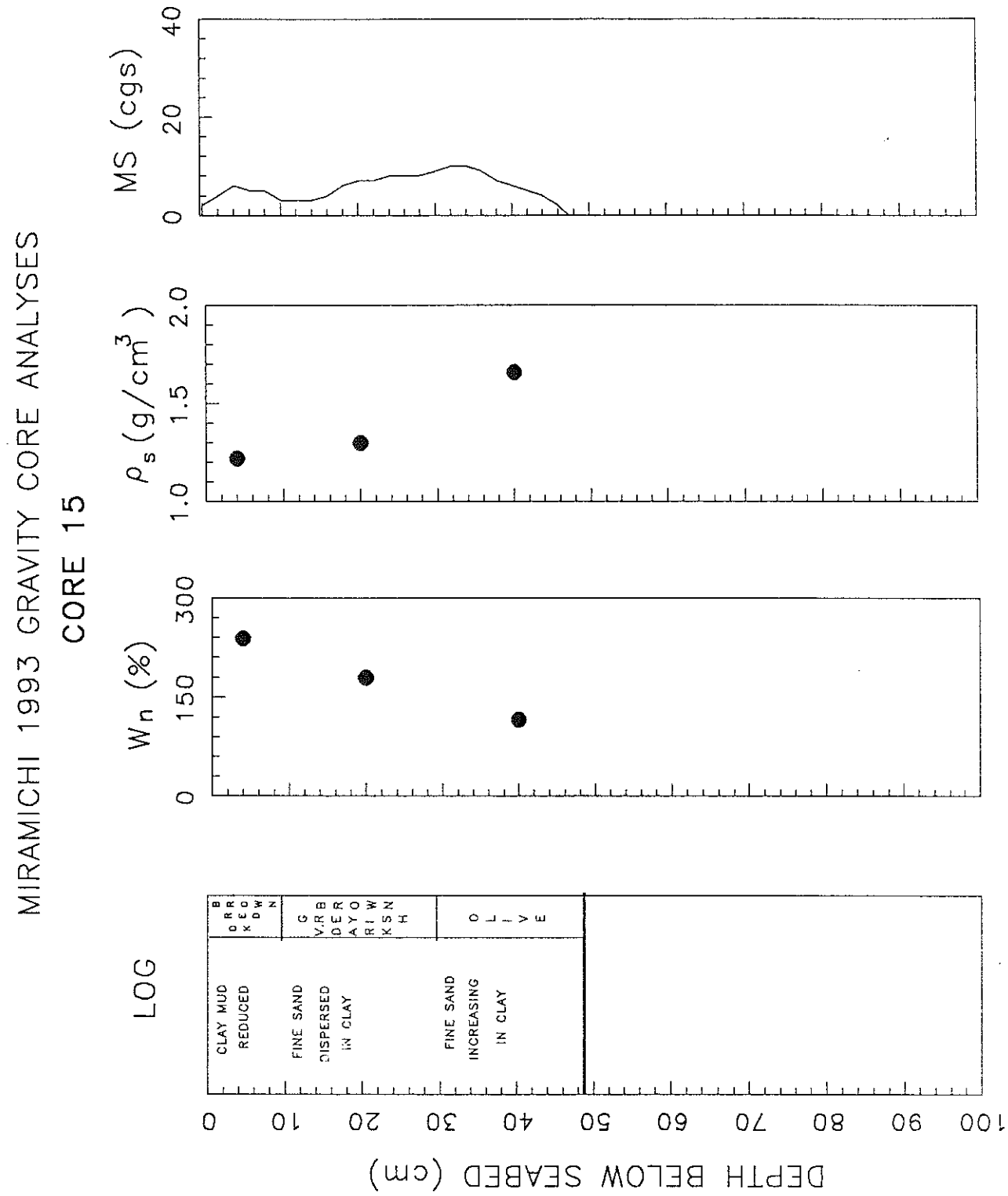
MIRAMICHI 1993 GRAVITY CORE ANALYSES
CORE 15
LOG
CLAY MUD
REDUCED
BROWN
FINE SAND
DISPERSED
IN CLAY
GRAY
FINE SAND
INCREASING
IN CLAY
OLIVE
W_n (%)
0
150
300
ρ_s (g/cm^3)
1.0
1.5
2.0
MS (cgs)
0
20
40
DEPTH BELOW SEABED (cm)
0
10
20
30
40
50
60
70
80
90
100

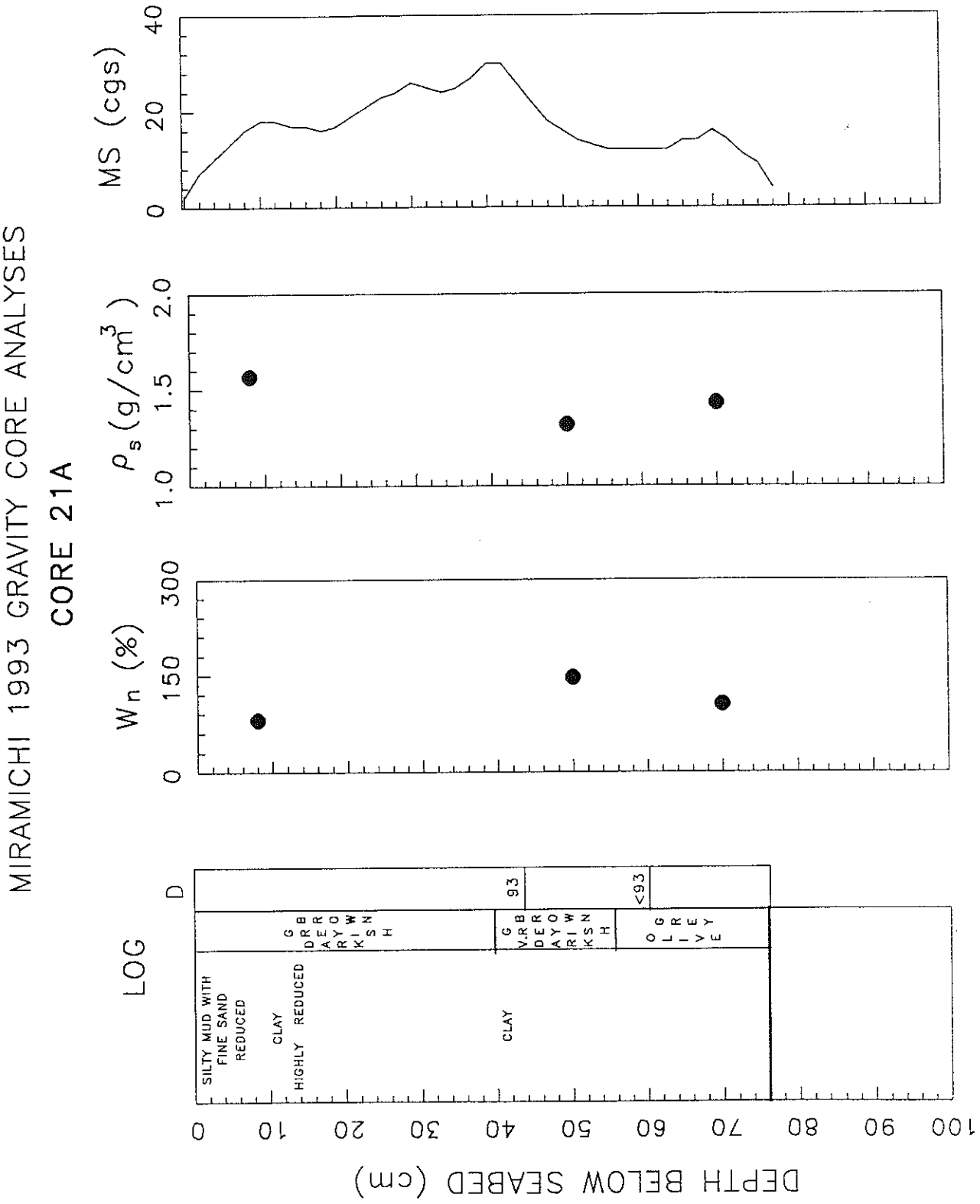
MIRAMICHI 1993 GRAVITY CORE ANALYSES
CORE 21A
MS (cgs)
0
20
40
ρ_s (g/cm^3)
1.0
1.5
2.0
W_n (%)
0
150
300
LOG
D
93
<93
GRADE RAYWASH
GRADE RAYWASH
OGLIVEY
SILTY MUD WITH FINE SAND
REDUCED
CLAY
HIGHLY REDUCED
CLAY
0
10
20
30
40
50
60
70
80
90
100
DEPTH BELOW SEABED (cm)

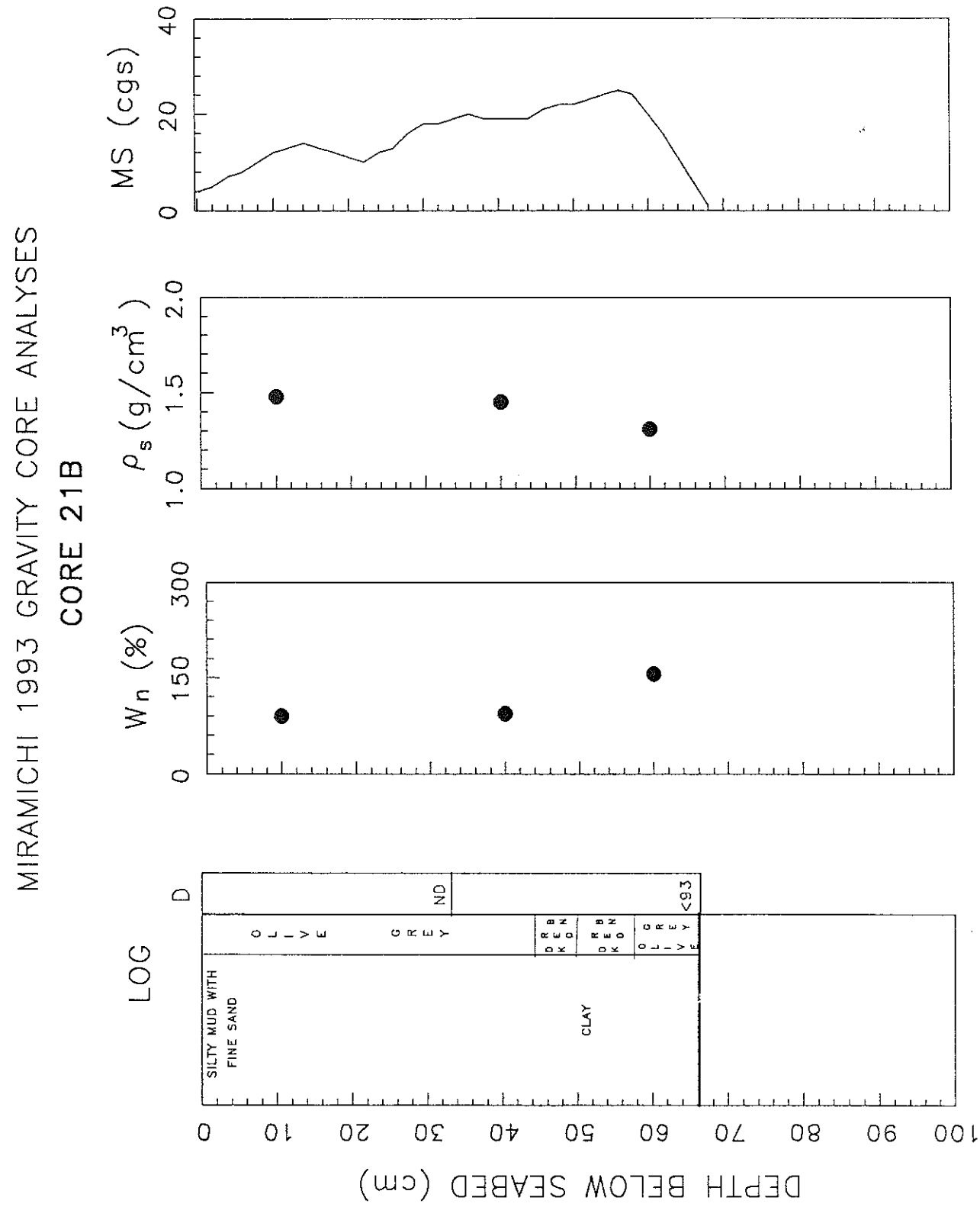
MIRAMICHI 1993 GRAVITY CORE ANALYSES
CORE 21B
MS (cgs)
0
20
40
ρ_s (g/cm^3)
1.0
1.5
2.0
W_n (%)
0
150
300
LOG
D
ND
<93
OLIVE GREY
DRB KD
DRB KD
OLIVE GREY
SILTY MUD WITH FINE SAND
CLAY
0
10
20
30
40
50
60
70
80
90
100
DEPTH BELOW SEABED (cm)

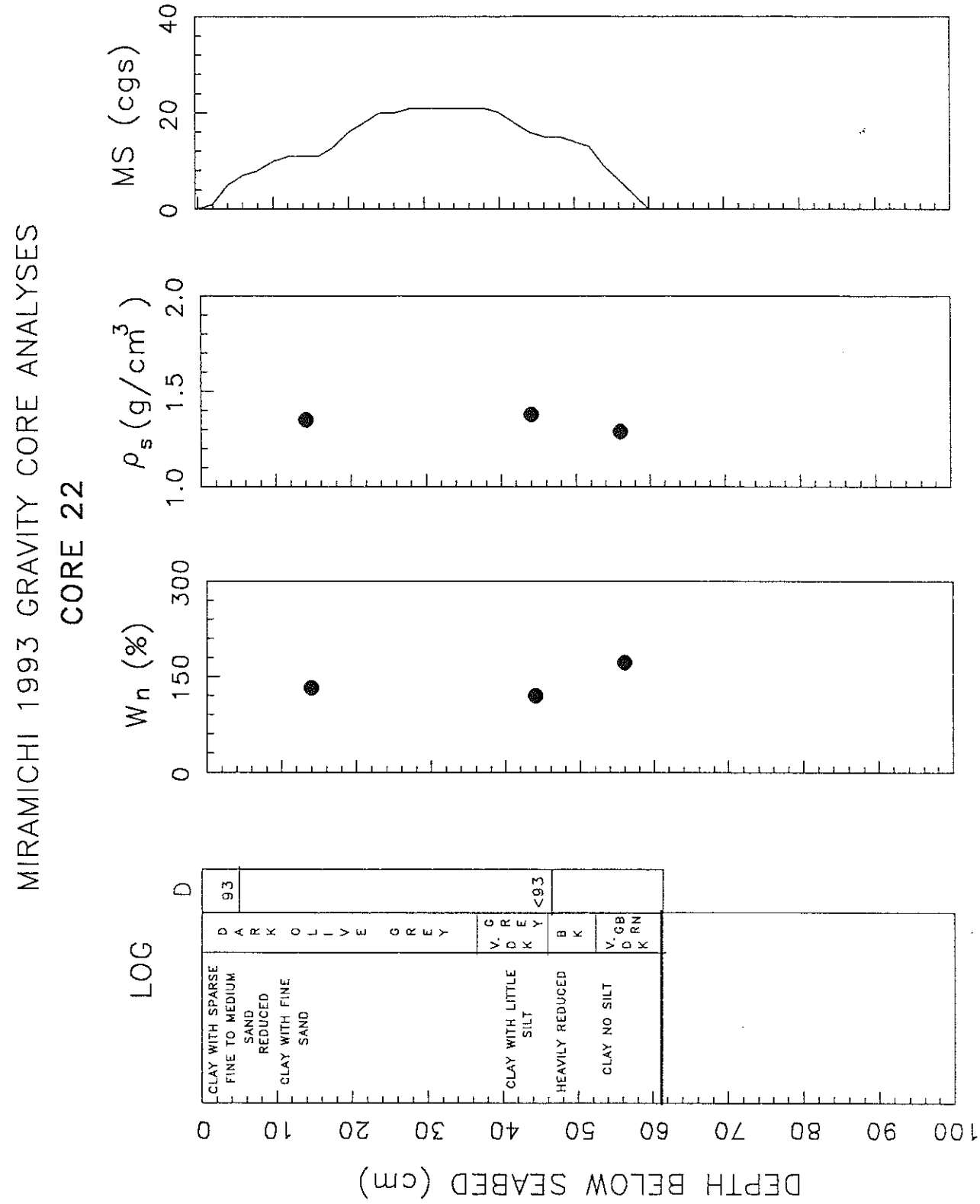
MIRAMICHI 1993 GRAVITY CORE ANALYSES
CORE 22
LOG
D
93
<93
D ARK OLIVE GREY
V. G DK GREY
BK
V. GB DRN
CLAY WITH SPARSE FINE TO MEDIUM SAND REDUCED
CLAY WITH FINE SAND
CLAY WITH LITTLE SILT
HEAVILY REDUCED
CLAY NO SILT
W_n (%)
0
150
300
ρ_s (g/cm^3)
1.0
1.5
2.0
MS (cgs)
0
20
40
DEPTH BELOW SEABED (cm)
0
10
20
30
40
50
60
70
80
90
100

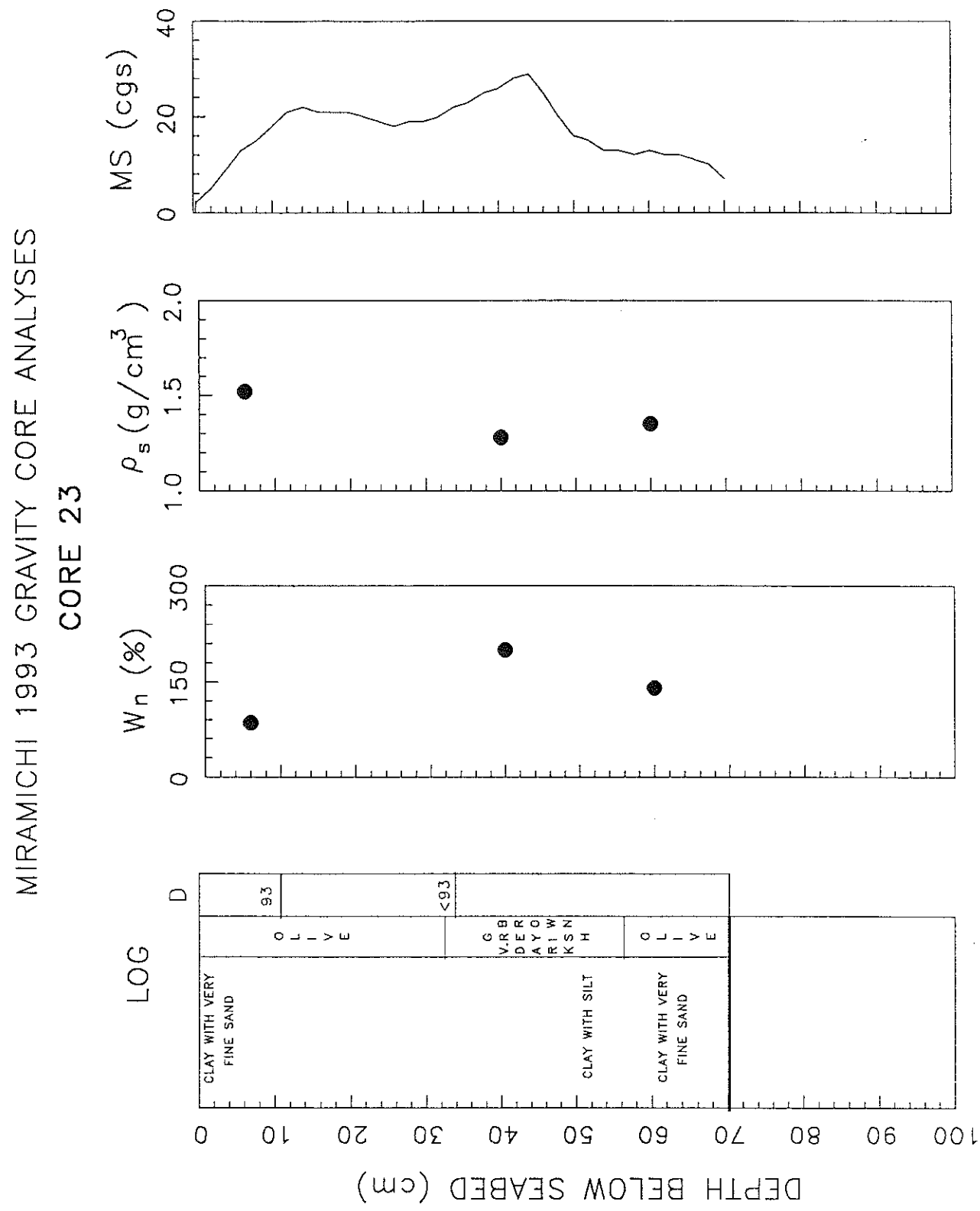
MIRAMICHI 1993 GRAVITY CORE ANALYSES
CORE 23
MS (cgs)
0
20
40
ρ_s (g/cm^3)
1.0
1.5
2.0
W_n (%)
0
150
300
LOG
D
93
<93
OLIVE
GRAVELLY MUDDY SAND
OLIVE
CLAY WITH VERY FINE SAND
CLAY WITH SILT
CLAY WITH VERY FINE SAND
0
10
20
30
40
50
60
70
80
90
100
DEPTH BELOW SEABED (cm)

MIRAMICHI 1993 GRAVITY CORE ANALYSES

CORE 25

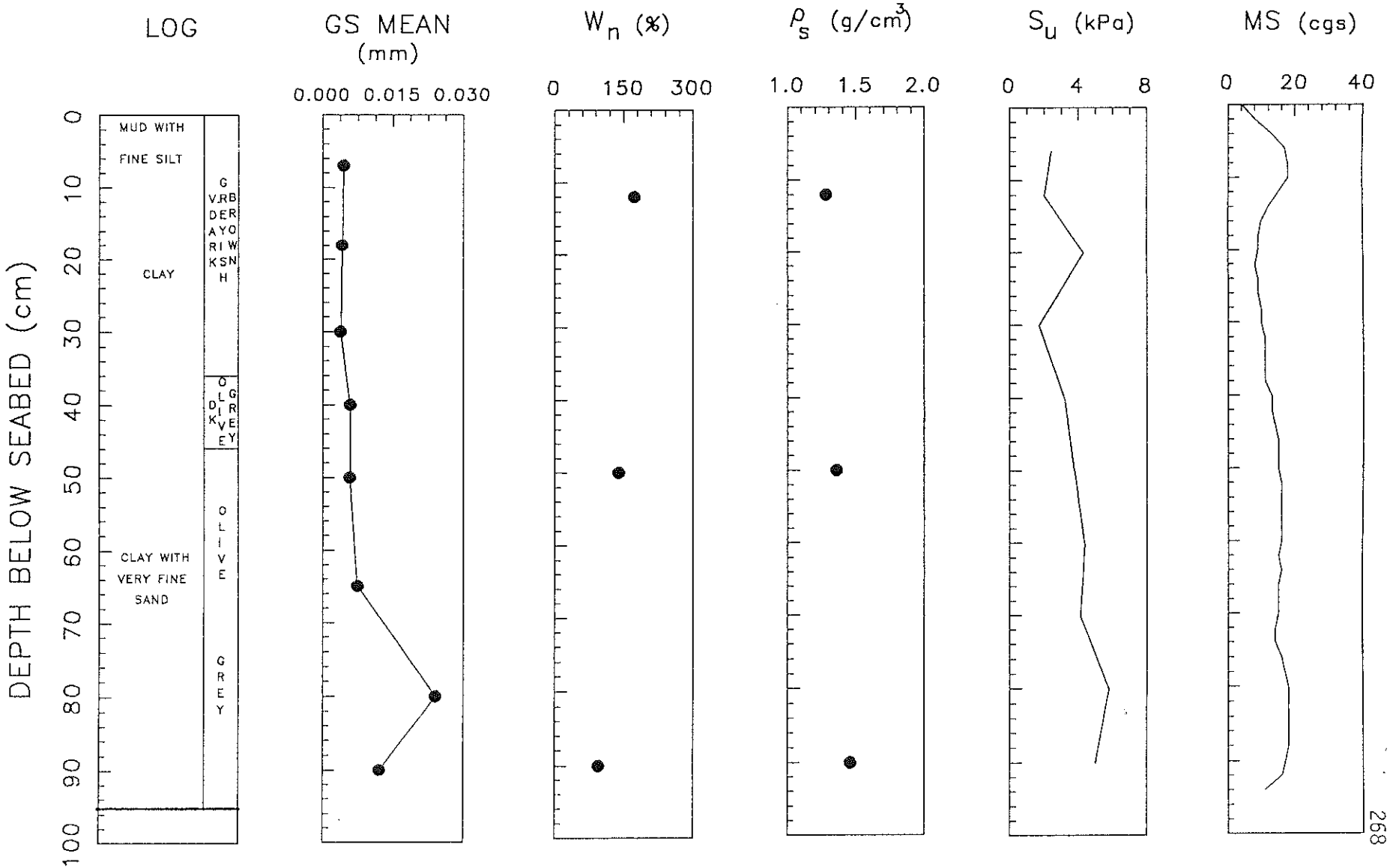

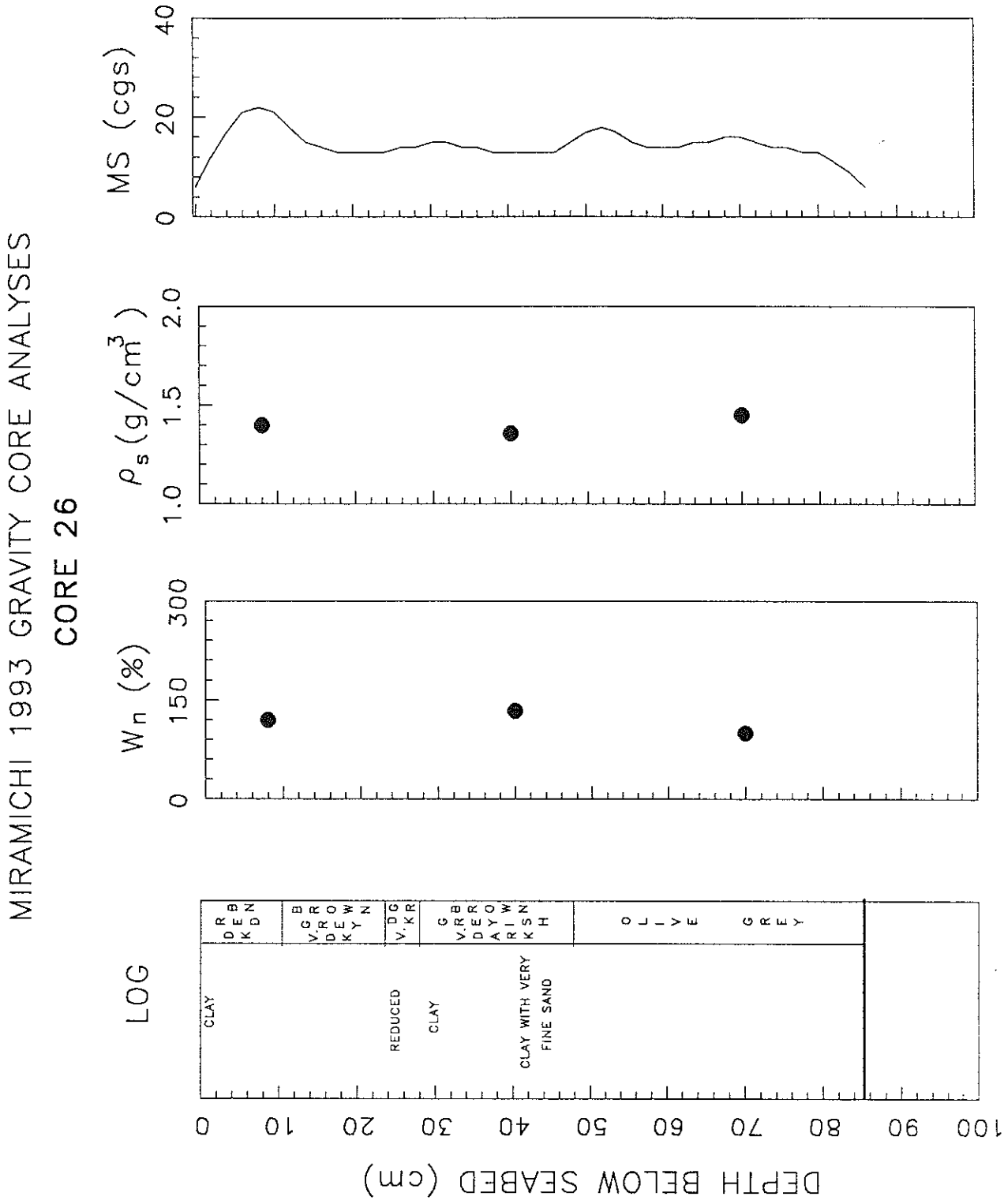
MIRAMICHI 1993 GRAVITY CORE ANALYSES
CORE 26
LOG
CLAY
REDUCED
CLAY
CLAY WITH VERY FINE SAND
OLIVE GREY
W_n (%)
0
150
300
ρ_s (g/cm^3)
1.0
1.5
2.0
MS (cgs)
0
20
40
DEPTH BELOW SEABED (cm)
0
10
20
30
40
50
60
70
80
90
100

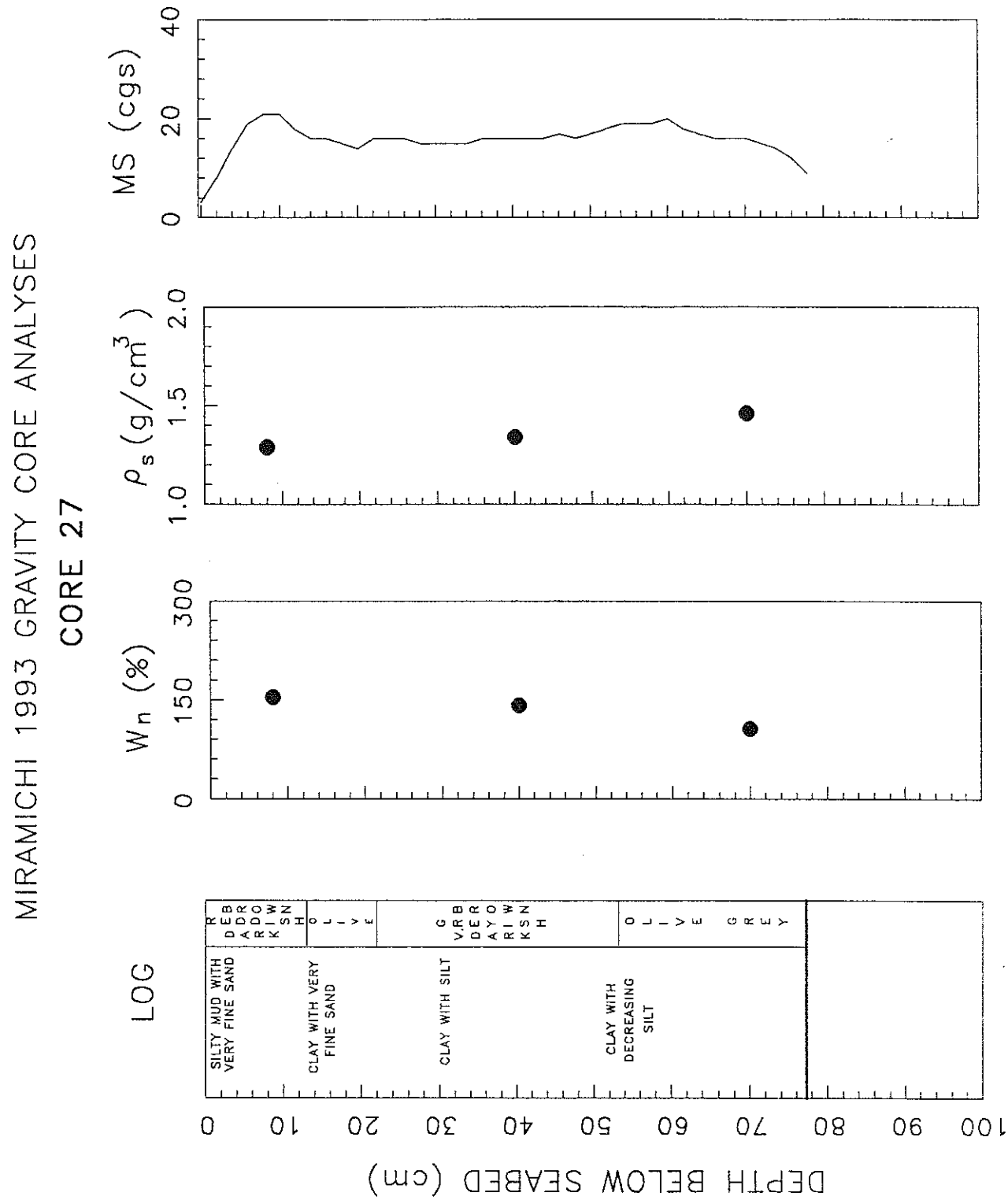
MIRAMICHI 1993 GRAVITY CORE ANALYSES
CORE 27
LOG
SILTY MUD WITH VERY FINE SAND
CLAY WITH VERY FINE SAND
CLAY WITH SILT
CLAY WITH DECREASING SILT
DEBRIS
LIVE
GRAVEL
W_n (%)
0
150
300
ρ_s (g/cm^3)
1.0
1.5
2.0
MS (cgs)
0
20
40
DEPTH BELOW SEABED (cm)
0
10
20
30
40
50
60
70
80
90
100

MIRAMICHI 1993 GRAVITY CORE ANALYSES

CORE 28

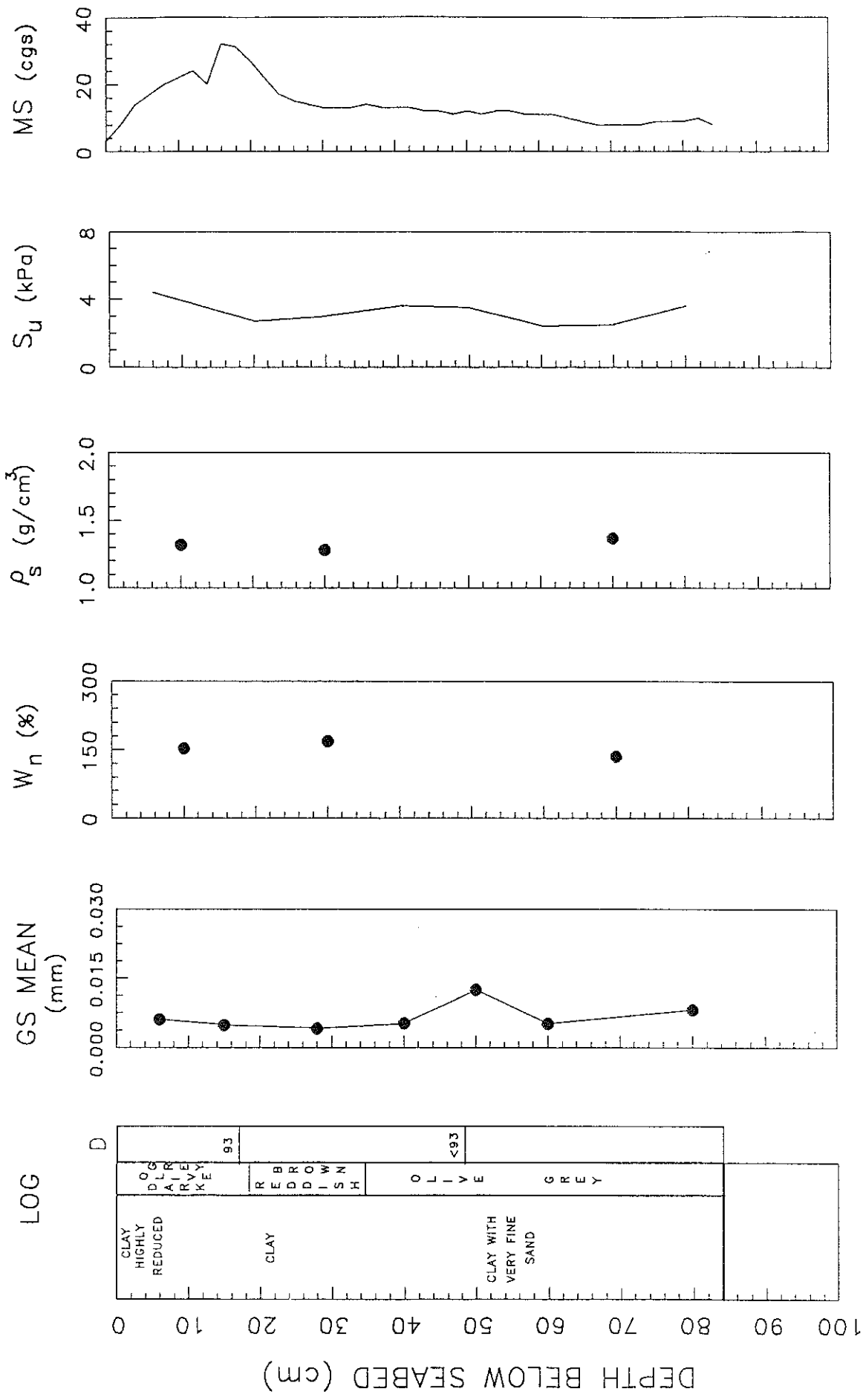

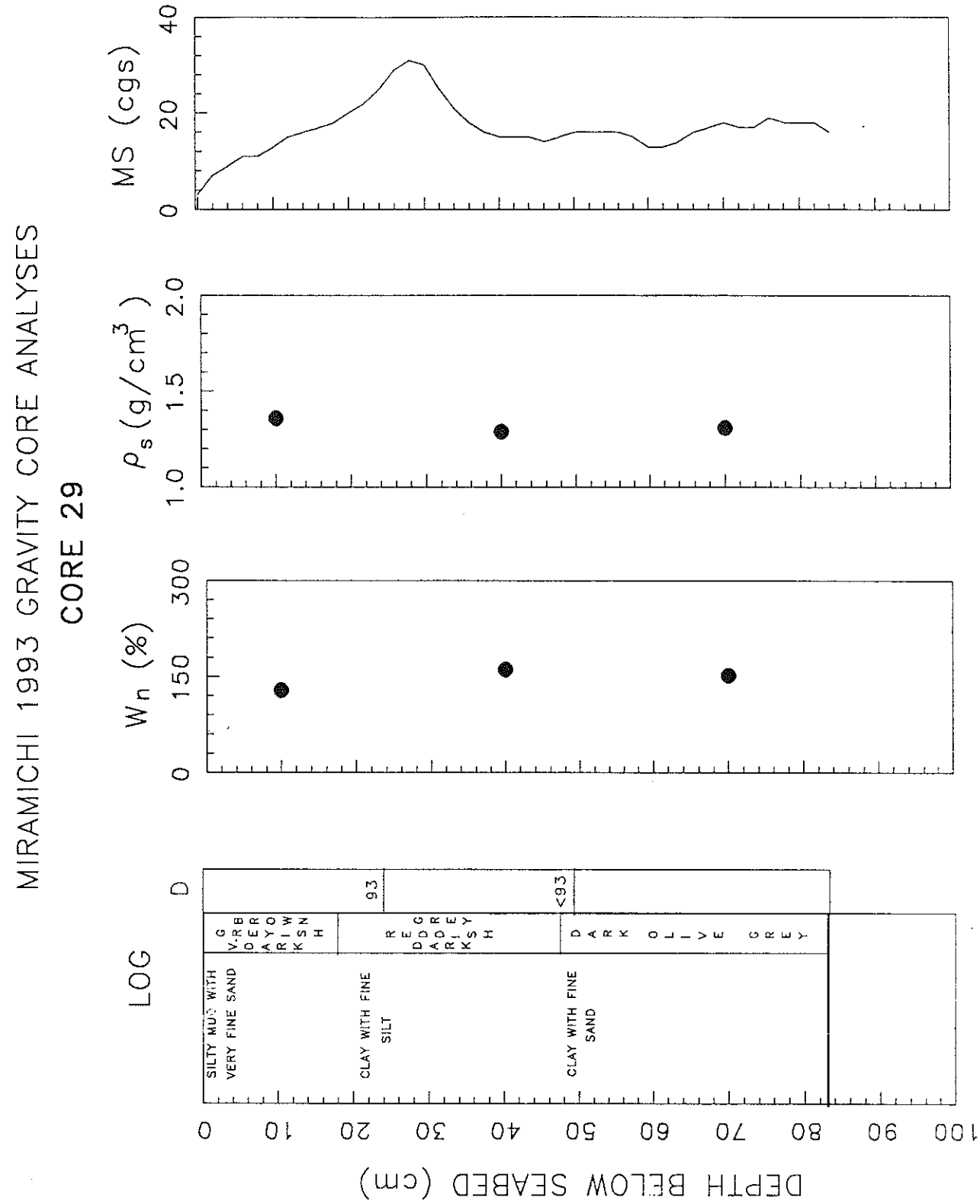
MIRAMICHI 1993 GRAVITY CORE ANALYSES
CORE 29
MS (cgs)
0
20
40
ρ_s (g/cm^3)
1.0
1.5
2.0
W_n (%)
0
150
300
LOG
D
93
<93
SILTY MUD WITH VERY FINE SAND
CLAY WITH FINE SILT
CLAY WITH FINE SAND
GRAYISH BROWN
REDDISH BROWN
DARK OLIVE GREY
0
10
20
30
40
50
60
70
80
90
100
DEPTH BELOW SEABED (cm)

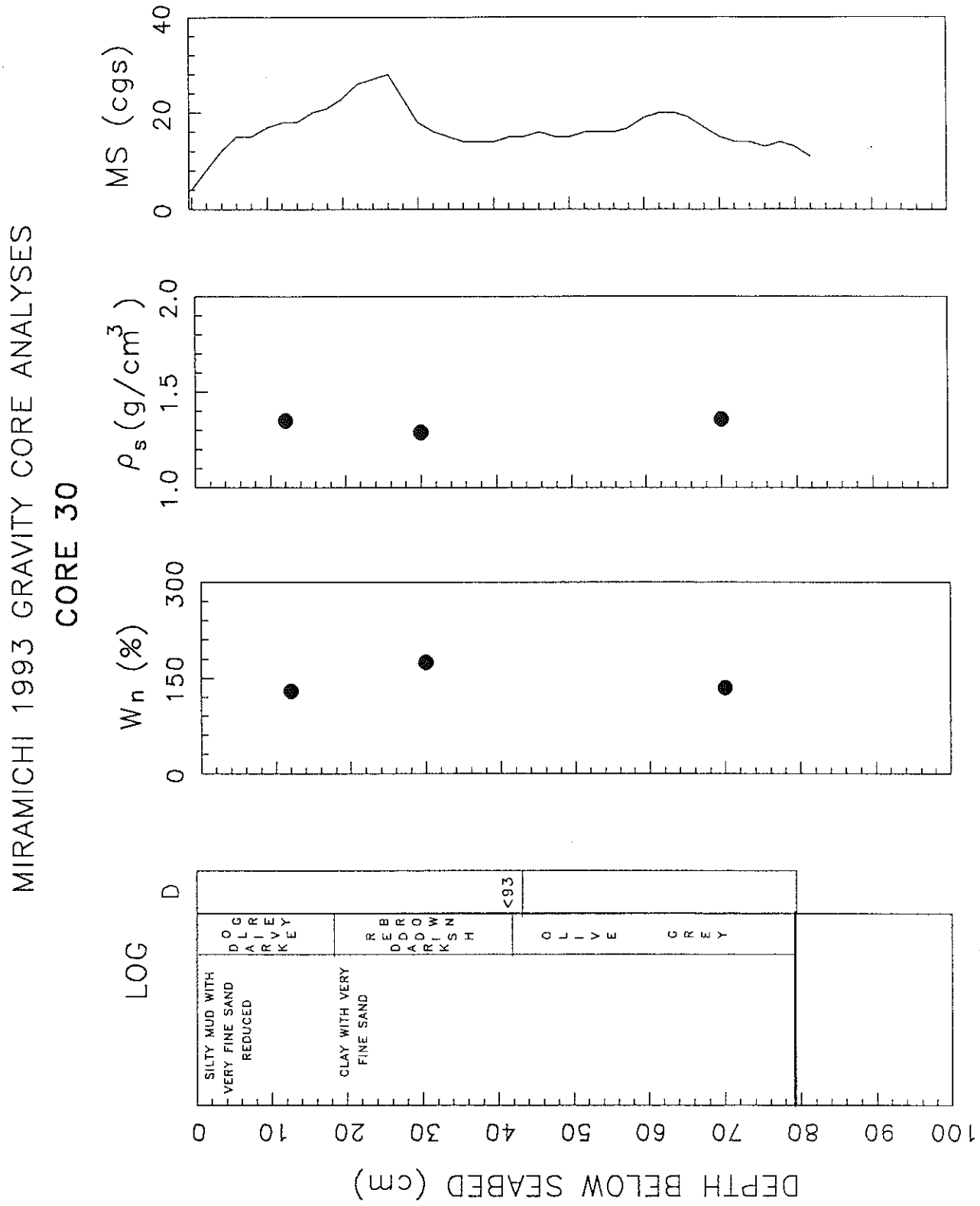
MIRAMICHI 1993 GRAVITY CORE ANALYSES
CORE 30
MS (cgs)
0
20
40
ρ_s (g/cm^3)
1.0
1.5
2.0
W_n (%)
0
150
300
LOG
D
<93
DOG AIR REVE KEY
REDDO RIVER KISH
OLIVE GREY
SILTY MUD WITH VERY FINE SAND REDUCED
CLAY WITH VERY FINE SAND
0
10
20
30
40
50
60
70
80
90
100
DEPTH BELOW SEABED (cm)

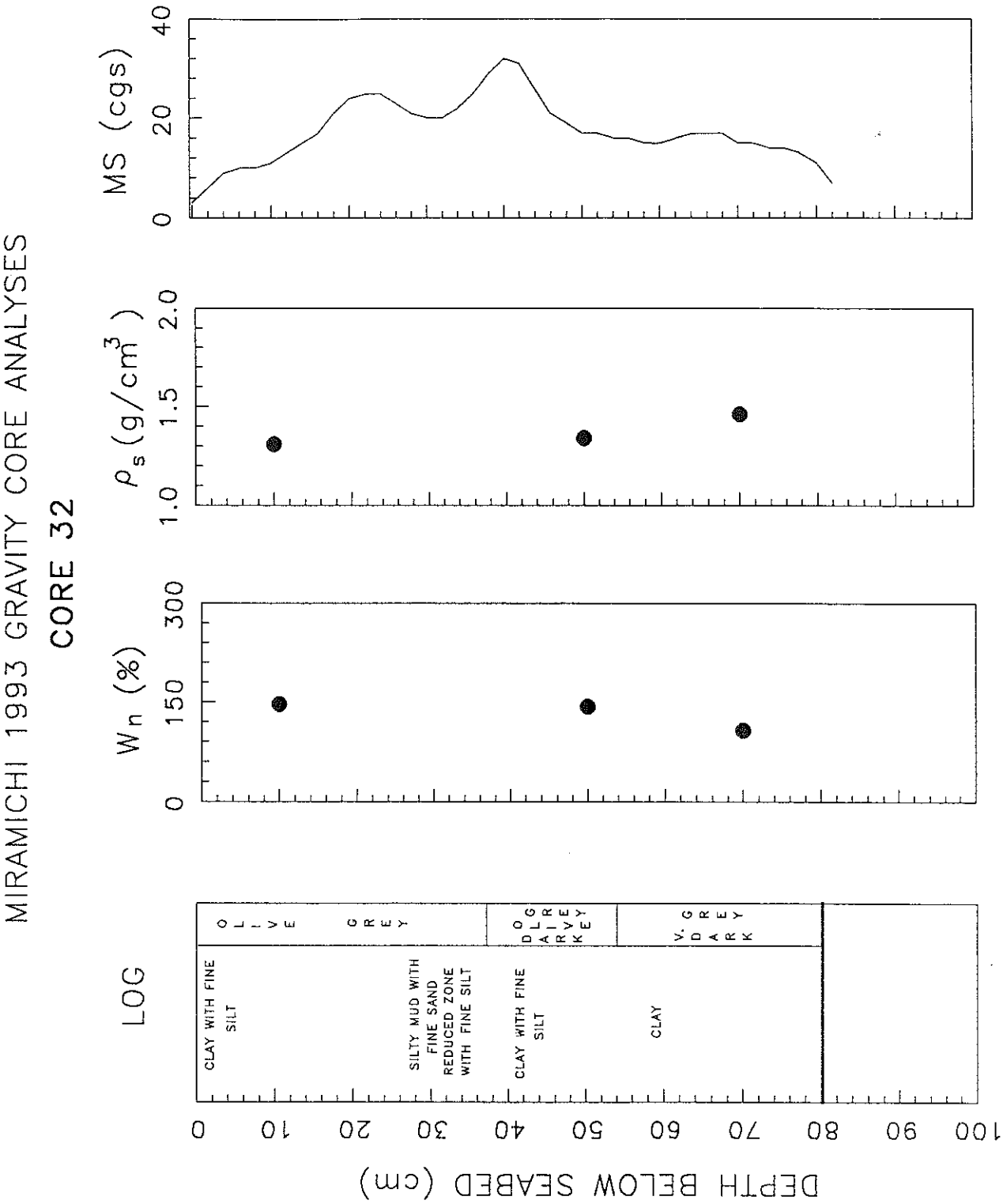
MIRAMICHI 1993 GRAVITY CORE ANALYSES
CORE 32
MS (cgs)
0
20
40
ρ_s (g/cm^3)
1.0
1.5
2.0
W_n (%)
0
150
300
LOG
OLIVE GREY
DOG AIR RVE KEY
V. G DR AE RY K
CLAY WITH FINE SILT
SILTY MUD WITH FINE SAND REDUCED ZONE WITH FINE SILT
CLAY WITH FINE SILT
CLAY
DEPTH BELOW SEABED (cm)
0
10
20
30
40
50
60
70
80
90
100

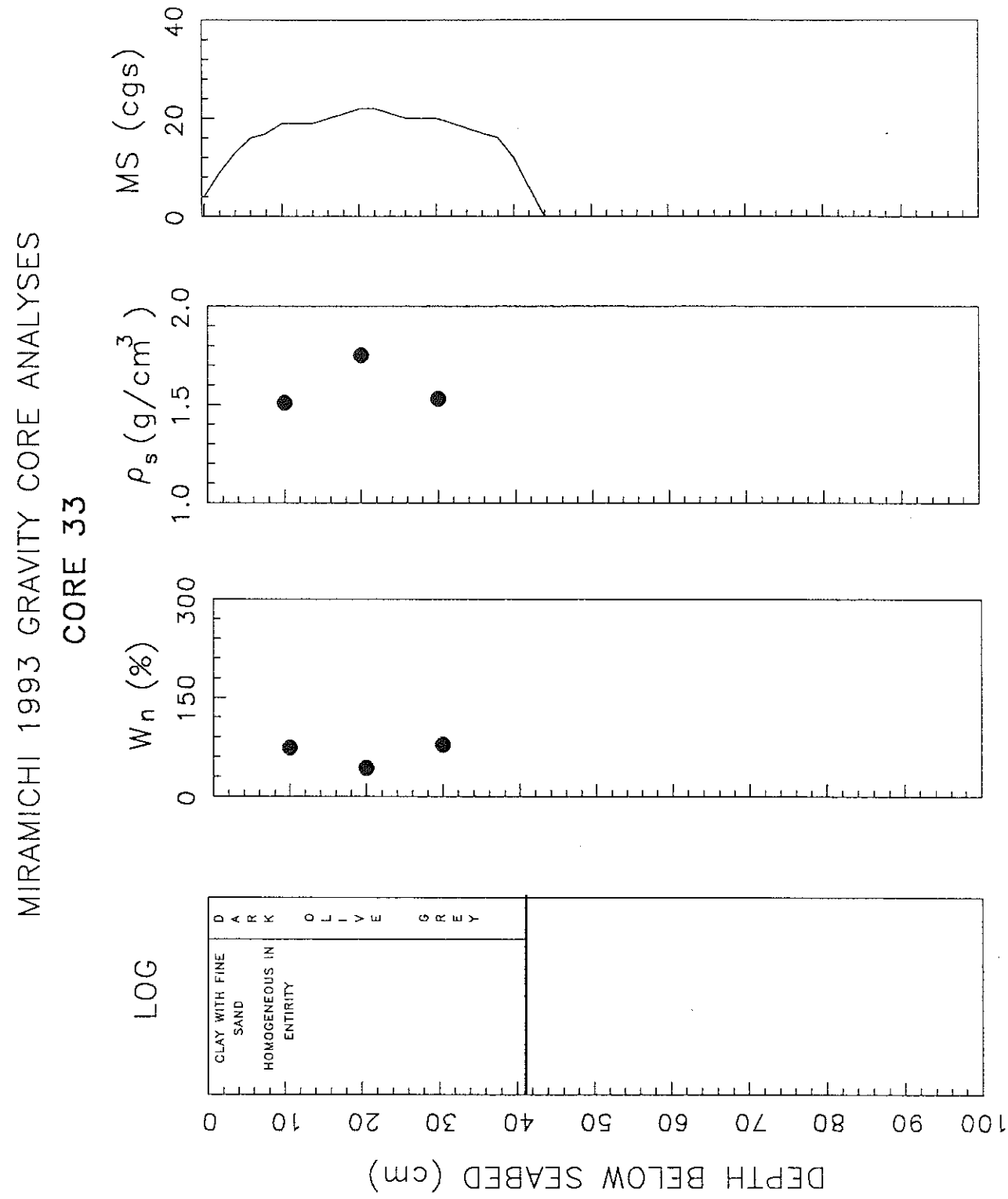
MIRAMICHI 1993 GRAVITY CORE ANALYSES
CORE 33
LOG
CLAY WITH FINE SAND
HOMOGENEOUS IN ENTIRITY
DARK OLIVE GREY
W_n (%)
0
150
300
ρ_s (g/cm^3)
1.0
1.5
2.0
MS (cgs)
0
20
40
DEPTH BELOW SEABED (cm)
0
10
20
30
40
50
60
70
80
90
100

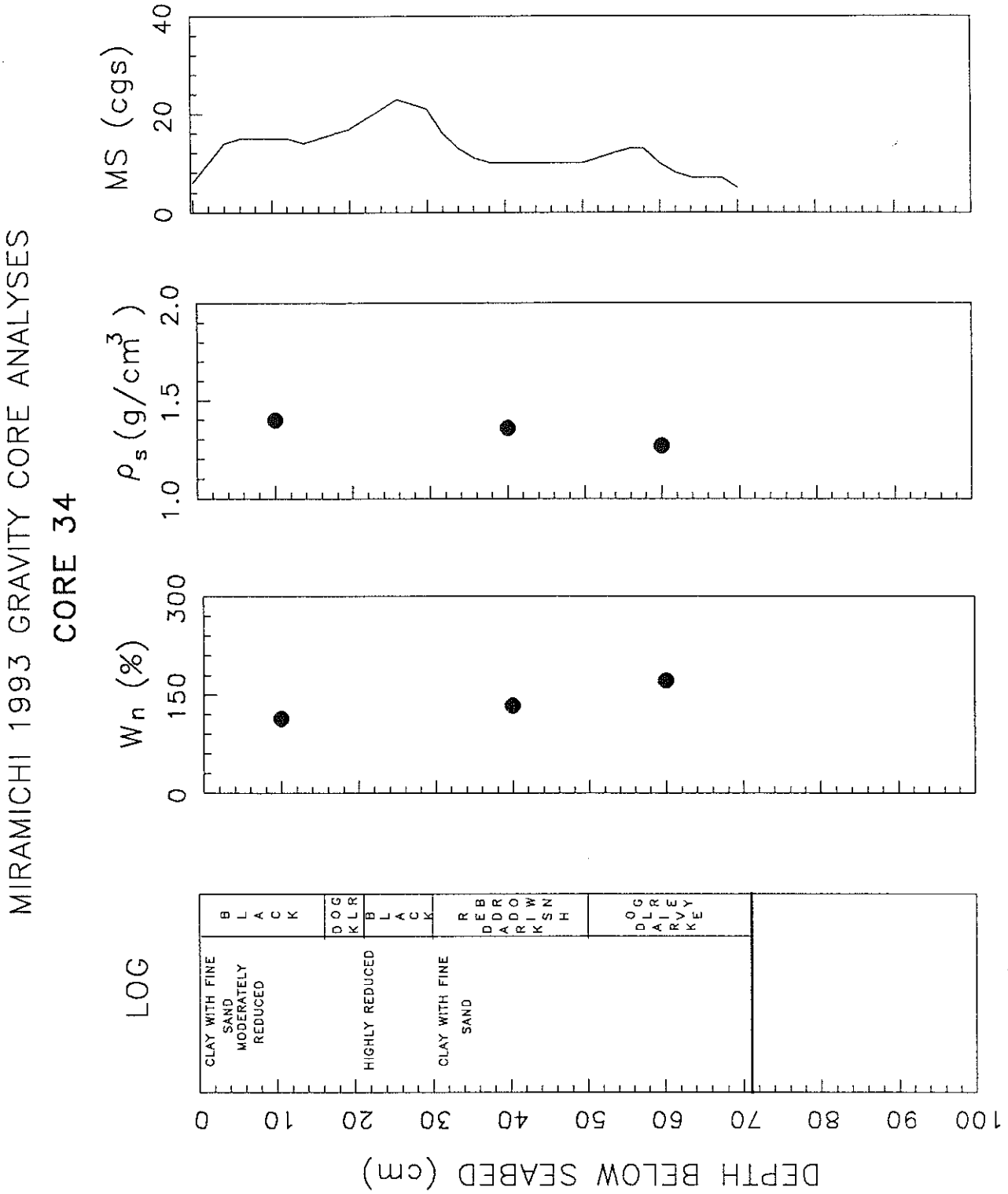
MIRAMICHI 1993 GRAVITY CORE ANALYSES
CORE 34
LOG
CLAY WITH FINE SAND MODERATELY REDUCED
HIGHLY REDUCED
CLAY WITH FINE SAND
BLACK
DOG KLR
BLACK
REDDRADO RIWKSNH
OGDLRAIERVYKE
W_n (%)
0
150
300
ρ_s (g/cm^3)
1.0
1.5
2.0
MS (cgs)
0
20
40
DEPTH BELOW SEABED (cm)
0
10
20
30
40
50
60
70
80
90
100

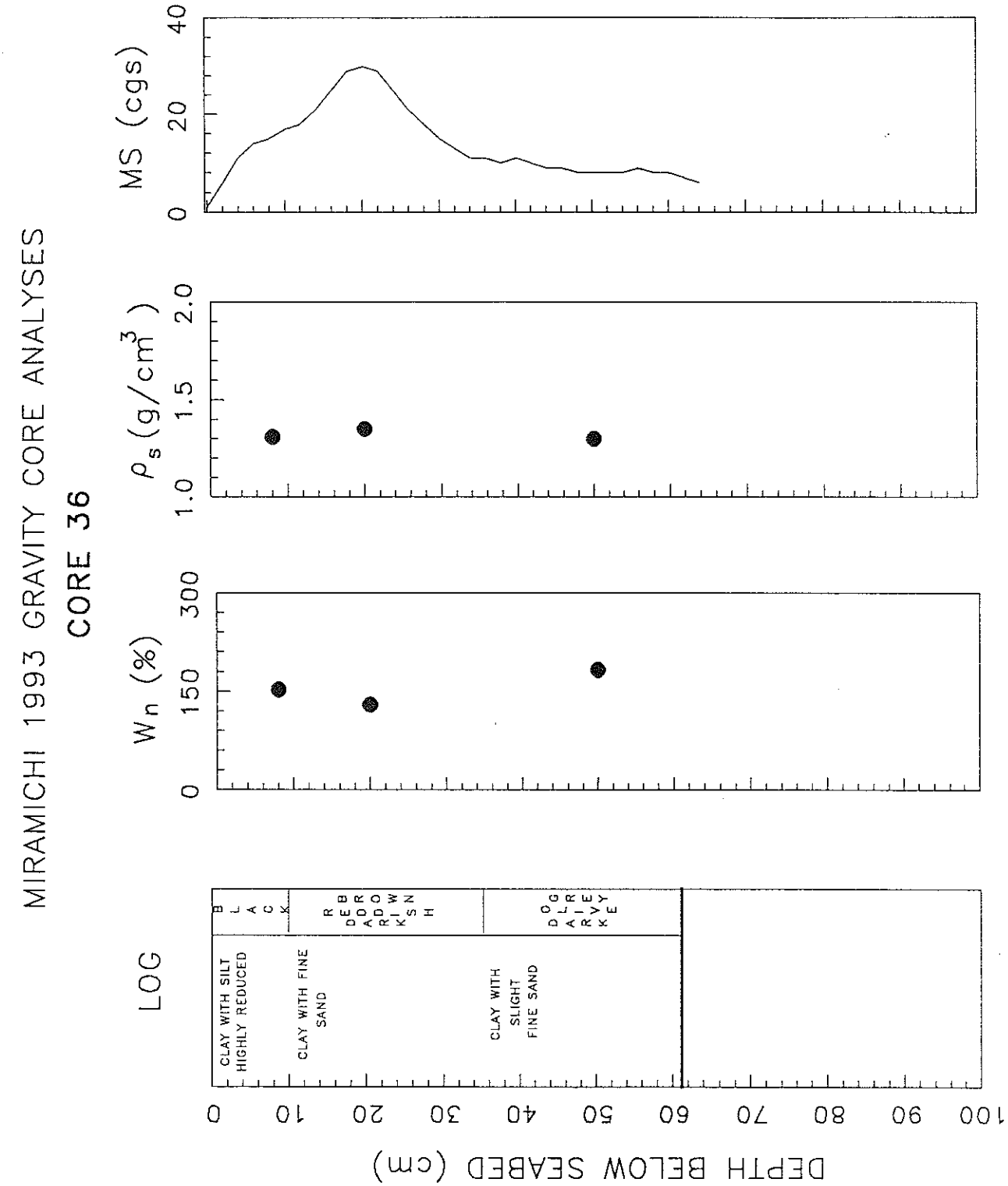
MIRAMICHI 1993 GRAVITY CORE ANALYSES
CORE 36
LOG
CLAY WITH SILT HIGHLY REDUCED
BLACK
CLAY WITH FINE SAND
REDEBADRO KIWSNH
CLAY WITH SLIGHT FINE SAND
OGDLRAIEVYKE
W_n (%)
0
150
300
ρ_s (g/cm^3)
1.0
1.5
2.0
MS (cgs)
0
20
40
DEPTH BELOW SEABED (cm)
0
10
20
30
40
50
60
70
80
90
100

APPENDIX D

Colour Photographs of Sediment Cores

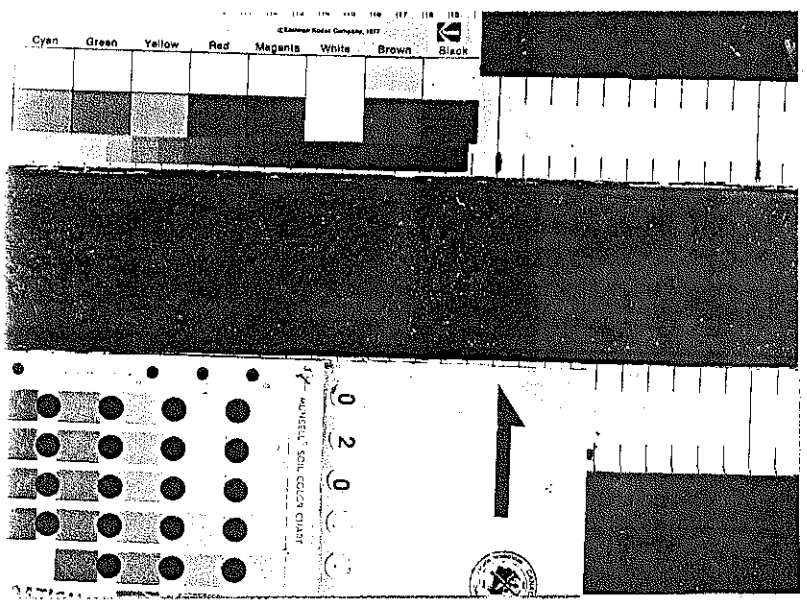
Cyan
Green
Yellow
Red
Magenta
White
Brown
Black
MUNSELL SOIL COLOR CHART

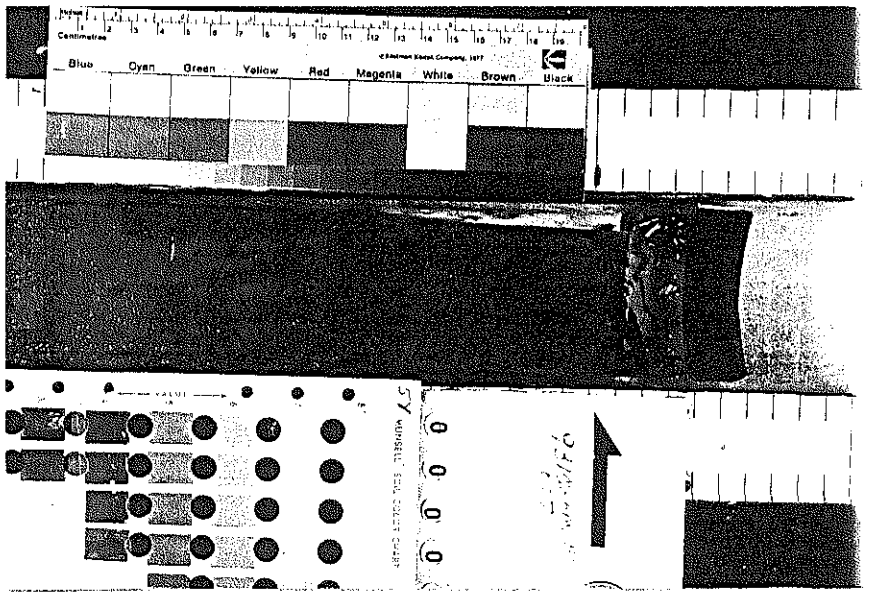
Blue
Cyan
Green
Yellow
Red
Magenta
White
Brown
Black

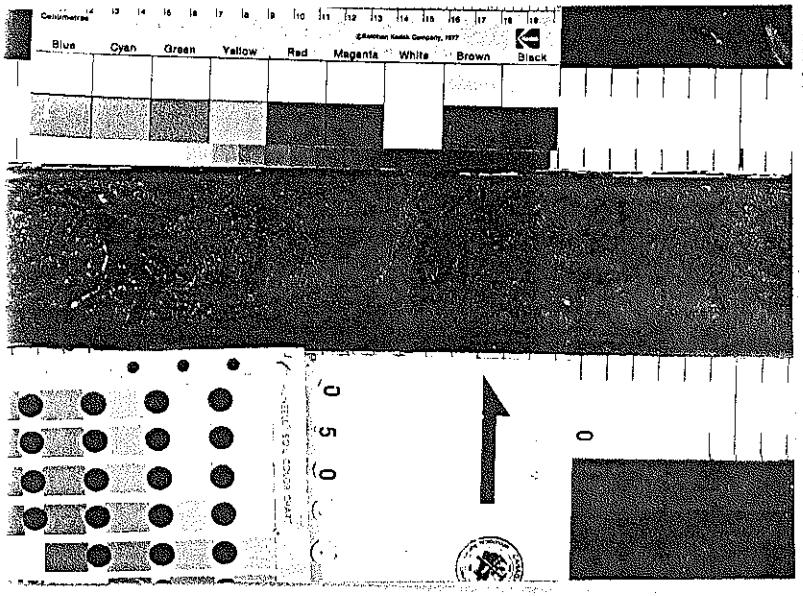
Blue
Cyan
Green
Yellow
Red
Magenta
White
Brown
Black

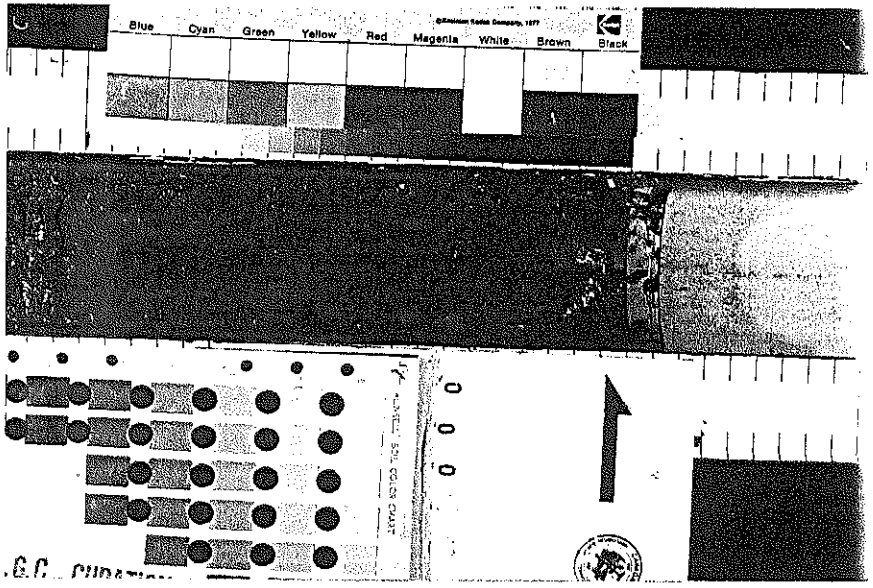
Blue
Cyan
Green
Yellow
Red
Magenta
White
Brown
Black

0200
5Y MUNSELL SOIL COLOR CHART
0500
5Y MUNSELL SOIL COLOR CHART
012
0700
5Y MUNSELL SOIL COLOR CHART
0000
5Y MUNSELL SOIL COLOR CHART

93MIRAMICHI
009
0 2 0 0
5Y MUNSELL SOIL COLOR CHART
Blue
Cyan
Green
Yellow
Red
Magenta
White
Brown
Black

93MIRAMICHI
009
0 0 0 0
5Y MUNSELL SOIL COLOR CHART
Blue
Cyan
Green
Yellow
Red
Magenta
White
Brown
Black

93MIRAMICHI
008
0 5 0 0
5Y MUNSELL SOIL COLOR CHART
Blue
Cyan
Green
Yellow
Red
Magenta
White
Brown
Black

93MIRAMICHI
008
0 2 0 0
5Y MUNSELL SOIL COLOR CHART
Blue
Cyan
Green
Yellow
Red
Magenta
White
Brown
Black

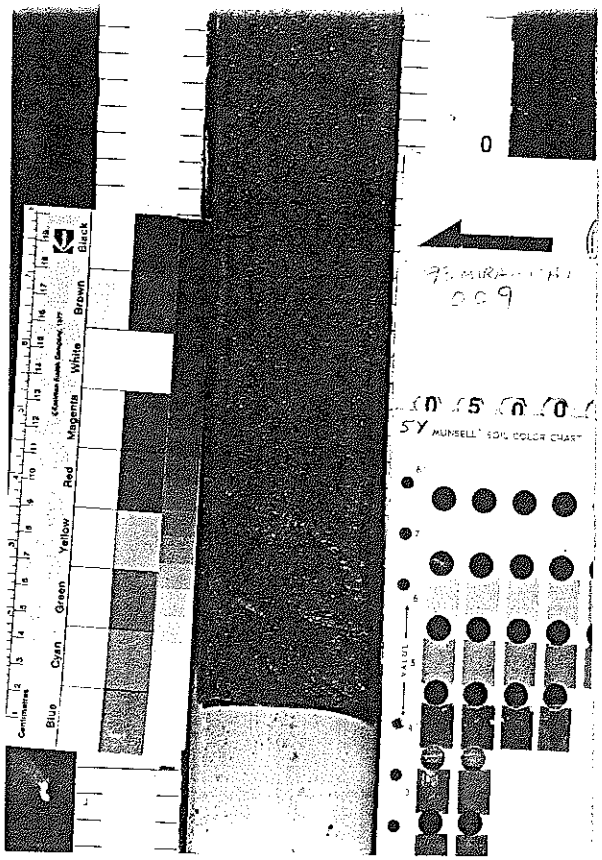
0
5Y MUNSELL SOIL COLOR CHART
Blue
Cyan
Green
Yellow
Red
Magenta
White
Brown
Black

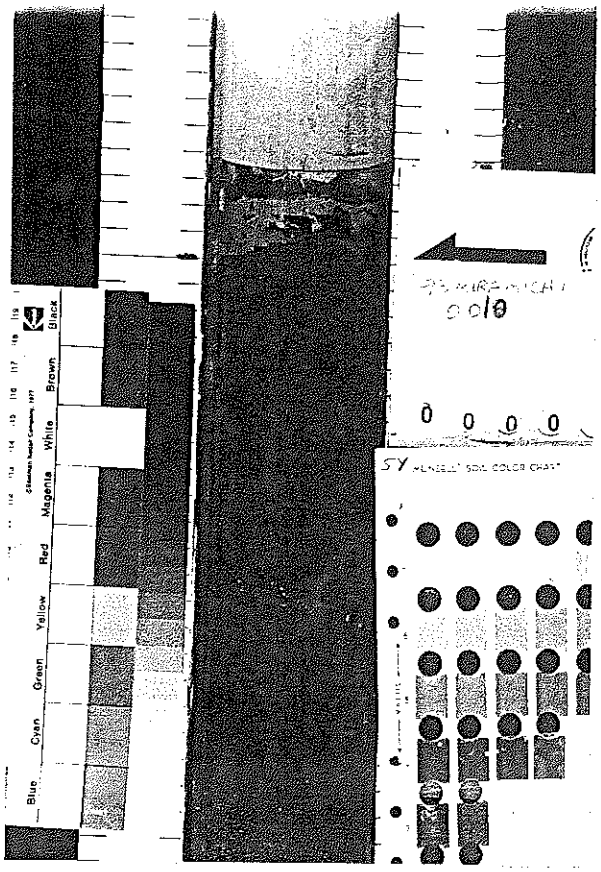
0 0 0 0
5Y MUNSELL SOIL COLOR CHART
Blue
Cyan
Green
Yellow
Red
Magenta
White
Brown
Black

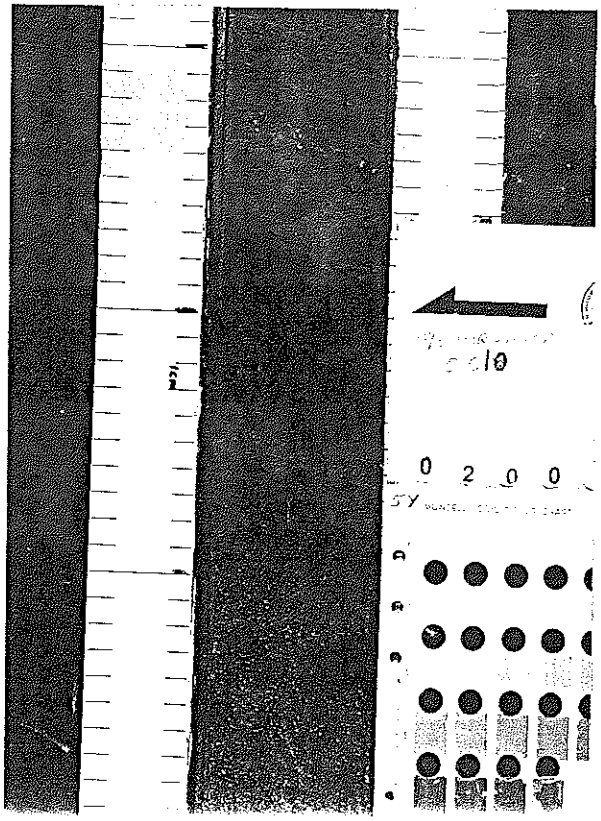
0 2 0 0
5Y

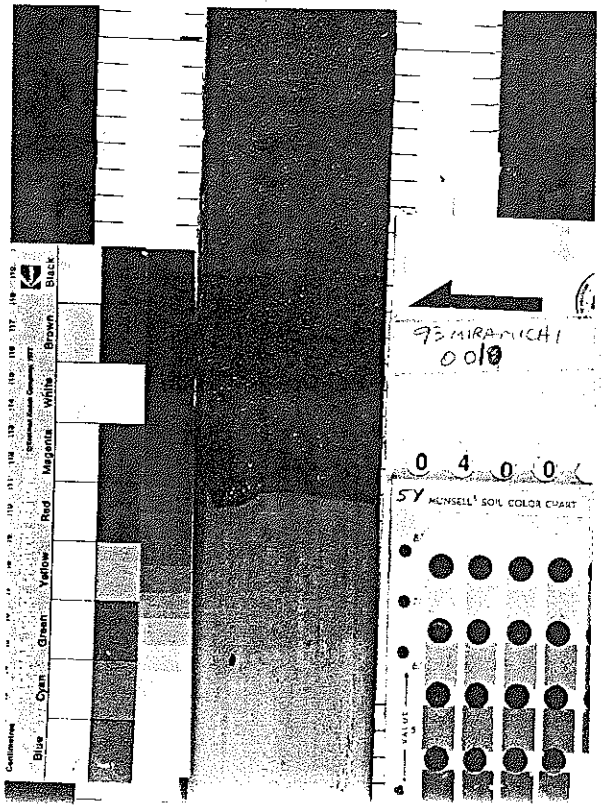
0 4 0 0
5Y MUNSELL SOIL COLOR CHART
Blue
Cyan
Green
Yellow
Red
Magenta
White
Brown
Black

Blue
Cyan
Green
Yellow
Red
Magenta
White
Brown
Black
0 0 0 0
0 0 0 0
2 0 0
0 5 0 0
0

1
2
3
0 8 0 0
5Y MUNSELL SOIL COLOR CHART

0
93 MIRAMICHI
013
0 5 0

93 MIRAMICHI
013
0 0 0

93 MIRAMICHI
013
0 2 0

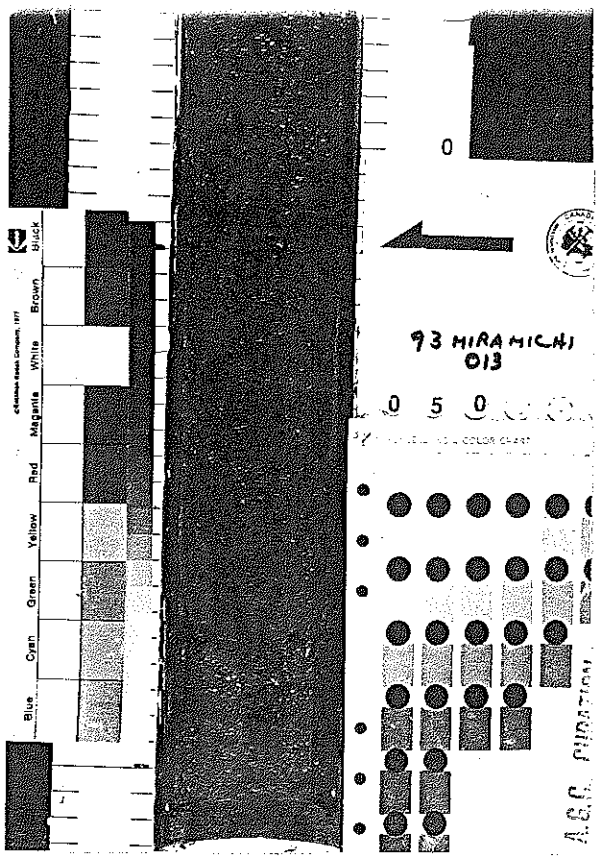
93 MIRAMICHI
013
0 5 0
10 YR MUNSELL SOIL COLOR CHART
Blue
Cyan
Green
Yellow
Red
Magenta
White
Brown
Black

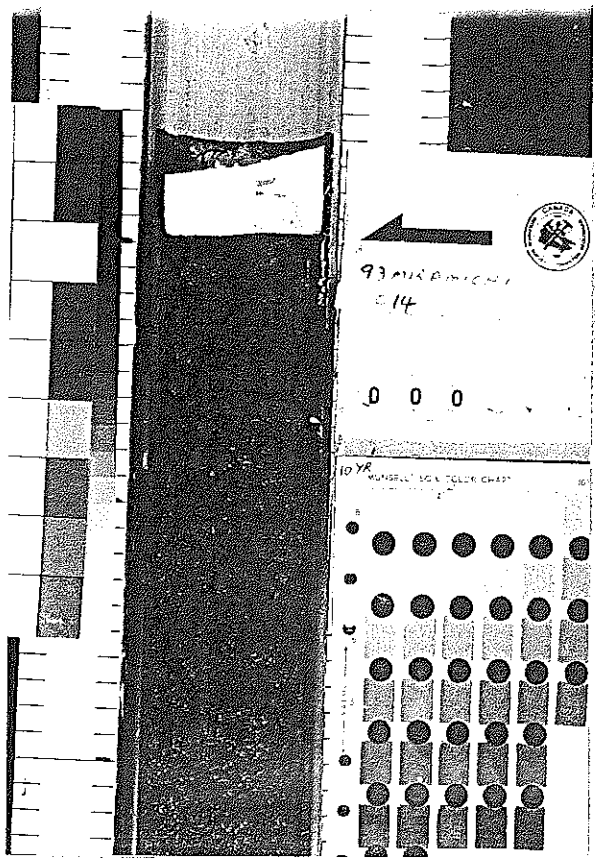
93 MIRAMICHI
14
0 0 0
10 YR MUNSELL SOIL COLOR CHART

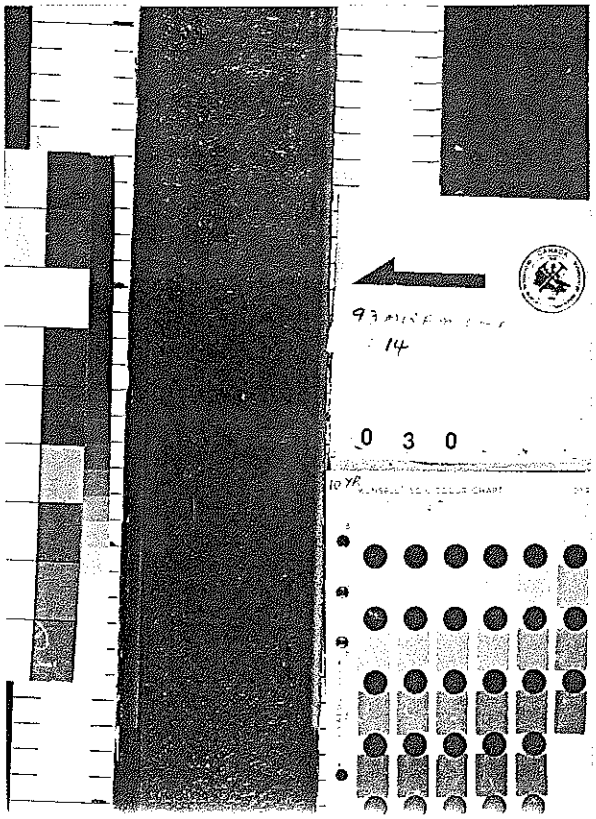
93 MIRAMICHI
14
0 3 0
10 YR MUNSELL SOIL COLOR CHART

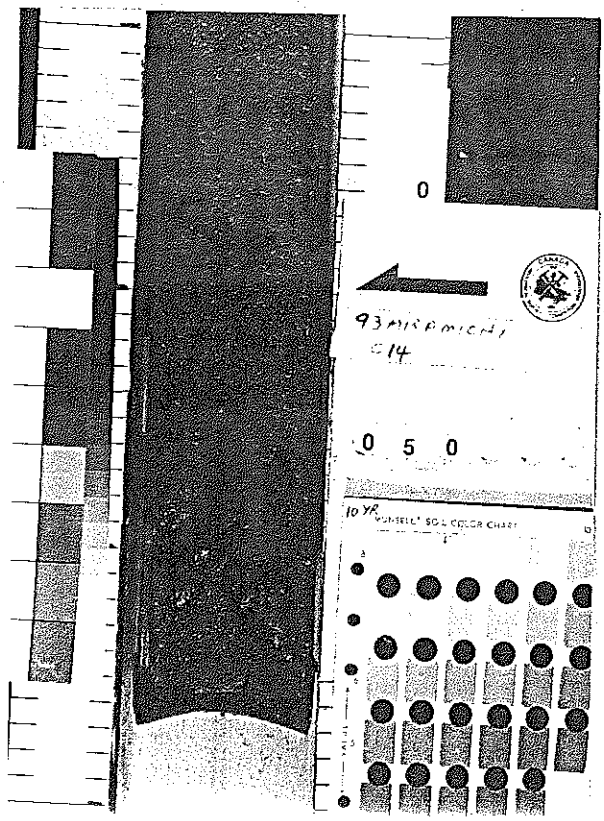
93 MIRAMICHI
14
0 5 0
10 YR MUNSELL SOIL COLOR CHART

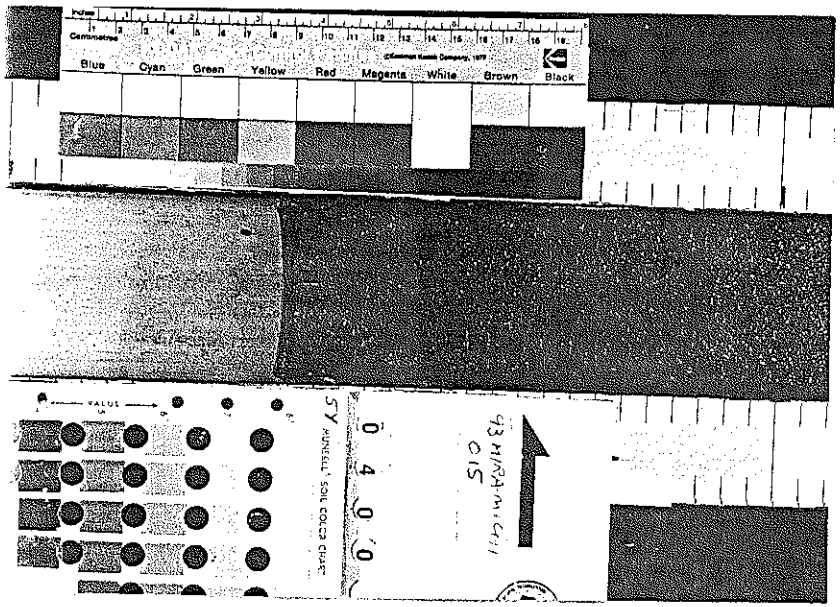
Blue Cyan Green Yellow Red Magenta White Brown Black
5Y MUNSELL SOIL COLOR CHART
0 4 0 0
43 HRA mi C11
C15

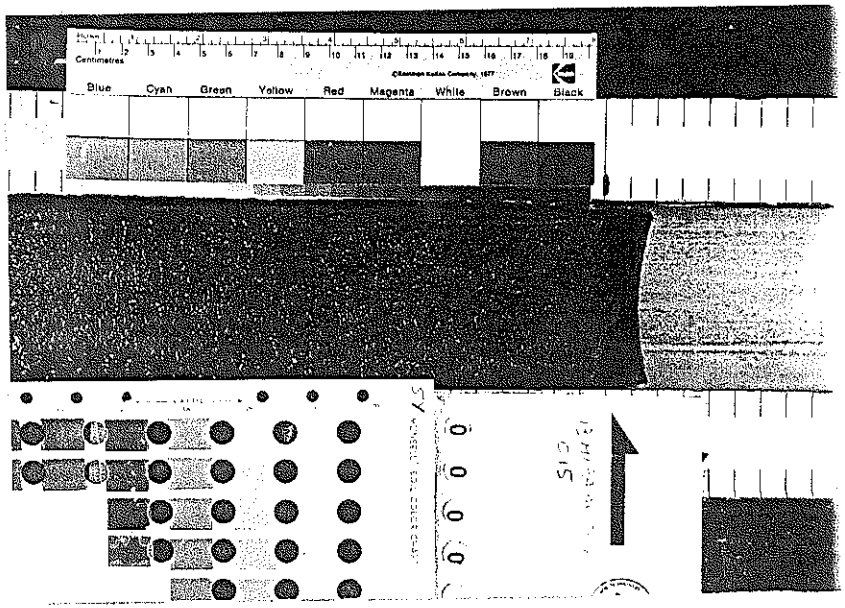
Blue Cyan Green Yellow Red Magenta White Brown Black
5Y MUNSELL SOIL COLOR CHART
0 0 0 0
C15

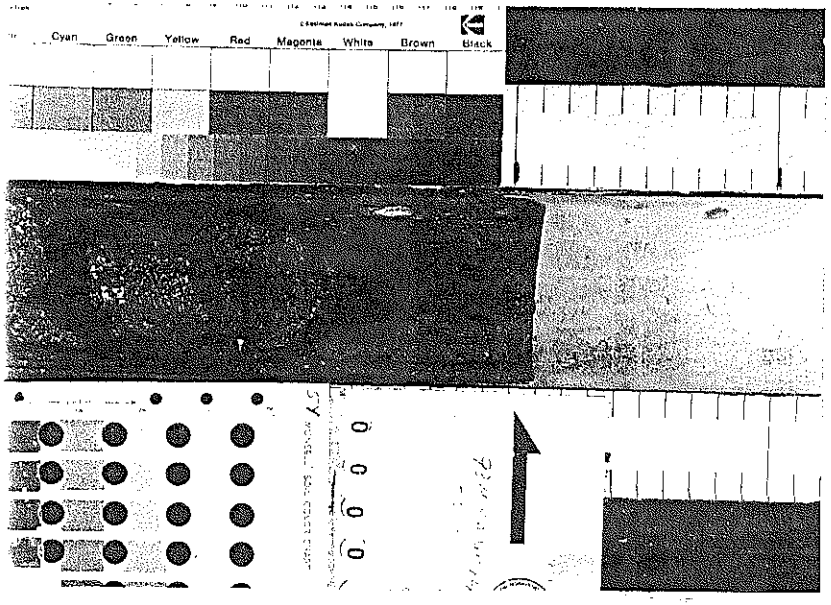
Cyan Green Yellow Red Magenta White Brown Black
5Y MUNSELL SOIL COLOR CHART
0 0 0 0

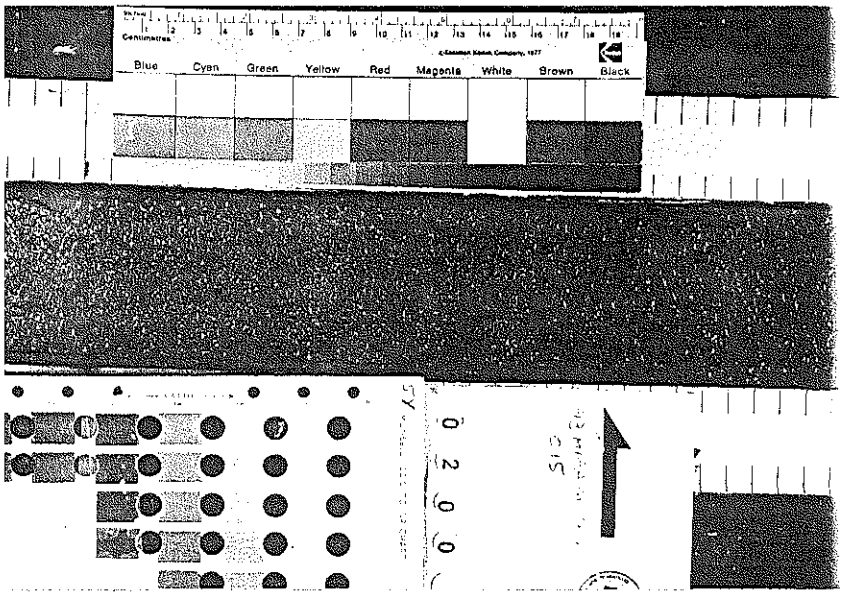
Blue Cyan Green Yellow Red Magenta White Brown Black
5Y MUNSELL SOIL COLOR CHART
0 2 0 0
C15

0 2 0 0
5Y
Blue
Cyan
Green
Yellow
Red
Magenta
White
Brown
Black

0 5 0 0
5Y
Blue
Cyan
Green
Yellow
Red
Magenta
White
Brown
Black

0 7 0 0
5Y MUNSELL SOIL COLOR CHART
Blue
Cyan
Green
Yellow
Red
Magenta
White
Brown
Black

0 0 0 0
5Y MUNSELL SOIL COLOR CHART
Green
Yellow
Red
Magenta
White
Brown
Black

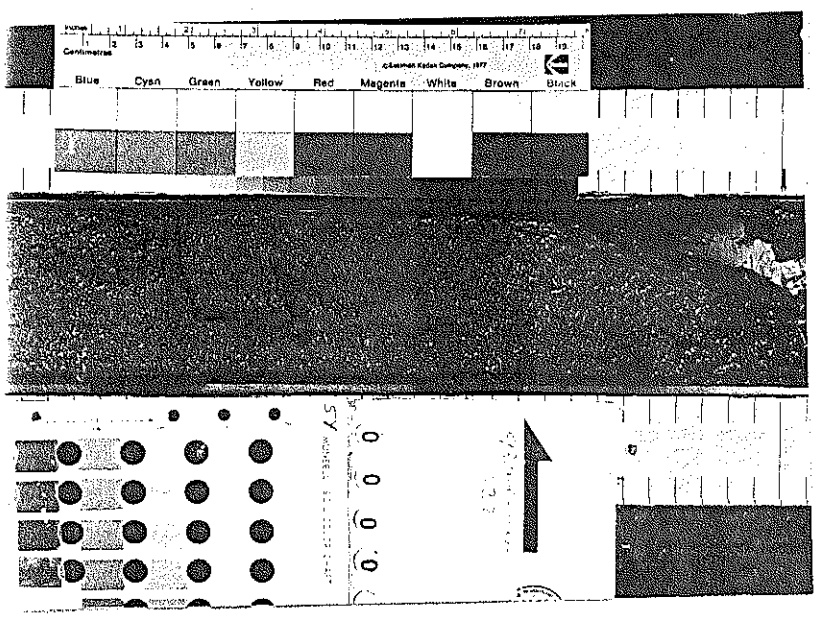
Blue Cyan Green Yellow Red Magenta White Brown Black

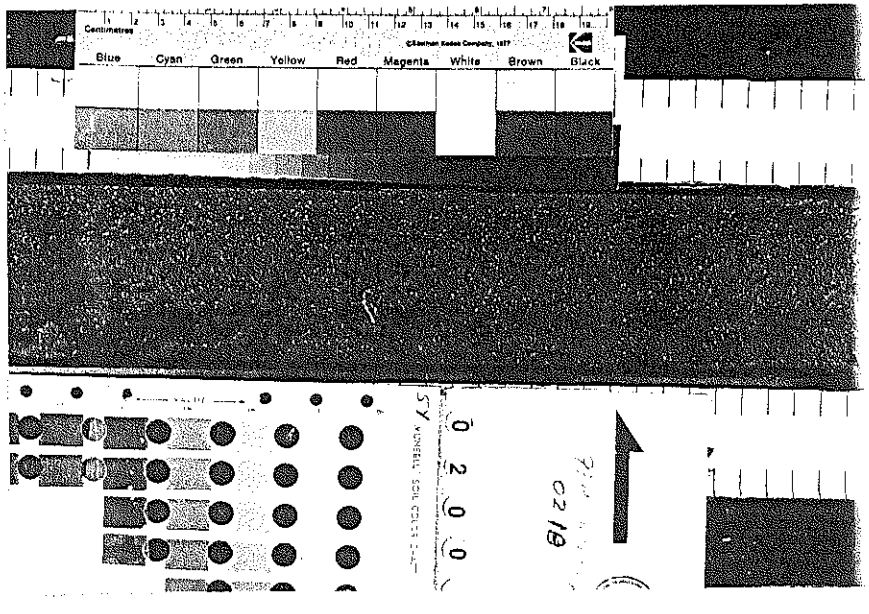
Blue Cyan Green Yellow Red Magenta White Brown Black

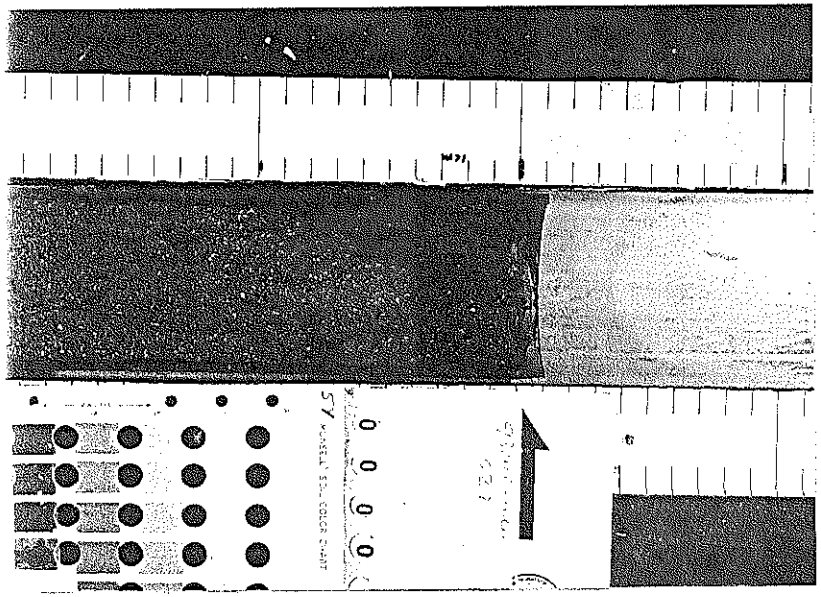

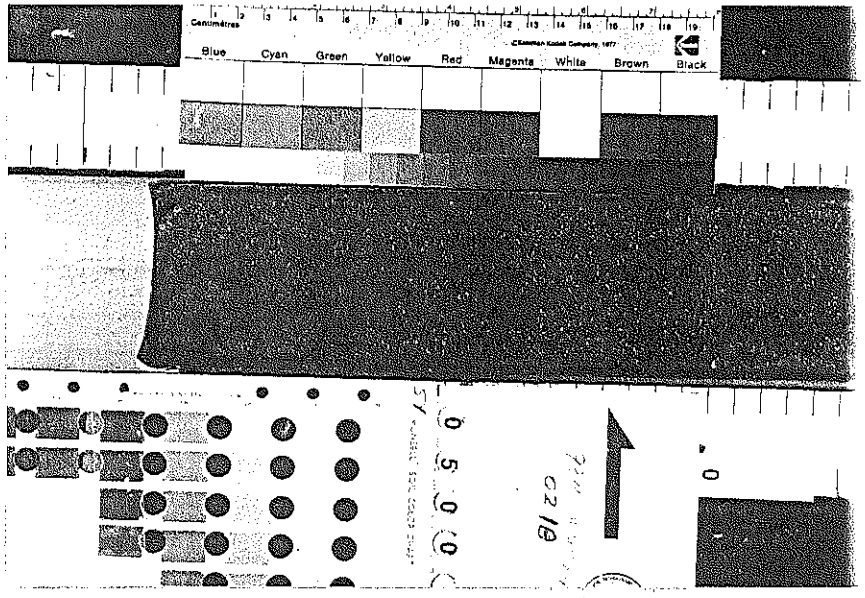
Blue Cyan Green Yellow Red Magenta White Brown Black

Blue
Cyan
Green
Yellow
Red
Magenta
White
Brown
Black
0 0 0 0
5Y MUNSELL SOIL COLOR CHART

Blue
Cyan
Green
Yellow
Red
Magenta
White
Brown
Black
0 2 0 0
5Y MUNSELL SOIL COLOR CHART

Blue
Cyan
Green
Yellow
Red
Magenta
White
Brown
Black
0 5 0 0
5Y MUNSELL SOIL COLOR CHART

Cyan
Green
Yellow
Red
Magenta
White
Brown
Black
0 0 0 0
5Y MUNSELL SOIL COLOR CHART

93 McFarlane
c23
0 2 0
5Y MUNSELL SOIL COLOR CHART
Blue
Cyan
Green
Yellow
Red
Magenta
White
Brown
Black

93 McFarlane
c23
0 2 0
5Y MUNSELL SOIL COLOR CHART
Blue
Cyan
Green
Yellow
Red
Magenta
White
Brown
Black

93 McFarlane
c23
0 5 0
5Y MUNSELL SOIL COLOR CHART
Blue
Cyan
Green
Yellow
Red
Magenta
White
Brown
Black

93 McFarlane
c23
0 2 0
5Y MUNSELL SOIL COLOR CHART
Blue
Cyan
Green
Yellow
Red
Magenta
White
Brown
Black

93 MIRAMICHI
025
0500
5Y MUNSELL® SOIL COLOR CHART
VALUE
Blue Cyan Green Yellow Red Magenta White Brown Black

93 MIRAMICHI
025
0800
5Y MUNSELL® SOIL COLOR CHART
VALUE
Blue Cyan Green Yellow Red Magenta White Brown Black

93MIRAMICHI
026
0000
5Y MUNSELL® SOIL COLOR CHART
VALUE
Blue Cyan Green Yellow Red Magenta White Brown Black

93MIRAMICHI
026
0200
5Y MUNSELL® SOIL COLOR CHART
VALUE

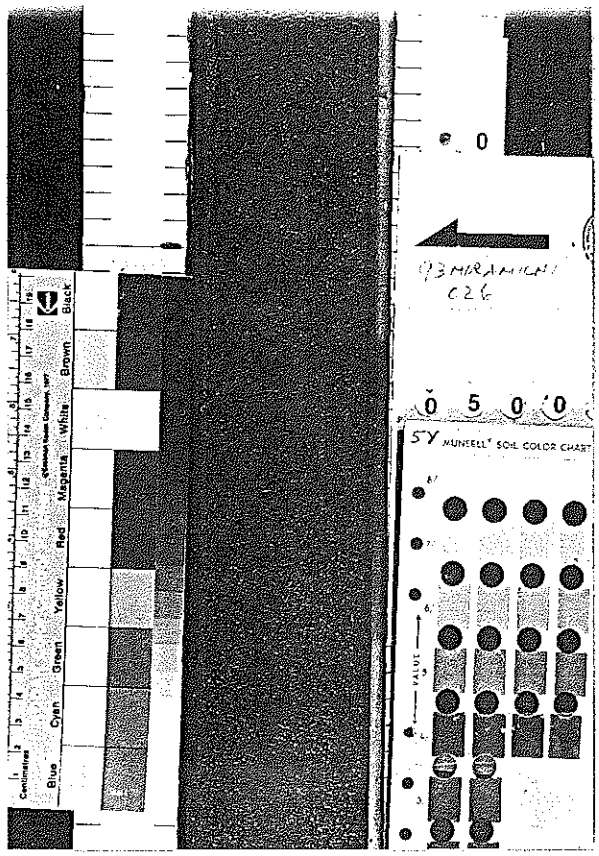
93 MIRAMICHI
026
0 5 0 0
5Y MUNSELL SOIL COLOR CHART

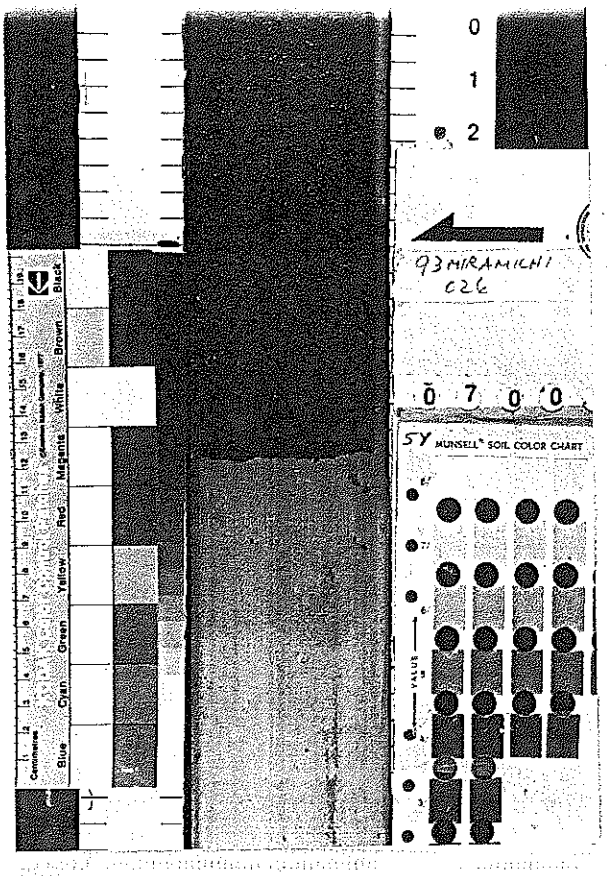
93 MIRAMICHI
026
0 7 0 0
5Y MUNSELL SOIL COLOR CHART

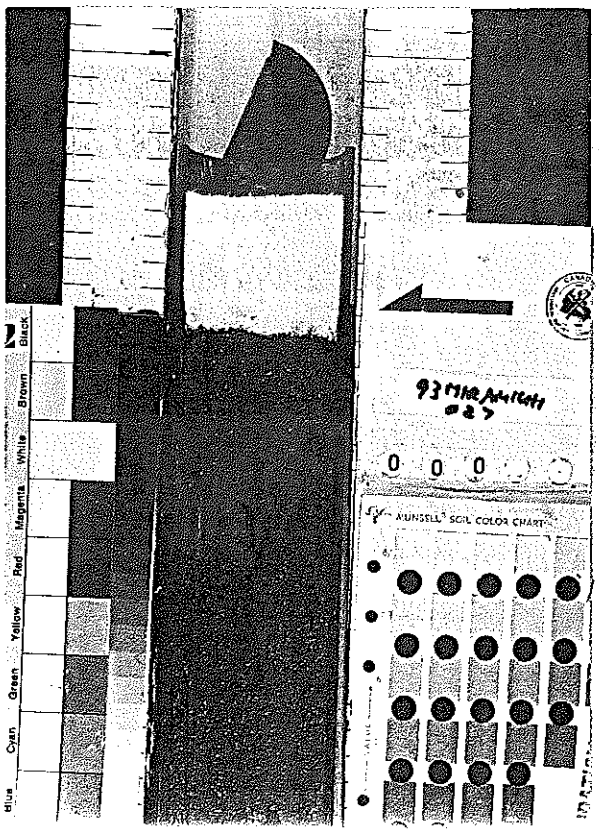
93 MIRAMICHI
027
0 0 0
5Y MUNSELL SOIL COLOR CHART

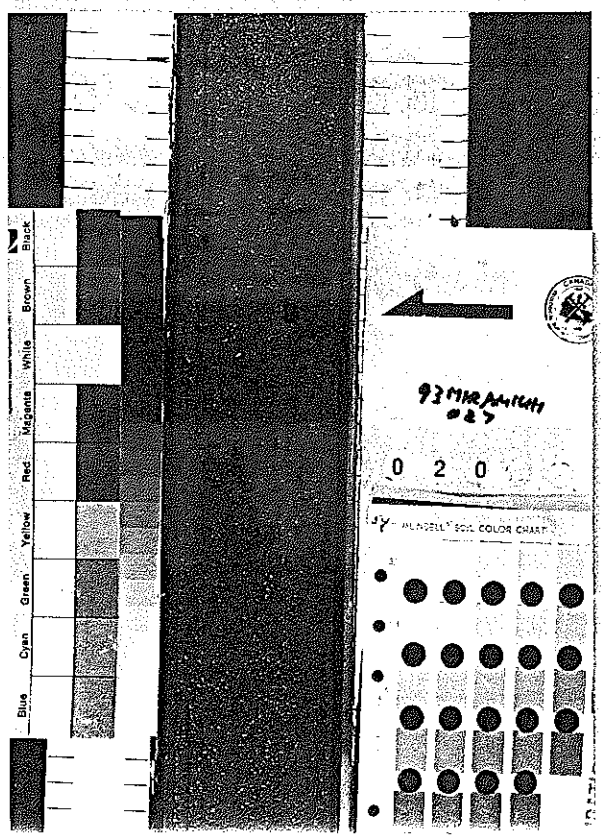
93 MIRAMICHI
027
0 2 0
5Y MUNSELL SOIL COLOR CHART

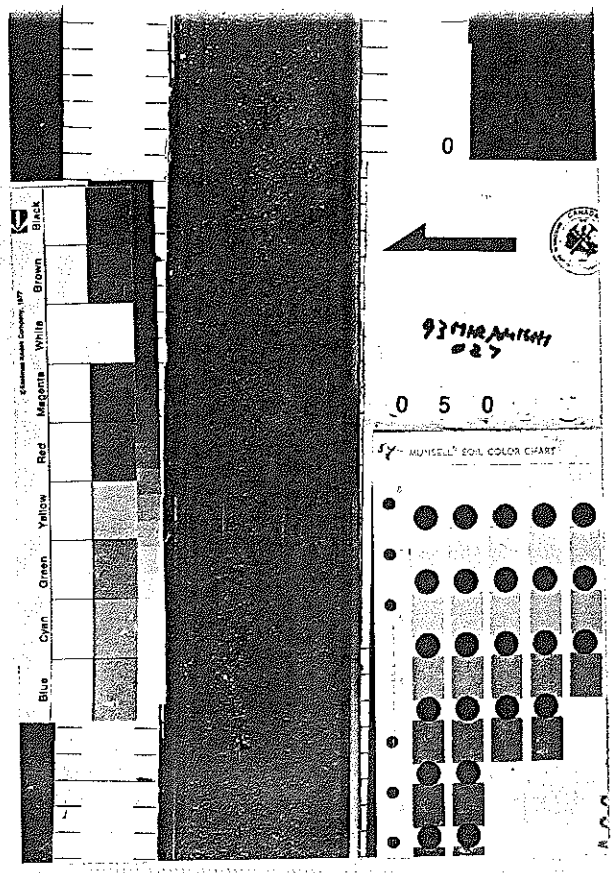
0
93MIRAMICHI
027
0 5 0
5Y MUNSELL® SOIL COLOR CHART
Black
Brown
White
Magenta
Red
Yellow
Green
Cyan
Blue

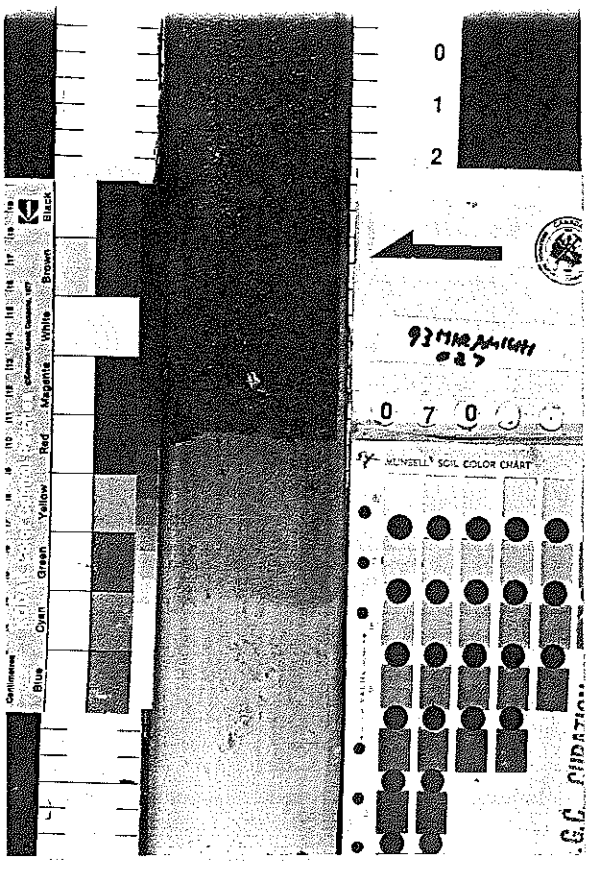
0
1
2
93MIRAMICHI
027
0 7 0
5Y MUNSELL® SOIL COLOR CHART
Black
Brown
White
Magenta
Red
Yellow
Green
Cyan
Blue

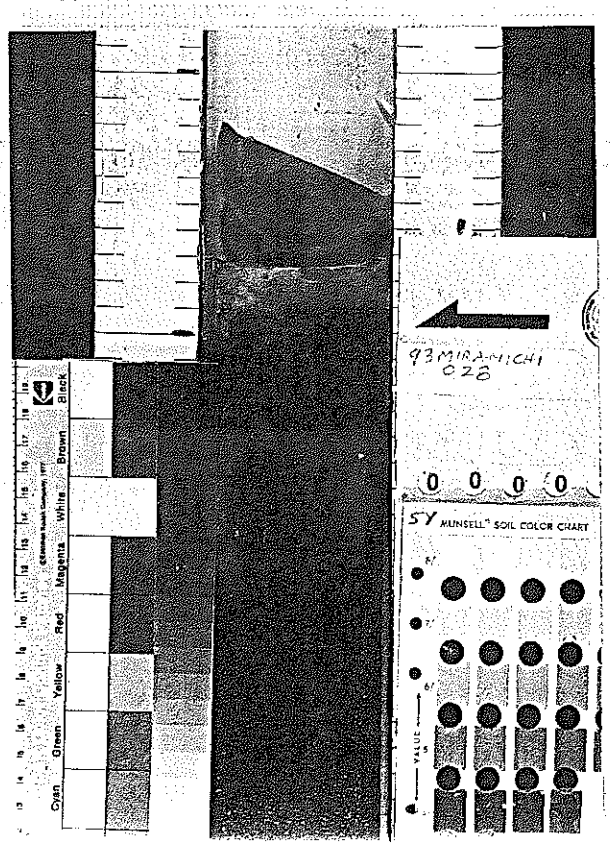
93MIRAMICHI
028
0 0 0 0
5Y MUNSELL® SOIL COLOR CHART
Black
Brown
White
Magenta
Red
Yellow
Green
Cyan
VALUE

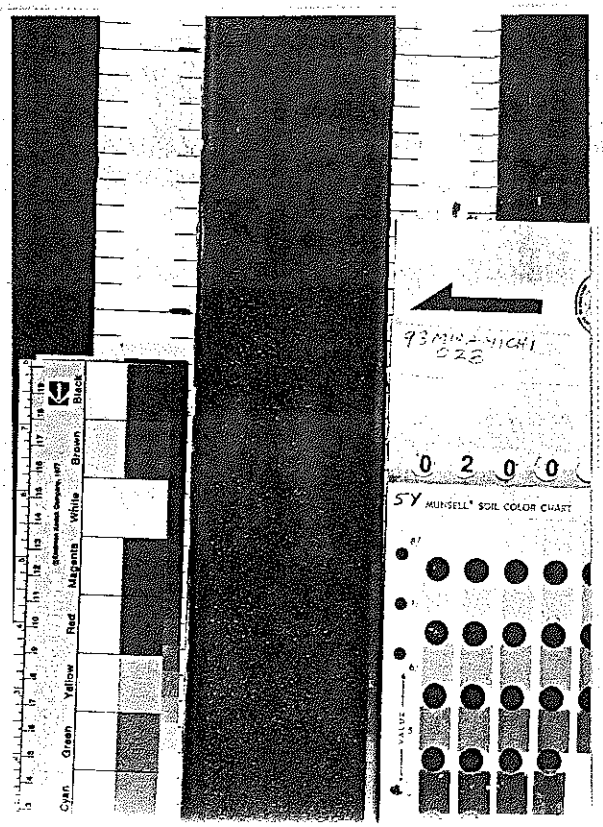
93MIRAMICHI
028
0 2 0 0
5Y MUNSELL® SOIL COLOR CHART
Black
Brown
White
Magenta
Red
Yellow
Green
Cyan
VALUE

10
93MIRAMICHI
028
0500
5Y MUNSELL® SOIL COLOR CHART

012
93MIRAMICHI
028
0700
5Y MUNSELL® SOIL COLOR CHART

93MIRAMICHI
029
0000
5Y MUNSELL® SOIL COLOR CHART

93MIRAMICHI
029
0200
5Y MUNSELL® SOIL COLOR CHART

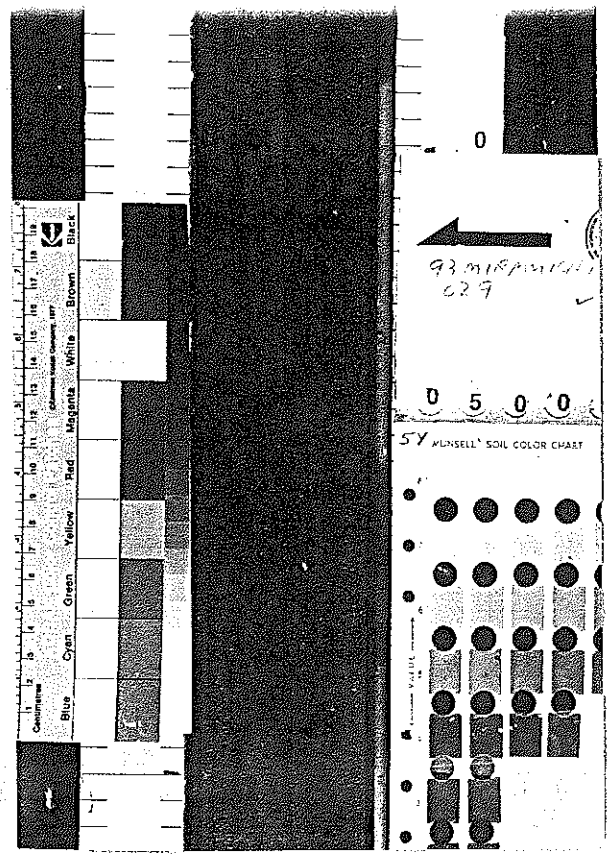
93MIRAMICHI
C29
0 5 0 0
5Y MUNSELL SOIL COLOR CHART

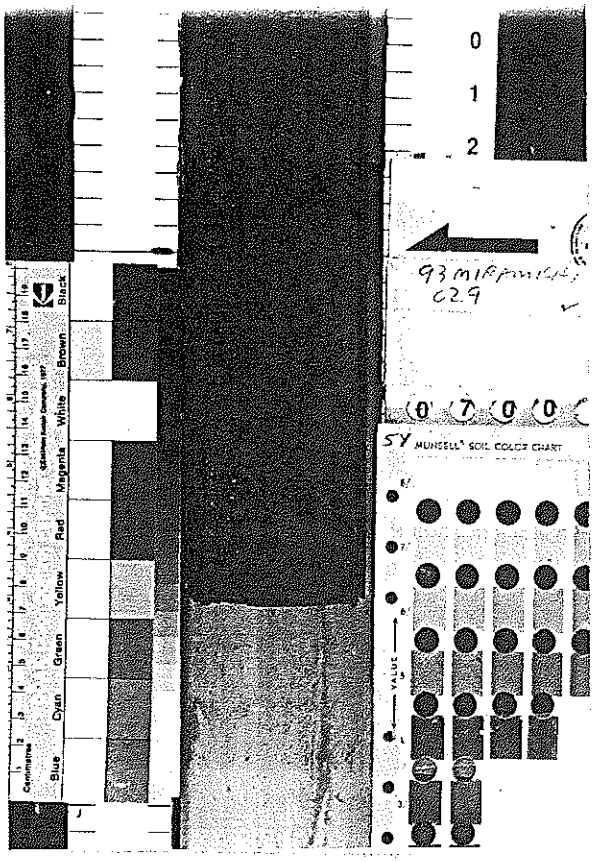
0
1
2
93MIRAMICHI
C29
0 7 0 0
5Y MUNSELL SOIL COLOR CHART

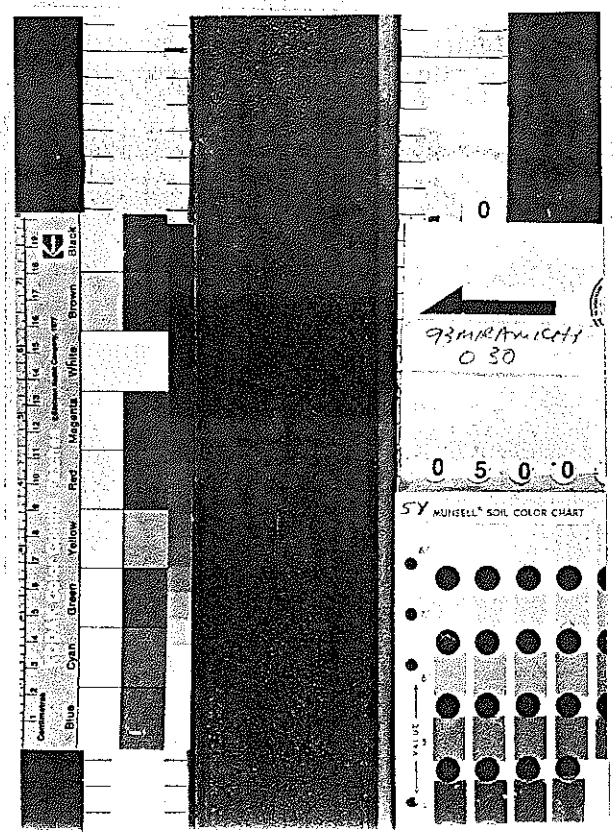
93MIRAMICHI
0 30
0 5 0 0
5Y MUNSELL SOIL COLOR CHART

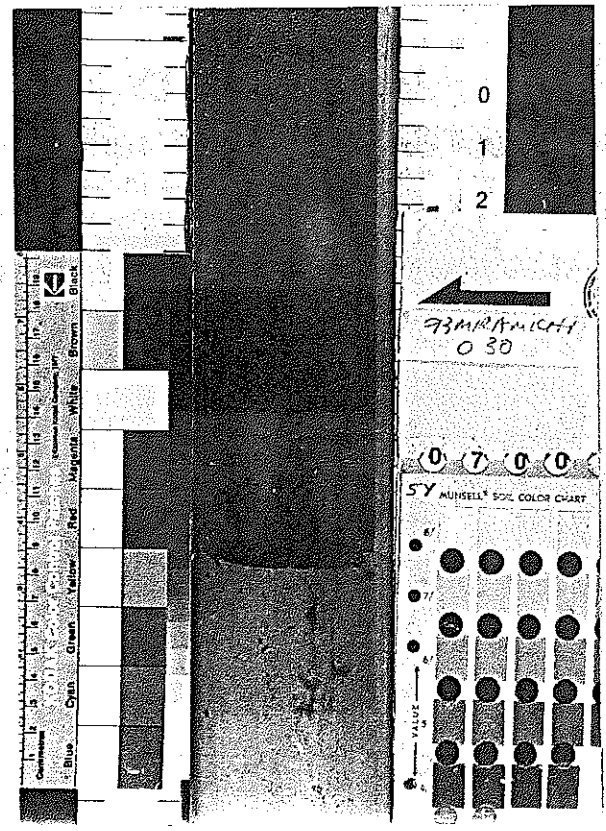
0
1
2
93MIRAMICHI
0 30
0 7 0 0
5Y MUNSELL SOIL COLOR CHART

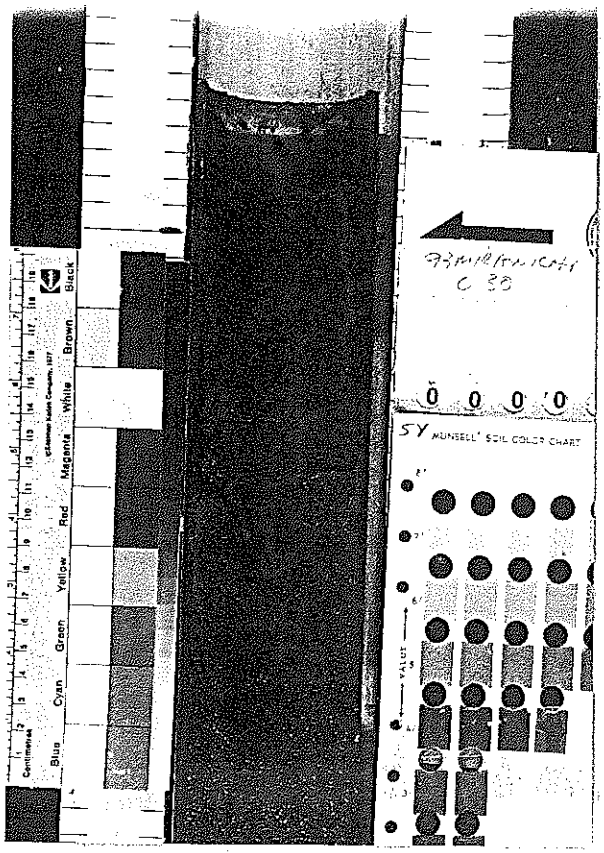
93MIRAMICHI
C 30
0 0 0 0
5Y MUNSELL SOIL COLOR CHART

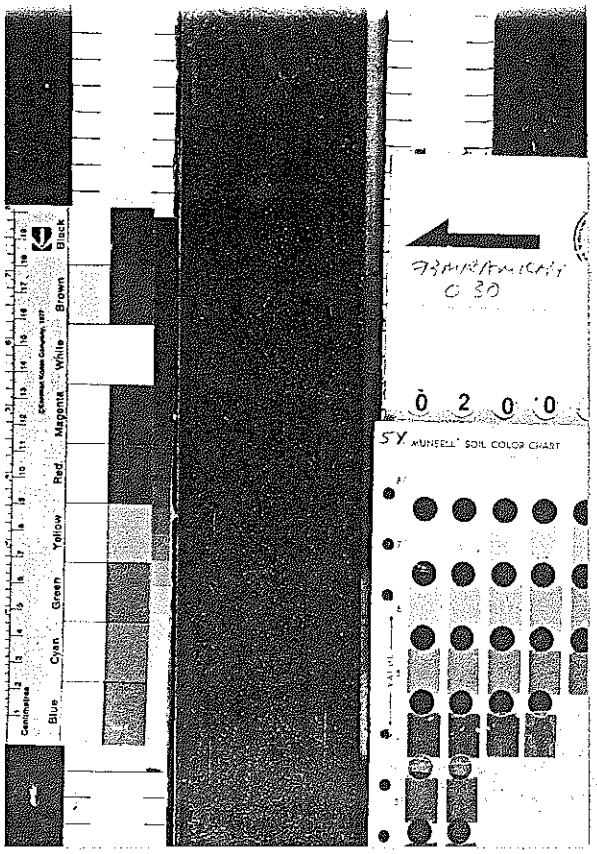
93MIRAMICHI
C 30
0 2 0 0
5Y MUNSELL SOIL COLOR CHART

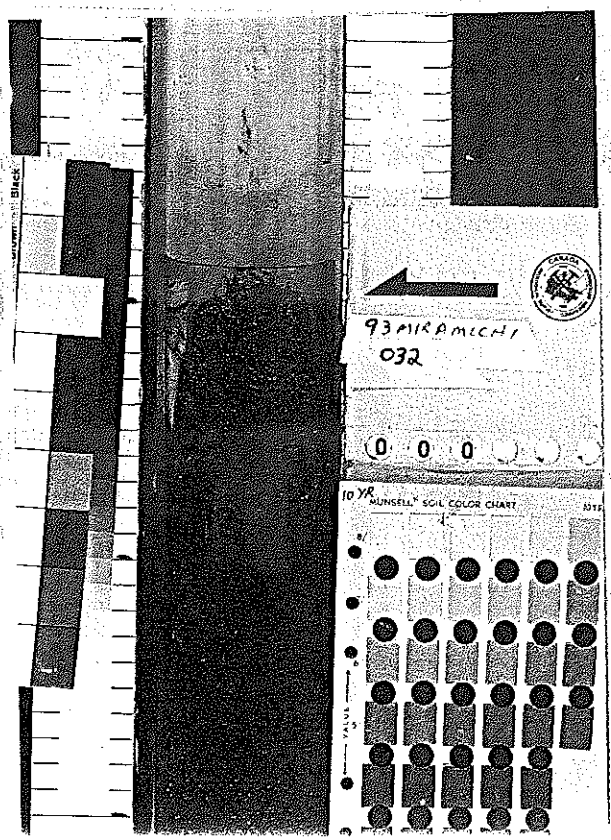
93MIRAMICHI
032
0 0 0
10YR MUNSELL SOIL COLOR CHART

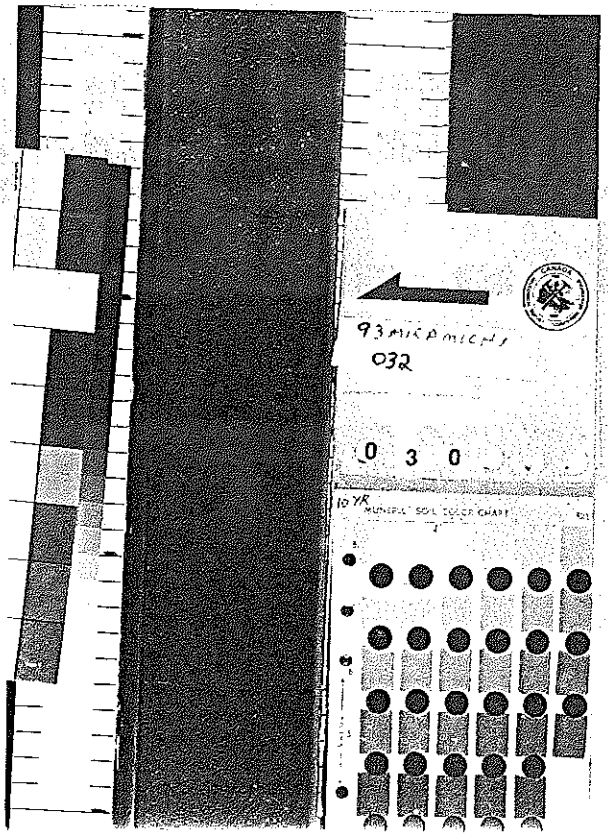
93MIRAMICHI
032
0 3 0
10YR MUNSELL SOIL COLOR CHART

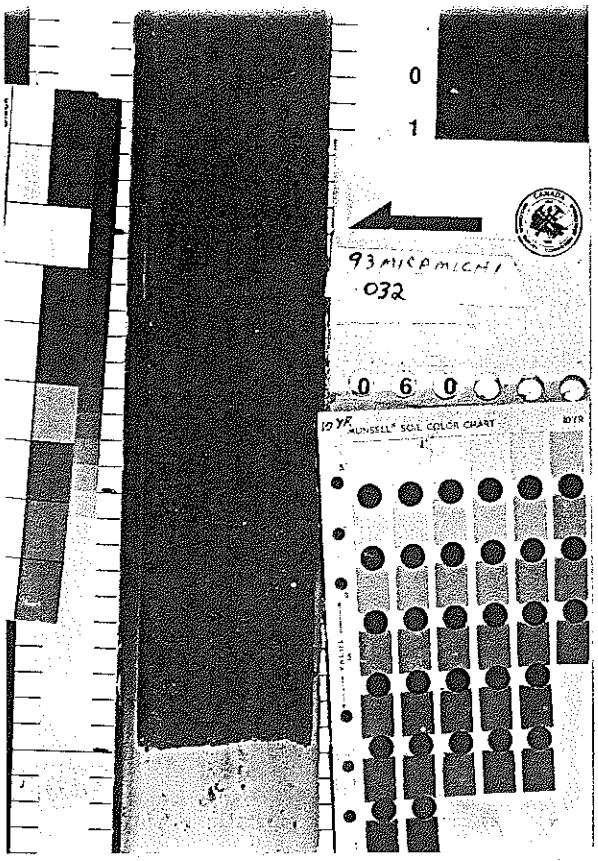
93 MIR AMICH 1
032
0 6 0
10 YR MUNSELL SOIL COLOR CHART

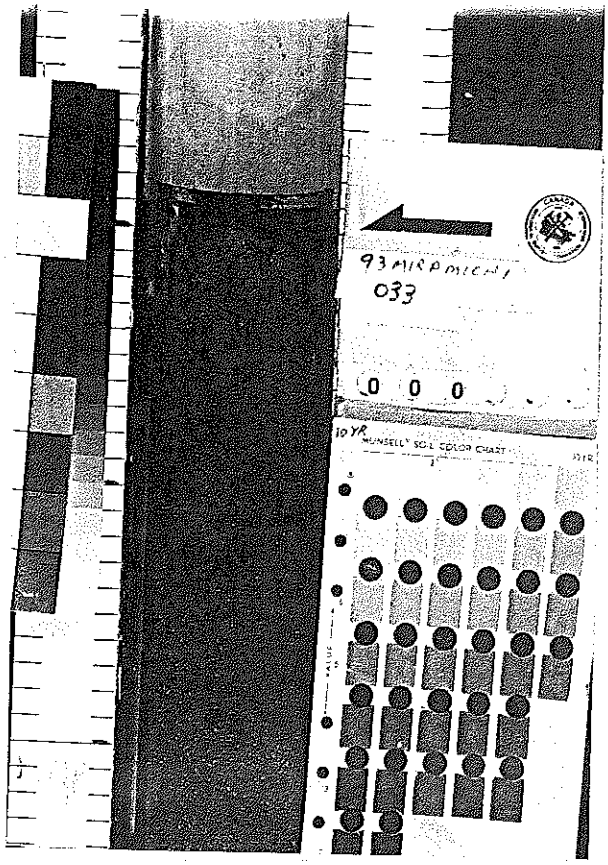
93 MIR AMICH 1
033
0 0 0
10 YR MUNSELL SOIL COLOR CHART

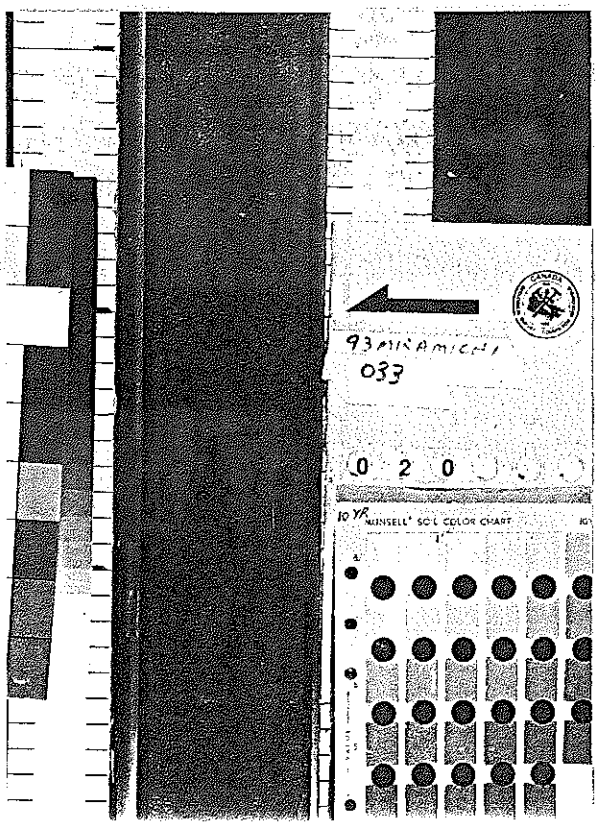
93 MIR AMICH 1
033
0 2 0
10 YR MUNSELL SOIL COLOR CHART

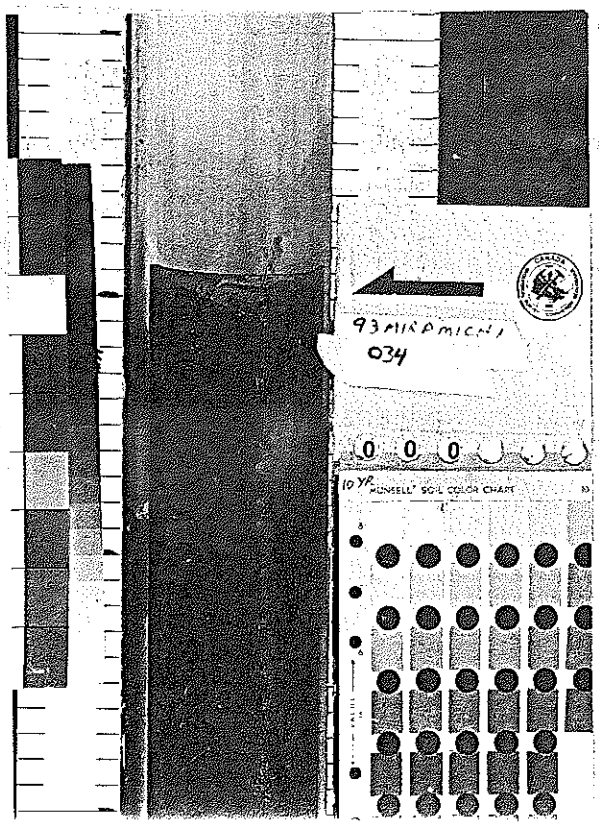
93 MIR AMICH 1
034
0 0 0
10 YR MUNSELL SOIL COLOR CHART

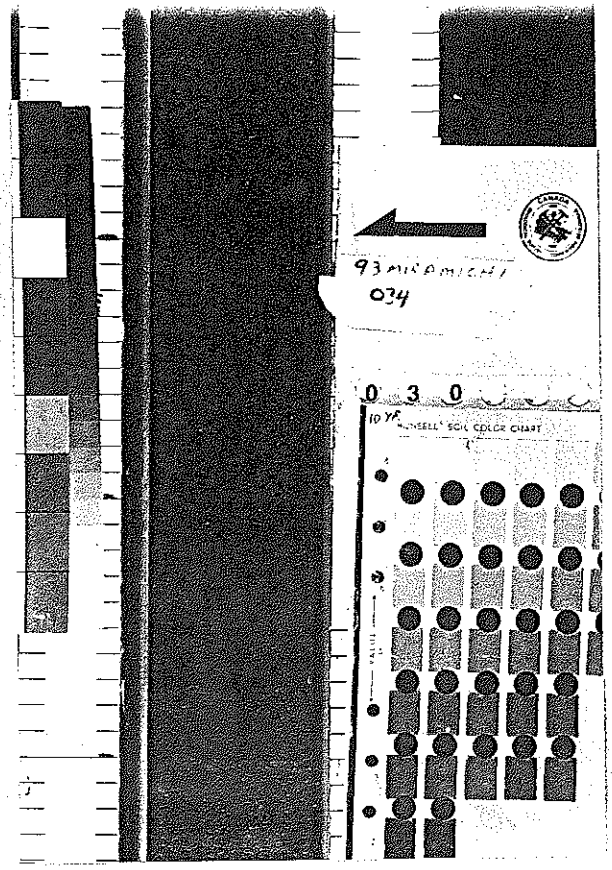
93MIRAMICHI
034
0 3 0
10 YR MUNSELL SOIL COLOR CHART

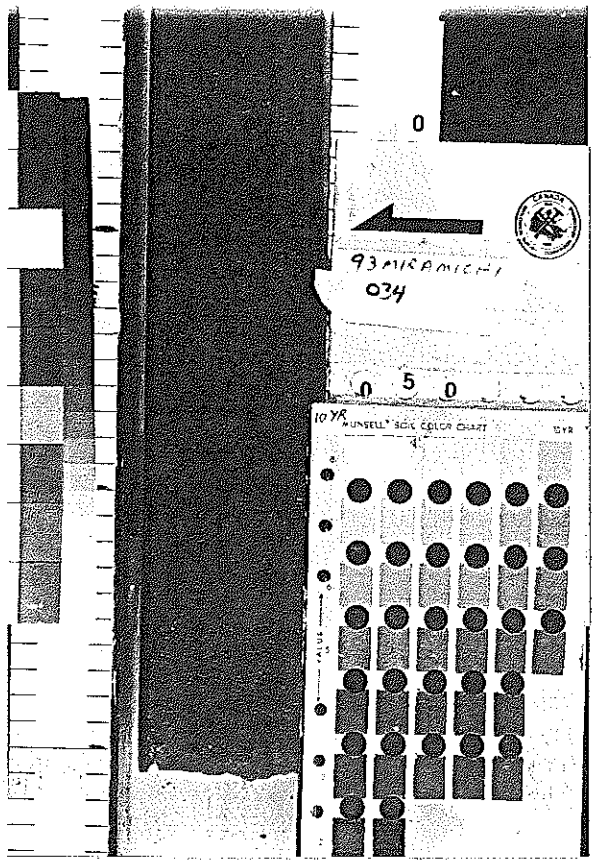
93MIRAMICHI
034
0 5 0
10 YR MUNSELL SOIL COLOR CHART

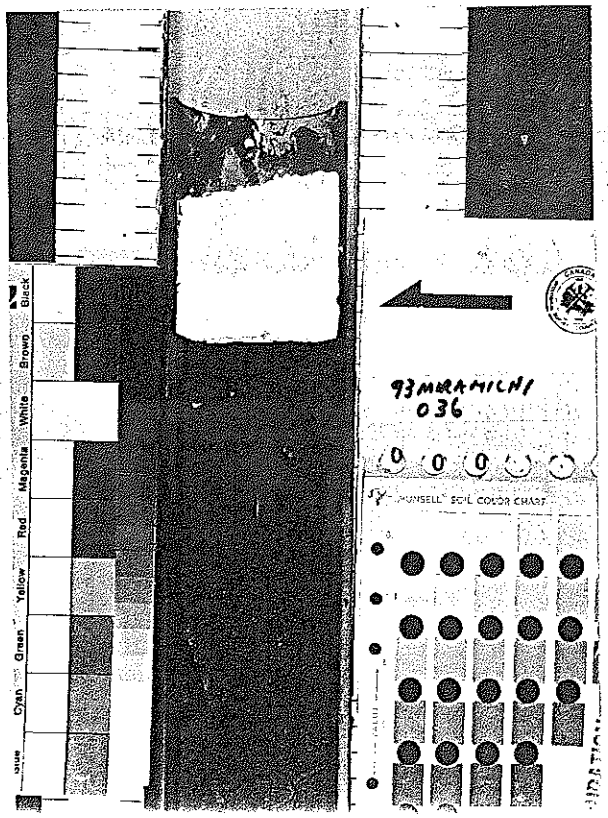
93MIRAMICHI
036
0 0 0
5Y MUNSELL SOIL COLOR CHART
Black
Brown
White
Magenta
Red
Yellow
Green
Cyan
Blue

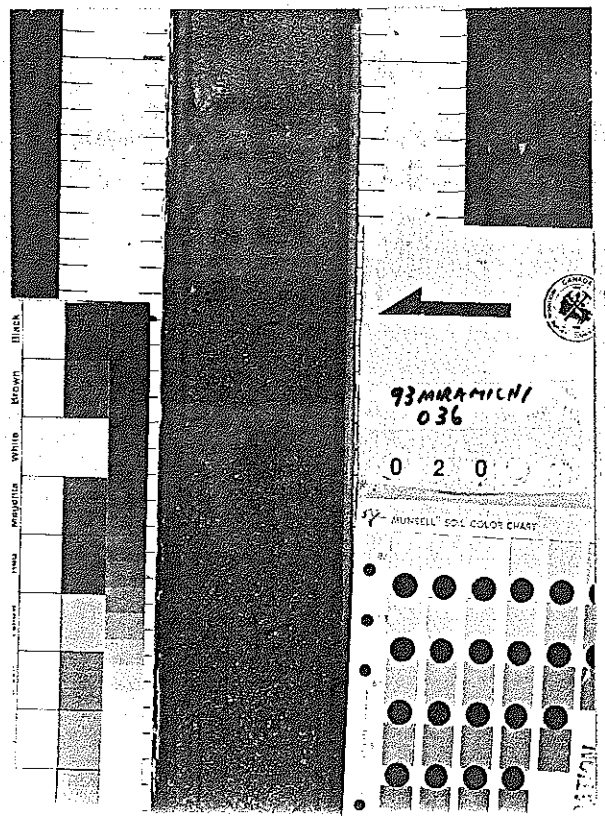
93MIRAMICHI
036
0 2 0
5Y MUNSELL SOIL COLOR CHART
Black
Brown
White
Magenta

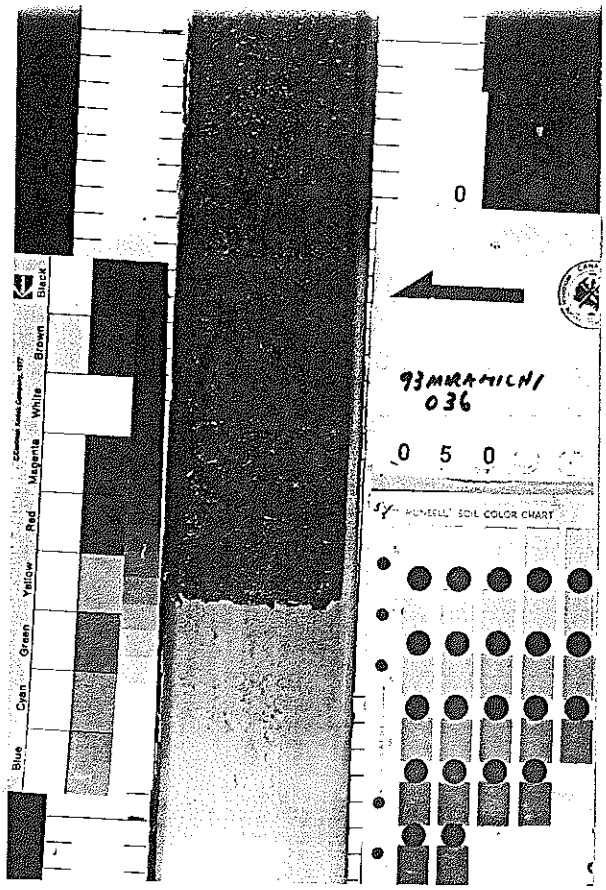
0
Black
Brown
White
Magenta
Red
Yellow
Green
Cyan
Blue
93MRAMICN1
036
0 5 0
MUNSELL SOIL COLOR CHART

APPENDIX E

Relationship Between Sea Carousel OBS Voltage and Suspended Sediment Concentration for Each Sea Carousel Deployment

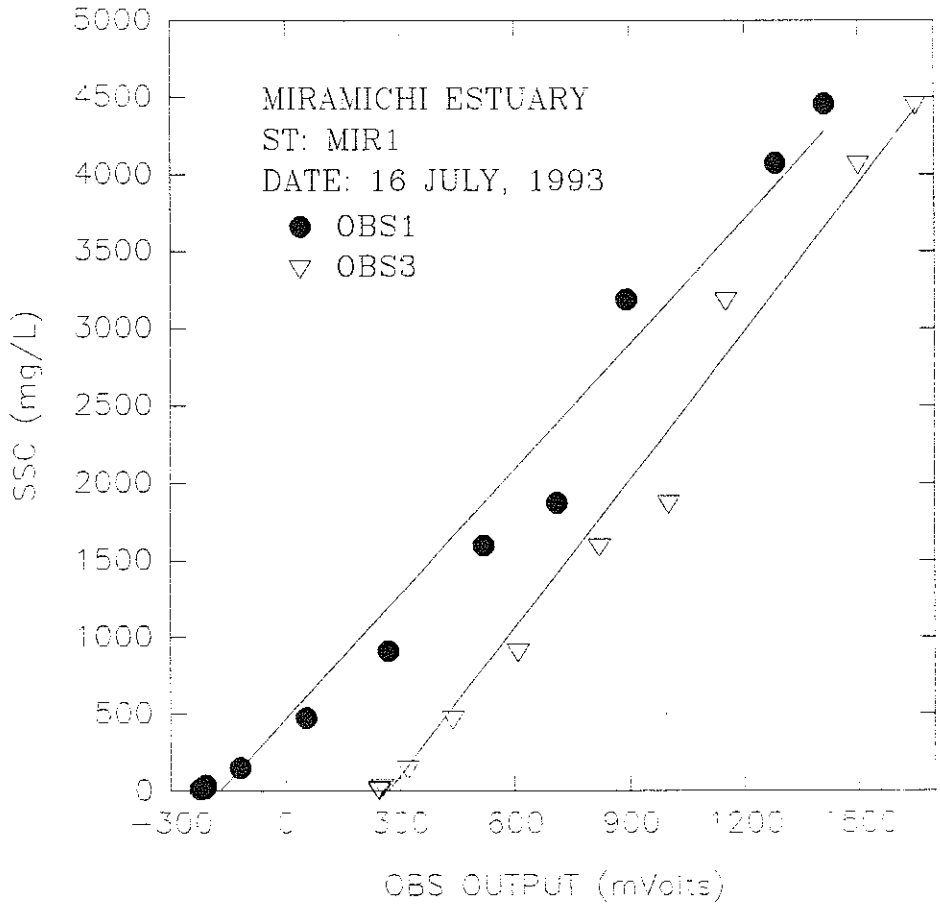
MIRAMICHI ESTUARY
ST: MIR1
DATE: 16 JULY, 1993
OBS1
OBS3
SSC (mg/L)
OBS OUTPUT (mVolts)
5000
4500
4000
3500
3000
2500
2000
1500
1000
500
0
-300
0
300
600
900
1200
1500

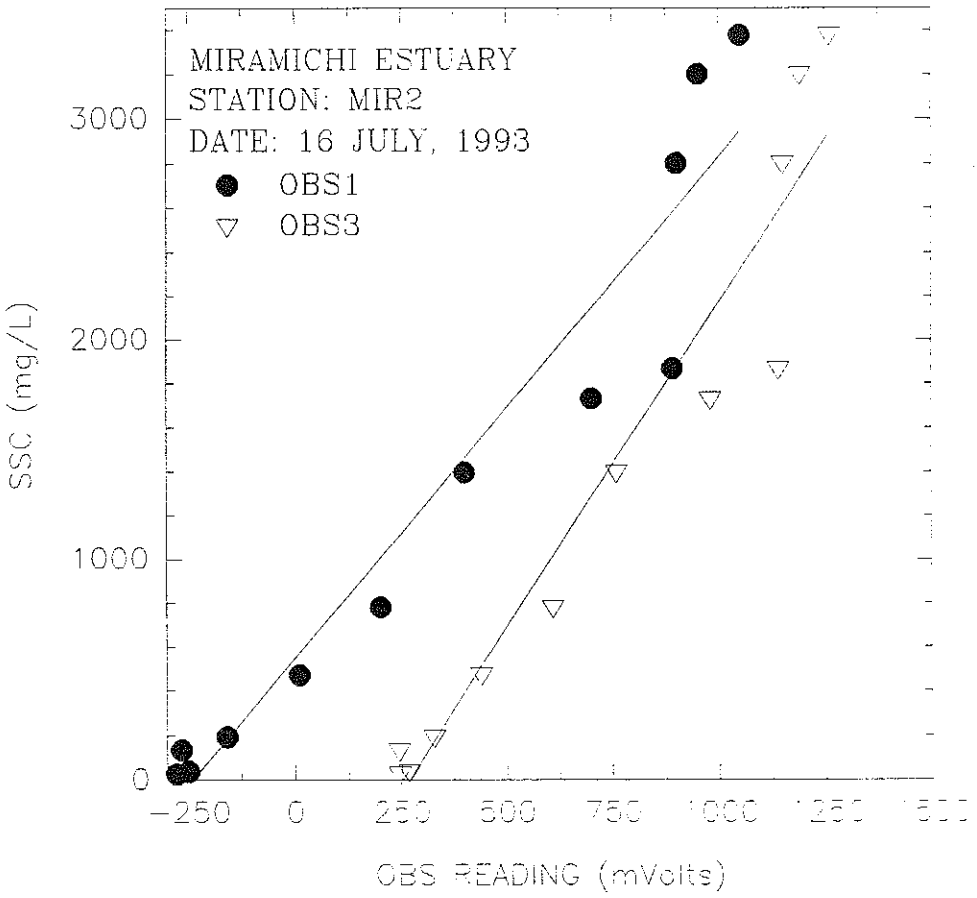
MIRAMICHI ESTUARY
STATION: MIR2
DATE: 16 JULY, 1993
OBS1
OBS3
SSC (mg/L)
3000
2000
1000
0
−250
0
250
500
750
1000
OBS READING (mVolts)

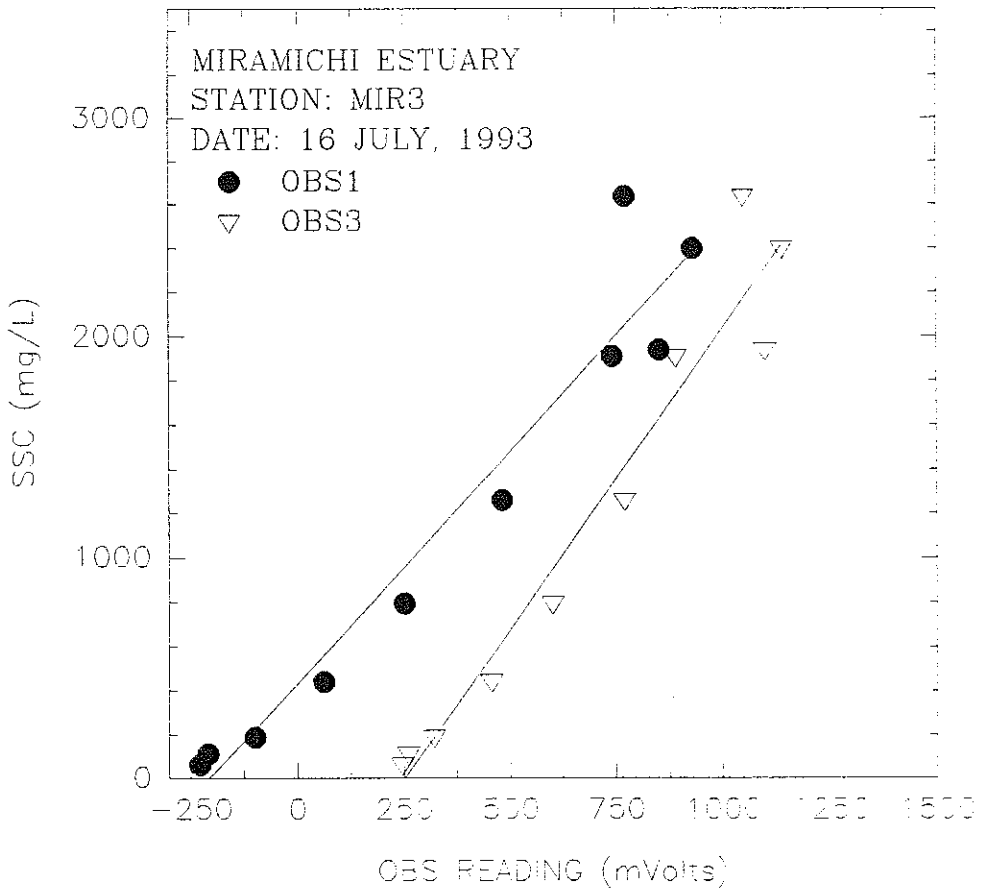
MIRAMICHI ESTUARY
STATION: MIR3
DATE: 16 JULY, 1993
OBS1
OBS3
SSC (mg/L)
3000
2000
1000
0
−250
0
250
500
750
1000
1250
1500
OBS READING (mVolts)

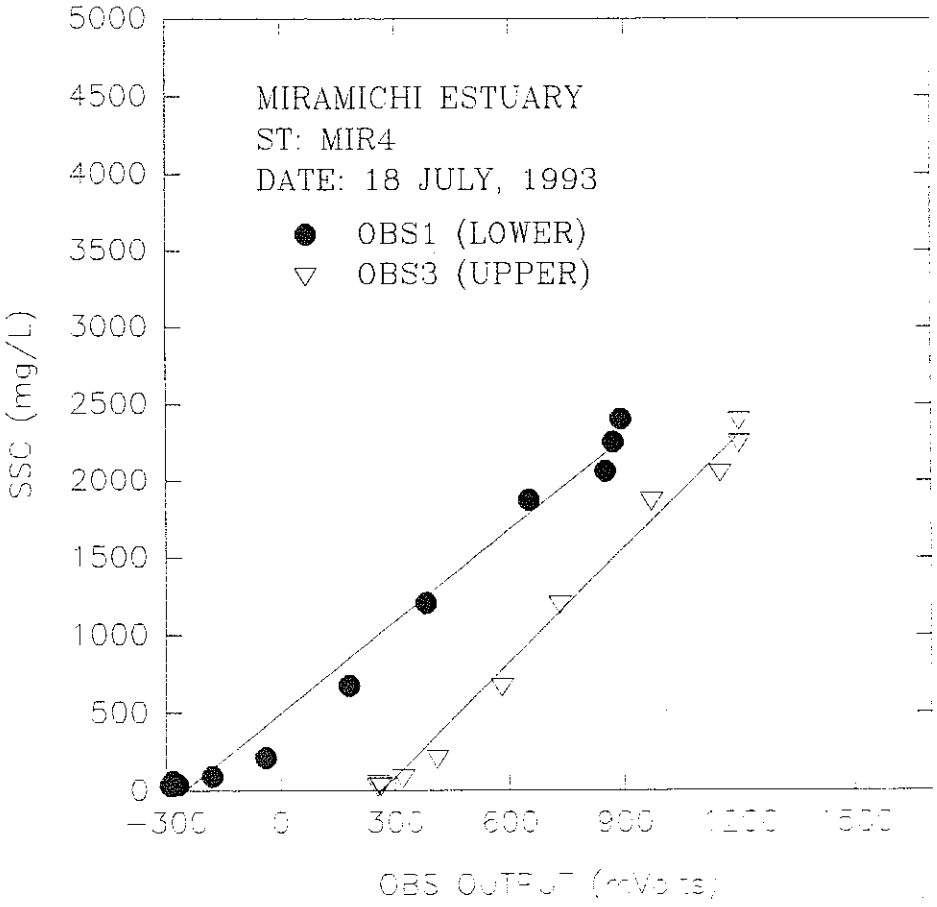
MIRAMICHI ESTUARY
ST: MIR4
DATE: 18 JULY, 1993
OBS1 (LOWER)
OBS3 (UPPER)
SSC (mg/L)
5000
4500
4000
3500
3000
2500
2000
1500
1000
500
0
-300
0
300
600
900
1200
1500

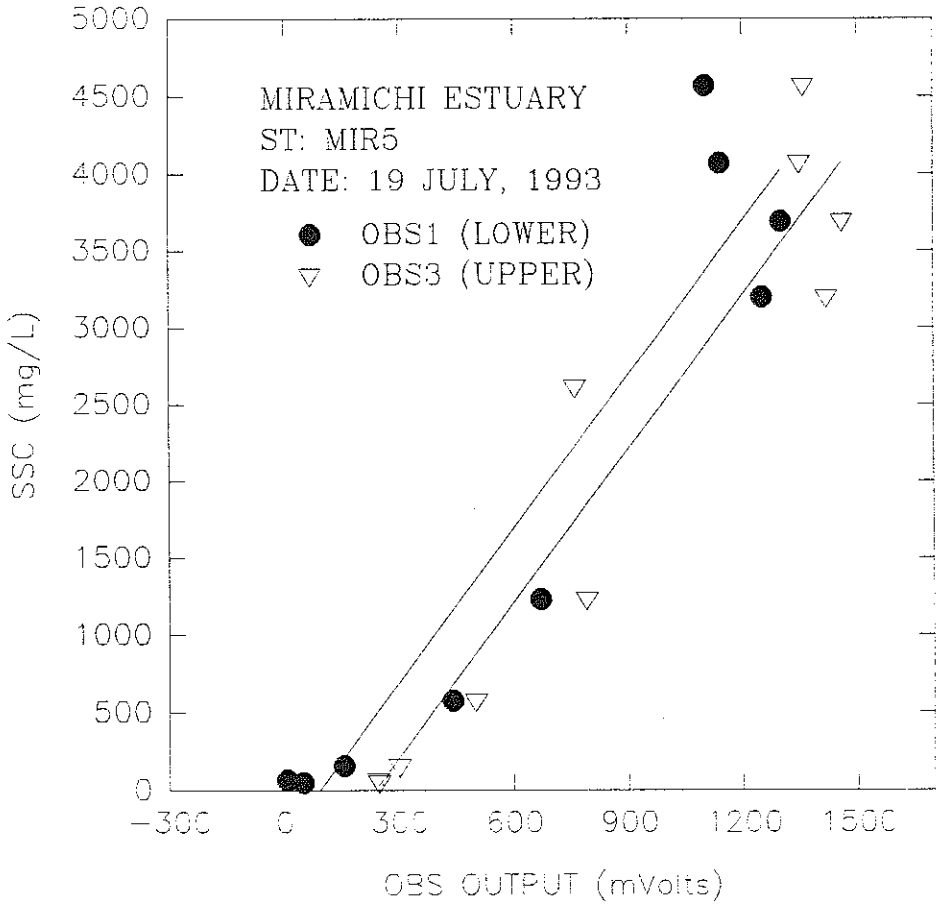
MIRAMICHI ESTUARY
ST: MIR5
DATE: 19 JULY, 1993
OBS1 (LOWER)
OBS3 (UPPER)
SSC (mg/L)
OBS OUTPUT (mVolts)
5000
4500
4000
3500
3000
2500
2000
1500
1000
500
0
-300
0
300
600
900
1200
1500

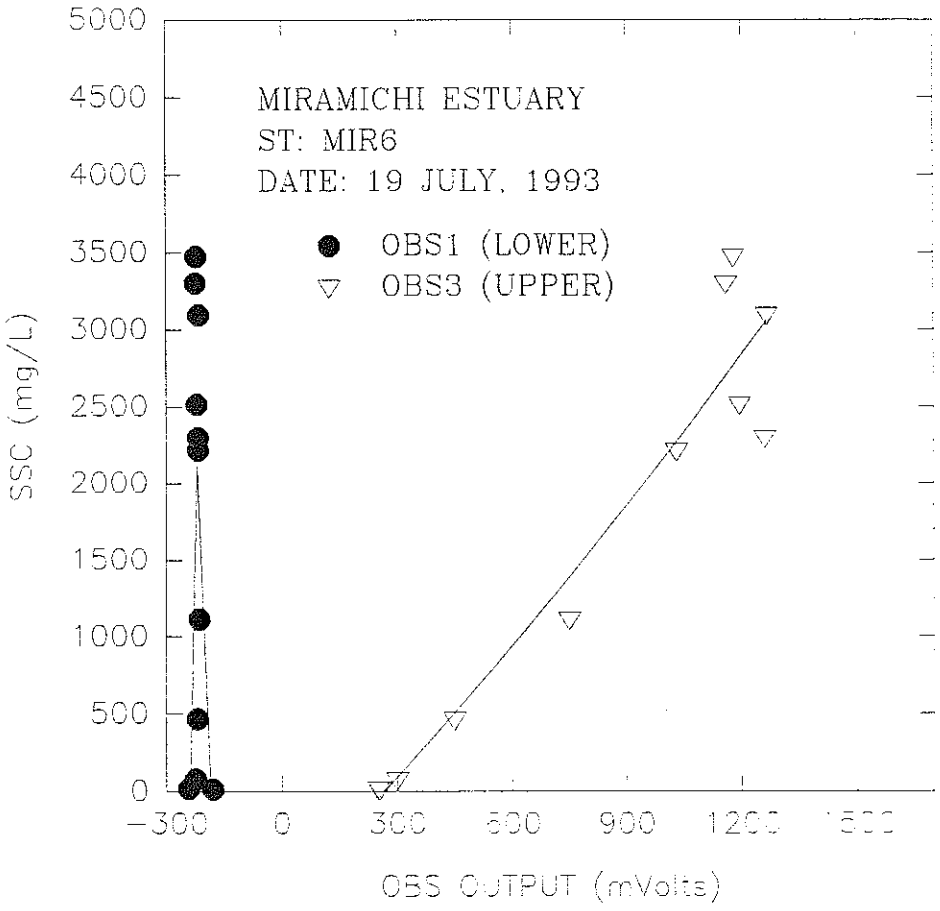
MIRAMICHI ESTUARY
ST: MIR6
DATE: 19 JULY, 1993
OBS1 (LOWER)
OBS3 (UPPER)
SSC (mg/L)
OBS OUTPUT (mVolts)
5000
4500
4000
3500
3000
2500
2000
1500
1000
500
0
-300
0
300
600
900
1200

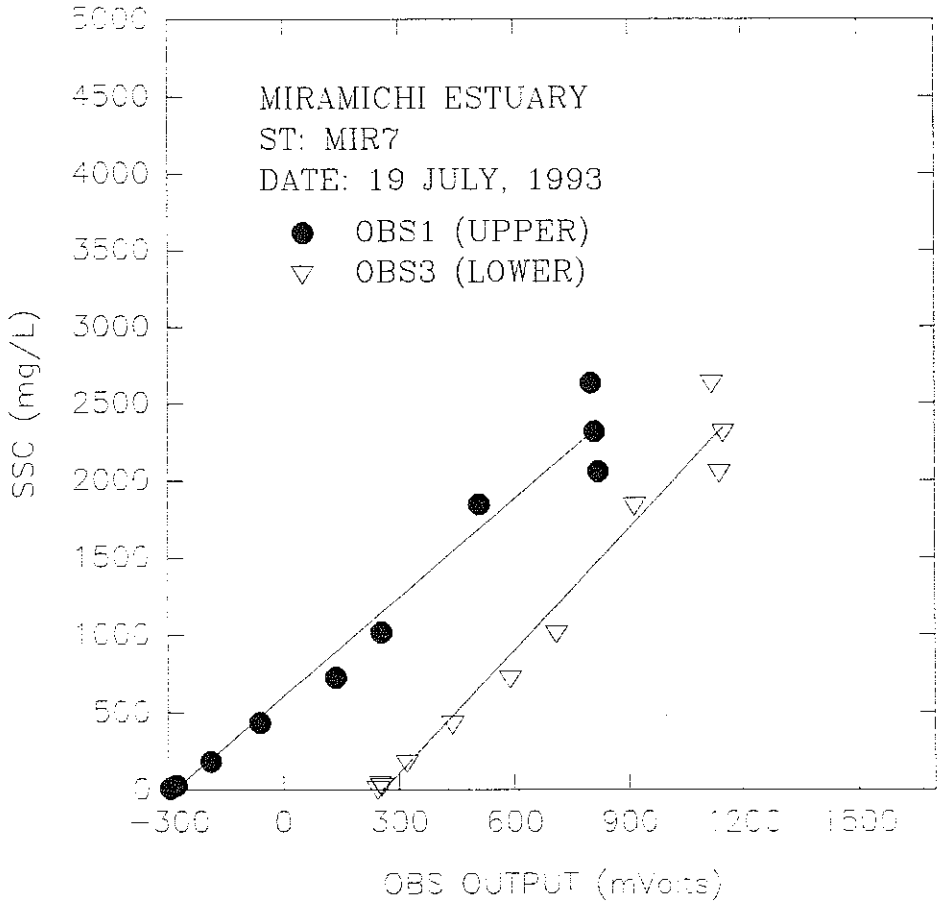
MIRAMICHI ESTUARY
ST: MIR7
DATE: 19 JULY, 1993
OBS1 (UPPER)
OBS3 (LOWER)
SSC (mg/L)
OBS OUTPUT (mVolts)
5000
4500
4000
3500
3000
2500
2000
1500
1000
500
0
-300
0
300
600
900
1200
1500

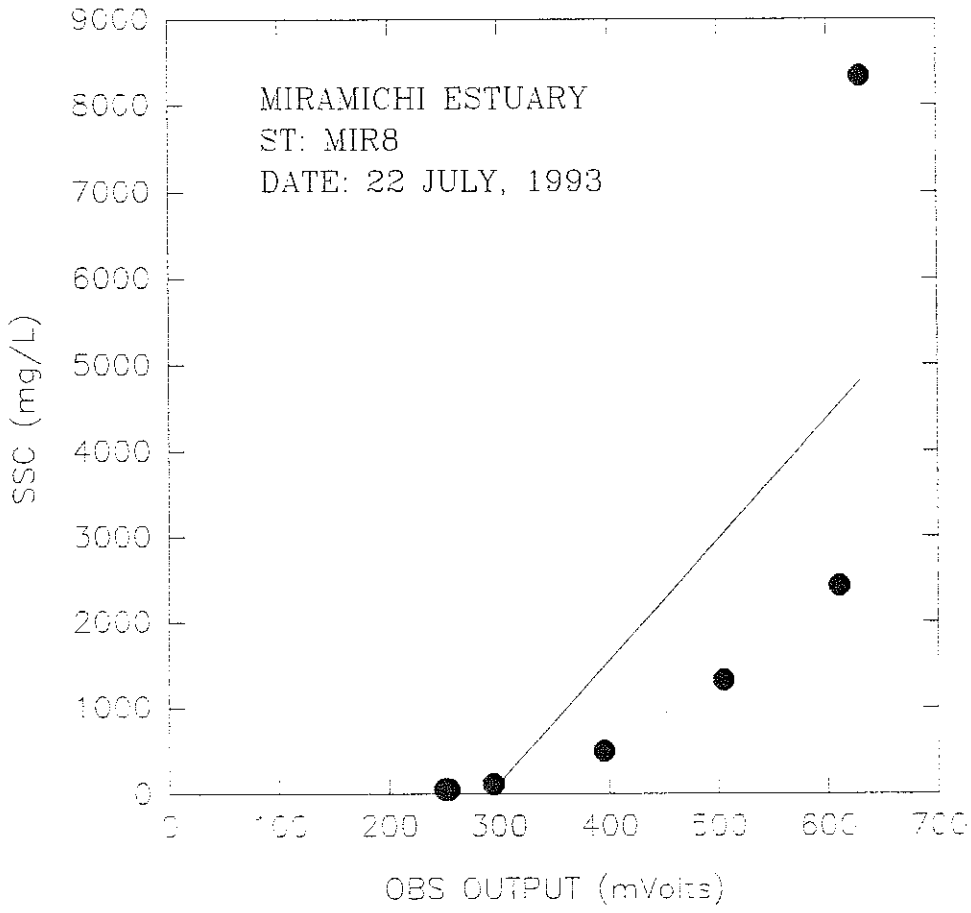
MIRAMICHI ESTUARY
ST: MIR8
DATE: 22 JULY, 1993
SSC (mg/L)
OBS OUTPUT (mVolts)
9000
8000
7000
6000
5000
4000
3000
2000
1000
0
0
100
200
300
400
500
600
700

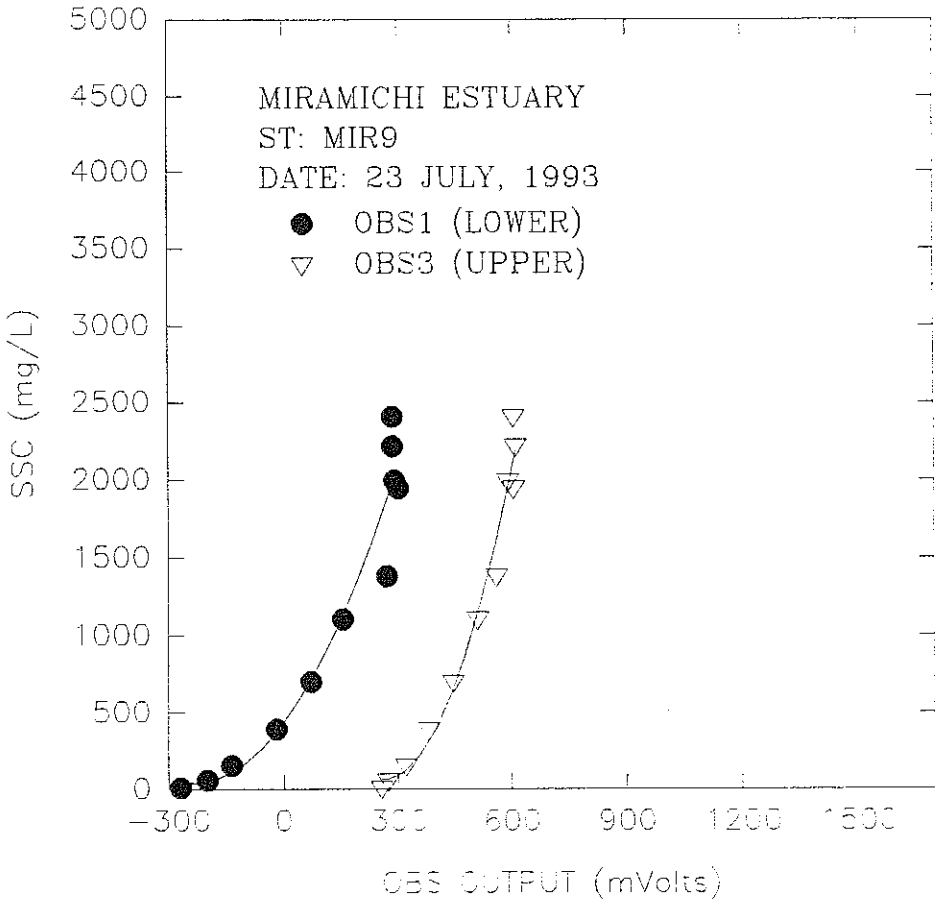
MIRAMICHI ESTUARY
ST: MIR9
DATE: 23 JULY, 1993
OBS1 (LOWER)
OBS3 (UPPER)
SSC (mg/L)
OBS OUTPUT (mVolts)
5000
4500
4000
3500
3000
2500
2000
1500
1000
500
0
−300
0
300
600
900
1200

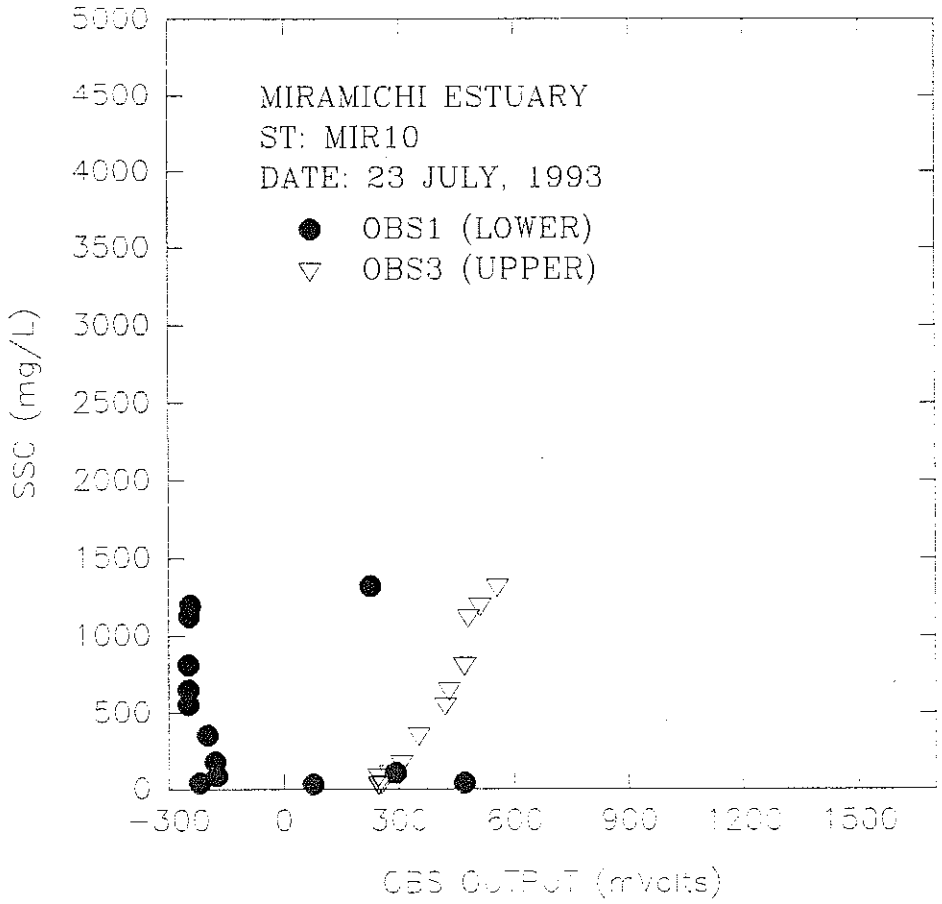
MIRAMICHI ESTUARY
ST: MIR10
DATE: 23 JULY, 1993
OBS1 (LOWER)
OBS3 (UPPER)
SSC (mg/L)
OBS OUTPUT (mVolts)
5000
4500
4000
3500
3000
2500
2000
1500
1000
500
0
-300
0
300
600
900
1200
1500

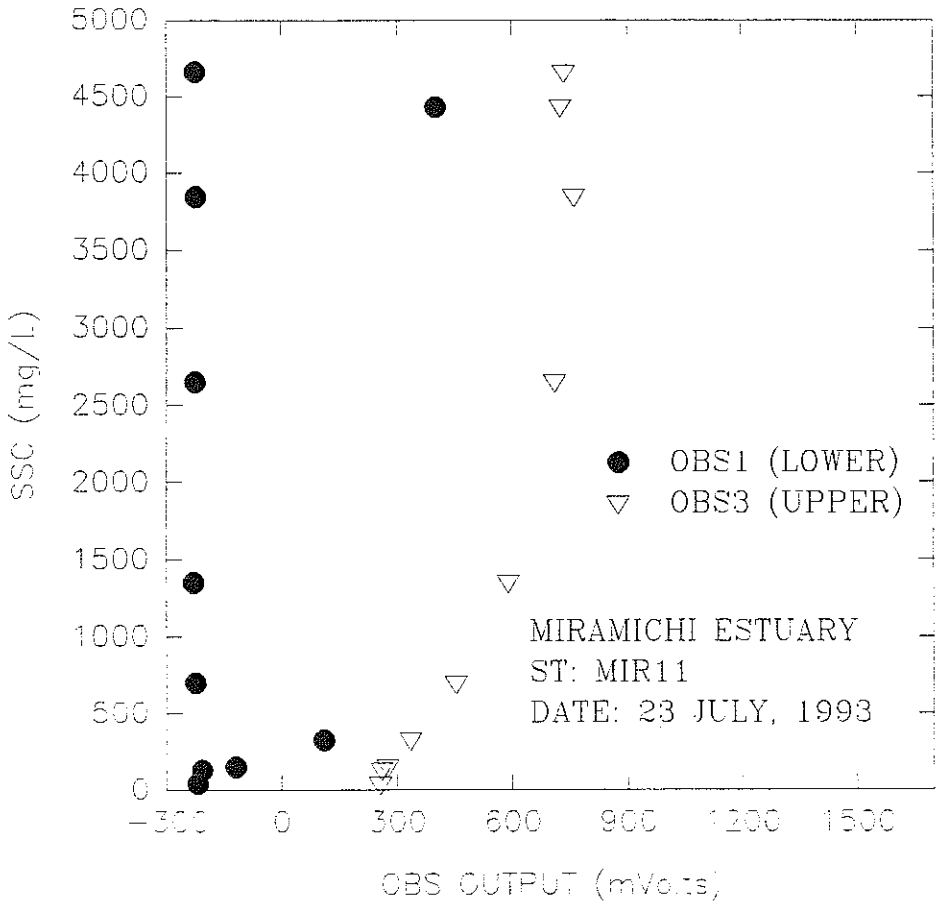
5000
4500
4000
3500
3000
2500
2000
1500
1000
500
0
SSC (mg/L)
−300
0
300
600
900
1200
1500
OBS OUTPUT (mVolts)
OBS1 (LOWER)
OBS3 (UPPER)
MIRAMICHI ESTUARY
ST: MIR11
DATE: 23 JULY, 1993

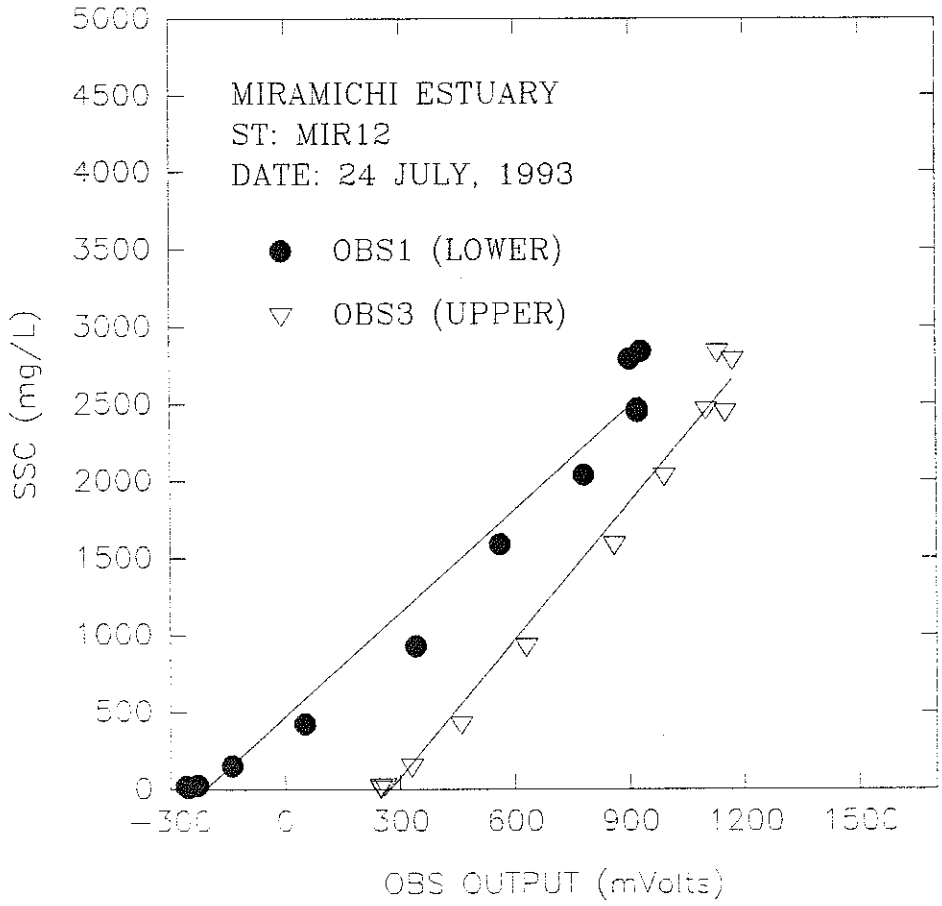
MIRAMICHI ESTUARY
ST: MIR12
DATE: 24 JULY, 1993
OBS1 (LOWER)
OBS3 (UPPER)
SSC (mg/L)
OBS OUTPUT (mVolts)
5000
4500
4000
3500
3000
2500
2000
1500
1000
500
0
-300
0
300
600
900
1200
1500

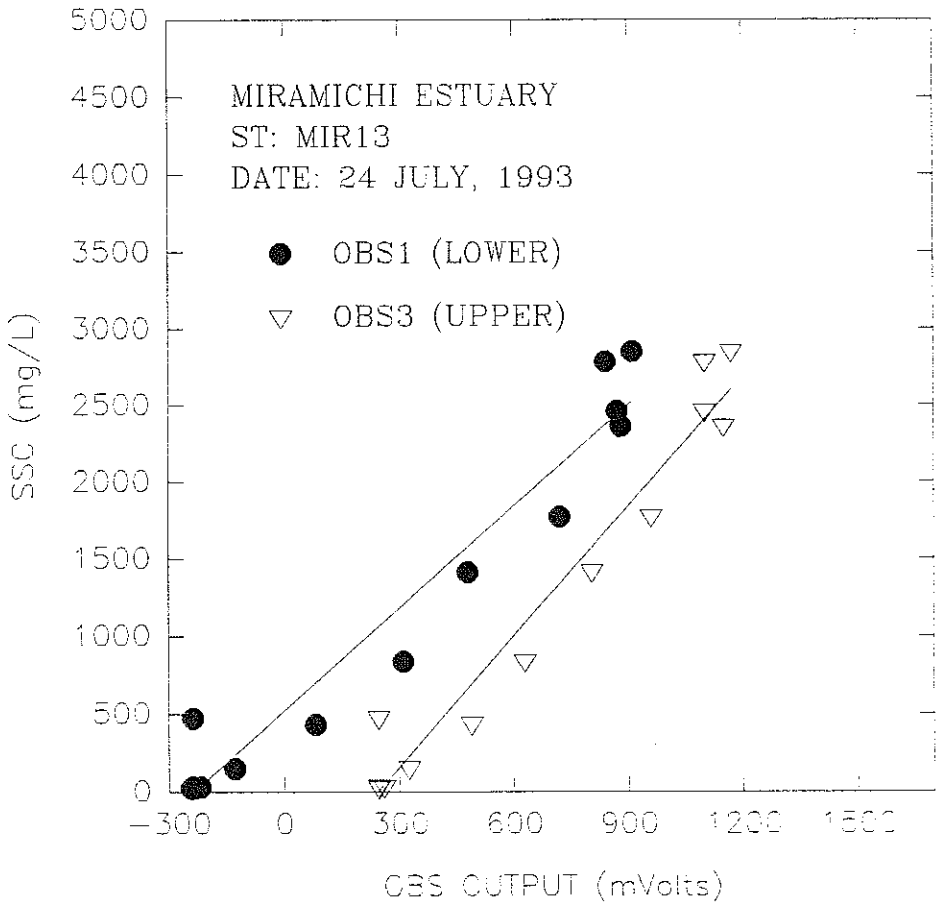
MIRAMICHI ESTUARY
ST: MIR13
DATE: 24 JULY, 1993
OBS1 (LOWER)
OBS3 (UPPER)
SSC (mg/L)
OBS OUTPUT (mVolts)
5000
4500
4000
3500
3000
2500
2000
1500
1000
500
0
−300
0
300
600
900

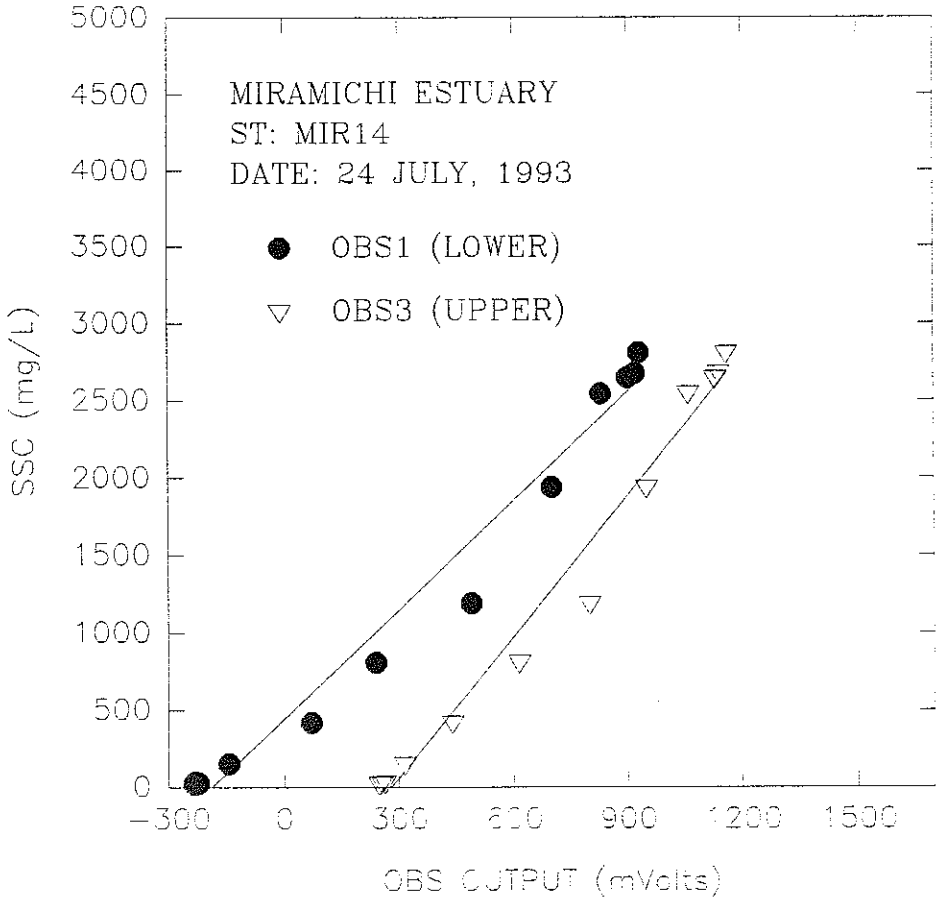
MIRAMICHI ESTUARY
ST: MIR14
DATE: 24 JULY, 1993
OBS1 (LOWER)
OBS3 (UPPER)
SSC (mg/L)
OBS OUTPUT (mVolts)
5000
4500
4000
3500
3000
2500
2000
1500
1000
500
0
−300
0
300
600
900
1200
1500

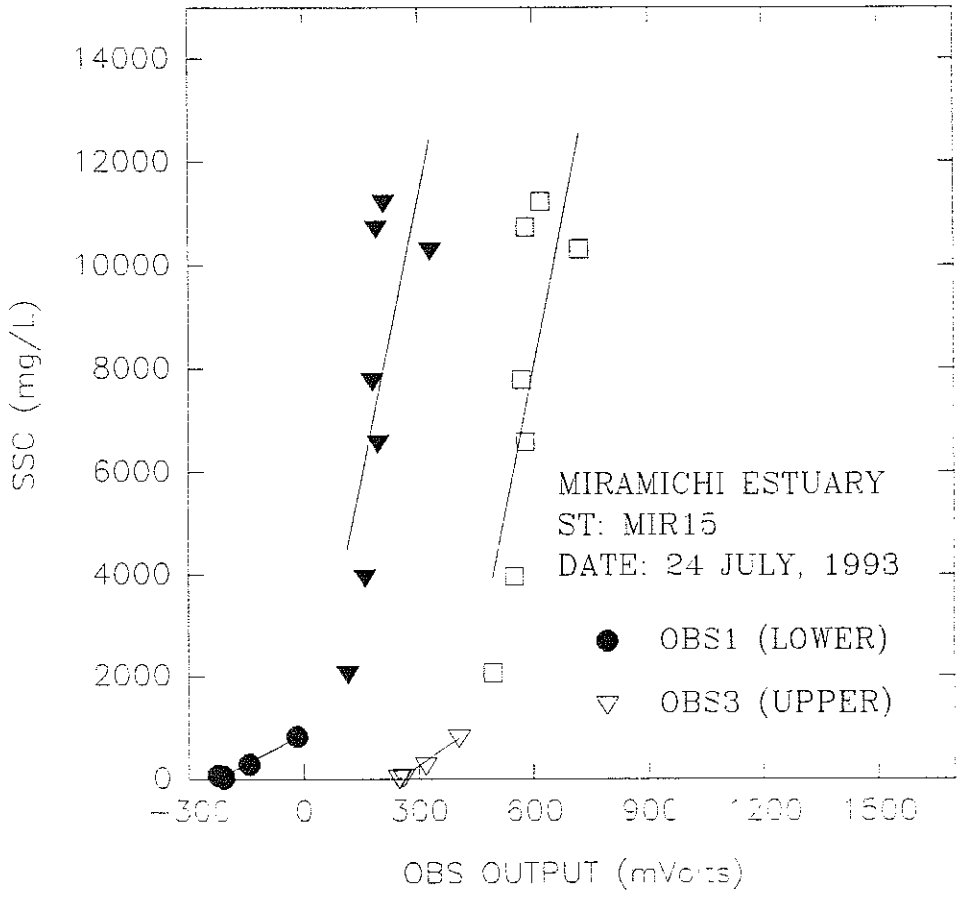
14000
12000
10000
8000
6000
4000
2000
0
SSC (mg/L)
-300
0
300
600
900
1200
1500
OBS OUTPUT (mVolts)
MIRAMICHI ESTUARY
ST: MIR15
DATE: 24 JULY, 1993
OBS1 (LOWER)
OBS3 (UPPER)

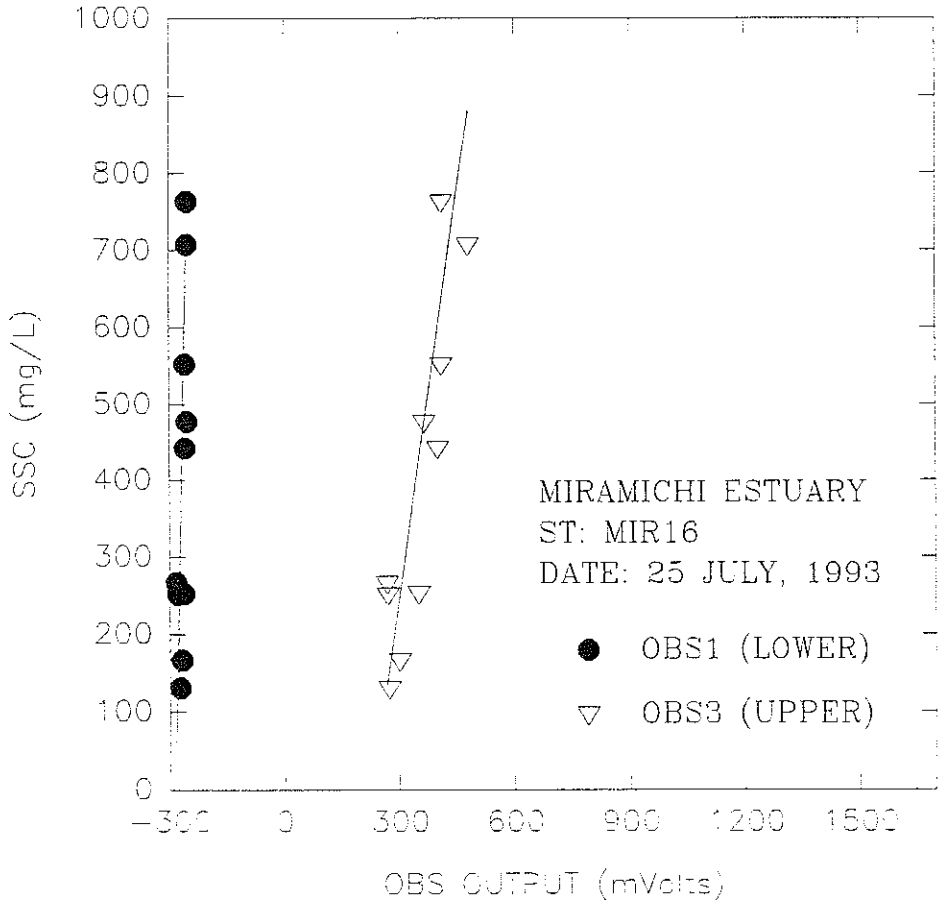
1000
900
800
700
600
500
400
300
200
100
0
SSC (mg/L)
−300
0
300
600
900
1200
1500
OBS OUTPUT (mVolts)
MIRAMICHI ESTUARY
ST: MIR16
DATE: 25 JULY, 1993
OBS1 (LOWER)
OBS3 (UPPER)

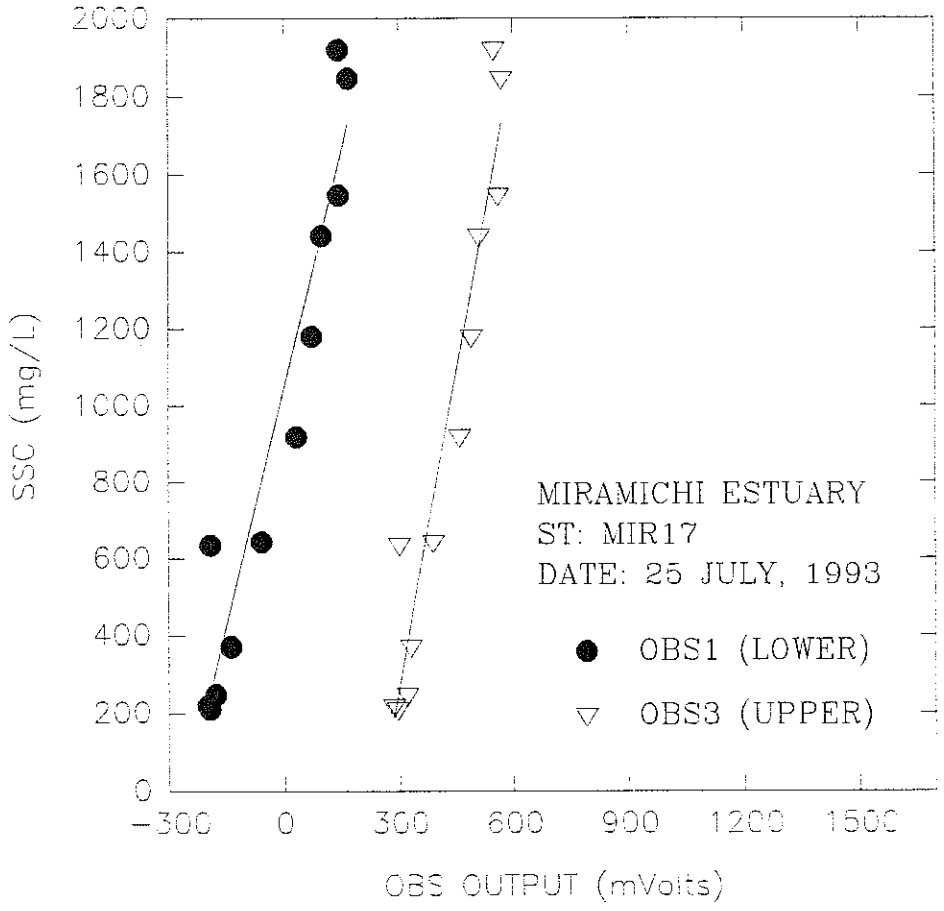
2000
1800
1600
1400
1200
1000
800
600
400
200
0
SSC (mg/L)
−300
0
300
600
900
1200
1500
OBS OUTPUT (mVolts)
MIRAMICHI ESTUARY
ST: MIR17
DATE: 25 JULY, 1993
OBS1 (LOWER)
OBS3 (UPPER)

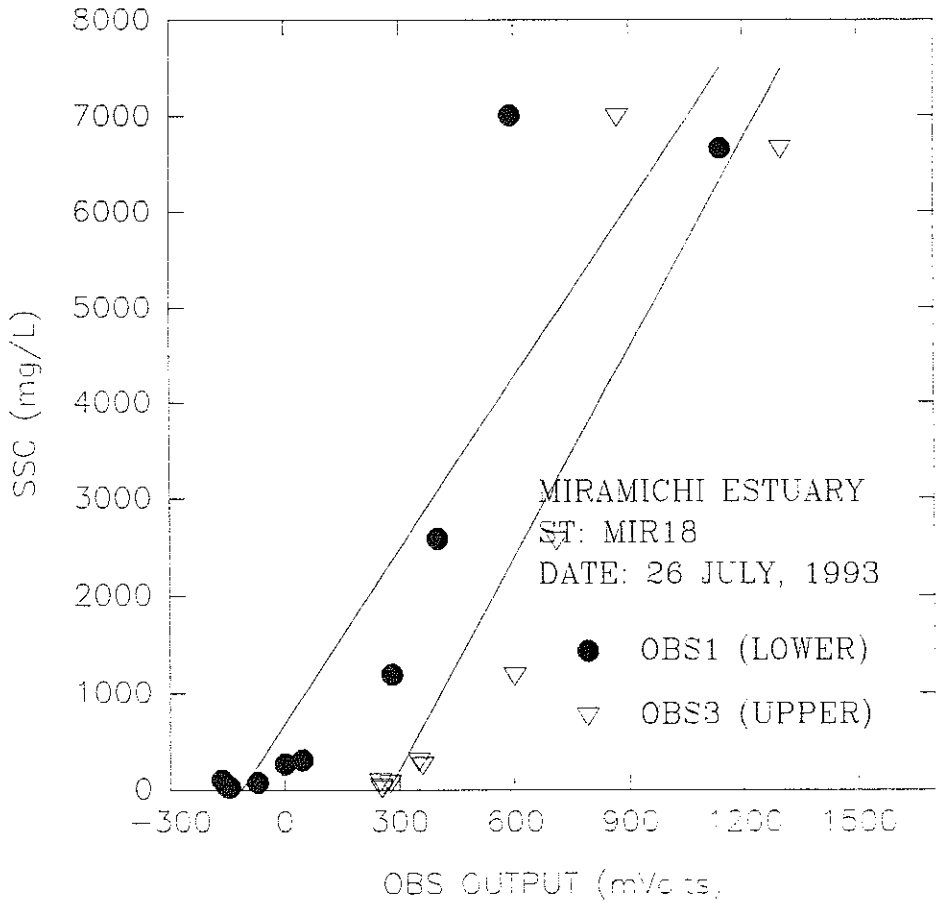
8000
7000
6000
5000
4000
3000
2000
1000
0
SSC (mg/L)
−300
0
300
600
900
1200
1500
OBS OUTPUT (mVolts)
MIRAMICHI ESTUARY
ST: MIR18
DATE: 26 JULY, 1993
OBS1 (LOWER)
OBS3 (UPPER)

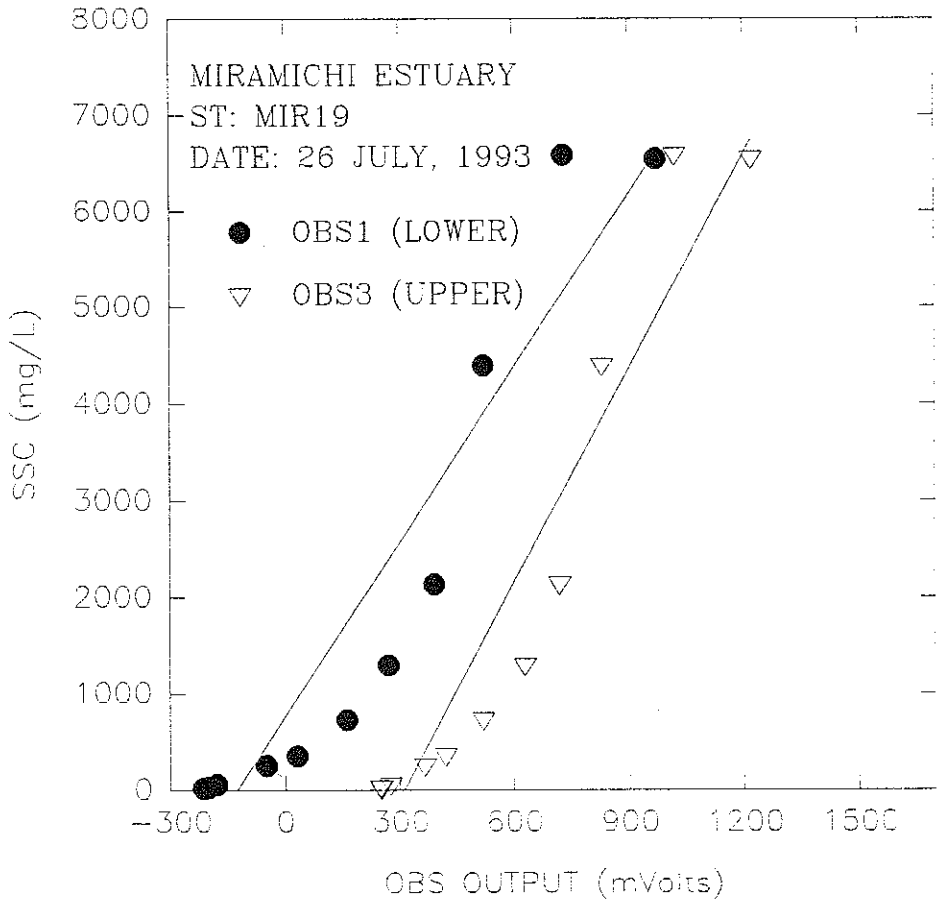
MIRAMICHI ESTUARY
ST: MIR19
DATE: 26 JULY, 1993
OBS1 (LOWER)
OBS3 (UPPER)
SSC (mg/L)
OBS OUTPUT (mVolts)
8000
7000
6000
5000
4000
3000
2000
1000
0
-300
0
300
600
900
1200
1500

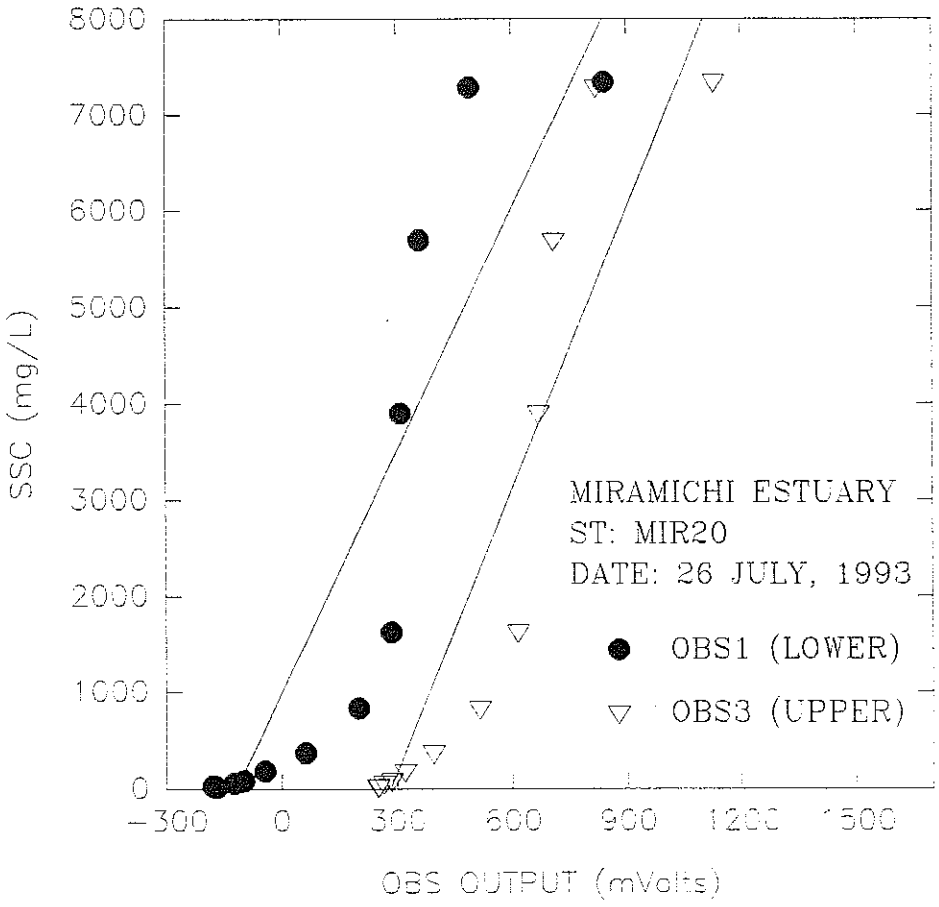
8000
7000
6000
5000
4000
3000
2000
1000
0
SSC (mg/L)
−300
0
300
600
900
1200
1500
OBS OUTPUT (mVolts)
MIRAMICHI ESTUARY
ST: MIR20
DATE: 26 JULY, 1993
OBS1 (LOWER)
OBS3 (UPPER)

APPENDIX F

Operational Log for Lancelot and Excalibur Deployments

SEA CAROUSEL – MIRAMICHI ESTUARY

STATION MIR1 – 16 JULY, 1993

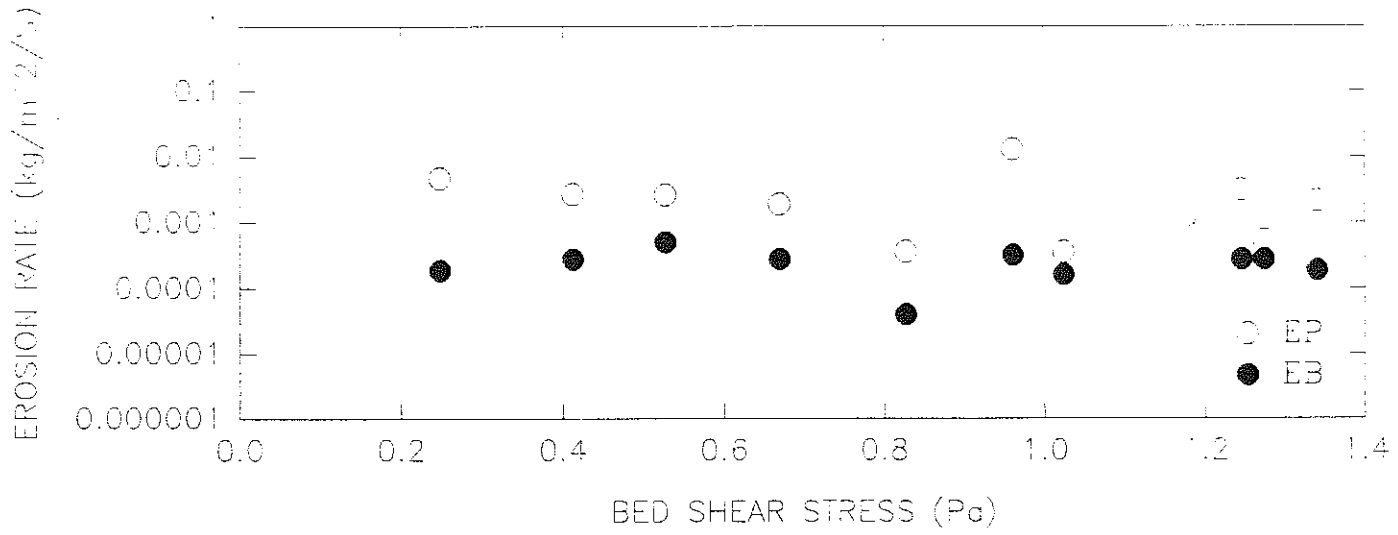

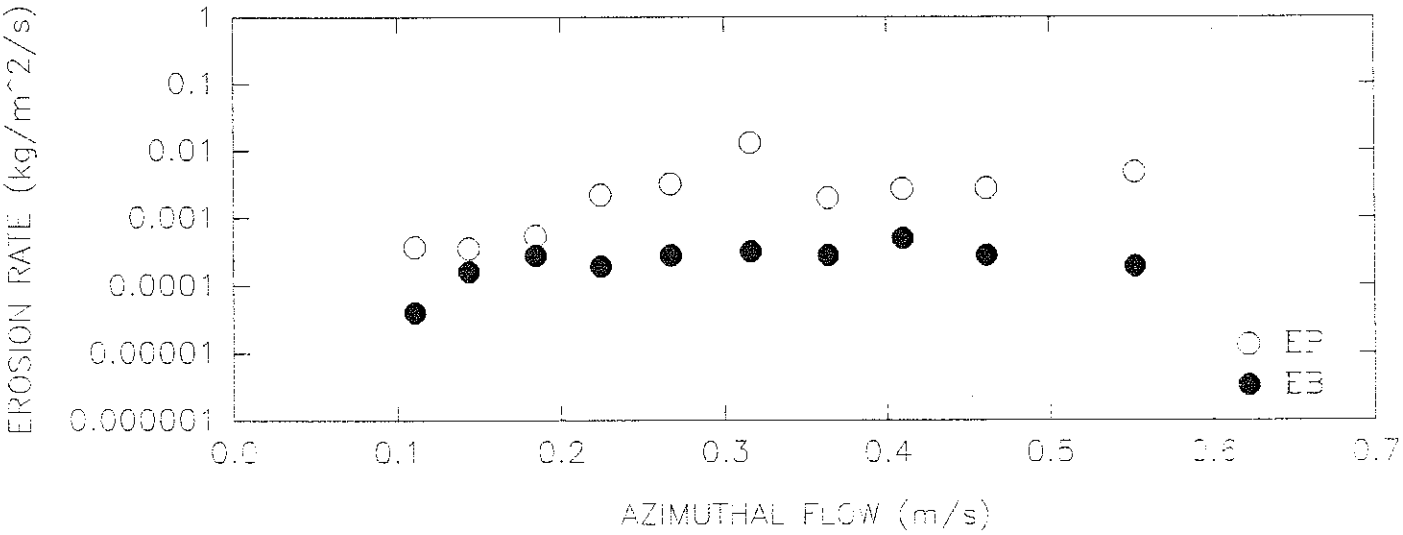

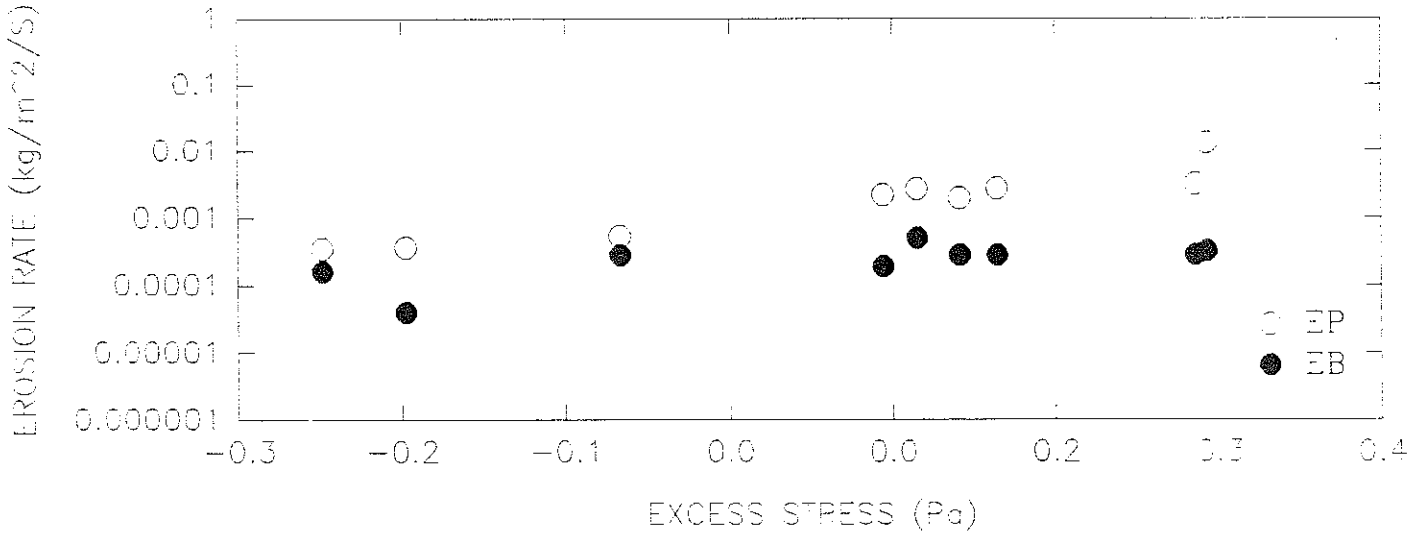

SEA CAROUSEL – MIRAMICHI ESTUARY

STATION MIR2 – 16 JULY, 1993

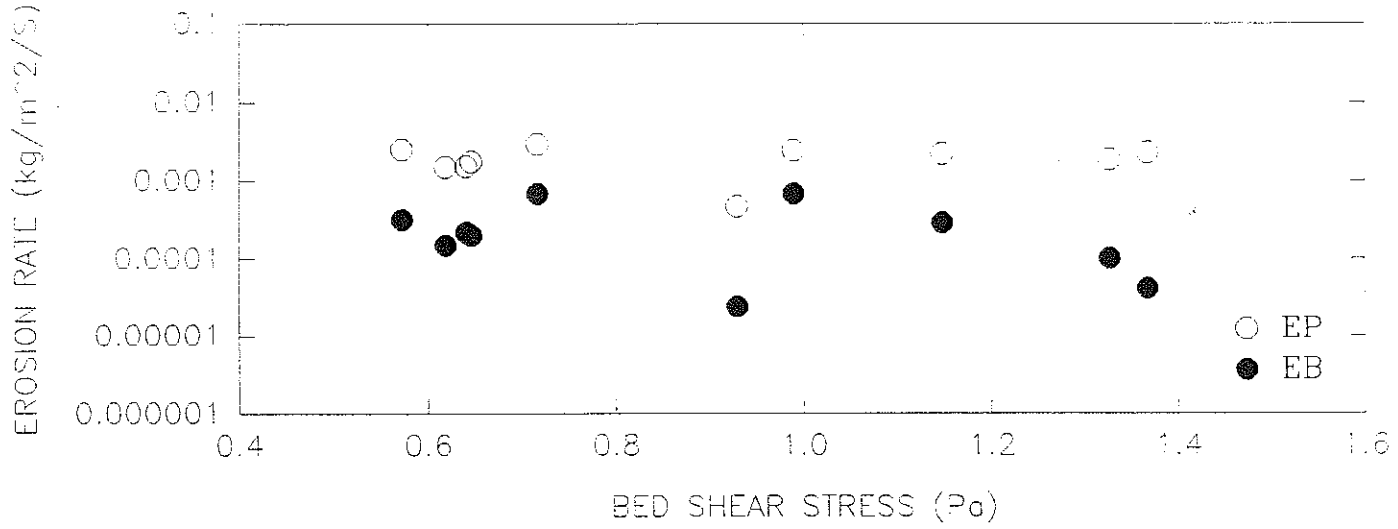

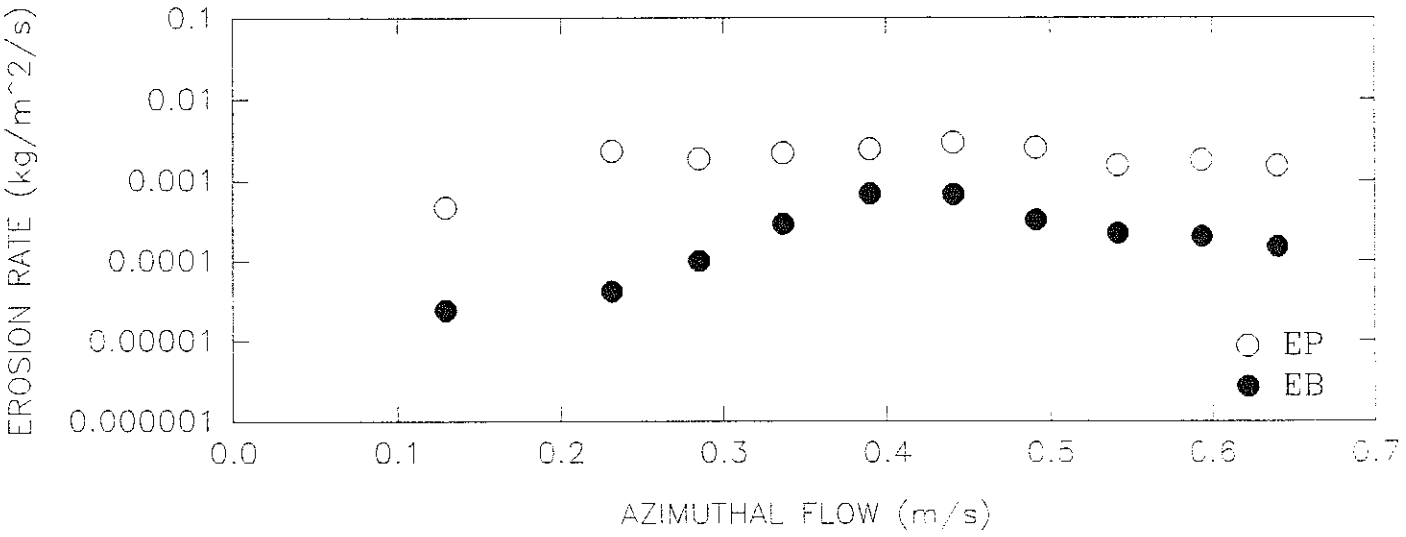

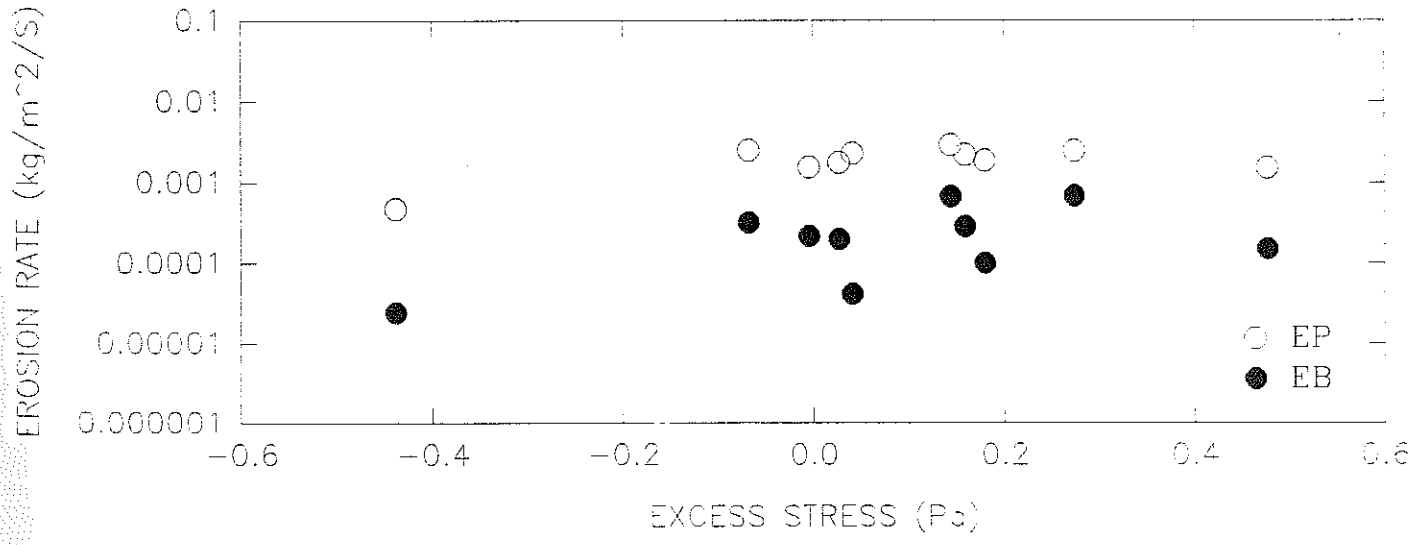

SEA CAROUSEL – MIRAMICHI ESTUARY

STATION MIR3 – 16 JULY, 1993

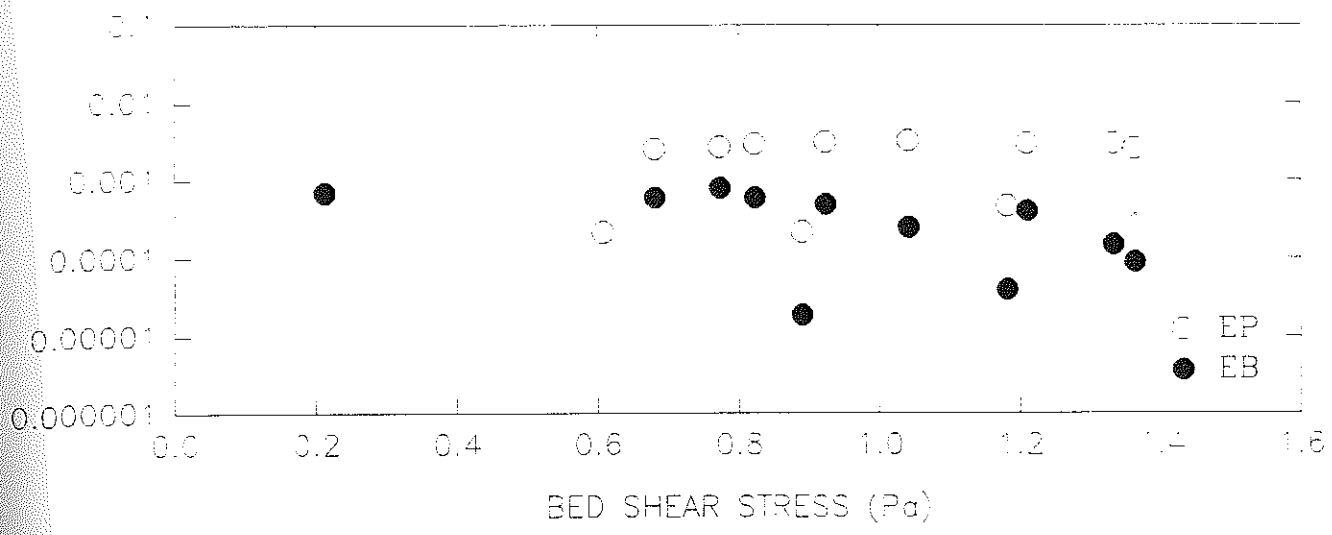

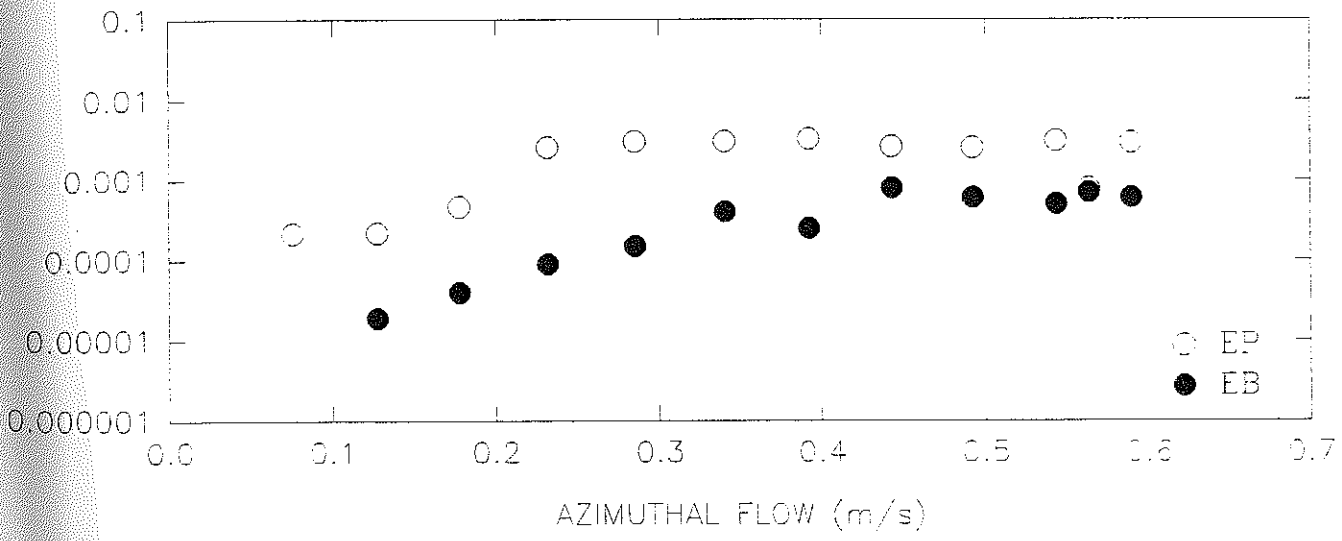

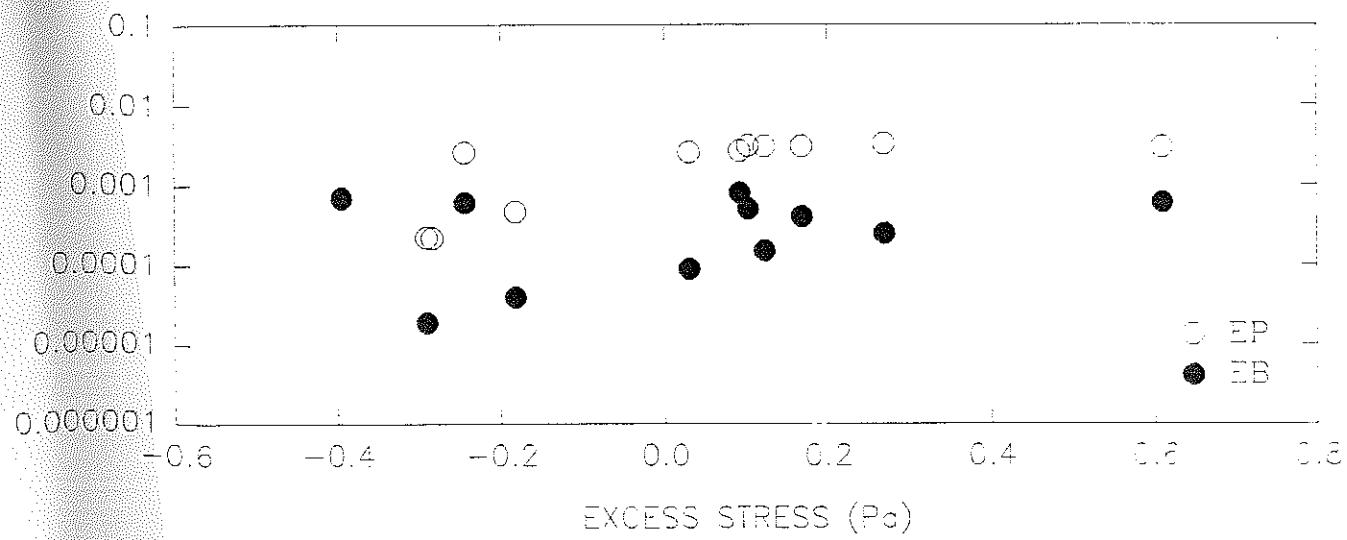

SEA CAROUSEL – MIRAMICHI ESTUARY

STATION MIR4 – 18 JULY, 1993

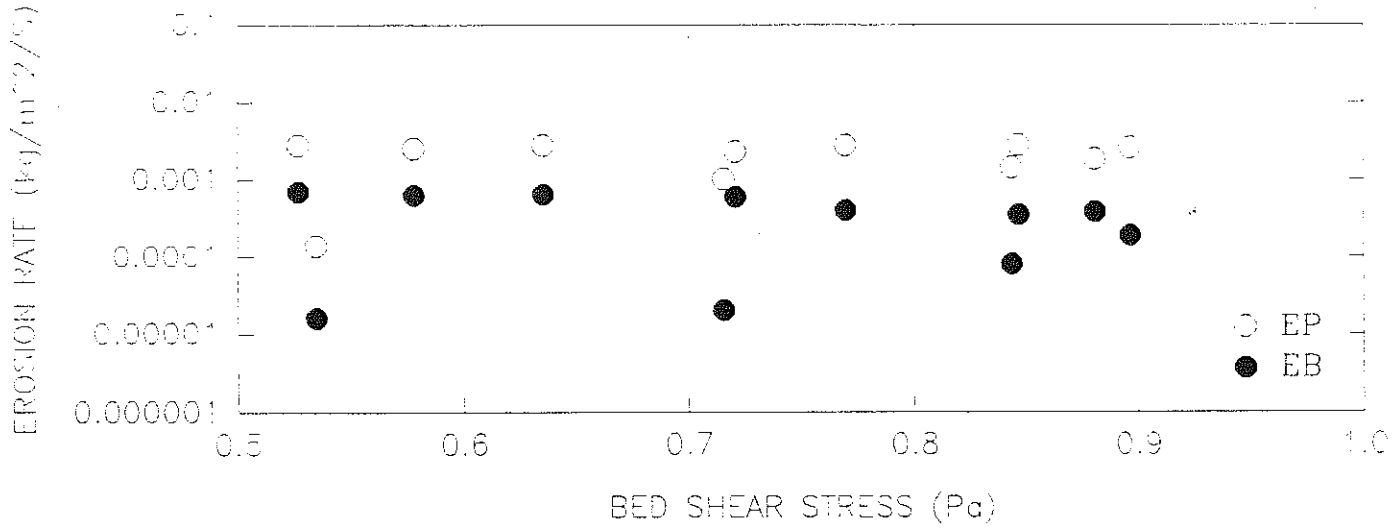

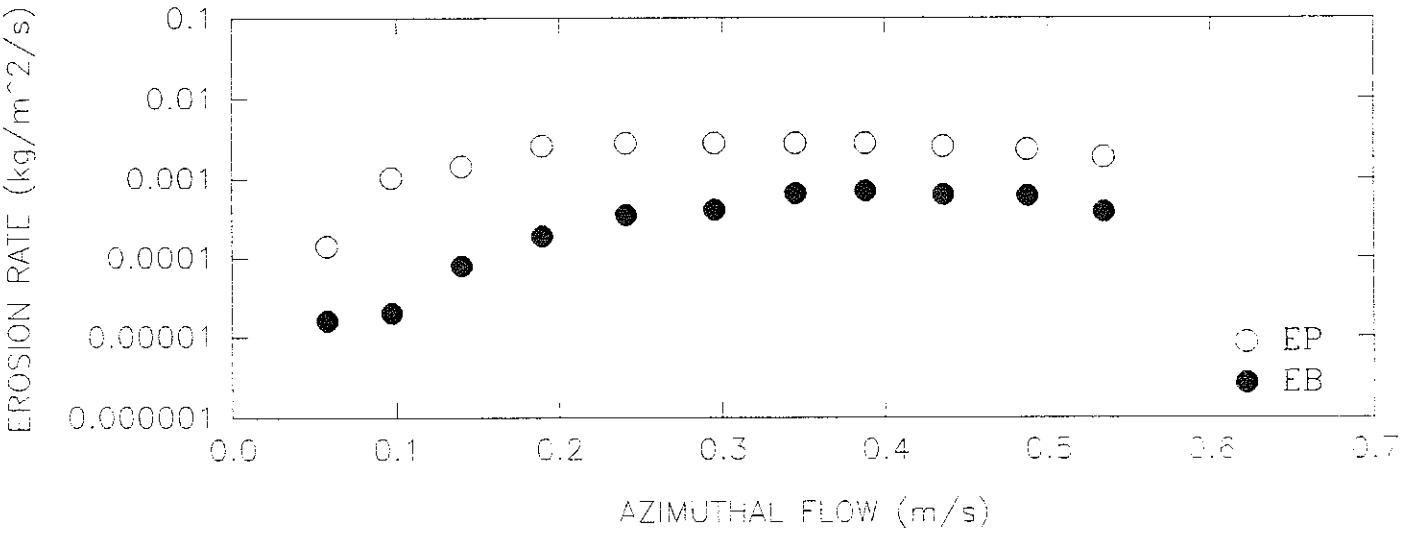

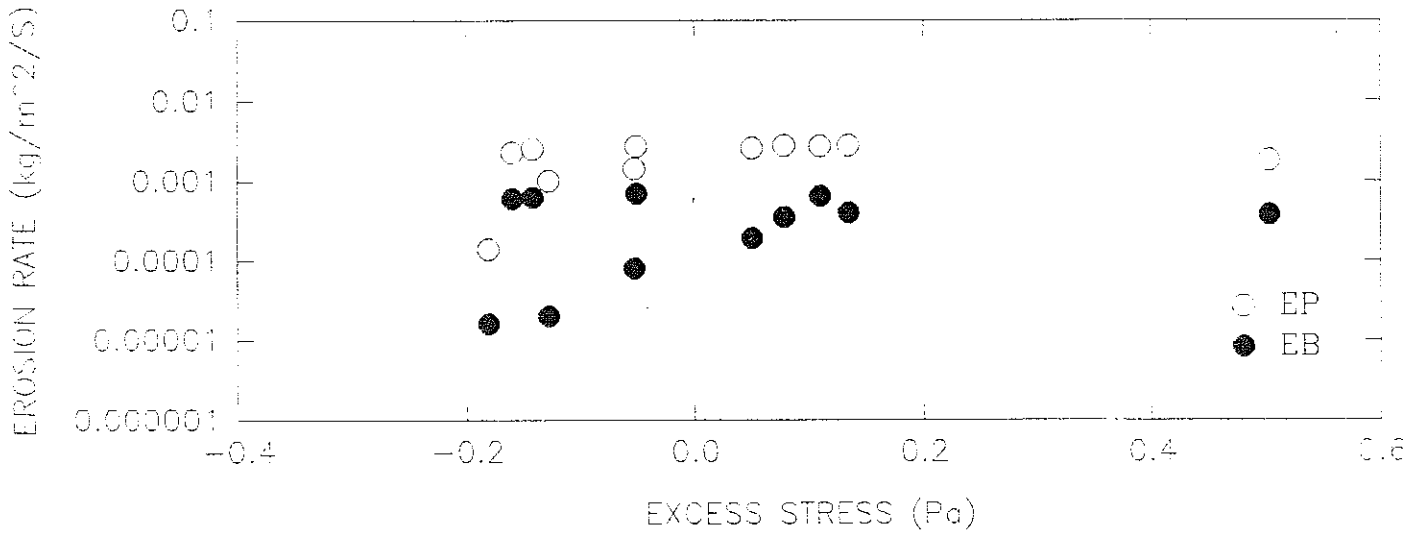

SEA CAROUSEL -- MIRAMICHI ESTUARY

STATION MIR5 - 19 JULY, 1993

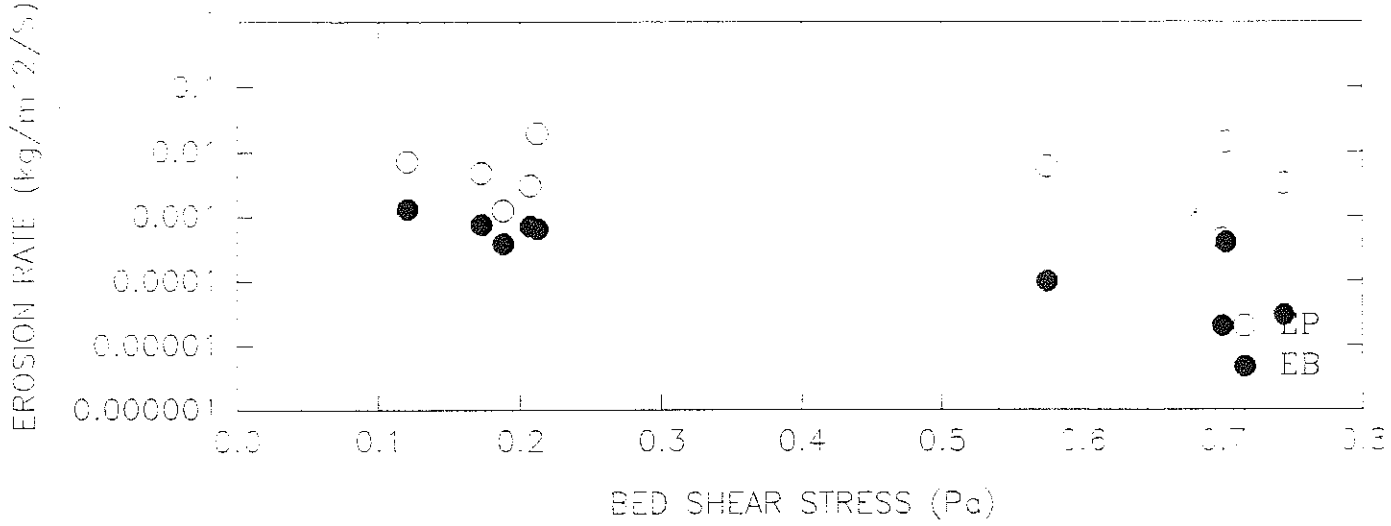

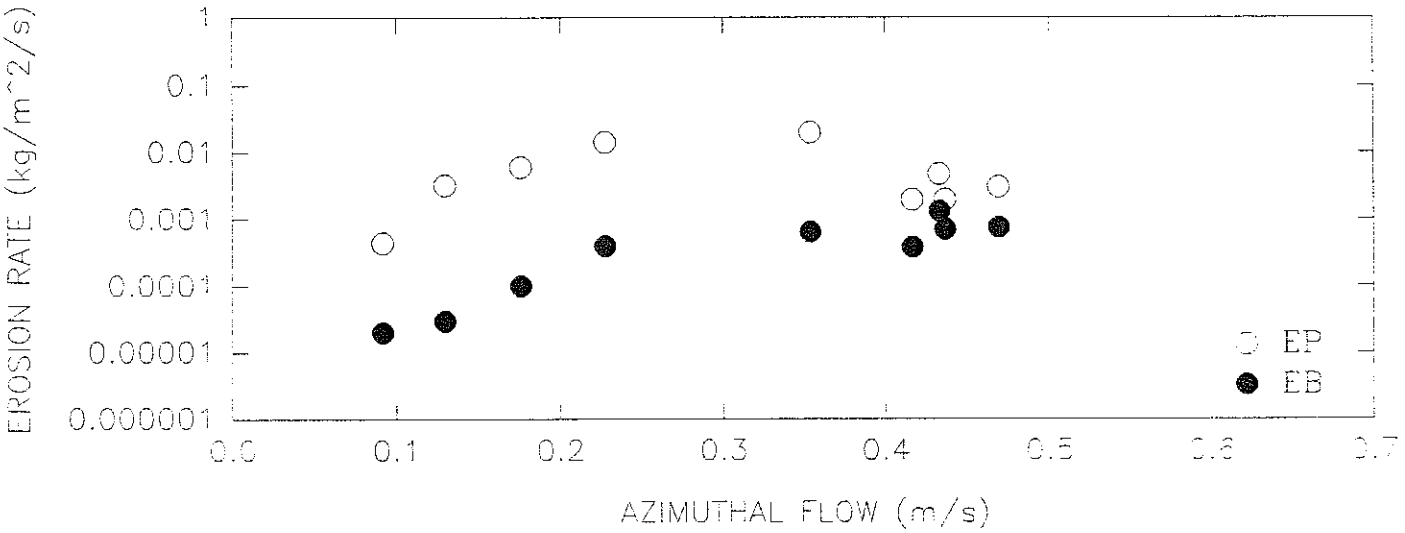

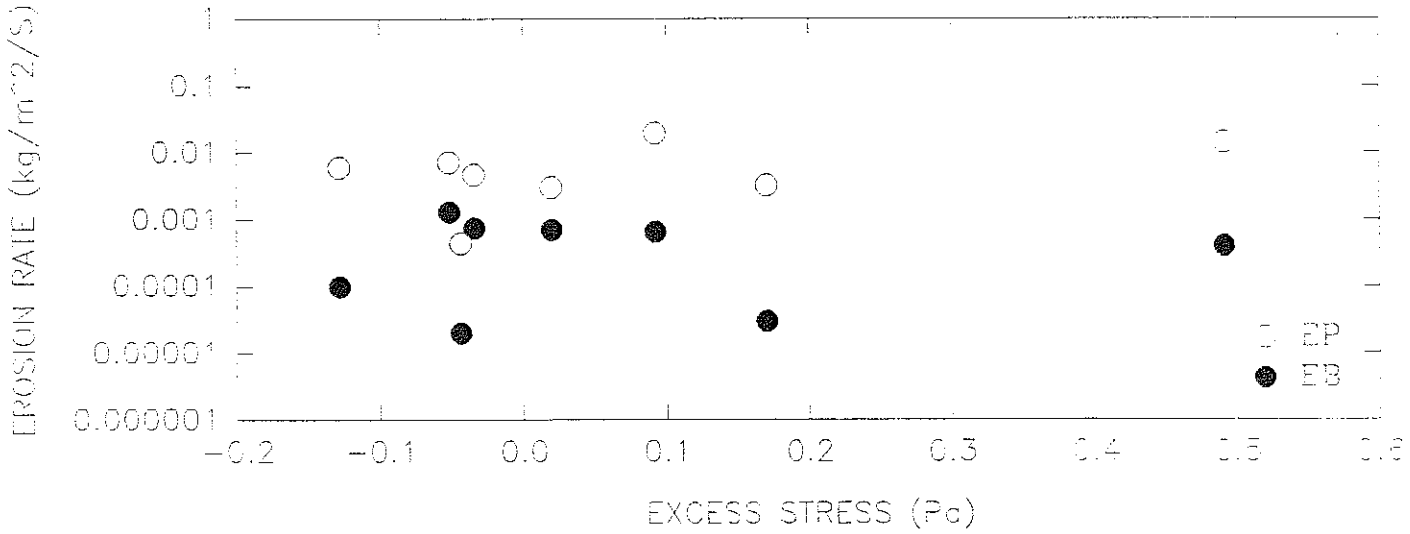

SEA CAROUSEL – MIRAMICHI ESTUARY

STATION MIR6 – 19 JULY, 1993

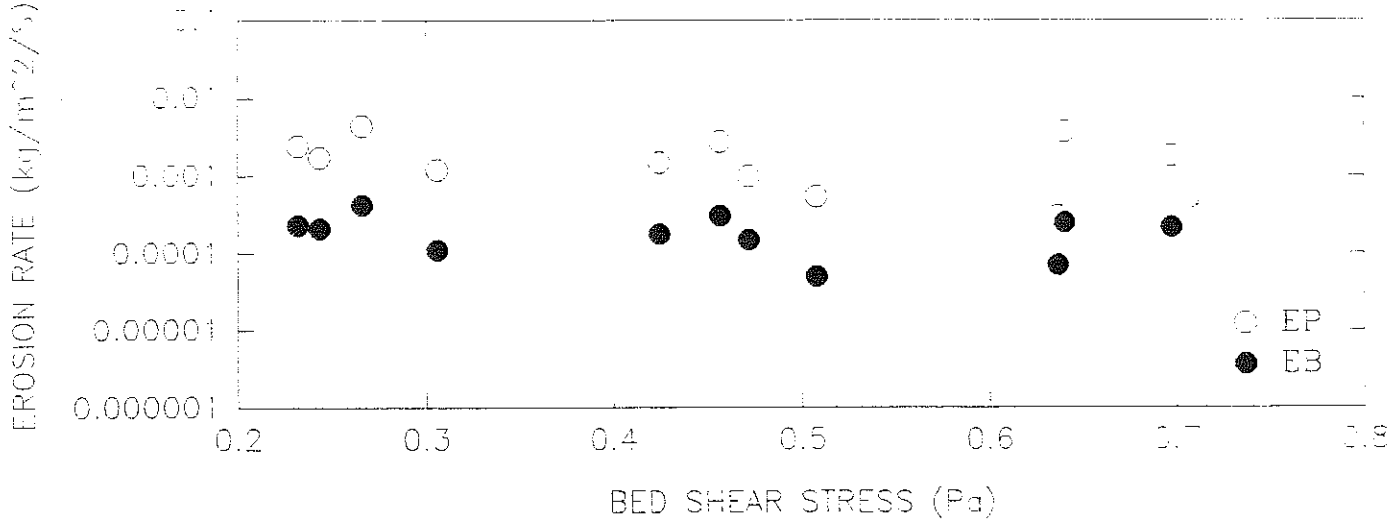

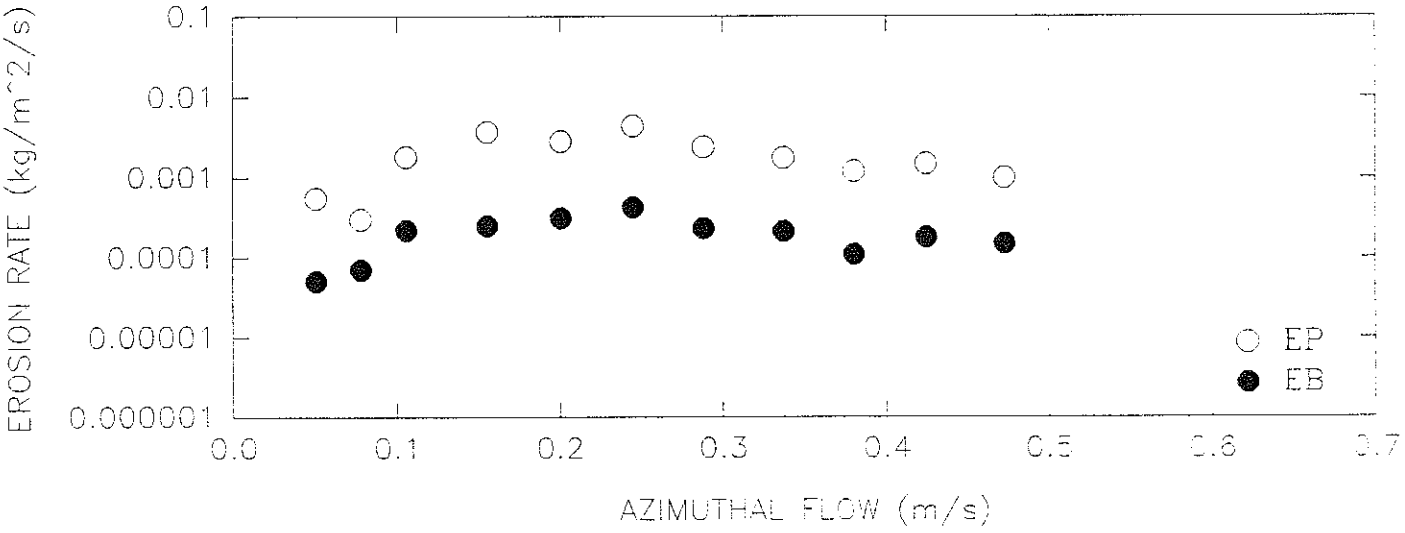

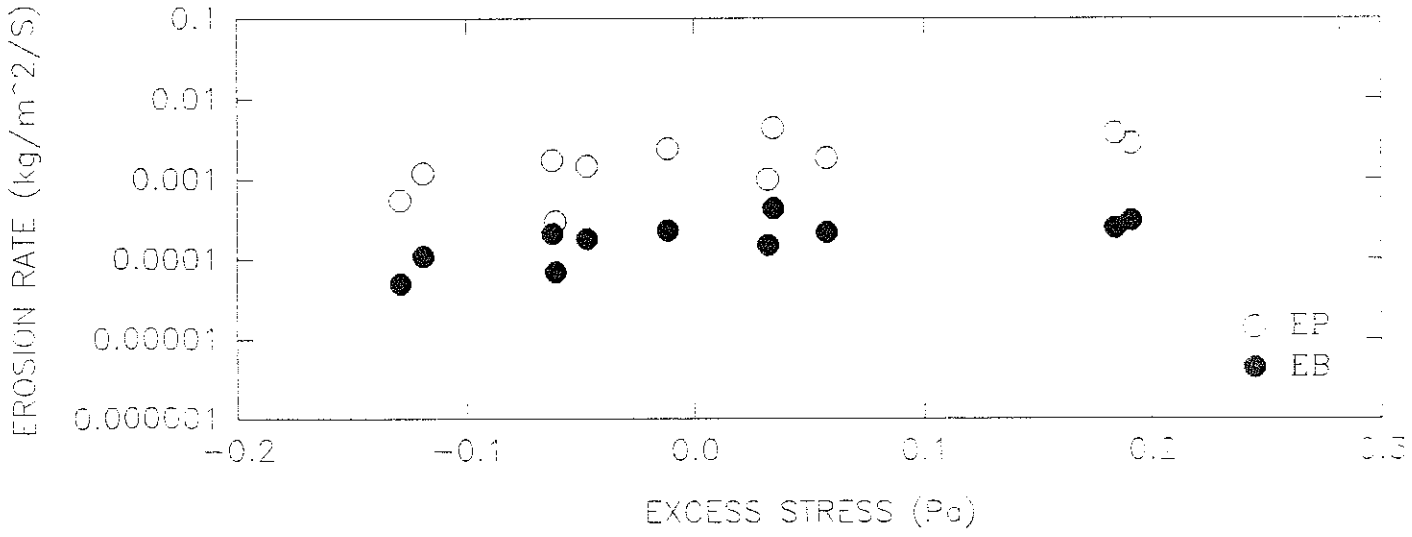

SEA CAROUSEL – MIRAMICHI ESTUARY

STATION MIR7 – 19 JULY, 1993

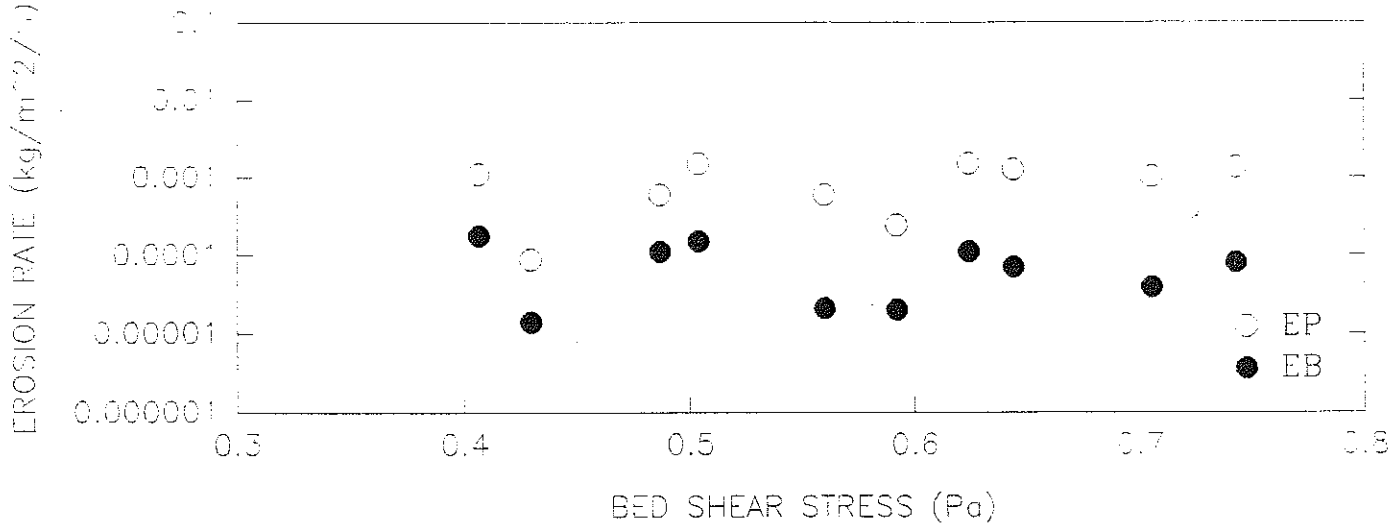

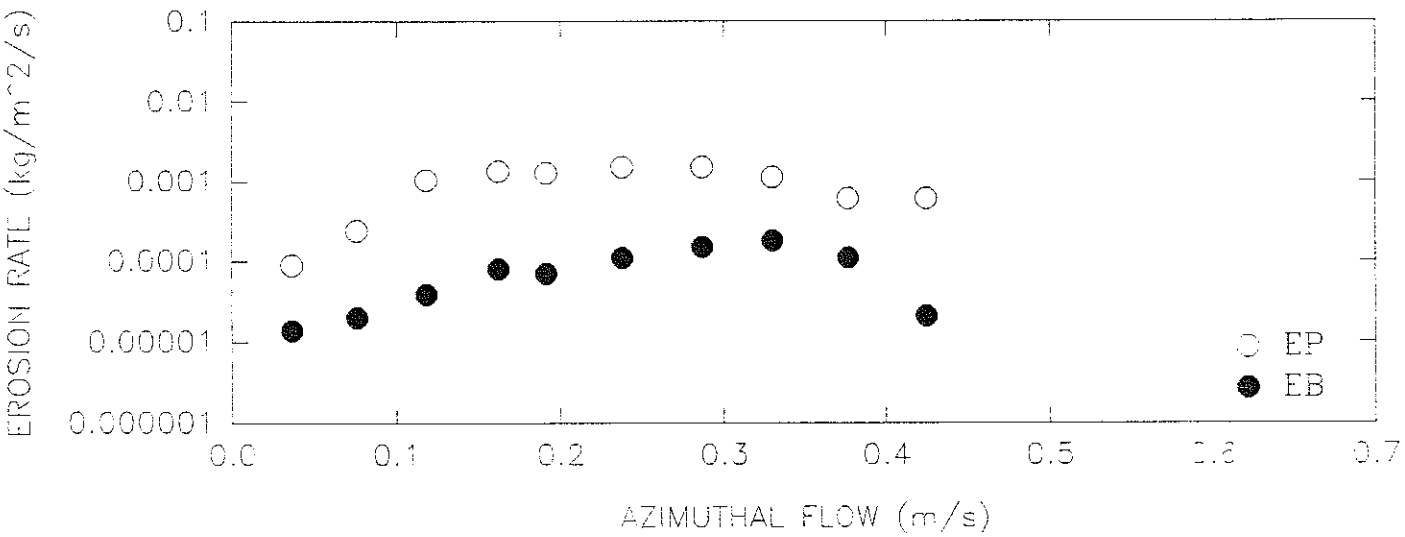

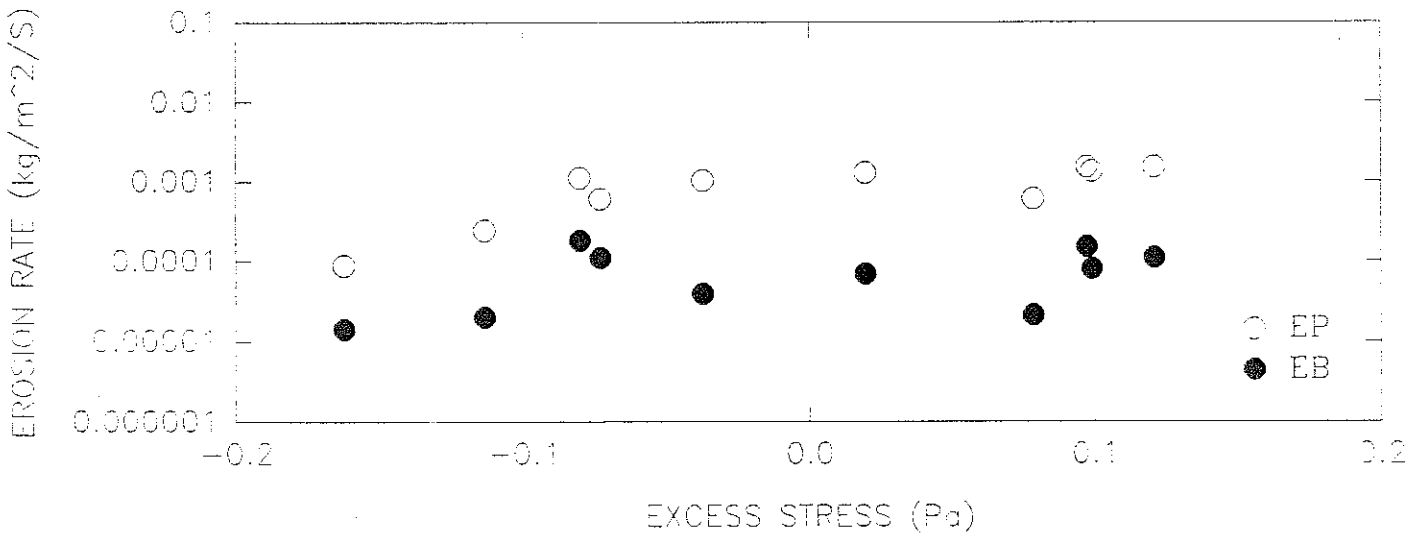

SEA CAROUSEL - MIRAMICHI ESTUARY

STATION MIR8 - 22 JULY, 1993

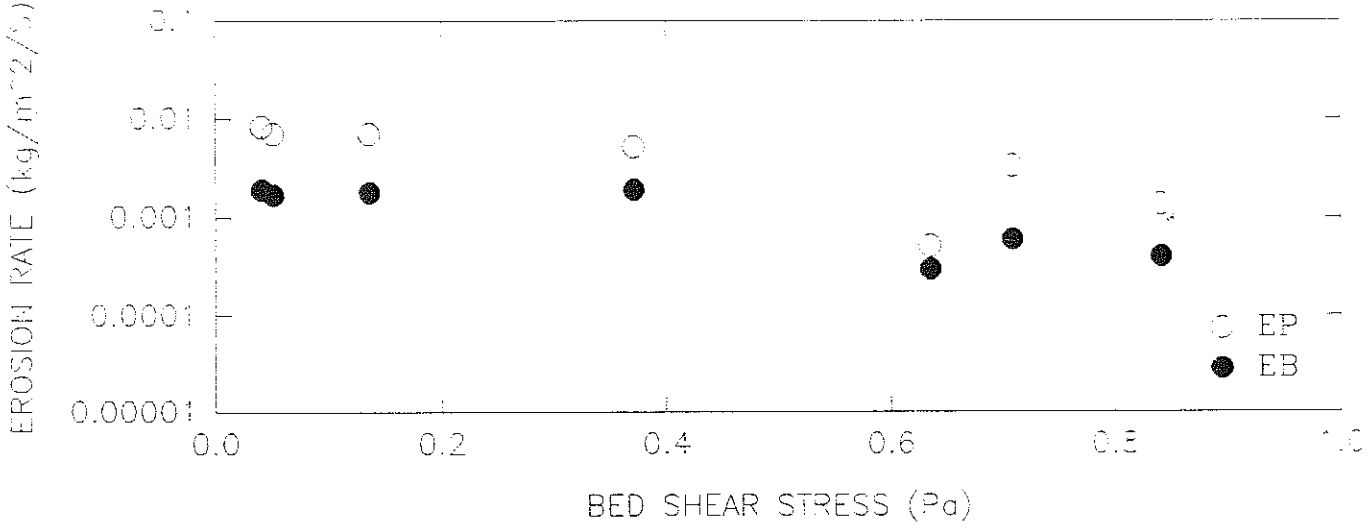

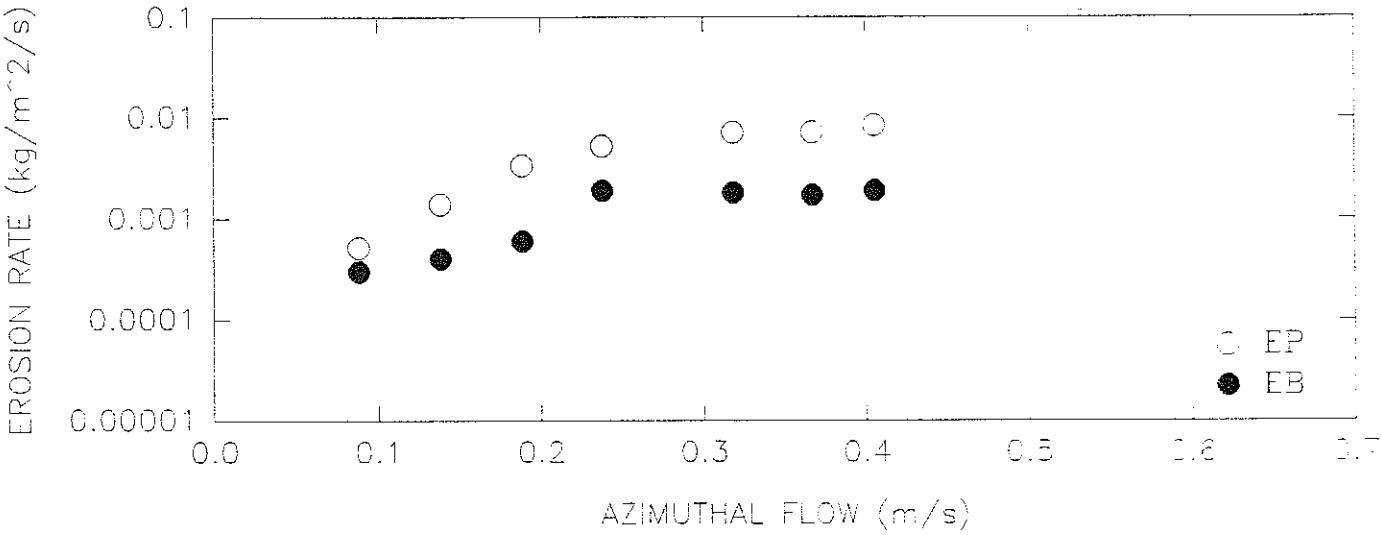

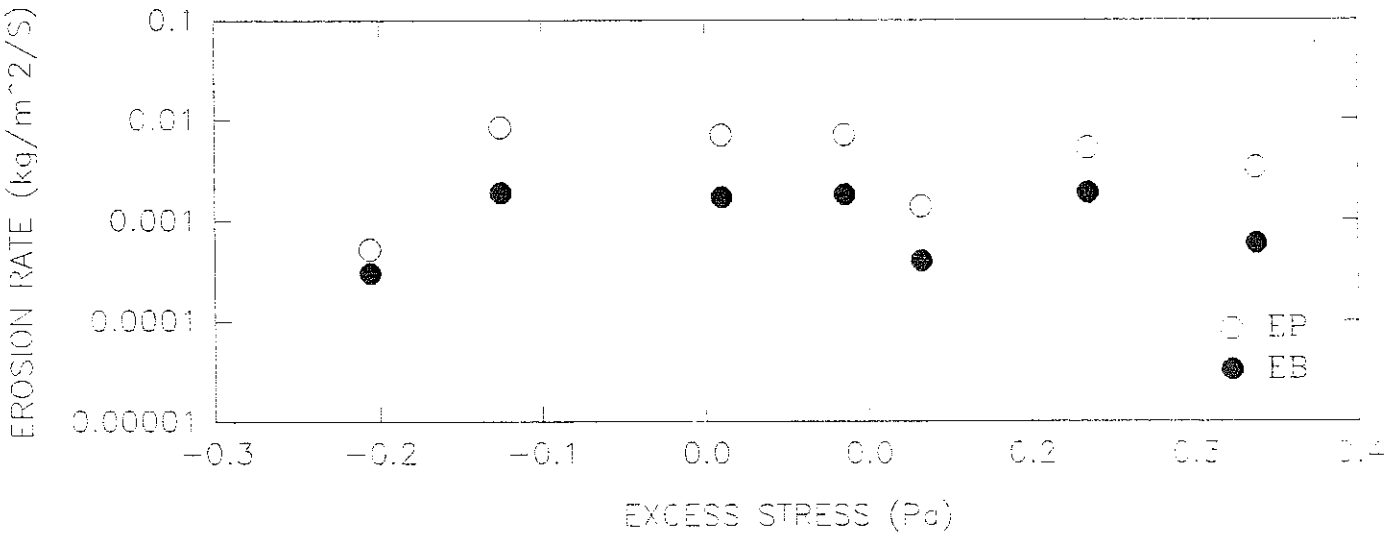

SEA CAROUSEL – MIRAMICHI ESTUARY

STATION MIR9 – 23 JULY, 1993

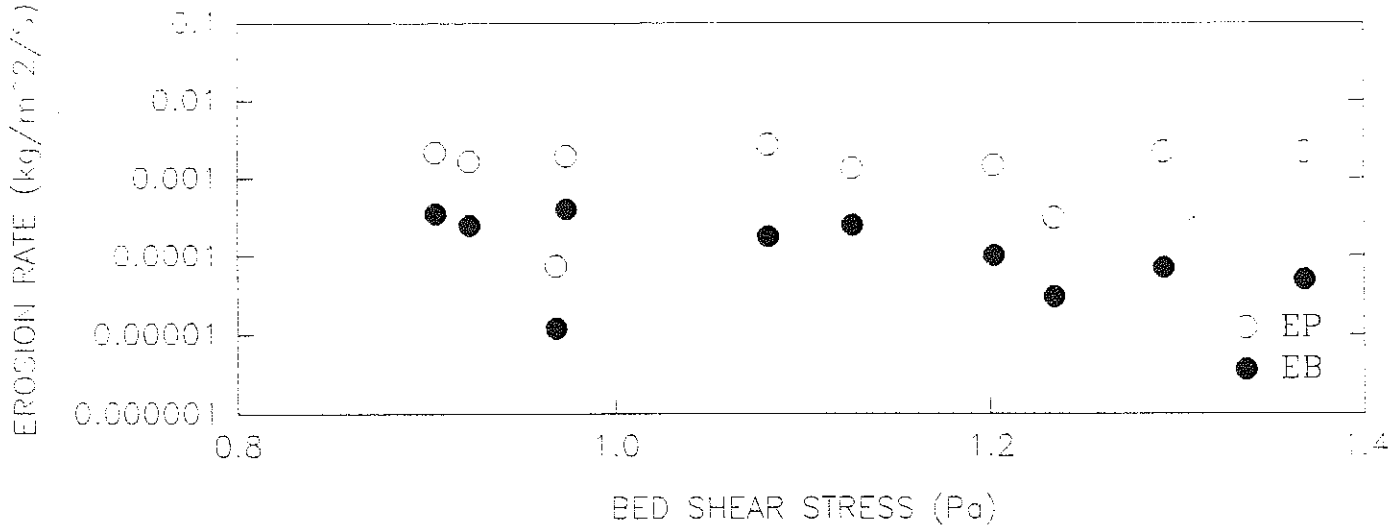

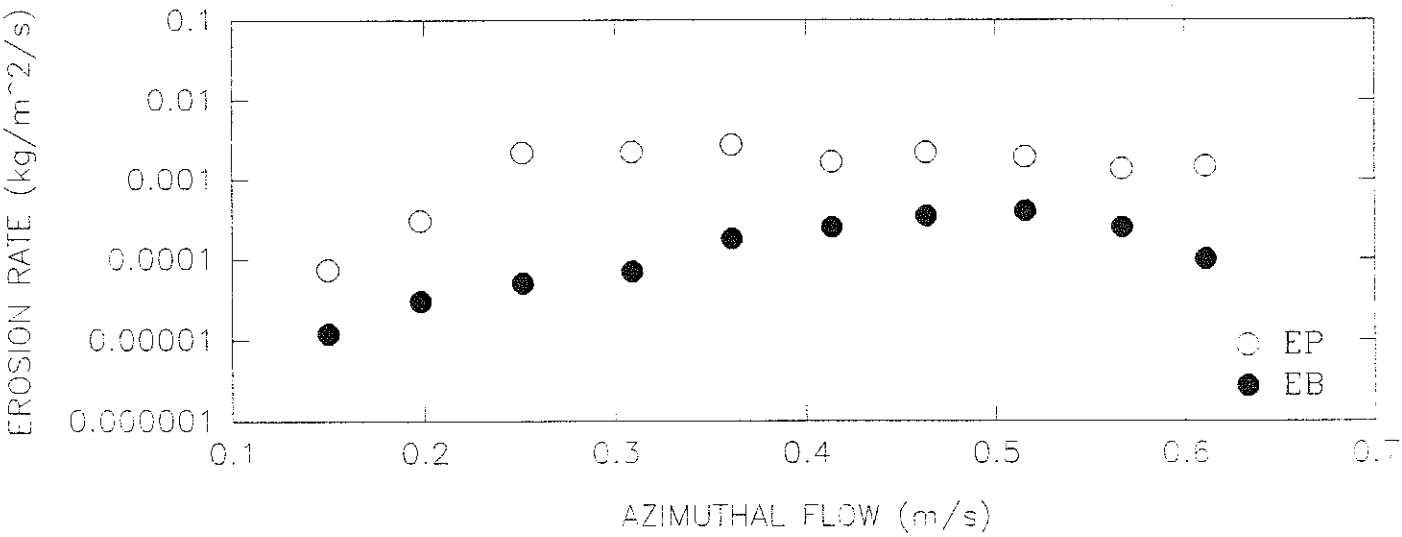

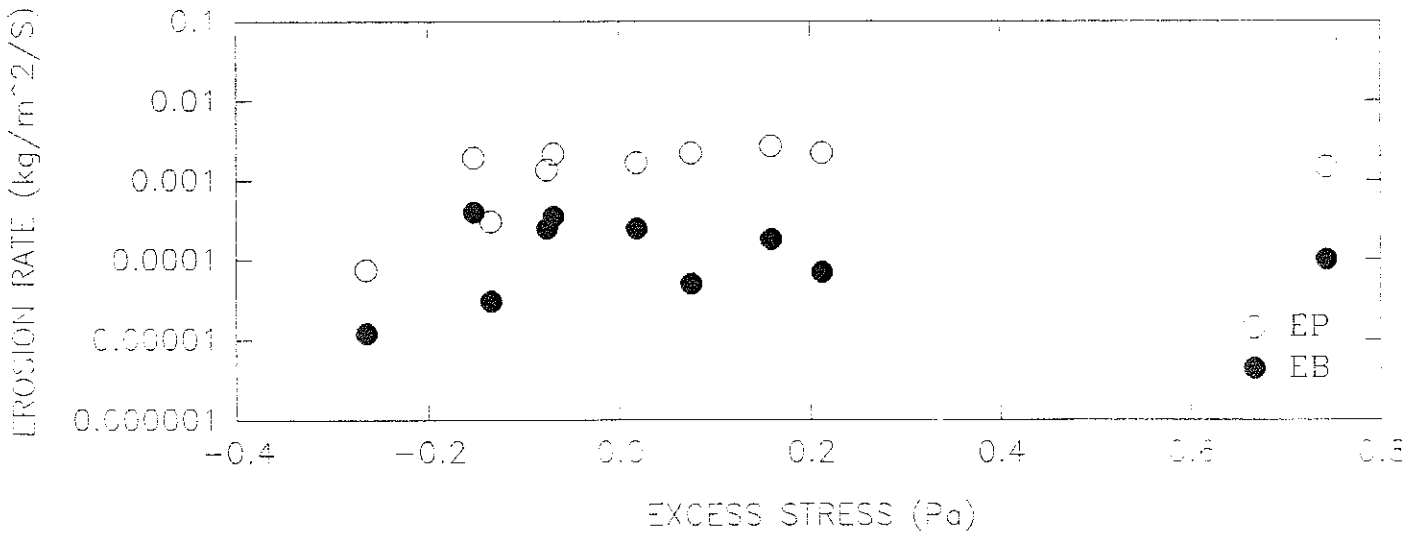

SEA CAROUSEL – MIRAMICHI ESTUARY

STATION MIR10 – 23 JULY, 1993

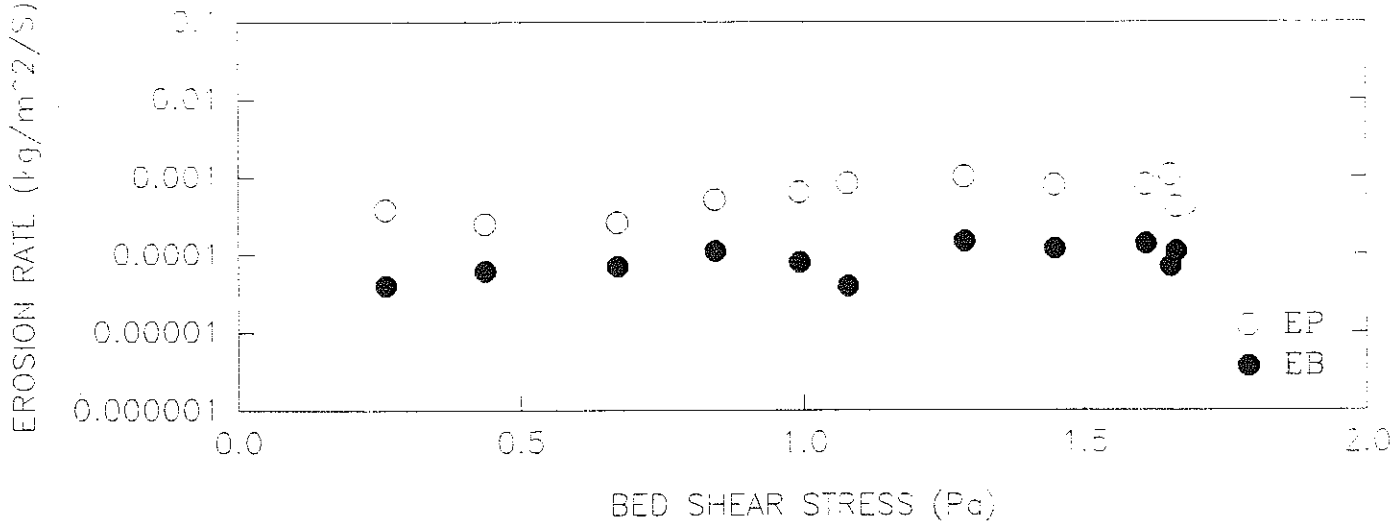

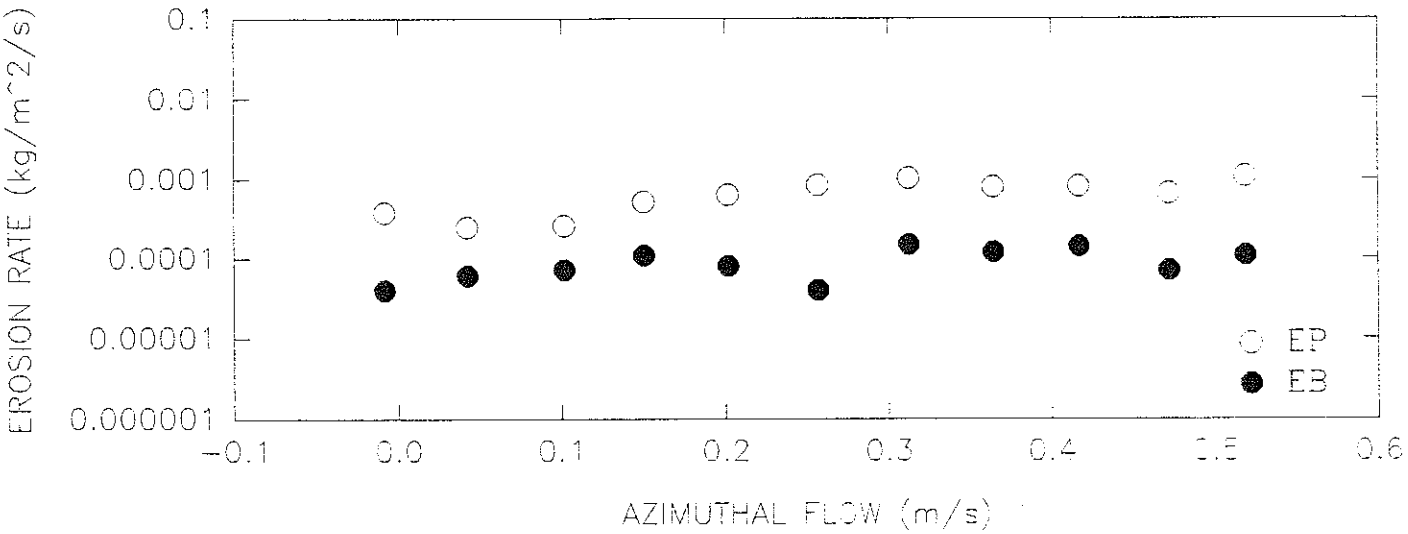

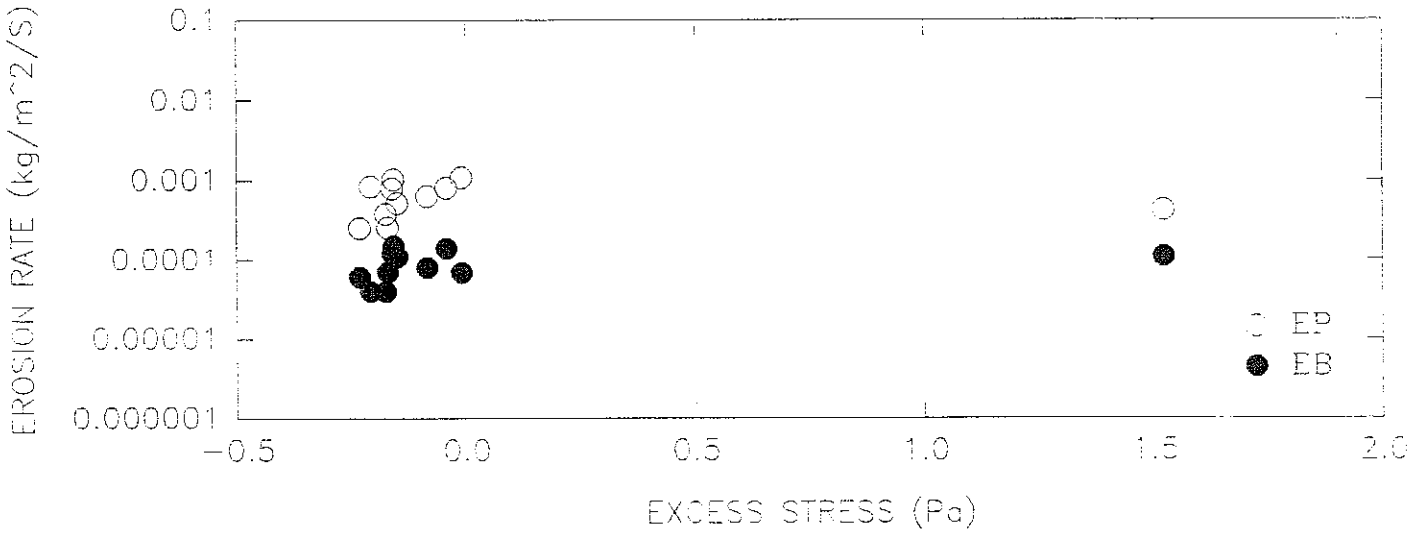

SEA CAROUSEL – MIRAMICHI ESTUARY

STATION MIR11 – 23 JULY, 1993

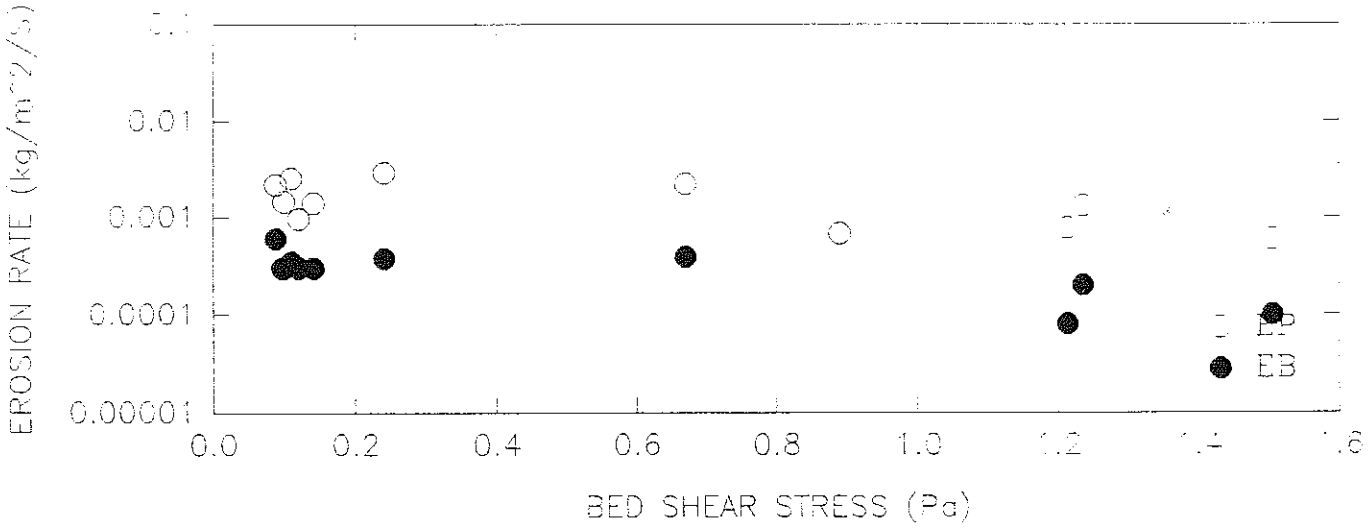

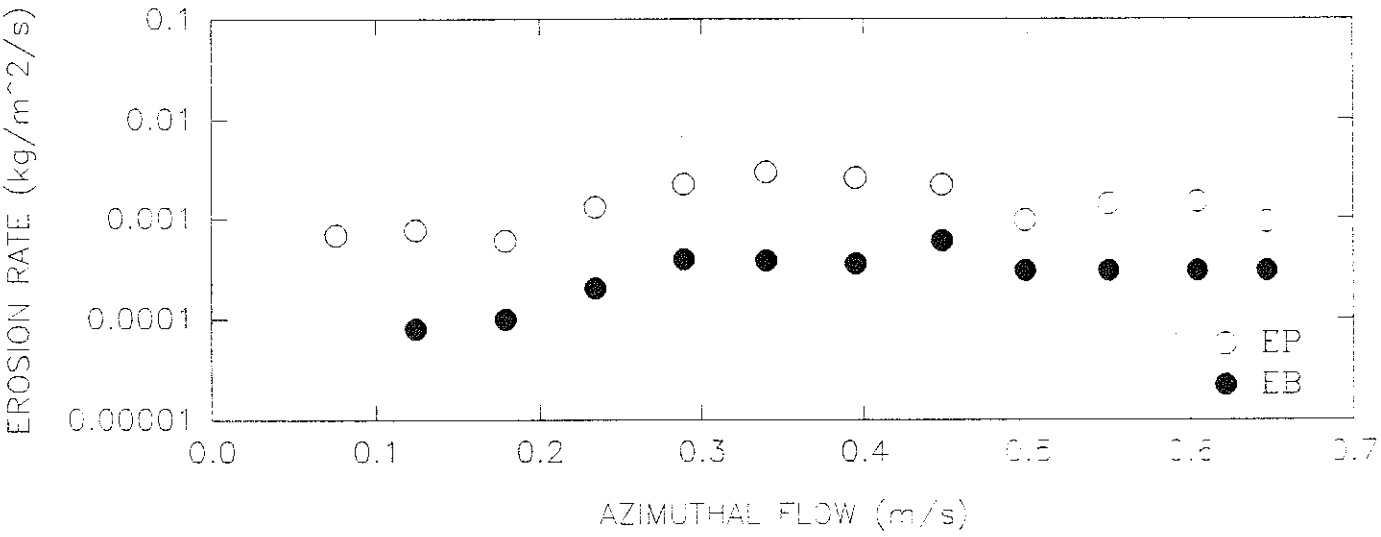

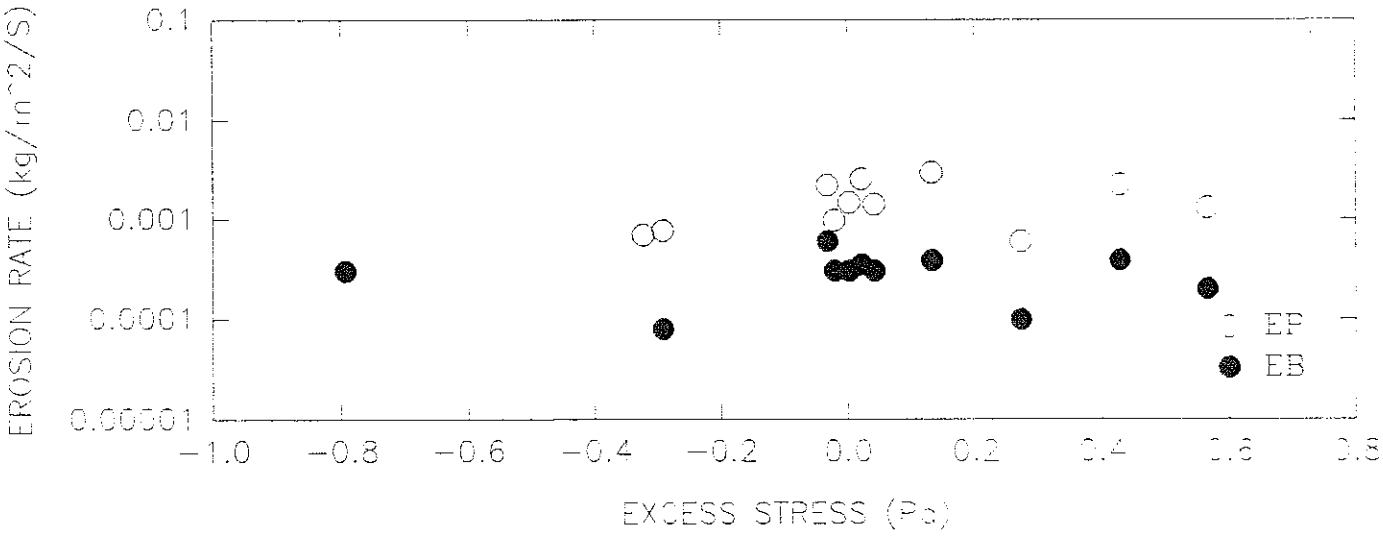

SEA CAROUSEL – MIRAMICHI ESTUARY

STATION MIR12 – 24 JULY, 1993

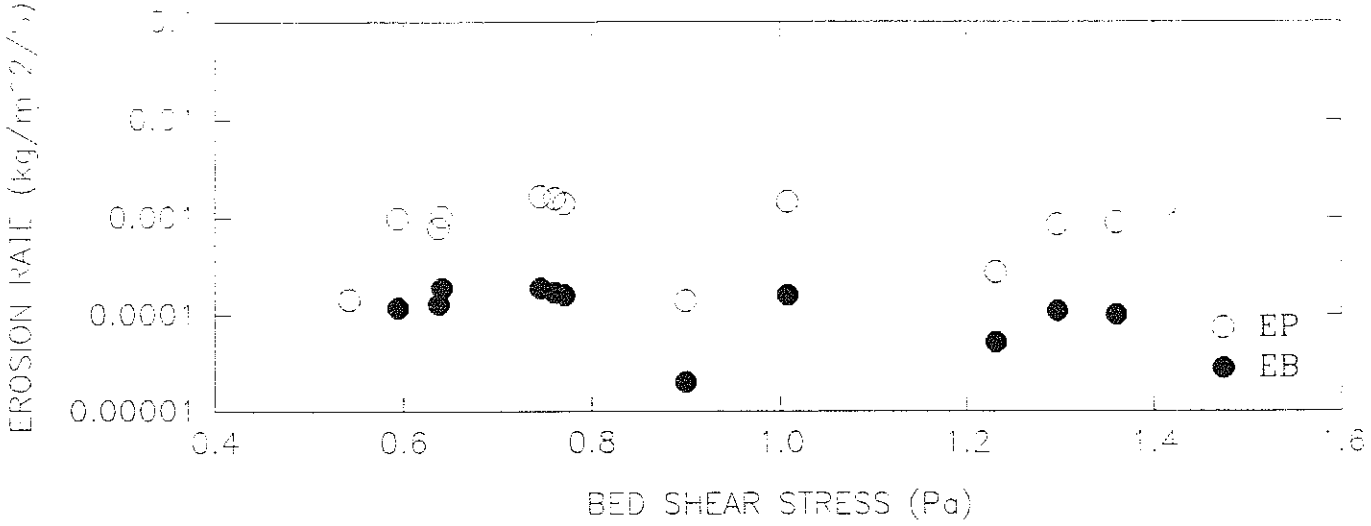

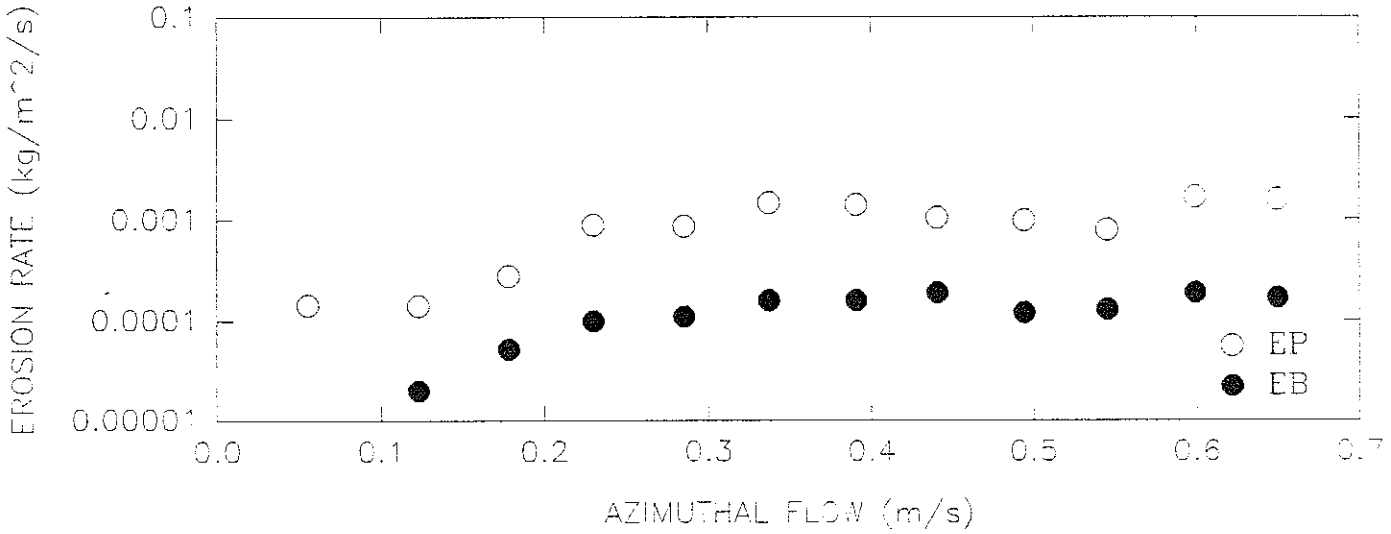

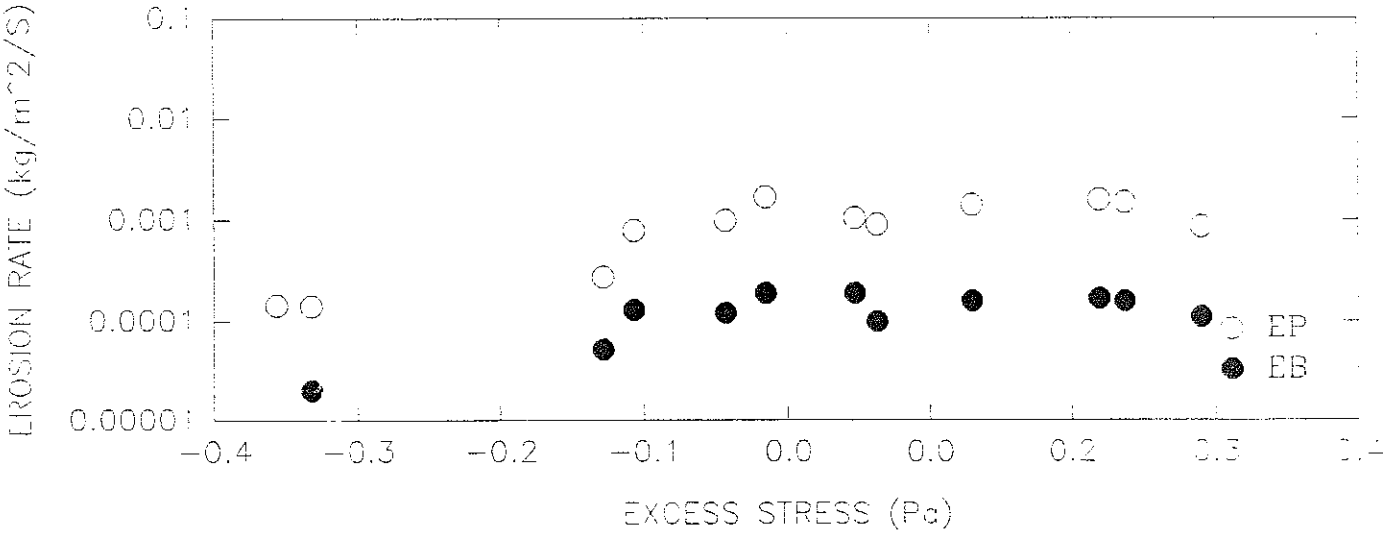

SEA CAROUSEL – MIRAMICHI ESTUARY

STATION MIR13 – 24 JULY, 1993

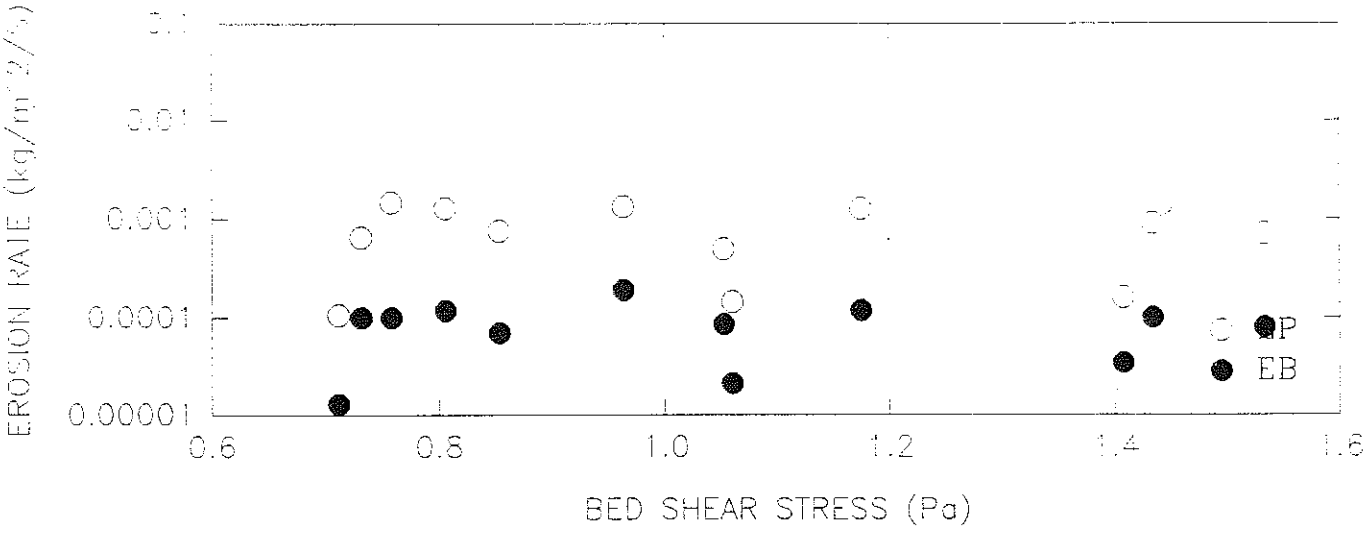

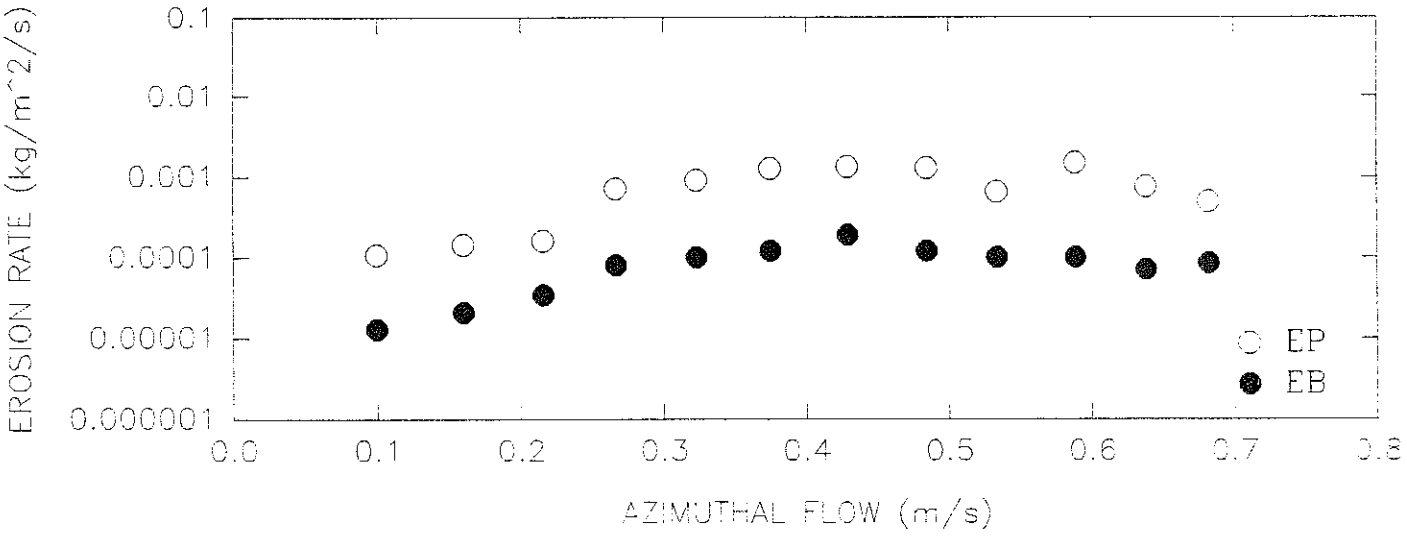

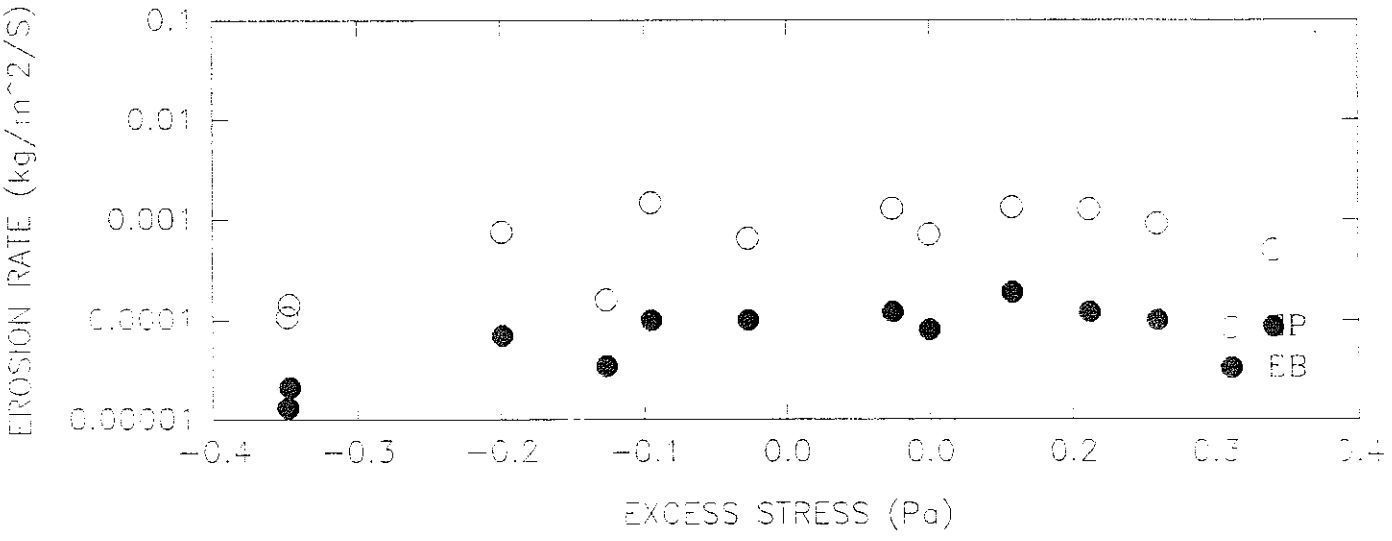

SEA CAROUSEL – MIRAMICHI ESTUARY

STATION MIR14 – 24 JULY, 1993

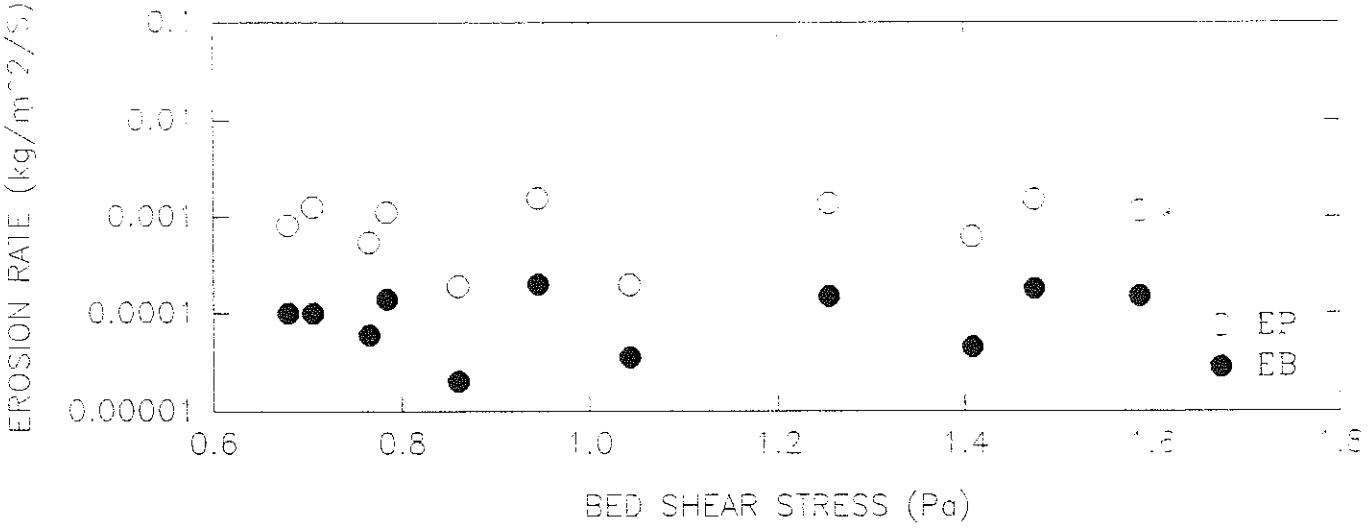

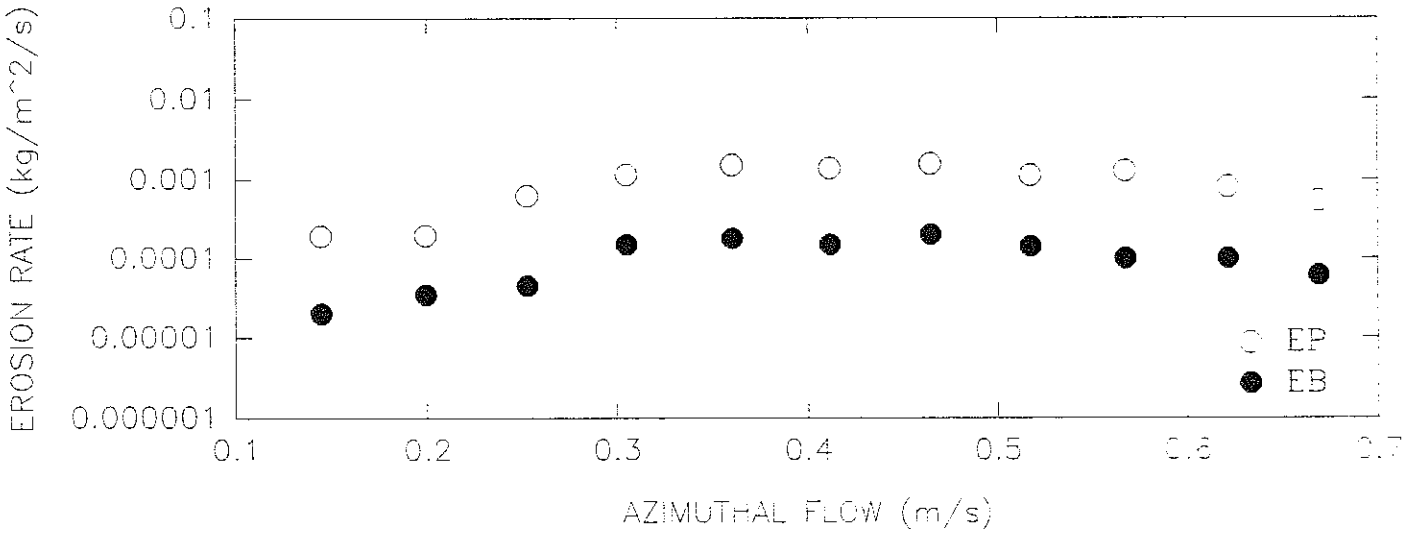

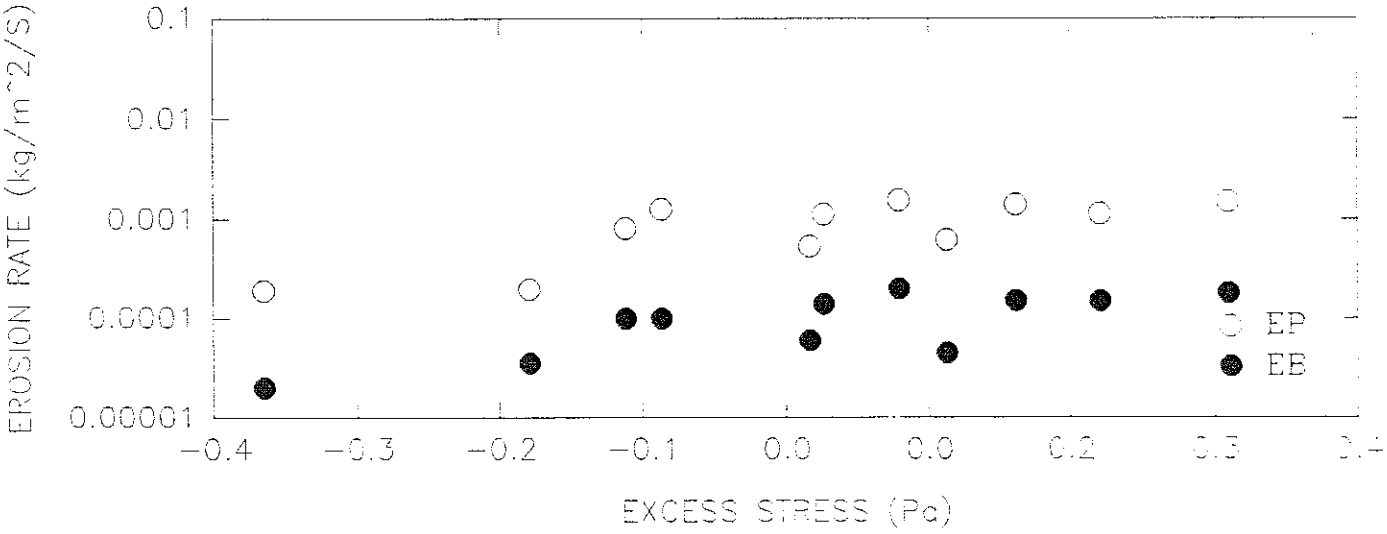

SEA CAROUSEL – MIRAMICHI ESTUARY

STATION MIR15 – 24 JULY, 1993

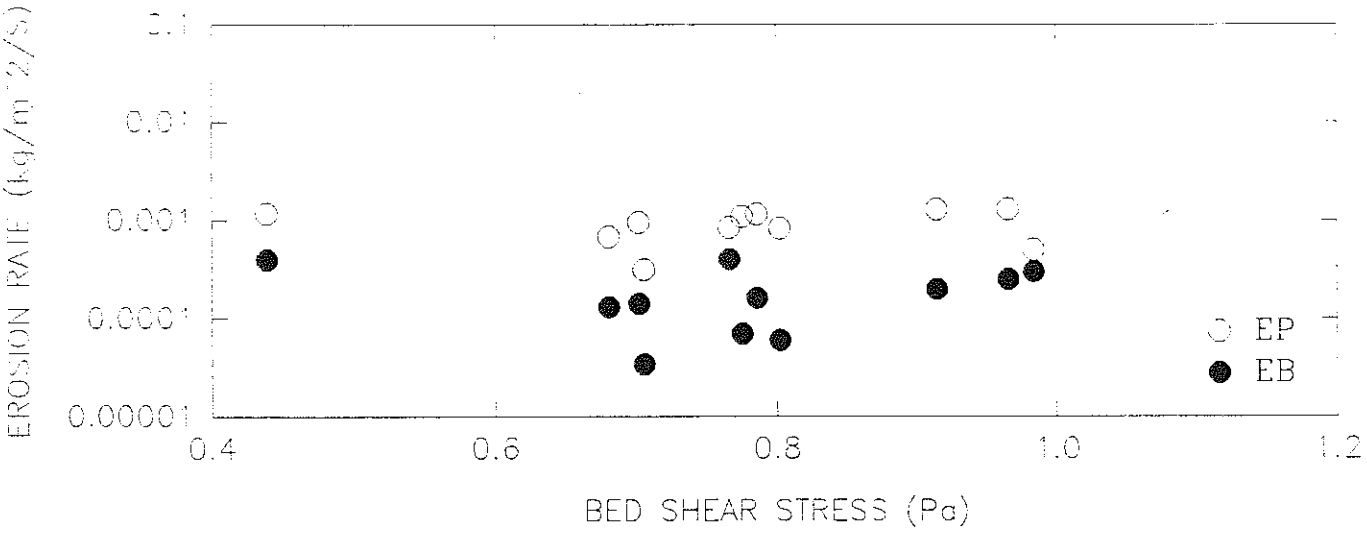

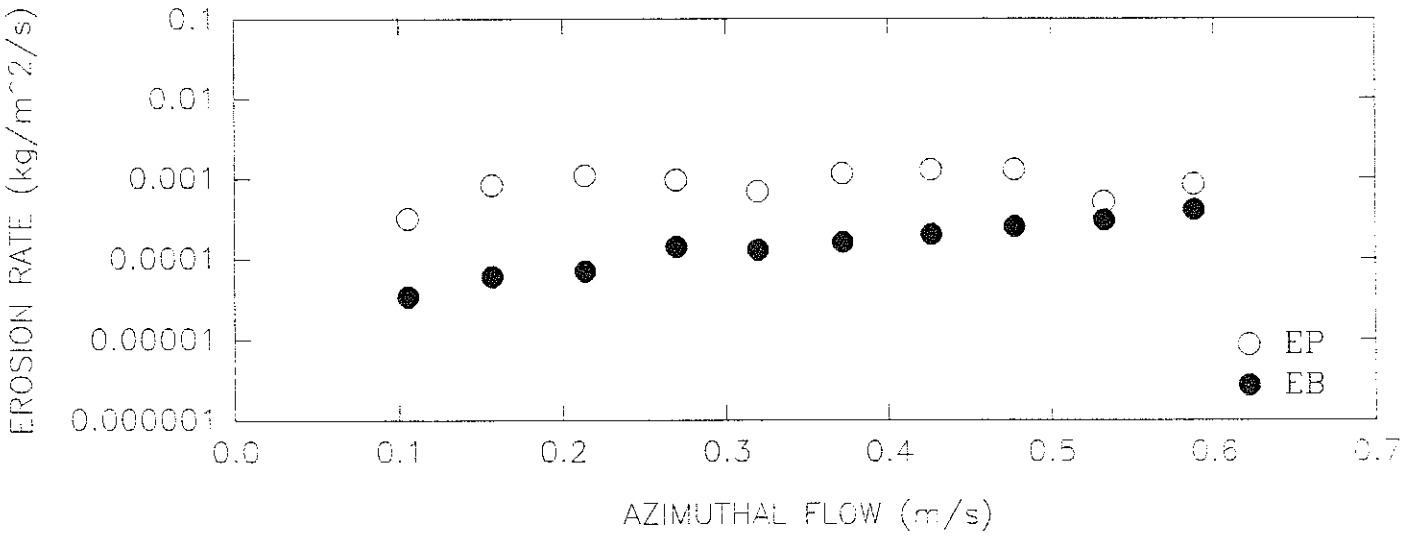

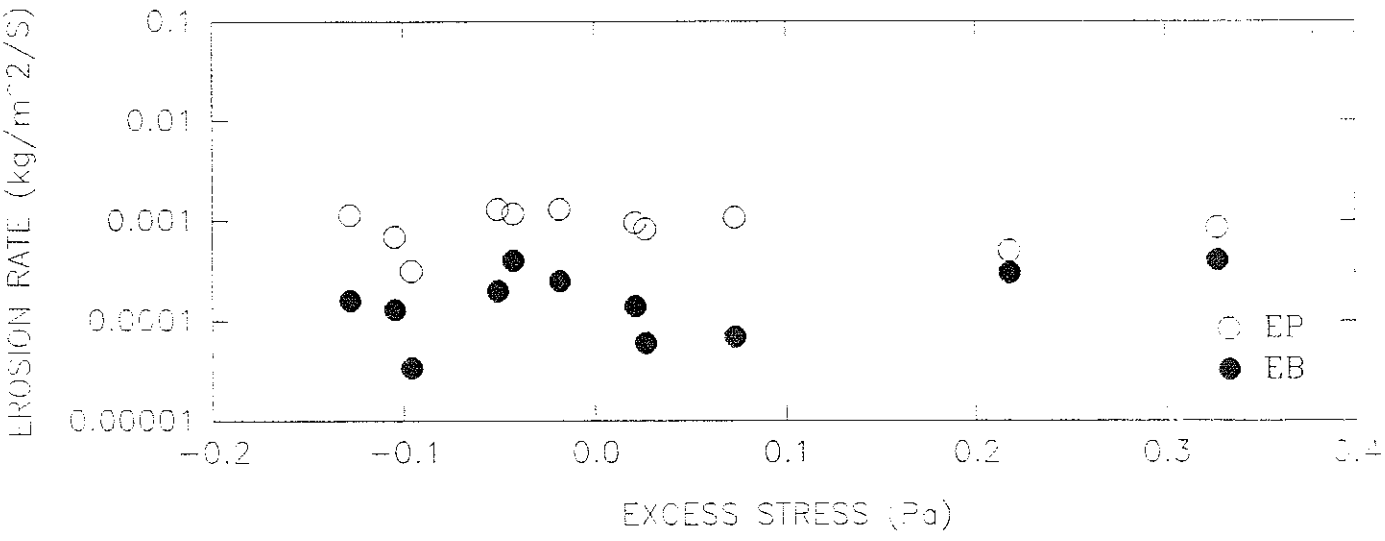

SEA CAROUSEL – MIRAMICHI ESTUARY

STATION MIR16 – 25 JULY, 1993

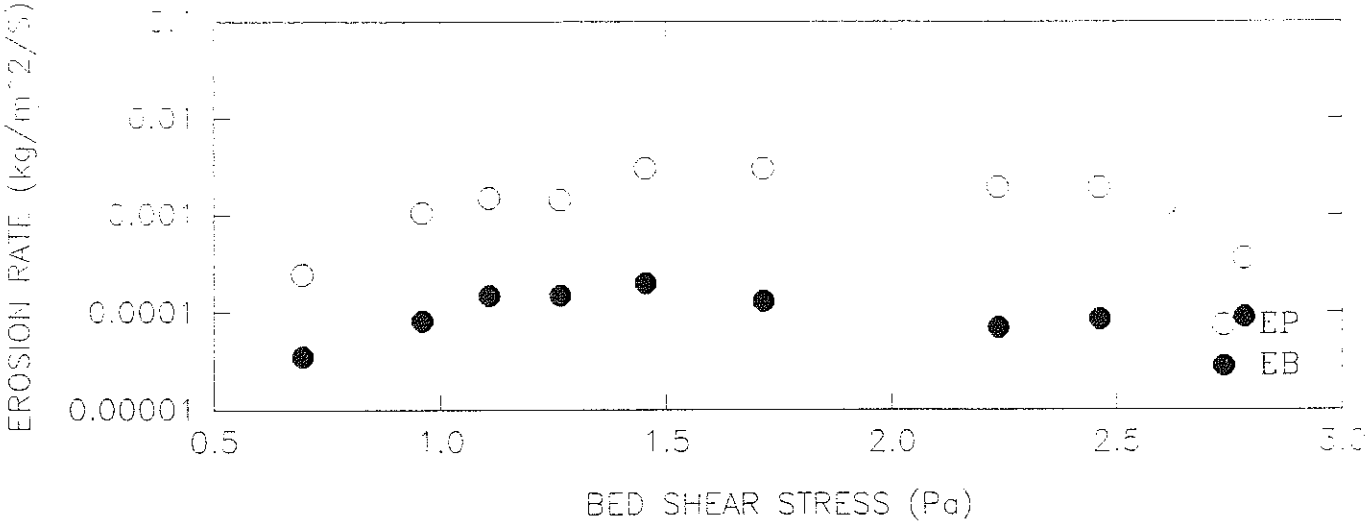

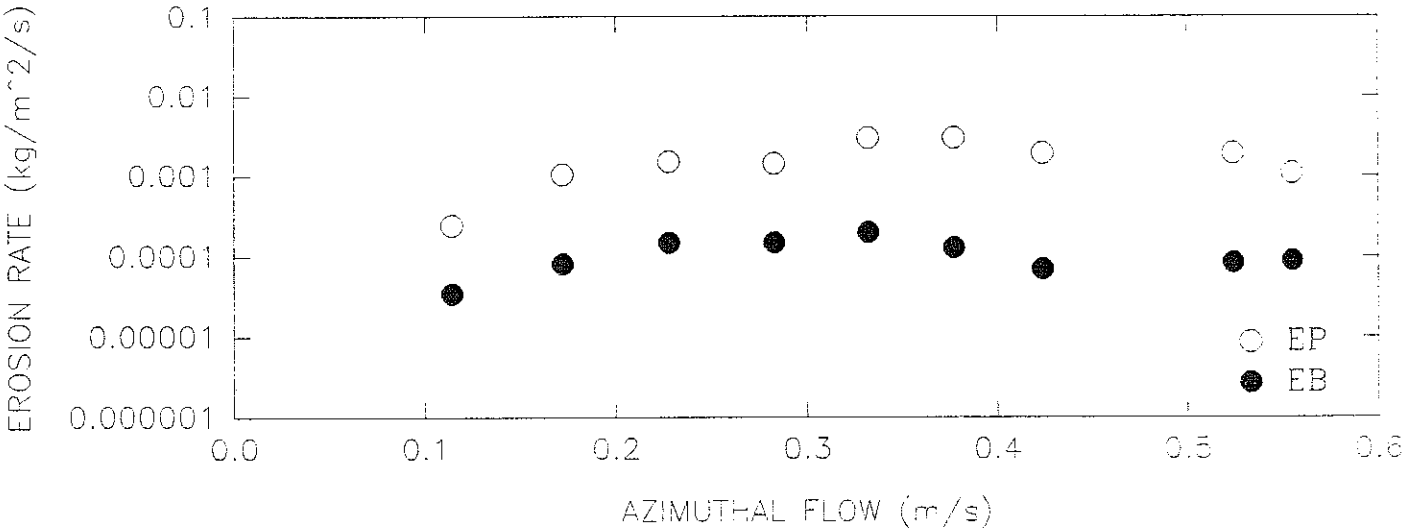

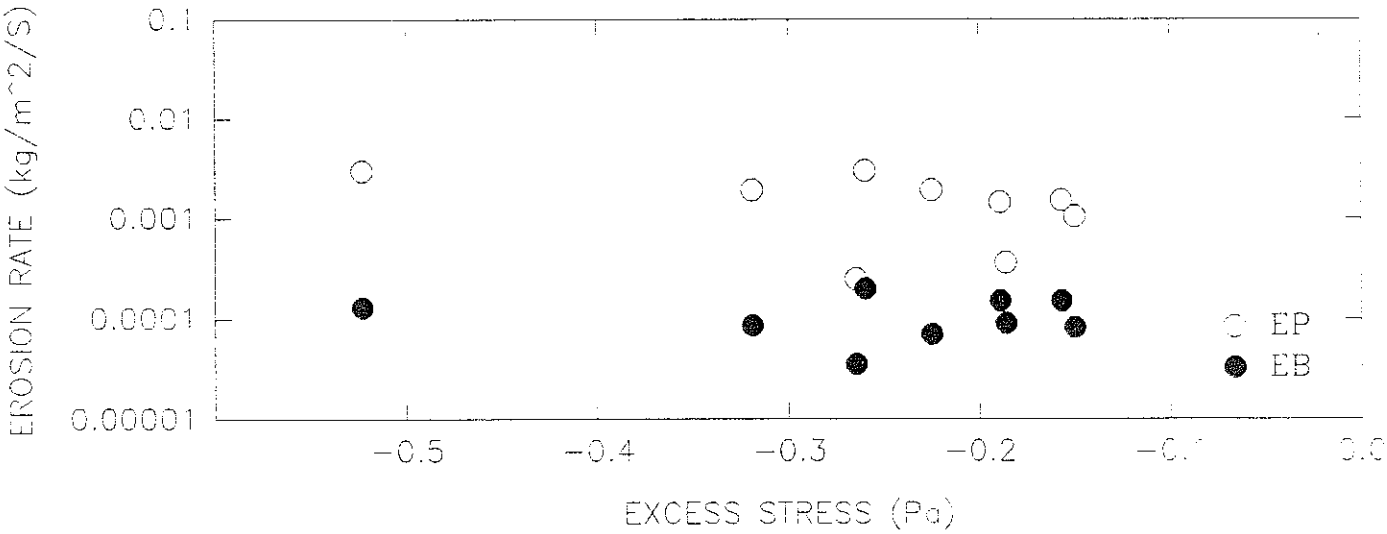

SEA CAROUSEL – MIRAMICHI ESTUARY

STATION MIR17 – 25 JULY, 1993

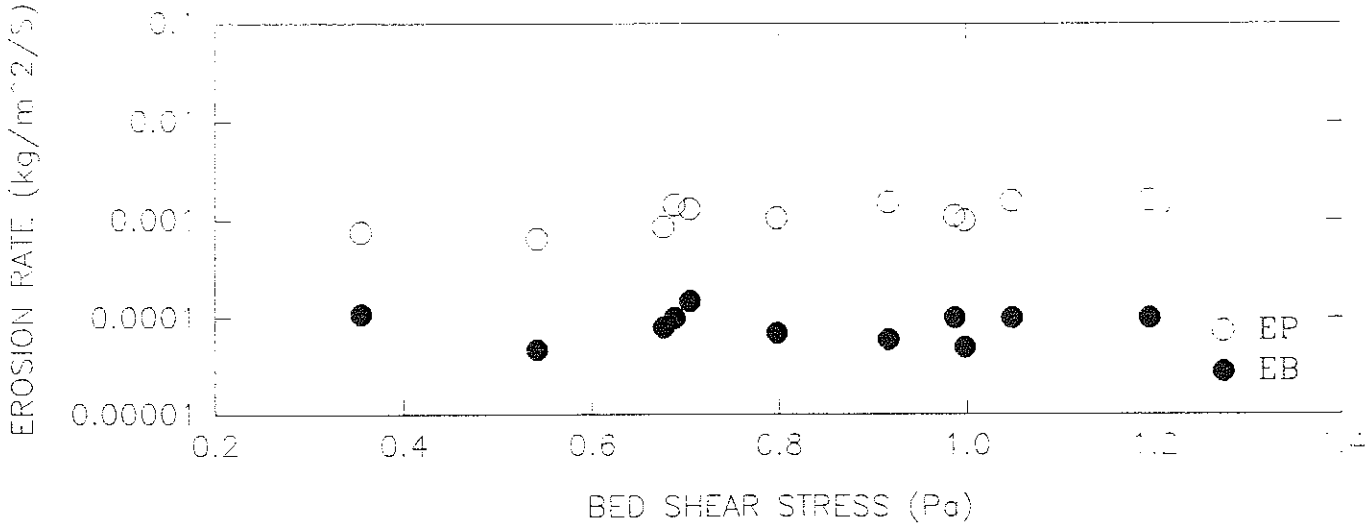

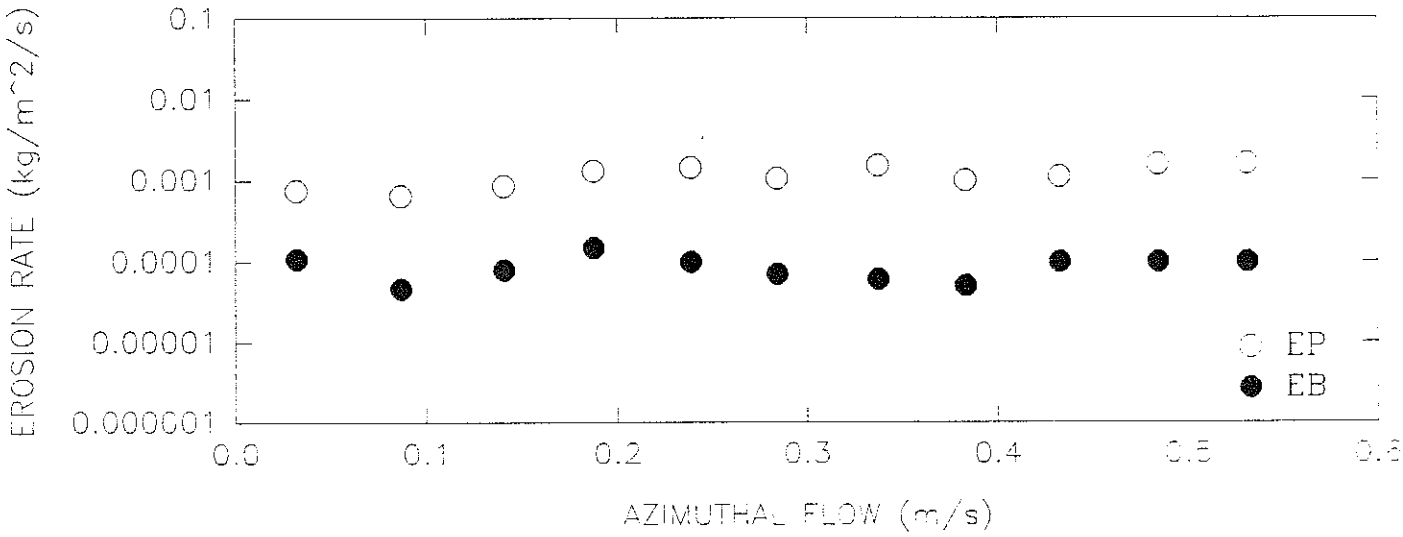

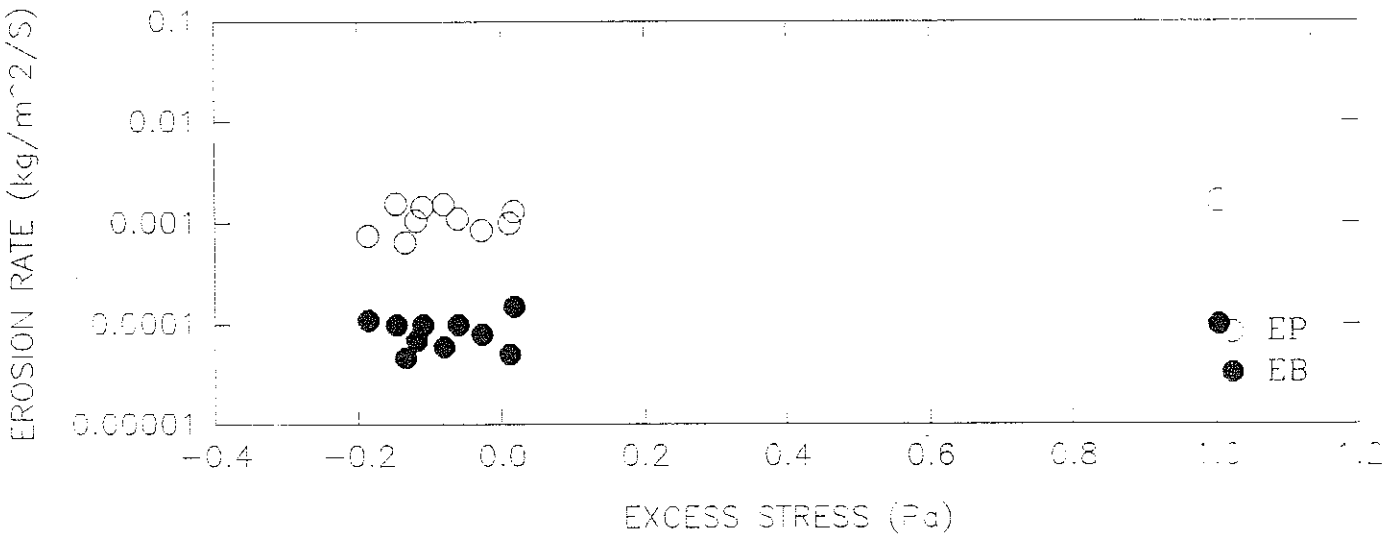

SEA CAROUSEL – MIRAMICHI ESTUARY

STATION MIR18 - 26 JULY. 1993

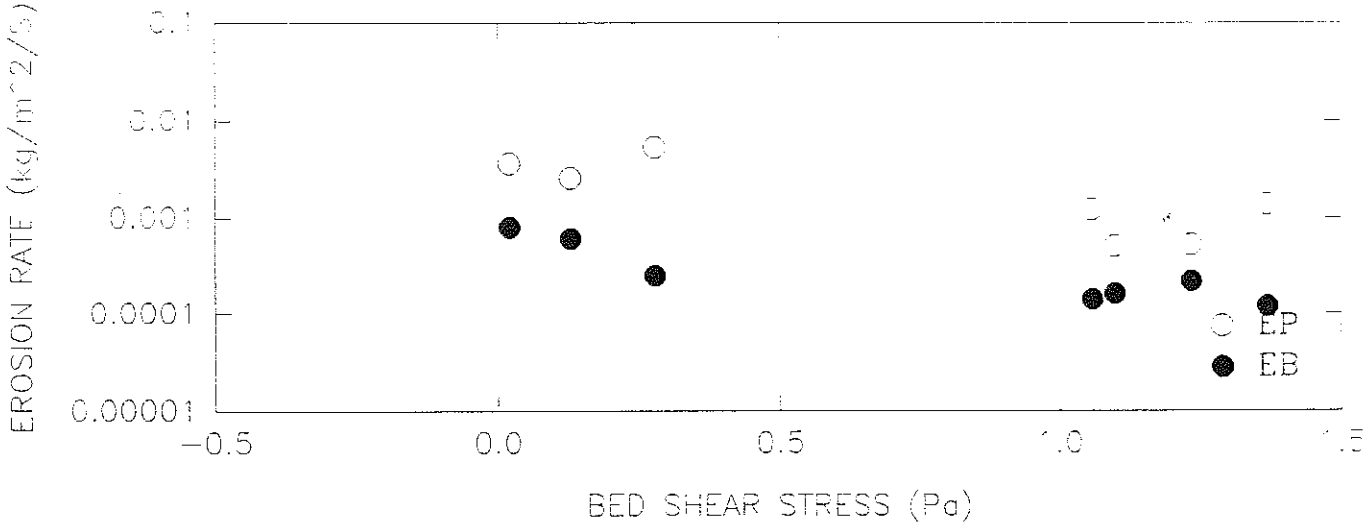

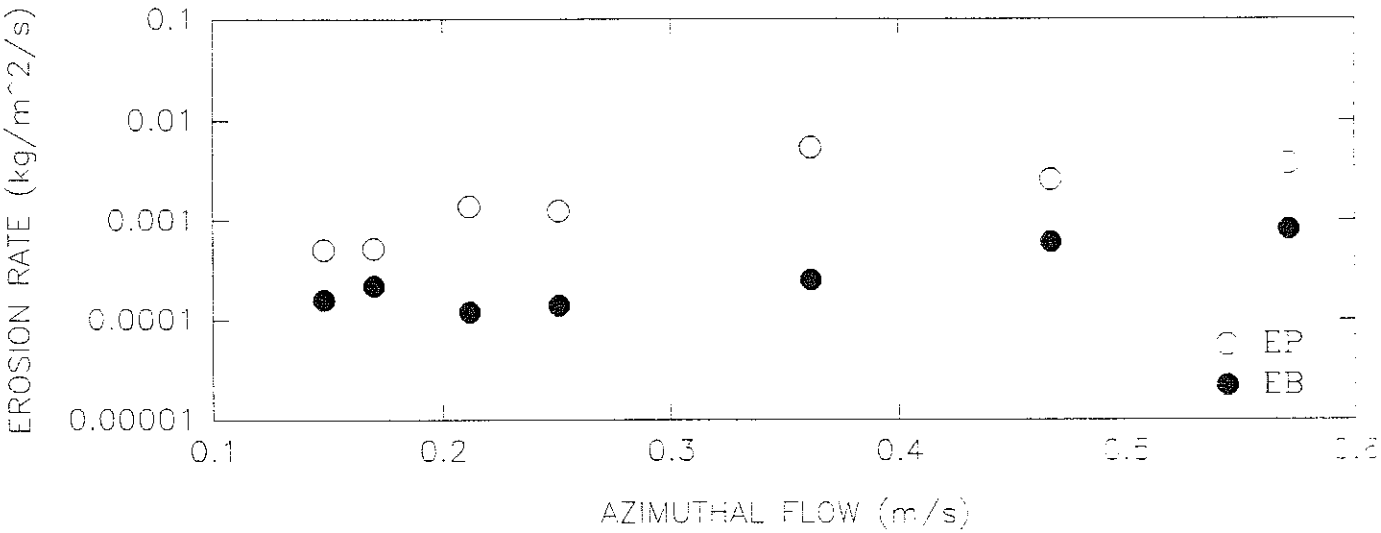

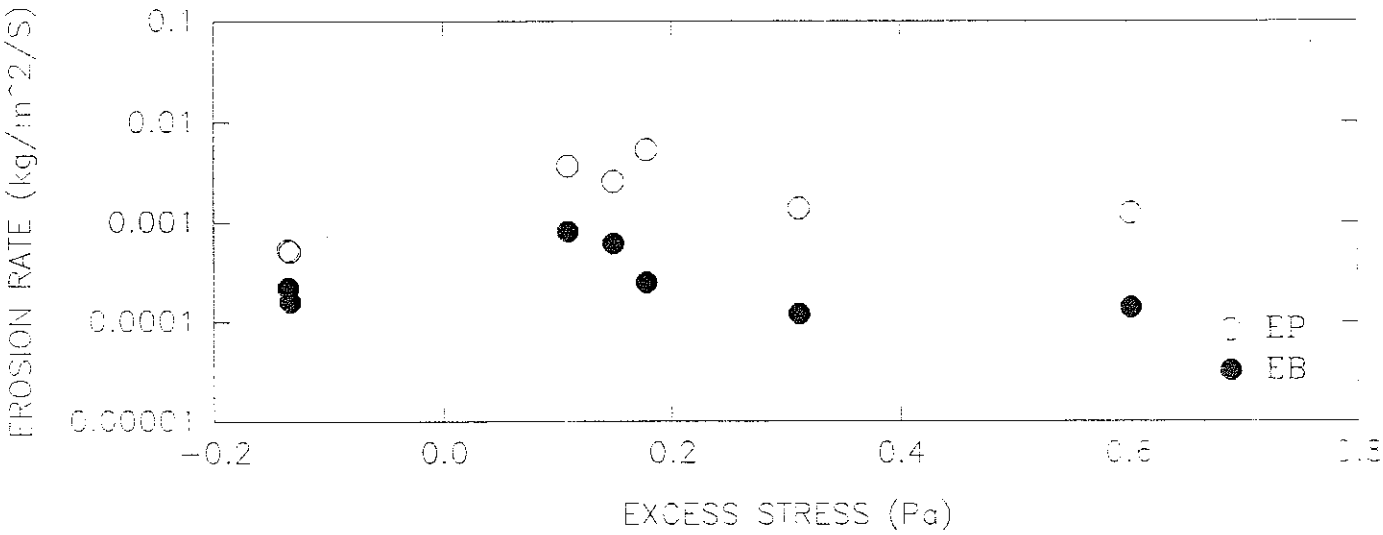

SEA CAROUSEL – MIRAMICHI ESTUARY

STATION MIR19 – 26 JULY, 1993

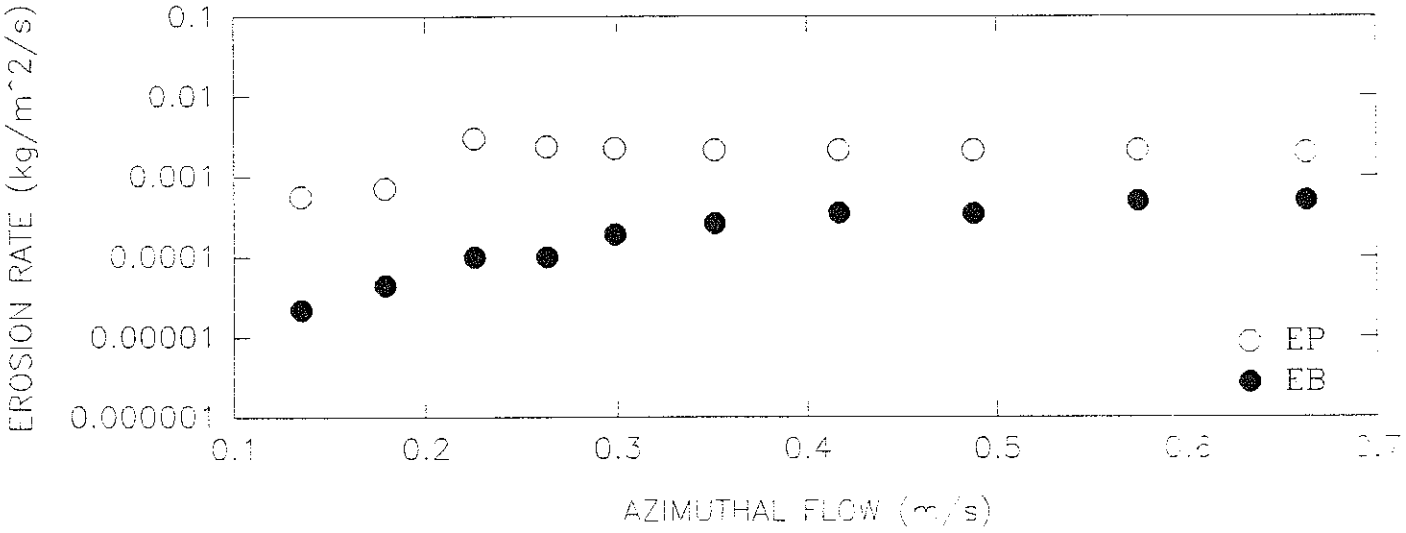

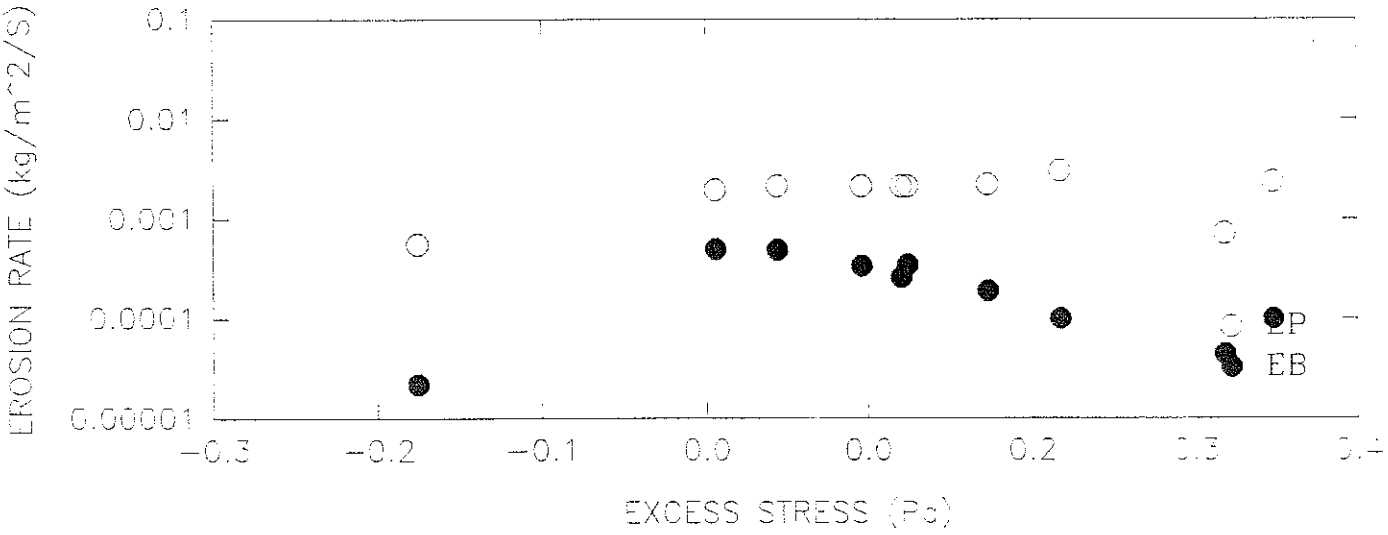

SEA CAROUSEL – MIRAMICHI ESTUARY

STATION MIR20 – 26 JULY, 1993

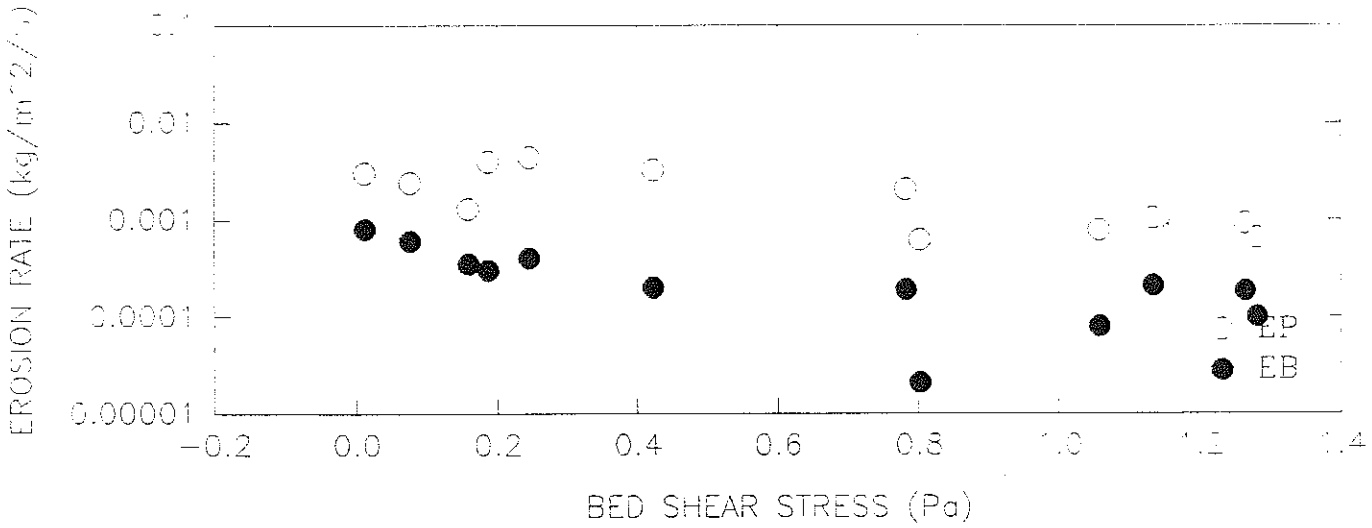

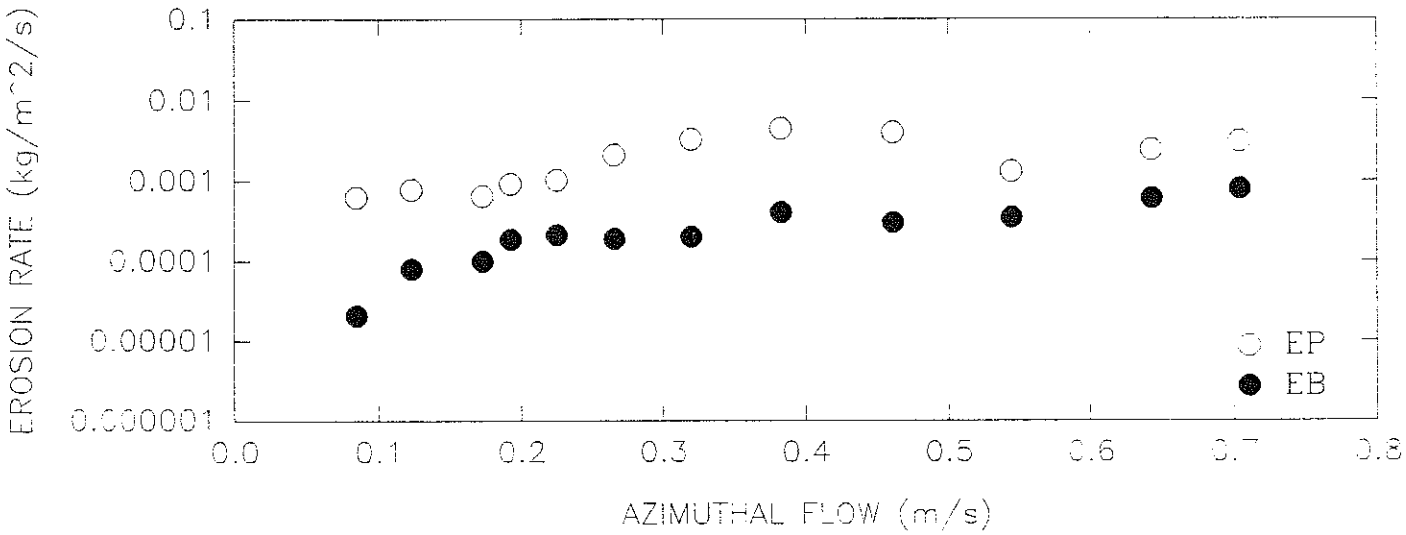

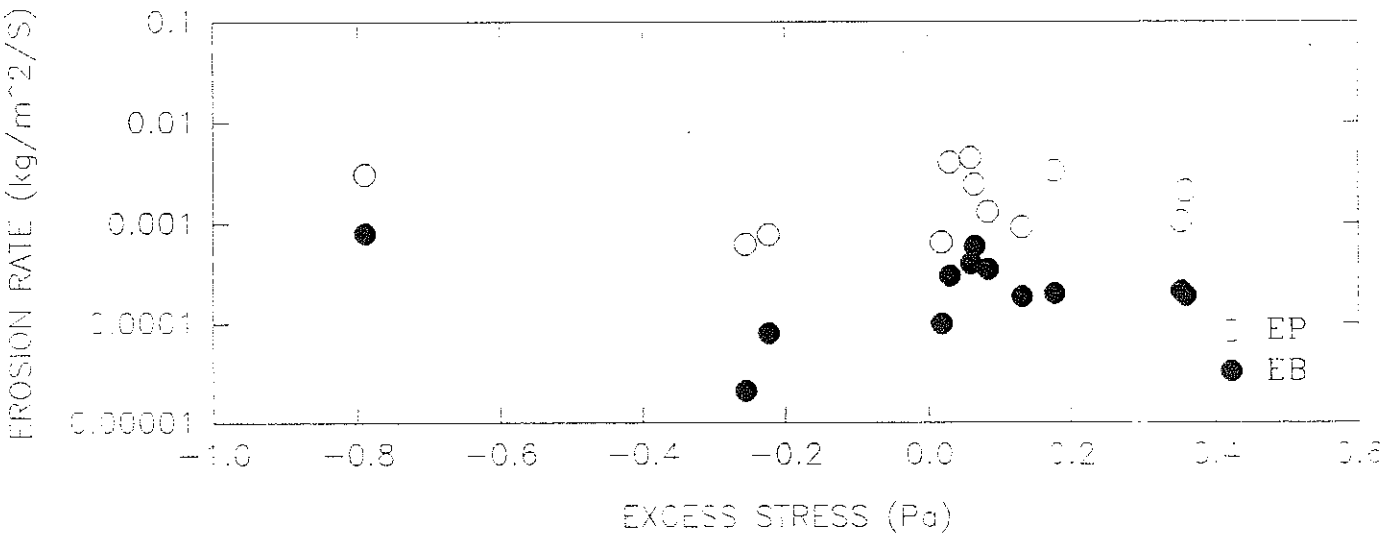

APPENDIX G

Relationship Between Bed Shear Stress, Azimuthal Flow and Excess Stress With Erosion Rate for Each Sea Carousel Deployment

(All times are ADT)

July 14 Lancelot 1 Station 4 (LAN001-21) Water Depth=5.2m

Water Cal @ 1518 for 10 min., in bot	60 scans/min.
Water Cal @ 1530 for 5 min.	45 cm bsb.
In Bottom @ 1537 for days hrs. min.	250 um stone
Pullout @ 1438 on July 20	3/16 in. tip
Water Cal @ 1439 for 10 min. on July 20	

(Deployed at channel margin for ship passage, accidentally set on bottom during 1st calibration.)

July 15 Excalibur 1 Station 6 (EXC06) Water Depth=5.5m Do=39m

Water Cal @ 1439 for 10 min.	120 scans/min.
In Bottom @ 1450 for 2 hrs. 39.4 min.	55 cm bsb.
Pullout @ 1705 on July 15	250 um stone
Water Cal @ 1706 for 5 min.	3/16 in. tip

July 15 Excalibur 2 Station 11 (EXC11) Water Depth=5.2m Do=0m

Water Cal @ 1735 for 10 min.	60 scans/min.
In Bottom @ 1746 for 21 hrs. 12.0 min.	55 cm bsb.
Pullout @ 1431 on July 16	250 um stone
Water Cal @ 1432 for 1 min.	3/16 in. tip
Valve opened after 120 min.	36.3cc recovered
Valve closed after 120 + 240 min.	21.7 deg. C (on deck)
Pi=0m (vacuum-deaired)	

July 16 Excalibur 3 Station 7 (EXC07) Water Depth=5.5m Do=39m

Water Cal @ 1710 for 10 min.	60 scans/min.
In Bottom @ 1721 for 42 hrs. 5.6 min.	55 cm bsb.
Pullout @ 1024 on July 18	35 um stone
Water Cal @ 1024 for 15 min.	3/16 in. tip

(Boat swung over instrument at 2030 hrs.)

July 19 Excalibur 4 Station 13 (EXC13) Water Depth=8.2m Do=39m

Water Cal @ 1052 for 10 min.	60 scans/min.
In Bottom @ 1103 for 2 hrs. 39.8 min.	55 cm bsb.
Pullout @ 1322 on July 19	35 um stone
Water Cal @ 1322 for 5 min.	3/16 in. tip

(Accidentally tugged on instrument while dropping anchor weight.)

July 19 Excalibur 5 Station 12 (EXC12) Water Depth=8.5m Do=39m

Water Cal @ 1350 for 10 min.	60 scans/min.
In Bottom @ 1405 for 2 hrs. 43.1 min.	55 cm bsb.
Pullout @ 1621 on July 19	35 um stone
Water Cal @ 1622 for 5 min.	3/16 in. tip

(Short chop, 0.5 sec. waves, our boat wake at 1744-1745 hrs.)

July 19 Excalibur 6 Station 8 (EXC08) Water Depth=5.3m Do=39m

Water Cal @ 1702 for 5 min.	300 scans/min.
In Bottom @ 1709 for 2 hrs. 11.3 min.	55 cm bsb.
Pullout @ 1902 on July 19	35 um stone
Water Cal @ 1902 for 5 min.	3/16 in. tip

(Deployed at same site as Station 06.)

July 19 Excalibur 7 Station 17 (EXC17) Water Depth=5.5m Do=2m

Water Cal @ 1952 for 10 min.	30 scans/min.
In Bottom @ 2004 for 16 hrs. 27.6 min.	55 cm bsb.
Pullout @ 1202 on July 22	35 um stone
Water Cal @ 1203 for 10 min.	3/16 in. tip
Valve opened after 70 min.	40.8 cc recovered
Valve closed after 70+360 min.	22 deg C (on deck)
Po=0m (vacuum-deaired)	

(Deployed near Lancelot 1 at channel margin.)

July 22 Lancelot 2 Station 18 (EXC18) Water Depth=7.0m

Water Cal @ 1009 min. for 5 min.	120 scans/min.
In Bottom @ 1016 for days	45 cm bsb.
Pullout @ 1014 on July 27	70 um stone
Water Cal @ 1015 for 5 min.	3/16 in. tip

(Deployed on control site with new plywood baseplate.)

July 22 Excalibur 8 Station 20 (EXC20) Water Depth=5.5m Do=39m

Water Cal @ 1112 for 10 min.	60 scans/min.
In Bottom @ 1118 for 3 hrs. 47.4 min.	55 cm bsb.
Pullout @ 1441 on July 22	70 um stone
Water Cal @ 1442 for 5 min.	3/16 in. tip

(Deployed on dumpsite, possible leak putting senosrs off-scale.)

July 23 Excalibur 9 Station 21 (EXC21) Water Depth=4.9m Do=39m

Water Cal @ 1047 for 10 min.	60 scans/min.
In Bottom @ 1058 for 4 hrs. 5.9 min.	55 cm bsb.
Pullout @ 1438 on July 23	70 um stone
Water Cal @ 1439 for 5 min.	3/16 in tip

(On dumpsite, deployed at high tide, previously was 20 ft. of water before dumping.)

July 23 Excalibur 10 Station 23 (EXC23) Water Depth=4.3m Do=39m

Water Cal @ 1505 for 15 min.	120 scans/min.
In Bottom @ 1520 for 2 hrs. 19.5 min.	55 cm bsb.
Pullout @ 1714 on July 23	70 um stone
Water Cal @ 1714 for 5 min.	3/16 in. tip

(On dumpsite, deployed at low tide.)

July 23 Excalibur 11 Station 24 (EXC24) Water Depth=5.3m Do=1m

Water Cal @ 1731 for 5 min.	60 scans/min.
In Bottom @ 1737 for 16 hrs. 47.6 min.	55 cm bsb.
Pullout @ 1002 on July 24	70 um stone
Water Cal @ 1003 for 5 min.	3/16 in. tip
Valve opened after 240 min.	36.6 cc recovered
Valve closed after 240+120 min.	22 deg C (on deck)

July 24 Excalibur 12 Station 25 (EXC25) Water Depth=6.4m Do=38m

Water Cal @ 1221 for 5 min.	60 scans/min.
In Bottom @ 1228 for 3 hrs. 42.5 min.	55 cm bsb.
Pullout @ 1552 on July 24	70 um stone
Water Cal @ 1553 for 5 min.	3/16 in. stone

July 24 Excalibur 13 Station 28 (EXC28) Water Depth=5.2m Do=38m

Water Cal @ 1642 for 5 min.	60 scans/min.
In Bottom @ 1650 for 18 hrs. 17.4 min.	55 cm bsb.
Pullout @ 1050 on July 25	70 um stone
Water Cal @ 1050 for 5 min.	3/16 in. tip

July 25 Excalibur 14 Station 29 (EXC29) Water Depth=5.5m Do=38m

Water Cal @ 1132 for 20 min.	120 scans/min.
In Bottom @ 1154 for 9 hrs. 8.7 min.	55 cm bsb.
Pullout @ 1614 on July 25	70 um stone
Water Cal @ 1615 for 5 min.	3/16 in tip

July 25 Excalibur 15 Station 31 (EXC31) Water Depth=5.5m Do=38m

Water Cal @ 1641 for 5 min.	60 scans/min.
In Bottom @ 1646 for hrs. min.	55 cm bsb.
Pullout @ 1016 on July 26	70 um stone
Water Cal @ 1017 for 5 min.	3/16 in. tip

July 26 Excalibur 16 Station 32 (EXC32) Water Depth=5.5m Do=38m

Water Cal @ 1040 for 15 min.	60 scans/min.
In Bottom @ 1057 for hrs. min.	55 cm bsb.
Pullout @ 1222 on July 26	70 um stone
Water Cal @ 1322 for 5 min.	3/16 in. tip

(Brushed bottom during 1st calibration?)

July 26 Excalibur 17 Station 33 (EXC33) Water Depth=4.6m Do=38m

Water Cal @ 1238 for 8 min.	60 scans/min.
In Bottom @ 1246 for hrs. min.	55 cm bsb.
Pullout @ 1619 on July 26	70 um stone
Water Cal @ 1619 for 5 min.	3/16 in. tip

(Located on freshly-dumped material about 1m in thickness, based on sounder.)

July 26 Excalibur 18 Station 36 (EXC36) Water Depth=5.5m Do=3m

Water Cal @ 1649 for 10 min.	60 scans/min.
In Bottom @ 1700 for hrs. min.	55 cm bsb.
Pullout @ 0943 on July 27	70 um stone
Water Cal @ 0949 for 5 min.	3/16 in. tip
Valve opened after 80 min	40.8 cc recovered
Valve closed after 80+180 min.	22 deg C (on deck)
Po=0m (vacuum-deaired)	

(Strong smell of hydrogen disulphide, ship leaving harbour in morning (unloaded), located on channel margin near Lancelot 1.)